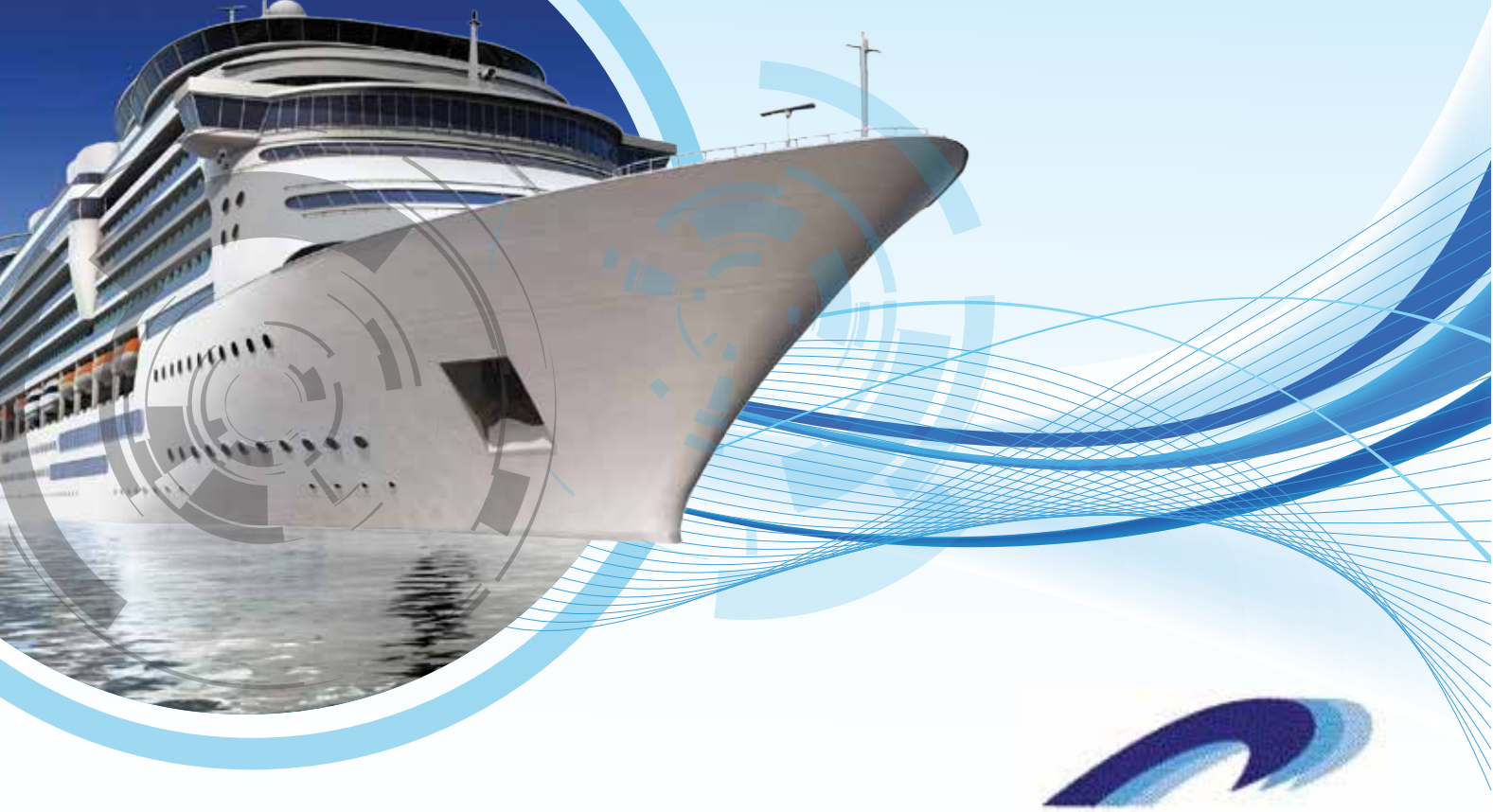

ISSW 2014

14th International Ship Stability Workshop

29 September - **1** October 2014

UTMSPACE Kuala Lumpur, Malaysia

Hosted by:

UTM
UNIVERSITI TEKNOLOGI MALAYSIA

Marine Technology Centre,
Universiti Teknologi Malaysia

Co-Sponsor:

MALAYSIA JOINT BRANCH

Malaysia Joint Branch
Royal Institution of Naval Architects (RINA)
& Institute of Marine Engineering, Science
and Technology (IMarEST)

PROCEEDING BOOK

TABLE OF CONTENT

SESSION 1: DYNAMICS OF LARGE AMPLITUDE MOTIONS & DESIGN IMPLICATIONS

Development of Minimum Bow Height Formula for Indonesian Waters
Mochammad Zaky (Indonesia) 1

What is Surf-Riding in Irregular Seas?
Kostas J. Spyrou, Nikos Themelis, Loannis Kontolefas (Greece) 12

Quantitative Assessment of Ship Behaviour in Critical Stern Quartering Seas
Maria Acanfora, Jerzy Matusiak (Finland) 19

Regulatory Use of Nonlinear Dynamics: An Overview
William S.Peters, Vadim Belenky (USA), Kostas Spyrou (Greece) 28

Applicability of the Difference between Population Statistics as an
Acceptance Criteria Metric for Seakeeping Validation
Aurore V. Zuzick, Arthur M. Reed, William F. Belknap, Bradley L. Campbell (USA) 36

SESSION 2 : NAVAL SHIPS STABILITY

Features Architecture of Mean Ship to Navigation in Heavy,
Stormy and Ice Conditions on the Northern Seas
Vasily N. Khramushin (Russia) 47

A New Approach to the Derivation of V-Line Criteria for a Range of Naval Vessels
Andrew Peters, Rick Goddard, Nick Dawson (UK) 58

Small Combatant Accidental Damage Extents
Steve Marshall, Rick Goddard, Dominic Horner, Ian Randles (UK) 67

SESSION 3 : NEW EXPERIMENTAL TECHNIQUES FOR SHIP STABILITY ASSESSMENT

Remarks on Experimental Validation Procedures for
Numerical Intact Stability Assessment with Latest Examples
Naoya Umeda, Daichi Kawaida, Yuto Ito, Yohei Tsutsumi, Akihiko Matsuda, Daisuke Terada (Japan) 77

Model Experiments in Following and Quartering Seas using a Small Size Ship Model
Mitsuhiro Nakamura, Yasuo Yoshimura, Daisaku Shiken (Japan) 85

Experimental Database for Surf-Riding and Broaching-to
Quantification based on Captive Model Tests in Waves
Boris Horel, Pierre-Emmanuel Guillerm, Jean-Marc Rousset, Bertrand Alessandrini (France) 94

Air Pressure Scale Effects during Damage Model Tests
Gyeong Joong Lee (Korea), Frans van Walree (Netherlands), Arthur M. Reed (USA), Andrew Peters (UK),
Paola Gualeni (Italy), Toru Katayama (Japan), WenYang Duan (China) 105

Forensic Study of BOUVET Capsizing
Jean-Yves Billard, François Grinnaert, Isabelle Delumeau,
Pierre Vonier, Paul Creismeas, Jean-François Leguen (France), Larrie D. Ferreiro (USA) 110

Experimental and Numerical Study on Predicting Method of Parametric Rolling in Regular Head Seas
Jiang Lu, Min Gu (China), Naoya Umeda (Japan) 117

Experimental and Numerical Study on Roll Restoring Variation using the C11 Containership
Min Gu, Jiang Lu, Tianhua Wang (China) 126

SESSION 4: STOCHASTIC DYNAMICS OF SHIPS AND ASSESSMENT OF PROBABILITY OF STABILITY FAILURES

Calculation Scheme for Wave Pressures with Autoregression Method
Alexander Degtyarev, Ivan Gankevich (Russia) 135

Example of Validation of Statistical Extrapolation
Timothy Smith (USA) 140

Critical Distance on a Phase Plane as a Metric for the Likelihood of Surf-Riding in Irregular Waves
Vadim Belenky, Kenneth Weems (USA), Kostas Spyrou (Greece) 144

On the Application of the Generalized Pareto Distribution for Statistical Extrapolation
in the Assessment of Dynamic Stability in Irregular Waves
Bradley Campbell, Vadim Belenky, Vladas Pipiras (USA) 149

SESSION 5: STABILITY OF OFFSHORE FLOATING PLATFORMS

An Experimental Investigation on Reduction of List Angle of a Semi-submersible Platform in Head Sea
Nam Woo Kim, Bo Woo Nam, Young Myung Choi, Sa Young Hong (Korea) 157

SESSION 6: MANEUVERABILITY AND STABILITY CONSIDERATIONS IN ADVERSE CONDITIONS

A Numerical Study on Maneuverability under Steady Equilibrium
Condition in Waves for Free-running Model Ship
Ryosuke Suzuki, Michio Ueno, Yoshiaki Tsukada (Japan) 167

Criteria for Minimum Powering and Maneuverability in Adverse Weather Conditions
V. Shigunov (Germany), A. Papanikolaou (Greece) 174

SESSION 7: NUMERICAL APPROACHES TO SHIP STABILITY

Design and Construction of Computer Experiments in Fluid Mechanics and Ship Stability
Alexander Degtyarev, Vasily Khramushin, Vladimir Mareev (Russia) 187

The Inertia Contributions due to Floodwater Mass
Gyeong Joong Lee (Korea), Arthur M. Reed (USA), Frans Van Walree (Netherlands), Andrew Peters (UK),
Paola Gualeni (Italy), Toru Katayama (Japan), Wenyang Duan (China) 199

Numerical Estimation and Validation of Shallow Draft Effect on Roll Damping
Toru Katayama, Jun Umeda (Japan), Burak Yildiz (Turkey) 204

Modelling of Extreme Waves Related to Stability Research
Janou Hennig, Frans van Walree (Netherlands) 210

An Analysis of Bilge Keel Effects using RANS with Overset Grids Method
Motoki Araki, Kunihide Ohashi, Nobuyuki Hirata (Japan) 216

Numerical Investigation into Ship Stability Failure Events in Quartering Seas Based on Time Domain Weakly Nonlinear Unified Model
Liwei Yu, Ning Ma, Xiechong Gu (China) 229

Deriving the Linear-Wave Spectrum from a Nonlinear Spectrum
Arthur M. Reed, John G. Telste (USA) 236

High Performance Algorithms for Multiphase and Multicomponent Media
Bogdanov A, Stankova E, Mareev V (Russia) 242

SESSION 8: HIGH SPEED AND SPECIALIZED CRAFT STABILITY AND SAFETY

A Study on Spinout Phenomena of Planing Craft in High Speed Turning with Radio Control Small Model
Toru Katayama, Shun Ohashi (Japan) 249

Stability Analysis of Hybrid Catamaran Fishing Vessel
Pramudya I Santosa, I K A P Utama, T W Wuruk Pribadi (Indonesia) 254

Selecting Monohull, Catamaran and Trimaran as Suitable Passenger Vessels Based on Stability and Seekeeping Criteria
Richard B Luhulima, D Setyawan, I K A P Utama (Indonesia) 262

SESSION 9: DAMAGE STABILITY STANDARD OF OLD SHIPS

Application of Second Generation IMO Intact Stability Criteria to Medium – Sized Fishing Vessels
Marcos Míguez González, Vicente Díaz Casás, Luis Pérez Rojas, Fernando Junco Ocampo, Daniel Pena Agras (Spain) 269

Consideration of Risk Level in Terms of Damage Stability of Old Ship
Tomohiro Yuzui, Yoshitaka Ogawa (Japan) 278

Stability of Grounded Ship
Apurba Ranjan Kar (India) 286

Regulatory, Design, Operational and Emergency Response Measures for Improving the Damage Survivability of Existing RoPax
Dracos Vassalos, Evangelos Boulougouris, Luis, Guarin, Andrzej Jasionowski, John Garner (UK) 292

- SESSION 1 -

DYNAMICS OF LARGE AMPLITUDE MOTIONS & DESIGN IMPLICATIONS

Development of Minimum Bow Height Formula for Indonesian Waters

Mochammad Zaky

Dept. Research and Development, PT. Biro Klasifikasi Indonesia (Persero), Indonesia

Abstract: Freeboard was considered long ago as an important element of ship safety. It was recognized that in order to maintain seaworthiness ships must possess some amount of reserve buoyancy, i.e. some volume above the water-plane and below the watertight deck. Indonesian Bureau Classification, known as BKI (Biro Klasifikasi Indonesia) has authorized by the Government to carry out the survey and certification of load line. The study of minimum freeboard and bow height will be performed on ships register BKI for Indonesian waters are later become a reference in the calculation on load line. Bow height correction is performed based on probability of deck wetness analysis using strip theory. Both analysis of ship response (RAO) are performed at two positions are amidships position by beam sea condition that affect rolling motion and stem position by head sea condition that affect coupled motion of heaving and pitching. Probability of deck wetness was taken from the stern, amidships and particularly on stem position for 22 ship models. Development of the bow height calculation was modified using 4 scenarios that resulted linear regression formula of bow height minimum by ships length and wave height as parameters where the optimum results are in scenario 3 which assumes when the longer of the ships makes the wave higher and these results allow to reduce of bow height minimum up to 35 % from bow height minimum calculation according to Regulation 39 ILLC 1966 as amended Protocol 88.

Key words: freeboard, BKI, bow height, deck wetness, seakeeping, strip theory, beam sea, rolling, head sea, heaving, pitching

1. Introduction

Various kinds of marine transportation operating in indonesian waters to support the mobility both of people and goods, as well as a mode of transportation for connecting inter islands. Increased of national marine transportation activities will have an impact on the increasing incidents and accidents. It was shown by the high of ship accident in Indonesian waters. Based on the data from ministry of sea transportation during the period of 2007-2011there has been 27 ship accidents in Indonesian waters caused by sinking 37%, fire/explosion 41%, and 22% of collision [1]. One of the ship safety is affected by the freeboard and bow height parameters according to load line regulation, where one of the causes of sinking is shipping of green water is caused primarily by the relative deck motion [2]. Several countries have been involved in studies related to the revision of load line regulation ILLC 1966. The revision consists of several parts regarding the regulation of freeboard and bow height minimum related with deck wetness, and also issue of watertight integrity, the size and location of openings, crew safety, and the interpretation of the regulations relating to other IMO instruments. In Indonesia, some researchers have conducted a study related to the characteristics of the ship motion when operating in Indonesian waters, one of the largest studies that have been done is cooperation between several universities in Indonesia and Japan, as well as ministry of research and technology of Indonesia [3].

1.1 BKI Ship Register

BKI as the national classification bodies which classifying Indonesian flag ship have been authorized by the Indonesian government to carry out survey and issue load line certificates for national voyage, KM 3 Decree Year 2005 [4] and international voyage, ICLL 1966 [5]. That it is extremely necessary for BKI to contribute by giving a suggestion to the administration in the formulation of domestic rules especially on load line through by study of ship behavior or seakeeping

when operating in Indonesian waters, especially for ships that have been registered in BKI.

According to the ship registered in Ministry of sea transportation, the number of Indonesian flag ship up to April 2010 is 52.890 units consisting of gross tonnage < 500 GRT amount to 46.076 units and gross tonnage ≥ 500 GRT amount to 6.814 units [6]. Another data from BKI informed that the ship registered up to July 2012 with total amount 8192 units, with the total gross tonnage of 12.911.545 GRT, by population of 34% pusher and tug boat, pontoon and barge is 32%, general cargo is 10.5%, tanker 5%, passenger and ro-ro ferries 4.5% and 14% for other types [7]. Furthermore BKI ship registered based on ship age expressed that mostly at the age of 0-5 years and the age of the vessel > 25 years, for 0-5 years mostly barge and tug boat and for the ship age > 25 years are the second hand ships imported from abroad.

1.2 Indonesian Vessels Overview

Currently the conditions of vessel in Indonesia in particular related with the freeboard and bow height minimum can be classified that ships with large ratio B/D and low freeboard are ro-ro ferries, landing craft, and self propulsion barge generally do not have forecastle, then bow height is calculated to the main deck as upper deck. And general cargo ship especially those imported from Japan mostly draught increased by ship owners to add the cargo, which initially the maximum draft position below the tween deck as freeboard deck, then after draft increased the position of freeboard deck changed to the upper deck. This affected in a reduction of the minimum bow height so it does not complies with the minimum bow height requirements according to regulation of ICCL 1966.

2. Bow Height and Probabilistic Deck Wetness Approach

Bow height (Fb) defined as the vertical distance at the forward perpendicular between the waterline corresponding to the assigned summer freeboard and the designed trim and the top of the exposed deck at side, based on the international load line regulation 39 ICCL 1966 with the standard ICLL ships (C_b = 0.68 at d = 0.85D), shall be not less than:

$$56L\left(1-\frac{L}{500}\right)\cdot\frac{1.36}{C_b+0.68} \quad \text{mm for L < 250 m} \qquad (1)$$

$$7000\frac{1.36}{C_b+0.68} \quad \text{mm for L > 250 m} \qquad (2)$$

Development of the revision of bow height formula has been done by some studies based on probability deck wetness [8]. Some results and recommendations submitted to the IMO especially on Sub Committee Stability and Load Line on Fishing Vessel (SLF) by the regulation which contained on the regulation 39 ICLL as amended protocol 88, where the bow height shall not be less than:

$$F_b=\left(6075\cdot\left(\frac{L}{100}\right)-1875\cdot\left(\frac{L}{100}\right)^2+200\cdot\left(\frac{L}{100}\right)^3\right)\times\left(2.08+0.609C_b-1.603C_{wf}-0.0129\cdot\left(\frac{L}{d_1}\right)\right) \qquad (3)$$

Where F_b is bow height minimum, L is length at draught d_1, B is moulded breadth, d_1 is draught at 85% of the depth D, C_b is block coefficient at d_1, C_{wf} is waterplane area coefficient forward of LPP/2.

The phenomenon of shipping of water on deck or green water is caused primarily by the relative deck motion, that is the motion of the forward deck relative to the surface, but depends also on the height of the freeboard. It is often important to be able to predict the probability of deck wetness in a particular cycle of motion. The probability that the immersion exceeds the effective freeboard [9] is defined as:

$$P_S = P\{S_a > F_b\} = \exp\left[\frac{-H_b{}^2}{2m_{0s}}\right] \qquad (4)$$

Where Ps is the probability of deck wetness, S_a is the vertical relative motion amplitude at the bow, F_b is the freeboard effective, m0s is area relative motion spectrum, Hb is the bow height minimum. This yields for the bow height Hb:

$$Hb = \sqrt{-2m_{0s}.\ln(P_S)} \qquad (5)$$

There are some wave spectrum which has developed, one of which was applied to this study is the Pierson Moskowitz spectrum [10] with the spectrum formula:

$$S_{\zeta}(\omega) = 172.8 \bullet T_1 \bullet (\zeta_{w1/3})^2 (T_1 \bullet \omega)^{-5} \bullet \exp\left[-691(T_1 \bullet \omega)^{-4}\right] \quad (6)$$

Where ω is the circular frequency, $\zeta_{w1/3}$ is the significant wave height, T_1 is the average wave period, T_p is the peak period, where $T_p/T_1 = 1.296$. The selection of this spectrum based on the parameter of spectrum measurements which was taken from closed sea in the gulf Mexico that having similarities with the geographical conditions in Indonesian waters.

Furthermore the ship response was obtained by the solution numerically of ship motion equations using SHIPMO software with 2D strip theory, particularly analyze on *heaving*, *pitching* and *rolling* motions. The formula for the solution of motion equation based on Newton's second law in six degree of freedom can be written as follows:

$$\sum_{n=1}^{6}(M_{jk} + A_{jk})\ddot{\varsigma}_k + B_{jk}\dot{\varsigma}_k + C_{jk}\zeta = F_j e^{i\omega t} \quad j,k = 1,2,3,4,5,6 \qquad (7)$$

Where M_{jk} is vessel mass matrice, A_{jk} is added mass matrice, B_{jk} is damping coefficient, C_{jk} is restoring force coefficient, $\zeta, \dot{\zeta}, \ddot{\zeta}$ are displacement, velocity, acceleration amplitude, $\zeta_1 = \zeta_x$ is displacement of x direction or *surge* motion, $\zeta_2 = \zeta_y$ is displacement of y direction or *sway*, $\zeta_3 = \zeta_z$ is displacement of z direction or *heave*, $\zeta_4 = \zeta_\phi$ is angular motion amplitude towards x direction or *roll*, $\zeta_5 = \zeta_\theta$ is angular motion amplitude towards y direction or *pitch*, $\zeta_6 = \zeta_\psi$ is angular motion amplitude towards z direction or *yaw*, F_1, F_2, $F_3 = F_x$, F_y, F_z are exciting or encountering forces which resulting the translation motions *surge*, *sway* and *heave*, F_4, F_5, $F_6 = F_\phi$, F_θ, F_ψ are exciting or encountering momets which resulting the angular motions *roll*, *pitch* dan *yaw*.

To determine the bow height minimum for Indonesian waters required a clarification through a ship model experiment to analyze the deck wetness that can be known the quantity of green water, with some constraints on the ship speed, wave heading, and point of deck wetness. Furthermore, the results of should be meet with the seakeeping criteria according to NordForsk, 1987 [11].

3. Experiment and Numerical Simulation

The selection of vessel models in this study were taken from BKI ship register which includes the type of vessels are general cargo, passenger and ferry, landing craft, self propelled barge and pontoon, fishing boats and speed boat. Then each type of vessel is taken one sample model with a length parameter based on the largest population for each type of vessel. The results are various ship models based on ship length 7 up to 250 meters. The ship data and body plans are expressed in Table 1 and Figure 1.

Table 1 Ships data taken from BKI Ship Register

No	Initial	Tipe	LOA (m)	LBP (m)	Bmld (m)	Hmld (m)	T (m)	Cb	Disp. at T (Tonne)	Vs (knot)
1	KI -1	Speed Boat	7.2	6.35	2.36	1.2	0.6	0.649	5.561	23
2	KI -2	Sea truck	10.75	10.75	3.36	1.3	0.75	0.736	18.31	23
3	KI -3	Crew Boat	16	14.32	4	2	0.67	0.45	14.28	28
4	KI -4	Tug Boat	28	26.34	7.8	3.5	2.75	0.65	390	10
5	KI -5	General Cargo	42	38	7.8	3.7	2.72	0.73	603	11.27
6	KI -6	SPOB	48.32	45.5	9	3	2.4	0.831	886.8	10
7	KI -7	Fishing Vessel	53.51	46.9	8.7	3.75	3.4	0.7	948	11.5
8	KI -8	Ferry Ro-Ro	55.5	47.25	13	3.45	2.45	0.65	1006	12
9	KI -9	General Cargo	57.6	53	9.3	5.55	3.5	0.69	1273	10
10	KI -10	LCT	60	51.73	11	3.2	2.56	0.83	1235	10
11	KI -11	Tanker	75.78	71.25	11.5	5.1	4.65	0.69	2694	12.5
12	KI -12	Cement Carrier	77.97	72	12.3	5.8	5.2	0.72	3524	11
13	KI -13	Passenger	89.58	83.4	16	5.5	4.5	0.503	3132	17
14	KI -14	Pontoon	91.44	87.78	24.38	5.48	4.295	0.88	8650	10
15	KI -15	General Cargo	113.63	103.43	19	8.91	6.55	0.71	9400	15
16	KI -16	Container	115.5	105.6	17	9	5.8	0.794	8485	12
17	KI -17	Cement Carrier	122.68	115	18	9.1	7.331	0.766	11911	13.5
18	KI -18	Passenger	123	115.5	18	12.3	6.25	0.603	8283	17
19	KI -19	General Cargo	127.73	119.8	18	8.2	6.2	0.821	11536	12
20	KI -20	Tanker	158	151.8	27	11.7	7	0.817	24025	14
21	KI -21	Bulk Carrier	223.13	213	32.2	17.9	13	0.803	73387	14.7
22	KI -22	Tanker	244.5	233	44	21.5	12.7	0.818	109417	15

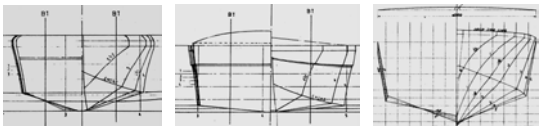

KI-1 KI-2 KI-3

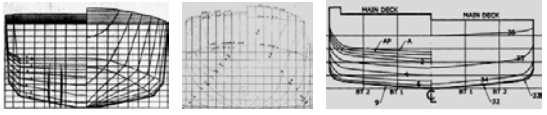

KI-4 KI-5 KI-6

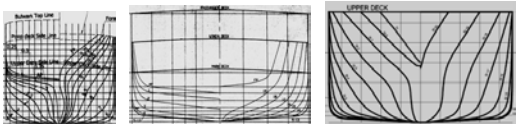

KI-7 KI-8 KI-9

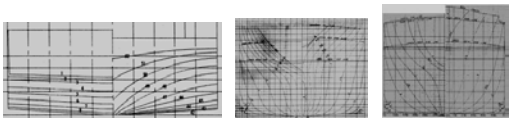

KI-10 KI-11 KI-12

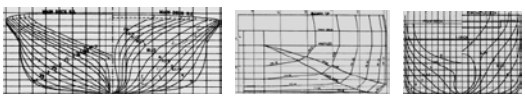

KI-13 KI-14 KI-15

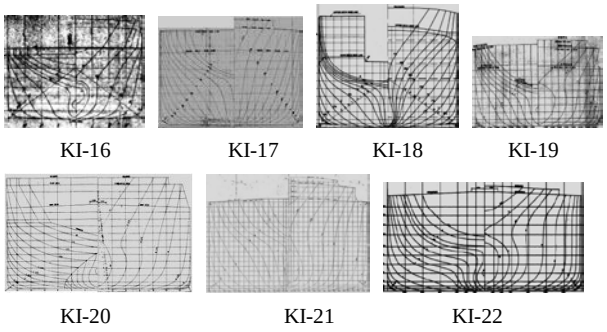

Fig. 1– Body Plan of 22 ship models

The wave data were retrieved by wave recording obtained from the Indonesian Meteorology, Climatology and Geophysics (BMKG) during 7.5 years from 2000 to 2007. Then divided the Indonesian territorial waters to 18 zones with boundaries of grid areas 10 latitude and 10 longitudinal, which is presented according to Figure 2, the area of each zone is taken 5 waves data points that are positioned at the corners of the zone and one point is positioned of the center of the zone, so if the position of these points to be connected to form a diagonal line and the five points will represent all the data within the zone. The number of waves data recording for 7.5 years at each point a number of (24 hours x 365 days x 7.5 years = 65,000 wave recording data for each point).

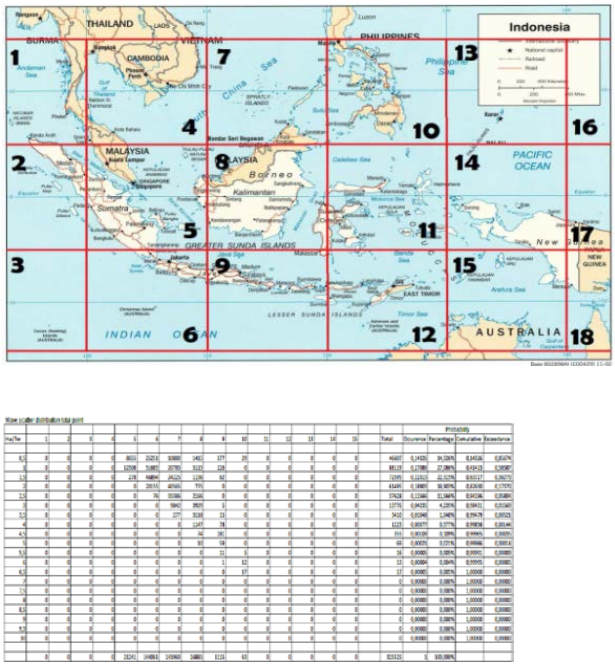

Fig. 2–Indonesian waters zone and scatter diagram zone 1

Furthermore, the overall wave data grouped in the form of a scatter diagram with parameters of wave height and period. From the scatter diagram calculated significant wave height (H1/3) and the largest number of periods in each area are displayed according to Table 2.

Table 2 Significant wave height and the largest period for each zone

Area	Hs (1/3) m	Period (T) sec	Area	Hs (1/3) m	Period (T) sec
1	2.382	6	10	2.445	6
2	2.154	6	11	1.750	6
3	2.679	7	12	1.786	6
4	2.137	6	13	2.465	6
5	1.907	6	14	1.998	6
6	2.318	6	15	2.266	6
7	2.495	6	16	2.241	6
8	1.709	6	17	1.834	6
9	1.925	6	18	2.456	6

To validate the numerical calculations performed physical model experiment using general cargo type which increased of ship draft when operating in waters of Indonesia, where the initial full load draft 3.3 meters to 3.5 meters, the ship particular according to Table 3. Probability deck wetness analysis done using model experiment for free running condition. The experiment was done at maneuvering and Ocean Basin (MOB) Hydrodynamics Laboratory with a size of 60 m x 35 m x 2.5 m for each length, width and depth. MOB is equipped with a wave generator for generating regular and irregular waves and wave absorber to dampen the reflected wave. The experiment conducted using irregular waves with a duration equivalent to about 2 hours in full scale.

Table 3 Ship Particular

Item	Ship	Model
LOA (m)	57.600	2.504
LPP (m)	53.000	2.304
Breadth, B (m)	9.300	0.404
Depth, H (m)	5.550	0.241
Draft, T Full Load (m)	3.500	0.152
Block Coefficient, Cb	0.690	0.690
Displasement (Tonne)	1273	0.102
LCG fromTransome (m)	26.077	1.134
VCG fromBaseline (m)	3.331	0.145
Roll Gyration, kxx (m)	2.530	0.110
Pitch Gyration, kyy (m)	13.800	0.600
Vessel Speed (knot)	10 (Fn=0.22)	2.085

The scale model of the ship is 1: 23 according to Figure 3, the deck is assumed straight from front to back without sheer, no chamber, no bulwark and without forecastle (no effective length). Ship model was ballasted to meet the draft, trim, radius of gyration in longitudinal and transversal using balance swinging.

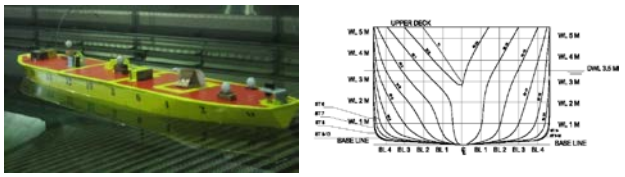

Fig. 3–Model and Body Plan

The experiment were conducted at irregular wave both of head seas (180 degrees) and beam sea (90 degrees) and using the Pierson Moskowitz wave spectrum [10], with the number of wave cycles of about 200, the peak period and significant wave height used in the experiment are peak period Tp = 8 sec and Hs = 1.3 meters, ship speed assumed of 10 knots (Fn = 0:22).

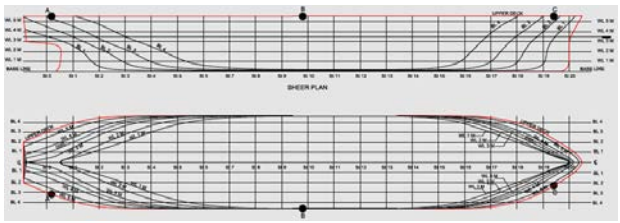

Fig. 4 – Point of Deck Wetness

The calculation both of the relative vertical motion and the probability of deck wetness measured at the position of the stem, middle and stern of the position of the point A, B and C according to Figure 4. The equipment used to capture the motion of the ship response in 2D and 3D that uses Qualisys Track Manager (QTM) software, then during the running experiment together with making a video recordings and photographs to see the visualization of the ship model motion.

The comparison of bow height (H_b) based on experimental and numerical for these model in accordance with the probability of deck wetness Ps ≤ 0.05 which assume of significant wave height 1.3 meters, are shown on Table 4. Where the probability of deck wetness calculated on the direction of head sea and beam sea with ship speed 10 knots (Fn = 0:22).

Table 4 Bow height comparison between experiment and numeric for each point based on Ps ≤ 0.05

Description	Heading	Ps 0.05 Hb Poin A (m)	Hb Poin B (m)	Hb Poin C (m)
Eksperiment	Head Sea	0.230	0.900	1.750
	Beam Sea	0.630	1.000	1.300
Numerical	Head Sea	1.286	0.694	1.457
	Beam Sea	0.939	0.775	0.674

While the probability of deck wetness value (Ps) for each point A, B and C on the existing bow height (H_b) is 2.05 meter, for head seas and beam sea condition as shown in Table 5.

Table 5 The comparison of Ps for existing bow height (H_b) 2.05 meter

Description	Heading	Bow Height (H_b) 2.05 meter Ps Poin A (%)	Ps Poin B (%)	Ps Poin C (%)
Eksperiment	Head Sea	0.000	0.000	2.000
	Beam Sea	0.000	0.000	0.000
Numerical	Head Sea	0.050	0.000	0.266
	Beam Sea	0.000	0.000	0.000

From the comparative results of experimental and numerical values with the similar parameters of the wave and ship, it can be known that for head sea condition noted especially at point C in stem position caused having the highest frequency of occurrence of deck wetness due to couple motions heaving and pitching, then for beam sea condition at point B in amidships position which has a high probability of deck wetness due to the rolling motion. From the comparison of the two (experimental and numerical) points C and B, the difference both of them was not significant and the further analysis of ship models can be performed using numerical calculation by SHIPMO software. The minimum bow height analysis to be concentrated on the probability of deck wetness to point C.

4. Result and Discussion

4.1 Bow Height Minimum Evaluation

The bow height calculation according to regulations 39 ILLC 1966 (ILLC, 2005) on some ship models shown at Figure 5 expressed that the longer ship required increasing bow height gradually, as linear curve. This is affected the parameters used in calculating of the bow height only consists variables of length and shape of the ship hull/block coefficient by assuming the same wave height for the difference ship length.

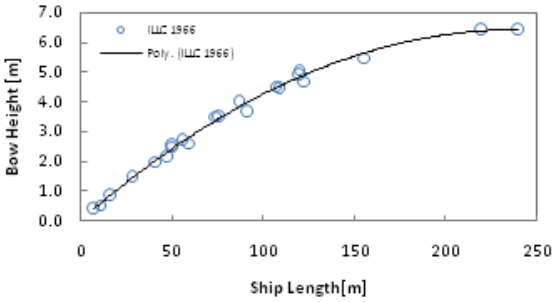

Fig. 5–Bow height minimum according to ILLC 1966

Furthermore, the bow height calculation according to Regulation 39 ILLC 1966 as amended by the Protocol 88, which expressed that the updated formula is analyzed using probability of deck wetness approach, where the value of bow height consist of some variables such as ship length, width, draft, block coefficient (C_b), coefficient of waterplane area forward (C_{wf}) and waterplane area forward (A_{wf}), if compared with previous bow height (according ILLC 1966) which only uses a ship length and block coefficient Cb 0.68 parameters. The results of bow height calculation for 22 vessels according to Figure 6 shows that the curvature shape of bow height decrease for some vessels with large hull size and length (with parameter function of block coefficient and coefficient of waterpalane forward), this is caused of ship motion or ships response due to couple motions heaving and pitching will be decreased for some vessels with large displacement and length.

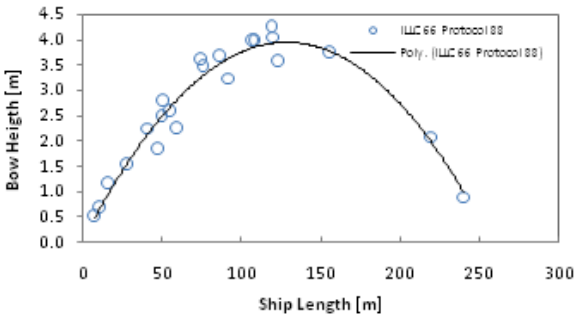

Fig. 6–Bow height minimum according to ILLC1966 as amended by protocol 88

Next in Figure 7 shows the bow height existing of 22 ship models. From the regression results can be known that the same trend with previous curve on Figure 11 where the bow height proportionally to the length the ship, the curve shape tends to linear.

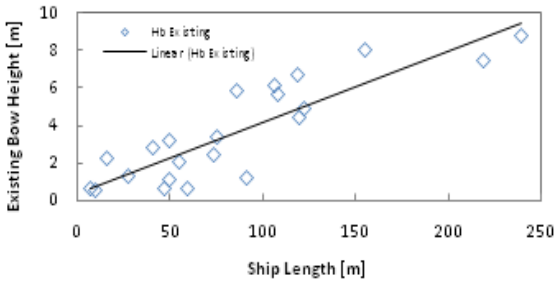

Fig. 7–Existing bow height of 22 ship models

4.2 Probability of Deck Wetness According to Several of Significant Wave Height

Probability of deck wetness is calculated by varying the wave height 0.5 meters to 9 meters, and it can be seen the value of the probability of each ship model by wave height variations. Probability of deck wetness at stem position (point C) toward the wave height variation with head seas condition, are presented as per Figure 8.

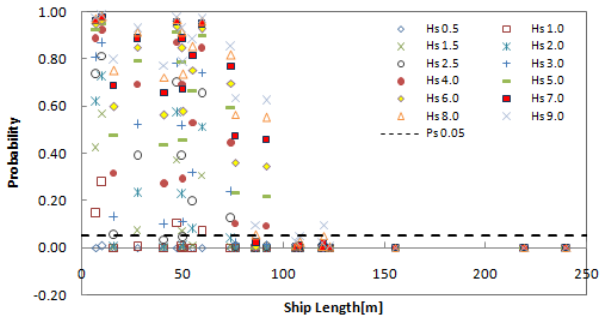

Fig. 8–Probability of deck wetness for various wave heights, Hs

For wave height Hs 0.5 meters the probability values for all ships below the safety margin by using deck wetness probability criteria Ps ≤ 0.05. Furthermore, for wave height Hs 0.5 meters to 2 meters for small ships (speed boat), Ro-Ro ferry, LCT, SPOB and vessels length below 60 meters, the probability values have exceeded the probability criteria. For wave height Hs 2 meters to 7 meters have exceeded the criteria on vessels up to 100 meters length, and for ships above 100 meters the probability exceeded Ps 0.05 occurs in wave height over 7 meters.

In general it can be concluded that the ship length and displacement (ship shape) affects the occurrence of deck wetness phenomenon, where the longer of ships then the smaller the probability of deck wetness, this is because the ratio of vessel length to the wavelength to be greater and the frequency encounter between wave crest and trough against the ship hull is relatively high so that the ship response to be smaller and the possibility of resonance is also getting smaller. Then the effect of low freeboard or the large ratio B/D, causing the value of probability of deck wetness to be high.

4.3 Bow Height Minimum Formula Modification

Determination of minimum bow height formula for Indonesian waters has been conducted through several simulations and scenarios based on parameters wave height and length of the vessel (22 models with variations in ship shape) with criteria of deck wetness probability Ps ≤ 0.05 of the total cycle of motions. The deck wetness position to be reviewed at point C (stem position) with head sea condition for irregular waves.

In scenario 1 the bow height minimum calculated up to a maximum probability of deck wetness criteria Ps ≤ 0.05 that will get the value of the maximum wave height is allowed, according to Table 6. From Figure 9 shown the comparison between the values of existing bow height, bow height according ILLC 1966 as amended Protocol 88 and bow height as scenario 1.

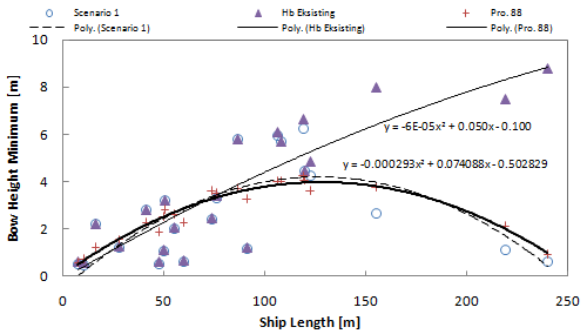

Fig. 9–The comparison of bow height existing, protocol 88 and scenario 1on Ps ≤ 0.05 by wave height maximum

For existing bow height values tend to be linear where bow height value is proportional to the ship length of the while the calculation results of bow height minimum scenario 1 by using criteria of Ps ≤ Ps 0.05 these value almost equal with the bow height in accordance ILLC Protocol 1988. And the regression results can be formulated as follows:

$$F(L_{pp}) = 7.409\left(\frac{L_{pp}}{100}\right) - 0.503 - 0.0293\left(\frac{L_{pp}^{\ 2}}{100}\right) \qquad (8)$$

In Table 6 shows that the maximum wave height for varying values of Ps ≤ 0.05, which for small ships and vessel with large ratio B/D (i.e. LCT, SPB and Fery R-Ro) maximum allowable wave height less than 1.5 meters (sea state on calm waters and moderate). As for ships with large displacement and length, the value of the maximum permissible wave height is high.

Table 6 Maximum wave height for probability of deck wetness Ps ≤ 0.05

Initial	Ship Type	Lpp (m)	Allowable Maximum Hs (m)	Existing Bow Height (m)	Bow Height Scenario 1 (m)
KI-1	Speed Boat	7.100	0.672	0.600	0.502
KI-2	Sea truck	10.250	0.581	0.540	0.480
KI-3	Crew Boat	16.000	2.479	2.230	2.224
KI-4	Tug Boat	27.600	1.335	1.260	1.201
KI-5	General Cargo	41.000	2.614	2.810	2.785
KI-6	SPOB	47.300	0.733	0.600	0.509
KI-7	Ferry Ro-Ro	49.900	1.343	1.106	1.056
KI-8	Fishing Vessel	50.300	2.551	3.200	3.185
KI-9	General Cargo	55.100	1.794	2.050	1.991
KI-10	LCT	59.500	0.861	0.650	0.593
KI-11	Tanker	73.950	2.063	2.450	2.429
KI-12	Cement Carrier	76.000	3.393	3.400	3.297
KI-13	Passenger	86.400	7.930	5.800	5.791
KI-14	Pontoon	91.440	3.458	1.191	1.153
KI-15	General Cargo	106.390	9.900	6.081	5.933
KI-16	Container	108.200	8.977	5.684	5.682
KI-17	Passenger	119.334	9.900	6.650	6.247
KI-18	Cement Carrier	119.700	7.957	4.449	4.444
KI-19	General Cargo	122.770	9.900	4.850	4.263
KI-20	Tanker	155.200	9.900	8.000	2.643
KI-21	Bulk Carrier	219.300	9.900	7.500	1.129
KI-22	Tanker	239.900	9.900	8.800	0.609

In scenario 2 the bow height minimum is determined by the variation of wave height based on vessel length, the longer of the vessel then the larger wave height is assumed, the probability of deck wetness criterion may not exceed Ps ≤ 0.05.

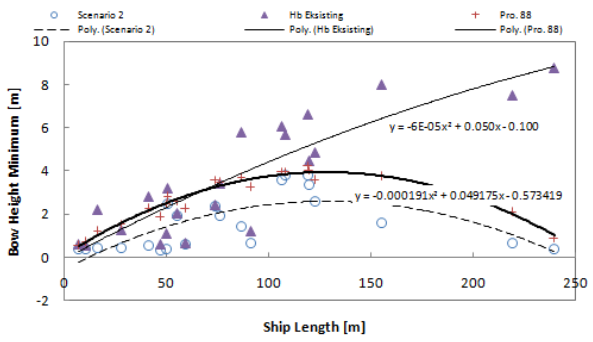

Fig. 10–The comparison of bow height existing, protocol 88 and scenario 2 by wave height variations

Figure 10 shows the same comparison between the value of the existing bow height, bow height according to ILLC 1966 Protocol 88 and bow height minimum scenario 2. Existing bow height values is the same, while the results of bow height calculation of scenario 2 for Ps ≤ 0.05 there is an average reduction of 47.037% compared with the bow height values according ILLC Protocol 1988. The regression results of bow height can be formulated as follows:

$$F(L_{pp}) = 4.917\left(\frac{L_{pp}}{100}\right) - 0.573 - 0.0191\left(\frac{L_{pp}^{\ 2}}{100}\right) \qquad (9)$$

In Table 7 shows the variation of wave height in accordance with the vessel length by criteria Ps ≤ 0.05. The wave height variations are intended as a vessel operating limitation with wave height parameters. The lowest wave height 0.5 meters (calm waters/smooth water condition) was applied to vessels with a length up to 50 meters. And wave height up to 2 meters (moderate) was applied to vessels over 50 meters up to 100 meters high and wave height above 2 meters (high and very high condition) for ships over 100 meters up to 250 meters. For ships with the large ratio B/D and low freeboard assumed wave height up to a maximum wave height with deck wetness criterion Ps ≤ 0.05.

Table 7 Wave height variations with ship length parameter, scenario 2

Initial	Ship Type	Lpp (m)	Wave Height Hs (m)	Bow Height Existing (m)	Ps	Bow Height Min (m)	Ps 0.05	Status Ps ≤ Ps 0.05
KI-1	Speed Boat	7.100	0.500	0.600	0.044%	0.373	5%	OK
KI-2	Sea truck	10.250	0.500	0.540	0.589%	0.412	5%	OK
KI-3	Crew Boat	16.000	0.500	2.230	0.000%	0.449	5%	OK
KI-4	Tug Boat	27.600	0.500	1.260	0.000%	0.450	5%	OK
KI-5	General Cargo	41.000	0.500	2.810	0.000%	0.533	5%	OK
KI-6	SPOB	47.300	0.500	0.600	0.013%	0.348	5%	OK
KI-7	Ferry Ro-Ro	49.900	0.500	1.106	0.000%	0.393	5%	OK
KI-8	Fishing Vessel	50.300	2.000	3.200	0.729%	2.497	5%	OK
KI-9	General Cargo	55.100	1.750	2.050	4.408%	1.942	5%	OK
KI-10	LCT	59.500	0.850	0.650	4.845%	0.585	5%	OK
KI-11	Tanker	73.950	2.000	2.450	3.911%	2.355	5%	OK
KI-12	Cement Carrier	76.000	2.000	3.400	0.010%	1.944	5%	OK
KI-13	Passenger	86.400	2.000	5.800	0.000%	1.460	5%	OK
KI-14	Pontoon	91.440	2.000	1.191	0.007%	0.667	5%	OK
KI-15	General Cargo	106.390	6.000	6.081	0.019%	3.596	5%	OK
KI-16	Container	108.200	6.000	5.684	0.122%	3.797	5%	OK
KI-17	Passenger	119.334	6.000	6.650	0.010%	3.786	5%	OK
KI-18	Cement Carrier	119.700	6.000	4.449	0.509%	3.351	5%	OK
KI-19	General Cargo	122.770	6.000	4.850	0.003%	2.583	5%	OK
KI-20	Tanker	155.200	6.000	8.000	0.000%	1.602	5%	OK
KI-21	Bulk Carrier	219.300	6.000	7.500	0.000%	0.685	5%	OK
KI-22	Tanker	239.900	6.000	8.800	0.000%	0.369	5%	OK

In scenario 3 same as scenario 2, but there are differences in assumptions of wave height variation with the value of the ship length range to be smaller, where the bow height minimum was determined by the variation of wave height based on vessel length, the longer the vessel then the larger wave height is assumed, with probability of deck wetness criterion may not exceed Ps ≤ 0.05.

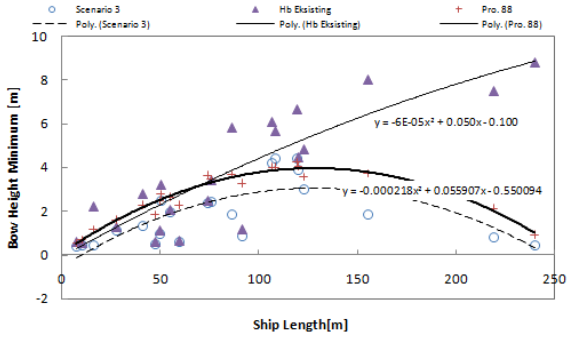

Fig. 11–The comparison of bow height existing, protocol 88 and scenario 3 by wave height variations

Figure 11 shows the same comparison between the value of the existing bow height, bow height according to ILLC 1966 Protocol 88 and bow height minimum scenario 3. Existing bow height values is the same, while the results of bow height calculation of scenario 3 for Ps ≤ 0.05 there is an average reduction of 36.619% (35%) compared with the bow height values according ILLC Protocol 1988. The regression results of bow height can be formulated as follows:

$$F(L_{pp}) = 5.591\left(\frac{L_{pp}}{100}\right) - 0.550 - 0.0218\left(\frac{L_{pp}^{\ 2}}{100}\right) \qquad (10)$$

In Table 8 shows the variation of wave height in accordance with the vessel length ≤ Ps 0.05 with a range of ship length to be smaller, by assuming the lowest wave height 0.5 meter (waters calm/smooth water condition) was applied to vessels with a length of up to 20 meters. For wave height up to 1.25 meters (slight) was applied for ship length 20 meter up to 50 meter, wave height up to 2 meters (moderate) was applied to vessels above 50 meter up to 75 meters, wave height up to 2.5 meters (moderate) was applied to vessels over 75 meter up to 100 meter and wave height above 2.5 meter up to 7 meter (high and very high) was applied for vessels above 100 meter up to 250 meters. For ships with the large ratio B/D and low freeboard values assumed up to wave height maximum with deck wetness criterion Ps ≤ 0.05.

Table 8 Wave height variations with ship length parameter, scenario 3

Initial	Ship Type	Lpp (m)	Wave Height Hs (m)	Bow Height Existing (m)	Ps	Bow Height Min (m)	Ps 0.05	Status Ps ≤ Ps 0.05
KI-1	Speed Boat	7.100	0.500	0.600	0.044%	0.373	5%	OK
KI-2	Sea truck	10.250	0.500	0.540	0.589%	0.412	5%	OK
KI-3	Crew Boat	16.000	0.500	2.230	0.000%	0.449	5%	OK
KI-4	Tug Boat	27.600	1.250	1.260	3.799%	1.124	5%	OK
KI-5	General Cargo	41.000	1.250	2.810	0.005%	1.332	5%	OK
KI-6	SPOB	47.300	0.700	0.600	4.302%	0.487	5%	OK
KI-7	Ferry Ro-Ro	49.900	1.250	1.106	3.718%	0.983	5%	OK
KI-8	Fishing Vessel	50.300	2.000	3.200	0.729%	2.497	5%	OK
KI-9	General Cargo	55.100	1.750	2.050	4.408%	1.942	5%	OK
KI-10	LCT	59.500	0.850	0.650	4.845%	0.585	5%	OK
KI-11	Tanker	73.950	2.000	2.450	3.911%	2.355	5%	OK
KI-12	Cement Carrier	76.000	2.500	3.400	0.283%	2.429	5%	OK
KI-13	Passenger	86.400	2.500	5.800	0.000%	1.825	5%	OK
KI-14	Pontoon	91.440	2.500	1.191	0.220%	0.833	5%	OK
KI-15	General Cargo	106.390	7.000	6.081	0.184%	4.195	5%	OK
KI-16	Container	108.200	7.000	5.684	0.722%	4.430	5%	OK
KI-17	Passenger	119.334	7.000	6.650	0.112%	4.417	5%	OK
KI-18	Cement Carrier	119.700	7.000	4.449	2.067%	3.910	5%	OK
KI-19	General Cargo	122.770	7.000	4.850	0.043%	3.014	5%	OK
KI-20	Tanker	155.200	7.000	8.000	0.000%	1.869	5%	OK
KI-21	Bulk Carrier	219.300	7.000	7.500	0.000%	0.799	5%	OK
KI-22	Tanker	239.900	7.000	8.800	0.000%	0.431	5%	OK

In scenario 4 wave height was taken from highest H1/3 of18 zones Indonesian waters, so that all ships length applied with the same wave height.

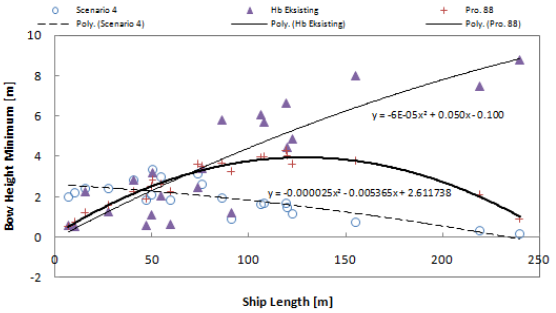

Fig. 12–The comparison of bow height existing, protocol 88 dan scenario 4 with Hs 2.679 meter

Figure 12 show a comparison between the value of the existing bow height, bow height according to ILLC 1966 Protocol 88 and bow height minimum scenario 4. In the calculation of scenario 4 where the probability value for the ship length up to 75 meters exceeded the existing bow height and bow height on ILLC 1966 Protocol 88. Based on the figure above that the curve of bow height scenario 4, the minimum value is inversely proportional to the existing bow height. Thus the regression results can be formulated as follows:

$$F(L_{pp}) = 0.536\left(\frac{L_{pp}}{100}\right) - 2.611 - 0.0025\left(\frac{L_{pp}^{\ 2}}{100}\right) \qquad (11)$$

In Table 9 shows the results of calculation bow height minimum by assuming wave height from the highest significant wave height H1/3 of 18 zones in Indonesian waters, with a value of 2,637 meters. From the calculation can be evaluated that by assuming the same wave height then the probability of deck wetness of ships length up to 75 meters did not meet the criteria, due to the probability value exceeded the criteria requirement Ps ≤ 0.05. However ships with a length of 75 meters above the probability value have a large margin than required. It is caused by the ratio of vessel length to the wavelength where for small ships with a small ratio having large response of the vessel due to wave motion (relative motion direction), if compared with the large ships.

Table 9 Probability of deck wetness by assuming the highest wave height H1/3 of 18 zones Indonesian waters

Initial	Ship Type	Lpp (m)	Wave Height Hs (m)	Bow Height Existing (m)	Ps	Bow Height Min (m)	Ps 0.05	Status Ps ≤ Ps 0.05
KI-1	Speed Boat	7.100	2.679	0.600	75.968%	1.999	5%	FAIL
KI-2	Sea truck	10.250	2.679	0.540	83.339%	2.211	5%	FAIL
KI-3	Crew Boat	16.000	2.679	2.230	7.898%	2.403	5%	FAIL
KI-4	Tug Boat	27.600	2.679	1.260	43.676%	2.409	5%	FAIL
KI-5	General Cargo	41.000	2.679	2.810	5.826%	2.855	5%	FAIL
KI-6	SPOB	47.300	2.679	0.600	72.845%	1.862	5%	FAIL
KI-7	Ferry Ro-Ro	49.900	2.679	1.106	43.397%	2.106	5%	FAIL
KI-8	Fishing Vessel	50.300	2.679	3.200	6.770%	3.344	5%	FAIL
KI-9	General Cargo	55.100	2.679	2.050	23.991%	2.972	5%	FAIL
KI-10	LCT	59.500	2.679	0.650	68.490%	1.844	5%	FAIL
KI-11	Tanker	73.950	2.679	2.450	16.538%	3.155	5%	FAIL
KI-12	Cement Carrier	76.000	2.679	3.400	0.790%	2.603	5%	OK
KI-13	Passenger	86.400	2.679	5.800	0.000%	1.956	5%	OK
KI-14	Pontoon	91.440	2.679	1.191	0.652%	0.893	5%	OK
KI-15	General Cargo	106.390	2.679	6.081	0.000%	1.605	5%	OK
KI-16	Container	108.200	2.679	5.684	0.000%	1.696	5%	OK
KI-17	Passenger	119.334	2.679	6.650	0.000%	1.690	5%	OK
KI-18	Cement Carrier	119.700	2.679	4.449	0.000%	1.496	5%	OK
KI-19	General Cargo	122.770	2.679	4.850	0.000%	1.154	5%	OK
KI-20	Tanker	155.200	2.679	8.000	0.000%	0.715	5%	OK
KI-21	Bulk Carrier	219.300	2.679	7.500	0.000%	0.306	5%	OK
KI-22	Tanker	239.900	2.679	8.800	0.000%	0.165	5%	OK

4. Conclusions

Modification of the minimum bow height Indonesian waters conducted through 4 scenarios by assuming the wave height with the criterion of deck wetness probability Ps ≤ 0.05. Scenario 1 bow height values calculated up to Ps ≤ 0.05 in order to obtain the maximum wave height for each vessel, and the result is the bow height minimum curve close to the bow height value according to ILLC 1966 Protocol 88. Scenario 2 and 3 assumes the wave height according to the ship length where the longer and larger ships and the greater freeboard then the wave height assume to be higher. Scenario 4 assumes the highest wave height H1/3 of 18 zones Indonesian waters is 2.679 meters, the result is that the longer of ship length then the smaller of bow height minimum. According to 4 scenarios of development of bow height for Indonesian waters, the scenario 3 is recommended to be applied because suitable with the operating conditions of the vessel and the assumption of wave height will be used as the operational constraints of ships at sea. The minimum bow height formula and the proposed restrictions as follows:

$$F(L_{pp}) = 5.591\left(\frac{L_{pp}}{100}\right) - 0.550 - 0.0218\left(\frac{L_{pp}^{\ 2}}{100}\right)$$ or

35% reduction of bow height values according to Regulation 39 ILLC 1966 Protocol 88.

$$F_b = 0.35x\left[6075\left(\frac{L}{100}\right) - 1875\left(\frac{L}{100}\right)^2 + 200\left(\frac{L}{100}\right)^3\right]x\left[2.08 + 0.609C_b - 1.603C_{wf} - 0.0129\left(\frac{L}{d_1}\right)\right]$$

or $$F(L_{pp}) = 0.057 + 3.924\left(\frac{L_{pp}}{100}\right) - 0.015\left(\frac{L_{pp}^{\ 2}}{100}\right)$$

Meanwhile vessel operating restrictions are as follows:

Ship Length (m)	Wave Height, Hs (m)	Sea State
≤ 20	0.5 - 1.25	Slight
21 – 75	1.25 – 2.5	Moderate
76 – 100	2.5 - 4	Rough
≥ 100	6 - 9	High

Exemption for vessels with large B / D (B/ > 3 meter) eg: LCT, Barge, and Ro-Ro ferry. Where the bow height correction value is greater than the values calculated by the freeboard, then the provisions of the bow height correction calculation can be ignored by the terms of ship operations are at a maximum wave height of 1 meter (slight).

Acknowledgments

This work supported by management of PT. Biro Klasifikasi Indonesia (Persero) as Indonesian ship classification society, Jakarta Indonesia

References

[1] National Transportation Safety Committee (2011), Marine Safety Digest, Improving safety at sea, Buletin KNKT Ministry of Transportation, Jakarta.

[2] Battacharya R (1978), Dynamics of Marine Vehicles, John wiley & sons, Canada.

[3] JSPS-DGHE Program on Marine Transportation Engineering (2006), Collection of Wave Data and Safety of Ships Operating in Indonesian Domestic Seas, Final Report, Jakarta.

[4] Ministry of Transportation of Indonesia (2005), Minister Decree (KM) 3 Year 2005, Jakarta.

[5] International Maritime Organization (2005), International Convention on Load Line, and Protocol of 1988, as amended in 2003, Consolidated Edition, 2005, London.

[6] Directorate of Sea Transportation of Indonesia (2010), Indonesian Ship Register Year 2010, Jakarta.

[7] Biro Klasifikasi Indonesia (2012), BKI Ship Register, 2012, Jakarta.

[8] Alman P., Cleary Jr. W.A., Dyer M.G., Paulling J.R., Salvesen N. (1992), The International Load Line Convention: cross road to the future, Marine Technology, June.

[9] Journeé J.M.J, Zhu Yonge, de Kat J.O, Vermeer H. (2001), Joint Development of Bow Height Formula by China and the Netherlands Based on Probabilistic Deck Wetness Analysis, Delft University of Technology, Technical Report 1270-P, DUT.

[10] W. Pierson and L. Moskowitz (1964), A proposed Spectral Form for Fully Developed Wind Seas Based On Similarity Theory of S.A Kitaigorodski, Journal of Geophisical Research, Vol. 69 No. 2, December 1964.

[11] Faltinsen, O.M. (1990), Sea Loads on Offshore Structures. Number ISBN 0-521-37285-2, 1990

What is Surf-Riding in Irregular Seas?

Kostas J. Spyrou , Nikos Themelis and Ioannis Kontolefas

School of Naval Architecture and Marine Engineering, National Technical University of Athens

Abstract: The concept of surf-riding in irregular seas is enquired and two calculation schemes are implemented in order to create upper and lower bounds of the probability of surf-riding. The first scheme is focused on the identification of the generation and disappearance of surge equilibria. Due to the time-varying nature of the dynamical system, these are finite-time objects, departing from the conventional notion of an equilibrium. The other scheme is aimed to determine time segments of ship motion where the mean speed is higher than expected. The probability values obtained by the two schemes are compared against each other and conclusions are drawn.

Key words: surf-riding; high-run; irregular waves;

1. Introduction

Phenomenologically, one could characterize as "surf-riding" a ship's prolonged run in waves with speed higher than the speed sustained by her propulsive thrust. For regular "seas" such behavior is owed to the generation of equilibrium conditions in the surge dynamics which create capture and a "push" of the ship on the down-slope of a steep wave. In irregular seas however, the meaning of an "equilibrium state" is questionable given the time-varying nature of system dynamics. Moreover, any plausible notion of ship dynamic equilibrium in surge could claim its relevance only for finite time segments during ship runs. One wonders therefore if what is established for regular seas could reasonably be extended to the irregular seas; and moreover, whether new phenomena distinctively identified with the time-varying nature of the system can also emerge.

In the current paper, the concept of "surf-riding equilibrium" in a multi-frequency wave field was enquired and a suitable scheme for the identification of such points was developed, involving calculation of the instantaneous celerity.

A numerical scheme was implemented for identifying these time segments in a long simulation record where the ship performs "high-runs" (she moves with a mean velocity that is higher than the nominal). A massive campaign of simulations was subsequently performed for contrasting apparent surf-riding occurrences against equilibria existence.

2. Time segments of equilibria existence in multi-chromatic sea

2.1 Concept

Large-scale simulation results reveal finite time intervals over which instantaneous celerity (calculated at ship's position) and surge velocity, strongly relate to each other. Based on this, one could infer that some kind of point attractors can arise in the phase plane, advancing with velocity relating to the instantaneous celerity. These attractors (we will henceforth call them surf-riding equilibria for convenience) have finite life-spans over which they can invoke ship "high runs" if the ship is found within the basin of attraction of anyone of them.

To identify stable and unstable surf-riding equilibria in the vicinity of the ship, we introduce a non-inertial frame of reference that moves with the instantaneous celerity (it is evident that such equilibria will, in general, not constitute solutions of the surge equation; rather they lie inside bounded regions in the time-extended phase space that contain trajectories qualified as "high-runs"). The ratio of the time that the scheme returns "positives" for the existence of equilibria, to the total time of exposure to a specified wave environment, should comprise an upper bound of the "probability of surf-riding".

2.2 Mathematical model and identification scheme

Consider the mathematical model of surge motion in following seas, written with respect to an earth-fixed observer, see for example [1]

$$\begin{aligned}&\left(m-X_{\dot u}\right)\ddot{\xi}\ +\ \left(r_1-\tau_1 n\right)\dot{\xi}\ +\ \left(r_2-\tau_2\right)\dot{\xi}^2\\&+\ r_3\dot{\xi}^3-\sum_{i=1}^{N} f_i\sin\left(k_i\xi-\omega_i t+\varepsilon_i+\varepsilon_{fi}\right)\ =\ \tau_0 n^2\end{aligned}\qquad(1)$$

where ξ is the longitudinal position of the ship, m and $X_{\dot u}$ are her mass and "added mass" respectively, while n is the propeller rate. In the forcing term, k_i, ω_i and ε_i denote, respectively, the wave number, wave frequency and the random phase of the ω-harmonic component; f_i denote the amplitude and ε_{fi} the phase of the ω-harmonic wave force component.

Let us conceive a transformation that, in analogy to the one used for the harmonic case, would allow us to identify stationary points. This could be feasible if a new, non-inertial system of axes was introduced moving with the instantaneous celerity $c[\xi(t);t]$ at ship's position. Let us suppose that instantaneous celerity satisfies some appropriate smoothness conditions over some finite time interval (despite knowing that, the more the sea becomes "broad–banded", the more difficult will be to satisfy these conditions over such an interval). The location of the ship with respect to the new origin can be expressed by a new distance variable χ as follows,

$$\chi=\xi-z\qquad(2)$$

The variable z is the abscissa of the moving origin with respect to the earth - fixed frame, expressed as,

$$z=z_0+\int_{t_0}^{t} c\left[\xi(s);s\right]ds\qquad(3)$$

For the existence of surf-riding equilibria the following condition must hold,

$$\begin{aligned}&\sum_{i=1}^{N} f_i\sin\left[k_i\left(\chi+z\right)-\omega_i t+\varepsilon_i+\varepsilon_{fi}\right]+\left(\tau_2 c^2+\tau_1 cn+\tau_0 n^2\right)\\&-\left(r_1 c+r_2 c^2+r_3 c^3\right)-\left(m-X_{\dot u}\right)\dot c\ =\ 0\end{aligned}\qquad(4)$$

Should surf-riding equilibria be located, their paths are traced, under the condition however of remaining always within the close vicinity of the ship (only nearby equilibria pose a threat).

The ship selected for applying the above scheme is the ONR "tumblehome topside" that has been used in our previous studies ($L_{\mathrm{WL}}=159$ m, $B_{\mathrm{WL}}=18.802$ m, $T_{\max}=7.605$ m) [2, 3]. A JONSWAP spectrum is assumed. It is discretized by applying a fixed frequency increment $\delta\omega=2\pi/t_{\mathrm{sim}}$ where $t_{sim}=300\ s$ is the basis simulation time. To assess the effect of band-width, four scenarios are investigated in terms of the considered range around spectrum's peak. Several simulations were carried out, for parameters values shown below in Table 1.

Table 1 Parameters of the simulations carried out

Parameter	Value
u_{nom} (m/s)	(12,13)
$u(0)$ (m/s)	10
H_{S} (m)	(3,6)
T_{p} (s)	(9.5,10)
Considered range around ω_{p} (% ω_{p})	(10,20,30,40)
Total simulation time T_{sim} (s)	1200

The detection scheme comprises of finding real roots of equation (4), if any, during the simulation, lying within a moving spatial window centered amidships, whose size is pre-specified and is used as a parameter of the investigation.

When a real root is detected, starting from a time instant let's say t_i and existing for n_i consecutive time steps, then the time interval $\left(t_i,\ t_i+\left(n_i-1\right)\delta t\right)$ represents a segment of existence of a threatening surf-riding equilibrium (nonetheless, it is not necessary the attraction to be felt by the ship and her motion to be affected). A time ratio of existence of

equilibria is subsequently calculated by diving with the simulation time,

$$a = \frac{1}{T_{sim}} \sum_{i=1}^{N} \left(n_i - 1 \right) \delta t \qquad (5)$$

The results obtained are visualized in the form of animated series of figures (Fig. 1) in an attempt to gain better insight into the mechanism of "engagement to" and "disengagement from" surf-riding. We were able to recognize two different scenarios of entrapment,

1. The ship is initially attracted by the inset of an unstable equilibrium. Likewise regular sea scenarios, the trajectories in the neighborhood of this unstable state seem to be organized in such a way that the ship is engaged to a chase with the coexisting stable equilibrium.

2. A stable equilibrium appears suddenly in the close vicinity of the ship capturing her in the surf-riding condition.

In Fig.1 red circles correspond to equilibria identified using condition (3) while black circles correspond to roots of (3) when the last term of the lhs (accounting for the accelerating reference frame) is neglected. On the bottom part of these figures one can observe the time history of surge velocity (black line) versus that of instantaneous celerity calculated at ship's position (gray line).

3. Realizations of "high runs"

3.1 Definitions

In this part we have considered phenomenological realizations of surf-riding through simulation. Such events are evidenced by the up-crossing of a certain high velocity threshold and the later down-crossing of the same (or another selected) velocity threshold. In general, these two thresholds need not be identical and a subjective element is inevitable. Individual times of such events ("high runs) are summed up, then they are divided by the total time of the run in order to obtain the "time ratio of high run".

$$P_{\text{surf-riding}} = \frac{\sum_i t_{(i)\text{high run}}}{T_{sim}} \qquad (6)$$

Two different specifications of the "high run" have been evaluated:

Definition 1: The two thresholds are identical and they are defined by the instantaneous celerity. In Fig. 2, such "high runs" are indicated by the dashed line arrows.

Definition 2: The threshold of up-crossing is the instantaneous celerity and the threshold of down-crossing is the nominal speed. This allows dealing with the fluctuations of the motion during surf-riding. This definition includes surge velocity fluctuations that may be below the instantaneous celerity but higher than nominal speed. Such time intervals are indicated in Fig. 2 with continuous line arrows. The condition the surge velocity to be higher than nominal speed is still invoked to exclude cases that qualitatively, should not qualify as high runs.

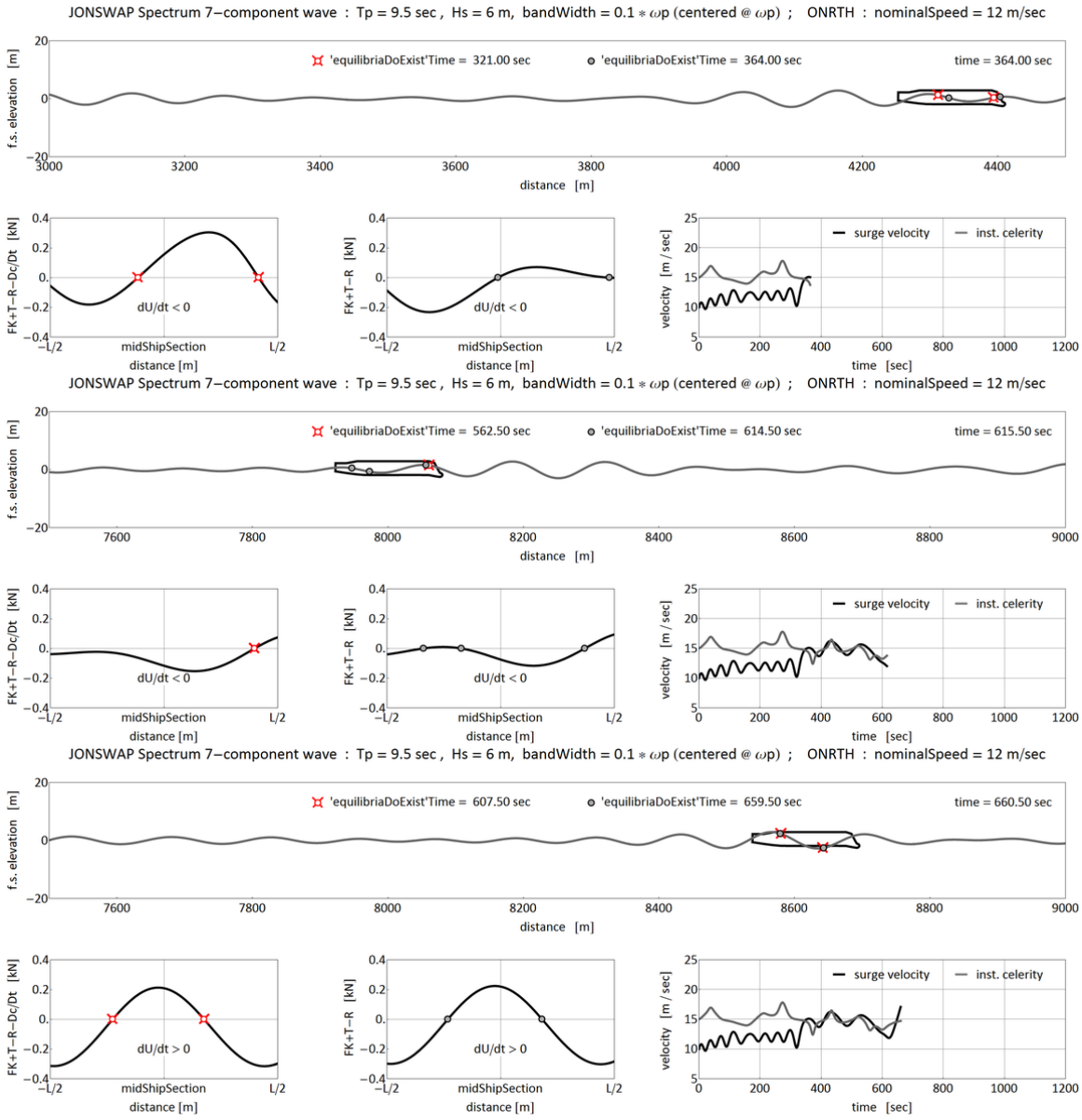

Fig. 1 - Time instants of an animated simulation [H_S=6 m, T_P=9.5 s, frequency range 10% ω_P (one side), u_{nom}=12m/s. The detection scheme was applied on a spatial window of one ship length.

3.2 Simulation settings

The simulation time was a multiple of the basis time $t_{sim} = 300$ s and specifically it was varied from t_{sim} to $40 \times t_{\text{sim}}$. Four ranges around spectrum's peak have been considered. Table 2 presents the considered ranges of the simulation parameters. Sensitivity studies related to the sea state, narrowness of the spectrum and simulation time were carried out. The number of wave components that participate in the simulation (basis time) depends on the frequency range (Table 3). We run 100 wave realizations per scenario. The nominal and the initial speed of the ship in each scenario were unchanged (details are provided in [4]).

Table 2 Ranges of values of parameters

Parameter	Value
u_{nom} (m/s) - *Fn*	12 – 0.308
$u(0)$ (m/s)	10
wave realizations per scenario	100
H_S (m)	(3 – 6)
T_P (s)	(8.5 – 13)
(% ω_P one side)	(5 – 30)
Total simulation time T_{sim} (s)	$(t_{sim} - 40 \times t_{sim})$

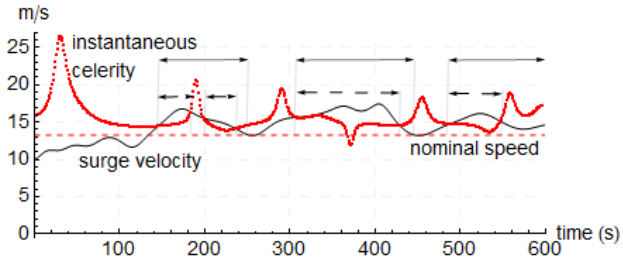

Fig. 2 – Schematic definitions of "high run".

3.2 Results

Fig. 3 shows time histories of surge velocity and instantaneous celerity for a "high-run" occurrence according to the 2nd definition. The lower diagram of Fig.3 shows the calculated time segments of "high-run". The convergence of the statistics was examined (see Fig. 4) and the simulation time per run was selected appropriately.

Effect of different "high run" definitions

In Fig. 5 are shown the obtained time ratios (loosely called "probabilities" although they can be regarded as such only in a crude sense) by varying the peak period and keeping constant the significant wave height. As expected, the first definition produces lower probabilities than the second. There is significant influence on probability by a 10% increase of the down-crossing threshold.

Table 3 Number of wave components per scenario for t_{sim} = 300 s.

T_P (s)	5% ω_p	10% ω_p	20% ω_p	30% ω_p
8.5	4	8	15	22
9	4	7	14	21
9.5	4	7	13	19
10	4	7	13	19
10.5	3	6	12	18
11	3	6	11	17
11.5	3	6	11	16
12	3	6	11	16
12.5	3	5	10	15
13	3	5	10	14

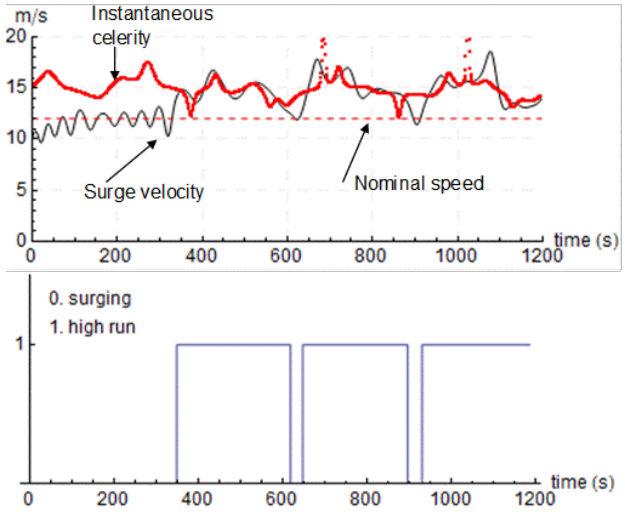

Fig. 3 – Sample simulation of a "high-run" and the respective time segments (low diagram) [H_S=6 m, T_P=9.5 s , u_{nom}=12m/s , frequency range 10% ω_P (one side)].

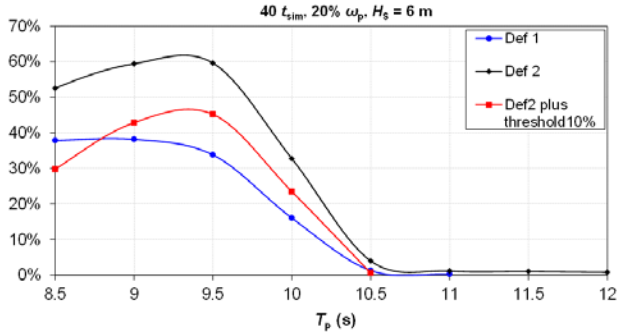

Fig. 4 – Convergence of statistics per simulation time and varying T_P for 20% ω_P (one side), H_S=6 m.

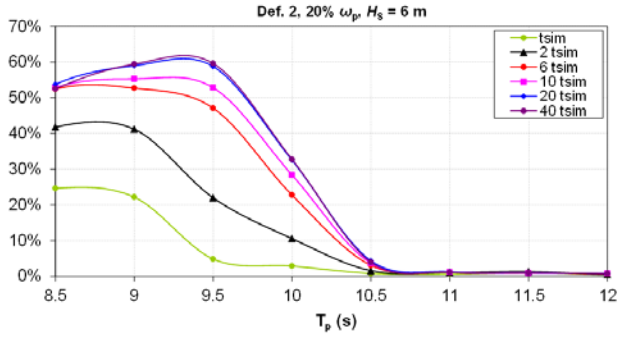

Fig. 5 – Probability of "high-run" as function of the peak period T_P. The duration of the simulations was 40 t_{sim} = 12 x 10^3 s., the frequency range (one-side) was 20% ω_P and the significant wave height was H_S=6 m.

Effect of the frequency range

We have varied the peak period by keeping constant the significant wave height (Fig. 6). It was derived that in all cases, there is a peak period value below which there is sharp increase of the probability. By increasing the considered frequency range, high probabilities of surf-riding appear for a broader range.

3.3 Cross-comparison of calculated time ratios

A comparison study on the calculated time segments based on the methods of equilibria existence and "high runs" was carried out. Both results correspond to the same wave realizations, while a range of spatial window lengths (from $L/32$ up to L, where L is the ship length) has been considered. Furthermore, four sea states and three frequency ranges were studied and the simulation time was fixed to $4\times t_{sim}$.

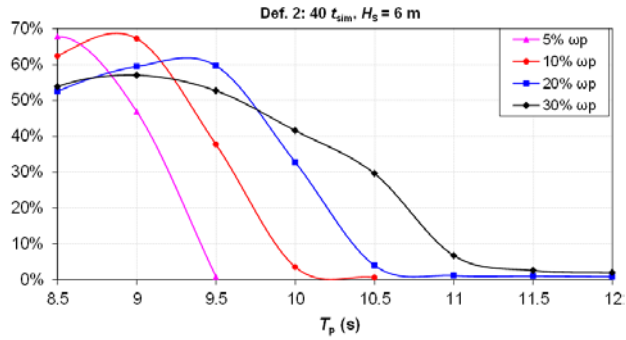

Fig. 6 - Probability of "surf-riding" (2nd definition) per % ω_P and varying T_P for 40 t_{sim} = 12 x 10^3 s, H_S=6 m.

The comparison results are summarized in Fig. 7. One can note a similar trend regarding the effect of the spatial window in the time ratios. However, higher differences are noted for the higher sea states.

Additionally, in Fig. 7 are included the time ratios according to the 2nd definition, but with a 10% increase of the down-crossing velocity threshold. As the time segments of equilibrium existence are not always felt by the ship, the two methods are not expected to produce directly comparable time-ratio results, a fact reflected by the diagrams.

6. Concluding remarks

The notion of surf-riding equilibrium was extended from the regular to a multi-chromatic sea where such "features" can exist for a finite time interval. A numerical scheme that is based on the concept of instantaneous celerity was developed to determine the time-ratio upper bound regarding the exposure to the danger of surf-riding. A more empirical approach for surf-riding prediction was subsequently applied, based on a campaign of numerical simulations, in order to calculate time intervals of 'high run.

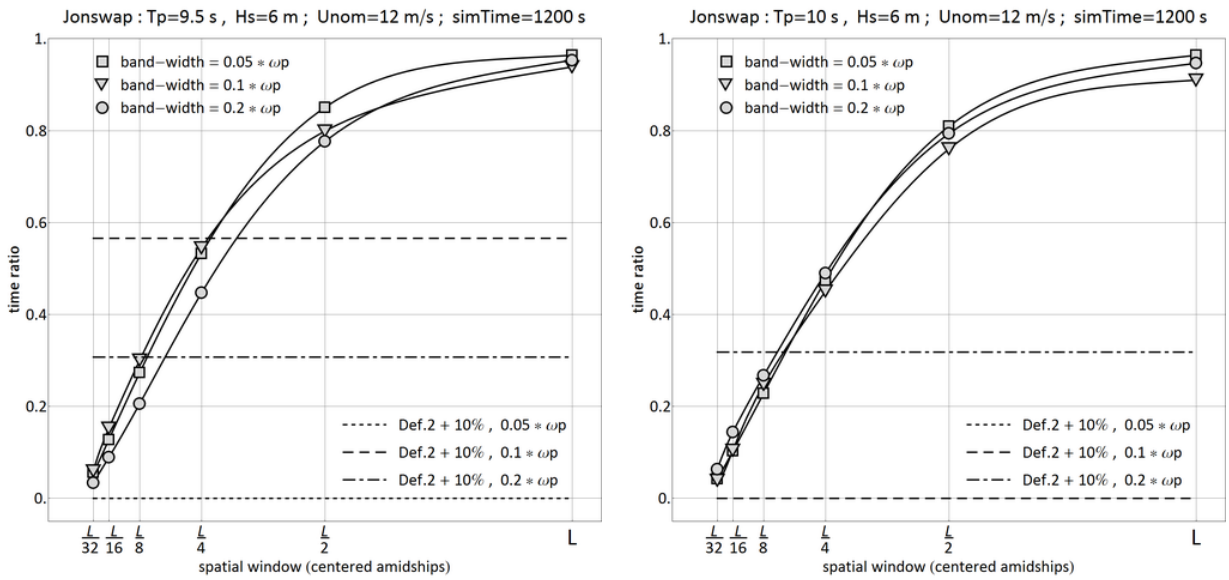

Fig. 7 - Effect of the different size of spatial windows on the upper bound of the time ratio of attraction to surf-riding and comparison with similar ratios corresponding to high runs.

Various up-crossing and down-crossing velocity thresholds that can determine a "high run" have been investigated. Statistical measures such as the mean time ratio and mean time duration of "high runs" were obtained. Moreover, sensitivity studies related to the sea state, narrowness of the spectrum and simulation time duration were carried out. Lastly, a preliminary comparison study on the time ratio of equilibrium existence and "high run" duration was performed, seeking a relation between these two quantities which, whilst related, they produce quantitatively very different time ratios of exposure to danger.

Acknowledgments

This work has been funded by the Office of Naval Research, on the basis of a contract with the university of Strathclyde, under Dr. Ki-Han Kim and Dr. Woei-Min Lin. This support is gratefully acknowledged.

The authors acknowledge also the contribution of Dr. Vadim Belenky of David Taylor Model Basin with whom there is continuous scientific interaction in this line of work.

References

[1] K. Spyrou, V. Belenky, N. Themelis & K. Weems, Detection of Surf-riding Behavior of Ships in Irregular Seas, Nonlinear Dynamics, (2014) (accepted), DOI 10.1007/s11071-014-1466-2.

[2] K. Spyrou, V. Belenky, N. Themelis, K. Weems, Conditions of surf-riding in an irregular seaway, Proceedings, 11th International Conference on Stability of Ships and Ocean Vehicles, (2012), Athens, Greece.

[3] K. Spyrou, N. Themelis, Wave celerity in a multi-chromatic sea: a comparative study, Proceedings, 13th International Ship Stability Workshop, (2013), Brest, France.

[4] K. Spyrou, N. Themelis, I. Kontolefas, Development of Probabilistic Models for Evaluating the Dynamic Stability and Capsizing Tendency of Naval Vessels with Respect to Broaching-to, Technical Report to the Office of Naval Research (2014), ONRG grant number: N62909-13-1-7.

Quantitative Assessment of Ship Behaviour in Critical Stern Quartering Seas

Maria Acanfora* and Jerzy Matusiak
Dept. of Applied Mechanics, School of Engineering, Aalto University of Espoo, Finland

Abstract: Following and stern quartering seas, combined with a relatively high speed of vessel, represent the operational conditions which may lead the ship to dangerous situations in adverse weather. Recently, IMO efforts were addressed to the development of the Second Generation Stability Criteria, based on three different safety levels.
The third level requires a direct assessment of ship stability, based mainly on numerical simulation of ship motions in waves. The numerical simulation tool is expected to reproduce vessel dynamics, in order to allow detailed design analysis when assessing ship safety.
The proposed paper presents an application of the numerical model called LaiDyn to the investigation of ship large amplitude motions, in critical conditions typical for a conventional RoPax vessel.
LaiDyn is a six-degree of freedom dynamic model, in time domain, that works on a discrete representation of the hull, using panels. The non-linear restoring generalized forces and the Froude-Krylov wave loads are evaluated, at each time, on the instantaneous ship wetted surface. Radiation and diffraction forces are derived using linear model. The ship resistance and the propeller thrust are also implemented into LaiDyn.
For the purpose of the numerical applications, stern quartering irregular sea is assumed.

Key words: Ship stability, roll resonance, parametric rolling, dynamic simulation.

1. Introduction

The need to upgrade the General Stability Criteria led to a revision of the Intact Stability Code [1], trying to focus more on ship dynamics, with particular emphasis on nonlinear aspects. The so-called Second Generation of Intact stability criteria have been planned to have a multi-tiered structure consisting of three levels [2]. The criteria in level 1, named vulnerability criteria consist of relatively simple methodologies to be applied at the very preliminary phase of the stability assessment in the design process. If a possible vulnerability is detected, then the vulnerability second level criteria are used, referred also as severity criteria.

The final third level, to be applied in case of failure of the previous ones, is called direct assessment, based on numerical simulation tools or, as alternative, experimental tests.

Stability criteria should address three fundamental modes of stability failures [3]: restoring arm variation problems, (such as parametric excitation and pure loss of stability), stability under dead ship condition and maneuvering related problems in waves (such as broaching-to).

Despite several research works dealt with various proposals for the first two levels regarding the several stability failures [4] [5] [6] [7], the third one is still under development.

Direct assessment procedures for stability failure are intended to employ the most advanced state-of-the art technology available being sufficiently practical to be uniformly applied, verified, and validated [8].

* **Corresponding Author:** Maria Acanfora, research fellow; research field in marine engineering, ship stability.
E-mail: maria.acanfora@aalto.fi

The numerical simulation tool is expected to reproduce vessel dynamics, in order to allow detailed design analysis when assessing ship safety [9]. Moreover, simulation is expected to provide ship-wise guidance for a safe operation also in adverse sea conditions. The operational limitations came out during SLF 55 [10], with the proposal to use operational limitations if the ship fails to comply with the second level vulnerability criterion.

Some proposal for simulation tools to be used for the direct assessment criteria have been developed by several authors [11] [12] [13] [14], regarding parametric rolling analysis.

Parametric rolling is perhaps the most complicated phenomena to understand and manage by officers onboard, partly because it may lead to a sudden heavy roll, from nowhere, in otherwise apparently calm and controllable conditions.

The proposed paper presents an application of the numerical model called LaiDyn to the investigation of ship large amplitude motions, with particular attention to the parametric rolling resonance in stern quartering sea. Following and stern quartering seas, combined with a relatively high speed of vessel, represent the operational conditions which may lead the ship to dangerous situations in adverse weather [15] [16].

LaiDyn is a six- degrees of freedom dynamic model, in time domain, that works on a discrete representation of the hull [17] [18] [19]. The ship resistance in still water and the propeller characteristics are also implemented into LaiDyn, while the ship resistance due to the wave pressure, is computed during the simulation.

Ship speed is obtained by taking into account the propeller behavior in waves; this allows performing a more realistic simulation of ship operational conditions. In the following sections a brief description of LaiDyn architecture is presented, with particular attention on the propeller implementation.

Experimental tests and numerical simulations for a turning circle manoeuvre, in irregular long-crested waves, are carried out and the results by the two different approaches are compared. This investigation is intended to qualitatively validate LaiDyn result, by checking ship rolling behaviuor for several encounter frequencies.

For the purpose of the applications, stern quartering irregular sea is assumed by means of JONSWAP spectrum. The operational conditions that yield to resonant roll motion and to parametric rolling are identified and then analyzed through the simulation.

2. The LaiDyn Simulation Code

The LaiDyn code has been developed for the ship dynamics in waves; the ship is regarded as a rigid intact body.

It could be defined as a hybrid non-linear simulation model in six- degrees of freedom in time domain, for regular and irregular seas.

Wave action on ship hull is represented by two components: the so-called Froude-Krylov component and the so-called diffraction component. The former is evaluated by integrating the pressure over the wetted portion of hull surface. In the linear approximation the integration is conducted up to the still water level and a steady ship motion is assumed. The non-linear model, implemented in LaiDyn, allows instead six-degrees-of-freedom for ship motions. The same non-linear approach is applied in computing the hydrostatic actions.

The diffraction component takes into account the disturbance caused by a ship to oncoming wave. The diffraction actions are evaluated instead according to the linear model for small amplitude oscillatory motions. Radiation forces, i.e. added mass and damping terms come out from the same linear model.

LaiDyn implements also rudder actions, allowing to simulate manoeuvring tasks [18].

The main coordinate systems used for describing ship motion are presented in Fig.1, i.e the inertial system fixed to Earth, with the X-Y plane coincident with

the still water level, and the body-fixed reference frame having its origin at ship center of gravity.

For more details about the code, please refer to the following papers [17] [18].

2.1 Propeller Model

There are two ways to model ship resistance and propeller action. The simplest way is to assume that resistance and thrust are of the same magnitude and do not change. The other model takes into account the resistance with an operating propeller.

One of the main goals achieved by LaiDyn is the capability to simulate the ship operational condition taking into account the ship velocity given by the propeller behavior, together with ship resistance in wave.

The code gives the possibility to implement several kinds of propellers as: fixed pitch or controllable pitch propellers and podded propulsion system. The following elaboration refers mainly to fixed pitch propeller, used for the carried out applications.

For still water condition, the thrust that the propellers have to supply for keeping the ship at the operational speed V is given by:

$$X_{resistance} = -R_T/(1-t) = -0.5\rho u^2 S C_T/(1-t) \quad (1)$$

where R_T is the total resistance, t is the thrust deduction factor, S is the wetted surface and u is the forward velocity of the ship in the body-fixed co-ordinate system.

The total resistance coefficient C_T is given in tabular form as a function of Froude number.

The total thrust provided by the propellers is evaluated from a known open water characteristic of the propeller, $K_T = K_T(J)$, as follows:

$$X_{prop} = Z\rho n^2 D^4 K_T \quad (2)$$

where J is the advance number, Z is the number of the propellers, n is the propeller revolutions per second and D is the propeller diameter.

The required propeller revolution, for still water and constant forward speed, is set in order to obtain the condition:

$$X_{prop} = X_{resist} \quad (3)$$

The propeller characteristic curve $K_T(J)$, in the application model, has been assumed and implemented as a linear function.

$$X_{prop} = \frac{P_D \eta_0 \eta_R}{V(1-w)} \quad (4)$$

Keeping in mind that X_{prop} depends on propulsion power P_D, according to (4), it may happen to have unrealistic high thrust values at low speed. The terms η_0 and η_R that figures in (4) are respectively the open water and the rotational efficiencies of the propeller, while w is the wake fraction.

The maximum attainable thrust of a propeller, known as the bollard pull, is evaluated and checked by applying:

$$T = 0.5\rho \frac{\pi}{4} D^2 \left(\frac{16 P_D}{\rho \pi D^2} \right)^{2/3} = \sqrt[3]{\frac{\rho\pi}{2}} (P_D D)^{2/3} \quad (5)$$

Once the initial propeller set up in still water is made, the simulated ship dynamics in waves will affects also propeller behavior.

Propeller actions are expressed in body fixed reference frame and move with the hull (see Fig.1). If the propeller, due to ship motions and wave profile, is instantaneously out of the water, its thrust is set as zero. Moreover, when evaluating thrust, the kinematics of water flow in waves are taken into account.

Added resistance in waves is evaluated as a result of dynamic pressures forces, acting on the wetted panel on the ship, projected on x-direction.

There are two possible approaches to deal with the ship resistance in wave: one possible way is to keep the revolution, set for the still water conditions, as constant. In this way the added resistance in wave will reduce the initial ship speed according to (3).

In order to keep the desired velocity as constant, a different approach can be used. It consists of introduc-

ing a feedback control law on the ship speed, adjusting the revolutions during the simulation. For the purpose of the application a simple proportional controller is used.

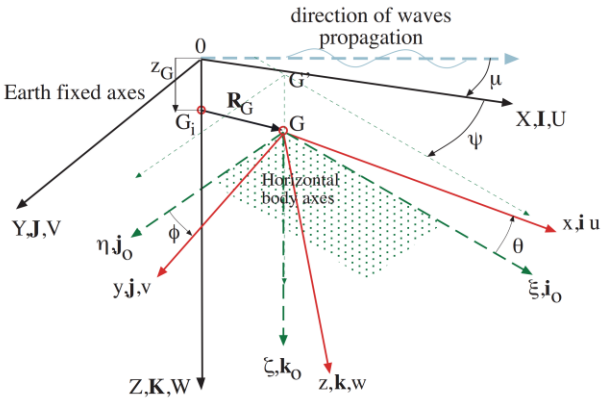

Fig. 1 – Co-ordinate systems used in ship dynamics

3. Roll Resonance in Quartering Sea

Parametric rolling is a critical phenomenon that leads ship, under certain conditions, to quickly develop large roll amplitudes, due to parametric excitations. Hulls with large bow and stern flare, such as container and Ro-Ro vessels, are especially sensitive to this phenomenon: this is link to the significant variation of the metacentric height in waves.

Ordinary linear strip theory in the frequency domain does not capture this phenomenon. One of the possible ways of predicting and assessing parametric rolling is by means of nonlinear simulation model in the time domain.

A ship can experience resonance between the natural period of roll and stability variation if the wave encounter period is half (or less critical, equal to) the roll period [7].

Parametric roll is a resonance phenomenon but it is distinct from "normal" resonance between external periodical forces and natural period of the system, characterized by $T_e=T_n$ [20].

Parametric roll resonance for a ship is driven out by the variation in time of the restoring moment, usually expressed as change of the metacentric height (GM) in wave, together with low roll damping and high wave amplitude. The resonance between stability variation and ship's natural period of roll requires $T_e=0.5T_n$. It is clear that this kind of unstable behavior cannot be predicted by applying linear analysis.

Linear method, assuming a constant GM value, can instead predict roll resonance but only a non-linear simulation would give a quantitative assessment of ship behavior in that condition. In particular the roll resonance in stern quartering sea coupled with the variation in time of the restoring actions in wave, would lead to unexpected higher amplitude rolling motions.

The applications of LaiDyn code have been performed on a modern fast twin-screw Ro-Pax vessel, named SeatechD, whose main characteristics are shown in Table 1.

Table 1 Main particulars of the vessel SeatechD

	Full Scale	Model Scale
L (m)	158.0	4.049
B (m)	25.0	0.123
T (m)	6.1	0.156
D (m)	15.0	0.384
∇ (m^3)	13766	0.232
S (m^2)	4356	2.860
C_B	0.571	0.571

An extensive experimental research study was carried out at the Ship Laboratory of the Helsinki University of Technology on SeatechD model (see Fig.2), concerning with the dynamic stability.

Fig. 2 – SeatechD model

These model test series allowed validating LaiDyn regarding pure loss of stability and parametric roll resonance in regular and irregular waves [21] [22].

In irregular seas, as the roll response is very sensitive to the period of excitation, only the part of the encountered wave spectrum that coincides with the natural period of roll will be effective.

In order to evaluate an approximate value of the mean period of the encountered waves, the following formula can be used:

$$T_e = \frac{T_1}{1 - 2\pi V \cos\mu / (gT_1)} \qquad (6)$$

The inception of parametric roll depends on the frequency of encounter being in the frequency range where the parametric roll is possible [4]. Therefore, the development of parametric roll depends on speed and heading.

According to (6) it is possible to tune velocity and heading of the vessel in order to get an encounter period that would lead to parametric roll. This analysis set the initial condition of the simulated cases in LaiDyn.

3.1 Turning circle manoeuvre

Experiments and simulations regarding a turning circle manoeuvre in irregular long-crested waves were conducted, in order to observe the ship rolling behaviuor for several encounter frequencies, checking the agreement of the LaiDyn responses with the experimental ones.

The model tests were carried out on the SeatechD model in the multifunctional model basin of Aalto University.

The turning circle tests were run with selfpropelled and radio-controlled model, in irregular waves, given by the Jonswap-type wave spectrum; the significant wave height and the average period were assume respectively H_S=4.8 (m) and T_1=5.9 (s). The speed of the model, with a target value of V_S=16.5 (kn) in full-scale, was controlled manually by adjusting the revolutions of propellers.

The height of Center-Of-Gravity for the model was adjusted to obtain a natural roll period close to its natural rolling period. In performing the turning circle, this creates a dangerous situation of roll resonance in stern quartering seas.

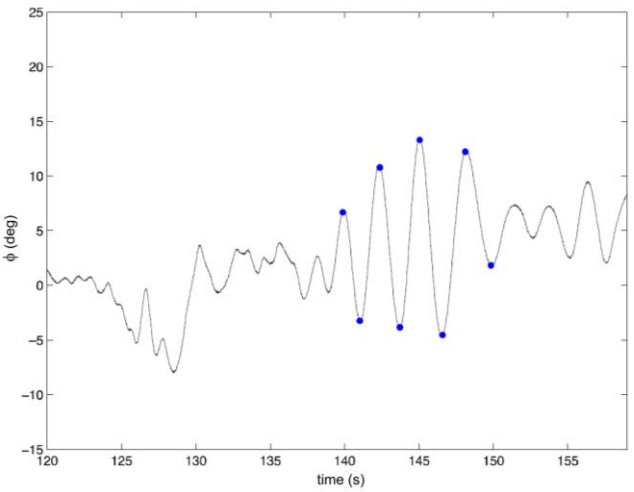

Fig. 3 – Experimental turning circle sample

A sample of the roll motion in turning circle manoeuvre, measured for a single realization of irregular waves, is presented in Fig. 3; roll motions develop in stern quartering seas as an unfavourable effect of change in encountered frequency. The simulated maxima and minima of roll amplitude, for the critical encounter condition, are marked with blue dots; peak-to-peak roll angles exceed 8°.

The simulated ship motion, corresponding to the condition of the model test, was obtained by means of LaiDyn, for a qualitatively comparison of the results. The numerical simulation of the turning circle test is presented in Fig.4. As can be noticed, roll motion, obtained from the same wave spectrum, but for a different wave realizations, develops according to the behavior of the experimental result, showing simulated maxima close to the measured ones.

More details, about the turning circle manouvre investigation, can be found in [18].

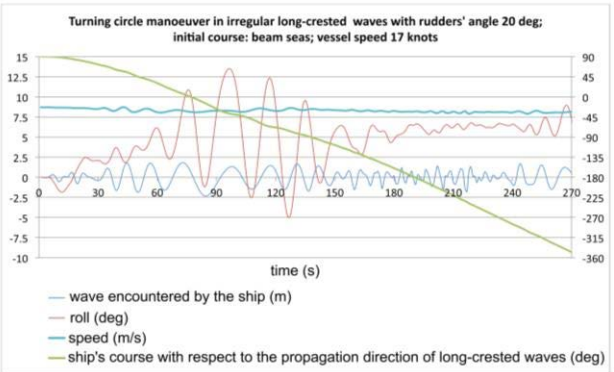

Fig. 4 – Simulated turning circle sample

4. Application and Results

The numerical applications carried out on SeatechD model regard roll resonance, with $T_e=T_n$ and parametric roll resonance with $T_e=0.5T_n$.

The simulation was performed by assuming a stern quartering irregular sea, described by the JONSWAP spectrum of significant wave height H_S=4.6 (m) and mean period T_1=6.5 (s).

The critical resonant situation were tuned, based on the considerations explained in the previous section (see Table 2).

Table 2 Simulated Conditions in LaiDyn

Case	Speed (m/s)	Heading (deg)	Encountered period (s)
1	8.5	42	16.3
2	8.5	22	22.6
3	5.65	42	11.8
4	2.85	42	9.3

In Fig.5 the results obtained from the application of the LaiDyn code to the Case 1 are shown.

The whole time history of ship motions is presented. Focusing on the rolling motion it is possible to observe the resonance that lead to large roll amplitudes.

Moreover, Fourier analysis of the encountered waves was conducted and the results are presented in Fig.6. It is possible to notice an interesting feature of the encountered waves: compared to the stationary spectrum, the amplitude of the encountered wave changes while the period of the wave train seems to be nearly constant. Its mean value is close to the natural roll period of the ship, as expected by applying (6).

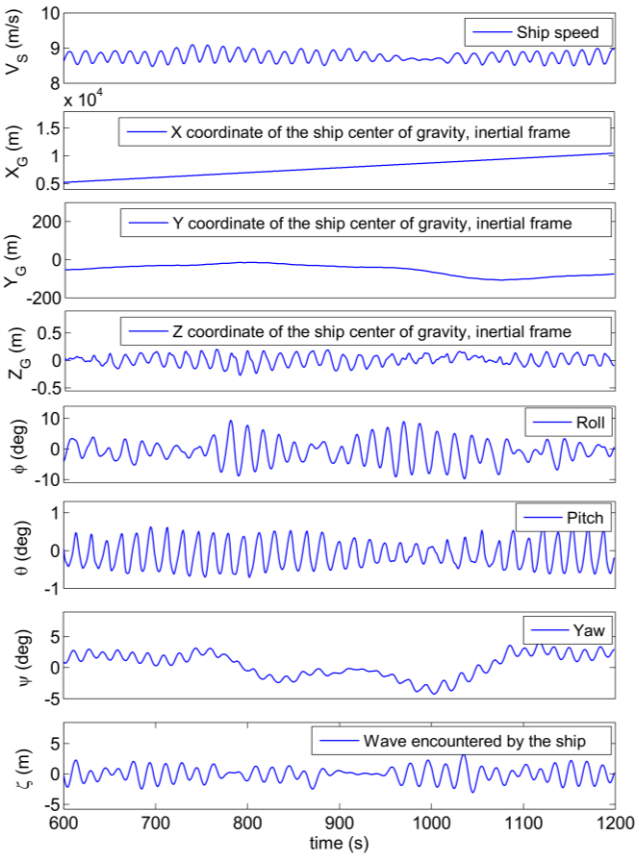

Fig. 5 – Time History of Ship Behavior for Case 1

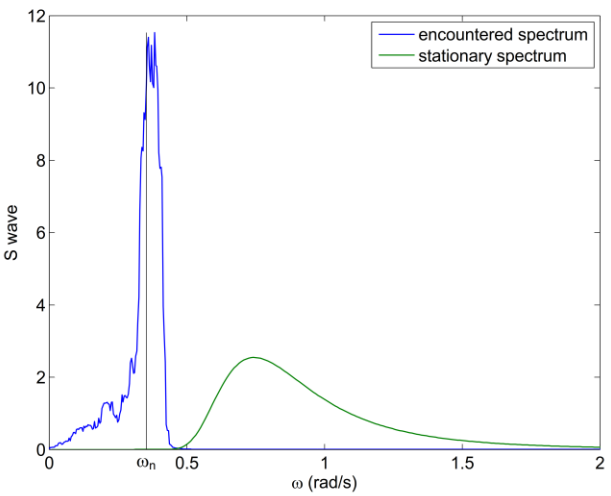

Fig. 6 – Spectral Analysis of irregular sea for Case 1

Further simulations, named Case 2 and Case 3 (see Table 2), were carried out with LaiDyn in order to drive the ship out of the resonant condition, by changing respectively the heading and the speed.

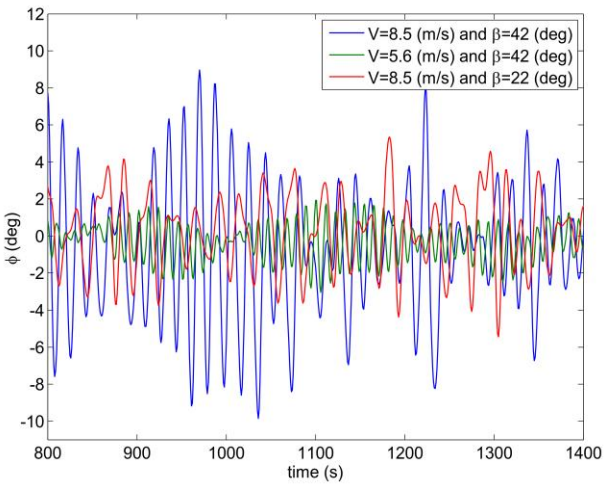

Fig. 7 – Roll Response Comparisons

The main results are shown in Fig.7, where the rolling responses for the three cases are compared.

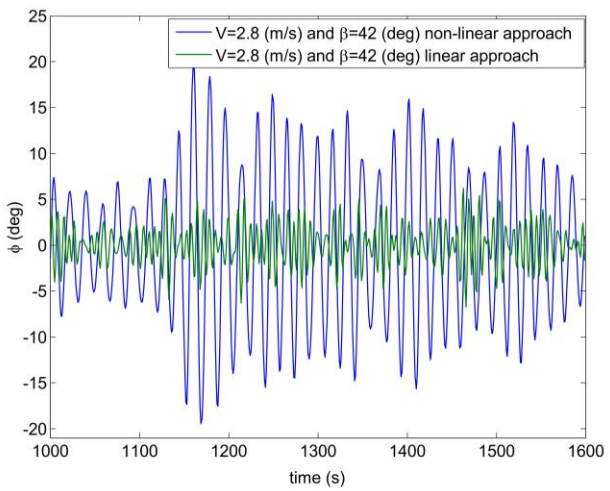

Fig. 8 – Simulated Parametric Roll

As could be noticed, the rolling motions are significantly mitigated, out of the resonant region, in particular for the reduced speed case.

For the Case 4 simulation, with lower speed and with $T_e \approx 0.5 T_n$, the phenomenon of parametric rolling can be easily observed in Fig.8. The parametric resonance was checked by means of the spectral analysis and reported in Fig.9.

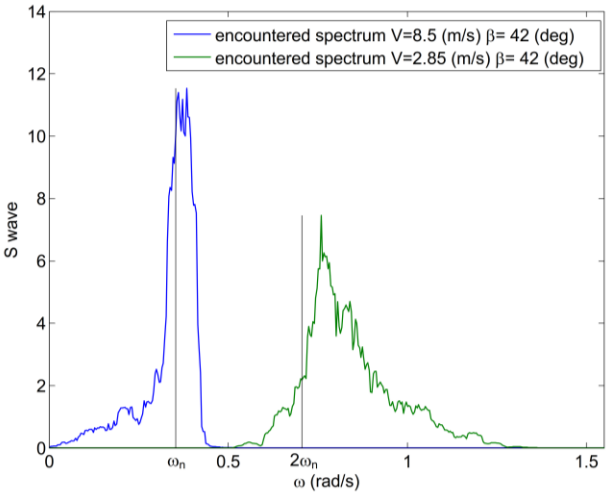

Fig. 9 – Spectral Analysis with resonance frequency

Due to the lower speed of the vessel, the decreased effects of the rolling damping, together with the parametric resonance, lead the ship to larger amplitude rolling motions (see Fig. 8). Moreover the showed results confirm that the linear analysis is not capable to simulate parametric resonance.

From the application of the numerical simulation it is possible to notice that the parametric rolling started for a lower value of T_e, compared to the theoretical value, in terms of frequencies, of $\omega_e \approx 2\omega_n$.

6. Conclusions

In this study a proposal, regarding direct assessment numerical tool, for stability failure, was presented. The numerical simulation tool is expected to reproduce vessel dynamics and provide ship-wise guidance for a safe operation also in adverse sea conditions.

The non-linear numerical model in six- degrees of freedom, LaiDyn was briefly presented and applied to simulate roll resonance in stern quartering irregular waves.

The simulations were performed by assuming a stern quartering irregular sea, described by the JONSWAP spectrum and critical resonant situations were tuned by means of speed and heading.

In order to allow a more realistic simulation of ship operational conditions, the ship speed was obtained by taking into account the propeller behavior in waves.

The applications were carried out on a Ro-Ro vessel. The roll resonance, with $T_e=T_n$ and parametric roll resonance with $T_e=0.5T_n$ were simulated in time domain. The same ship was also used, in previous research works, to validate LaiDyn, by means of experimental test, regarding pure loss of stability and parametric roll resonance in regular and irregular waves.

Fourier analysis of the encountered waves was conducted and the results analyzed. For the roll resonance condition, with $T_e=T_n$, a large amplitude rolling motions were observed in time domain. From the spectral analysis it was possible to notice that the encountered waves spectrum, presented its mean value close to the natural roll period of the ship.

The application of the numerical simulation on parametric rolling, with $T_e\approx0.5T_n$, for a lower speed and thus for a lower damping condition, showed larger rolling motions. By means of the spectral analysis it was also possible to observe that the parametric rolling started for a value of T_e, a somewhat lower than the theoretical value.

References

[1] A. Francescutto, Intact ship stability code: present status and further developments, Proc. of the 2nd Int. Conf. on Marine Research and Transportation, Naples, (2007), Session A, 199-208.

[2] IMO, Development of new generation intact stability criteria, SLF 52/INF.2, (2009).

[3] IMO, Report to the maritime safety committee, SLF 48/21, (2005).

[4] V. Belenky, C. Bassler, K. Spyrou, Development of second generation intact stability criteria, NSWCCD-50-TR-2011/065, Hydrodynamics Department Report, Bethesda, Naval Surface Warfare Center, (2011).

[5] C. Bassler, V. Belenky, G. Bulian, A. Francescutto, K. Spyrou, N Umeda, A review of available methods for application to second level vulnerability criteria, Proc. of the 10th Int. Conf. on Stability of Ships and Ocean Vehicles, Saint Petersburg, (2009), 111-128.

[6] N. Umeda, Current status of second generation intact stability criteria development and some recent efforts, Proc. of the 13th Int. Ship Stability Workshop, Brest, (2013), 138-157

[7] ABS, Guide for the assessment of parametric roll resonance in the design of container carriers, American Bureau of Shipping, Houston, (2008).

[8] W. Peters, V. Belenky, A. Reed, On regulatory framework of direct stability assessment, Proc. of the 11th Int. Conf. on Stability of Ships and Ocean Vehicles, Athens, (2012), 115-128.

[9] D. Spanos, A. Papanikolaou, Benchmark study on numerical simulation methods for the prediction of parametric roll of ships in waves, Proc. of the 10th Int. Conf. on Stability of Ships and Ocean Vehicles, Saint Petersburg, (2009), 627-636.

[10] C. Wandji, P. Corrignan, Sample application of second generation imo intact stability vulnerability criteria as updated during SLF 55, Proc. of the 13th Int. Ship Stability Workshop, Brest, (2013),

[11] R. Silva, G. Soares, Prediction of parametric rolling in waves with a time domain non-linear strip theory model, Ocean Engineering, Vol. 72, (2013), 453-469

[12] V. Belenky, H. Yu, K. Weems, Numerical procedures and practical experience of assessment of parametric roll of container carriers, Proc. of the 9th Int. Conf. on Stability of Ships and Ocean Vehicles, Rio de Janeiro, (2006), 119-130.

[13] B. Chang, On the parametric rolling of ships using a numerical simulation method, Ocean Engineering, Vol. 35, Iss. 5-6, (2008), 447-457

[14] Y. Ogawa, A study on numerical modelling for the parametric rolling, Proc. of the 10th Int. Conf. on Stability of Ships and Ocean Vehicles, Saint Petersburg, (2009), 533-540

[15] IMO, Revised guidance to the master for avoiding dangerous situations in adverse weather and sea conditions, IMO Maritime Safety Committee, (2007).

[16] J. Panjaitan, A study on ship motions and capsizing in severe astern seas, Doctoral Dissertation at Department of Naval Architecture and Ocean Engineering, Faculty of Engineering, Osaka University, (1998).

[17] J. Matusiak, Dynamics of a Rigid Ship, Aalto University, http://urn.fi/URN:ISBN:978-952-60-5205-2, publ. series SCIENCE + TECHNOLOGY, (2013).

[18] J. Matusiak, C. Stigler, Ship motion in irregular waves during a turning circle manoeuvre, Proc. of the 11th Int. Conf. on Stability of Ships and Ocean Vehicles, Athens, (2012), 291-298.

[19] O. Faltinsen, Sea loads on ships and offshore structures, Cambridge University Press, (1990).

[20] C. Holden, Modeling and Control of Parametric Roll Resonance, Doctoral Theses at NTNU, ISSN 1503-8181, (2011).

[21] J. Matusiak, On the effects of wave amplitude, damping and initial conditions on the parametric roll resonance, Proceedings of the 8th Int. Conf. on Stability of Ships and Ocean Vehicles, Madrid, Spain, (2003), 341-348.

[22] M. Mattila, An investigation of the dynamic stability of a fast RoPax vessel in waves (in Finnish), Helsinki University of Technology, Mechanical Engineering Department, Master Thesis, (1999)

Regulatory Use of Nonlinear Dynamics: an Overview

William S, Peters[1], Vadim Belenky[2] and Kostas Spyrou [3]

1. *USCG Office of Design and Engineering Standards, Washington DC, USA*
2. *David Taylor Model Basin, USA*
3. *School of Naval Architecture National Technical University of Athens, Greece*

Abstract: The paper is focused on the physical background of the second level vulnerability criterion for surf-riding /broaching-to as a part of the second generation IMO intact stability criteria. The criterion is based on Nonlinear Dynamics, homoclinic bifurcation, in particular, and uses the Melnikov method for calculations. While, well understood in the scientific community, these concepts may present a challenge for regulatory use as most practicing Naval Architects are not familiar with these concepts. The paper presents an explanation of the criterion background using conventional Naval Architecture physical concepts, and gives an overview of the dynamical aspects of the calculation procedure.

Key words: Surf-riding, dynamical system, equilibrium attraction, t

1. Introduction

Current development of the IMO second generation intact stability criteria brought a number of new problems and solutions that are not familiar to a practicing Naval Architect [1]. The reason is not as much new physical phenomena of stability failures, but rather related to the fact that the new criteria are based on first principles. Thus, the new criteria have to rely on a mathematical model of the stability failure; the only input is hull geometry, propulsion and environment characteristics. The development experience has shown that one of the least familiar mathematical techniques is the Melnikov method [2] used in the second level vulnerability criteria for surf-riding and broaching-to [3, 4]. The objective of this paper is bring this subject to the attention of the expert community at the Workshop, as the regulatory use of this technique requires an explanation accessible for practicing Naval Architect.

* **Corresponding author:** William Peters,work area: development and support of intact stability regulation.
E-mail: william.s.peters@uscg.mil

The work described in this paper has been funded by the USCG Office of Engineering Standards) under Mr. Jaideep Sirkar. The scientific background of this work was a result of a research funded by ONR under Dr. Patrick Purtell and Dr. Ki-Han Kim and ONR Global under Dr. Woei-Min Lin This support is gratefully acknowledged by the authors.

2. The Description of the Failure Mode

2.1 General

Broaching-to is a violent uncontrollable turn, occurring despite maximum steering effort in the opposite direction. As with any other sharp turn event, broaching-to is frequently accompanied with a large heel angle, which may lead to partial or total stability failure. Broaching-to occurs in following and stern-quartering seas. Broaching-to is usually preceded by surf-riding. Surf-riding occurs when a wave, approaching from the stern, captures a ship and accelerates her to the speed of the wave profile - wave celerity. While surf-riding, the wave profile does not move relative to the ship. Most ships are directionally unstable in the surf-riding situation; and this leads to the uncontrollable turn, defined as broaching-to (or often, just “broaching”). Therefore, the likelihood of surf-riding can be used to formulate vulnerability criteria for broaching-to [5].

2.1 Surf-Riding Equilibria

When a ship sails in longitudinal waves, three main forces act in the axial direction: thrust, resistance and surging wave force. Since the surf-riding occurs with the speed equal to wave celerity, it is convenient to

locate the frame of reference on the wave crest. As the reference frame moves with the wave, the ship remains unmovable in this frame of reference while she surf-rides.

For most practical cases, the surf-riding phenomenon is associated with acceleration of a ship to wave celerity. Thus, the thrust is not sufficient to provide speed equal to the wave celerity in calm water. Consider the difference between the thrust and resistance in calm water within the accepted frames of references; this difference is negative, when the resistance is greater than thrust.

The value of the wave force depends on the location of the ship on the wave. The front slope of the wave pushes a ship forward; while the back slope does the opposite. Indeed, there are neutral points around the wave crest and wave trough. If the wave is sufficiently long and steep, the pushing action of the wave force is sufficient to compensate the negative balance between thrust and resistance and create two equilibria. See Fig. 1 where the wave force, taken with opposite sign, is shown for different positions of a ship on a wave.

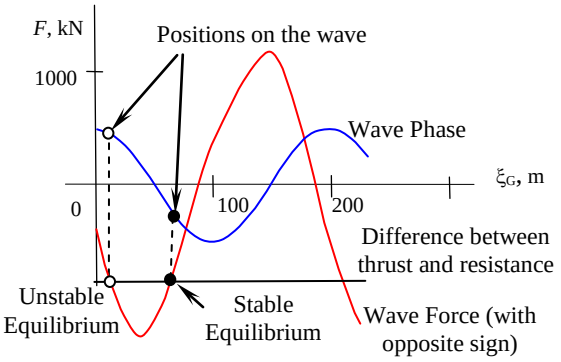

Fig. 1 – Wave forces and balance between thrust and resistance shown for different positions of ship on a wave.

Superimposed with the difference between thrust and resistance, the crossings with the wave force mark the position of two equilibria along the wave. One could note that the difference between thrust and resistance is referred to as "balance between thrust and resistance" in some literature, *e.g.* [4], however this term will not be used here.

3. Mathematical Model of Ship Motions

3.1 Mathematical Model of Resistance and Propulsion

Given wave parameters (length and height), calculating the position of these equilibria does not go beyond conventional Naval Architecture calculations. The first element needed is the approximation of the calm water resistance with a cubic polynomial:

$$R(V_S) = r_1 V_S + r_2 V_S^2 + r_3 V_S^3 \qquad (1)$$

Here V_S is ship speed in m/s, while r_1, r_2 and r_3 are curve-fitting coefficients. Curve fitting is a standard operation, available from a number of software packages, including Microsoft Excel.

The second element is thrust in calm water as a function of commanded number of revolution n and V_S is ship speed in m/s

$$T(V_S, n) = \tau_0 n^2 + \tau_1 V_S n + \tau_2 V_S^2 \qquad (2)$$

The coefficients τ_0, τ_1, τ_2 for thrust are defined as

$$\tau_0 = c_0 (1 - t_p) \rho D^4 \qquad (3)$$

$$\tau_1 = c_1 (1 - t_p)(1 - w_p) \rho D^3 \qquad (4)$$

$$\tau_2 = c_2 (1 - t_p)(1 - w_p)^2 \rho D^2 \qquad (5)$$

Here t_p is the coefficient for thrust deduction, while w_p is the wake fraction coefficient. Both coefficients are evaluated for calm water. D is the propeller diameter and ρ is mass density of water. Coefficients c_0, c_1, c_2 came from polynomial presentation of the coefficient of thrust K_T:

$$K_T = c_0 + c_1 J + c_2 J^2 \qquad (6)$$

Where J is the advance ratio

$$J = \frac{V_S (1 - w_p)}{nD} \qquad (7)$$

Thrust and resistance are plotted in Fig 2. Indeed, the curves are crossing in self-propulsion point in calm water; Fig. 2 also shows the balance between thrust and resistance as the difference at the speed corresponding to wave celerity.

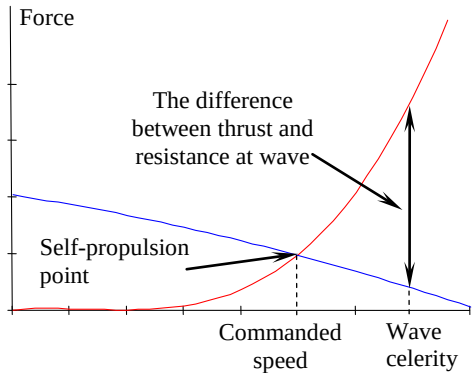

Fig. 2 – Resistance and propulsion showing self-propulsion point and thrust-resistance difference

3.2 Mathematical Model of Wave Surging Force

The surging wave force is a result of the projection of the wave pressure on the longitudinal axis. When a ship is moving in waves, the wave pressure are usually influenced by the presence of the ship. The ship generates waves because of her motions; these waves radiate from the ship and interfere with in incoming waves. Also, the waves that reach the ship, will be reflected from her as from any other obstacle (diffraction). These reflected (or diffracted) waves will also interfere with incoming waves changing the wave pressure on the hull.

However, when considering surf-riding, the ship speed is close to wave celerity. Thus, the encounter frequency is close to zero; no significant ship motions can be expected. Hence, the influence of radiated waves cannot be significant either. Also, if an obstacle moves with a wave, the reflection is going to be weak. Thus diffraction and radiation wave forces can be assumed small and excluded from the consideration.

This simplifies the problem: integrating the pressures along the hull lead to the following formula for the wave surging force:

$$F_W(\xi_G) = -\rho g k \zeta_A [A_S \sin(k\xi_G) - A_C \cos(k\xi_G)] \quad (8)$$

Where ρ is the density of water; g is gravity acceleration; ζ_A is the amplitude of the wave, ξ_G is the position of a ship on the wave; k is the wave number, also known as the spatial frequency of a wave of length λ:

$$k = \frac{2\pi}{\lambda} \quad (9)$$

A_S and A_C are sine and cosine amplitudes of the wave force, respectively:

$$A_S = \sum_i S_i \exp(-0.5kd_i) \cdot \cos(kx_i)\Delta x \quad (10)$$

$$A_C = \sum_i S_i \exp(-0.5kd_i) \cdot \sin(kx_i)\Delta x \quad (11)$$

Here x_i are the distance to station i, measured from the amidships, Δx is the distance between the stations and S_i is the submerged area of station i and d_i is the draft at the station i.

The amplitude of the surging wave forces shown in Fig. 1 is calculated as:

$$A_F = \rho g k \zeta_A \sqrt{A_S^2 + A_C^2} \quad (12)$$

Usually, the value A_S is about 10 times larger than A_C, thus the latter can be safely neglected from equations (8) and (12)

4. The Physics behind the Criterion

4.1 The Mechanics of Surging

The mechanics of surging can be illustrated using just the curves of thrust and resistance. Consider relatively small surging motion while the curves of thrust and resistant are not very different from the tangent lines plotted at the self-propulsion point in calm water, see Fig. 3.

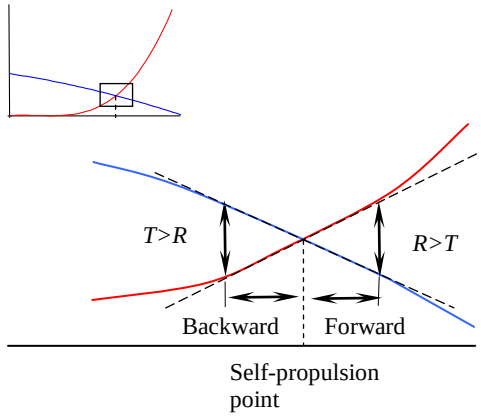

Fig. 3 – Small surging motions around self-propulsion point

Once the surging force pulls the ship backwards, the instantaneous speed decreases and the resistance becomes less than the thrust. The difference between thrust and resistance is directed forward, against the surging speed. When the wave surging force pushes the ship forward, the instantaneous speed increases and the resistance exceeds the thrust. The difference between thrust and resistance is directed against the surging speed again.

Consider the case where the wave force pushes the ship forward. The ship continues motion in the same direction even when the wave force changes sign. Now both wave force and the difference pulls the ship backward. Eventually, the ship changes the direction and surges backward. Once the self-propulsion point is passed the difference between the thrust and resistance changes sign and the surge starts to slow down. Then the surging force also changes the sign and start pushing the ship forward.

We now need to consider how the surging motion is stabilized, i.e. how the steady state amplitude is established?

One can consider the energy balance: the wave transfers to the ship some kinetic energy through the wave force. The difference between thrust and resistance disperses this energy; the balance between the work of these forces establishes the amplitude of surge.

4.2 Stability of Surf-riding Equilibrium

The surf-riding equilibria were referred to as stable and unstable in Fig.1. How it can this be shown?

Consider a ship in a surf-riding mode; midship is located around 70 m forward of the wave crest (marked as stable equilibria near wave trough in Fig. 1) and has a speed that is equal to the wave celerity.

Let the ship be perturbed from this location forward, towards the wave trough. The surge force is smaller there and the difference between thrust and resistance pulls back, since the wave celerity is larger that the commanded speed. Thus, the instantaneous speed of the ship decreases and the wave starts overtaking the ship. Once the ship slips back towards the wave crest, the wave surge force increases and pushes her back to the equilibrium.

Now, let the ship be perturbed from the equilibrium backwards, *i.e.* towards the wave crest. The wave force becomes larger than the difference between thrust and resistance. Thus, the ship will be pushed back to the surf-riding equilibrium (trough).

These simple considerations show that if one tries to perturb the ship from the equilibrium near wave trough, a resultant force pushes it back to the equilibrium. Thus, the equilibrium near the wave trough is stable.

Consider a ship in a surf-riding mode; she is located around 30 m forward of the wave crest (marked as unstable equilibria near wave crest in Fig. 1) and has a speed equal to wave celerity.

Let the ship be perturbed from this location forward, towards the wave trough. The wave surging forces is increasing there; it will push the ship further forward, until she ends up at the stable equilibrium near the wave trough.

If the ship is perturbed from this location backward, towards the wave crest, the wave force is decreased and the instantaneous speed also starts to decrease. The difference between thrust and resistance pulls the ship back and nothing keeps the wave from overtaking the ship. There are several scenarios that consider what may happen next (to be considered in the next

subsection), but one thing is clear, the ship does not return back to the equilibrium.

These considerations show that as one tries to perturb the ship from the equilibrium near wave crest, a resultant force takes it away from that equilibrium. Thus, the equilibrium near the wave crest is unstable.

4.3 Attraction to Surf-riding Equilibrium

If surf-riding equilibria do not exist, surf-riding is not possible and the ship will simply surge. That means that all the combinations of instantaneous speed and position on the wave lead to the same outcome *i.e.* it does not matter where the motion has started from.

However, once the equilibria points appear at certain positions on the wave, not all the combinations of the wave position and instantaneous speed lead to the same response.

If a ship is "placed" exactly at the location of the stable equilibrium near wave trough and accelerated to the wave celerity, indeed, she will stay there indefinitely. Any small perturbation from this position will return the ship back to equilibrium (see the discussion in the previous subsection). If a ship is placed to the unstable equilibrium near wave crest, accelerated to wave celerity and then perturbed towards the wave trough, she will end up at the stable surf-riding equilibrium as well.

Thus, there is a set of combinations of wave positions and instantaneous speeds that will lead to surf-riding. One can say that these combinations form a "domain of attraction to surf-riding equilibrium." What happens to a ship outside of this domain?

For translating ship motions in the longitudinal direction, two options are possible: surging or surf-riding. So, in principle, once outside of the attraction domain, the ship either continues to surge or is attracted to surf-riding equilibrium on some other wave. How is the choice between these options determined?

Consider again the energy/work balance of the wave surging force and the difference between thrust and resistance. As it was discussed in the subsection 4.1, the latter disperses the kinetic energy obtained from wave. Once the balance between these two works is established, the ship's response is surging. What if a wave provides the ship with more kinetic energy than the difference between thrust and resistance can disperse?

Eventually, this excessive kinetic energy leads to acceleration and to attraction to the surf-riding equilibrium. The surf-riding becomes a new energy balance between the works of wave surging force and the difference between thrust and resistance. The ship is captured by the wave. Once the surf-riding equilibria appear, is surf-riding inevitable and will occur on one of the succeeding waves?

As it was discussed in the beginning of this section not all the combinations of position on the wave and instantaneous speed lead to the same result. Indeed, the front slope of the wave provides more chances for surf-riding because the wave surging force is directed forward. If started on the back slope of the wave, the wave surging force is directed backward and the surging energy balance still may be achieved. That means: surging and surf-riding may co-exist for the same speed setting and wave parameters. How this can be explained?

If the initial energy level can be dispersed by the difference between thrust and resistance, surging will occur. If the initial energy level is too high (say, front slope of the wave and/or high instantaneous speed) to be dispersed, surf-riding will occur.

If the wave adds too much kinetic energy (say, wave is steep) to ship motions that it cannot be dispersed by the difference between thrust and resistance (say, commanded speed is too large), then surging motions are no longer possible. Even when starting with low initial energy level on the back slope of the wave and commanded speed, each sequential wave will add a bit of kinetic energy that cannot be dispersed; then sooner or later the surf-riding will occur as the ship moves towards stable equilibrium.

4.4 Influence of the Commanded Speed

The discussion in the previous subsection led to the conclusion that if a ship cannot disperse kinetic energy by the difference between thrust and resistance, then surf-riding becomes inevitable. Thus, the commanded speed defines the surf-riding likelihood for the given wave parameters.

If the commanded speed is low, the difference between thrust and resistance (at the speed of wave celerity) is larger than the amplitude of the wave surging force, the intersection (like in Fig.1) does not exist, and the surf-riding is impossible.

Increase of commanded speed leads to appearance of surf-riding equilibria (seen as the intersection in Fig. 1). Surf-riding may be possible for some combinations of wave position and instantaneous speed. Other combinations with lower initial energy level still lead to surging as the difference between thrust and resistance still is capable of dispersing the additional energy. This is the case with the co-existence of surging and surf-riding. The minimal commanded speed corresponding to appearance of the equilibria (i.e. leading to the difference between thrust and resistance equal to the amplitude of the wave surging force) is commonly referred as "the first threshold."

Further increase of the commanded speed will illuminate the surging mode of motions, because the difference between the thrust and resistance becomes too small to disperse additional kinetic energy obtained from the wave surging force. Surf-riding becomes inevitable. The lowest commanded speed leading to inevitable surf-riding is commonly referred as "the second threshold."

5. The Reasoning behind the Criterion

5.1 Choice of the Criterion

Two thresholds described at the end of previous section seem to be natural candidates for the criterion. Given the wave parameters, one can find the commanded speed corresponding to one of these thresholds. If a ship cannot make this speed, there is no vulnerability for surf-riding and broaching-to. Which threshold should be used for the criterion?

Use of the first threshold seems to be more conservative as the surf-riding is impossible for the commanded speed below it. However, a simple calculation with formulae (1), (2) and (12) show that the surf-riding equilibria may exist even for ships that have never been observed to surf-ride, such as bulk-carriers. Thus, the criterion based on the first threshold would lack the discriminating power to single out the ships vulnerable for broaching. Why?

Appearance of the surf-riding equilibria makes broaching possible, but requires a ship be placed into the domain of attraction to the stable surf-riding equilibrium. This domain is defined for combinations of wave positions and instantaneous speeds. So it is not enough for the ship to be on the front slope of the wave, but also needs to obtain an instantaneous speed close to wave celerity. For example, for a ship of 180 m length and the wave of the same length, the speed close to the wave celerity will be just above 30 knots. There is no real reason for a ship with the service speed of, say 18 knots, to be spontaneously accelerated up to 30 knots.

At the same time, the second threshold guarantees surf-riding for any ship that can make the speed above the threshold for a given wave. This gives the criterion its discriminatory power and this is why the second level vulnerability criterion is based on the second threshold.

5.2 Evaluation of the Criterion

Use of the criterion requires a way to calculate the commanded speed (setting of number of revolutions or the throttle setting) that corresponds to the second threshold. In principle, it can be done by numerical simulations [4]. The Melnikov analysis gives a process to do it quickly and easily [2].

Consider two or three sequential waves. Let's assume, one has found the boundaries of the domain of attraction to stable surf-riding equilibrium. If the commanded speed is below the second threshold and allows co-existence of surging and surf-riding, the

boundary of the attraction domains of sequential waves, must have some separation between them to allow combinations of position on a wave and instantaneous speed leading to surging.

There is a class of mathematical models, known as Hamiltonians, that provide analytical solutions for these boundaries. Unfortunately, they cannot be applied directly because they do not include any energy dispersion, which is essential for the problem at hand.

The Melnikov analysis is an asymptotic expansion, (similar to Taylor series) where the Hamiltonian is used as the first term. The influence of the energy dispersion terms is included in the higher order terms. This approach allows expressing the distance between the boundaries (Melnikov function, see [2] for derivation) for a given commanded number of revolutions *n*:

$$M(n) = -\frac{r(n)}{q} - \frac{4}{\pi} p_1(n) + 2 p_2 - \frac{32}{3\pi} p_3 \qquad (13)$$

The terms in this equation has the following meaning:

$$r(n) = \frac{k\left(T(c,n) - R(c)\right)}{\left(m + m_x\right)} \qquad (14)$$

Here $T(c,n)$ is the thrust at the speed equal to wave celerity, k is the wave number (spatial frequency, see formula 9), $R(c)$ is the resistance at the speed equal to wave celerity, m is mass of the ship and m_x is the added mass of the ship computed for zero-frequency.

$$q = \frac{k \cdot A_F}{m + m_x} \qquad (16)$$

The amplitude of the wave surging force, A_F, is defined by formula (12).

$$p_1(n) = \frac{3r_3c^2 + 2(r_2 - \tau_2)c + r_1 - \tau_1 n}{\sqrt{kA_F\left(m + m_x\right)}} \qquad (15)$$

$$p_2 = \frac{3r_3c + 2(r_2 - \tau_2)}{k\left(m + m_x\right)} \qquad (16)$$

$$p_3 = \frac{r_3\sqrt{A_F}}{\left(\sqrt{k\left(m + m_x\right)}\right)^3} \qquad (17)$$

The coefficient *r* and t are defined by formulae (1) through (5). The appearance of the Melnikov Function (13) is given in Fig. 4.

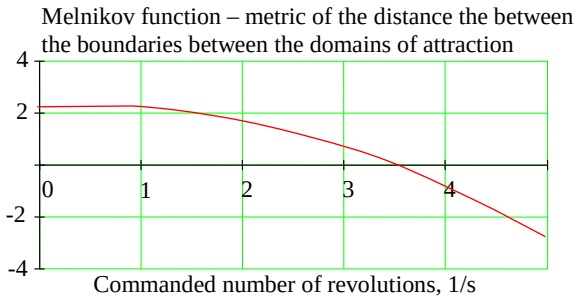

Fig. 4 – Melnikov function

The zero value of Melnikov function approximately corresponds to a zero distance between the boundaries of the domains of attraction to stable surf-riding equilibrium for the sequential waves. Indeed, the number of commanded revolutions is an approximation for the second threshold that was chosen as a criterion.

5.3 Wave parameters

The calculation described in the previous subsection is performed for a given set of wave parameters. How to choose these parameters to reflect a realistic seaway?

The idea is to approximate a realistic seaway as a series of regular waves with random lengths and heights. Then, the parameters of each wave become random numbers and can be obtained from known probability distributions, see [5] for details. In principle, the final form of the criterion is probabilistic and based on a critical wave/ wave group approach, see [6], and [7]. Discussion of the probabilistic aspects of the second level vulnerability criteria falls outside the scope of this paper.

6. Summary and Concluding Comments

The paper is focused on dynamical aspects of the second level vulnerability criterion for surf-riding / broaching-to. The criterion is based on the commanded speed corresponding to the second threshold, exceedance of which makes surf-riding inevitable on a given wave. The appearance of such a threshold is associated with a phenomenon known in nonlinear dynamics as "homoclinic bifurcation" [8]. However, its physical background can be explained without the vocabulary of Nonlinear Dynamics using physical concepts available in Naval Architecture.

The phenomenon of surf-riding is essentially the attraction to the surf-riding equilibrium created when the wave surging force is large enough to compensate for the difference of thrust at the commanded speed and resistance at the speed of the wave profile (wave celerity).

While surging, the difference between thrust and resistance disperses the additional kinetic energy obtained from the wave surging force. When the kinetic energy is too large or the difference between thrust and resistance is too small, the additional kinetic energy cannot be dispersed and the attraction to the surf-riding equilibrium becomes inevitable.

Calculation of the criterion, i.e. the commanded speed leading to inevitable surf-riding on a given wave, can be calculated using the Melnikov method, which is an asymptotic expansion of an analytical solution of this problem. These calculations involve a numerical solution of an algebraic equation, requiring approximate resistance, propulsion and hull geometry data.

Acknowledgements

The authors are grateful to Dr. A. Reed of the David Taylor Model Basin and Prof. N. Umeda of Osaka University for fruitful discussions.

References

[1] Peters, W., Belenky, V., Bassler C., Spyrou, K., Umeda, N., Bulian, G. and B. Altmayer "The Second Generation of Intact Stability Criteria An Overview of Development", SNAME Trans. (2011) Vol. 119.

[2] Spyrou, K.J. "Asymmetric Surging of Ships in Following Seas and its Repercussions for Safety," *Nonlinear Dynamics*, (2006) Vol. 43, pp. 149-172.

[3] IMO document SLF/54/3/3 "Summary of Research into Stability Failures Modes and associated Criteria Development", London, 2011

[4] Belenky, V., Bassler, C.C. and K.J. Spyrou Development of Second Generation Intact Stability Criteria, Naval Surface Warfare Center Carderock Division Report (2011) NSWCCD-50-TR-2011/065.

[5] Proposed Amendments to Part B of the 2008 IS Code to Assess the Vulnerability of Ships to the Broaching Stability Failure Mode, Appendix 15 of IMO document SDC-1-INF.8 "Information Collected by the Correspondence Group on Intact Stability Regarding the Second Generation intact Stability Criteria Development", London, 2013

[6] Themelis, N. and K.J. Spyrou "Probabilistic Assessment of Ship Stability," *SNAME Trans.* (2007) Vol. 115. pp. 181-206

[7] Umeda, N., Shuto, M. and Maki, A., "Theoretical Prediction of Broaching Probability for a Ship in Irregular Astern Seas", *Proc. of the 9th Intl Ship Stability Workshop*, Hamburg, (2007).pp. 1.5.1-1.5.7.

[8] Spyrou, K.J. (1995) Dynamic instability in quartering seas: the behavior of a ship during broaching. Journal of Ship Research, 40, 1, pp. 46-59.

Applicability of the Difference between Population Statistics as an Acceptance Criteria Metric for Seakeeping Validation

Aurore V. Zuzick*, Arthur M. Reed, William F. Belknap, and Bradley L. Campbell
David Taylor Model Basin (NSWCCD), USA

Abstract: The difference between population statistics is proposed as a primary acceptance criteria metric for the direct quantitative validation of ship simulation tools in support of accreditation for uses related to ship motions in irregular seas. The discussion is applicable to comparisons of statistical quantities calculated from ship motion time histories generated by simulations and benchmark data such as scale-model test results. The difference between population statistics provides several of the key characteristics desirable in acceptance criteria, including quantifiable measures of accuracy, completeness, and self-consistency. Further, this metric can be applied to a variety of statistical quantities of interest, provides an opportunity to extend parameter-level comparison results to a broader measure of overall accuracy, and allows for straightforward application of engineering margins traceable to simulation tool performance requirements. Use of the difference between values (often called the error) as the foundation of comparison metrics is not a new concept in the field of validation, but its use is not frequently associated with acceptance criteria for simulations of stochastic processes. Much work has been completed to characterize the total uncertainties from various sources associated with each data set in a comparison of this type. Extension of that body of work to the uncertainty associated with the comparison itself provides a robust measure of parameter accuracy and a flexible and adaptable acceptance criteria foundation.

Key words: Validation; Simulation; Seakeeping

1. Introduction

Validation and accreditation of simulation tools for modeling ship motions in irregular seas is a challenging endeavor for which no single straightforward methodology has been proven universally applicable. Rather, several key comparison approaches are typically employed through a multifaceted comparison of simulation results to benchmark data.

Belknap, *et al.* (2011) describes two categories of validation techniques: qualitative and quantitative. Qualitative validation methods examine trends and expected behaviors to provide confidence that the underlying assumptions within the code lead to reasonable, physical results. Quantitative validation methods establish the simulation tool's ability to meet specific performance requirements associated with the Specific Intended Uses (SIUs) for which accreditation is sought.

Acceptance criteria are typically implemented as part of quantitative validation to provide non-subjective assessment of desired simulation tool performance. Of course, subjectivity is inherently present in the development of acceptance criteria, themselves, but ideally the quantitative criteria are directly traceable to performance capabilities defined by the simulation tool user for each SIU.

Establishment of appropriate acceptance criteria for SIUs related to ship motions in irregular waves is not straightforward. Smith (2012) describes some of the complexities of this task, including the development of acceptance criteria structure. Validation methods should extend single parameter comparisons to overall assessment of the code through examination of multiple degrees of freedom and conditions. Smith (2012) proposes a three-tier structure of parameter

* **Corresponding author:** Aurore V. Zuzick, research fields: surface ship hydromechanics, computational hydrodynamics. E-mail: aurore.zuzick@navy.mil

criteria, condition criteria, and set criteria. Parameter criteria are applied to a single degree of freedom and a single condition; results from the parameter criteria form the inputs to condition criteria, and so forth.

The challenge of establishing appropriate parameter criteria is complicated by uncertainty associated with the data values compared. Statistical values calculated from ship motion time histories are not known exactly. Uncertainty associated with calculated time history statistics comes from several sources including stochastic process uncertainty, instrumentation uncertainty (if model results are used as benchmark data), and uncertainty in simulation results due to uncertainty in simulation input parameters (input sensitivity). Known uncertainties should be quantified and incorporated into acceptance criteria for robust comparison assessment.

Characteristics of good acceptance criteria for validation and accreditation of computer models have been identified by previous efforts within and beyond the field of ship dynamic stability. Oberkampf & Barone (2006) outline features of good validation metrics within their discussion of criteria development. Smith (2012) discusses the importance of many of these characteristics to the development of acceptance criteria for irregular seas ship motion prediction validation. Perhaps most significant among these characteristics is the ability to provide quantifiable measures accuracy through comparisons. Also notable are the importance of self-consistency (non-contradictory assessment outcomes) and completeness (consideration given for all relevant sources of uncertainty associated with validation data sets).

The quantitative acceptance criteria metric proposed in this paper is intended to be applied on a parameter level for direct validation through comparison with benchmark (model-test) data.

2. Definitions

Ship motion response in irregular seas can be characterized in many ways, the most common of which is the standard deviation (or square root of variance) of a particular ship motion parameter time history. The discussion below will be presented in the context of standard deviation comparisons, but the concepts are applicable for other statistical quantities which may be applicable to the SIUs (*e.g.* exceedence rate, percentile of peak amplitudes). Belenky, *et al.* (2013) provides discussion on the calculation of mean ensemble variance values from typical irregular seas model-test time histories.

2.1 Difference Between Data Points

The foundation of the proposed metric for this application is the difference between statistical quantities calculated from simulation and model test data sets.

$$\Delta = \sigma_{simulation} - \sigma_{benchmark} \quad (1)$$

A positive value is associated with simulation over-prediction, and a negative value denotes simulation under-prediction. This concept is certainly not new to the field of validation, but its use is often associated with largely deterministic processes. Both Oberkampf & Barone (2006) and ASME (2009) refer to this quantity as the error between model and experimental results, noting that the experimental results are only an estimated measure of the "true" parameter value.

2.2 Confidence Intervals

The confidence interval is an conventional mathematical quantity which NIST (2014) defines as a range of values which is likely to contain the population parameter of interest. Its purpose is to account for the possible difference between a discreet value derived from limited population samples from the underlying population value. The level of confidence associated with the interval defines its length and corresponds to the probability that the sampled value and intervals encompass the true population value.

When defined relative to a mean value and assuming a large sample size, the confidence interval is defined as

$$CI_{\mu} = z_{1-\alpha/2}\frac{s}{\sqrt{N}}$$

where s is the sample standard deviation, N is the number of samples, α is the desired significance level (corresponds to confidence level), and z is the two-tailed Gaussian distribution factor with significance level, α. The upper and lower bounds of the confidence intervals applied to the sample mean are defined as

$$\mu_{sample} \pm CI_{\mu} \tag{2}$$

where μ_{sample} is the sample mean. Belenky, *et al.* (2013) provides an extension of this theory to calculate the confidence interval on the ensemble mean standard deviation value from a set of time histories of ship motions for one parameter and one condition.

When comparing samples from two populations, the confidence interval on the difference between mean values is of interest. The confidence interval on the difference between mean values is defined as

$$CI_{\Delta\mu} = z_{1-\alpha/2}\sqrt{\frac{s_1^2}{N_1} + \frac{s_2^2}{N_2}} \tag{3}$$

where the subscripts 1 and 2 distinguish between data sets.

2.3 Combined Uncertainty

Additional sources of uncertainty may be applicable to the sample value, including uncertainty due to instrumentation limitations and uncertainty due to variability of the conditions under which the data was generated. Combined uncertainty intervals constructed from multiple sources of uncertainty are typically the root sum of squared intervals calculated separately for each source. While confidence intervals (based only on sampling characteristics) are symmetric, combined uncertainty intervals may be asymmetric.

To compare two data sets with equal number of samples (*i.e.* $N_1 = N_2$) and symmetric confidence intervals, (3) can be rearranged and described in terms of the confidence intervals associated with each data set value as

$$CI_{\Delta\mu} = z_{1-\alpha/2}\sqrt{\left(\frac{CI_{\mu\_1}}{z_{1-\alpha^*/2}}\right)^2 + \left(\frac{CI_{\mu\_2}}{z_{1-\alpha^*/2}}\right)^2}$$

where α^* refers to the level of significance associated with the sample intervals and α refers to the level of significance associated with the uncertainty in the difference.

Equation (3) lends itself to a definition of the combined uncertainty (*e.g.* statistical, instrument, etc.) in the difference between samples which is agnostic to the methods used to define the combined uncertainty intervals associated with each data set, assuming the uncertainties of each set are Gaussian distributed. Further, (3) can be adapted to account for asymmetric intervals by distinguishing between the upper and lower intervals associated with each set.

For validation purposes, consider the definition of the difference provided in (1) to compare two ensemble mean standard deviation quantities. Given combined uncertainty intervals associated with each data set of significance level α^*, the upper and lower combined uncertainty intervals on the difference can be calculated as

$$CI_{\Delta}^{+} = z_{1-\alpha/2}\sqrt{\left(\frac{CI_{bench}^{-}}{z_{1-\alpha^*/2}}\right)^2 + \left(\frac{CI_{sim}^{+}}{z_{1-\alpha^*/2}}\right)^2}$$

and

$$CI_{\Delta}^{-} = z_{1-\alpha/2}\sqrt{\left(\frac{CI_{bench}^{+}}{z_{1-\alpha^*/2}}\right)^2 + \left(\frac{CI_{sim}^{-}}{z_{1-\alpha^*/2}}\right)^2}$$

where the subscripts "bench" and "sim" refer to the benchmark and simulation data sets, respectively. Fig. 1 below illustrates the relationships between the uncertainty intervals on both data sets and the uncertainty interval on the difference.

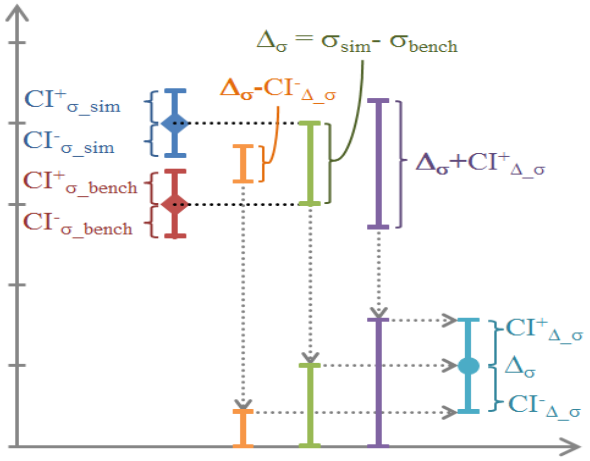

Fig. 1: Uncertainty Intervals On Two Data Sets and On the Difference Between Data Sets

3. Validation Utility

Quantitative validation for stochastic processes is often centered around traditional methods of statistical inference. Hypothesis testing and interval overlap examination address the question: "Could the underlying populations (described by the sample data sets) be the same?" Smith (2011) presents techniques to extend these types of statistical methods to continuous and non-independent samples, such as ship motion time histories. The level of significance associated with these statistical testing methods can satisfy a requirement for quantified accuracy. However, for engineering purposes, statistical similitude does not necessarily constitute a required level of correlation.

Some quantifiable differences between the simulation and the benchmark data may be acceptable for a given SIU. Further, the intended use of a simulation tool may allow for application of a margin to simulation results. If so, the validation effort may be most effective if it provides quantifiable measures of the demonstrated accuracy of the tool in lieu of a binary accreditation outcome (*i.e.* accredited or not accredited).

3.1 Interpretation of Results

The combined uncertainty intervals surrounding a difference between simulation and benchmark statistics enclose the region within which the "true" difference between populations is found. The level of confidence associated with interval calculations corresponds to the probability that the true difference is within the interval limit. For a 90% level of confidence, there is a 90% probability that the difference between the simulation and benchmark results is between the lower and the upper interval
extents.

Positive values denote a simulation value which is greater than the benchmark (over-prediction) while negative values denote under-prediction. A zero-crossing of an interval denotes the possibility that there is no difference between the underlying populations (similar to the objectives achieved through statistical inference tests). It should be noted, however, that the confidence level associated with the interval does not equal the probability that the difference is zero. In fact, there is equal likelihood that the true difference falls anywhere else within the interval extents.

For some purposes, a relative metric may be more suitable for comparison purposes. By dividing the difference (and interval limits) by the benchmark statistic value, a %-difference (and associated uncertainty) is generated. Both the difference and %-difference comparison measures can be used to apply parameter-level acceptance criteria for a single condition or can be used to examine simulation parameter accuracy trends over a range of conditions.

3.2 Parameter Acceptance Criteria

As noted above, when the uncertainty interval on the difference crosses zero, there may be no difference between the two populations. As a potential parameter-level acceptance criteria, a zero-crossing of difference intervals is most analogous to an overlap of

uncertainty intervals associated with two data sets. Note, however, that zero-crossing is a more "strict" measure of similitude than interval overlap. For same level of significance, it is mathematically possible for the intervals to slightly overlap without the corresponding interval on the difference crossing through zero. Comparison A in Fig. 2 below illustrates a case of the uncertainty interval on percent difference crossing through zero.

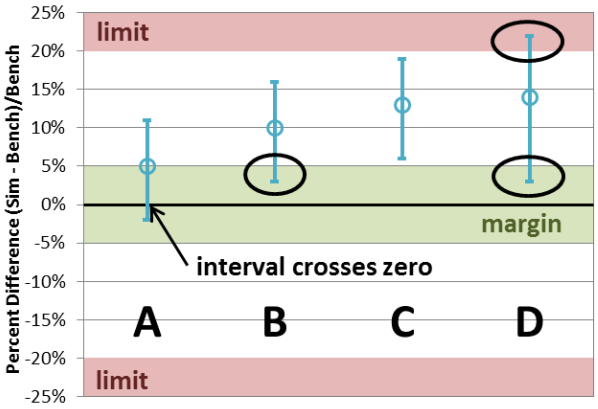

Fig. 2: Options for parameter-level criteria application based on the difference between population statistics

While zero difference is generally a goal for most validation efforts, a region around zero can be defined to capture a broader and more requirement-specific measure of successful agreement. A criterion which would require some part of the difference interval to fall within this region (*i.e.* margin) can be an effective way to link specific requirements to validation comparisons. For example, the acceptance criteria may state that simulation roll standard deviation values must potentially agree with benchmark values by 5%. For a specified significance level, any interval falling at least partially within –5% and +5% could satisfy the criterion. Comparisons A, B, and D in Fig. 2 illustrate cases in which the uncertainty intervals on the percent difference extend into a margin region defined about zero.

In additional to providing a test for statistical equivalence or good correlation, the difference can be used to investigate other aspects of comparison results. Based on the requirements associated with the SIUs, the application of a criterion to bound the differences (*i.e.* limit) may be a more applicable approach. This may be the case if the SIU is related to safety and potential differences are more important than potential similarities. For example, acceptance criteria may require that simulation results not differ from benchmark data by more than 20%. For a specified significance level, any interval falling entirely within the limits of –20% and +20% would satisfy the requirement. Further, if conservatism is a goal, the bounds on the difference could be asymmetric, such as requiring all parts of the interval to fall between –10% and +20%. Cases A, B, and C in Fig. 2 satisfy this type of limit criterion, while the uncertainty associated with case D suggests the differences could be greater than the limiting value.

If validation requirements are well-defined, a combination of limits and margins can be employed to form a multi-faceted parameter-level criterion. For example, the requirements associated with the SIUs may identify good correlation as standard deviation values within ±5% of benchmark results and unacceptable differences greater than ±20%. Cases A and B in Fig. 2 would satisfy both the margin and limit criteria. Case C passes the limit criterion but fails to demonstrate sufficient performance by not extending into the margin region.

Case D demonstrates sufficient correlation (interval extends into the margin region) while also suggesting the possibility of excessively large differences (interval extends into limit region). In this case, the uncertainty in the comparison is too large to adequately determine a successful comparison outcome. For validation purposes, it is important to distinguish between the outcomes of cases C and D. While case C demonstrates a lack of correlation, case D provides evidence of good correlation, but the comparison is hindered by the large uncertainty in the validation data sets.

3.3 Broad View of Simulation Accuracy

The acceptance criteria methodologies based on the differences between benchmark and simulation statistics described in the previous section are most useful as part of a multi-level acceptance criteria structure. Typically, for a given condition, several key parameters (*e.g.* roll, pitch, etc.) must pass parameter criteria in order to consider the overall comparison of the condition a success. The purpose of this requirement is to provide evidence that the overall physics underlying a given condition are adequately captured by the simulation tool. While this methodology is sound, the information provided as a result of multi-level criteria application is limited in value. A condition, or some percentage of conditions, is determined to pass or fail the criteria. The question answered through accreditation is, "Is the tool accurate enough to be used for the SIUs?". The question which cannot be answered by this approach is, "How accurate is the simulation tool?".

A particularly useful attribute of the difference between statistics is its ability convey information about a simulation's accuracy for a given parameter across a range of conditions. The following section provides an example of this utility using notional comparison data.

4. Sample Data

Fig. 3 below presents notional data similar to results which may be used for simulation tool validation. The values shown have been generated using typical ship response in large seas, but are not attributable to any particular ship. Standard deviation values are plotted with 90% confidence intervals for ten different environmental conditions. Benchmark results are shown in red and simulation results are shown in blue. The data presented are assumed to share the same operational condition (*e.g.* head seas, 10kts full-scale ordered speed) with varying wave characteristics.

Application of an interval overlap criterion would result in the passing of all conditions except for B and D. However, the differences between standard deviation values in those cases may still be small enough to satisfy the requirements of the SIUs. Fig. 4 shows the difference (and 95% confidence interval on the difference) for the same ten cases.

Examination of the comparison difference results provides additional quantifiable comparison results. For example, there is at least a 95% probability that the difference in all conditions is less than +1.5 deg (over-prediction) and –1.0 deg (under-prediction). Also, all ten comparisons show evidence of possible correlation within ±0.5 deg. Note that cases B and D, whose individual data set intervals do not overlap, are the only conditions whose interval on the difference does not pass through zero.

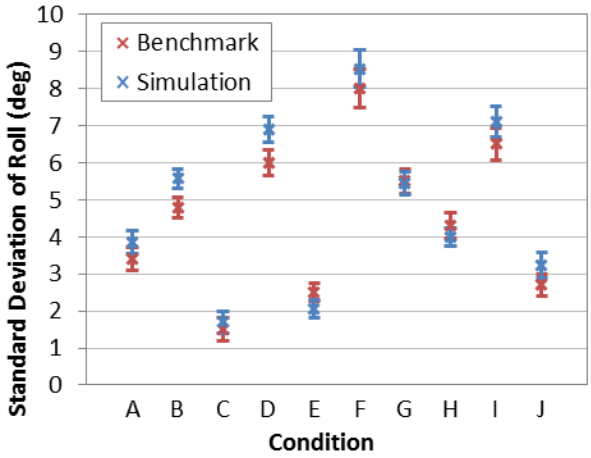

Fig. 3: Notional Validation Data Sets for Roll Standard Deviation of Ship In Heavy Seas

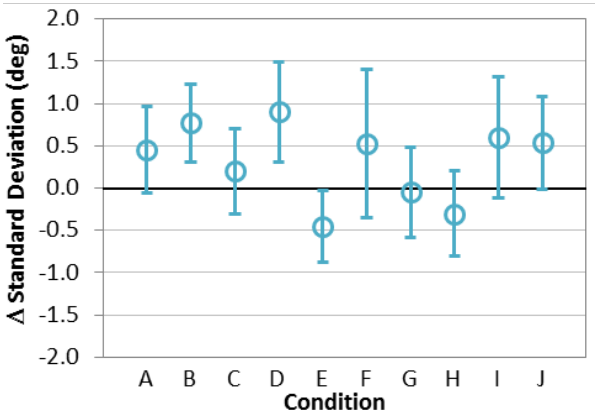

Fig. 4: Difference in Roll Standard Deviation Values (Notional Validation Data)

Fig. 4 provides the viewer the opportunity to focus on the quantified accuracy of each comparison. However, presented this way, the context of each comparison is not apparent. Specifically, Fig. 4 does not allow the viewer to draw inferences about the simulation accuracy as it relates to ship response. By plotting the difference values for all conditions (A–J) as a function of the benchmark standard deviation value, this context is returned to the comparison. Fig. 5 illustrates this approach.

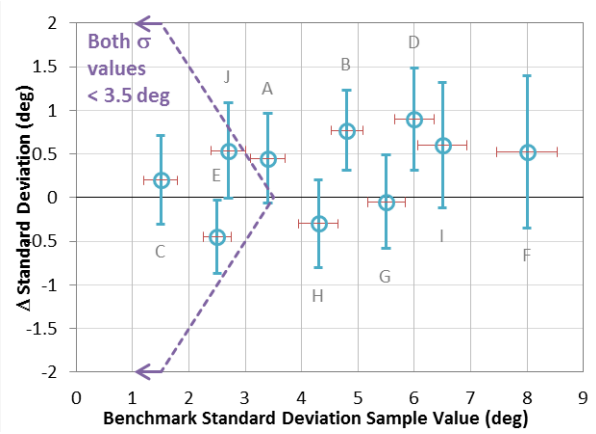

Fig. 5: Difference in Roll Standard Deviation Values as a Function of Benchmark Value (Notional Data)

Horizontal red error bars are added to the difference values plotted in Fig. 5 to indicate the 90% uncertainty associated with the benchmark standard deviation value (*x*-axis). The overall quantified accuracy is unchanged from that described in discussion of Fig. 4, but additional insight is provided by the plotting technique of Fig. 5. For example, the simulation tends to over-predict when the ship is most excited (*i.e.* differences are more positive than negative at higher *x*-values).

The ability to distinguish between conditions as a function of expected ship motion response may be important if, for example, the SIU is directly tied to safety. In this case, simulation accuracy may be most important for conditions in which the roll standard deviation values are large. As such, it may be determined that conditions with "small" expected responses are not desired for validation. The purple dashed line in Fig. 5 identifies the threshold between values (both simulation and benchmark) which are less than and greater than 3.5 deg. This line is analogous to a horizontal line on Fig. 3 at y = 3.5 deg. Using this metric, conditions C and E are denoted as small response conditions, while conditions J and A may or may not be considered small motions.

The comparisons presented in Fig. 4 and Fig. 5 can be modified to reflect the percent difference between the simulation and benchmark results, as shown in Fig. 6 and Fig. 7. The purple dashed line in Fig. 7 again identifies the threshold between values less than and greater than 3.5 deg.

As indicated in Fig. 6, the simulation correlates with benchmark data to within ±30% for most cases, but conditions C, E, and J display larger percent differences. Fig. 7 shows that these conditions coincide with the smallest ship motion response cases. If these cases are not of interest for accreditation, the simulation can be said to agree with benchmark results within –20% and +30%.

5. Conclusions

The difference between population statistics is proposed as a primary acceptance criteria metric for the direct quantitative validation of ship simulation tools in support of accreditation for uses related to ship motions in irregular seas. This metric can be used to achieve traditional goals of this type of validation, including investigation of statistical similitude. It provides a quantifiable measure of comparison accuracy, which incorporates a level of significance associated with the uncertainty in the data as well as a quantified measure of agreement between benchmark and simulation statistical results. This metric can be used to generate acceptance criteria linked to the requirements of the SIUs by incorporating margins and limits on simulation accuracy. Finally, this metric can be used for parameter level criteria application (*i.e.* resulting in pass/fail conclusions) as well as across multiple conditions simultaneously to provide a broad view of simulation accuracy.

Use of the difference between population statistics (including uncertainty) as an acceptance criteria metric builds upon established validation techniques typically reserved for deterministic processes while also utilizing the body of work associated with the quantification of uncertainty of ship motion responses in irregular seas.

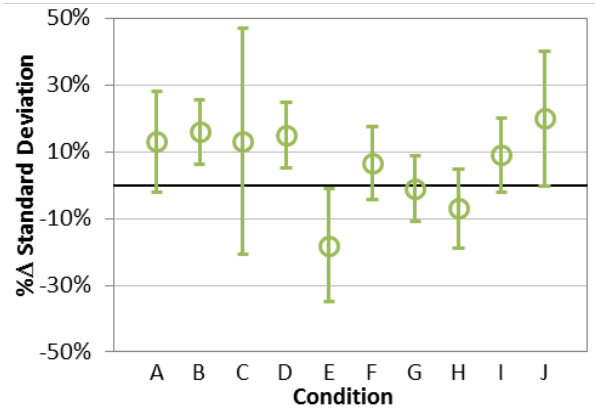

Fig. 6: Percent Difference in Roll Standard Deviation Values (Notional Validation Data)

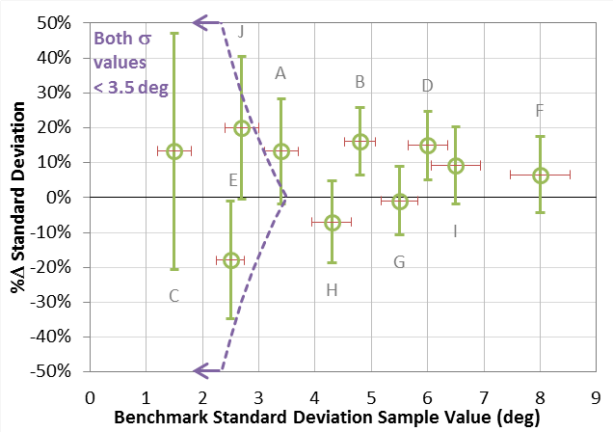

Fig. 7: Percent Difference in Roll Standard Deviation Values as a Function of Benchmark Value (Notional Data)

Acknowledgments

The authors would like to thank Timothy Smith and Vadim Belenky and for their encouragement throughout the development of this paper and their efforts to facilitate attendance of this workshop.

References

ASME (2009) "Standard for Verification and Validation in Computational Fluid Dynamics and Heat Transfer." American Society of Mechanical Engineers, New York.

Belenky, V., V. Pipiras, C. P. Kent, M. Hughes, B. L. Campbell & T. C. Smith (2013) "On the Statistical Uncertainties of Time-domain-based Assessment of Stability Failures: Confidence Interval for the Mean and Variance of a Time Series." *Proc. 13th Int'l. Ship Stability Workshop*, Brest, France.

Belknap, W. F., T. C. Smith & B. L. Campbell (2011) "Addressing Challenges in the Validation of Dynamic Stability Simulation Tools." *Proc. 12th Int'l. Ship Stability Workshop*, Washington, DC

NIST/SEMATECH (2014) e-*Handbook of Statistical Methods*, http://www.itl.nist.gov/div898/handbook/, 20 June 2014.

Oberkampf, W. L. & M. F. Barone (2006) "Measures of Agreement Between Computation and Experiment: Validation Metrics." *J. Comp. Physics*, 217: 5–36

Smith, T. C. (2011) "Statistical Data Set Comparison for Continuous, Dependent Data," *Proc. 12th Int'l. Ship Stability Workshop*, Washington DC.

Smith, T. C. (2012) "Approaches to Ship Motion Simulation Acceptance Criteria." *Proc. 11th Int'l. Conf. Stability of Ships & Ocean Vehicles*, Athens, Greece.

- SESSION 2 -

NAVAL SHIPS STABILITY

Features Architecture of Mean Ship to Navigation in Heavy, Stormy and Ice Conditions on the Northern Seas

Vasily Khramushin [1]

1. Applied mathematics and control processes faculty, St. Petersburg State University,

ships seaworthiness in stormy conditions subsection of Russian science-engineering society of shipbuilders named Alexey Krylov

Abstract: These studies in a stormy seaworthiness are most relevant for vessels with a mean displacement, for which the length and height of storm waves comparable with the main dimensions of a marine vessel. As an analytical tools is activated synthesis of good seamanship technical experience and new engineering justification to build outside appearance (ship's architecture) and the main elements of the hull shape, which directly affect the seaworthiness of the ship maneuvering and conditions in difficult, storm and ice conditions for the navigation.

Key words: Hull structure, stormy seakeeping, noncontradictory design of ship

1. Introduction

Conditions of seafaring in the northwestern Pacific, Far East Russia, do not effectively use the fleet calm weather, even for coastal navigation, widely represented in foreign offshore temperate latitudes. Conceptual ship design provisions consistent with findings of the mechanics of harmonious dialogue with the ship in stormy sea navigation specific conditions, good seamanship bound axiom technical aesthetics of the absence of which it would be superfluous on a beautiful ship.

Far away ocean campaigns between regions of fisheries and open the Sakhalin-Kuril port point abound storm winds, with moving ice floes and heavy icing decked devices and superstructures the cold seasons. All classes of fishing and auxiliary fleets should be designed to reflect the actual absence of reliable harbors on Sakhalin and the Kuril Islands, which requires crews constant readiness to leave the port harbors for the inevitable meeting of all storms and hurricanes in the open sea – in deep water away from the shore.

Contrary of a large sealiners, for designing fishing, rescue and survey vessels, the most important requirements are all-weather effectiveness and safety at work of the deck crew, possible routine use of all ship arrangements and mechanisms in conditions of storms and icing. Purpose of this fleet is fully determined by the initial design decisions to achieve the best storm seaworthiness of vessels, strictly coordinated with experienced sailors on the bridge watch; on the upper decks and fishing, in the ship's machine and industrial environments. Navigation conditions in the Far East of Russia should be evaluated winds exceeding 30 m/s; large progressive wave front height of 10 meters and the slope of the order of 30°, with periods of 6-8 s on the Sea of Okhotsk and on the Sea of Japan, and to 15 s – in the Pacific Ocean; and regularly the standing ninth waves of dangerous cross with steep ridge more than 45°.

Preliminary proposals of the design problem

Optimization techniques based on private engineering solutions in the absence of "sufficient conditions" to determine the only true conclusion of the project. Freedom and necessity of a creative

choice associated with fundamental contradictions and insufficiency of initial requirements to promising vessel is permitted solely in good seamanship and literacy mariners in formulating design requirements and evaluation of technical solutions for special cases of the new marine equipment.

Consistent design effective seagoing vessels is possible with the aid connected in reverse stages exploratory research targeted at consistent harmonization of requirements for the ship as a unified engineering structures [1]. Target design with verification of selected engineering solutions may be submitted counterclaims passes (steps), as the analysis of "top-down" - from the total project prerequisites for private technical solutions; and synthesis of "bottom-up" - from the technological capabilities available to the optimal intended project of the new ship as a whole.

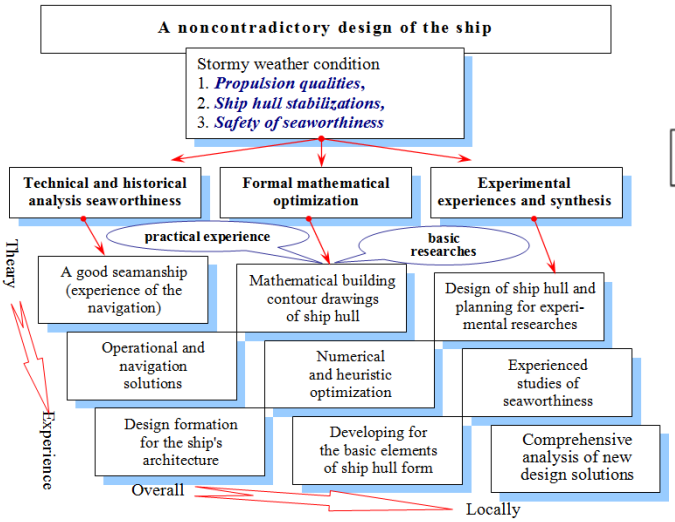

Fig. 1-a. Ternary hieroglyph of the project under the scheme of synthesis of new technical solutions, "top-down" – from the generalized theoretical prerequisites for optimal engineering developments. The columns are coupled variants historically approved seamanship techniques (in left) and the latest achievements in the field of fluid mechanics ship (in right), which forms the rows levels stages adaptation engineering design in limited technological capabilities of modern shipbuilding

Noncontradictory design optimization reduces to harmonize operational requirements for promising ship running on a pass by logical synthesis stages of the project: "top-down" (Fig. 1-a), then the reverse sequence verification analysis of decisions on the way: "bottom - up" (Fig. 1-b). New technical solutions accompanied concept exploratory synthesis "top - down", where based on the wishes of seafarers occurs coordination technological capabilities of modern shipbuilding and projected long-term seaworthiness of the ship. Private layout analysis and sturdy engineering decisions on the design phase, "bottom - up" completes perfecting instruction to Mariners, with a detailed experimental study of all modes of navigation and seagoing documenting special properties and proven recommendations for optimal resolution of dangerous situations at sea, with instructions on Regulatory crew actions under difficult, ice and stormy weather offshore activities, including given features and benefits of the project implemented innovations.

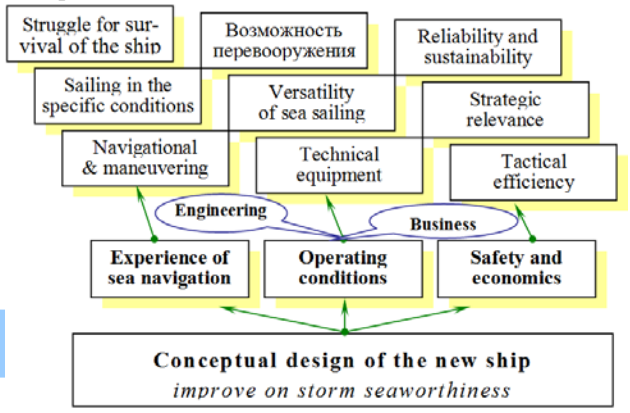

Fig. 1-b. Inverse matrix shows directions the verification analysis of design decisions "bottom-up" from many technical innovations to the assessment of technical efficiency and economic optimality vessel as a unified engineering structures, adapted for exploitation in specific navigation and geographical conditions.

Prerequisites for promising project of the ship

Unlike the midlatitude navigation of warm seas, the Russian Far East requires highly specialized vessels for special stormy and ice sailing conditions, operational efficiency which is determined by minimizing the lead time to loss of storming active (waiting for good weather by the sea). Actual absence ports of refuge also serves as the initial condition to achieve unlimited storm seaworthiness as necessary design background to ensure continuous and all-weather conducting fishing, rescue or exploratory operations on the high seas.

Effectiveness of all-weather for marine works is due: - habitat crew comfort smoothness and small stormy pitching or rolling; - Protected deck crew from squalls and chilling northern winds; - The possibility of heating compartments for stable operation of marine services and decked teams in the winter fisheries or hydrographic expeditions. Then the functional goals of design optimization proceed from navigation requirements for propulsion arbitrary courses relative to of storm excitement and winds caused by the optimal distribution of mass and volume of ship compartments, with convenient access to the operating deck; linking different ship deck operations and efficiency of marine processes and comfort of everyday living conditions for the crew.

Conceptual design prerequisites for classes thereunder ships and vessels [1], according to conditions of operation, are reduced to the necessity of achieving generalized conditional seaworthiness:

- patrol, rescue and fishing vessels provided propulsion any courses relatively of storm excitement and winds; for mandatory stabilization pitching or rolling to maintain deck operations in all weather conditions;

- rescue vessels and patrol must have a minimum of rolling and be stable to storm course; and at the same time be able to actively maneuver in difficult weather conditions and difficult navigation;

- all three classes of vessels must have a minimum pitching and provide non sweep the stern working deck on the move forward under the main (marching) engines, possibly due to excessive wave sweeping, heave and yaw in the bow of the ship hull;

- unconditional safety of emergency on storming sea without motion is not put essential condition, because in emergency situations qualified crew can take active steps to install storm sails and floating anchors.

In practice, this design tasks related aerohydromechanic the ship in heavy wind and storm waves, with the target to achieve functional: 1 - propulsion; 2 - stabilization of the ship hull; 3 - ability to conduct deck operations in all weather conditions. Conclusion of the project limited to the following features and ship's hull form and superstructures architecture:

1. Reduction of the area, the transverse and longitudinal moments of inertia waterplane and sharpen it bow and stern to reduce the power impact of storm waves and saving propulsion with low pitching.

2. A significant decrease the volume of ship's hull of surface bow and stern, and tumblehome of sterns and boards in the middle of the hull at waterplane, which stabilizes the progress in cutting mode of storm waves.

3. Exclusion and the general flare of boards of continuous upper deck that will prevent excessive pitching waves with punches on the sides and decks, to create opportunities for active management course in stormy conditions, and takes the edge off the problem deicing.

These rules are not contrary to the natural shape of the hull constructions in general engineering optimization and navigation requirements for prospective ship seaworthy increased:

- propulsive quality on calm water due to sharp waterlines bulbous bow and rounded contours of frames in the middle of the hull, enclosing the largest volume in minimal surface ship plating;

- exclusion of boundary layer separation near the rudder and propulsion is achieved by cruiser stern with smoothing rib lines on a theoretical line drawing, contributing to small gradients and low vorticity near area of the propulsion;

- passableness in the ice at the autonomous navigation can be improved in the cutting regime and break under ice fields below, which partly solves the problem of ice protection propulsion.

Fishing waters are often characterized smaller depths of marine and offshore shallow water where storm danger are compounded by long sea level oscillations, killer waves and extreme currents, resulting from the transformation of storm waves and swell with their active interference, increase the dispersion wavelengths, against density stratification of water near the mouths of rivers and in areas of bottom waters rise. Such adverse hydrodynamic processes observed in the narrows, at anchorages on raids and on the approaches to the gate of the seaports where danger to mariners grow even at moderate winds and long-wave responses to remote coasts storm.

Undecidable difficulties arise in finding design solutions with the aim of harmonizing the safe sailing hydrodynamic regimes in stormy ways on a shallow water. Then, each project for promising and existing vessels must be undergo sea trials with complex remote-controlled towing models at the surf zone in shallow water, for example, and then submitted at teachings of navigators, and in the algorithms for automatic control of a vessel is fast deep water.

Vessels enhanced storm seaworthiness, capable of maneuvering arbitrary storm passages and courses at nominal (or minimum) available power, as a result, are exempted from the excessive costs for fuel and maintenance of the main engines, which is more than cover one-time expenses of the target design, sturdy construction and sea trials of ships for work in the northern latitudes of the Far Eastern seas.

Conceptual project development of fishing vessels

Conditions of industrial activity of the fishing vessel is not fishery abound with originality schemes and methods of deployment fishing gears, from which also should not be following variety of technical solutions in the construction and arrangement of ship's contours architecture.

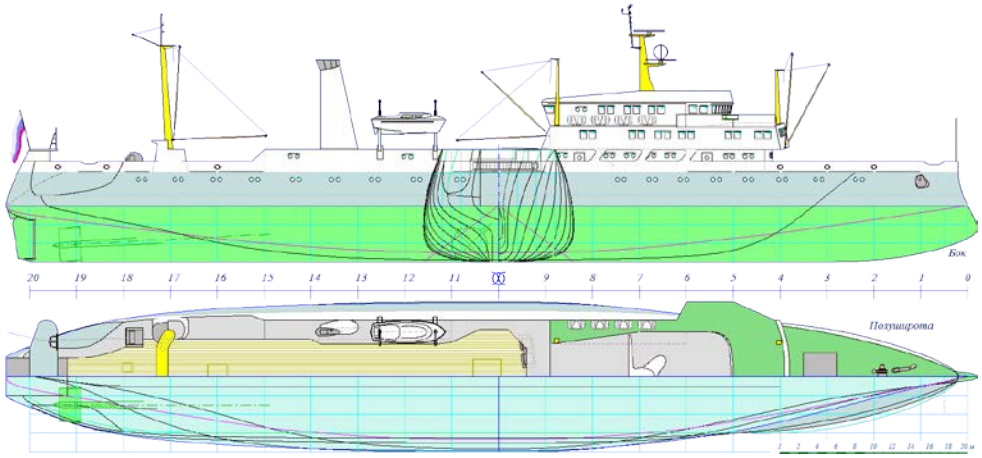

Fig. 2. The large fishing trawler, arranged according to the prototype "Prometheus" (Superatlantik), which has traditional relations the main dimensions, hull form and features of the historic ship architecture from late XIX - early XX centuries. L=100 m; B=16 m, T=6 m; W=4500 m^3; S=1500 m^2; δ=0,55 (W - displacement; S - wetted surface; δ - block coefficient)

The criterion of designing of perspective vessel can be establish that fishing trip seaworthy qualities should be in full operation crew at the conditions of storms and icy winds of the northern seas:

1. Habitability quality, whose adequate for action with fishing gear on the upper deck, and for continuous shipboard operations and production processes for fish industry:

– free movement of arbitrary courses with the trawl, in the fishfinding regime and by transitions between the fishing areas;

– possibilities for active maneuvering with trawl team on the upper deck, during work when setting / pulling of fishing trawl net.

2. Modes of moving or drift fishing gear when folded and stopped fishery and manufacturing operations:

– mooring operations in the open sea for receiving and transfer ready stocks of fish products;

– emergency modes of navigation and storming awaiting calm weather.

Mighty prototype promising trawler with enhanced seaworthiness can be traditional Superatlantik [2] that is configured at a similar case in displacement of the historic ship the XIX century (Fig. 2). Superatlantik able for 24 days to produce the fishery and take on board some 1.200 tons of fish products.

Fishing fleet usually does not have the technical capacity to safely holding fishing operations in a stormy sea. In the shipbuilding industry, this means that as at the dawn the Great Geographical Discoveries, in the design of promising types of ships should be used Navigational experience and knowledge of good seamanship, which is especially important to actually achieve all-weather efficiency of fishing operations. Participation reputable captains mentors capable of perceiving engineering innovation with many years of experience of command positions of fishing vessels in the far fishing voyages, it is extremely important in the search for optimal design solutions, initially need to be agreed with the practical development and effective use of the latest models of marine equipment.

To improve storm seaworthiness, useful historically experience embodiment cruiser stern aft, not perceiving impacts of large ridges of storm waves. Compensation will be improved hydrodynamic loads assuming of unimpeded flooding forecastle deck that will become a special freeboard dampers pitching, and contribute to improving the conditions of marine operations and safety of seafarers on the open aft a deck fishing:

1. In the stern is arranged two level decks above the main watertight deck of fishing vessel hull:

- shelter deck of the fish processing plant, which is discharged through semi-portico flows used in the production of sea water;

- upper deck provides simultaneous operation of two fisheries trawls (doubles) at their rising / setting; fully shelter from wind effects and tumblehome inward to reduce the rolling under the blows of the wave crests and squall winds.

2. Narrowed (cruiser) stern deck do restrict access to the danger zone under the trawl bridge and load portal, makes it possible to full mechanization for a heavy operations with trawl boards in the side cut-sections under cargo hooks between stern transom and portal bridge, with marching mounting boards in these cut-sections board in close proximity to dragrope winches.

3. Ship contours provide stabilization stern of the hull on the move forward, and when trawl towing, settings/arising fishing gears in heavy storming. Stern part of ship hull made heavier by building the stern draught, and the completeness of bow contours reduced to avoid capture body wave crests, which frees yaw and promotes the smooth flow of flooding forecastle deck of the wave crests. Stormy stabilization stern deck also shown intensive outboard dynamics of the wave ridges, which board cut-sections partly compensate the rolling.

On the navigating bridge is provided wide overview of trawl, deck, which is important for safety

monitoring team trawl, then vessel is maneuvering in the storm. Continuous upper deck allows the master to deploy trawl fishing gear on the entire length of the trawler at their repair or modernization; Simplifies migration of ship's stores or goods between the forward and the middle holds the high seas; and promotes compensation rolling with a side tie-storm waves on the upper deck.

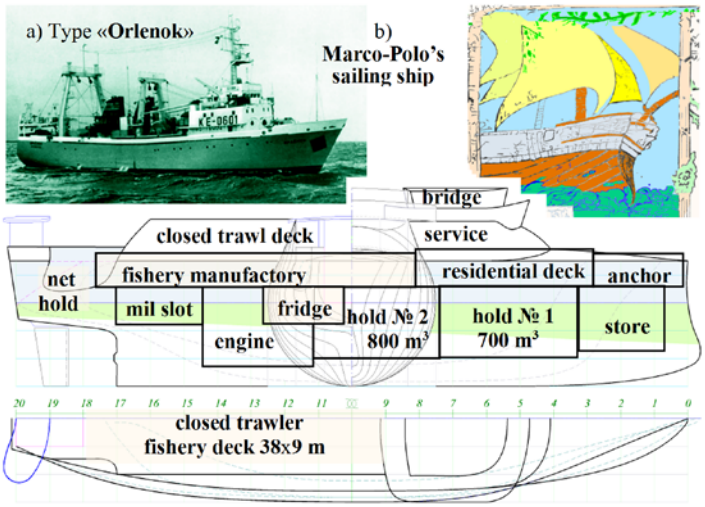

Fig. 3. The trawler-seiner freezer with fishing manufactory equipments by using the prototype: "Atlantic-333" ("Orlyonok"), arranged in the hull of an ancient Chinese ship, which Marco Polo represented in the XIII century. L = 60 m; B = 15 m, T = 7.5 m; W = 3444 m^3; S = 1500 m^2; δ = 0.55. ("engine" – *engine and boiler room*, "mil slot" – *fishmeal plant*)

Believing as a prototype average freezer trawler-seiner type "Eaglet" (Project 333 Atlantic): L - 62,25 m; B - 13,8 m; T - 5,2 m; W - 2400 m3 (2467 m); load capacity of 230 tons; crew of 40 seamans. Ship's hull lines constructed by analogy with a picture of the ship Marco Polo from the XIII century (Fig. 3), which would mean using all the key technical solutions to optimize the hull form and the ship's architecture to achieve the best medium-tonnage fishing vessel with a best stormy seaworthiness.

Anchor-mooring device placed indoors forepeak (fig. 3), shelter from winds and spray ice fishing deck, which is important for the effective operation of the crew in the winter cold seas of Russia. Minimum area forecastle deck is arranged for open access to the hold manhole number 1, which is necessary for unloading of frozen fish products in the open sea at calm weather or in the shelter of high boards transport refrigerator.

In the contours of the trawler used technical solution for hydrodynamic compensation pitching when the vessel is relatively arbitrary course of storm waves a trochoidal nature [4]. In the process of superposition and proportional counter storm ship waves force effect is concentrated in the area of bilge contours contours, where the trim points degenerate into translational force vertical ascent / dive of ship hull. A prerequisite of this process is to maintain plane floating and lack of running trim in calm water, even during the test model at supercritical high speed full ahead. In sea trials (Fig. 4) is confirmed as steady state course by teething with ridges of storm waves, which practically does not change trawler form dissecting wavefronts, which is the condition of conservation of propulsion and smooth pitching on a large storm waves.

Fig. 4. Trawler hulls balanced by the lack of running trim in calm water, and this dynamic stabilization is not affected on a large stormy waves, where the motion of the wave energy goes mainly in heave, with no direct impact on the propulsive quality and stability on the storm course

In sea trials also raised the issue of reducing the potentially dangerous effects of heaving, which course at high speeds (Fig. 4) is accompanied by a wave flouding bow deck and almost complete ascent of ship

hull between wave ridges[1]. For a predictable reaction to control actions trawler steering stabilizers and requires precise knowledge of at least the characteristics of stability at of ship hull at any time. Using rounded frames allows you to save the value of metacentric height [5] at different planting the conditions at then vessel is heave that can be used in the laws of the automatic steering-ahead to sending commands to rolling stabilizers to prevent uncontrolled roll by turning dangerous for trawl, fishing operations team at on the upper deck in heavy weather. If the active wing stabilizers installed in the flow propellers [6], their effectiveness will be maintained during fishing operations with trawl or other outboard gear.

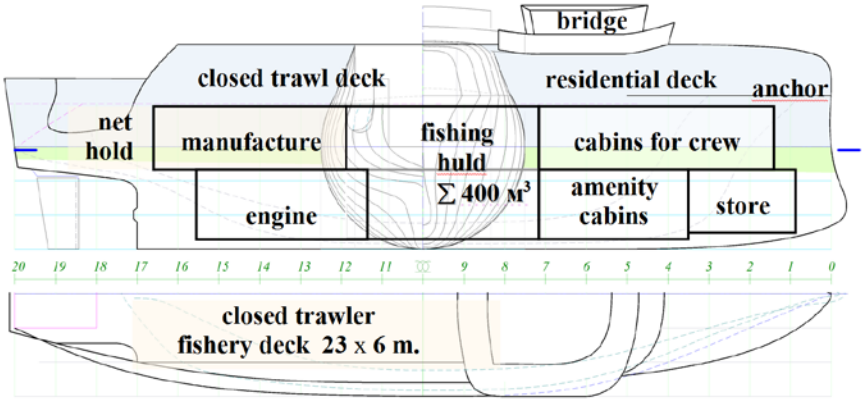

Fig. 5. Generalized scheme of arrangements the seiner-trawler with enhanced storm seaworthiness,. L = 40 m; B = 10 m; T = 5 m; W = 1,020 m^3

Overstated to 7.5 m draught trawler ensures its stable motion in a stormy sea with the largest proportionate ridges of wind waves and swell. Due to this displacement precipitation increases by more than 1,000 tons, which corresponds to the rank of a large trawler with initial average dimensions. Increasing the volume of ship's stores and cargo holds is required for autonomous operation fishery then vessel is in remote areas of the Pacific Ocean, not ensure a sustainable port of refuge, which is an important operational requirement for promising project trawler.

Traditional fishing vessels for the Russian Far East are seiners trawlers with a displacement about 800 m3. Possible to build a similar medium variant trawler providing shelter deck crew in storm conditions winter seasons northwestern Pacific. As the prototype uses modern trawler STR-420 type "Nadezhny(Reliable)»: L - 44,9 m; B - 9,5 m; T - 3,8 m; W - 806 m^3 (781 t); hold 200 m^3 (100 t), cooled to -7°C; crew - 22 mariners.

In modern conditions in the Far East of Russia is difficult organized fishing expedition with the support of large fish processing bases. Extra in comparison with the prototype of a new displacement trawler used to increase the capacity of freezing equipment, of the fish processing plant unit, as well as to increase the volume and the number of freezing hold of ship's stores to operate autonomously away from the fishing ports.

Contours of the hull similar to the previous project trawler (Fig. 3). The main difference is the absence of layer of shelter deck (Fig. 5), which makes the fishing trawl deck by main deck watertight hull of fishing vesssel. Deck of fishing plant accommodation and amenity rooms falls below the waterline. To ensure emergency flooding living deck included in sealed circuit freeboard reserve buoyancy. Forecastle deck with anchor-mooring devices locked superstructure, with output the mooring roller through at shelter from the wind and waves semi-porticus that is necessary for the prevention of icing, preservation of stability and minimize rolling in heavy storm wave flouding on the bow of ship hull.

[1] In the non-optimized shipvhull heave no less intense, and only exacerbated by the dynamics of pitching, loss of speed and yaw under direct blows waves. Ship had reduced speed to small and loses functionality at the highest level of danger of badly managed vessel.

Rounded frames serve to preserve the stability of the same draught in different of ship hull conditions on vertical heaving [5], which is important for stabilizing by control of ship hull in storm conditions to the predicted pitching control and safety deck works and fishery operations at different loadings of the trawler. Narrow cruiser stern minimizes external loads on the move on a wave or rising of trawl gear. To work with trawl boards in the stern sections of the shell are arranged cut-sections. Trawl slip has overlapping scheme for the restructuring of fishing nets to work with.

Deep hold allows you to choose stacking height of made of fish products, thereby adjusting the initial hydrostatic stability change in depending on the current amount of fuel and ship stocks of the trawler.

Seaworthiness of fishing vessel underlie its effectiveness on high seas fisheries. Yet to achieve the desired course mode navigator has some freedom in choosing the course and on the main thrust engines (usually on a wave), which also allows a significant diversity in the contours of the ship's construction and the principles of the architecture of the fishing vessel. Consider the case of the rescue ship, the project brief for which specifies the possibility of confident maneuvering and stable motion with respect to an arbitrary course by stormy waves.

Maritime rescuer

Small ocean-going vessels of the auxiliary fleet used for various purposes, including the extremely difficult conditions of navigation. It can be life-saving operations, emergency towing vessels in stormy conditions, special delivery mail and small packages into cruises, as well as conducting search operations and marine researches at complex, and the ice storm sailing conditions.

Medium ship may have rugged hull enough for the active maneuvering in heavy waves and under the blows of hurricane winds. Active stabilization of pitching, as well as a dynamic influence on the draught, roll and trim of the vessel with the use flapping wing stabilizers and automatically controlled rudders and propellers are possible in principle, provided that the form of the hull and superstructure architecture provide passive reduction in the intensity of force interaction of ship hull with marine waves and wind (fig. 6).

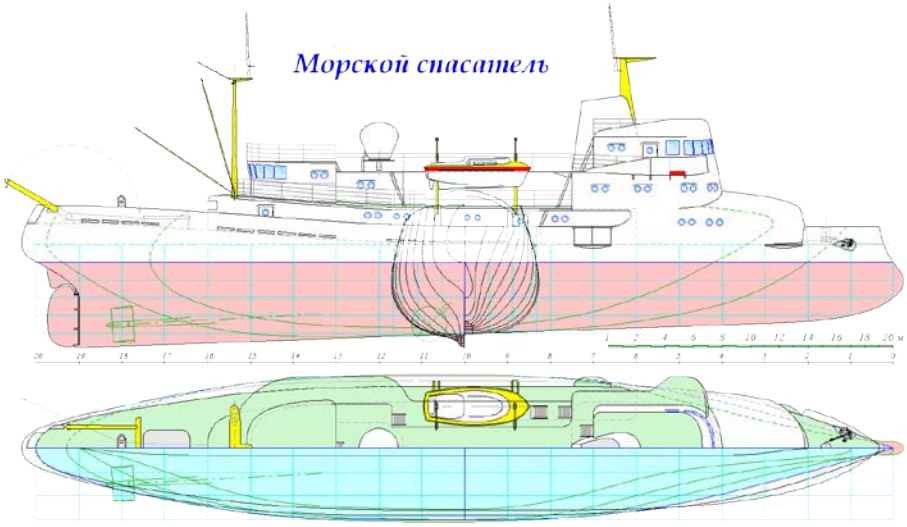

Fig. 6. Hull form and the conceptual scheme of the general arrangement of the sea rescuer - research vessel, capable of active positioning in heavy waves and hurricane winds. L = 62.8 m; B = 10.3 m; $T_{B/S}$ = 4/6 m; W = 1.74 m^3, S = 809 m^2; δ= 0.58.

Believing that the rescue fleet is formed exclusively from professional sailors, will not impose specific requirements for habitability and comfort for the crew, placing major demands only the unconditional fulfillment of marine tasks in any weather conditions. Using as a prototype historical Arab ships from the Age of Discovery, define hull shape and layout of these devices ship design and technical features:

1) ship hull as a whole is similar a circular cylinder, which minimizes the rolling in rescue operations in a stormy sea;

2) main volume of ship hull and the center of buoyancy shifted to stern part, that shifts to stern the center of pitching and yawing, approaching them to the area of the rudder and propeller;

3) narrowed and sharpened bow waterline not provide a wave of floating and heawing, making surfacing and center axis of pitching while the vessel shifted to the stern, closer to the middle of the hull;

4) full stern with high castle and deeply immersed fin sternpost for best levels of manageability in storm conditions, it is allowing for crew to work operations on flush deck at the stern;

5) main displacement of the ship is concentrated in the middle of the of ship hull, which reduces the transverse moment of inertia of the vessel and allows the use of horizontal rotary movable control shroud [6] on the propellers to calm pitching and trim alignment when positioning in stormy waves;

6) form a surface volume bow of the hull adapted to the cutting of ridges of storm waves under conditions of high wave flouding, which reduced the maximum forecastle deck, superstructure and bow included in the circuit durable waterproof of ship hull.

Round-shaped ship stability diagram form without the angle of sunset and off-center area and off-center area (the maximum righting moment) beyond 90 °. On real roll angles arises large righting moments, respectively, and there is no dangerous rolling moments when the sea surface wave slopes that allows to stabilize the rocking ship with active stabilizers (eg, horizontal movable control shroud allow to control both the roll and trim of the vessel at the same time).

Practically, this means that the concept of non-contradictory following storm nature is the universal rule of designing ships and vessels (Fig. 7), provided as passive as a safe sailing and active technical facilities to achieve the complexity marine tasks.

Fig.7. Rounded ship hull and lower deck of the vessel reduces the intensity of all types of storm rolling on deep water

Itself does not need a rescue ship in maintaining particularly high speed ahead; in operating costs provided for nominal consumption for maximum autonomy and cruising range; and on board ship there is only equipment specifically designed for regular use in accordance with the scheduled services jobs or planned expeditionary requirements.

Shall consider a variant a high-speed ship at the destination which are not optimized design and technical solutions to meet the operational requirements of economically feasible, and are on board complex weapons systems, dangerous both for the ship and for all others.

Fast ship (patrol and hydrographic vessel)

Patrol and hydrographic ship is designed for continuous duty weatherproof waters of Sakhalin and the Kuril Islands North Pacific ocean, with healthy shipboard weapons and existing complexes constantly monitoring the situation on the open ocean and offshore, ready for fast transitions in heavy and stormy navigation. Besides the protection of maritime borders, the ship is given the responsibility to ensure safety of navigation and saving life at sea, active monitoring and early warning Sakhalin and Kurily

offshore services for early prediction of potentially dangerous marine phenomena. [7] [2].

A noncontradictory design of the ship means comprehensive research of modern technical solutions, operating experience and good seamanship of a ship maneuvering in difficult sailing conditions, as well as develop of all aspects of navigation in complex, ice and storm sailing conditions.

As the main requirements for a high-speed ship hull form identifies the need to maintain effective go ahead arbitrary course relatively intense sea wave, provided the maximum stabilizing of ship hull as a platform for all types of weapons and control systems environment of the sea.

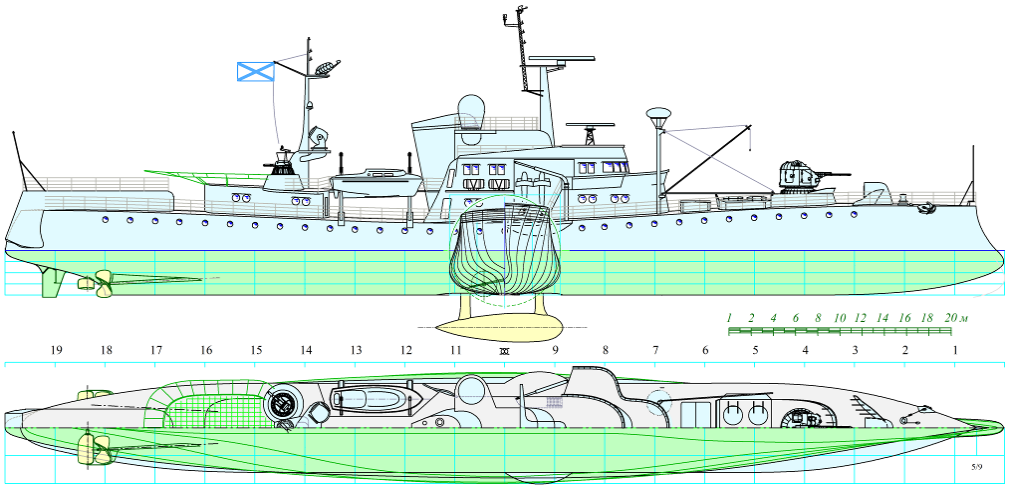

Fig. 8. The project for a fast patrol and hydrographic ship. L = 90 m; B = 10 m; T = 4 m; W = 1920 m^3, S = 1050 m^2, δ= 0,473, V = 25 knots

To achieve good seaworthiness into the contours and external architecture of the ship made the following design features:

1) surface sealed enclosure of ship hull is less than the displacement of ship;

2) tumblehome board into middle of the hull side of the ship has a maximum angle at waterline level;

3) the initial metacentric height has a minimum value in a constructive draught and increases as when afloat, and when immersed of ship hull [5];

4) static stability diagram has an S-shape with an angle of sunset 180 °;

5) inseparable space of the upper deck minimized by longitudinal arrangement of superstructures and foundations for a decked devices and mechanisms;

6) in storm conditions on any section of the deck along the board of the ship is filled with approximately the same amount of water, indicating damping of pitching;

7) surface part of the stem of the ship tilted to the stern, and in the underwater part the stem is made inclined undercut the need to avoid yaw and onboard slamming on the move by storm excitement;

8) has a cruiser stern tumblehome and minimum freeboard stern afterrake overhang allowed by the scheme using two-shaft propeller-rudder system;

9) restricted area fin of sternpost lets slide (yaw) with a passing wave, avoiding hard blows of waves in the area of stem bowl;

10) directly behind the propellers mounted horizontal wings of active stabilizers on spring loaded Baller [6], which in the case of stopping of the main machines begin to work as emergency storm propulsion;

11) the geometry of the ship's hull with deckhouse determined covering a circular cylinder, and the underwater part of the of ship hull is smooth and does not contain or bilge contours longitudinal keels of

[2] The project was developed on the instructions and under the supervision of the cap. I rank Sergei Ivanovich Krolenko (Higher Naval Engineering Institute, St. Petersburg).

bottom and along the sides of the upper deck is arranged an open passage, in which water flows from ridges of storm waves kept using for a decked logging and longitudinal coamings;

12) all household and office space ship located under the upper deck, which is also by main deck watertight hull of the ship.

Only after successful minimization of force action by storm waves on the hull, the ship can be used active dampers for rolling and pitching. Installing the wing stabilizers into the zone of active water flow action after propellers needed for predictable working out commands to stabilize the ship hull [6]. In the case of stopping of the main machines such stabilizers will automatically be started into emergency mode by the storm propulsion, thrust which can be used to hold the ship in a safe storm course.

Conclusion

Operational efficiency is determined by the vessel's ability to perform tasks into specific geographic region of storm conditions and ice floating. At the core of the new design and technical solutions used Navigational experience of the active storm maneuvering, agreed with the knowledge of good seamanship, realy deck works in complex, storm and icing environments, with checking developments in severe restrictions consistent of designing concept of all-weather ocean vessel. Patents and video tests published in the ship's portal: Shipdesign.ru.

Acknowledgements

The author expresses his sincere gratitude to really authors of this actual maritime researches: the naval officers - the teachers Kaliningrad Marine College of Fisheries – A.A. Kamyshev, G.S. Malenko, E.V. Mironov, D.Ya. Bronstein, and their careful attitude to the maritime and naval engineering history, which found as the basis for creating new ships projects for enhanced seaworthiness, and passed the first experimental verification with their participation into the 1975-1979 years. The main series of analytical and experimental researches performed in 1986 under the guidance of A.N. Kholodilin – professor of ship theory Leningrad Shipbuilding Institute. In creating these ship designs took an active part S.V. Antonenko, V.G. Bugaev from Far Eastern Federal University; N.A. Mytnik and S.A. Chizheumov – department of shipbuilding Technical University in Komsomolsk-on-Amur. Actually known and formal recognition of the research ship to the greatest extent due to creative discussions and selfless help of captain I rank S.I. Krolenko – teacher shipbuilding department of Naval Engineering Institute, for your many useful ideas, which are usefull into study of new ship projects, and in a variety of interesting marine engineering solutions.

References

[1] Khramushin V.N. Exploratory studies storm seaworthiness of the ship. Lambert Academic Publishing, Germany, 2011. – 288 (in russian).

[2] Kamensky E.V., Terent'ev G.B. Trawlers and Seiners. - Leningrad: Shipbuilding, 1978. – 216 (in russian).

[3] Bronstein D.Y. Device and Basic Theory of Vessel. - Leningrad: Shipbuilding, 1988. – 336 (in russian).

[4] Khramushin V.N. Ship without pitching on the go in stormy waves // Rospatent: reg. Number 2007133625/11. Bulletin number 8 from 20.03.2009. (www.shipdesign.ru/Invent/02.html)

[5] Khramushin V.N. The Ship stability in a stormy voyage // Patent № RU2487043 on 12.07.2011 – (www.shipdesign.ru/Invent/06.html)

[6] Khramushin V.N. Active stabilizer pitching and rolling of the ship – the stormy emergency propulsion // Patent № RU2384457 from 20.03.2010 (www.shipdesign.ru/Invent/04.html).

[7] Khramushin V.N. Hydrographic and Patrol Ship // Patent № RU2384456 from 20.03.2010 – (www.shipdesign.ru/Invent/05.html).

A New Approach to the Derivation of V-Line Criteria for a Range of Naval Vessels

Andrew Peters[1], Rick Goddard[2] and Nick Dawson[1]

1. *QinetiQ, Haslar Marine Technology Park (UK)*
2. *Steller Systems Ltd., Nailsworth (UK)*

Abstract: Previous work has gone some way to understanding the applicability of the current naval V-lines standards to modern day naval designs by carrying out damaged vessel simulations using the CRN developed time-domain ship motion program FREDYN. The work presented in this paper seeks to further this understanding of V-lines by analysing the damaged motions of six vessel types, varying from a small Mine Counter Measure Vessel (MCMV) to a large auxiliary, and implementing a new methodology for the calculation of probabilistically derived dynamic motion allowances for heave and roll. Furthermore, analysis has been conducted in sea states up to a sea state 6 in order to understand the applicability of V-line criteria at greater wave heights and periods. This paper compares heave and roll allowances derived from the probability of exceeding water heights on the bulkheads bounding the damage in varying sea states for each vessel type, each with two damage cases at eight wave headings and at two speeds. Conclusions are drawn regarding the suitability of current criteria for vessels of varying size and design and their sensitivity to sea state.

Key words: V-lines, Naval Standards, FREDYN, Numerical Simulation, Time Domain Simulation, Red-Risk Lines, Damaged Stability

1. Introduction

Significant subdivision is common practice in naval ship design. These internal arrangements introduce both symmetric and asymmetric flooding when damaged. Traditional damage stability analysis using quasi-static approximations cannot predict in a seaway the head of water on a bulkhead bounding a damaged region. For many navies around the world including the UK's Royal Navy, a dynamic allowance over and above the static damage waterline is included in order to account for heave and roll in a seaway (Red Risk and V Lines).

The Red Risk and V-line criteria found in most current naval standards are based on criteria originally presented by Sarchin and Goldberg in 1962. It is recognised that more refined understanding of the criteria could be developed using the latest tools and knowledge; it is also recognised that vessel design has changed significantly since the initial development of V-line criteria.

An assessment of V-line and red risk criteria has been conducted on six distinct vessel types, from a small MCMV to a large auxiliary. Each model has been simulated in two damage cases. Static stability analysis of the two damage scenarios can be performed using standard static stability software; however, this does not take account of the vessel motions or consequential progressive flooding which can occur as the vessel moves in waves.

The use of the time domain simulation tool FREDYN (De Kat et al 2002, MARIN 2011, MARIN 2010) enables the dynamic performance of the damaged vessel to be analysed in a seaway, allowing

the water heights on the bulkheads bounding the damage to be monitored in the time domain. This water height data can then be compared with the Sarchin and Goldberg static criteria in varying sea conditions to identify the applicability and limitations of these criteria to a range of modern vessel designs.

The current Sarchin and Goldberg based criteria are the foundation of the standard used by the UK MoD, defined in Defence Standard 02-900 (DefStan) and MAP 01-024. V-line requirements take the general form of the following dynamic allowances over the worst case static damaged waterline:

- A roll allowance above the static damaged list angle to account for dynamic roll motion. (Angle from upright to out)
- A heave allowance above the damaged water level to account for the ship's heave motion and the relative wave height.

Table 1 compares the current UK Naval standards with the original Sarchin and Goldberg suggested criteria:

Table 1 Sarchin and Goldberg dynamic allowance as compared to DefStan 02-900

Allowance	Sarchin and Goldberg (1962)	UK MOD and other navies (DefStan 02-900)
Angle of list	15 degrees static list assumed following asymmetric damage.	Worst case damage angle of heel (limited by 20 degree list/loll criteria).
Angle of Roll	Related to displacement as per graph in published paper.	15 degrees above static damaged angle of heel.
Heave	4 foot heave allowance.	1.5m heave allowance.

This work focused its investigation on the probability of exceedence of water heights on the bounding bulkheads of the damage region and compares the results with the current V-line criteria requirements. Using the probability of exceedance data and an acceptable probability of exceedence associated with naval standards, it is possible to evaluate both heave and roll values for comparison with current criteria.

2. Modelling Approach

The six vessels were categorised into combatant and non-combatants with three generic designs produced for each category. The six vessel types modelled were:

- Combatant 1 – Destroyer
- Combatant 2 – Mine Counter Measure Vessel (MCMV)
- Combatant 3 – Offshore Patrol Vessel (OPV)
- Non-combatant 1 – Small auxiliary
- Non-combatant 2 – Large auxiliary
- Non-combatant 3 – Tanker

The models were created in the software package Paramarine with indicative hull form coefficients and internal subdivision in order to create a set of modern representative hullform models. Light and deep loading conditions were generated and all models were checked for compliance with both intact and damaged Def Stan 02-900 stability criteria. The small auxiliary, large auxiliary, and tanker were modelled with typical double bottom arrangements. Damage cases were generated using DefStan 02-900 extents for combatant and non-combatant vessels as appropriate. Accidental damage templates were used in Paramarine to generate a full range of damage scenarios in order that suitable severe damage cases could be selected. Two damage cases were modelled for each vessel, one representing an asymmetric damage case with damage to the centreline and the other a fully symmetric damage case. The asymmetric damage case was simulated in a light seagoing loading condition and the symmetric damage case was modelled in a deep sea going load condition. This was done to attempt to capture the worst case roll and heave motions in these damage cases. Powering characteristics, roll damping and natural roll periods

were all selected based on data from similar real vessels to ensure realistic vessel motions were obtained.

Initially each vessel was statically assessed with all tanks and compartments modelled. The results of the static assessment allowed the identification of the worst case asymmetric and symmetric damage case and load condition combination, as well as identification of any load condition tanks with significant free surface moment that had to be modelled. The impact of this modelling was checked through the comparison of intact GZ curves; this approach ensured that the condition modelled in the time domain simulation captured the essential characteristics of the vessel whilst minimising computational time.

Tanks with large free surface moments and damaged compartments were modelled in FREDYN using the standard QinetiQ approach (Dawson 2013) with damage openings defined to the centerline and with full vertical damage extent. Static validation of the damage case was conducted against the results of the Paramarine analysis using a new Matlab based GZ generator tool, which uses FREDYN to produce GZ moment and trim plots for comparison to the static tool.

Fig. 1 shows an example of a damaged GZ validation and the level of correlation between the FREDYN flooding module and Paramarine. As can be seen, there is excellent agreement across the entire heel range.

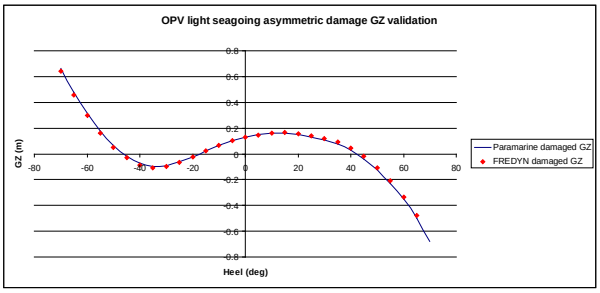

Figure 1: OPV light seagoing asymmetric damage GZ validation

3. Simulation Details

The analysis simulated conditions from a sea state 4 to sea state 6. Previous work (Peters 2004) has focused on the assumptions of the initial Sarchin and Goldberg work which aligned with a sea state 4. Waves were modelled in the simulation using a JONSWAP spectrum (Hasselmann et al., 1973) with a peak enhancement factor of 3.3. Ten one-hour simulations were run for each wave height and period modelled, each with a different wave realisation. Long crested seas were used in all the simulations. A summary of the wave definitions used in the simulations, derived using the World Meteorological Organisation sea state code (Ewing 1974) as guidance, is seen in Table 2:

Table 2 Simulation wave definitions

Sea State	Modal wave period (s)	Significant wave height (m)
SS4 mean	7.35	1.88
SS4 max	7.35	2.50
SS5 mean	8.10	3.25
SS5 max	8.10	4.00
SS6 mean	10.35	5.00
SS6 max	10.35	6.00

Each vessel and damage case combination was simulated at zero (free to drift) and five knots. Eight headings were simulated, from head to stern seas with the damage opening facing into and away from the waves. The models were free to drift in the waves however constant heading was achieved by freezing yaw in order to fully understand the impact of wave heading on internal bulkhead water heights.

In total 960 hours of simulations were performed for each vessel, equating to 40 days of damaged sea time.

4. Calculation Methodology

Previous V-line investigations have compared water height cumulative distribution functions (CDF) at the centerline and outboard points to water heights generated from the existing V-lines, in order to understand the probability of exceedence water heights defined by the current V-line criteria. The work conducted for this study deviates slightly from this approach in so far as the required output is a set of V-line roll and heave allowances varying with the probability of the water level exceeding the line. This approach allows the simple selection of V-line and red risk criteria based on an acceptable probability of exceedence.

Throughout this paper the measure 'percentile water height' is used in place of a probability of exceedence in order to align with convention. For example the 95th percentile water line refers to a line with a 5% probability of exceedence; i.e. a line that provides coverage of 95% of recorded water heights.

In order to calculate the V-line allowances, water height sensors were placed on the bounding bulkheads of the damage regions arising from each of the damage scenarios. Sensors were placed at the centreline and at outboard points within the damaged compartments. Where subdivision was present in the deck plane, multiple sensors were required in order to provide coverage of the full range of water heights. An example of water height sensor placement is seen in Fig. 2.

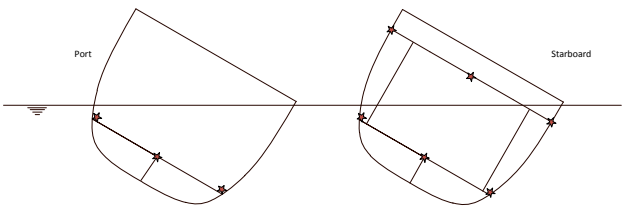

Figure 2 - Placement of water height sensors

The data was then combined into a single time history at the centreline and at outboard points. From these histories both centreline and outboard CDF were calculated. In order to generate V-lines allowances with varying probabilities of water exceedence, corresponding outboard and centreline percentile water heights were joined to form a percentile V-line, the angle of which could then be calculated from the transverse position of the outboard water height sensor. This approach is seen illustrated in Fig. 3.

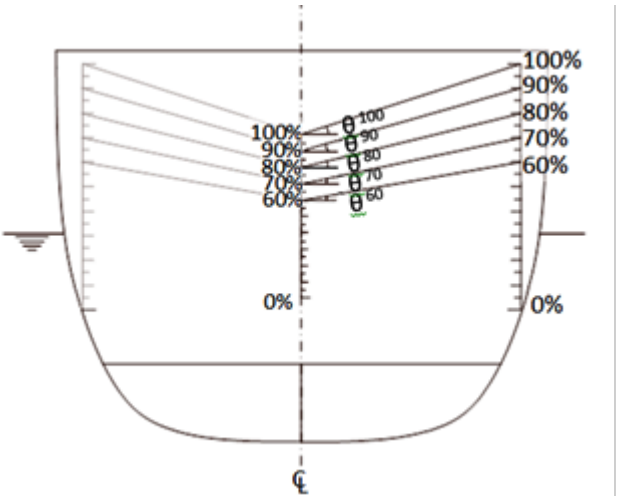

Figure 3 –Lines of probability of exceedence of water heights for the calculation of V-line criteria

The resulting percentile relative water height allowances are referred to as heave and roll allowances in line with the terminology of the V-line standard, however in reality these terms are not conceptually accurate. By combining the centreline and outboard water height probabilities, the vessel heave allowance directly impacts the roll allowance calculated; for example maximum roll motions may predominantly occur as the vessel is at the peak of its heave oscillations, meaning the outboard 95th percentile water height may only be fractionally higher than the centreline point, despite the vessel rolling significantly. This results in a 'roll' allowance of only a few degrees despite the vessel rolling

significantly more than this. Fundamentally, the approach adopted succeeds in combining both roll and heave motions to give a probabilistic V-line which reflects the actual waterline as opposed to modelling it through independent criteria where the worst case roll and worst case heave are assumed to occur simultaneously.

In order to further understand the relationship between vessel motion and local water height, global vessel motions, taken from vessel earth axis motions, were calculated, highlighting where the vessel was contouring the waves in heave and roll or where waves were affecting the local water height at each bulkhead.

5. Results

Tables are presented giving a summary of the worst case 95th percentile heave and roll allowances for the combatants and non-combatant vessels. The results for the maximum sea state 4 and a maximum sea state 6 are presented. In conjunction with these results statistical measures of the vessel roll and heave motions are also presented.

In the tables of results the vessel designators are followed by either a H, corresponding to the vessel heave allowance, or by an R, corresponding to the vessel roll allowance.

Table 3 outlines the static damaged list angles of all vessels following damage allowing an understanding of the final Red Risk and V-line levels.

Table 3 Damaged list angles

Sea State	Symmetric damage list angle (deg)	Asymmetric damage list angle (deg)
OPV	0	17.4
MCMV	0	17.3
Destroyer	0	7.2
Small Auxiliary	0	18.1
Large Auxiliary	0	17.9
Tanker	0	6.3

5.1. Combatant Results

Table 4 summarises the worst case heave and roll allowance results of the OPV, MCMV and the Destroyer (DEST) in sea state 4 conditions following symmetric and asymmetric damage.

Table 4 Summary of combatant heave and roll allowances (angle from upright) in a maximum sea state 4

Ship/ allowance	Damage	Heading (deg)	95% V-line criteria		95% Vessel motions	
			Heave (m)	Roll (deg)	Heave (m)	Roll (deg)
OPV H	Sym	178	0.70	0.18	0.50	0.32
OPV R	Sym	090	0.40	10.20	1.10	12.28
OPV H	Asym	315	0.98	0.70	0.66	19.72
OPV R	Asym	090	0.55	5.70	1.13	25.10
MCMV H	Sym	002	0.74	0.15	0.64	0.29
MCMV R	Sym	090	0.40	7.02	1.12	8.55
MCMV H	Asym	002	0.84	2.62	0.73	20.58
MCMV R	Asym	090	0.44	5.77	1.10	23.10
DEST H	Sym	002	1.00	0.08	0.50	0.20
DEST R	Sym	090	0.28	3.54	1.09	4.07
DEST H	Asym	002	0.77	0.00	0.39	7.52
DEST R	Asym	090	0.30	2.69	1.06	10.53

In sea state 4 conditions the heave allowances can be seen to be below both the original Sarchin and Goldberg dynamic heave allowance of 1.22m and the larger DefStan 02-900 allowance of 1.5m. The worst case 95th percentile heave allowances are seen to occur predominantly in following sea and head sea conditions, as expected, where pitching motions are at their greatest, contributing to waterline height on the bulkhead centre point.

In all cases the worst case roll allowance is also substantially below the 15° defined in DefStan 02-900. Even where large vessel roll motions are seen, the corresponding roll allowance is seen to be small, suggesting that the smaller vessels are contouring the beam sea waves. It is important to note that where high roll allowances are seen following symmetric damage, these are unlikely to drive final V-line angle

as following symmetrical damage the mean list angle is negligible. This is illustrated in Fig 4:

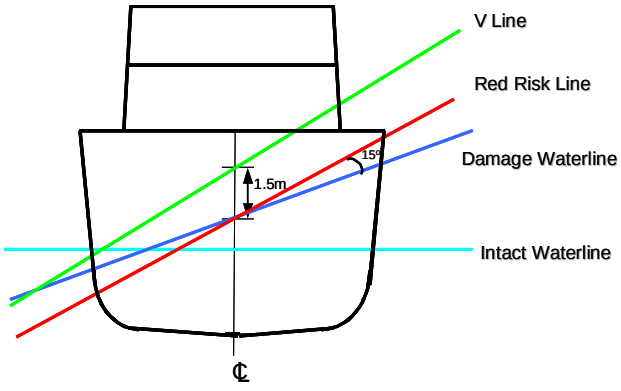

Figure 4 – V-line and Red Risk line composition

Table 5 presents the results of the three combatants following damage in a maximum sea state 6. Due to the significant damage cases (worst cases under DefStan 02-900) the OPV was found to capsize in a number of heading in these large sea state 6 waves and as a consequence results are not available for these runs.

Table 5 Summary of Combatant heave and roll allowances in a maximum sea state 6

Ship/ allowance	Damage	Heading (deg)	95% V-line criteria		95% Vessel motions	
			Heave (m)	Roll (deg)	Heave (m)	Roll (deg)
OPV H	Sym	Vessel capsized – no results available				
OPV R	Sym	Vessel capsized – no results available				
OPV H	Asym	Vessel capsized – no results available				
OPV R	Asym	Vessel capsized – no results available				
MCMV H	Sym	045	1.16	8.89	2.40	16.49
MCMV R	Sym	270	0.40	**17.58**	2.39	19.03
MCMV H	Asym	135	1.45	7.44	2.39	25.43
MCMV R	Asym	270	0.56	11.73	2.42	30.92
DEST H	Sym	002	1.32	0.24	1.70	0.92
DEST R	Sym	225	0.57	13.38	1.76	12.15
DEST H	Asym	178	1.27	0.00	1.65	8.88
DEST R	Asym	090	0.58	8.48	2.63	16.98

The MCMV and Destroyer are both seen to experience large vessel roll angles, indicated by the 95th percentile vessel motion statistics. Despite this, roll allowances are again seen to be predominantly low.

Following symmetric damage to the MCMV a roll allowance of 17.6° was seen. Whilst this is outside the roll allowance found in DefStan 02-900, the DefStan allowance is applied to the worst case damaged waterline, i.e asymmetric heel up to 20 degrees. Therefore, a DefStan V-line angle would be 35° under current rules compared to 17.6° using the results of the analysis, despite a larger roll allowance being used.

In all cases heave allowances were seen to fall below current naval V-line standards despite large heave motions being seen. Once again worst case heave allowances were calculated in head and following seas.

5.2. Non-combatant Results

The non-combatants examined were all large vessels with greater freeboard and reserves of buoyancy than their combatant counterparts. In addition the relative wave size of a sea state 6 when compared to vessel size is less onerous than those seen in the smaller combatant vessels.

Table 6 outlines the worst case roll and heave allowance for the three non-combatants in sea state 4 conditions.

Table 6 Summary of non-combatant heave and roll allowances in a maximum sea state 4

Ship/ allowance	Damage	Heading (deg)	95% V-line criteria		95% Vessel motions	
			Heave (m)	Roll (deg)	Heave (m)	Roll (deg)
Small Aux H	Sym	002	1.06	0.05	0.43	0.53
Small Aux R	Sym	090	0.34	2.66	1.00	3.59
Small Aux H	Asym	270	**1.83**	0.00	0.57	22.52
Small Aux R	Asym	090	1.06	2.63	1.15	24.63
Large Aux H	Sym	002	1.05	0.04	0.32	0.47
Large Aux R	Sym	090	0.30	1.03	0.87	1.71
Large Aux H	Asym	178	**1.66**	0.00	0.31	15.76
Large Aux R	Asym	090	0.95	0.86	0.93	15.45
Tanker H	Sym	045	1.30	0.08	0.69	1.18
Tanker R	Sym	090	0.61	2.31	0.79	3.24
Tanker H	Asym	090	**1.51**	0.00	0.92	7.15
Tanker R	Asym	270	0.67	3.65	0.62	13.89

In all cases the DefStan 02-900 roll allowance was not exceeded by the simulation results; this is despite relatively large roll motions being seen in the case of the small auxiliary (24.63°). Worst case roll allowances were seen to occur in beam sea conditions and were seen following symmetric damage, with the exception of the tanker whose worst case roll allowance was seen following asymmetric damage (13.89 degrees).

The DefStan heave allowance was seen to be exceeded by all three vessels, the worst being the small auxiliary with 0.33 metre exceedence following asymmetric damage. In these cases vessel global heave motions were low, suggesting that the vessel did not react in heave to the incident wave, resulting in the centreline water height being water inflow through the damage. These results suggest that for a larger vessel, reacting more slowly to incoming waves, the current naval standards do not provide coverage of likely centreline water levels.

Table 7 outlines the worst case roll and heave allowance for the three non-combatants in sea state 6 conditions. The results presented in table 7 (* correspond to a mean sea state 6).

Table 7 Summary of non-combatant heave and roll allowances in a maximum sea state 6

Ship/ allowance	Damage	Heading (deg)	95% V-line criteria		95% Vessel motions	
			Heave (m)	Roll (deg)	Heave (m)	Roll (deg)
Small Aux H	Sym	002	**1.93**	0.14	1.54	1.01
Small Aux R	Sym	090	0.64	8.79	2.78	10.08
Small Aux H	Asym	270	**2.66**	0.00	2.08	24.37
Small Aux R	Asym	045	**1.53**	2.33	1.93	22.48
Large Aux H	Sym	135	**1.75**	3.79	1.44	2.75
Large Aux R	Sym	225	1.09	6.38	1.32	2.29
Large Aux H	Asym*	178	**2.59**	0.00	0.77	17.90
Large Aux R	Asym*	090	1.17	3.29	2.09	18.13
Tanker H	Sym	002	**3.48**	0.03	0.26	1.59
Tanker R	Sym	225	**2.15**	8.45	1.61	21.37
Tanker H	Asym	002	**2.48**	0.00	1.37	6.10
Tanker R	Asym	270	1.05	6.45	1.93	19.40

In sea state 6 conditions roll allowances are still seen to fall substantially below the current DefStan requirement, suggesting that for these larger vessels the criteria could potentially be relaxed from the 15 degree roll allowance.

The worst case heave V-line allowances are seen to be very high when compared to the current 1.5m standard. In most cases these high allowances correspond to relatively low global vessel heave motions, aligning with the results seen in the sea state 4 analysis. The 95th percentile heave allowance for the large auxiliary was found to exceed current standards in all conditions greater than a sea state 4 with a 25% probability of the 1.5m allowance being exceeded seen in a sea state 4. In the sea state 6 the internal water level heave allowance was between 1 and 2m above the current V-line standard.

6. Conclusions

It has been shown that following this methodology and using a suitable time-domain code that the Red Risk and V-lines criteria can be evaluated for different sized vessels.

Current Def Stan 02-900 V-line criteria are based upon the original Sarchin and Goldberg work of 1962 which was based around the seakeeping characteristics of frigate sized vessels of that time. By examining water heights at the bounding bulkheads of damage cases across a range of modern indicative vessel designs, the suitability of these historic criteria has been assessed.

The new approach of forming a probabilistic water height line, which covers probability percentiles of bulkhead submergence, leads to heave and roll being considered together to form allowances that represent the actual percentage of time that points on the bounding bulkhead spend submerged. This is in contrast to current criteria which are based on the individual consideration of maximum roll angles and maximum heave motions, and do not account for the fact that these two occurrences are unlikely to manifest themselves at the same time.

It is clear that the vessels considered in this report must be assessed as two groups to truly understand the applicability of the existing standards; namely smaller combatants and larger non-combatants. Unsurprisingly, vessel size is seen to significantly affect the probabilistic heave and roll allowances of a vessel as a direct result of the different seakeeping behavior the vessels exhibit in larger sea states.

The current naval standards, based around World War 2 frigates, appear conservative when applied to a modern day destroyer design. Maximum roll allowance angles are predominantly seen following symmetric damage cases and the application of these allowances to an asymmetric list angle results in an additional level of conservatism. All the vessel-damage scenario combinations examined have a 95th percentile probabilistic roll allowance in a sea state 4 of less than 11°, showing the current criteria is suitable for sea state 4 for modern vessels.

The heave allowance is seen to be significantly more sensitive to vessel size than roll allowance. The current heave allowance is not exceeded by any of the smaller combatant vessels in a sea state 4, with the maximum 95th percentile heave allowance of 1.0m in the case of the destroyer.

In a maximum sea state 6 the highest combatant 95th percentile heave allowance was seen to be 1.45m. However in the case of the larger non-combatant ships examined, these heave allowances do not appear to be as suitable. The larger ships are seen to experience greater bulkhead water heights, not as a result of the vessel global vertical motions, but instead as a result of local water height as the vessel experiences small vertical motions and large flows in and out of the damage region. A heave allowance of 1.9m is required in order to ensure a 95% probability of compliance in a sea state 4 for the vessels and damage cases examined. This allowance increases to 3.5m in a sea state 6.

It appears evident that applying the current V-line standard roll allowance of 15° and heave to modern combatant designs is conservative up to a sea state 6. Similarly the current heave allowance of 1.5m also appears conservative when applied to modern combatants up to the sea state 6 conditions examined. The roll allowance standard for large non-combatants is seen to be very conservative and could be reduced significantly whilst still maintaining a 95% probability of compliance in a sea state 6, however, the non-combatant heave allowance may require a significant increase over current standards.

Acknowledgments

The authors would like to gratefully acknowledge the permission granted by QinetiQ and CRN Navies for allowing the publication of the findings from the investigation.

References

Sarchin, T.H. and Goldberg, L.L., Stability and Buoyancy Criteria for US Naval Surface Ships, Transactions SNAME, 1962

De Kat, J.O., Peters A.J. Damage Stability of Frigate Sized Ships, International Maritime Association of the Mediterranean Conference, Crete, 2002

MARIN, FREDYN – A computer program for the simulation of a steered ship in extreme seas and wind, User's Manual Version 10.3, Part I – Intact Hull, May 2011

MARIN, FREDYN Flooding Module – version 3.2.0.0 User Manual, March 2010

United Kingdom Defence Standard 02-900, General Naval Standard Part 1: Ship Safety & Environmental Protection, Issue 1, Aug 2013

United Kingdom Maritime Acquisition Publication No 01-024, Stability of Surface Ships Part 1 Conventional Ships, Issue 4, October 2010

Dawson, N.A. Work Package 2 – Damage Sensitivity Analysis QINETIQ/MS/MAR/CR1303691, September 2013.

Andrew J. Peters QinetiQ, Haslar Marine Technology Park, (UK), An Investigation into the V-Line Criteria for Naval Vessels, 2004

Hasselmann K. et al., Measurements of wind-wave growth and swell decay during the Joint North Sea Wave Project (JONSWAP). Ergnzungsheft zur Deutschen Hydrographischen Zeitschrift ReiheA(8) (Nr. 12): 95, 1973

Ewing J, Some results from the Joint North Sea Wave Project of interest to engineers, First international symposium on the dynamics of marine vehicles in waves, IMechE, 1974.

Small Combatant Accidental Damage Extents

Steve Marshall[1], Rick Goddard[2], Dominic Horner[2], Ian Randles[3]

1. *Naval Authority Group, UK Ministry of Defence*
2. *Steller Systems Ltd.*
3. *Maritime Platform Systems, UK Ministry of Defence*

Abstract: A cost benefit analysis has been conducted to understand how the extent of transverse watertight subdivision as a result of accidental damage extent requirements drives vessel cost, and where the balance lies between cost of increasing survivability and cost of vessel loss. The results of this investigation suggest that a 15% accidental damage extent is appropriate for a small naval combatant.

A great deal of work has been conducted in recent years concerning the derivation of appropriate accidental damage extents for naval vessels; this work has focussed predominantly on extents determined as a percentage of vessel length. Traditionally however, small vessels less than 90 metres in length have struggled to comply with such a standard and have consequentially been certificated against an extent based on number of compartments.

This paper explores the impact on small combatant design of moving from a two compartment damage requirement to a 15% length damage extent through a series of design explorations on four current small combatants. The implication of a 15% extent is examined with regard to the respective changes in ship size and watertight definition required to achieve compliance, and corresponding conclusions are presented.

Key words: Damaged Stability, Accidental Damage Extents, Damage Templates, Longitudinal Damage Extent, Damaged Stability Standards

1. Introduction

An ongoing package of work is being undertaken by the UK MOD Naval Authority to assess the suitability and applicability of current naval damage extents, split into accidental and hostile categories. As part of this work a method for conducting a cost benefit analysis to determine accidental longitudinal damage extents has been developed [1][2][3]. This work had previously focused on longitudinal accidental damage extents for vessels above 92m waterline length and uses factors such as vessel value, cost of transverse subdivision and estimates of annual probability of an accident.

Under current UK MOD stability standards [5], vessels below 92 metres waterline length are not required to comply with a percentile accidental longitudinal damage extent; instead a damage extent is defined with regards to number of compartments, where a compartment is considered to be a minimum of 6 metres in length. Current UK MOD longitudinal accidental damage extents are seen as:

Vessels of length less than 30 metres:

- *Any single main compartment*

Vessels of waterline length between 30 metres and 92 metres:

- *Any two adjacent main compartments, a main compartment is to have a minimum length of 6 metres*

The design and cost impact of moving from such a standard to a standard defined by percentage of waterline length was previously unclear. It was not known if a percentage damage extent, output from the

cost benefit analysis, would be prohibitively expensive to comply with, or lead to an increase in the size of small combatants in order to achieve compliance.

As the next phase of the derivation of accidental longitudinal damage extents the following work has been conducted and is presented herein:

- A sensitivity study to understand the sensitivity of the cost benefit approach to key inputs.
- An assessment of a suitable longitudinal extent for a vessel under 92 metres.
- A study to assess the design implications of a damage extent defined by percentage of waterline length on four in-service small naval combatants.

Cost Benefit Analysis Sensitivity Study

2.1 Cost Benefit Approach

A study was conducted, to assess whether the upfront cost of increased subdivision, and hence survivability is a worthwhile investment to reduce the risk of losing a vessel to accidental damage. This increased subdivision is linked to the design longitudinal damage extent such that the best value for money design standard can be applied. Figure 1 shows a typical example of the cost-benefit curves produced, and shows a point of inflection where the additional cost of designing to a higher standard does not represent worthy investment. This point of inflection is therefore the optimum damage extent to which a ship should be designed.

As the cost benefit approach is based on ship specific cost assumptions, it is an unsuitable method for the development of a generic standard; instead the method is suited to the development of standards for specific classes or individual ships. The cost benefit study undertaken by the UK MOD looked at three different classes of vessels: a destroyer, a high capability frigate, and a small combatant. A full explanation of the approach with underpinning assumptions is laid out in [1].

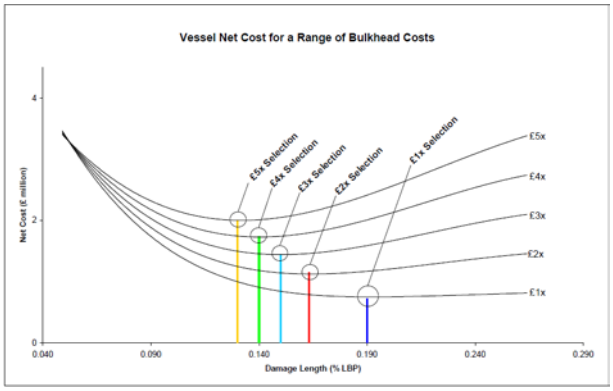

Fig. 1 - Example of a vessel net cost for a range of bulkhead costs

2.2 Sensitivity Study

There are several key assumptions upon which the cost benefit analysis is dependent; there were further scrutinized in order to provide assurance that the model is robust. These three areas are:

- Likelihood of loss
- Cost of additional bulkheads
- Unit Procurement Cost (UPC)

2.2.1 Likelihood of loss

The likelihood of vessel loss is a function of the probability of the vessel experiencing an accident multiplied by the probability of the damage length being exceeded. This was derived from merchant vessel collision statistics which are discussed in detail in [1]. The applicability of using merchant data to derive naval standards is outlined in [3] where the conclusion states that using merchant vessel accidental damage is credible due to the accident rates being found to be similar. As the sample size for Naval vessels is small, the calculated accident rate varies greatly with each individual incident; as a result, it is appropriate to assess the impact that this variance has

on the overall calculated optimum design damage length. The baseline value used is derived from the average of the mercantile sources available which is an accident rate of 1.6 x 10^{-02} per annum. The upper bound was 1.5 times the baseline level, and the lower limit half the baseline level with the RN average accident rate used by way of comparison.

2.2.2 Cost of additional bulkheads

In order to determine the cost of introducing additional bulkheads into an established design a design study was conducted. The starting point for the study was that the design of the vessel had been developed and that the drawing work was complete. Uncertainty in bulkhead cost estimates arise from more indeterminate factors such as the potential complexity of rearranging a general arrangement and re-routing ship systems around a new bulkhead. For a small combatant, the baseline cost per bulkhead was assumed as £130k however it was significantly increased to £500k when input into the sensitivity study in order to encompass all unaccounted costs.

2.2.3 Unit Procurement Cost

A large spread (±25%) was assumed from the baseline values as the confidence in an assumed cost of procuring a new ship is low. It is likely to be cheaper to procure ships produced as part of a class than a one-off replacement vessel built after all sister vessels have been constructed. For a small combatant, £25m was considered the baseline value.

2.3 Sensitivity Results

Varying the parameters outlined above, each of the net cost benefit curves were produced and the optimum design damage extents were tabulated into look up tables with an example shown in Table 1.

Table 1 - Sensitivity table of varying UPC and likelihood of loss

		Likelihood of Loss			
	Relative	0.5 x Baseline	RN Statistics	Baseline (UK Vessel Damage Baseline)	1.5 x Baseline
UPC	-25%	17.30%	17.70%	17.80%	18.20%
	-10%	17.40%	17.80%	18.00%	18.50%
	-5%	17.40%	17.90%	18.10%	18.50%
	Baseline	17.50%	18.00%	18.10%	18.60%
	5%	17.50%	18.00%	18.20%	18.70%
	10%	17.60%	18.10%	18.20%	18.70%
	25%	17.70%	18.20%	18.40%	18.90%

The output of the study is shown in Table 2. It can be seen that within the bounds of the variation in the sensitivity analysis, the design damage extent is always greater than the current DEF STAN 02-900 15% damage extent standard.

Table - 2 Output of sensitivity study

Vessel	Baseline cost	Optimum cost-benefit damage extent	Range
Destroyer	£1b	22.7%	19.9%-26.1%
Frigate	£500m	21.0%	18.4%-25.2%
Small Combatant	£25m	18.1%	16.5%-24.9%

One conclusion drawn from the data above is that with the upfront cost of building warships, it is prudent to design the vessel to be more survivable due to the relatively small cost of increased survivability through subdivision at the design stage even when assuming the worst case bulkhead cost.

The sample size for the RN accident rate was considerably smaller than the merchant vessel statistics and showed that there was a reduced accident rate meaning individual incidents have a much larger effect on the calculated accident rate. As the optimum design points for all classes were found to be above the current DEFSTAN 02-900 requirements, the next step of the study was to consider what annual

accident rate would result in a standard of 15% representing the optimum solution from a cost-benefit perspective. Table 3 shows the output of this work and shows that for smaller vessels the annual probability of vessel loss would need to be an order of magnitude less than mercantile statistics, and for larger, more expensive vessels two orders of magnitude.

Table - 3 Likelihood of loss required for 15% damage extent to be optimum

	Optimum cost-benefit damage extent	Likelihood required for 15% damage extent
DD	22.7%	$\approx 2.1 \times 10^{-4}$
FF	21.0%	$\approx 3.8 \times 10^{-4}$
OPV	18.1%	$\approx 2.0 \times 10^{-3}$
Baseline accident probability		1.6×10^{-2}

The analysis was all carried out theoretically and showed that the current standards should perhaps be in excess of that which is currently being used. Given the reduced flexibility of internal subdivision on smaller ships, it was assumed that this would be the most challenging increased standard to achieve. In order to validate that the outputs of the cost benefit analysis can be achieved, a study looking at the feasibility of achieving an increased standard was undertaken. A 15% waterline damage length is deemed the most appropriate starting point to align with the current standard for larger vessels and to avoid a step change between small and large ships' damage extents. It is perhaps also conceivable to say that naval vessels are 10 times less likely to have an accident than their mercantile counterparts which would result in a 15% damage extent.

3. Design Implication of a 15% Waterline Length

3.1 Approach

A study was conducted to investigate the degree of design change required to existing in-service naval vessels below 92m in order for them to comply with a 15% longitudinal damage extent. The vessels selected for the study range from 50m to 90m and have commissioned dates ranging from 1979 through to 2003. As such the vessels selected span a range of sizes and ages all of which must comply with a current two compartment standard.

Damage analysis was conducted using the naval architecture design and analysis software Paramarine and making use of the MOD recommended Damage Template functionality which semi-automates the process of applying damage to a vessel. The ships were considered in both a deep and a light condition for all damage cases in order to capture the worst case combination of damage case and loading condition. The damage extent was set to 15% and the location of the damage templates was defined working forward to aft and then aft to forward with the forward or aft face being placed 0.001m in front and behind of each transverse watertight bulkhead respectively (Fig 1). This approach ensured that the maximum number of bulkheads were breached by the damage extent and that correspondingly the worst case damage location was likely to be included in calculations.

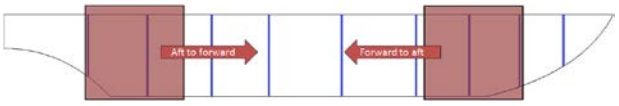

Fig. 1 - Application of damage templates

Damage was simulated at three transverse extents measured as a fraction of maximum beam (B); damage to but not including the centreline (B/2), damage to 20% of the maximum beam (B/5) and full symmetric damage (B). In all asymmetric cases the damage penetration is measured relative to the vessel outer shell at the longitudinal position being examined. Damage was applied to both Port and Starboard sides to identify the worst case scenario arising from design asymmetry.

Two independent assessments of the small ship designs were conducted: The first of these investigated the required change to basic ship vertical centre of gravity (VCG) required to comply with DefStan 02-900 damage stability GZ criteria following 15% damage. This information illustrates the level of ballasting or liquid loading restrictions which would be required in order to ensure that the existing vessel can pass damaged stability criteria with a 15% damage extent applied.

Secondly, subdivision changes were considered in order to achieve compliance. During this process it was felt important to limit the design changes as far as possible so as to minimize deviation from the original design intent and balance. To achieve this, local changes to subdivision were employed first, followed by global changes only where local changes did not result in compliance with damaged stability criteria. The following steps were considered to be local subdivision changes and are listed in the order in which they were applied:

- Increase the height of down-flooding points where practical
- Change tank and void layout to reduce asymmetry whilst maintaining tank volumes as per the original design
- Movement of small internal watertight boundaries

If the above process failed, the global subdivision would be examined and altered until compliance was achieved. This process is outlined below:

- Identify the zones which represented the most onerous stability cases when damaged and investigating small adjustments to the bounding watertight bulkheads
- Investigate global changes to the position of the transverse watertight bulkheads throughout the design whilst maintaining volumes in key functional spaces
- Investigate increases in key characteristics (length, beam depth etc.) to allow compliance with damaged stability criteria

3.2 Assumptions

In order to reduce the complexity of the analysis a number of assumptions were made regarding the nature of the applied damage. These assumptions are seen below:

- Worst case damage is assumed to occur at one of the three transverse extents examined, no additional worst case damage scenarios, unique to each damage location were identified. This includes additional trapped buoyancy cases. The assumption being justified by the expectation that individual cases such as these could be dealt with by adjusting the local design detail, e.g. intentional down-flooding, openings designated ‘to be left open following damage’ etc.
- Vertical damage extent was modelled as full, i.e. no lesser vertical extents were considered.
- Intermediate flooding cases were not considered, where intermediate refers to partial flooding of compartments as a result of non-watertight boundaries (rated to a 1m pressure head) retaining fluid for a short period of time.
- Worst case damage scenarios where non-watertight subdivision completely withstands flood water were not considered.

3.3 Findings

It was shown that the four vessels considered in this analysis can all meet DefStan 02-900 damage criteria with a 15% longitudinal damage extent applied without the requirement for major changes to vessel

principal dimensions. Two of the classes considered required changes to internal subdivision in order to comply with the standard however it is important to note that neither sets of changes involved the movement of major transverse bulkheads or global changes to the vessels dimensions.

Where changes to subdivision were necessary these were predominantly centred on reducing the magnitude of flood water asymmetry. In most cases, the driving load condition was seen to be light seagoing, consequentially the arrangement of water ballast tanks to be outboard of fuel oil tanks dramatically reduces the contribution of the fuel oil tanks to floodwater transverse centre of mass (Fig. 2). In all cases B/5 or B/2 damage were seen to constitute the worst case transverse extent and rearranging the transverse location of tanks was seen to significantly improve stability following damage.

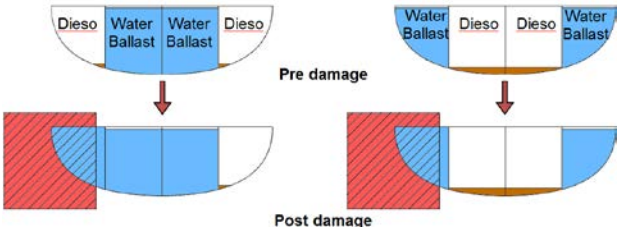

Figure 2 - Layout of water ballast and fuel oil tanks

The configuration of void spaces was found to impact damage asymmetry; a number of instances of asymmetry in void spaces, particularly below machinery spaces, were found to drive poor stability following damage. The rearrangement of these voids, whilst maintaining the functionality of pipe and cable runs, in order that they had minimal transverse subdivision was seen to significantly improve damaged stability (Fig. 3).

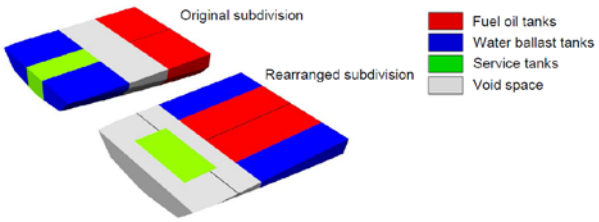

Figure 3 - Arrangement of void spaces

The most substantial changes to internal subdivision were required when compartments above the damage control deck were not subdivided by watertight boundaries. This situation lead to longitudinal progressive flooding and excessively large damage cases causing widespread criteria failure. This issue was found to be the case with one of the classes examined. Almost all other bulkhead changes were confined to the tank top primarily concerning void spaces, fuel oil and ballast tanks. Where tanks were rearranged the overall fluid volumes were maintained as closely as possible to those in the original design.

In all four of the vessels examined compliance was reached with the proposed 15% standard without the requirement for changes to vessel size. The smaller vessels were found to require little or no change to their subdivision to achieve compliance. Both of the larger vessels required local changes to subdivision in way of tank and void space arrangements. Furthermore downflooding points were seen to significantly impair the ability of the designs to meet stability criteria by truncating the damaged GZ curves. It was found that in most cases this effect was completely removed through raising downflooding points by small amounts, with little impact on the overall design.

The relative damage stability performance of the vessels in question can be best examined by converting the two compartment standard to an equivalent percentile damage length for each vessel. The percentile damage lengths can then be compared to the proposed 15% damage lengths. In Fig. 4 the

average damage length for each of the vessels has been plotted along with error bars representing the maximum and minimum damage lengths represented by the current two compartment standard. For each zone the damage length was calculated as the maximum length beyond which a three compartment damage scenario would result. The maximum and minimum values of these resulting damage lengths were then calculated and plotted. In the figure we can see that the average two compartment damage length of the two smaller classes are close to the 15% damage extent line with the error bars falling either side. This shows that the increase in damage length is unlikely to require significant, if any, changes to the current design, as was borne out in the results of the analysis. Conversely the proposed 15% extent represents a significant increase in damage capability over current standards for the larger vessels where the average and maximum two compartment damage length was seen to be significantly below the proposed 15% extent, a hypothesis which was also borne out by the significant changes to subdivision required in order for these vessels to achieve compliance.

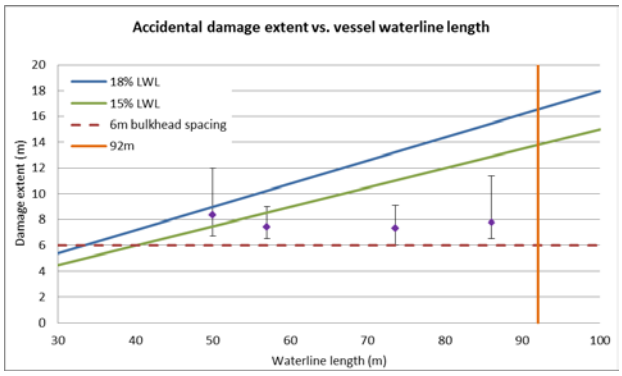

Fig. 4 – Accidental damage extent vs. vessel waterline

From the analysis conducted it is clear that not only is it possible to pass a more onerous 15% damage extent criteria but it is relatively easily achieved and in many cases does not impact the ship significantly. As mentioned previously the one exception to this conclusion is the case in which the damage control deck required the addition of watertight bulkheads. It is unlikely that the additional bulkheads will affect individual compartment volumes and may not significantly affect layout. However the changes proposed may have a detrimental effect on the ability of the crew to move through the ship, but this is considered in line with current naval design convention.

4. Conclusions

The sensitivity study outlined in this paper has shown that despite the subjective nature of some of the cost inputs and the difficulties faced in their estimation, the output of the cost benefit analysis does not vary greatly with variation of key inputs. Furthermore, the lowest calculated value of optimum accidental collision damage extent over the range of inputs examined is seen to be greater than current standards, suggesting that even with the accepted uncertainty in the calculation the current standards fall below the most cost effective extent. In the case of small vessels, the results of the cost benefit analysis suggest that a damage extent of 18.1% represents the most cost effective solution for a vessel less than 92 metres in length. That being said it is important to assess the findings and conclusions in the context of the global ship design and its affordability. It is worth bearing in mind that for any procurement project there is an ultimate maximum price that can be borne and as such further gains in benefit cannot necessarily be realised due to their cost. Furthermore there are numerous tradeoffs that must be addressed throughout the design of a naval combatant and ultimately decisions may have to be taken which would see survivability move away from the optimal damage extent in order to achieve a required capability elsewhere in the design.

Based on these findings, the adoption of a 15% accidental longitudinal damage extent, in line with vessels over 92 metres in length is not conceptually extreme and is a valid assessment point.

Individually, none of the design changes made to the current vessel designs in order to achieve compliance with a 15% damage extent represented significant or costly alterations nor were they revolutionary in terms of small combatant design. It is also notable that none of the vessels examined required changes to the global subdivision in order to obtain compliance, with the most significant changes being damage control deck subdivision. Interestingly only one of the vessels examined required the addition of watertight bulkheads and only on one deck. This could imply that the assumed correlation between damage extent compliance and the addition of transverse watertight bulkheads is more complex than accounted for in the research to date. With that said there is no question that a correlation exists however it is likely to be a stepped relationship, with each step representing an additional watertight bulkhead, and in the analysis to date a significant step has not been encountered.

The comparison of a two compartment standard and a 15% LWL standard demonstrates that vessels closer to the 92 metre delineation will see the largest increase in equivalent damage extent and this is borne out in the results of the design study.

It is clear that in terms of the four vessels examined, the answer to whether a vessel less than 92 metres can meet a 15% damage extent without significant cost is a resounding yes within the limitations of the analysis presented in this paper.

Acknowledgments

The authors would like to thank the UK Ministry of Defence for permission to publish in part the findings of the small ships damage extents study.

References

[1] Ministry of Defence, Work Package 1: Non-hostile damage extents for Naval ships, R Goddard and A Peters January 2013.

[2] MOD publication, Tolerable Safety of Damaged Ships, UK, S Marshall.

[3] Ministry of Defence, Accidental Damage Extents sensitivity analysis, I Randles, unpublished.

[4] D. Smith, M. Heywood, Accidental Damage Templates (ADTs), a basis for the future of Naval Ship Safety Certification. Proceedings of the 10th International Conference on Stability of Ships and Ocean Vehicles, 2009.

[5] Ministry of Defence, Defence Standard 02-900 Part 1 Issue 1, Ship Safety & Environmental Protection August 2013.

- SESSION 3 -

NEW EXPERIMENTAL TECHNIQUES FOR SHIP STABILITY ASSESSMENT

Remarks on Experimental Validation Procedures for Numerical Intact Stability Assessment with Latest Examples

Naoya Umeda[1*], Daichi Kawaida[1], Yuto Ito[1], Yohei Tsutsumi[1], Akihiko Matsuda[2] and Daisuke Terada[2]

1. *Dept. of Naval Architecture and Ocean Engineering, Osaka University*
2. *National Research Institute of Fisheries Engineering, Fisheries Research Agency*

Abstract: For facilitating development of the guidelines of direct stability assessment as a part of the second generation intact stability criteria at the IMO (International Maritime Organization), this paper provides examples of comparison between model experiments and numerical simulations for stability under dead ship condition and for pure loss of stability in astern waves. As a result, some essential elements for reasonable validation were identified. For dead ship stability, adequate selection of representative wind velocity generated by wind fans is crucial. For pure loss of stability, accurate Fourier transformation and reverse transformation of incident irregular waves are important. These remarks should be reflected in the guidelines as appropriate.

Key words: second generation intact stability criteria, direct stability assessment, IMO, dead ship condition, pure loss of stability

1. Introduction

At the IMO, the second generation intact stability criteria, which consist of three level criteria, are now under development. Here its highest level means direct stability assessment using time-domain numerical simulation tools and the tools should be validated with physical model experiments. For this purpose, the IMO started to develop draft guidelines of direct stability assessment procedures under the initiative of the United States and Japan as SDC 1/INF. 8, annex 27 [1]. For finalizing the guidelines, particularly their quantitative acceptance criteria, it is indispensable to examine their feasibility by comparing model experiments with numerical simulations. Thus it is important to collect comparisons between model experiments and numerical simulations for the relevant stability failure modes.

The second generation intact stability criteria deal with five failure modes, i.e, parametric rolling, pure loss of stability in astern waves, broaching, stability under dead ship condition and excessive acceleration. Among them, relatively large number of validation reports for parametric rolling (e.g. Hashimoto et al., [2]) and broaching (e.g. Hashimoto et al., [3]) are available but only the limited number of reports for stability under dead ship condition [4] and pure loss of stability [5]. Since few published experimental data are available, even the experimental procedures for dead ship stability have not yet been established by the ITTC (International Towing Tank Conference) [6].

Therefore, this paper reports recent attempts to validate numerical simulation codes for dead ship stability in irregular beam wind and waves and for pure loss of stability in irregular astern waves. The authors presumes that these information could facilitate finalization of the IMO guidelines for direct stability assessment as well as the revision of the ITTC recommended procedure for intact stability model test.

* **Corresponding author**: Naoya Umeda, Dr. Eng, research fields: ship stability, optimal control. E-mail: umeda@naoe.eng.osaka-u.ac.jp

2. Current draft guidelines of direct stability assessment procedures

The current draft guidelines of direct stability assessment procedures drafted by the United States and Japan consist of requirements for numerical modelling, qualitative and quantitative validation of software and extrapolation procedures. For the quantitative validation, numerically simulated results are requested to be compared with the model experiments based on the ITTC recommended procedures [6]. Its acceptance criteria are shown in Table 1. In this table, it was widely accepted that all quantitative numbers appeared as the acceptance standards here should be considered as tentative unless the sufficient evidence of their feasibility is submitted to the IMO. It is noteworthy here that these requirements do not refer to irregular wind at all. This is because it is not so easy to find a literature describing ship model experiments with both artificial irregular wind and waves except for T. Kubo et al. [4]. It can be also remarked that no acceptance criteria for pure loss of stability in astern waves exists. This is because only recently mechanism of "pure loss of stability" was discussed as Umeda et al. [7] and H. Kubo et al. [5]. They experimentally and numerically confirmed that large roll triggered by loss of restoring moment due to longitudinal waves could usually induce lateral motions because of asymmetric underwater hull due to heel. Centrifugal force due to such lateral motions could induce further roll motion. Thus, the phenomenon known as "pure loss of stability" could be theoretically dealt with both restoring reduction and centrifugal force due to lateral motions. These raised points have already been adopted by the IMO for the vulnerability criteria as a part of the second generation intact stability criteria. Therefore, it is an urgent issue to provide examples of comparison in artificial irregular waves between model experiments and numerical simulation.

3. Stability failure in irregular beam wind and waves

3.1 experimental procedures

For examining the validation procedures for dead ship stability, experiments using a 1/70 scaled model of the 205.7m-long CEHIPAR2792 vessel were conducted at a seakeeping and manoeuvring basin of National Research Institute of Fisheries Engineering. The ship model has a flat plate on the upper deck for realising the windage area and its area centre height of the super structure but without additional buoyancy. It was not equipped with bilge keels, propellers, shaft brackets and rudders. An optical fibre gyroscope inside the model is used for detecting the roll, pitch and yaw angles. For sway and heave motions, the total station system, which will be described in Chapter 3, was used.

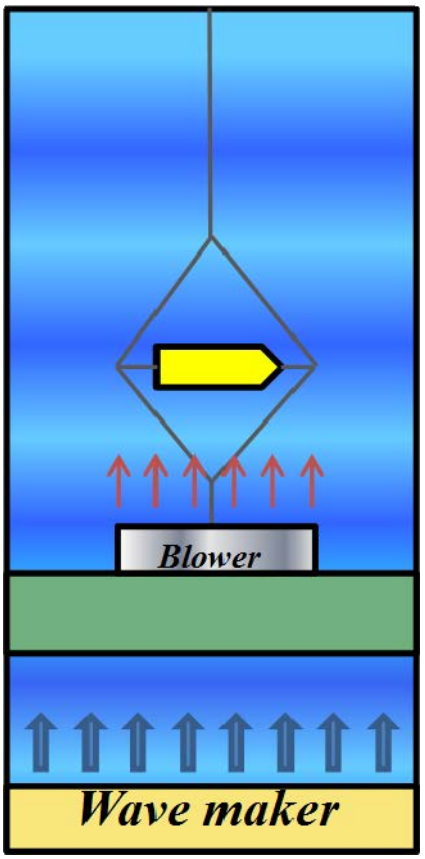

Fig. 1 – Overviews of experimental set-up

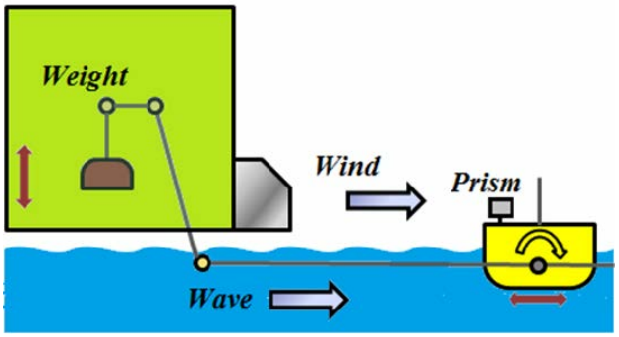

Fig. 2 – Lateral views of experimental set-up

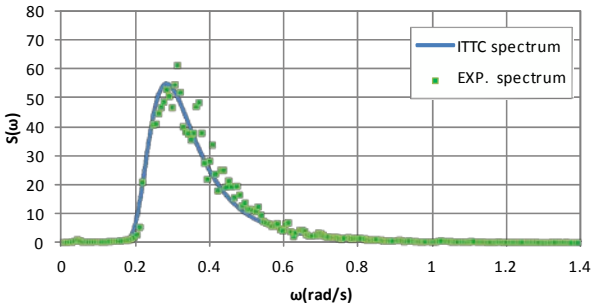

Fig. 3– Comparison of wave spectra

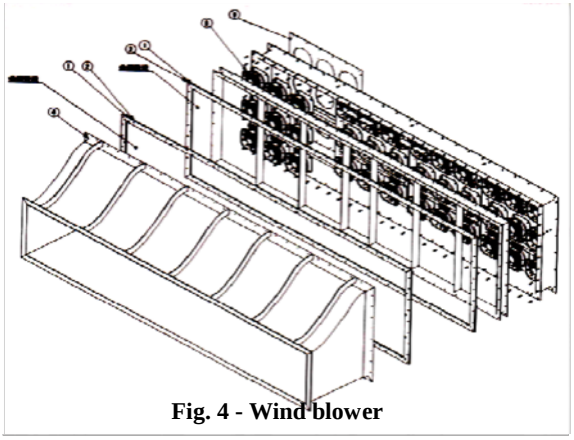

Fig. 4 - Wind blower

The model was kept to be orthogonal to the wind and wave direction by a wire system, which softly restrains drift and yaw, as shown in Figs. 1-2. Here the wire system was connected to the ship model at bow and stern where the height was set to be equal to calm water surface based on measured hydrodynamic reaction force and moment in a captive model test of the subject ship. The mean of fluid dynamic force in the sway direction was cancelled out by a counter weight.

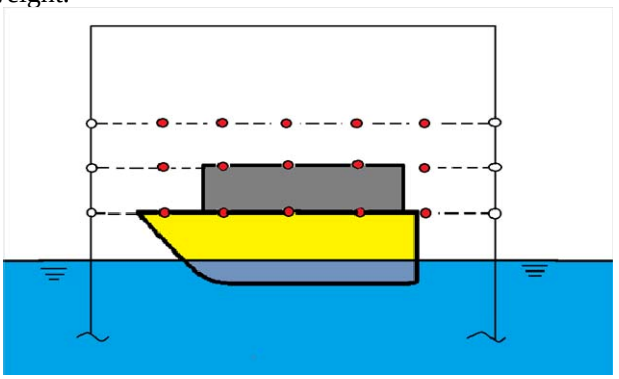

Fig. 5 – Measurement points for wind velocity

Irregular water waves were generated by plunger-type wave makers with the ITTC spectrum. As shown in Fig. 3 the specified spectrum was satisfactorily realized. Fluctuating wind was generated by a wind blower in the wave direction. The wind blower, as shown in Fig. 4 consists of 36 axial flow fans and is controlled by invertors with a v/f control law.

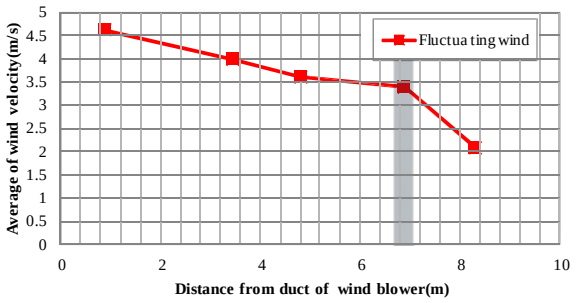

Fig. 6 – Measured wind velocity as a function of the distance from the blower. Here the shaded zone indicates ship position during the experiments in wind and waves.

Although in our previous experiment [4] the relationship between the drive frequency for this control and the wind velocity was adjusted by measuring steady heel angle of the ship model under non-fluctuating wind, the wind velocity was directly measured with a hot wire anemometer in this experiment. This wind measurement was executed without the ship model and 15 measured points we

used as shown in Fig. 5. Further, the distance between the wind blower and the ship position were changed with the shift of the position of the blower. These measured data as shown in Fig. 6, the wind velocity gradually decreases with the distance from the blower. In this study the data where the ship model position measured during the experiment is used so that the mean wind velocity used here is about 28 metres per second in full scale. The wind velocity has some spatial non-uniformness as shown in Fig. 7 because the ratio of blower breadth to ship length of 1.327 is not so sufficiently small. The use of wider blower or smaller ship model is preferable. The wind velocity spectrum is designed with the Davenport one without the transfer function between the drive frequency and the wind velocity. The measured spectrum was slightly larger than the specified one, as shown in Fig.8. In our previous experiment [4] better agreement between the two but with its mean wind velocity of 22.5 metres per second was obtained. In case of high wind velocity it seems to be appropriate to take account of the transfer function.

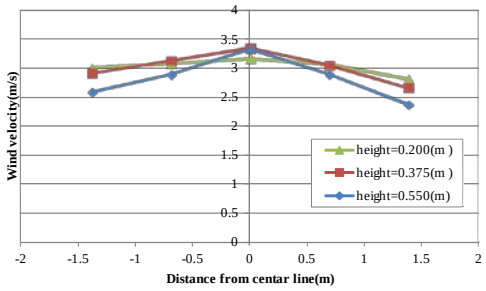

Fig. 7 – Mean wind velocities measured at different positions

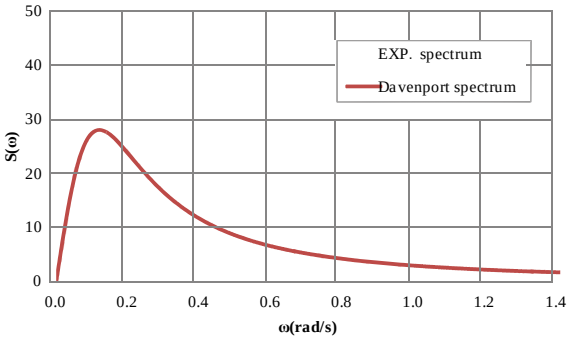

Fig. 8 – Comparison of wind spectra

3.2 numerical modelling

For a comparison with the model experiment, uncoupled roll model [7] was used in this study. As usual, the nonlinear roll damping coefficients in calm water and the effective wave slope coefficient were estimated with roll decay model tests and the roll response model tests in beam regular waves, respectively. The wind-induced moment was estimated with measured wind drag and heel angle only with constant beam wind velocities. As shown in Figs. 9-10, the estimated wind drag and heel angle reasonably agrees with the measured data so that the estimation of wind velocity from these ship data, which was used in our previous work [4], can be judged as reliable.

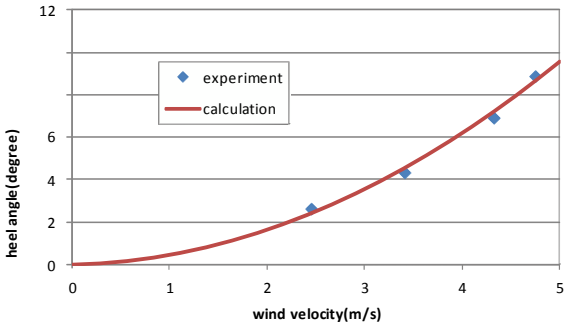

Fig. 9 – Steady heel angle with constant wind velocity

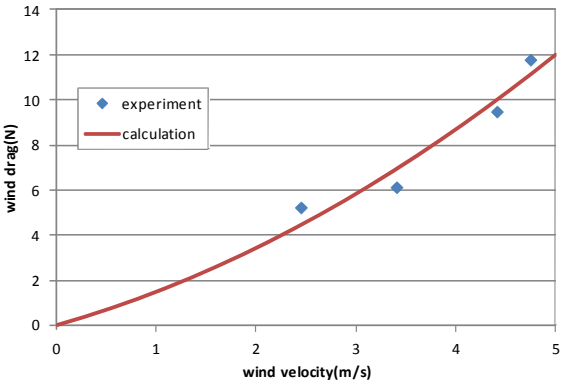

Fig. 10 – Wind drag with constant wind velocity

3.3 Comparison of experiment and simulation

Following the current draft guidelines, the ensemble average of variance of roll angle obtained by

the model experiment was compared with that by the numerical simulation with 5 % confidential intervals using *t* distribution as shown in Fig. 11. Here 20 realizations were used for both model experiment and numerical simulation and the duration is 3600 seconds in full scale. The initial heel angle due to cargo shift was 6 degrees towards leeside. In the numerical simulation, the mean wind velocity was set to that from the central points for wind velocity measurement except highest one. Since the two confidential intervals are overlapped, we could conclude that the numerical model was validated with the model experiment.

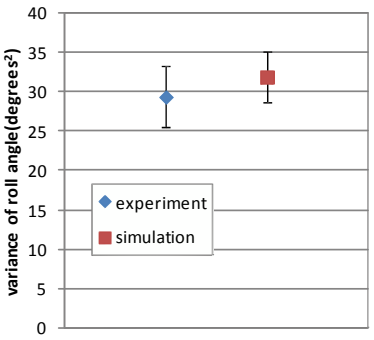

Fig. 11 – Comparison of variance of roll angle between experiment and simulation

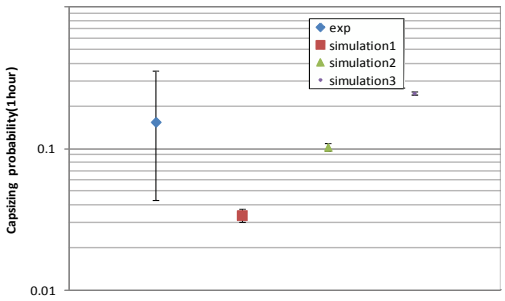

Fig. 12 – Comparison of capsizing probability of experiment and simulation

As a next step, the comparison of capsizing probability between the model experiment and numerical simulations is shown in Fig. 12 with 5% confidence intervals using binomial distribution. Here three different ways for determining the mean wind velocity are used. The "simulation 2" indicates the way that used in the comparison of variance of roll angles. The "simulations 1 and 2" use the mean of three central points and that of the central point at the middle height, respectively. The results indicate that both the "simulation 2 and 3" shows acceptable agreement and the "simulation 1" provides too low probability. Thus, appropriate selection of measured points for wind velocity is crucial for validation of numerical models.

4. Stability failure due to pure loss of stability

For validating a numerical model for pure loss of stability in irregular astern waves, experiments using a 1/48.8 scaled model of the 154m-long ONR flare topside vessel were executed at the seakeeping and manoeuvring basin of National Research Institute of Fisheries Engineering, based on the ITTC recommended procedure on intact stability model test [6]. The position of the ship model was observed by a total station system, which consists of the theodolite, an optical distance and direction measuring device and the prism which reflects light rays from the theodolite is on the ship model, as shown in Fig. 13. By synchronizing data of the total station system and gyroscope which is on the vessel, the ship position in inertia coordinate system was obtained. Ship velocity was calculated by differentiating the position of centre of gravity of the ship.

For precise comparison in time series between the experiment and the simulation, estimation of wave height at each ship position is indispensable. The wave elevation was measured by a servo-needle-type wave height metre near the wave maker. The Fourier spectrum from these measured wave data was converted with the ship position data and then it was inversely transformed so that the wave elevation at the

ship position was obtained. This converted Fourier spectrum was also used for numerical simulation as its input.

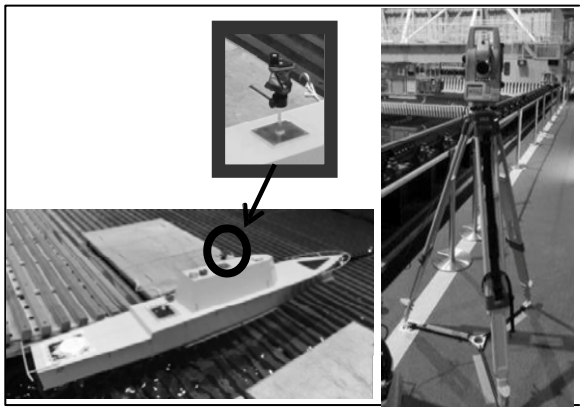

Fig.13 - Total station system (left; prism right; theodolite) used in the model experiment

The wave elevation at the ship centre was calculated by the above procedure and is shown in Fig. 14 with measured roll and pitch data. This result indicates that roll angle becomes large whenever the ship meets a wave crest, which is defined as minima of the wave elevation. Here the significant wave height is 0.2066m, the mean wave period is 1.627 s, the rudder gain is 1.0, the Froude number is 0.25 and the autopilot course from the wave direction is -15 degrees. Earlier and similar procedures and results were published in [8].

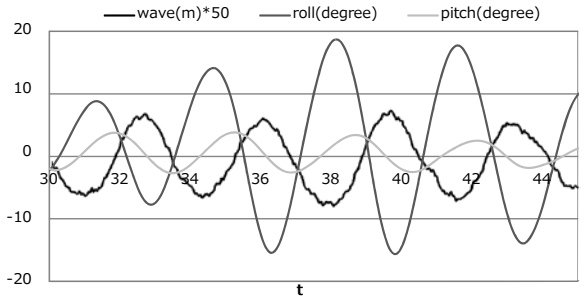

Fig. 14 - Wave height at the ship position and measured roll and pitch angle in irregular waves

The numerical model proposed by H. Kubo et al. [5] is based on nonlinear manoeuvring model with linear wave forces and nonlinear restoring variation. The manoeuvring, roll damping and propulsion coefficients were obtained by conventional model tests such as CMT. The linear wave forces were estimated with a slender body theory with very low encounter frequency and nonlinear restoring variation was predicted with Grim's effective concept and the Froude-Krylov assumption.

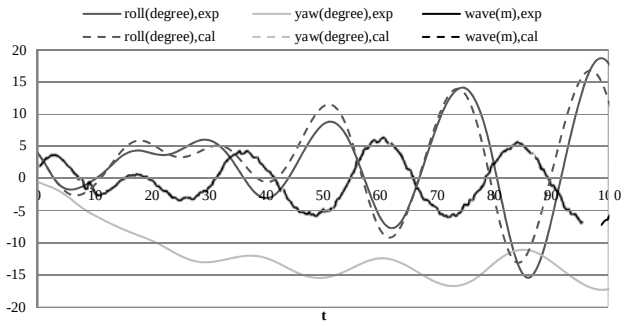

Fig. 15 - Comparison in time series between experiment and calculation in irregular waves

As shown in Fig. 15, this numerical model was well validated with the present model experiment in irregular waves. This validation procedure could be useful for developing standard guidelines of validation of direct stability assessment at the IMO.

5. Concluding remarks

The main remarks from this work are summarized as follows:

(1) For dead ship stability, adequate selection of representative wind velocity generated by wind fans is crucial.

(2) For pure loss of stability, accurate Fourier transformation and reverse transformation of incident irregular waves are important.

Acknowledgements

This work was supported by a Grant-in Aid for Scientific Research of the Japan Society for Promotion of Science (No. 24360355). It was partly carried out as a research activity of Goal-Based Stability Criterion Project of Japan Ship Technology Research Association

in the fiscal year of 2013, funded by the Nippon Foundation.

References

[1] SDC 1/INF.8, 2013: Information Collected by the Correspondence Group on Intact Stability, submitted by Japan, IMO (London).

[2] Hashimoto, H., Umeda, N. and Sogawa, Y. 2012: Prediction of Parametric Rolling in Irregular Head Waves, Proceedings of the 12th International Ship Stability Workshop，pp.213-218.

[3] Hashimoto, H., Umeda, N. and Matsuda, A., 2012: Broaching prediction of a wave-piercing tumblehome vessel with twin screws and twin rudders, Journal of Marine Science and Technology，pp.448-461.

[4] Kubo, T., Umeda, N., Izawa, S., Matsuda, A., 2012: Total Stability Failure Probability of a Ship in Beam Wind and Waves: Model Experiment and Numerical Simulation, Proceedings of the 11th International Conference on Stability of Ships and Ocean Vehicles，pp.39-46.

[5] Kubo, H., Umeda, N., Yamane, K. and Matsuda, A. 2012: Pure Loss of Stability in Astern Seas -Is It Really Pure?-, Proceedings of the 6th Asia-Pacific Workshop on Marine Hydrodynamics, Johor, pp. 307-312.

[6] ITTC, 2008: Recommended Procedures, Model Tests on Intact Stability, 7.5-02-07-04.

[7] Umeda, N., Izawa, S., Sano H., Kubo, H. and Yamane, K., 2011: Validation Attempts on Draft New Generation Intact Stability Criteria, Proceedings of the 12th International Ship Stability Workshop，pp.19-26.

[8] Clauss, G.F. and Hennig, J., 2004: Deterministic Analysis of Extreme Roll Motions and Subsequent Evaluation of Capsizing Risk, International Shipbuilding Progress. Vol. 51. No. 2/3, pp. 135-155.

Table 1 Quantitative validation requirements [1]

	Required for:	Objective:	Acceptance criteria:
Response Curve for Parametric Roll	parametric roll and excessive accelerations	to demonstrate reasonable agreement between numerical simulation and the models test on both bandwidth of parametric resonance and the amplitude of the roll response.	[1/10] of natural roll frequency for the bandwidth and [10%] of amplitude if below angle maximum of GZ curve in calm water and [20%] if above the angle of maximum of the GZ curve in calm water
Response Curve for Synchronous Roll	all modes	to demonstrate reasonable agreement between numerical simulation and the models test on the amplitude of the roll response	[10%] of amplitude if below angle maximum of GZ curve in calm water and [20%] if above the angle of maximum of the GZ curve in calm water
Variance Test / Synchronous Roll	software for numerical simulation of dead ship condition and excessive accelerations	demonstrate correct (in terms of statistics) modelling of roll response in irregular waves	probability that the difference between the ensemble estimates of variance of roll is caused by the random reasons is above the significant level of [5%].
Variance Test / Parametric Roll	software for numerical simulation of dead ship condition and excessive accelerations	demonstrate correct (in terms of statistics) modelling of roll response in irregular waves	probability that difference between the ensemble estimates of variance of roll is caused by the random reasons is above the significant level of [1%].
Wave Conditions for Surf-Riding and Broaching	software for numerical simulation of surf-riding and broaching	demonstrate correct modelling of surf-riding broaching dynamics in regular waves	wave steepness causing surf-riding and broaching at the wave length [0.75-1.5] of ship length is within [15%] of difference between model test and numerical simulation; speed settings are also within [15%] difference between model test and numerical simulation.

Model Experiments in Following and Quartering Seas using a Small Size Ship Model

Mitsuhiro Nakamura [1], Yasuo Yoshimura [1], Daisaku Shiken [1]

1. Dept. of Fisheries Sciences, Hokkaido University, Japan

Abstract: In case of performing a free-running model test, a large scale of ship model and basin are conventionally required because of the need of installing a lot of driving and measuring apparatus. They generally need the large cost for the model test. Therefore, it would be better and convenient if a small free-running ship model could be realized.

The authors have been trying to develop the small size of driving and measuring apparatus for such a small size ship model, and trying to carry out free-running model tests in waves at a small basin. Although there are significant problems about weight and space for the onboard apparatus, the small size of servo driving unit of propulsion motor as well as steering gear have been developed. The electric power for these apparatus is supplied by only one small lithium-polymer battery. Meanwhile, for the measurement of ship trajectory and speed, a total station system is utilized.

Using such ship model, the authors have successfully measured the ship motion of surf-riding and broaching, and reveal the occurrence condition of these phenomena as an example. From these data, initial conditions of surf-riding and broaching also can be clarified even in such small ship model and towing basin.

Key words: small size ship model, free-running model test in waves, surf-riding, broaching.

1. Introduction

Free-running model tests are essential and important for the study of maneuvering and sea-keeping performances. When these tests are performed, a lot of driving and measuring apparatus must be installed on a ship model. They are, for example, radio control receiver, battery, propulsion motor, steering gear; motion sensor, data logger and so on. Therefore, a large scale of ship model should be arranged, which requires a large model basin and also introduces a large cost for model testing.

In particular performing a free-running test in waves, the sufficient water proof device should be provided against the deck water caused by waves and sometimes the capsizing of ship model. This makes the ship model heavier, which introduces the larger cost for model tests.

In this paper, some method of free-running test using the small size ship model is proposed. Then, the results of model tests are shown, particularly in the following and quartering waves.

2. Method of free-running model test

Firstly, the methods of free-running model tests using a small ship model are shown. In order to install all the apparatus into the small model, smaller and lighter instruments have been developed. At the same time, the hull structure of ship model also has become lighter construction using some frames and FRP hull. As for the measurement of ship trajectory and speed, a total station system is applied.

2.1 Ship model

In this paper, 135GT purse seiner is investigated. The photograph of the ship model is shown in Fig.1. This kind of purse seiner is one of the typical fishing vessels in Japan and some of them caused the capsize accidents.

*** Corresponding author:** Yasuo Yoshimura, Professor, research fields: naval architects and fishery engineering. E-mail: y-yoshi@fish.hokuda.ac.jp

Fig. 1 – Ship model for free-running tests

The principal particular is shown in Table 1. It may be remarkable that the ship model length and the displacement are only 1.1m and 11kg, respectively.

Table 1 Principal particulars of the ship mode

		full-scale		model	
scale				1/35	
L_{pp}	m	37.00		1.057	
B	m	7.90		0.226	
D	m	3.22		0.092	
d	m	2.90		0.083	
DISP.		483.60	(t)	11.056	(kg)
KM	m	4.56		0.130	
KG	m	3.09		0.096	
GM	m	1.47		0.034	

2.2 Driving apparatus

1. Battery

Conventionally, lead batteries or nickel-cadmium batteries were used as a power supply of a ship model. However, these batteries are too heavy to install into a small ship model. Therefore, a lithium-polymer battery that is called a Li-Po battery is applied to the power source of the small ship model. This kind of battery is now widely used in the hobby airplane or helicopter. The size of 6 cell type battery as shown in Fig.2 is only 150mm×50mm×50mm, and the weight is less than 800g. The electric power is 22.2V and 5,800mAh at full charge.

This small but powerful battery can realize the experiment by means of supplying the electric power for all apparatus on board. The important points for using this battery are concerning to the electric charging and discharging. A computer controlled charger as shown in Fig.2 should be used for the battery charging. While the operation of model tests, the voltage of the battery should be carefully monitored and checked in order not to make over discharging condition that may break the battery.

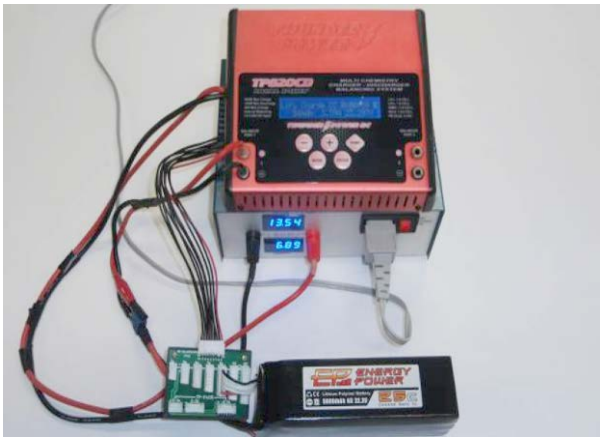

Fig. 2 – Lithium-polymer battery and its charger

Fig. 3 – Propulsion motor (60W DC motor)

2. Propulsion motor

In order to reduce the weight and space of a propulsion motor, a small size DC motor shown in Fig.3 has been used. The maximum power is 60W and the weight is only 0.7kg.

For the connection between propeller shaft and motor shaft, one helical coupling has been used as shown in Fig.4. This coupling can absorb the vibration caused by the small off center among these shafts.

3. Steering gear

As for the steering gear, the conventional servo motor of a proportional radio controller has been connected to the rudder pintle using one set of link lever. Rudder angle is detected by a small potentiometer which is connected by another link levers from the rudder pintle. These mechanisms are shown in Fig. 5.

4. Propulsion motor controller

The revolution of the propulsion motor is precisely kept constant during the model test. For this purpose, PDI controlled power driver including ahead/astern controller has been specially manufactured and mounted in a compact box as shown in Fig.6.

2.3 Measuring devices on board

Measuring devices on board and data recorder have been selected and used from the market.

1. 6DOF inertial sensor

In order to measure the ship motions, a 6DOF inertial sensor (Crossbow AHR5400MA) shown in Fig.7 has been used. It is able to measure the accelerations in 3 directions and roll, pitch, yaw angle and rate. The size is 75mm×75mm×100mm and weight is 720g.

2. Data recorder

As there is little space to install PC on board, a small size data logger (Keyence NR-2000) has been used. The size is 165mm×110mm×30mm. It can simultaneously record 16 measuring channels. This recorder has been stored in a watertight plastic box for food and fixed on the deck to operate it easily.

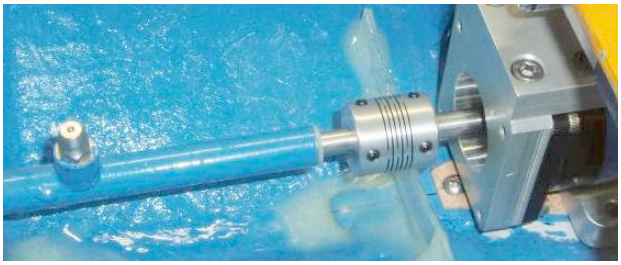

Fig. 4 – Connection of motor and propeller shafts

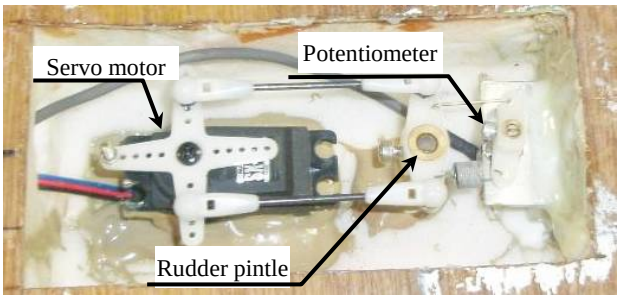

Fig.5 – Steering gear

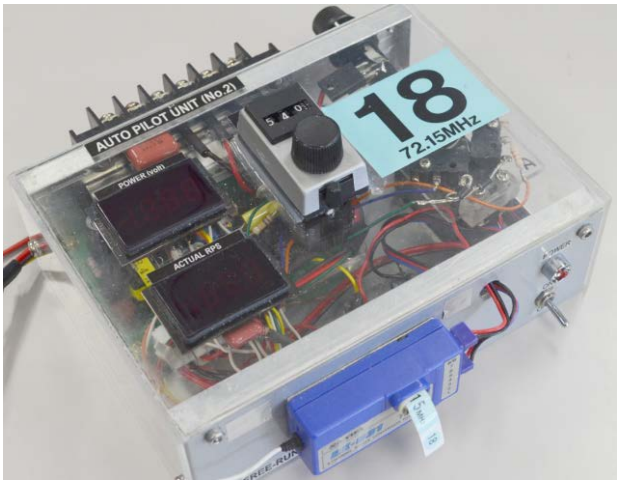

Fig. 6 –Compact control box

Fig. 7 –Data logger and 6DOF inertial sensor

2.4 Measurement of ship trajectory and speed

Although ship motions can be measure from the 6DOF inertial sensor, the ship trajectory and speed can not be obtained from the onboard data. The ship trajectory and speed should be measured from the shore. In this paper, a total station system shown in Fig.8 (Topcon / Power Station) is utilized. It is now widely used in civil engineers. This device can automatically track the laser lay reflected by the prism which is located on the top center of ship model, and calculate in 20Hz the 3D position of the prism that is the center of ship model.

Using the above 3D position data, ship's speed can be obtained by means of time differentiating these data. However, there are some small noises and errors in these 3D position data, this makes the large scatters in the calculated speed data. One example is shown in the pink line of Fig. 9. Therefore, some filtering technique should be applied.

In this paper, a simple differential digital filter has been used to eliminate the noise. The algorism of this filter is explained as in (1).

$$\left.\begin{aligned} u(k\Delta t) &= \Delta t \sum_{i=-N}^{N} x((k-i)\Delta t)W(i\Delta t) \\ v(k\Delta t) &= \Delta t \sum_{i=-N}^{N} y((k-i)\Delta t)W(i\Delta t) \\ U(k\Delta t) &= \sqrt{u^2(k\Delta t)+v^2(k\Delta t)} \end{aligned}\right\} \quad (1)$$

Where, $x(t)$, $y(t)$: measured position data

$u(t)$, $v(t)$: calculated speed

$U(t)$: resultant ship's speed

$W(t)$: impulse response of differential and low-pass filter with window function

Δt: sampling interval of data

This simple digital filter can realize an arbitral frequency response if necessary.

The obtained ship's speed using the above differential low-pass filter (cutoff frequency: 1Hz) is shown in straight bold line in Fig.10. It is found that the scatters can be well eliminated instead of phase-lag.

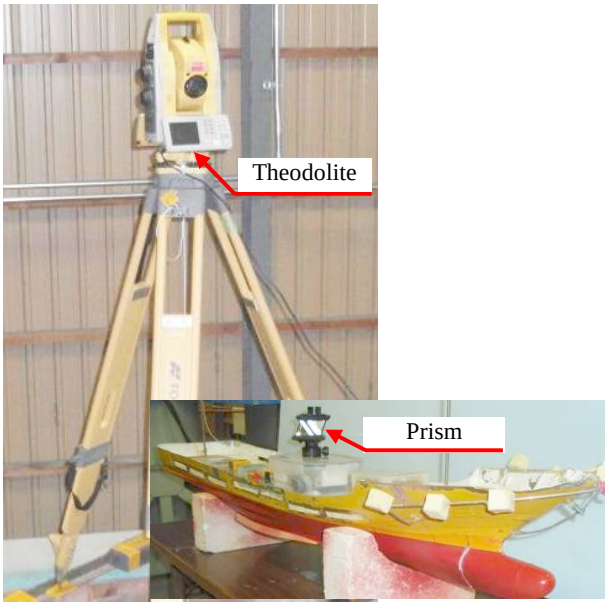

Fig. 8 – Total station system

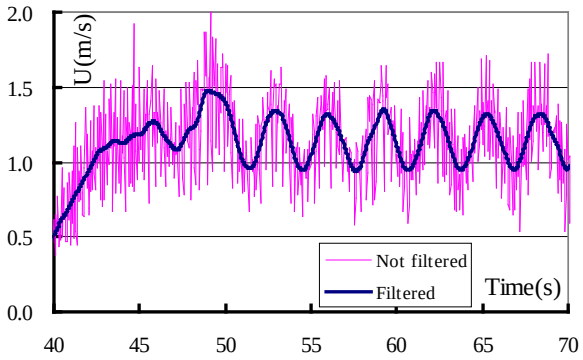

Fig. 9 – Comparison of a ship's speed between simple differentiation and digital filtering

3. Model experiments in following and quartering seas

Model tests have been performed concerning to reveal the occurrence condition of surf-riding and broaching. A small towing basin in Hokkaido University whose size is 50m×3.5m×1.5m has been used. Model tests have been carried out in following and quartering seas. The ship model is accelerated to a certain speed by a towing carriage, and then it is released from the carriage. After that, it is course-kept by a manual steering. According to the Ref. [1], surf-riding is divided into under any initial condition and under certain initial condition. Therefore, the

experiments in this paper become the surf-riding under certain condition. F_n and χ_c are adopted as the test parameters. F_n means a nominal Froude number that indicates non-dimensional ship speed in calm water with the specified propeller rps, and χ_c course keeping angle from wave direction, respectively.

3.1 Patterns of test results

Test results are classified to 4 patterns that are periodic motion, surf-riding, nearly broaching and broaching.

In case of a ship running high speed in following seas, the ship is sometimes caught by waves and accelerated to the same speed of wave celerity. It is called as surf-riding. During this surf-riding, the ship tends to fall into the severe condition that she can not maintain her course and until at last she quickly turns. It is known as broaching that often causes a capsizing. Therefore, surf-riding has to be considered as a necessary condition of broaching.

In order to categorize these 4 patterns, ship's motion are determined using the coordinate systems as shown in Fig.10. Typical examples of each time series are also shown in Fig.11.

1. Periodic motion

When a ship is running in following seas, the ship is generally overtaken by waves. Pitching angle is varying periodically. Therefore it is defined as periodic motion and expressed as in (2).

$$\theta \neq const. \tag{2}$$

2. Surf-riding

In case of surf-riding, pitching angle becomes to be not periodic and substantially constant in negative angle, since the ship almost locates a down slope of the same wave successively. It is defined as surf-riding and expressed as in (3)

$$\theta \approx const. < 0 \tag{3}$$

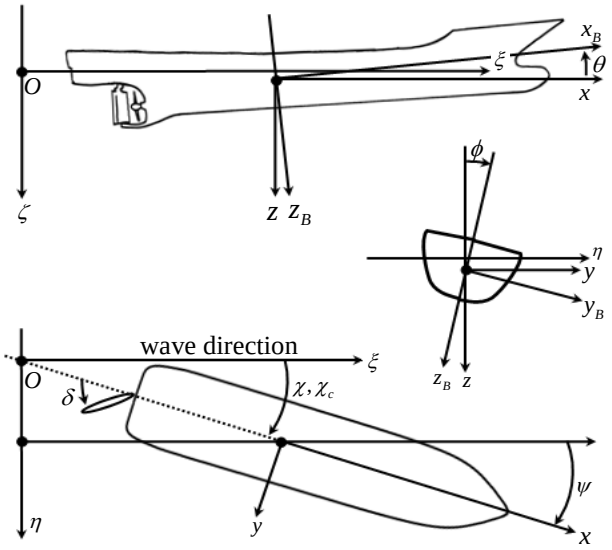

Fig. 10 – Coordinate systems

3. Nearly broaching

In spite of the maximum steering effort, the ship does not promptly respond; it is regarded as nearly broaching and expressed as in (4). The previously mentioned surf-riding condition is also added in this pattern.

$$\begin{aligned} &\theta \approx const. < 0 \\ &\delta = +\delta_{\max}, r = 0 \quad or \quad \delta = -\delta_{\max}, r = 0 \end{aligned} \tag{4}$$

where, δ_{max}=35 is maximum rudder angle

This pattern may reach to broaching. Particularly, the results of experiment in a small basin sometimes can not determine whether the ship will turn to the steering side or not, since the ship model has been running just a limited distance. This pattern is including such result.

4. *Broaching*

In case of the ship turning to the opposite direction against to the steering side in spite of the maximum steering effort, it is defined to be broaching. Broaching is defined as in (5) according to Ref. [2].

$$\begin{aligned} &\delta = +\delta_{\max}, r < 0, \dot{r} < 0 \quad or \\ &\delta = -\delta_{\max}, r > 0, \dot{r} < 0 \end{aligned} \tag{5}$$

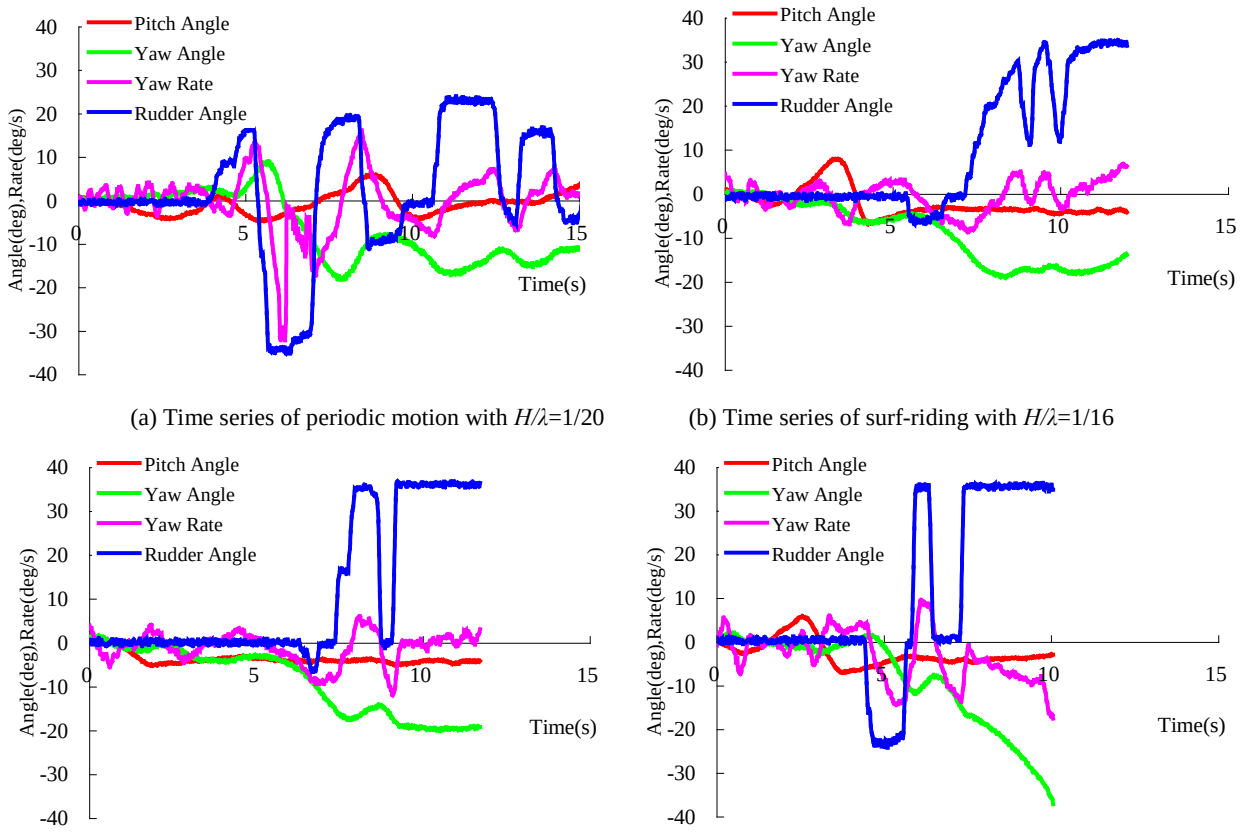

(a) Time series of periodic motion with H/λ=1/20

(b) Time series of surf-riding with H/λ=1/16

(c): Time series of nearly broaching with H/λ=1/15.5

(d) Time series of broaching with H/λ=1/15

Fig.11 – An example of each definition (Every examples are carried out with λ/L=2.1, χ_c=-10degrees and F_n=0.43.)

3.2 Occurrence condition of broaching

Experiments have been carried out in quartering seas. The wave condition is λ/L=2.1 and H/λ=1/19, 1/17 and 1/15.5. The ship model has been course-kept to χ_c=-5, -10 and -15 degrees; propeller rps has been set to be F_n=0.35, 0.40 and 0.43.

Results of the experiments are categorized to the previous mentioned patterns and the probability of broaching are obtained and plotted in Fig.12 for various test parameters. From this figure, it is clear that the probability of broaching is increased by the larger F_n, H/λ and χ_c.

However, as χ_c is limited to -15 degrees in this experiment and the probability can not be obtained over this angle. According to Ref.[3], it is expected that the ship model is overtaken by waves when χ_c is over -15 degrees, and then the occurrence of broaching may reduce.

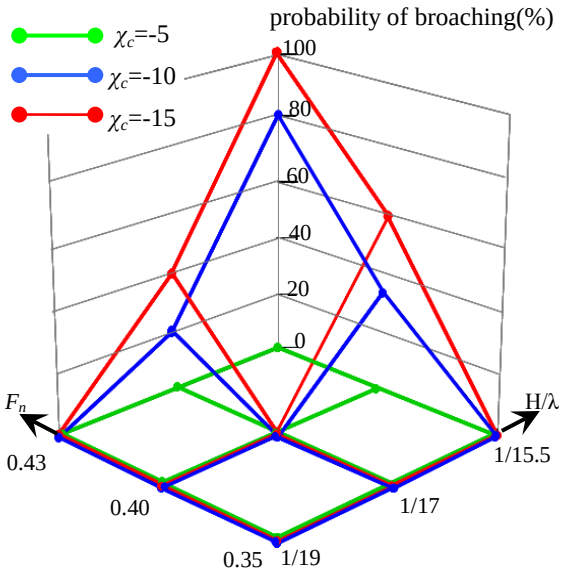

Fig. 12 – Occurrence condition of broaching

From the above results, it can be pointed out that the reduction of ship's speed or course-keeping direction to the wave is important in following seas.

3.2 ship speed in following seas

At the previously mentioned experiments, ship's speed is also measured. Fig.13 shows the measured ship's speed in following seas where χ_c=0 and various λ/L, H/λ and F_n. The horizontal axis indicates nominal Froude number that is corresponding to the propeller rps, and the vertical axis is actual ship speed converting to Froude number. Each figures show that the actual ship's speed becomes higher when propeller rps or H/λ increasing. Also, two different patterns can be seen. One is the case that the ship model has been overtaken by waves and then ship's speed changes periodically. The other is that the ship's speed has been accelerated and reached to the wave celerity that is shown by the dotted line in each figure. This is surf-riding condition. In case of approaching to the surf-riding condition, amplitude of ship's speed becomes larger. This tendency is known as a surging with large amplitude in Ref. [4]. It is considered to be the signal of a surf-riding.

4. For the future study

In order to perform model test more precisely, smaller size devices have been developed. These devices are shown in Fig.14. The total weight of altered devices is just 6kg. In order to adjust the ship's trim and moment of inertia easily, a little bit larger ship model is constructed. The length and displacement are about 1.2m and 14kg.

1. Auto-pilot device

In order to keep ship's course exactly and automatically, an intelligent auto-pilot unit is added in the compact control box. It is shown in Fig.14 (a). It is expected that the uncertainty at course keeping maneuver can be decreased by using this unit.

2. Compact size propulsion dynamometer

A conventional propulsion dynamometer in the market is too large and heavy for such a small ship model to measure the propeller thrust and torque.

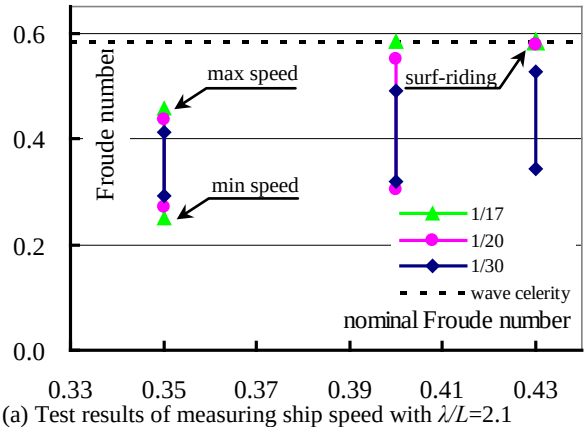

(a) Test results of measuring ship speed with λ/L=2.1

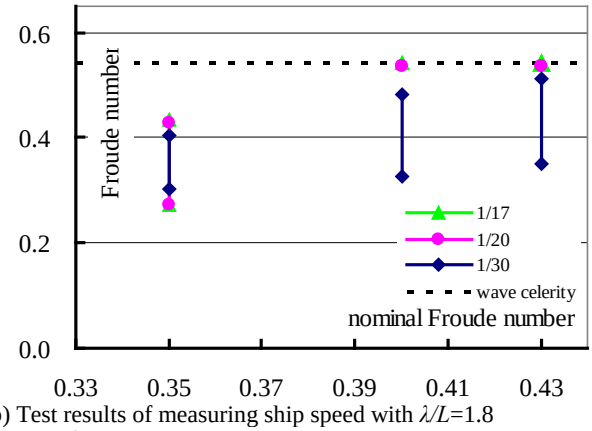

(b) Test results of measuring ship speed with λ/L=1.8

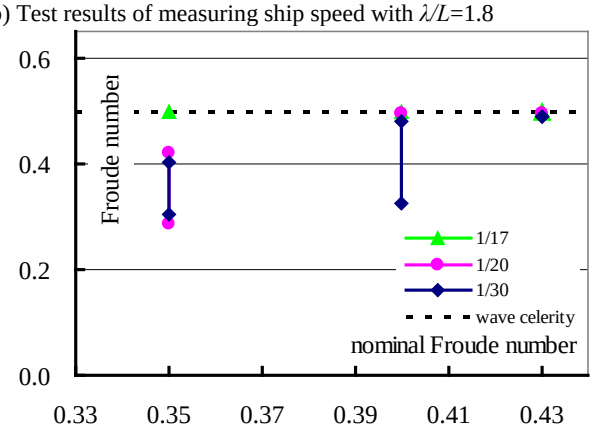

(c) Test results of measuring ship speed with λ/L=1.5

Fig. 13 – ship seed in following seas

For this purpose, a compact size propulsion dynamometer is developed. It is shown in Fig.14 (b). The previous mentioned compact propulsion motor is suspended by a dynamometer by which the propeller thrust can be directly measured. As for the propeller torque, the electric current of the propulsion motor is precisely converted to the torque. These electric circuits are additionally installed in the above auto-pilot unit.

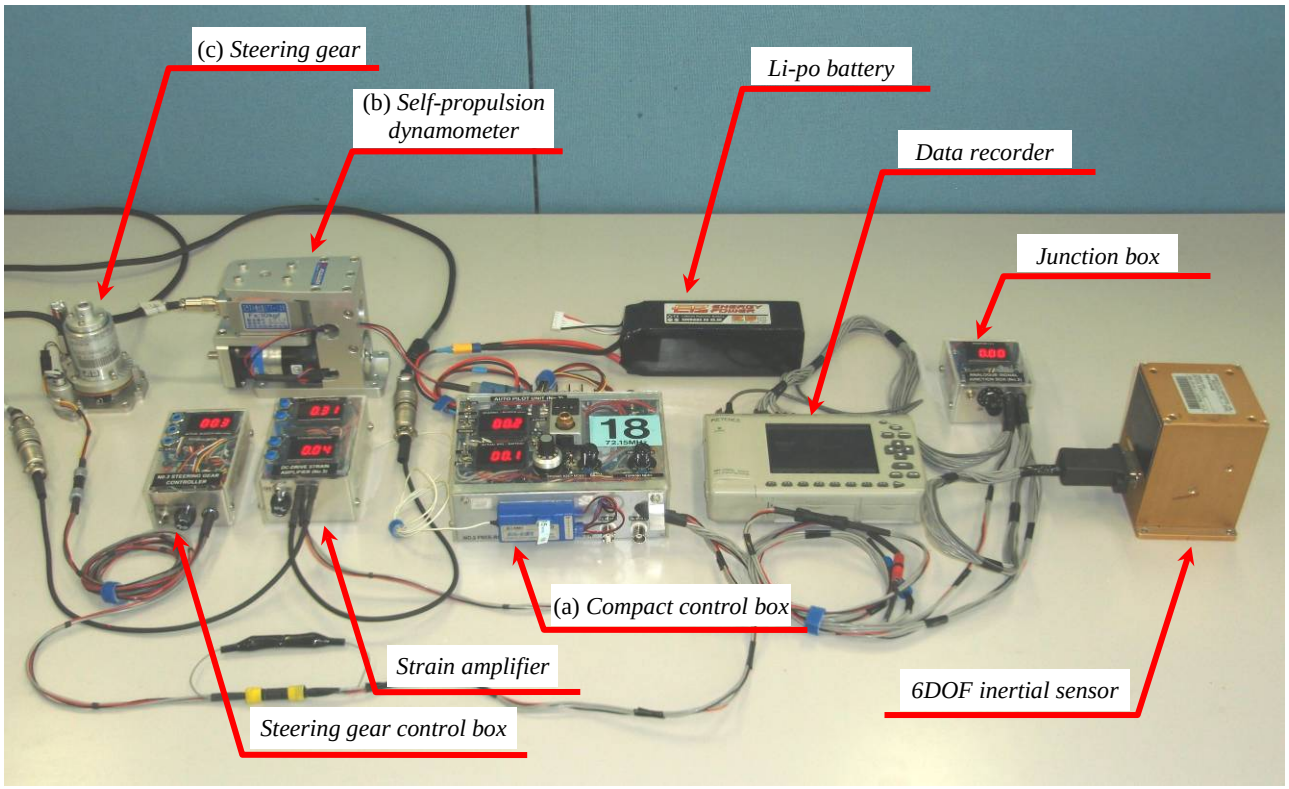

Fig.14 – Driving and measure devices for the future experiments

3. Small size steering gear

A servo controlled steering is essential for the auto-pilot steering. For this purpose, a small size of steering gear has been developed. It is shown in Fig.14 (c). Moreover, an accurate load cell can be attached on this steering gear, which can measure rudder normal force precisely.

5. Conclusions

The experimental technique using the small ship model is proposed here. Model tests have been carried out in the small towing basin. The concluding remarks are summarized as the following.

1. Utilizing a small size of ship model, ship motions during free-running in following and quartering seas can be obtained even in a small towing basin. As for broaching, however, only initial conditions have been clarified.
2. Although there are some uncertainties in the course keeping because of the manual steering, the outlines of broaching occurrence conditions can be clarified.
3. Ship speed and trajectory can be successfully measured using a total station system, and also the surging with large amplitude in waves can be measured.

As the results, a small ship model is considered to be an effective method. However, in case of the investigation of the capsizing due to broaching, a larger basin may be essential.

Acknowledgment

This research was financially supported by the Sasakawa Scientific Research Grant from The Japan Science Society. The authors would like to express many thanks to the grant.

References

[1] N. Umeda, T. Kohyama, Surf-riding of a Ship in Regular Seas, Journal of the Kansai Society of Naval Architects, Japan, 1990, 63-74.

[2] N. Umeda, and M.R. Renilson, Broaching – A Dynamic Behavior of a Vessel in Following seas, Maneuvering and Control of marine Craft, 1992, 533-543.

[3]N. Umeda, A. Matusda, M. Hamamoto, S. Suzuki, Stability assessment for intact ships in the light of model experiments, JMST, 1999, 4:45-57.

[4]M. Kan, T. saruta, M. Yasuno, Y. Yamakoshi, S. Suziki, Surging of large amplitude and surf-riding of ships in following seas, Journal of the Society of Naval Architects of Japan, 1987, 152-162

Experimental Database for Surf-Riding and Broaching-to Quantification based on Captive Model Tests in Waves

Boris Horel [1*], Pierre-Emmanuel Guillerm [1], Jean-Marc Rousset [1] and Bertrand Alessandrini [1]

1. *Hydrodynamic, Energetics and Atmospheric Environment Laboratory (LHEEA), Ecole Centrale de Nantes, Nantes, France*

Abstract: With the aim of better understanding the phenomena of surf-riding and broaching for small service ships, a 6DOF numerical-experimental hybrid model based on semi-captive model tests in following waves has been created. Since a system based model is used, experiments are required in order to bring the hydrodynamic interactions between hull and water. In this paper, several semi-captive model tests in calm water and in following waves using a 1/10 scaled model of a trawler's hull will be presented. When navigating in astern seas, three modes of motion can be observed: the ship is overtaken by a wave, the ship is surfing a wave and the ship overtakes a wave.

Key words: Broaching, Surf-riding, Semi-captive model tests in waves

1. Introduction

Recent works concerning the Second Generation IMO Intact Stability Criteria showed that almost all of the world's fleet (fishing vessel, military ship, Ropax vessel...) is vulnerable to surf-riding and broaching (C. Wandji, P. Corrignan, 2012, [1]). Previous study brought out the instability boundary for an ONR tumblehome. It appears that surf-riding and broaching can be experienced by this military vessel for a wavelength to ship length ratio λ/L_{wl}=1.25 and a wave height to wavelength ratio H/λ=0.05 (S. Hosseini et al., 2010, [2]). With the aim of better quantifying these phenomena for small ships, semi-captive model tests in calm water and in following waves were conducted at the LHEEA towing tank, Nantes, France.

2. State of the Art

In 1999, N. Umeda et al. [3] confirmed with experiments that even a ship complying with the current IMO IS code can capsize as a result of broaching. It appears that surf-riding is regarded as a prerequisite of broaching.

In 2003, N. Umeda, H. Hashimoto and A. Matsuka [4] carried out captive model experiments on a 1/17.25 scaled model of a 135-gross-tonnage purse seiner in order to measure the restoring moment acting on the hull. The model was free in heave and pitch and was towed with a heel angle of 10° in following and quartering waves.

In 2004, H. Hashimoto et al. [5] proposed a new procedure for captive model experiments to obtain hydrodynamic forces. All experiments were conducted in calm water at various heel angles and Froude numbers corresponding to the case of an encounter frequency of 0. Some cases were chosen because they corresponded to the condition of a ship capsizing due to broaching in the ITTC benchmark test. For captive model tests, the 1/25 scaled model was equipped with a rudder but not a propeller, and was completely fixed in all directions.

In 2005, in order to validate their numerical code, Z. Ayaz, D. Vassalos and K.J. Spyrou [6] used results

*** Corresponding author:** Boris Horel, PhD student, research fields: hydrodynamic of ships and marine structures. E-mail: boris.horel@ec-nantes.fr

From model experiments on a 712 ton Japanese fishing vessel in extreme random seas. The captive model tests were conducted with different speeds, heading angle, sinkage, trim and in some cases with different wave steepness. They observed that the extremity of the conditions of captive model runs was defined within limits and strength of model that was used.

In 2008, R. Skejic and Odd M. Faltinsen [7] highlighted that no well-documented appropriate experimental results for manoeuvring of a ship in waves are available.

Still in 2008, since applicability of simulation models depends on the prediction accuracy of hydrodynamic forces, N. Umeda, A. Matsuda and H. Hashimoto [8] conducted captive model test experiments on a 1/48.94 scaled model of the ONR tumblehome vessel. The model was free in heave and pitch, and was attached with the towing carriage via a 4 component dynamometer. Heave and pitch were measured by a potentiometer and a gyroscope respectively. Experiments were then performed in waves at low encounter frequency. In these conditions, the model was towed with heel angles of 0, 10 and 20 degrees.

In 2009, S. Hosseini [9] carried out experiments on an ONR tumblehome in the INSEAN Basin and in the Osaka University towing tank. Resistance tests in calm water, static heel in calm water, static drift in calm water and static heel in following waves were performed to collect seakeeping and manoeuvring parameters for the Non-linear Dynamic Analysis (NDA) model of broaching.

In 2010, H. Hashimoto et al. [10] again performed captive model tests on the ONR tumblehome. They conducted resistance tests and propeller open water tests to estimate the resistance and the thrust of the subject ship. Circular motion tests (CMT) were also conducted at the seakeeping and manoeuvring basin of the NRIFE for combinations of drift angles and yaw rate. These CMTs were done without the propellers and the rudders. Linear and non-linear manoeuvring coefficients were obtained from the measured data by the least squared method. They pointed out that heel-induced hydrodynamic forces are important for broaching prediction so they measure the heel-induced hydrodynamic forces in calm water with forward velocity and several heel angles up to 70 degrees. To examine the roll restoring variation, they also conducted towing tank tests in following waves with different heel angles up to 70 degrees. In the experiment, the model was free in heave and pitch.

Inspired by the above state of the art experiments, we decided to design a purpose-built apparatus to perform semi-captive model experiments in waves. Resistance tests, static heel, static drift, pure sway and pure yaw both in calm water and in following waves were carried out.

3. Experimental Technique

3.1 Facilities

All the experiments were conducted in the towing tank of the LHEEA laboratory. The basin is 148 meters long, 5 meters wide and 3 meters deep. From low to medium speed, several model attitudes can be tested in one run, thereby improving the efficiency of the experimental campaign. The tank breadth makes it possible to perform pure sway tests with an amplitude of up to 0.6 meters. The carriage can reach a maximum speed of 8m/s.

3.2 Model

Fishing vessels are well known to suffer damage caused by the appearance of the broaching-to phenomenon. Marine investigation reports illustrate the extreme sea states and weather conditions of such a catastrophic event (Transportation Safety Board of Canada, 2009, [11]). It reveals that while a ship was navigating in astern seas, she lost her intact stability and capsized very quickly without the helmsman being able to influence the ship's heading. But these

Reports only provide qualitative aspects about the occurrence of this phenomenon.

The model is a 1/10 scaled model of a fishing vessel built as part of a project called OPTIPERF. This project was a collaborative project with HydrOcean and co-funded by the European Fisheries Fund (EFF). As shown in figure 1, this is an optimized-shape trawler, designed with a bifid bow to reduce drag due to wave field and hard chines to increase stability.

Fig. 1 - Hull shape of the model

The ship's features and the 1/10 scaled model features are given in table 1.

Table 1 Ship features

	Ship	*Model*
Length overall, L_{OA}	22.3 m	2.23 m
Waterline length, L_{wl}	21.3 m	2.13 m
Draft, T	3 m	0.3 m
Displacement, ∇	164 ton	160 kg
Longitudinal position of centre of gravity, x_{CG}	11.2 m	1.12 m
Roll moment of inertia, I_{Gx}	880 t.m²	8.8 kg.m²
Pitch moment of inertia, I_{Gy}	4700 t.m²	47 kg.m²
Yaw moment of inertia, I_{Gz}	4800 t.m²	48 kg.m²

The model was equipped with propeller and rudder in order to measure the influence of appendages on resultant forces acting on the hull.

When performing tests, the propeller revolution rate was set to a constant value.

Since the friction forces at full scale are smaller than at model scale, the full scale self-propulsion point was chosen instead of the model scale self-propulsion point to avoid the overestimation of the viscosity effect on the rudder.

An important part of trying to understand dynamical phenomena and their simulation is to accurately adjust the moments of inertia values. Indeed, when performing tests in waves the model was free in heave, pitch and roll, thus the recorded forces, moments and attitude are highly influenced by the roll moment of inertia, the pitch moment of inertia and loading conditions in calm water *GM*.

The moments of inertia were adjusted in the air using the compound pendulum theory. Then, by measuring the period T_M of the model oscillations, the following formulation gives the value of the pitch moment of inertia I_{Gy} expressed at the centre of gravity:

$$I_{Gy} = \nabla g \left\| \overrightarrow{OG} \right\| \left(\frac{T_M}{2\pi} \right)^2 - \nabla \left\| \overrightarrow{OG} \right\|^2 \qquad (1)$$

When using this kind of adjustment, the higher the moment of inertia, the lower the uncertainty is.

3.3 Instrumentation

Because the broaching-to phenomenon is well known to be an abrupt change of the kinematic in the horizontal plane (K.J. Spyrou, 2000, [12]), we decided to design a measurement system inspired by a planar motion mechanism (PMM), making it possible to measure forces and moments acting on the ship while she was towed in following waves

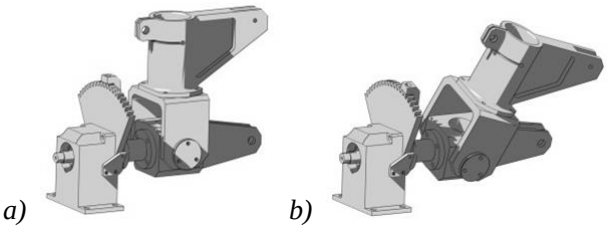

Fig. 2 - Articulation in upright position *a)*, articulation in a randomly adjusted position *b)*

As shown above in figure 2, new articulations have been designed in order to adjust the roll and pitch angles. According to the kind of test to be performed, roll, pitch and heave can be independently adjusted. Then, several combinations can be tested for roll (free or fixed), pitch (free or fixed) and heave (free or fixed).

a)

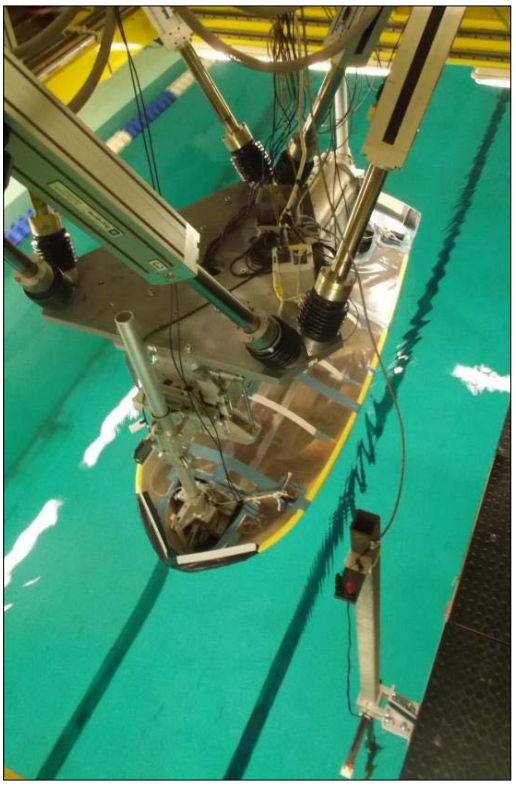

b)

Fig. 3 - *a)* Inertial setting and the mounting of the model on the dynamometer; *b)* Configuration with the *6DOF* hexapod

As shown in figure 3, the model was connected to a 6-component dynamometer by two vertical columns making possible the heave motion. The whole apparatus was mounted on a 6 degrees of freedom hexapod.

The main advantage of such a system is to make possible resistance tests, drift tests and harmonic tests (pure sway and pure yaw) both in calm water and in waves.

With the aim of studying their influence on forces and moments, following attitude parameters were measured: roll angle, pitch angle, heave motion. In parallel, surge force, sway force, heave force (if no heave motion), roll moment, pitch moment, yaw moment, thrust and torque on the propeller, lift and drag on the rudder were measured. Other parameters such as carriage velocity, motor angular rate and wave elevation were also measured at the ship's bow.

In our mathematical model, the rudder forces are modelled as external forces and there are no hydrodynamic derivatives relative to the rudder that will be defined (B. Horel et al., 2013, [13]). Thus we decided to create a 3D-printed rudder using a *NACA0015* profile whose lift and drag coefficients are knowledgeable in the literature.

4. Mathematical Model

The objective of the experiments is to express hydrodynamic derivative values of a manoeuvring model by post-processing the recorded signals. Inspired by the manoeuvring model of D. Obreja et al. [14], the mathematical model that has been established to model the broaching phenomenon is a *6DOF* model. However, towing tank tests were only used to create a *4 DOF* force model whose surge X_0, sway Y_0, roll K_0 and yaw N_0 components in calm water are defined using Taylor's series as follow:

$$X_0 = X_{\dot{u}}\dot{u} + X_u u + \frac{1}{2}X_{uu}u^2 + \frac{1}{6}X_{uuu}u^3 + X_{\dot{v}}\dot{v} + X_v v + \frac{1}{2}X_{vv}v|v| + X_{uv}uv + X_{\dot{r}}\dot{r} + X_r r + \frac{1}{2}X_{rr}r|r| + X_{ur}ur \quad (2)$$

$$Y_0 = Y_{\dot{v}}\dot{v} + Y_v v + \frac{1}{2}Y_{vv}v|v| + \frac{1}{6}Y_{vvv}v^3 + Y_{uv}uv + Y_{\dot{r}}\dot{r} + Y_r r + \frac{1}{2}Y_{rr}r|r| + Y_{ur}ur \quad (3)$$

$$K_0 = K_{\dot{v}}\dot{v} + Y_v v + \frac{1}{2}K_{vv}v|v| + K_{uv}uv + K_{\dot{r}}\dot{r} + K_r r + \frac{1}{2}K_{rr}r|r| + K_{ur}ur \quad (4)$$

$$N_0 = N_{\dot{v}}\dot{v} + N_v v + \frac{1}{2}N_{vv}v|v| + N_{uv}uv + N_{\dot{r}}\dot{r} + N_r r + \frac{1}{2}N_{rr}r|r| + N_{ur}ur \quad (5)$$

Those previous equations are the general expressions for forces acting on the hull in calm water. A significant change occurs when the vessel is navigating in following waves, so an encounter frequency dependent wave function is added to previous equations. The latter can be expressed as function of encounter frequency ω_e, relative position compared to the wave trough ξ_G/λ, wavelength to ship length ratio λ/L_{wl} and wave height to wavelength ratio H/λ.

5. Analysis Procedure

Both in calm water and while surfing in waves at zero encounter frequency, three main kinds of tests were performed and each of them has to be analyzed using one of the procedures described below.

5.1 Stationary Motion

Following stationary tests were performed for several trim and heel angles:

- Straight towing
- Straight towing with rudder deflection

X_u , X_{uu} and X_{uuu} are deduced from straight towing tests.

- Oblique towing
- Oblique towing with rudder deflection

X_v , X_{vv} , X_{uv} , Y_v , Y_{vv} , Y_{vvv} ,Y_{uv} , K_v , K_{vv} , K_{uv} ,N_v , N_{vv} and N_{uv} are calculated from oblique towing tests.

The analysis of these results is based on the averaging of the recorded signals. Samples are analysed for a minimum period of 15 seconds. The raw values are given in Volts at the reduction point of the dynamometer located around 1 meter above the model centre of gravity. Thus, once the dimensional values are calculated, it is necessary to express them in the ship coordinate system whose origin is at the centre of gravity instead of in the dynamometer coordinate system.

5.2 Harmonic Motion

Then, the following harmonic tests were also carried out for several trim and heel angles:

- Pure sway

$X_{\dot{v}}$, $Y_{\dot{v}}$, $K_{\dot{v}}$ and $N_{\dot{v}}$ are deduced from pure sway tests.

- Pure yaw

$X_{\dot{r}}$, X_r , X_{rr} , X_{ur} , $Y_{\dot{r}}$, Y_r , Y_{rr} , Y_{ur} , $K_{\dot{r}}$, K_r , K_{rr} , K_{ur} , $N_{\dot{r}}$, N_r , N_{rr} , N_{ur} are calculated from pure yaw tests.

For those tests, depending on the tank length, a minimum number of periods is needed to analyze the signals. Four sets of amplitudes A and periods T were tested: A=0.2m T=6s; A=0.2m T=9s; A=0.3m T=6s and A=0.3m T=9s.

Parts of the measured signal in-phase with acceleration and in-phase with velocity are determined using Fourier's series.

5.3 Accelerated Motion

In order to determine the added mass in surge, the following accelerated tests were performed only in calm water for several trim angles:

- Straight towing

$X_{\dot{u}}$ is deduced from straight towing tests.

This hydrodynamic derivative can only be determined once the hydrodynamic coefficients from straight towing tests are determined. In fact, the theoretical signal without acceleration is deducted from the measured signal. The remaining part is only due to acceleration and makes possible to compute $X_{\dot{u}}$.

6. Results

In this part of the paper, results in calm water and in waves will be presented. Experimental results are low pass filtered before being analyzed.

6.1 Calm Water

In the study of forces acting on the hull while performing straight towing at zero trim angle, zero heel angle and zero drift angle, figure 4 shows the comparison between measured values (blue dots) and the model. Hydrodynamic coefficients have been calculated using a polynomial regression method.

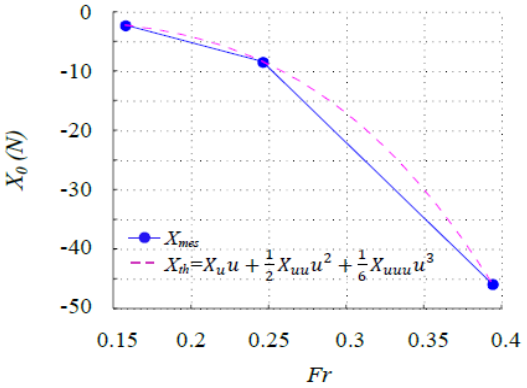

Fig. 4 - Resistance test: influence of the Froude number on the measured surge force

Then the post processing of oblique towing tests shows the influence of the sway velocity on the measured forces. From these tests, it is also possible to compute the coupling term between surge velocity u and sway velocity v. Indeed, previous studies reveal that coupling terms are relevant when trying to quantify the broaching-to phenomenon.

Oblique towing with drift angle β and constant carriage speed U_c means that sway velocity is not equal to zero, then:

$$u = U_C \cos\beta \tag{6}$$

$$v = -U_C \sin\beta \tag{7}$$

Figure 5 shows the mathematical model results compared to the experimental values. A good accordance is found when trying to fit the curves with non-linear terms. The graphs legend is as follows:

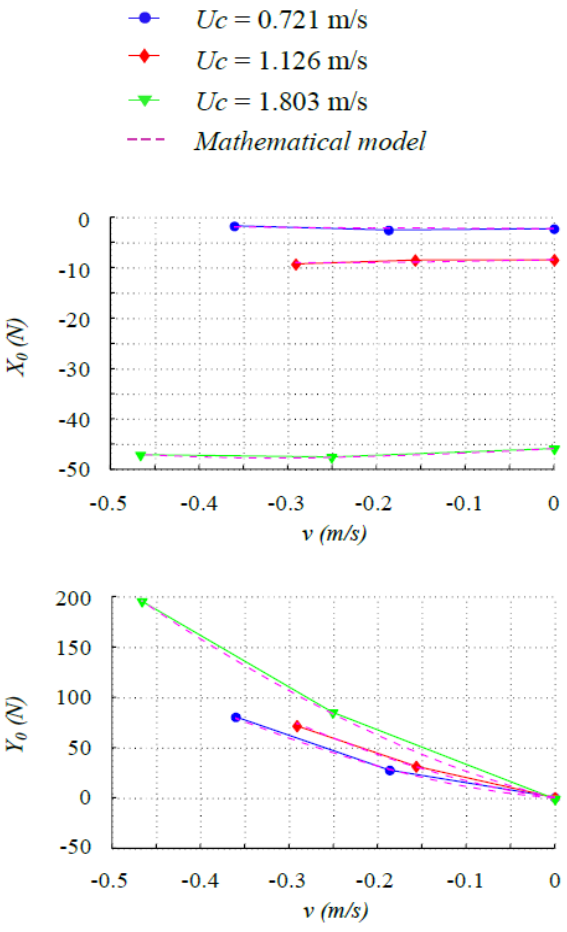

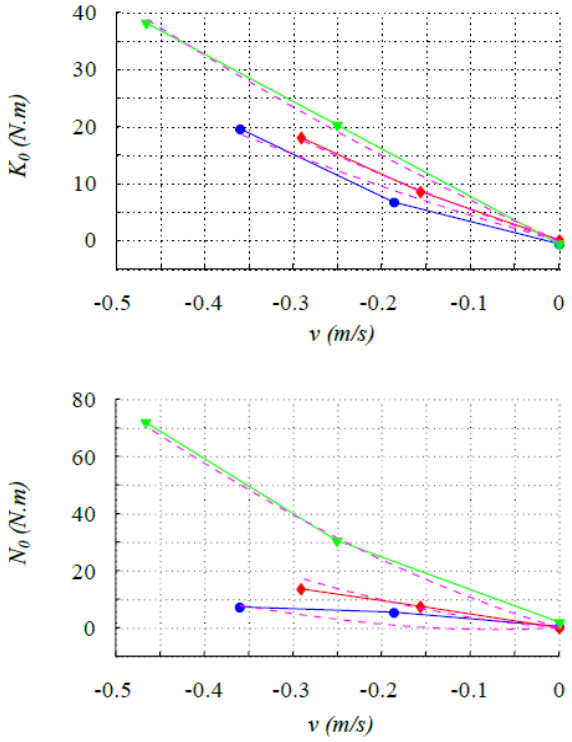

Fig. 5 - Oblique test: comparison between experimental results and mathematical model; surge force X_0, sway force Y_0, roll restoring moment K_0 and yaw moment N_0

Because our *6 DOF* model is a seakeeping and manoeuvrability coupled model, and also because the validation of the force model on the rudder is needed, we performed drift tests with rudder deflection. Influence of rudder angle δ on ship resistance for Uc=1.126m/s is shown in figure 6 below:

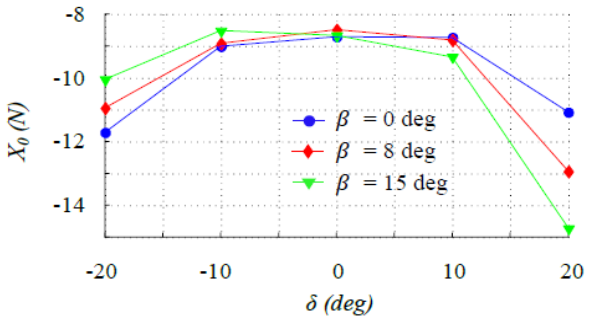

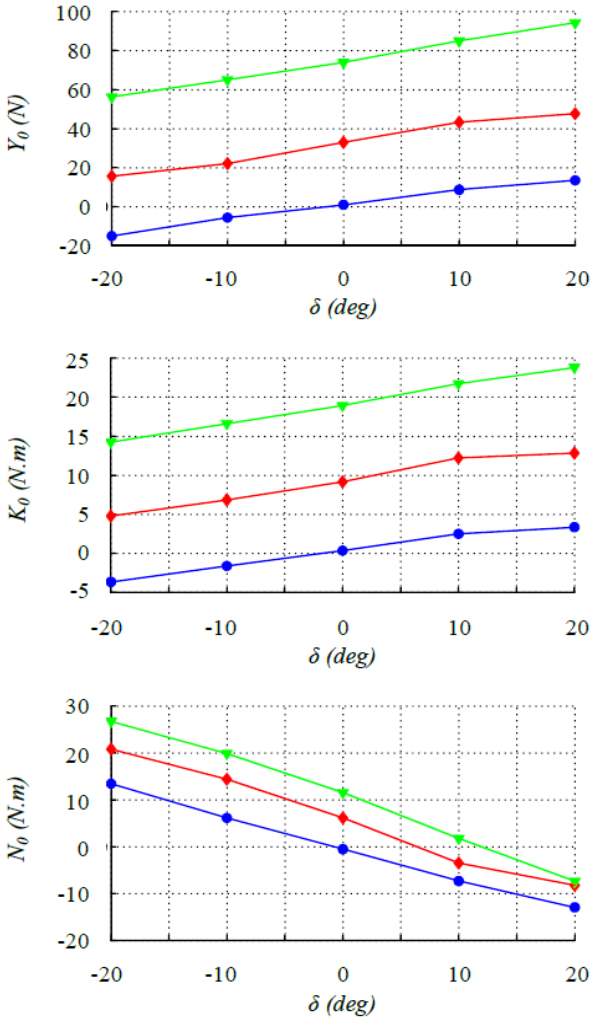

Fig. 6 - Drift tests with rudder deflection: Experimental results

The full determination of the model's hydrodynamic derivatives requires performing harmonic tests. Motions were generated using a *6 DOF* hexapod. Rotation in yaw was done at the centre of gravity around the vertical axis. Dynamometer's mass and inertia were first determined from pure sway and pure yaw tests without model. Then, deducing dynamometer effects from the recorded signal, figure 7 shows for A=0.3m and T=6s that for pure yaw tests, there is still a good agreement to be found between our model in calm water and experimental results.

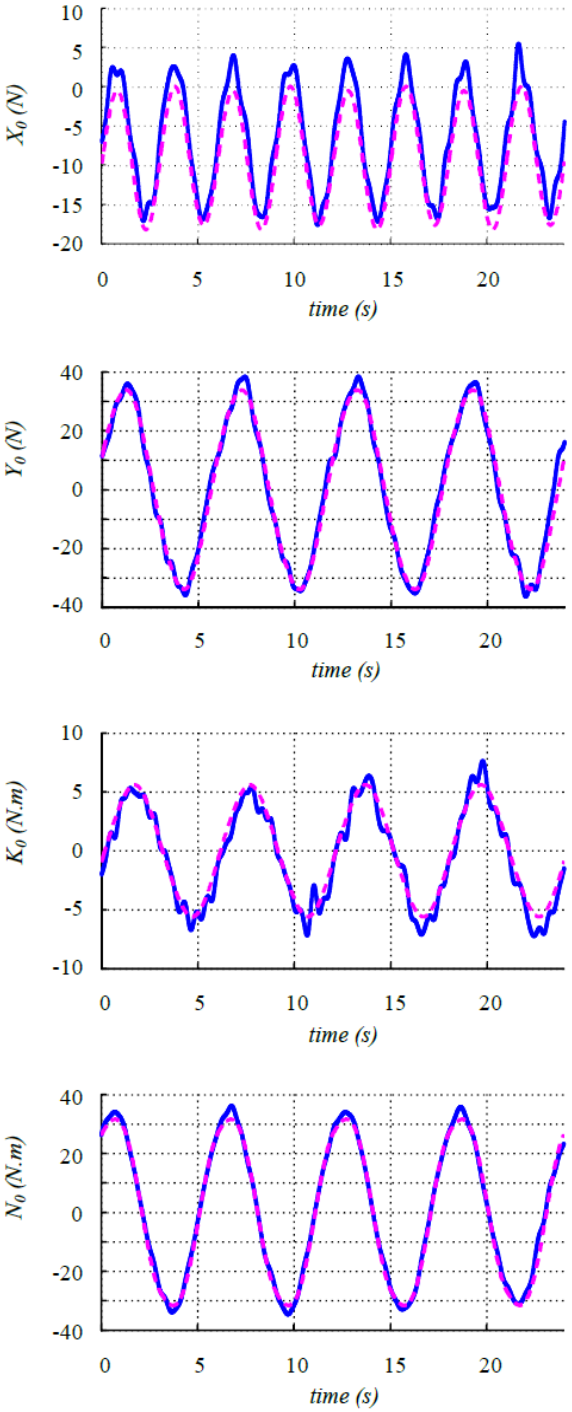

Fig. 7 - Pure yaw test: comparison between experimental results (blue line) and mathematical model (magenta dashed line)

This model in calm water is of importance because it is the basis of the mathematical model in waves.

6.2 Following Waves

Figure 8 shows a surf-riding test, while the centre of gravity of the model is located on a wave crest.

Fig. 8 - Surf-riding test while navigating on a wave crest

As previously mentioned, while surfing a wave, the experimental data have shown that forces acting on the hull can be derived from forces in calm water adding a function depending on wave parameters and encounter frequency. For instance, a first model has been developed in surge direction. The total resistance X can be expressed in terms of surge force in calm water X_0 as follow:

$$X = X_0 + \left[X_{Hc}\frac{H}{\lambda} + \frac{1}{2}X_{HHc}\left(\frac{H}{\lambda}\right)^2 + X_{\lambda c}\frac{\lambda}{L_{wl}} + \frac{1}{2}X_{\lambda\lambda c}\left(\frac{\lambda}{L_{wl}}\right)^2 + f_A(\omega_e)\right]\cos\left(2\pi\frac{\xi_G}{\lambda} + \frac{1}{2}\pi\left(20\frac{H}{\lambda} - 1\right) - f_\varphi(\omega_e)\right) + X_\lambda\frac{\lambda}{L_{wl}} + \frac{1}{2}X_{\lambda\lambda}\left(\frac{\lambda}{L_{wl}}\right)^2 - f_{offset}(\omega_e) \quad (8)$$

X_{Hc} , X_{HHc} , $X_{\lambda c}$, $X_{\lambda\lambda c}$, X_λ , and $X_{\lambda\lambda}$ are hydrodynamic derivatives.

Previous experimental tests have been done at low encounter frequency, but rarely at exact zero encounter frequency (H. Hashimoto et al., 2004 [4]). This has been possible by synchronizing the carriage start with the wave maker start. Using the dispersion

relationship for deep water waves, the wave phase celerity was known. Since the phase velocity is twice as big as the group velocity, a waiting time was needed after the wave maker started and before the carriage moved. This waiting time should be adjusted so that the centre of gravity of the model is located on a wave crest or on a wave trough.

Figure 9 shows the three different phases of a run: (1) zero carriage speed, the model is freely oscillating; (2) the carriage accelerates and the encounter frequency decreases; (3) the carriage speed is equal to the wave celerity, then the model is in surf-riding conditions.

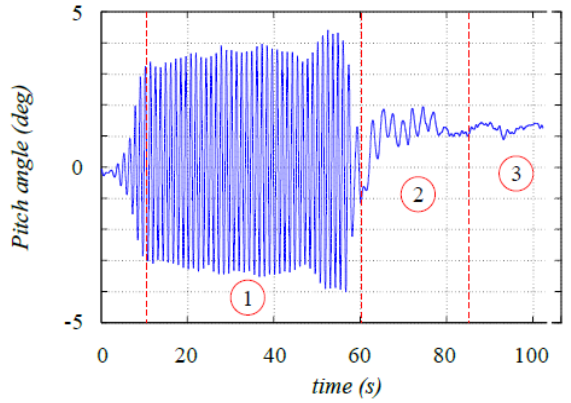

Fig. 9 - Pitch angle for $\lambda/L_{wl} = 1$ and $H/\lambda = 0.03$

Comparison between theoretical results and experimental results while the model was in surf-riding conditions is presented on figure 10.

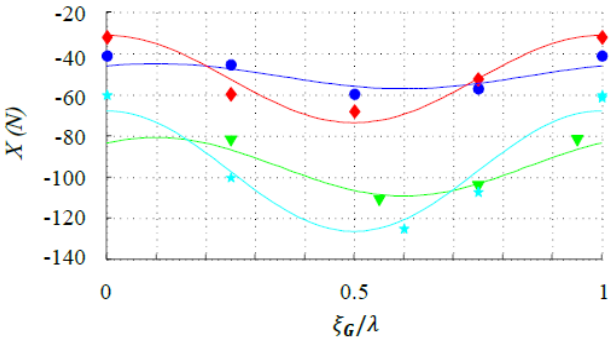

Fig. 10 - Straight towing in surf-riding conditions: surge force as a function of model position on the wave ($\xi_G/\lambda = 0$ at the wave trough; $\xi_G/\lambda = 0.5$ at the wave crest)

The legend used in the graph is as follow:

- *Experimental values for* $H/\lambda = 0.03$ *and* $\lambda/L_{wl} = 1$
- *Experimental values for* $H/\lambda = 0.05$ *and* $\lambda/L_{wl} = 1$
- *Experimental values for* $H/\lambda = 0.03$ *and* $\lambda/L_{wl} = 1.25$
- *Experimental values for* $H/\lambda = 0.05$ *and* $\lambda/L_{wl} = 1.25$
- *Mathematical model for* $H/\lambda = 0.03$ *and* $\lambda/L_{wl} = 1$
- *Mathematical model for* $H/\lambda = 0.05$ *and* $\lambda/L_{wl} = 1$
- *Mathematical model for* $H/\lambda = 0.03$ *and* $\lambda/L_{wl} = 1.25$
- *Mathematical model for* $H/\lambda = 0.05$ *and* $\lambda/L_{wl} = 1.25$

While the ship is surfing near the wave trough, it appears that the measured resistance force is lower than at the wave crest. This phenomenon can be explained since in that position, the ship is in stationary conditions where she is pushed forward by the wave from the stern.

Since our model is relatively accurate for zero encounter frequency, further analysis has been done in order to distinguish 3 main modes of motion: the ship is overtaken by the wave, the ship is in stable surf-riding and the ship slowly overtakes the wave. This implies taking into account the effect of the encounter frequency ω_e into the mathematical model. The encounter frequency is calculated as follow, with V_φ the phase velocity of the wave and λ the wavelength:

$$\omega_e = 2\pi \frac{|V_\varphi - U_C|}{\lambda} \qquad (9)$$

Then, figure 11 shows that a good correlation is obtained in terms of mean value, amplitude and phase with the experimental results. Thus, the effect of non-linear functions $f_A(\omega_e)$, $f_{offset}(\omega_e)$ and $f_\varphi(\omega_e)$ is relevant when trying to simulate the ship's behaviour in following seas.

- The ship is overtaken by the wave:
  - *Experimental values for* $\omega_e = 2.2\ rad/s$
  - *Experimental values for* $\omega_e = 0.8\ rad/s$
  - *Experimental values for* $\omega_e = 0.3\ rad/s$
  - *Mathematical model for* $\omega_e = 2.2\ rad/s$
  - *Mathematical model for* $\omega_e = 0.8\ rad/s$

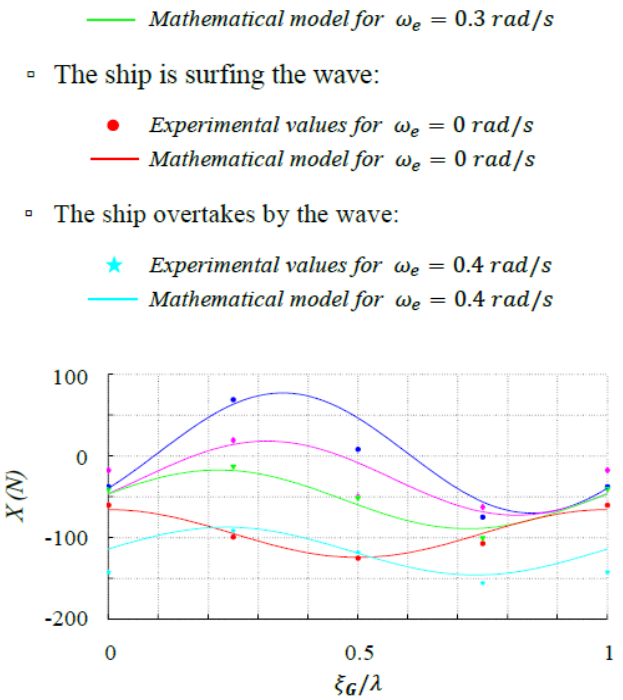

Fig. 11 - Straight towing in regular waves: surge force X plotted as function of ship position for $\lambda/L_{wl} = 1.25$ and $H/\lambda = 0.05$

7. Conclusions

Experimental and numerical studies are complementary when trying to understand a physical phenomenon since mathematical models are established from observations. There still are some recorded samples from the database that need to be post processed. For instance, pure sway and pure yaw tests while surfing regular waves need to be analyzed in order to give some quantified values to describe the broaching-to phenomenon.

However, a close correlation has been observed between the first results of our non-linear mathematical model and experiments. Once all measured data has been post-processed, and the hydrodynamic coefficients fully determined, it will be interesting to predict the ship's behaviour in following waves.

This work shows that captive model tests such as straight towing tests, oblique towing tests and several harmonic tests both in calm water and in following waves for different encounter frequencies and also at zero encounter frequency can be performed using the innovative measurement system we designed.

Future works will be done to validate our numerical-experimental *6 DOF* hybrid model by comparing the predicted behaviours with recorded behaviours from free-running model tests that will be carried out in the seakeeping and manoeuvring basin of the LHEEA. Then, quantitative values describing the surf-riding and broaching-to phenomena might be established and proposed to create new intact stability criteria.

Acknowledgments

This work is supported and funded with a PhD scholarship from DGA (Direction Générale de l'Armement) and the Pays de la Loire region.

Experiments have been performed thanks to the technical staff of the LHEEA basin.

References

[1] C. Wandji, P. Corrignan: Test Application of Second Generation IMO Intact Stability Criteria on a Large Sample of Ships, Proceedings of the 11th International Conference on the Stability of Ships and Ocean Vehicles, 2012.

[2] S. Hosseini, P. Carrica, F. Stern, N. Umeda, H. Hashimoto, S. Yanamura, A. Matsuda: CFD, system-based and EFD study of ship dynamic instability events: Surf-riding, periodic motion, and broaching, Ocean Engineering, Vol. 38, 2010, pp. 88-110.

[3] N. Umeda, A. Matsuda, M. Hamamoto, S. Suzuki: Stability assessment for intact ships in the light of model experiments, Journal of Marine Science and Technology, 1999, pp. 45-57.

[4] N. Umeda, H. Hashimoto, A. Matsuda: Broaching prediction in the light of an enhanced mathematical model, with higher-order terms

taken into account, Journal of Marine Science and Technology, 2003, pp. 145-155.

[5] H. Hashimoto, N. Umeda, A. Matsuda: Importance of several nonlinear factors on broaching prediction, Journal of Marine Science and Technology, 2004, pp. 80-93.

[6] Z. Ayaz, D. Vassalos, K.J. Spyrou: Manoeuvring behavior of ships in extreme astern seas, Ocean Engineering, 2005, pp. 2381-2434.

[7] R. Skejic, O.M. Faltinsen: A unified seakeeping and maneuvering analysis of ships in regular waves, Journal of Marine Science and Technology, JASNAOE, 2008.

[8] N. Umeda, S. Yamamura, A. Matsuda, A. Maki, H. Hashimoto: Model Experiments on Extreme Motions of a Wave-Piercing Tumblehome Vessel in Following and Quartering Waves, The Japan Society of Naval Architects and Ocean Engineers, 2008.

[9] S. Hosseini: CFD prediction of ship capsize: parametric rolling, broaching, surf-riding, and periodic motion, dissertation, University of Iowa, 2009.

[10] H. Hashimoto, N. Umeda, A. Matsuda: Broaching prediction of a wave-piercing tumblehome vessel with twin screws and twin rudders, Journal of Marine Science and Technology, 2011, pp. 448-461.

[11] Transportation Safety Board of Canada: Chavirement avec perte de vie du petit bateau de pêche Le Marsouin I, report number M09L0074, 2009.

[12] K. J. Spyrou: The nonlinear dynamics of ships in broaching, Marie Curie Fellowships Annals, Vol. 1, 2000.

[13] B. Horel, P.E. Guillerm, J.M. Rousset, B. Alessandrini: A method of immersed surface capture for broaching application, Proceedings of the ASME 2013 32nd International Conference on Ocean, Offshore and Arctic Engineering, 2013.

[14] D. Obreja, R. Nabergoj, L. Crudu, S. Pacuraru-Popoiu: Identification of hydrodynamic coefficients for manoeuvring simulation model of a fishing vessel, Ocean Engineering, Vol. 37, 2010, pp. 678-687.

Air Pressure Scale Effects during Damage Model Tests

[*]Gyeong Joong Lee[1], Frans van Walree[2], Arthur M. Reed[3], Andrew Peters[4], Paola Gualeni[5], Toru Katayama[6], and WenYang Duan[7]

1. *KRISO, Korea*
2. *MARIN, Netherlands*
3. *NSWC, USA*
4. *QinetiQ, UK*
5. *University of Genoa, Italy*
6. *Osaka Prefecture University, Japan*
7. *Harbin Engineering University, China*

Abstract: The Stability in Waves committee of the 27th ITTC has investigated the significance of scale effects in air pressure on flooding model tests under atmospheric conditions. For this purpose, the committee classified the flooding cases into the trapped air case and vented air cases, and investigated the flooding process for a simple geometry using the state equation of air and the orifice equation. As a result, the committee concluded that the scale effect is large for the case of trapped air and small vent area. For the other cases, the effect is small and can therefore be neglected in the model test of a damaged ship. The committee further proposed some guidelines that can be used to reduce the scale effect of air pressure.

Key words: Scale effect of air, damage model test, depressurised wave basin

1. Introduction

One of the tasks of the committee on Stability in Waves of the 27th ITTC is to investigate the scale effect due to air pressure on damage model test and to update the ITTC Recommended Procedure 7.5-02-07-04.2 "Model Tests on Damage Stability in Waves". The procedure provides guidelines for carrying out model tests on a damaged ship in irregular waves to determine the probability of capsizing or the significant wave height that will cause the model to capsize in a fixed time period. If there is a compartment of the model which is not vented, and this compartment has a large effect on damage stability, scale effects due air pressure may be important. However, most damage model tests are carried out in atmospheric conditions. Model testing under scaled air pressure is not customary; there is one facility suited for such tests among the ITTC member facilities. Ypma (2010) reported a comparison of the model test in atmospheric and reduced air pressure conditions and the difficulties of model testing in such conditions.

The Stability in Waves committee has investigated the significance of scale effects in air pressure on flooding model tests under atmospheric condition. For this purpose, the committee classified the flooding cases into the trapped air case and the vented air case, and investigated the flooding process for a simple geometry using the state equation of air and the orifice equation.

In the case of trapped air, the scale effect due to air pressure is significant regardless of the damage opening size. In the case of vented air, the scale effect is dependent of the size of the vent area. The ratio of the vent area to the damage area plays an important role in the flooding process. When this ratio is large, i.e. a large vent area, the scale effect turns out to be small. For the small vent area, the scale effect is large

*** Corresponding author:** Gyeong Joong Lee, Principal Researcher, research fields: ship dynamics. E-mail: gjlee@kriso.re.kr

during the initial stage, and as time passes the scale effect becomes small. In order to reflect the damage model test procedure, in which the model is initially set in equilibrium condition, the effects of assuming the air compression process to be isothermal or adiabatic were investigated after setting the inner air pressure to be equal to the outside water pressure at the position of damage opening. The scale effect is small in this case for both isothermal and adiabatic processes.

As a result, the committee concluded that the scale effect is large for the case of trapped air and a small vent area. For the other cases, the effect is small and can therefore be neglected during model tests. Furthermore the committee proposed some guidelines that can be used to reduce the scale effect of air pressure.

2. Model Test and Scale Factor

Damage model testing is carried out under the Froude hypothesis. If the Froude number is set to be the same in full scale and model test, there is a dynamic similitude. The Froude number,

$$F_n = \frac{V}{\sqrt{gL}} \tag{1}$$

is the ratio of inertia force and gravitational force. Let the scale factor λ be the ratio of ship length to model length. Then the physical quantities follow the scale laws below.

$$\frac{L_s}{L_m} = \lambda, \quad \frac{V_s}{V_m} = \sqrt{\lambda}, \quad \frac{t_s}{t_m} = \sqrt{\lambda}$$
$$\frac{\omega_s}{\omega_m} = \frac{1}{\sqrt{\lambda}}, \quad \frac{p_s}{p_m} = \lambda \tag{2}$$

where L is length, V velocity, t time, ω frequency, p pressure, and the subscript 's' means the full scale ship and 'm' means the model. In order to follow the scale rule, the pressure head of the model should be reduced by 1/λ, and the atmospheric pressure should reduce accordingly.

The water flow through an opening is usually represented by the orifice equation

$$q = C_D \rho_w A \sqrt{2(g\Delta h + \Delta p_a / \rho_w)}, \tag{3}$$

where C_D is the discharge coefficient of the opening, ρ_w the density of water, A the area of opening, Δh the difference of water pressure head, Δp_a the difference of air pressure in and out. Using water with the same density under the same gravity, the flow rate obeys the scale rule provided that the air pressure follows the scale rule of 1/λ.

The model scale pressure should be 1/λ of the atmospheric pressure in order to maintain dynamic similitude. This is possible only in a depressurised tank facility. Most model basins can only test in atmospheric air conditions, not under scaled air pressure. Figure 1 reveals conceptually the difference in pressure head between the scaled air pressure model test and atmospheric model test.

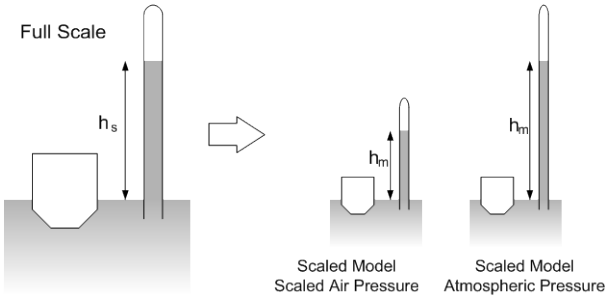

Figure 1 Concept of scaled model test

3. Scale Effects in Air Pressure

There are some cases in which the flooding of a ship is affected by the air pressure inside the vessel. The main contribution of air pressure takes place in the trapped air case and the vented air case with small vent area. In a model test with a damaged ship, if the air pressure is maintained at atmospheric pressure, then scale effects in air pressure occur.

For the trapped air case, the pressure of the model in atmospheric conditions is higher than in scaled pressure. Therefore, the flooding to that compartment is restricted as shown in the Figure 2.

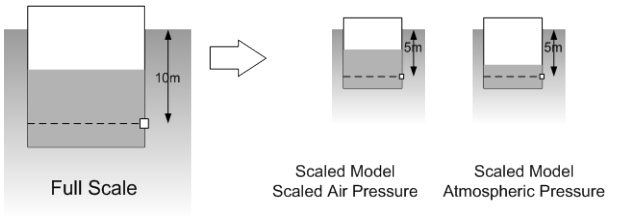

Figure 2 Flooding in trapped air case

For the vented air case, the air will be compressed and the internal pressure increases. The pressure in atmospheric conditions is higher than in scaled air pressure, so the flooding speed will be slower than in scaled air pressure. Therefore the following situation will occur, Figure 3.

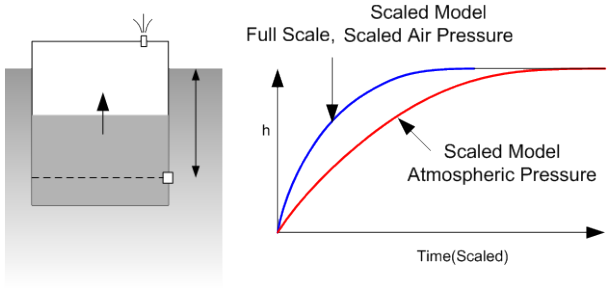

Figure 3 Flooding in vented air case

We can simulate the above situation by using the state equation of air.

$$PV^{\gamma} = const. \tag{4}$$

where P is absolute pressure of the air, V is the volume under consideration, and γ is the ratio of specific heat, in the case of air it is 1.0 for an isothermal process and 7/5 for an adiabatic process. The flow through an opening can be estimated by the orifice equation.

Figures 4, 5 and 6 show the water height as a function of the scaled time in the case of trapped air case for a small opening and a large opening in the compartment bottom.

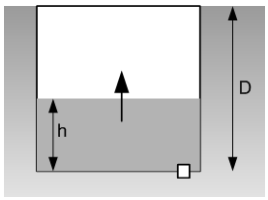

Figure 4 Schematic drawing for flooding in non-vented air case

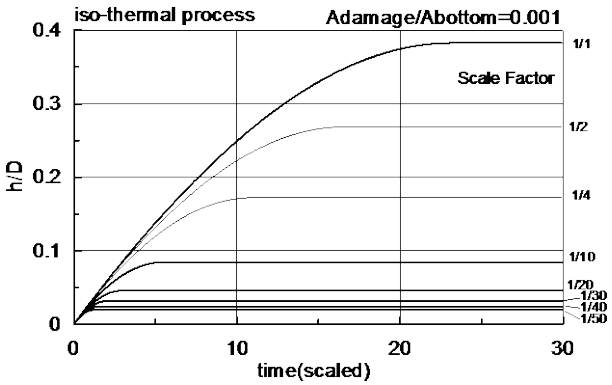

Figure 5 Flooding in non-vented air case for a small opening

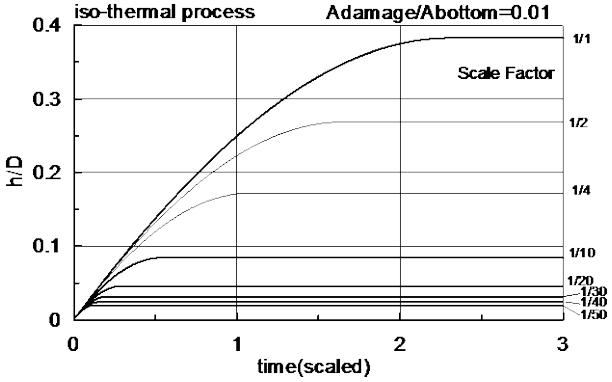

Figure 6 Flooding in non-vented air case for a large opening

The above two figures are exactly same except for the time scale. This time scale difference comes from the opening area ratio. As one over the scale ratio becomes small, the final water height reduces also. In this case, the scale effect of air pressure is significant regardless of the damage size.

For the vented case, Figures 7 to 10 show the density ratio of the air and the water height during the flooding process.

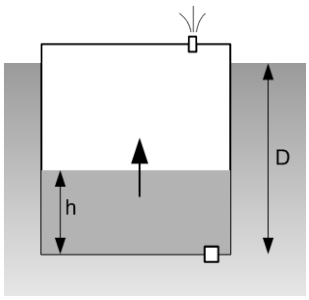

Figure 7 Schematic drawing for flooding in vented air case

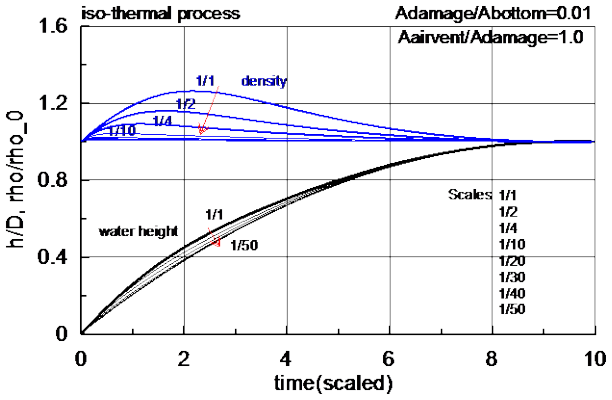

Figure 8 Flooding in vented air case for a large vent area

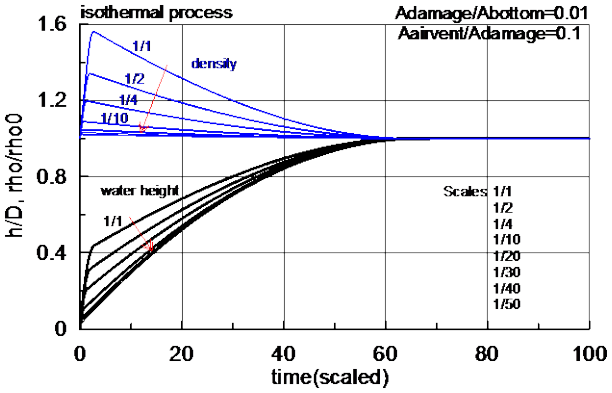

Figure 9 Flooding in vented air case for a medium vent area

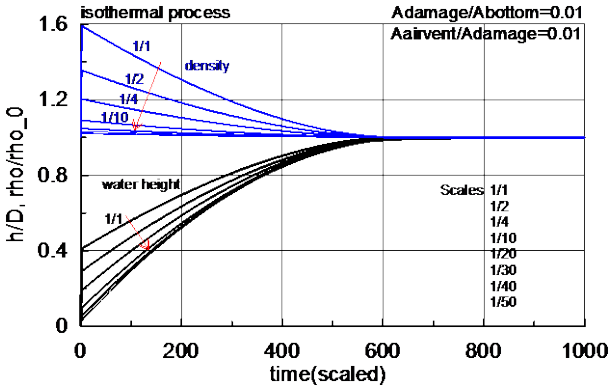

Figure 10 Flooding in vented air case for a small air vent area

The ratio of the vent area to the damage area plays an important role in the flooding process. When this ratio is large, i.e. a large vent area, the scale effect turns out to be small. For the small vent area, the scale effect is large during the initial stage, and as time passes the scale effect becomes small.

In order to reflect the damage model test procedure in which the model is initially set in equilibrium condition, the effects of assuming the air compression process to be isothermal or adiabatic can be simulated after setting the inner air pressure to be equal to the outside water pressure at the position of damage opening. For this purpose, the pressure of the compartment is set to the outside water pressure initially for the vented case. Figures 11 and 12 show the flooding process of the isothermal and adiabatic processes, respectively.

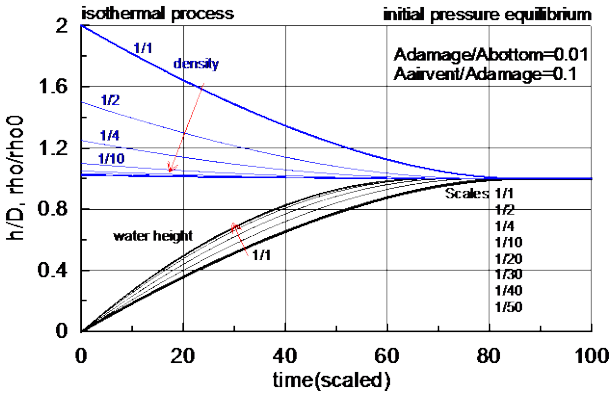

Figure 11 Flooding for the isothermal process; when the air pressure was initially balanced.

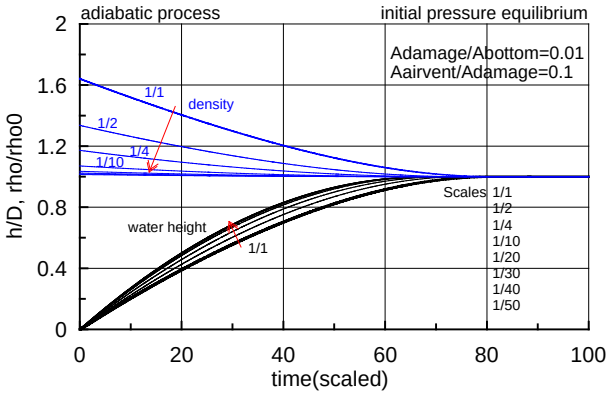

Figure 12 Flooding for the adiabatic process; when the air pressure was initially balanced.

If the flooding speed is low, the air compression process will be isothermal, and if the speed is high the adiabatic process can be applied. When a damaged ship with a large damage opening floats in waves, the flooding due to wave and ship motion is relatively fast, so an adiabatic process takes place in the air compression process. The Figures 11 and 12 show that then the scale effect is not large.

In line with the above discussion, it can be concluded that the scale effect is large for the case of trapped air and a small vent area. For the other cases, the effect is small and can therefore be neglected in the model test of a damaged ship.

In atmospheric conditions, it is possible to use alternative methods to reduce the scale effect due to the air pressure. For the case of a small vent area, the vent opening can be enlarged to an appropriate size in order to reflect the inflow and outflow of the full scale situation. For the case of trapped air, a simple solution would be to attach a balloon or a flexible membrane to the compartment in order to reduce the scale effect of air pressure, and to obtain realistic flooding results in the test condition.

4. Conclusions

In summary, if the damage opening is large and the compartment is well vented the scale effect of air pressure will be small, and model tests in atmospheric conditions are suitable. The scale effect will be large in the trapped air case and small vent area case. In that situation, if precise and accurate test results are required, the use of pressure regulation values on the compartments to control the internal pressure or model tests in a depressurised model basin are solutions. As a minimum, in the case of model tests under atmospheric conditions modifications are recommended to reduce the scale effects.

The ITTC model test procedure for damage stability experiments was updated to reflect the above discussion.

Acknowledgments

The aim of this paper is to introduce the work of ITTC Stability in Waves committee on the damage model test. The present paper is based on the SiW report to the 27th ITTC.

References

[1] Committee on Stability in Waves, 2014, Final Report and Recommendations to 27th ITTC, 27th ITTC.

[2] MARIN, 2013, Depressurised Wave Basin, Leaflet V2013/05/29, MARIN

[3] Ypma, E., (2010), “Model tests in atmospheric and vacuum conditions”, FLOODSTAND Project Report D2.5b

Forensic Study of *BOUVET* Capsizing

Jean-Yves BILLARD[1], François GRINNAERT[1], Isabelle DELUMEAU[1], Pierre VONIER[2], Paul CREISMEAS[2], Jean-François LEGUEN[2] and *Larrie D. FERREIRO[3]*

1. *Ecole Navale, Lanvéoc-Poulmic, France*
2. *DGA Hydrodynamics, Val de Reuil, France*
3. *Defense Acquisition University, Fort Belvoir, Virginia USA*

Abstract: The paper deals with the capsizing of the French pre-dreadnought *Bouvet* during World War One (WWI). If the circumstances of the drama were clear, the reasons for the capsizing -- both concerning the stability of the ship and the nature of the device -- were not, and few hypotheses can be found in the literature. The aim of this work is to clarify those hypotheses and to test modern tools against this rather well documented event. For that purpose both numerical computations and experiments have been planned. Part of them have been performed and reported in the present paper.

Key words: Damaged stability, History of naval architecture, stability criteria, experiments

1. Introduction

Bouvet was a French ironclad launched in 1896, she had been chosen with other ships of a similar design to fight an important battle in the Dardanelles Strait. She sunk after an explosion caused either by a mine or an artillery shell on the 18th of March 1915. According to all the testimonies she sunk in less than a minute. The rapidity of the drama revealed her very poor stability. During World War One many other ironclads shared the same fate. These problems had been considered as a proof that warships built prior to HMS *Dreadnought* were dangerous, because they were not able to survive damage to their intact stability, annulling their military value. With these ships, it was argued, all-out naval warfare in the Mahanian style was impossible.

A deep silence surrounding the utility of pre-dreadnoughts even after the war shrouded the sinking of ironclads. Many historians have described ironclad of the late XIXth century [1-3] but very few have tried to put them back into the context of the war they had to fought, questioning how their military value was perceived by strategists and headquarters.

2. Historical information

2.1 The ship

As shown on figure 1, *Bouvet's* hull form is characterized by considerable tumblehome and with a counter stern, seen today in the US destroyer DDG 1000 *Admiral Zumwalt*.

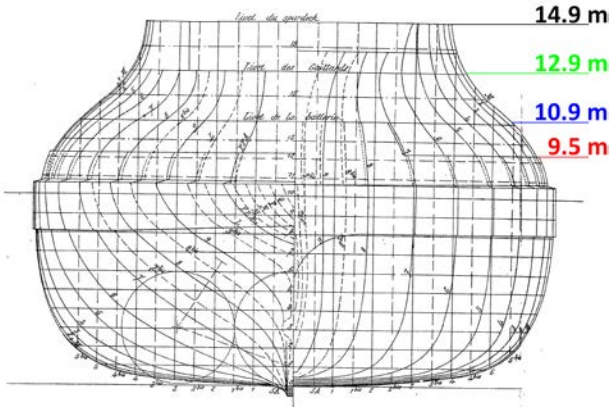

Fig.1: battleship Bouvet hull form.

Thanks to the SHD (Service Historique de la Défense, the historical service of the French ministry of defense) most of the plans are available and historical bibliography gives access to some

hydrostatics calculation [4]. The main particulars of the ship are given in table 1.

Table 1 Battleship *Bouvet*, main particulars

Length over all (m)	122.6
Full displacement (t)	12, 220
Beam over all (m)	21.4
Mean draft (m)	8.0

2.2 The dramatic battle

In fighting operations against Turkish coastal artillery the ship was struck either by a floating mine or an artillery shell, below the starboard 274 mm turret. According to the testimonies the ship capsized to starboard in 55 seconds with an initial forward speed of about 12 kts. Out of a total crew of 668 men, only 64 survived.

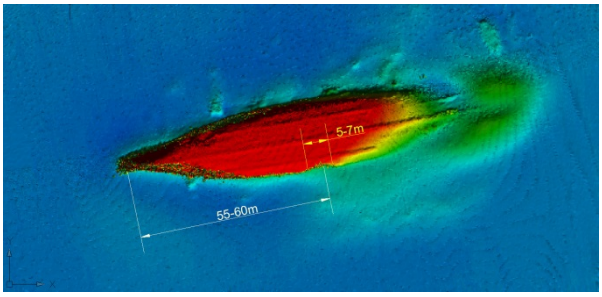

Fig. 2: Sonar image of the wreck from Turkish salvage team

This case study is very interesting because the ship sank in well-known conditions (there are even pictures of the disaster, see figure 3). Also, this case was among those of several other warships whose rapid capsize was to prove the necessity of developing damaged stability rules for warships.

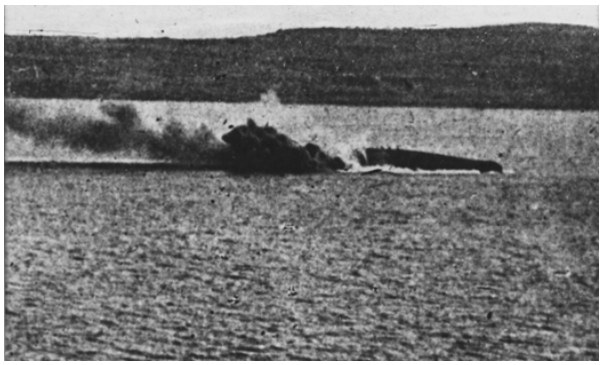

Fig. 3: Picture of the capsizing of Bouvet the 18th Mars 1915 taken from HMS Agamemnon.

2.3 The theory of stability in a military environment. The contribution of French engineers at the beginning of the XXth Century

At the verge of WW1 the Service de Construction Navale (SCN) of the French navy was divided over the use of models and theories to represent warships [5]. The first group, primarily older and experienced engineers, was still following empirical methods and doubted that the calculation of dynamic stability made with wooden models could be used to qualify a ship as stable or not. The second group of younger but capable engineers were developing new methods and were aware that dynamic stability was as much as determinant for safety as was intact stability. Chief among these engineers was Louis-Emile Bertin (fig. 4), who had defended and popularized this idea among the public and denounced the general design of warship built at the end of the XIXth Century, which he said had “feeble stability” [6]. He stated the theory that the military value of a warship depends on survivability, meaning stability after damage. Louis-Emile Bertin was the initiator of the first French towing tank, the *Bassin d’essais des carènes* build in 1906 in Paris (now named DGA Techniques Hydrodynamiques located in Val de Reuil). He had greatly contributed to ship construction. He developed the method of experiment on wooden model. The model is provided with a movable disc displaced transversely by a fixed screw in order to precisely measure the motion of a calibrated weight. There is also a long vertical arm pendulum in order to measure the angle of heel. To study the damaged case, as wooden model is constructed with floodable compartments. Unfortunately we have not yet found examples or pictures of these models.

In 1894, Bertin knew already that more mathematical methods existed, for example mechanical integrators, but he found his method of using models easier, more flexible, less expensive, no more time consuming (he expected 2 months to study a new design as with others methods) and more adapted to damaged stability.

Fig. 4: Louis-Emile BERTIN (1840-1924).

2.4 The drama of the *Bouvet* had been anticipated

The case of the *Bouvet* is interesting also because this is a good example to describe and understand how safety progresses in a military environment. The situation is different than the one that occurs in merchant navy where the market and the recommendation of insurance companies exert pressure on shipping. In the Navy the process of technical change in safety is rather different; in this case a dramatic event had been necessary to make decision-makers realize what the uselessness of the pre-dreadnought fleet. The loss of the *Bouvet* showed clearly the way but many hints could have been analyzed before the drama.

Before the war several commanding officers of the *Bouvet* had the intuition that the flooding of some compartments would endanger her. The longitudinal bulkheads had been pointed out as a particular hazard that would cause off-center flooding. In order to reduce the risk, transverse cross-flooding connection had been built to avoid heel angle after damage in the engine room. The crew made strong efforts to increase maximum initial stability by placing coal and heavy tackle low in the ship. Initial stability that was judged too small at the time would be seen as good enough from our modern eyes (GM greater than a meter). It seems that for them initial stability was more a matter of steadying the ship platform during gunfire than avoiding capsize. Moreover, the damaged stability of a ship compartmented as the *Bouvet* had been studied completely in 1899. The prescient conclusion of the engineer Maugas [7] was that the ship might sink if the hull suffered any damage.

During the Dardanelles fight, others warships had been damaged. One of them was the *Gaulois*, which had been hit by shellfire and repaired at Toulon. While in the shipyard, it was fitted with an above-water wooden caisson to improve the stability after damage, the direct result of the Navy's learning from the experience of the *Bouvet.* This happened just in time, as the *Gaulois* was torpedoed several months later on the 26th December 1916, and the caissons were credited with keeping the ship upright and afloat long enough to evacuate the crew [8].

3. The project

Main issues

From a technical point of view it was important to performed experiments to use the sinking of the *Bouvet* as a validation case for up-to-date damaged stability software codes. Moreover the example of the *Bouvet* is relevant for others reasons. It has brought to light how to study how military staff perceived the military value of the ships they had to engage in the Great War. The Dardanelles fight is for the French Navy the moment officers realized that

pre-dreadnoughts had no military value and the strategy had had to be totally revised. Finally, the example of the *Bouvet* is very relevant to model the process of technical change in safety procedures in a military environment especially at a time when market and insurance input were inexistent. It is clear that the dramatic fate of pre-dreadnought ships had been taken in account by engineers to create rules and norms for warship stability.

3.1 Ship configuration

A four-meter long model of the *Bouvet* was built and the static stability fully explored. Experiments have been performed in calm water without forward speed. The progressive flooding represents different configurations and internals arrangements. Experiments and numerical calculations have been performed on different cases. A view of the internal arrangement in the workshop is shown on figure 5 where the two starboard boiler rooms separate by a cofferdam (on axis) and starboard 274 mm ammunition room can be seen.

Fig. 5:Iinternal arrangement.

This arrangement represents the area of the ship shown on the original plan presented on figure 6 where all the compartments experimentally modeled have been underlined and the position of the explosion (mine or shell) positioned.

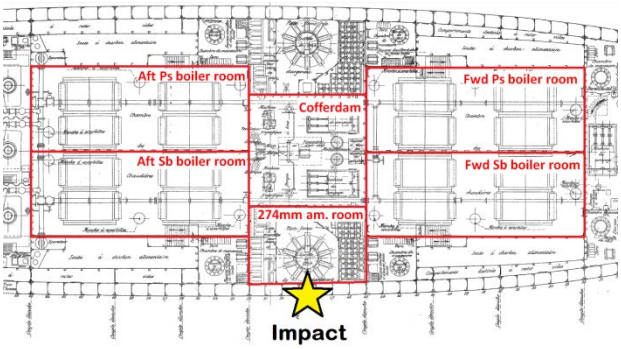

Fig. 6: Detail of the general arrangement in the area of impact.

At the location of the impact, a watertight door seals the ammunition compartment. At the beginning of the experiment the door is opened and the ammunition room open to flooding. Water can then flood a variety of compartments defined by bulkheads. Moreover to determine the movements of the ship, the model has been fitted with 6 reflecting spheres which can be seen in figure 12. We used a tracking system consisting of 4 infrared cameras and software that plots the position of the ship every 1/100 second.

3.2 Numerical computations

As we began the study, we attempted to determine how 19th century engineers defined watertight volume used for the determination of GZ curve. This proved very difficult to determine. Performing hydrostatic calculations it has been found that GZ original curves correspond to the whole closed volume of the ship. The same evidence has been found on other ships of the same period (*Gaulois*, *Charlemagne*), the first one has been hit by a shell during the same operation and went to ground on Rabbit Island and the second faced stability problems during turning experiments in the bay of Brest (about 30° of heel at 12 kts and 15° helm)[9]. To build a curve with the same shape and

the same vanishing stability angle we have progressively modified the watertight deck and obtained the result shown in figure 7 when the watertight volume has been limited by the uppermost deck. In these conditions (which seem rather optimistic...), we have obtained very similar curves even if in the range 20-40° the 1913 computations lead to underestimation of results obtained by modern numerical methods.

During this study the bibliography has been explored unsuccessfully to find regulations that applied to that kind of ship. From our computations we deduced that all the closed volume was used to define the GZ curve, even if this volume is far from watertight as determined by the criteria used today to define the watertight deck or the exposed deck.

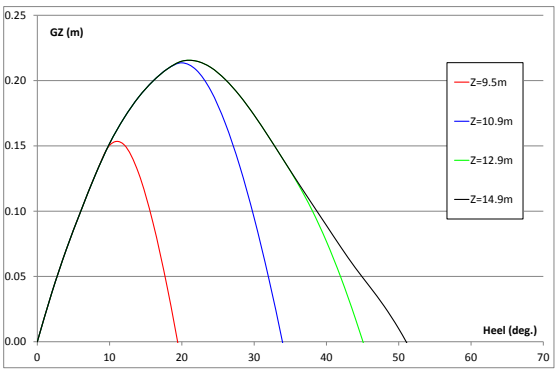

Fig. 7: Effect of watertight deck height on GZ curves.

The full GZ curve shown on figure 8 shows that the intact stability was quite poor, actually better when the ship was upside down! The estimated angle of vanishing stability was about 55° and the initial GM of about 1 m, but the GZmax value is of only 0.2 m. The two first parameters are not so bad but the third is catastrophic.

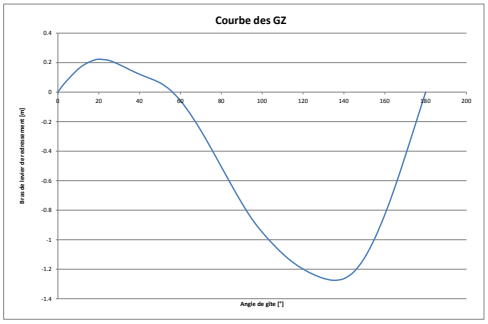

Fig. 8: Full GZ curve watertight deck at 14.9 m.

Stability in damaged conditions has been computed too. As discussed previously, the watertight intact volume is uncertain and the progressive flooding is unknown. Thus computations have been performed using different hypothesis concerning the watertight deck (10.5 m and 14.9 m) and the flooded volume (starboard ammunition room only and starboard ammunition room and cofferdam). The value of 10.5 m is adopted from the height of the armored deck which was fitted with a 1 m height coaming surrounding the deck. This value has been used to build the model. Watertight volumes corresponding to the different hypothesis are given on figure 9.

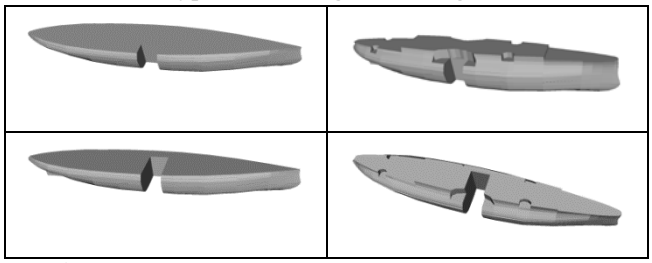

Left column: Watertight deck 10.5 m
Right column: Watertight deck 14.9 m
First row: Starboard ammunition room flooded
Second row: Starboard ammunition room and cofferdam flooded

Fig. 9: Watertight volumes.

Results are given on figures 10 and 11.

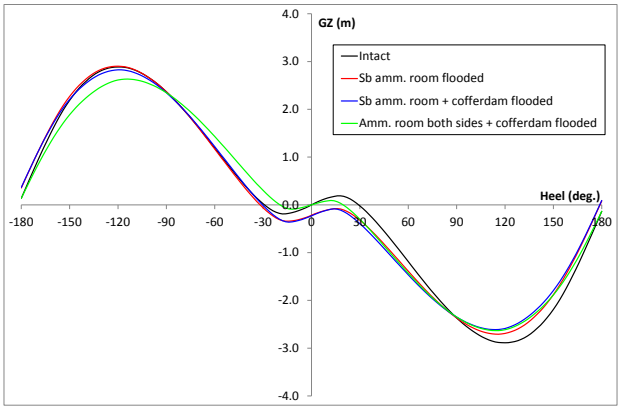

Fig. 10: GZ curves for watertight deck positioned at 10.5 m.

It can be seen that whatever the hypothesis the capsizing was certain; the only equilibrium position corresponds to 175° of heel. The experiments will give an insight, using the time to sink, to define the right hypothesis.

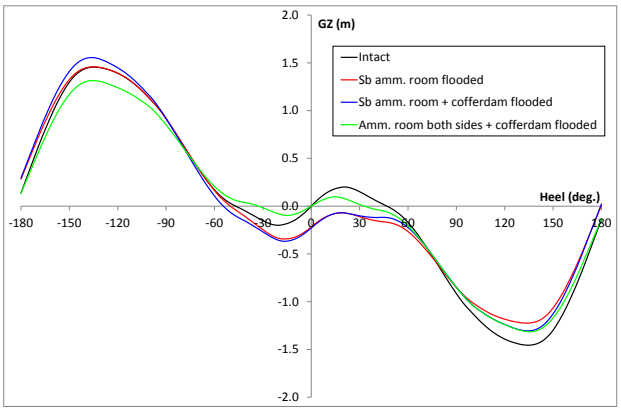

Fig. 11: GZ curves for watertight deck positioned at 14.9 m.

3.3 Experimental investigations

The model allows a modification of the internal arrangement that can lead to different flooding configurations. The model is shown on figure 12.

Fig. 12: Model during tests in the tank.

The flooding configurations that will be tested are the following:

Case 1 : Starboard ammunition room only

Case 2 : Starboard ammunition room with cofferdam

Case 3 : Case 2 + Starboard boiler rooms (fore and aft)

Case 4 : Case 2 + Starboard forward boiler room

Case 5 : Case 2 + both forward and aft boiler rooms

At this time, only succinct analysis has been performed. The repeatability of the measurement has been checked and is quite good as shown by figure 13 The heel angle versus time is reported on figure 13.

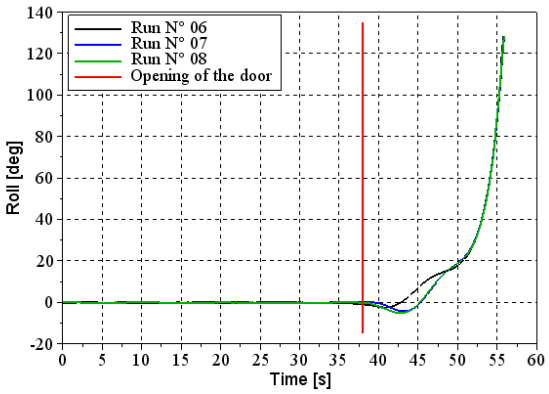

Fig. 13: Time history of the capsizing in case 2.

The roll angle was measured until a heel angle of about 130 degrees after what the markers are underwater. In case 2 the time to reach this angle is about 18s while 55 s have been reported by witnesses. Even if they report the duration of the full reversal – and not only till 130deg – the difference is quite large. As we can see on the figure 13 after beyond 20 degrees heel angle the capsize speed increase a lot. One could expect that after 90 degrees the deckhouse – not represented on our model – enter the water and slow down the motion because of drag effect and air locked in the decks.

If we now look at the results obtained with case 5 – a less favorable case as more compartment are flooded – but with a smaller opening size we can see that the capsizing time is closer from the 55s.

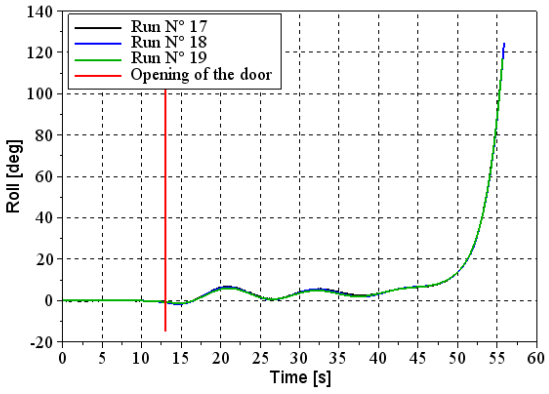

Further test and post-processing will be necessary to fully clarify and verify our hypothesis.

Conclusions

At several times, a few senior Navy officers had pointed to problems of stability, mainly concerning the longitudinal bulkheads which, in case of breach in the compartment, allow off-center flooding to induce a large heel angle. They recommended cross-flooding ducts to prevent this event, though these ducts were never fitted [10]. We have tested this possibility and their intuition was correct. As shown on figure 14, for a quasi-static flooding, an area remains under the GZ curve, whatever the watertight deck.

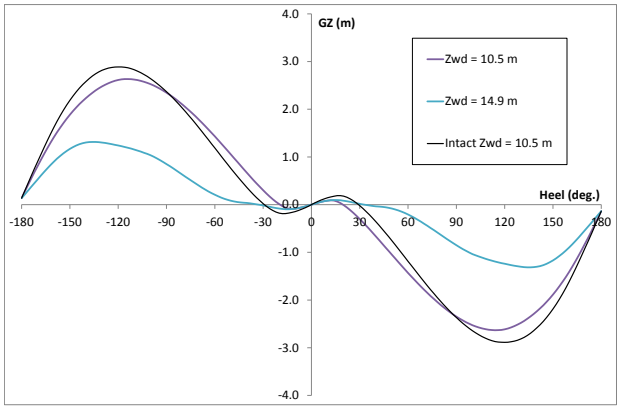

Fig. 14: GZ curves with a cross flooding duct.

Nevertheless the positive area under the curve is so tiny that the dynamic force of the capsizing would have overcome this feeble stability and led to capsize. Moreover, even had the ship been fitted with cross-flooding ducts in the three compartments, the dynamic nature of the flooding would still have led to the capsizing of the *Bouvet*.

This preliminary study has demonstrated that *Bouvet* was a doomed ship from the moment it was built. Further analyses will clarify the exact nature of the damage, including the likely weapon (mine or artillery shell) and the timeline of the capsizing.

Reference:

[1] Berry Warren, *The Pre-Dreadnought revolution: Developing the bulwarks of sea power*, The History Press, 2013.

[2] - Norman Friedman, *British Cruisers of the Victorian Era*, Seaforth Publishing, 2012.

[3] - Féron Luc, *Cuirassé d'escadre Bouvet*, Edimo, 1996.

[4] - Service historique de la Défense à Vincennes, division marine, dossier du *Bouvet* 7DD1 718

[5] - Ropp Theodore and Roberts Stephen *The Development of a Modern Navy: French Naval Policy, 1871-1904,* Annapolis, US Naval Institute Press, 1987, p. 235-259

[6] - Bertin Louis-Emile, « Evolution de la puissance défensive des navires de guerre », *Revue des deux mondes*, Paris, t. 31, 1906.

[7] - Maugas Gabriel, « Note sur la stabilité des bâtiments », *Mémorial du génie maritime*, 1ère livraison, 1900, p.105.

[8] - Doyère Charles, *Théorie du navire*¸ J.B Baillière et fils, 1927, p.225

[9] - Service historique de la Défense à Vincennes, division marine, 7 DD 1 951, Dossier du Charlemagne, Note du capitaine de vaisseau Étienne Raffier-Duffour à l'amiral commandant en chef la 1re Armée navale, 6 juin 1913.

[10] - Service historique de la Défense à Vincennes, division marine, 7 DD 1 718, Dossier du Bouvet, rapport d'inspection de 1899 et rapport de 1907.

Experimental and Numerical Study on Predicting Method of Parametric Rolling in Regular Head Seas

Jiang Lu [1*], Min Gu [1,] and Naoya Umeda [2]

1. *China Ship Scientific Research Center, Wuxi, China*
2. *Dept. of Naval Architecture & Ocean Engineering, Osaka University, Suita, Osaka, Japan*

Abstract: The methods to be used for direct stability assessment of parametric rolling are now under development by the International Maritime Organization (IMO) in the second generation intact stability criteria. In order to provide a reliable numerical method for predicting parametric rolling, firstly, free running experiments and partially restrained free running experiments were conducted to examine the effect of surge motion on parametric rolling and the effect of parametric rolling on heave and pitch motions in regular head seas. Secondly, the surge-roll coupled model with added resistance taken into account is used to predict parametric rolling in which the restoring variation is estimated with coupling from the vertical motion and diffraction effects, which are obtained with a strip theory. Thirdly, a coupled heave-roll-pitch mathematical model based on a nonlinear strip theory is used to calculate heave and pitch motions in regular head seas with parametric rolling taken into account. Finally, time-domain heave and pitch motions are analyzed in the frequency-domain by the Fourier transformation. The results of free running experiments, partially restrained free running experiments and simulations using the C11 containership show that the surge motion on parametric rolling is general small in regular head seas and heave and pitch motions are distinctly affected by parametric rolling and the pitch and heave motions in experiment include subharmonic component when parametric rolling occurs.

Key words: Parametric rolling, surge, heave, pitch, vulnerability criteria, IMO second generation intact stability criteria

1. Introduction

The methods to be used for direct stability assessment of parametric rolling are now under development by the International Maritime Organization (IMO) in the second generation intact stability criteria [1]. A predicting method for parametric rolling with quantitative accuracy is required in the criterion on parametric rolling. Parametric rolling in head seas as one of roll restoring variation problems is a nonlinear phenomenon with dynamic heave and pitch motions so that it is difficult to predict parametric rolling accurately in head seas. Therefore, it is urgent to develop a reliable method to predict parametric rolling in head seas.

In case of following waves, the encounter frequency is much lower than the natural frequencies of heave and pitch so that coupling with dynamic heave and pitch is not important. In addition, added resistance in following waves is generally small. Thus several successful predictions of parametric rolling in following waves were reported [2]. In case of head seas, however, prediction of parametric rolling is not so easy because coupling with heave and pitch is significant and added resistance cannot be simply ignored. Effect of dynamic heave and pitch motions on parametric rolling was investigated so far by many researchers and is well established: restoring arm variation in head waves depends on dynamic heave and pitch motions [3]. Germany also pointed out that speed variation in wave could have large influence on the results of direct assessment for parametric rolling [4], but two of the authors present that the effect of surge on parametric rolling in regular head seas is rather limited by numerical simulations[5]. The effect of surge motion with added resistance taken into account on parametric rolling was investigated by some researchers [6, 7, 8, 9], but experimental study with and without surge was not conducted in the above researches. So the effect of surge motion on

*** Corresponding author:** Jiang Lu, Dr., research fields: ship stability in waves and ship hydrodynamics. E-mail: lujiang1980@aliyun.com

parametric rolling should be validated by experiments with and without surge motion.

Since in a seakeeping theory the effect of roll on heave and pitch motions is small, coupling from heave and pitch to parametric rolling is usually taken into account but not vice versa in the published papers [5, 6, 7, 8, 9]. The effects of parametric rolling on heave and pitch motions in head seas, however, are not always negligibly small. Rodriguez et al. [14] observed in their model experiment that heave and pitch motions could have subharmonic components when parametric rolling occurs in head waves but did not reproduce them in their numerical simulations. Then Neves et al. [15] using their nonlinear heave-pitch-roll mathematical model numerically revealed bifurcation structure of heave and pitch motions together with parametric roll. Later the authors [11] observed subharmonic pitch motion together with parametric roll in free-running model experiment at zero forward velocity using the optical 6-DOF motion measuring system but failed to quantitatively explain it with a coupled heave-roll-pitch mathematical model [10] based on a nonlinear strip theory .

For providing a reliable predicting method for direct assessment of parametric rolling, the authors conducted partially restrained experiments with a newly designed equipment and used existing free running experiment data to investigate predicting methods for parametric rolling of a post Panamax C11 class containership which is provided by an IMO's intercessional corresponding group as one of standard ships for developing second generation intact stability criteria.

2. Mathematical Model

The mathematical model of the first approach for parametric rolling prediction in regular waves is expressed as (1).

$$\ddot{\phi}+2\mu\dot{\phi}+\gamma\dot{\phi}^3+\frac{W}{I_{xx}+J_{xx}}GZ(t,X_G,\zeta_G,\theta,\phi)=0 \qquad (1)$$

where ϕ: roll angle, μ: linear roll damping coefficient, γ: cubic roll damping coefficient, W: ship weight, Ixx: moment of inertia in roll, Jxx: added moment of inertia in roll, GZ: righting arm, t: time, ζ_G: heave displacement and θ: pitch angle, X_G: instantaneous ship longitudinal position. The dot denotes the differentiation with time.

In the first approach, heave and pitch motions obtained by a strip theory applied to an upright hull are used to estimate the restoring variation. In other words, coupling from heave and pitch to roll is taken into account but not vice versa. Coupling from parametric rolling to heave and pitch could also affect the prediction of parametric rolling. However, due to large roll amplitude and roll frequency of half the encounter frequency, coupling from parametric rolling to heave and pitch would be complicated, and here a coupled heave-roll-pitch mathematical model [10] based on a nonlinear strip theory as the third approach presented later. In the above two approaches, a constant speed is considered.

In the second approach, the added resistance in waves is calculated using Maruo's formula [16] for estimating speed loss and the surge motion, and then heave and pitch motions obtained by a strip theory applied to an upright hull are used to estimate the restoring variation.

The restoring variation consists of two components. One is the nonlinear Froude-Krylov component, which is calculated by integrating wave pressure up to wave surface with heave and pitch motions obtained by a strip theory. The other is the hydrodynamic effects which consist of radiation and diffraction components are extrapolated nonlinearly with regards to roll angle.

The first and second numerical approaches are based on the same principle, and here the formula on the second approach is shown as follows [5, 9]:

$$(M+M_x)\ddot{X}_G=T(\dot{X}_G,n)-R((\dot{X}_G)+F_x(X_G,t)-R_{AW}(\dot{X}_G,t) \qquad (2)$$

$$T(\dot{X}_G,n)=(1-t_p)\rho n^2 D_p^4 K_T\{\frac{\dot{X}_G(1-w_p)}{nD_p}\} \qquad (3)$$

$$\bar{\dot{X}}_G = \frac{1}{T_e}\int_0^{T_e} \dot{X}_G(t)dt \tag{4}$$

$$X_G = \int\int_0^t \ddot{X}_G(t)dtd \tag{5}$$

$$\varsigma_G(X_G,t) = \varsigma_{Ga}\cos(\omega t - kX_G\cos\chi + \delta_H) \tag{6}$$

$$\theta(X_G,t) = \theta_a\cos(\omega t - kX_G\cos\chi + \delta_\theta) \tag{7}$$

$$F_X(X_G,t) = F_{Xa}\cos(\omega t - kX_G\cos\chi + \delta_X) \tag{8}$$

where M_X : added mass in surge, *T*: propeller thrust, *R*: ship resistance in calm water, F_X: wave-induced surge force and R_{AW}: added resistance in waves. Furthermore, ζ_{Ga}: amplitude of heaving, δ_H: initial phase of heaving; θa: amplitude of pitching, δ_θ: initial phase of pitching; F_{Xa}: amplitude of wave force of surging, δ_X: initial phase of wave force of surging; ω wave frequency. The dot denotes the differentiation with time.

Initial values for numerical integration with time are set as follows:

$$t = 0\,;\, X_G = 0, \dot{X}_G = 0, n = n^* \tag{9}$$

where, n^*: denotes the desired revolution number of propeller.

Furthermore, the calculation method of restoring variation in waves should consider non-uniform forward speed. Its Froude-Krylov component is calculated by integrating the incident wave pressure around the instantaneous wetted hull surface. As a result, the following formula is used.

$$\begin{aligned} W\cdot GZ \;&= \rho g\int_L \dot{y}(x,X_G,t)\cdot A(x,X_G,t)dx + \rho g\sin\chi\cdot \\ &\int_L \dot{z}(x,X_G,t)\cdot F(x)\cdot A(x,X_G,t)\cdot\sin(\zeta_{G0}+(X_G+x)\cos\chi - c\cdot t)dx \end{aligned} \tag{10}$$

$$F(x) = \varsigma_a k\frac{\sin(k\frac{B(x)}{2}\sin\chi)}{k\frac{B(x)}{2}\sin\chi}e^{-kd(x)} \tag{11}$$

where, $A(x,X_G,t)$: the submerged area of local section of the ship; $\dot{y}(x,X_G,t)$: the transverse position of buoyancy centre of local section, $\dot{z}(x,X_G,t)$: the vertical position of buoyancy centre of local section, ξ_{G0}=0: the initial longitudinal position of a ship centre from a wave trough.

The radiation and diffraction components of the restoring variation are calculated as follows.

$$GZ_{R\&D} = -M_X / W \tag{12}$$

$$M_X = K - (KG - D)Y \tag{13}$$

$$M_X(X_G,t) = M_{Xa}\cos(\omega t - kX_G\cos\chi + \delta_{MX}) \tag{14}$$

$$Y = F_Y - (A_{23}\ddot{\varsigma} + B_{23}\dot{\varsigma} + C_{23}\varsigma + A_{25}\ddot{\theta} + B_{25}\dot{\theta} + C_{25}\theta) \tag{15}$$

$$K = M_\phi - (A_{43}\ddot{\varsigma} + B_{43}\dot{\varsigma} + C_{43}\varsigma + A_{45}\ddot{\theta} + B_{45}\dot{\theta} + C_{45}\theta) \tag{16}$$

where, *KG*: the distance from the keel to the gravity of ship; *D*: draft; M_{Xa}: amplitude of the restoring variation, δ_{MX}: the initial phase of the restoring variation.

Formulae of the wave exciting force, F_Y, and moment M_φ are available in the reference [12] as well as those for coupling coefficients in reference [13].

Due to large roll amplitude and roll frequency of half the encounter frequency, coupling from parametric rolling to heave and pitch would be complicated, and there is no theory can be used to investigate the effects of parametric rolling on heave and pitch motions in head seas, so the authors attempt to use a coupled heave-roll-pitch mathematical model [10] which is based on a nonlinear strip theory and based on same principle with the first and second approaches as the third approach. The mathematical model of the third approach for parametric rolling prediction in regular waves is expressed as (17), (18), (19).

$$\begin{aligned} &(I_{xx} + A_{44}(\phi)\ddot{\phi} + N_1\dot{\phi} + N_3\dot{\phi}^3 + A_{43}(\phi)\ddot{\zeta} \\ &+ B_{43}(\phi)\dot{\zeta} + A_{45}(\phi)\ddot{\theta} + B_{45}(\phi)\dot{\theta} \\ &= F_4^{FK+B}(\xi_G/\lambda,\zeta,\phi,\theta) + F_4^{DF}(\phi) \end{aligned} \tag{17}$$

$$\begin{aligned} &(I_{xx} + A_{44}(\phi)\ddot{\phi} + N_1\dot{\phi} + N_3\dot{\phi}^3 + A_{43}(\phi)\ddot{\zeta} \\ &+ B_{43}(\phi)\dot{\zeta} + A_{45}(\phi)\ddot{\theta} + B_{45}(\phi)\dot{\theta} \\ &= F_4^{FK+B}(\xi_G/\lambda,\zeta,\phi,\theta) + F_4^{DF}(\phi) \end{aligned} \tag{18}$$

$$\begin{aligned} &(I_{yy} + A_{55}(\phi)\ddot{\theta} + B_{55}(\phi)\dot{\theta} + A_{53}(\phi)\ddot{\zeta} \\ &+ B_{53}(\phi)\dot{\zeta} + A_{54}(\phi)\ddot{\phi} + B_{54}(\phi)\dot{\phi} \\ &= F_5^{FK+B}(\xi_G/\lambda,\zeta,\phi,\theta) + F_5^{DF}(\phi) \end{aligned} \tag{19}$$

Nonlinear Froude-Krylov forces are calculated by integrating the incident wave pressure around the instantaneous wetted hull surface. Radiation and

diffraction forces are calculated for the submerged hull considering time-dependant roll angle with the static balance of sinkage and trim. Two-dimensional hydrodynamic forces are calculated by strip theory. Hydrodynamic forces for the heave, pitch and diffraction models are calculated with the encounter frequency while those for roll mode are done with half the encounter frequency assuming parametric rolling. Linear and cubic roll damping coefficients are used in mathematic model which are obtained from roll decay test in experiment. Here in order to investigate the effect of parametric rolling on heave and pitch motions, roll damping coefficients is adjusted to tune amplitudes of parametric rolling. The model proposed by Neves et al. (2009) takes account of nonlinear hydrostatic coupling between roll and vertical motions as well as nonlinearity of both roll and vertical motions, while the model used here does also body-nonlinear hydrodynamic coupling between roll and vertical motions without nonlinearity of vertical motions.

3. Experiments

Both the free running experiment and the partially restrained experiment with a 1/65.5 scaled model of the post Panamax C11 class containership were conducted at the seakeeping basin (length: 69m, breadth: 46m, height: 4m) of China Ship Scientific Research Center, which is equipped a flap wave maker at the two adjacent sides of the basin.

The ship model was drove by a propeller in regular head seas in the free running experiment. Pitch and roll amplitude are measured by the MEMS (Micro Electro-Mechanical System)-based gyroscope placed on the ship model and wave elevation was measured by a servo-needle wave height sensor attached to the towing carriage. In order to directly measure the heave motion, an optical 6-DOF motion measuring system attached to the towing carriage is also used to measure ship motions. Here the optical system is only used to measure ship motion at zero speed because the towing carriage has mechanical vibrations with forward speed which affects the precision measure of the optical tracker.

The ship model was towed by the towing carriage in regular head seas in partially restrained experiment and a newly designed equipment was used to measure ship motions including roll, pitch and heave motions and excited wave moment/force including roll moment, yaw moment ,sway force and surge force. Roll and pitch motions are measure by potentiometer sensor. Heave motion are measured by displacement sensor. Roll moment, yaw moment, sway force and surge force are measured by four sensors based on electromotive strain gauge.

The principal particulars and body plan of the C11 class containership are shown in Table 1 and Fig.1, respectively. The ship model in free running experiment and partially restrained experiment are shown Fig.2 and Fig.3, respectively.

Table 1 Principal particulars of the C11 containership

Items	Ship	Model
Length:L	262.0m	4.000m
Draft:T	11.5m	0.176m
Breadth:B	40.0m	0.611m
Depth:D	24.45m	0.373m
Displ.:W	67508ton	240.2kg
C_B	0.560	0.560
GM	1.928m	0.029m
T_φ	24.68s	3.05s
K_{YY}	0.24L	0.24L

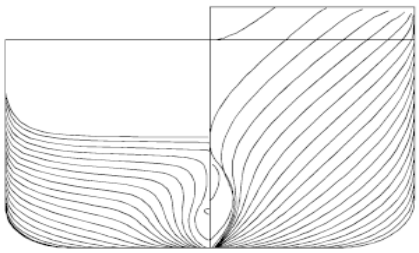

Fig. 1 Lines of C11 containership

Fig.2 The ship model in free running experiment

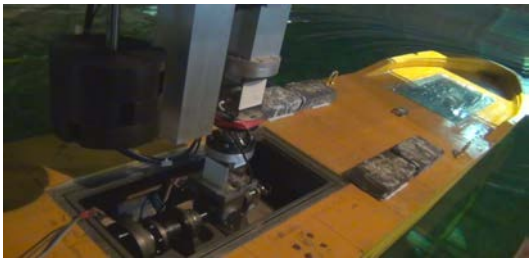

Fig.3 The ship model in partially restrained experiment

4. Results and Discussions

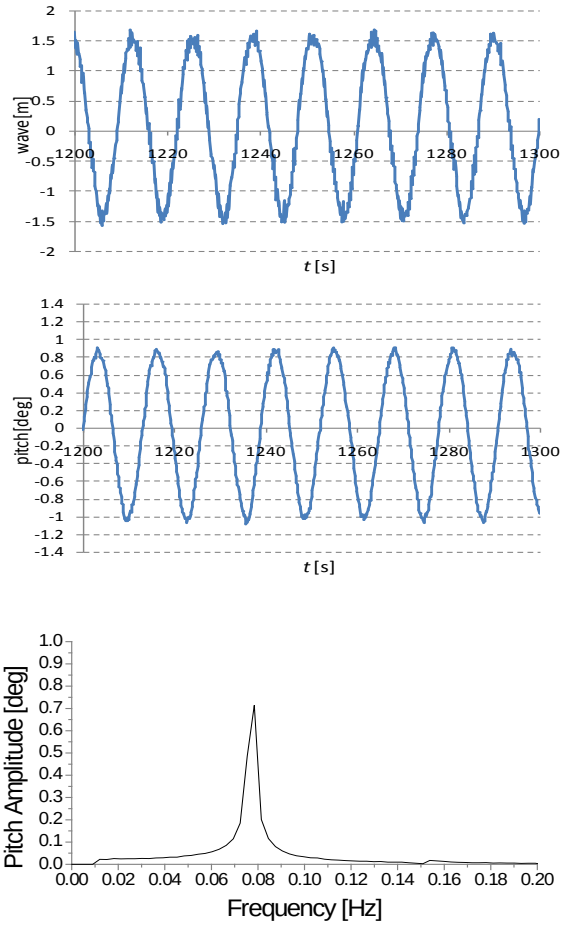

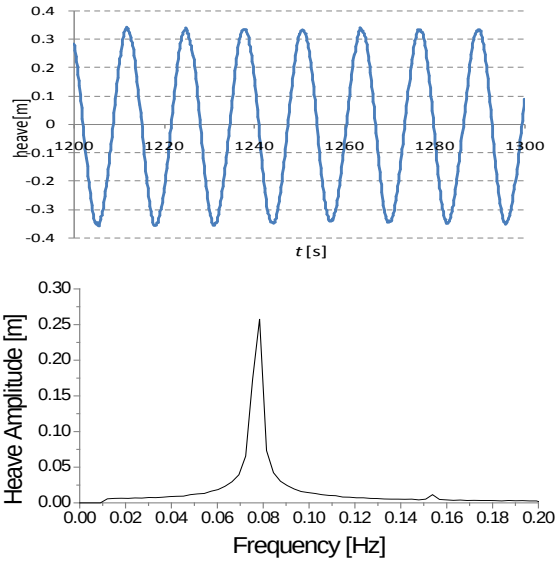

Fig.4 Wave, pitch and heave motions in time and frequency domains while heeling is restrained with λ/L_{pp}=1.0, H/λ=0.01, χ=180^0, Fn=0.0, 1/(Te) =0.0772HZ.(Exp2)

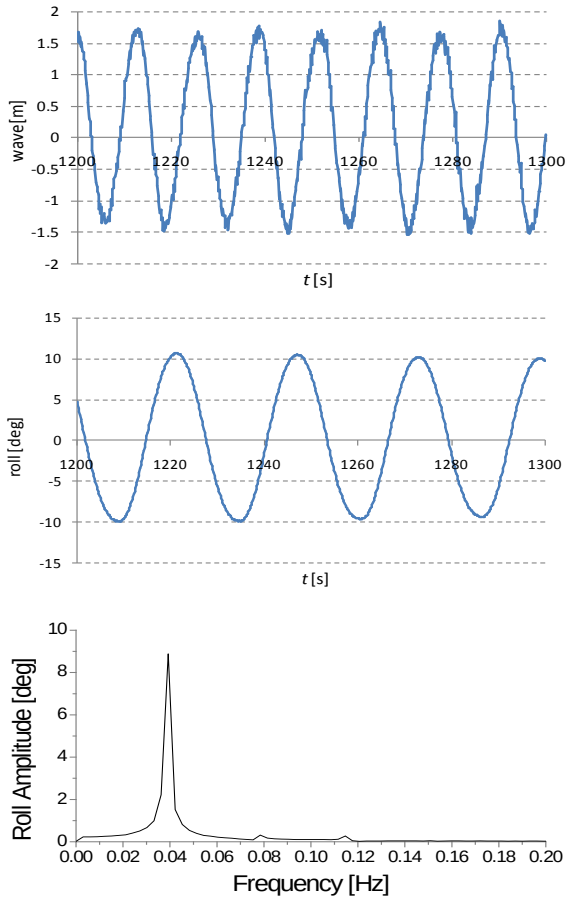

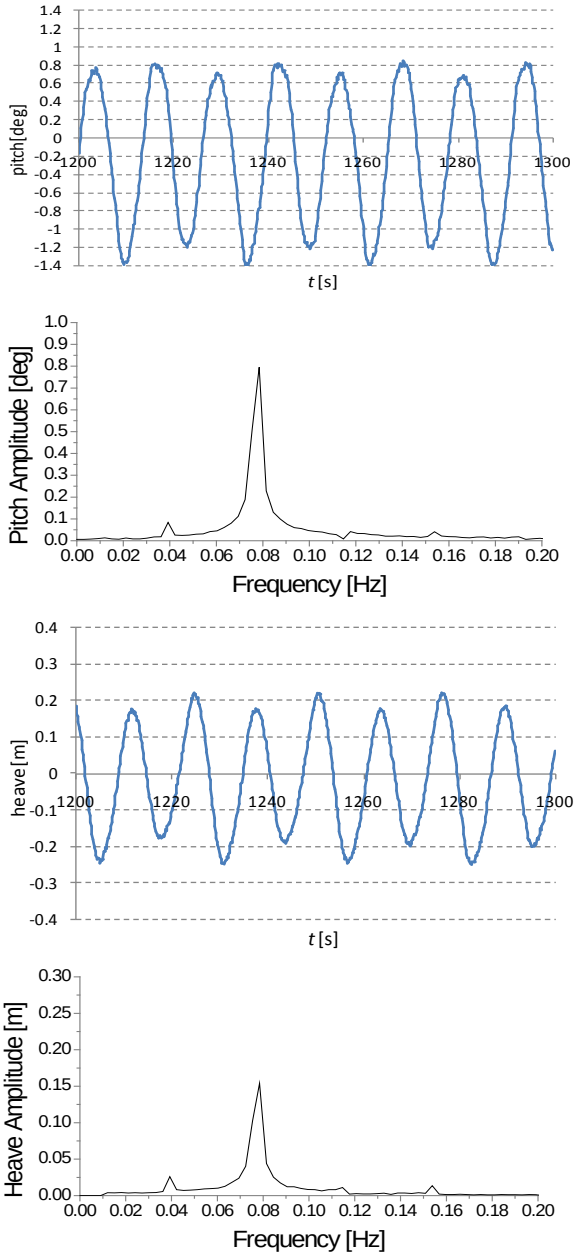

Fig.5 Wave, pitch and heave motions in time and frequency domains while parametric rolling occurs with λ/L_{pp}=1.0, H/λ=0.01, χ=180^0, Fn=0.0, 1/(Te) =0.0772HZ.(Exp2)

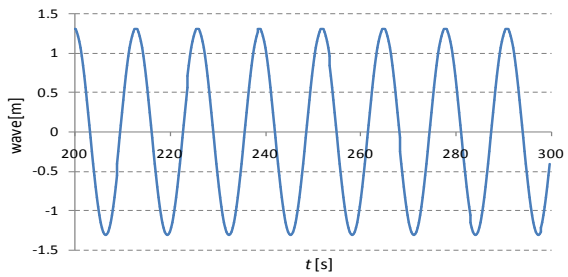

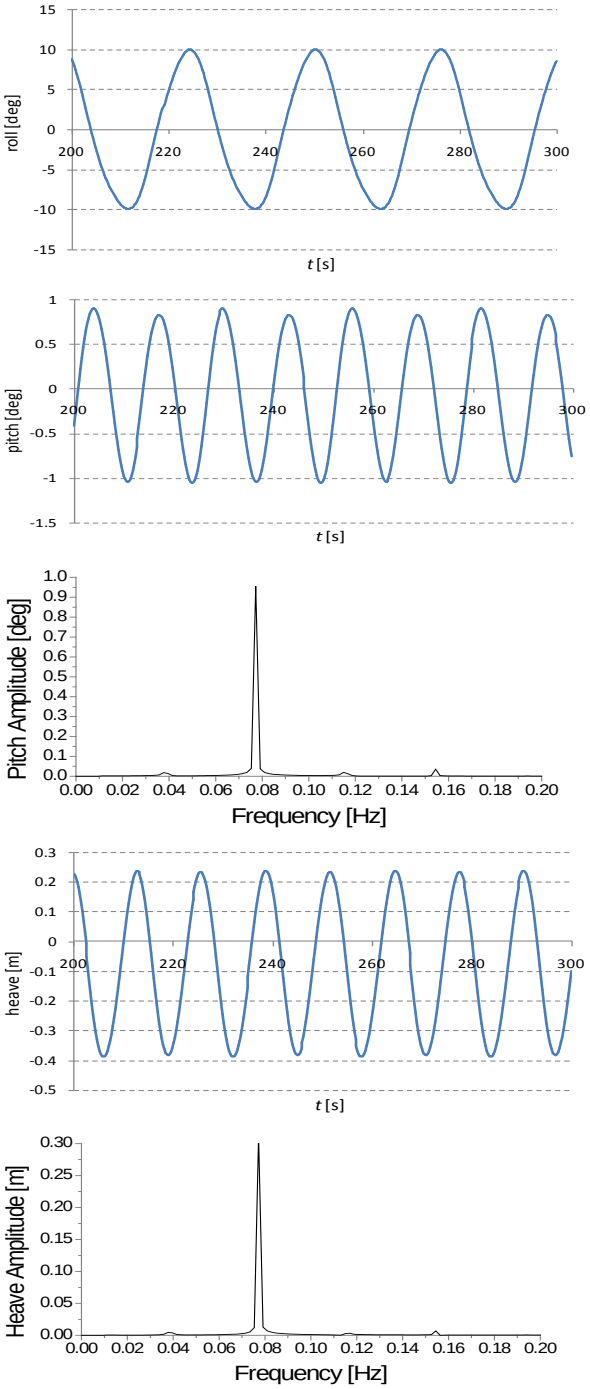

Fig.6 Wave, pitch and heave motions in time and frequency domains while parametric rolling occurs with λ/L_{pp}=1.0, H/λ=0.01, χ=180^0, Fn=0.0, 1/(Te) =0.0772HZ.(simulation of approach 3 with adjusted roll damping coefficients)

The results of experiments indicate the frequency of heave and pitch motions is equal to the encounter wave frequency in case without parametric rolling as shown in Figs.4 which coincide with a linear seakeeping theory. When parametric rolling occurs

with amplitudes of 10 degrees as shown Figs.5 in restrained experiments, heave and pitch motions are affected by parametric rolling and their large and small amplitudes alternatively appear. This phenomenon seems like "subharmonic pitch" and "subharmonic heave" [15]. The heave and pitch motions are analyzed in the frequency-domain by the Fourier transformation. One distinct phenomenon was observed that pitch and heave motions in the experiments has both half the encounter wave frequency and the encounter wave frequency components when parametric rolling occurs while this phenomenon is not obvious for heave motions in the reference[11] by the authors. This phenomenon in the simulation is not as distinct as that in the experiment as show in fig.6.

Although pitch and heave motions are lightly affected by parametric rolling in numerical simulations, the distinct phenomenon cannot reproduced in numerical simulations as show in fig.6. Therefore, in order to provide a reliable numerical method for predicting parametric rolling, the simulation model should be updated and the effects of parametric rolling on heave and pitch motions in head seas should be precisely taken into account.

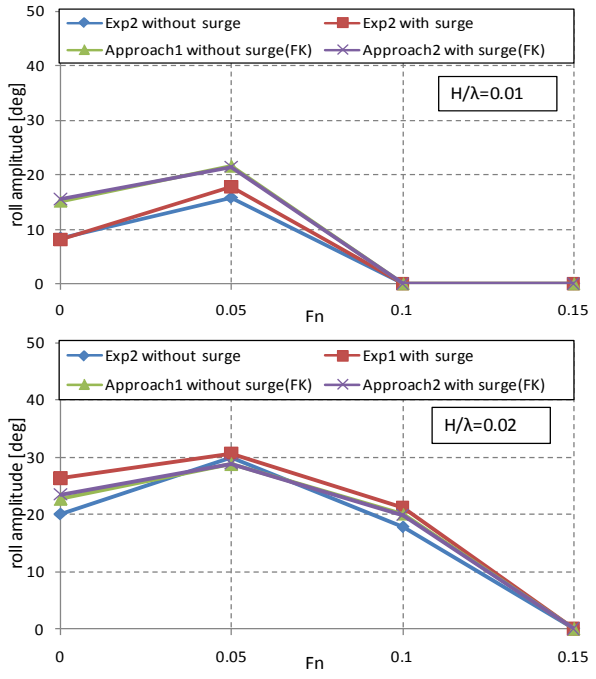

Fig.7 The effect of surge motion on parametric rolling as the function of the Froude number in experiments and simulations with λ/L_{pp}=1.0, χ=180^0(FK:only Froude-Krylov components of restoring variation are considered).

The surge motion is free in the free running experiment noted as Exp1 while the surge motion is restrained in the partially restrained experiment noted as Exp2. The effect of the surge motion on parametric rolling is generally small by comparing the results between the two experiments as show in figs.7. The results of simulations also indicate that the effect of the surge motion on the parametric rolling is generally small as show in figs.7 and 8. This is because the difference of XG is very small between with and without surge motion although ship forward speed is periodically varied while surge motion is considered in regular head seas, and then that results in the difference of wave profile as well as the change of GZ is very small [5].

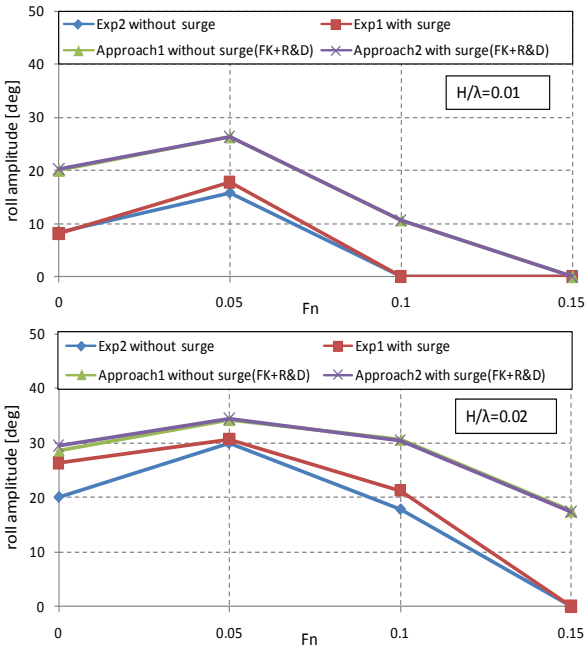

Fig.8 The effect of surge motion on parametric rolling as the function of the Froude number in experiments and simulations with λ/L_{pp}=1.0, χ=180^0(FK+R&D:the radiation and diffraction components of restoring variation are also considered).

The calculations in the restoring variation are executed both with and without the radiation and diffraction components. The prediction with Froude-Krylov, radiation and diffraction components is larger than that with the Froude-Krylov on its own. This is because the amplitude of GZ variation with Froude-Krylov, radiation and diffraction components

is larger than that with the Froude-Krylov on its own in regular head seas [5]. Therefore, for conservatively predicting parametric rolling, the dynamic effect of radiation and diffraction force should be taken into account.

5. Conclusions

As a result of experimental and numerical studies on predicting methods of parametric rolling in regular head seas, the following remarks and recommendations are noted:

1) The pitch and heave motions in the experiments consist of both half the encounter wave frequency and one the encounter wave frequency components when parametric rolling occurs, and the large and small amplitudes alternatively appear.

2) The effect of surge motion on parametric rolling in regular head seas is generally small in experiments and simulations and the surge motion could be ignored for providing a simple predicting method with quantitative accuracy on parametric rolling in direct stability assessment.

3) The dynamic effect of radiation and diffraction force should be taken into account for conservatively predicting parametric rolling in direct stability assessment.

4) The effects of parametric rolling on heave and pitch motions in head seas should be precisely taken into account for providing a reliable numerical method for direct stability assessment of parametric rolling.

Acknowledgments

Part of this research was once supported by China Scholarship Council [No.2008606031] for J. Lu's visit to Osaka University. The research is supported by Ministry of Industry and Information Technology of China (No. [2012] 533). The authors sincerely thank the above organizations.

References

[1] IMO SDC 1/WP.5, Development of Second Generation Intact Stability Criteria, Report of the working group. 2014.

[2] A. Munif, N. Umeda, Modeling Extreme Roll Motions and Capsizing of a Moderate-Speed Ship in Astern Waves. Journal of the Society of Naval Architects of Japan, (2000) 187: 405-408.

[3] H. Taguchi, S. Ishida, H. Sawada, M. Minami, Model Experiments of Ship Capsize in Astern Seas. Journal of the Society of Naval Architects of Japan, (1995)177: 207-217.

[4] IMO SLF53/INF.10 ANNEX 12, Replies to Comments on Draft New Generation Intact Stability Criteria Proposed by Japan. (2010)142-145.

[5] J. Lu, N. Umeda, K. Ma, Modeling Parametric Rolling in Regular and Irregular Head Seas with Added Resistance Taken into Account. Proceedings of the 5th Asia-Pacific Workshop on Marine Hydrodynamics, Osaka Pref Univ, (2010)93-98.

[6] N. Umeda, H. Hashimoto, F. Stern, S. Nakamura, H. Sadat-Hosseini, A. Matsuda, P. Carrica, Comparison Study on Numerical Prediction Techniques for Parametric Roll. Proceedings 27th Symposium on Naval Hydrodynamics, Seoul Nat Univ, (2008) 5-10.

[7] N. Umeda, A. Francescutto, Performance-Based Ship Operation. Proceedings 2nd International Workshop on Risk-Based Approaches in Maritime Industry, Univ. Strathclyde, (2008)2.2.1-2.2.9.

[8] J. Lu, N. Umeda, K. Ma, Predicting Parametric Rolling in Irregular Head Seas with Added Resistance Taken into Account . J Mar Sci Technol, (2011)16:462-471.

[9] J. Lu, G. Min, N. Umeda, Numerical Approaches on Parametric Rolling in Head Seas. The 10th International Hydrodynamics, Petersburg, Russia, (2012)83-88.

[10] H. Hashimoto, N. Umeda, Validation of a Numerical Simulation Model for Parametric Rolling Prediction using PCTC. Proceedings of the 11th STAB, (2012)141-149.

[11] J. Lu, G. Min, N. Umeda, A Study on the Effect of Parametric Rolling on Heave and Pitch Motions in Head Seas. Proceedings of the 13th International Ship Stability Workshop, Brest, France. (2013)185-191.

[12] M. Fujino, S. Sakurai, On the Evaluation of Wave Exciting Roll Moment by strip Method, J the Society of Naval Architects of Japan, (1982) 152: 125-137(in Japanese).

[13] M.C. Lee, K.H. Kim, Prediction of Motion of Ships in Damaged Condition in Waves, Proceedings of the 2nd STAB, the Society of Naval Architects of Japan, (1982)13-26.

[14] C. A. Rodriguez et al., Validation of a Container Ship Model for Parametric rolling, Proceedings of 9th International Ship Stability Workshop, Hamburg. (2007).

[15] Ma.A.S. Neves, J.E.M. Vivanco and C.A. Rodriguez, Nonlinear Dynamics on Parametric Rolling of Ship in Head Seas, Proceedings of the 10th STAB, (2009) 509-520.

[16] H. Maruo, Resistance in Waves, Chap.5 in Researches on Seakeeping Qualities of Ships in Japan, Soc. Nav. Arch. Japan 60th Anniv. Ser., No 8. (1963) pp67-102.

Experimental and Numerical Study on Roll Restoring Variation Using the C11 Containership

Min Gu, Jiang Lu, Tianhua Wang

China Ship Scientific Research Center, Wuxi, China

Abstract: The vulnerability criteria and direct stability assessment on parametric rolling and pure loss of stability are now under development by the International Maritime Organization (IMO) in the second generation intact stability criteria. Roll restoring variation is a key factor for both criteria and model experiments and simulations are conducted to study the roll restoring variation in waves. Firstly, captive model experiments in which heave and pitch motions are free and other motions are restrained with a constant heeling angle are conducted to measure roll restoring variation in following and head seas for parametric rolling and pure loss of stability. Secondly, the roll restoring variations of Froude-Krylov calculation by a static balance method and a strip method of heave and pitch motions are carried out in following and head seas,and the dynamic effect of radiation and diffraction force on restoring variation are also calculated. Finally,the rule of roll restoring variation in following and head seas is pointed out by experiments and simulations and the numerical methods are also validated through the comparisons between the model experiments and the simulations using the C11 containership for the vulnerability criteria and direct stability assessment on parametric rolling and pure loss of stability.

Key words: Roll restoring variation; pure loss of stability; parametric rolling; vulnerability criteria; direct stability assessment; IMO second generation intact stability criteria

1. Introduction

The vulnerability criteria and direct stability assessment on parametric rolling and pure loss of stability are now under development by the International Maritime Organization (IMO) in the second generation intact stability criteria [1]. The roll restoring variation in waves is allowed to use the Froude-Krylov assumption with static balance in heave and pitch in the vulnerability criteria of parametric rolling and pure loss of stability [2]. The roll restoring variation is a key factor for both criteria of parametric rolling and pure loss of stability . Therefore, it is necessary to conduct model experiments and simulations to validate the reliable of the method proposed in the vulnerability criteria for calculating roll restoring variation in waves and give out reasonable methods for direct stability assessment on parametric rolling and pure loss of stability.

Parametric rolling is induced by restoring arm variation in time. In case of following waves, the encounter frequency is much lower than the natural frequencies of heave and pitch motions so that coupling with heave and pitch is not significant. In addition, added resistance in following waves is generally small. Thus several successful predictions of parametric rolling in following waves were reported [3]. In case of head seas, however, prediction of parametric rolling is not so easy because coupling with heave and pitch is significant and added resistance cannot be simply ignored. Effect of dynamic heave and pitch motions on parametric rolling was investigated so far by many researchers and is well established: restoring arm variation in head seas depends on dynamic heave and pitch motions [4].

*** Corresponding author:** Jiang Lu, Dr., research fields: ship stability in waves and ship hydrodynamics. E-mail: lujiang1980@aliyun.com

Since in a ship seakeeping theory, the effect of roll on heave and pitch motions is small, coupling from heave and pitch to parametric rolling is taken into account but not vice versa in published papers, and here the roll restoring variation consists of two components. One is nonlinear Froude-Krylov component which is calculated by integrating the wave pressure up to the surface of the wave with the heave and pitch motions obtained by a strip theory. The other is the hydrodynamics effect which consists of radiation and diffraction components acting on a heeled hull as linear components with respect to wave height [5, 6, 7, 8, 9].

For validating the method proposed in the vulnerability criteria of parametric rolling and pure loss of stability and providing a reliable numerical method of calculating the roll restoring variation to accurately predict parametric rolling and pure loss of stability on a wave crest, the authors conduct partially restrained experiments with a newly designed equipment to investigate the roll restoring variation of a post Panamax C11 class containership which is provided by an IMO's intersetional corresponding group as one of standard ship for developing second generation intact stability criteria.

2. Mathematical Model

The mathematical model for the roll restoring variation of Froude-Krylov component in regular waves is expressed as (1), (2).

$$W \cdot GZ_{FK} = \rho g \int_L y'_{B(x)} \cdot A(x) dx + \rho g \sin\chi \cdot \int_L z'_{B(x)} \cdot F(x) \cdot A(x) \cdot \sin(\zeta_G + x \cdot \cos\chi) d\,x \quad (1)$$

$$F(x) = \varsigma_a k \frac{\sin(k\frac{B(x)}{2}\sin\chi)}{k\frac{B(x)}{2}\sin\chi} e^{-kd(x)} \quad (2)$$

where, W: ship weight, GZ_{FK}: Froude-Krylov components of the restoring variation, L: ship length, $A(x)$: the submerged area of local section of the ship; $y'_{B(x)}$: the transverse position of buoyancy centre of local section, $z'_{B(x)}$ *:* the vertical position of buoyancy centre of local section, ξ_G: the longitudinal position of a ship's centre of gravity from a wave trough, x: the longitudinal position from the ship's centre of gravity. Furthermore, ζa :wave amplitude, k:wave number, χ : heading angle, $B(X)$*:*breadth of x section, $d(x)$draught of x section, ρ: water density and g: gravitational acceleration.

When a ship has a heeling angle, static balance in heave and pitch should be satisfied, and heave and pitch could be calculate by follow static balance methods (3),(4).

$$W - \rho g \int_L A(x) dx + \rho g \cdot \int_L F(x) \cdot A(x) \cdot \cos(\zeta_G + x \cdot \cos\chi) d\,x = 0 \quad (3)$$

$$\rho g \int_L xA(x) dx + \rho g \cdot \int_L xF(x) \cdot A(x) \cdot \cos(\zeta_G + x \cdot \cos\chi) d\,x = 0 \quad (4)$$

A strip method is also used to calculated heave and pitch motions by follow equations (5), (6) as another method.

$$(M + A_{33})\ddot{\zeta} + B_{33}\dot{\zeta} + C_{33}\zeta + A_{35}\ddot{\theta} + B_{35}\dot{\theta} + C_{35}\theta = F_Z \quad (5)$$

$$A_{53}\ddot{\zeta} + B_{53}\dot{\zeta} + C_{53}\zeta + (I_{yy} + A_{55})\ddot{\theta} + B_{55}\dot{\theta} + C_{55}\theta = M_\theta \quad (6)$$

The radiation and diffraction components of the restoring variation are calculated as follows.

$$GZ_{R\&D} = -M_X / W \quad (7)$$

$$M_X = K - (KG - D)Y \quad (8)$$

$$M_X(X_G, t) = M_{Xa}\cos(\omega t - kX_G\cos\chi + \delta_{MX}) \quad (9)$$

$$Y = F_Y - (A_{23}\ddot{\zeta} + B_{23}\dot{\zeta} + C_{23}\zeta + A_{25}\ddot{\theta} + B_{25}\dot{\theta} + C_{25}\theta) \quad (10)$$

$$K = M_\phi - (A_{43}\ddot{\zeta} + B_{43}\dot{\zeta} + C_{43}\zeta + A_{45}\ddot{\theta} + B_{45}\dot{\theta} + C_{45}\theta) \quad (11)$$

where, KG: the distance from the keel to the gravity of ship; D: draft; M_{Xa}: amplitude of the restoring variation, δ_{MX}: the initial phase of the restoring variation.

Formulae of the wave exciting force, F_Y, and moment M_φ are available in the reference [10] as well as those for coupling coefficients in reference [11].

3. Experiments

The partially restrained experiment with a 1/65.5 scaled model of the post Panamax C11 class containership were conducted at the seakeeping basin (length: 69m, breadth: 46m, height: 4m) of China Ship Scientific Research Center, which is equipped a flap wave maker at the two adjacent sides of the basin. The ship model was towed by the towing carriage in regular head seas and newly designed equipment was used to measure roll restoring variation with pitch and heave motions free. Roll and pitch motions are measure by potentiometer sensor. Heave motions are measured by displacement sensor. Roll moments are measured by a sensors based on electromotive strain gauge.

The principal particulars and body plan of the C11 class containership are shown in Table 1 and Fig.1, respectively. The ship model in free running experiment and partially restrained experiment are shown Fig.2 and Fig.3, respectively.

Table 1 Principal particulars of the C11 containership

Items	Ship	Model
Length:L	262.0m	4.000m
Draft:T	11.5m	0.176m
Breadth:B	40.0m	0.611m
Depth:D	24.45m	0.373m
Displ.:W	67508ton	240.2kg
C_B	0.560	0.560
GM	1.928m	0.029m
T_φ	24.68s	3.05s
K_{YY}	0.24L	0.24L

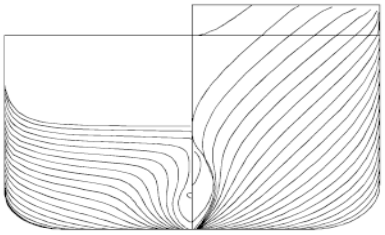

Fig. 1 Lines of C11 containership

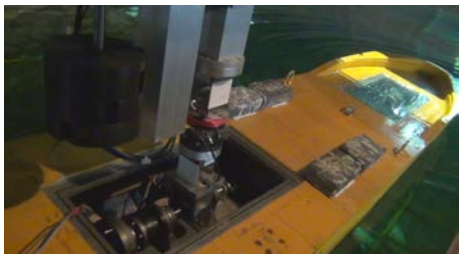

Fig.2 The ship model in partially restrained experiment

4. Results and Discussions

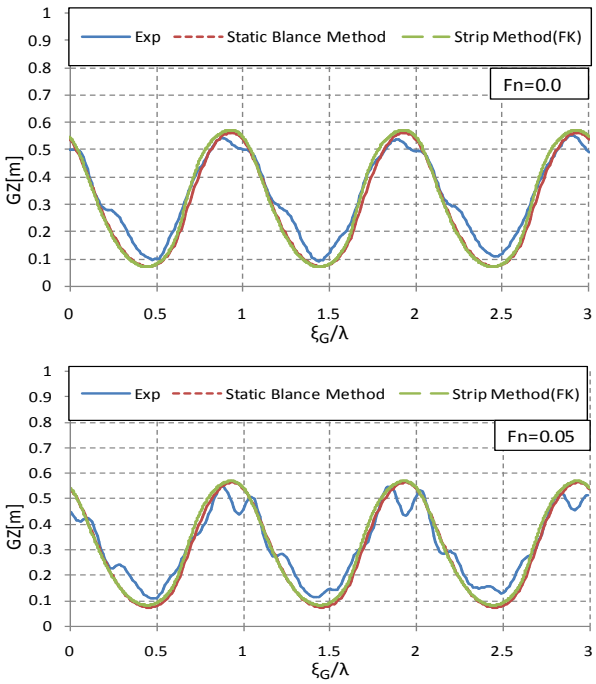

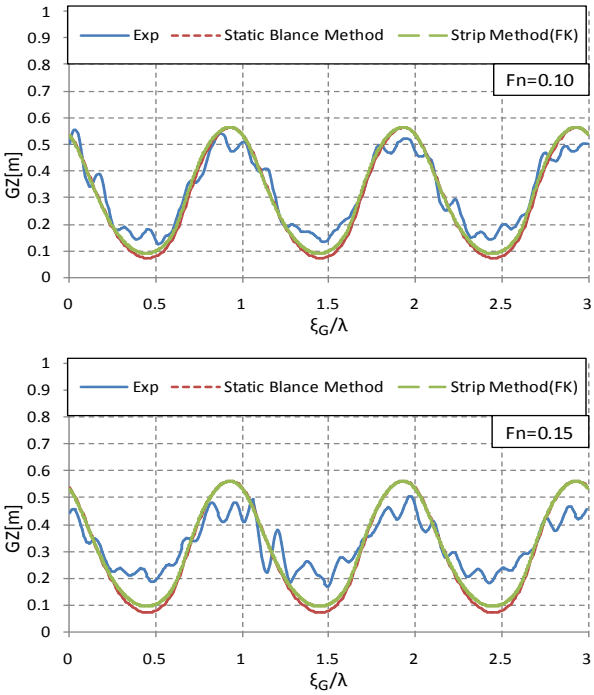

Fig.3 Comparison of roll restoring variation as the function of relative position of ship to wave between the experiment and the Froude-Krylov calculations with λ/L_{pp}=1.0, H/λ=0.02, $\chi=0^0$, $\Phi=8^0$.

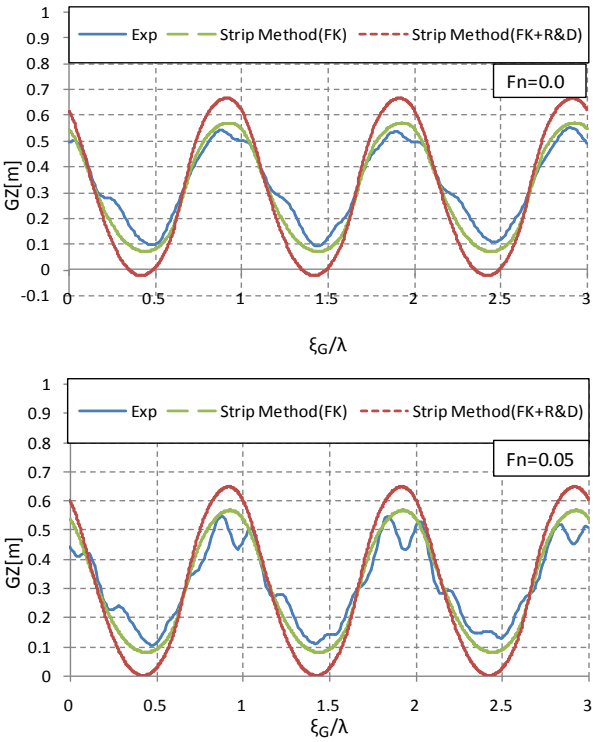

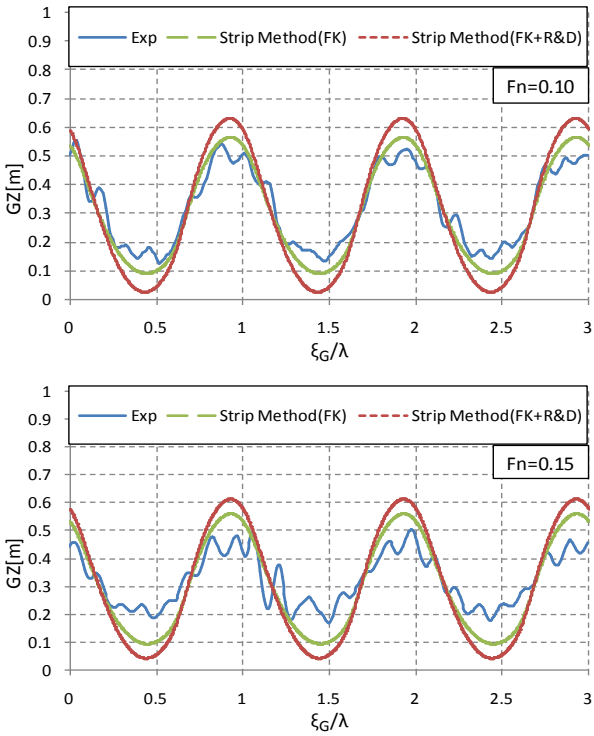

Fig.4 Comparison of roll restoring variation as the function of relative position of ship to wave between the experiment and the calculations with λ/L_{pp}=1.0, H/λ=0.02, $\chi=0^0$, $\Phi=8^0$.

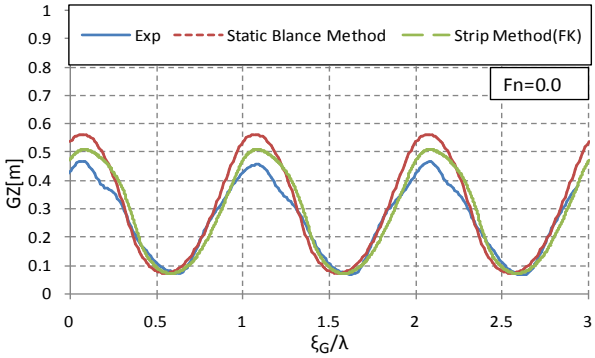

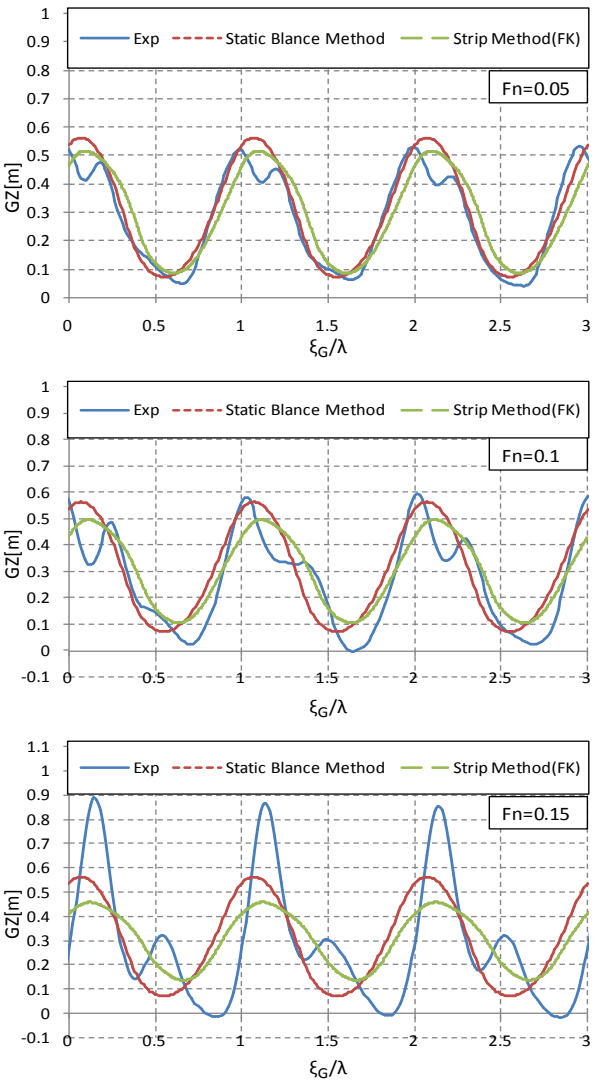

Fig.5 Comparison of roll restoring variation as the function of relative position of ship to wave between the experiment and the Froude-Krylov calculations with λ/L_{pp}=1.0, H/λ=0.02, χ=180^0, Φ =7.3^0.

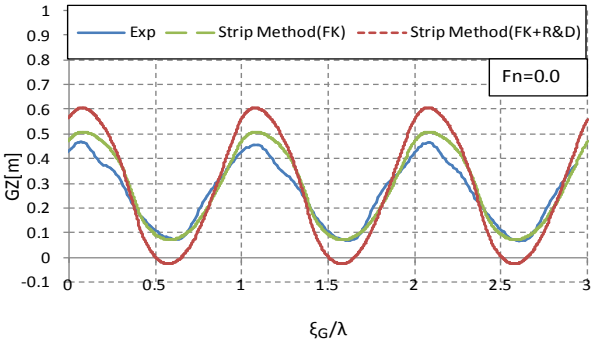

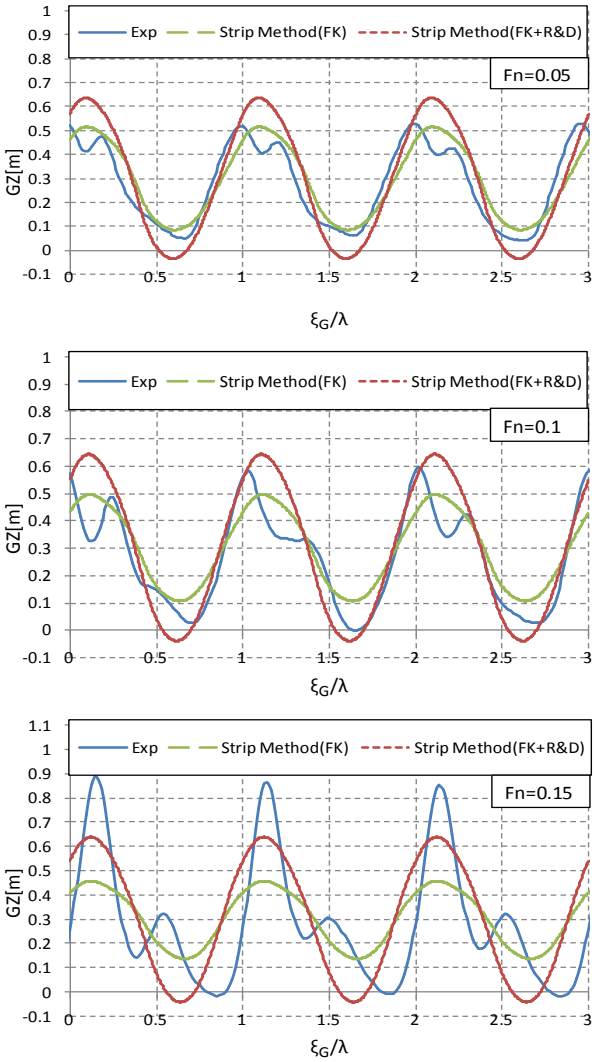

Fig.6 Comparison of roll restoring variation as the function of relative position of ship to wave between the experiment and the calculations with λ/L_{pp}=1.0, H/λ=0.02, χ=180^0, Φ =7.3^0.

The results of experiments indicate the roll restoring variations become small in following seas as ship forward speed increase and they could like first harmonic cosines curve although the signals are affected by the vibration of the carriage as shown in Fig.3. The roll restoring variations of Froude-Krylov calculation by the static balance method and the strip method are near same in following seas and they are also near same with that in experiment at zero ship forward speed while they are small larger than that in

experiment as ship forward speed increase as shown by Fig.3. The radiation and diffraction components of the restoring variation are also calculated. The roll restoring variations with he radiation and diffraction component become larger than that with Froude-Krylov on its own and that in experiment as shown by Fig.4. So the roll restoring variations of only Froude-Krylov calculation by static balance method and strip method should be allowed to predict parametric rolling and pure loss of stability in following seas while the roll restoring variations of only Froude-Krylov calculation by static balance method could be more suitable for providing a simple and conservative vulnerability criteria of parametric rolling and pure loss of stability in follow seas.

In case of head seas, prediction of parametric rolling is not so easy because coupling with heave and pitch is significant and heave and pitch motions are also distinct affected by parametric rolling [12, 13].The results of experiments indicate the roll restoring variations become large in head seas as ship forward speed increase and become complicated at a hight ship forward speed as shown in Fig.5. The roll restoring variations of Froude-Krylov calculation by static balance method and strip method are near same with that in experiment at zero ship forward speed while they are smaller than that in experiment as ship forward speed increase as shown by Fig.5. The radiation and diffraction components of the restoring variation are also calculated. The restoring variation with the radiation and diffraction component become larger than that with the Froude-Krylov on its own and also larger than that in experiment except Froude number 0.15 as shown by Fig. 6. This could be the reason why the parametric rolling with Froude-Krylov, radiation and diffraction components is larger than that in experiment while that with the Froude-Krylov on its own is near same with that in experiment[13]. So the dynamic effect of radiation and diffraction force should be taken into account for conservatively predicting parametric rolling in head seas with ship forward speed. However, the roll restoring variations of only Froude-Krylov calculation by static balance method could be also suitable for providing a simple vulnerability criteria of parametric rolling in head seas and keeping consistent with the method used in following seas .

5. Conclusions

As a result of experimental and numerical studies on the roll restoring variations in regular following and head seas, the following remarks and recommendations are noted:

1) The roll restoring variations become small in follow seas and become large in head seas as ship forward speed increase and they could like harmonic cosines curves in following seas while they become complicated in head seas at hight speeds.

2) The roll restoring variations of only Froude-Krylov calculation by the static balance method and the strip method should be allowed to predict parametric rolling and pure loss of stability in following seas, and the static balance method could be more suitable for providing a simple and conservative vulnerability criteria of parametric rolling and pure loss of stability in following seas.

3) The roll restoring variations of dynamic effect of radiation and diffraction force should be taken into account for conservatively predicting parametric rolling in head seas and the roll restoring variations of only Froude-Krylov calculation by the static balance method could be also suitable for providing a simple vulnerability criteria of parametric rolling in head seas and keeping consistent with the method used in following seas .

Acknowledgments

Part of this research was once supported by China Scholarship Council [No.2008606031] for J. Lu's visit to Osaka University. The research is supported by Ministry of Industry and Information Technology of China (No. [2012] 533). The authors sincerely thank the above organizations.

References

[1] IMO SDC 1/WP.5, Development of Second Generation Intact Stability Criteria, Report of the working group. 2014.

[2] IMO SLF55 1/IN.10, Draft Vulnerability Criteria on Parametric Rolling and Pure Loss of Stability with Their Sample Calculation Results, Submitted by Japan. 2010.

[3] A. Munif, N. Umeda, Modeling Extreme Roll Motions and Capsizing of a Moderate-Speed Ship in Astern Waves. Journal of the Society of Naval Architects of Japan, (2000) 187: 405-408.

[4] H. Taguchi, S. Ishida, H. Sawada, M. Minami, Model Experiments of Ship Capsize in Astern Seas. Journal of the Society of Naval Architects of Japan, (1995)177: 207-217.

[5] J. Lu, N. Umeda, K. Ma, Modeling Parametric Rolling in Regular and Irregular Head Seas with Added Resistance Taken into Account. Proceedings of the 5th Asia-Pacific Workshop on Marine Hydrodynamics, Osaka Pref Univ, (2010)93-98.

[6] N. Umeda, H. Hashimoto, F. Stern, S. Nakamura, H. Sadat-Hosseini, A. Matsuda, P. Carrica, Comparison Study on Numerical Prediction Techniques for Parametric Roll. Proceedings 27th Symposium on Naval Hydrodynamics, Seoul Nat Univ, (2008) 5-10.

[7] N. Umeda, A. Francescutto, Performance-Based Ship Operation. Proceedings 2nd International Workshop on Risk-Based Approaches in Maritime Industry, Univ. Strathclyde, (2008)2.2.1-2.2.9.

[8] J. Lu, N. Umeda, K. Ma, Predicting Parametric Rolling in Irregular Head Seas with Added Resistance Taken into Account . J Mar Sci Technol, (2011)16:462-471.

[9] J. Lu, G. Min, N. Umeda, Numerical Approaches on Parametric Rolling in Head Seas. The 10th International Hydrodynamics, Petersburg, Russia, (2012)83-88.

[10] M. Fujino, S. Sakurai, On the Evaluation of Wave Exciting Roll Moment by strip Method, J the Society of Naval Architects of Japan, (1982) 152: 125-137(in Japanese).

[11] M.C. Lee, K.H. Kim, Prediction of Motion of Ships in Damaged Condition in Waves, the 2nd STAB, the Society of Naval Architects of Japan, (1982)13-26.

[12] J. Lu, G. Min, N. Umeda, A Study on the Effect of Parametric Rolling on Heave and Pitch Motions in Head Seas. Proceedings of the 13th International Ship Stability Workshop, Brest, France. (2013)185-191.

[13] J. Lu, G. Min, N. Umeda, Experimental and Numerical Study on Predicting method of Parametric Rolling in Regular Head Seas. Proceedings of the 14th International Ship Stability Workshop, Kuala Lumpur, Malaysia. (2014).

- SESSION 4 -

STOCHASTIC DYNAMICS OF SHIPS AND ASSESSMENT OF PROBABILITY OF STABILITY FAILURES

Calculation Scheme for Wave Pressures with Autoregression Method

Alexander Degtyarev, Ivan Gankevich

Dept. of Computer Modelling and Multiprocessor Systems, Faculty of Applied Mathematics and Control Processes, Saint Petersburg State University, Russia

Abstract: In the problem of simulation of marine object behaviour in a seaway determination of pressures exerted on the object is often done on assumption of ocean wave amplitudes being small compared to wave height, however, this is not the best approach for real ocean waves. This was done due to underlying wind wave models (such as Longuet—Higgins model) lacking ability to produce large amplitude waves. The other option is to use alternative autoregressive model which is capable of producing real ocean waves, but in this approach pressure calculation scheme should be extended to cover large-amplitude wave case. It is possible to obtain analytical solutions for both two- and three-dimensional problem and it was found that corresponding numerical algorithms are simple and have efficient implementations compared to small amplitude case where the calculation is done by transforming partial differential equations into numerical schemes. In the numerical experiment it was proved that obtained formulae work for waves of arbitrary amplitudes whereas existing solutions work in small-amplitude case and diverge in large amplitude case.

Key words: Autoregressive model, hydrodynamic pressure, integral equation, wind wave model, marine object behaviour.

1. Introduction

For many years marine object behaviour in a seaway was investigated through experiments conducted in a towing tank and although in some cases this approach proved to be useful now it has some disadvantages compared to modern techniques. First of all, conducting a single experiment in a towing tank and collecting desired data takes as long as one month to complete. Second, towing tank provides machinery to generate only plane waves which propagate in at most one direction and process of propagation is disturbed by walls of a pool so that real three-dimensional sea waves cannot be generated in the experiment. Finally, all the simulations in a towing tank are carried out not for real-sized ship but for its model and using fitting criteria to generalise experimental results for the real ship is not always feasible; so not every aspect of real behaviour can be captured in a towing tank. As a result of these deficiencies and also as a consequence of development of high-performance computer machines more and more experiments are replaced by computer-based simulations conducted in a virtual testbed.

Virtual testbed being a computer program to simulate physical and anthropogenic phenomena can be seen as an evolution and virtual analogue of a towing tank and it not only lacks disadvantages of a towing tank mentioned above but also offers much broader set of simulation options. For example, in a computer program with help of a proper sea wave generator it is possible to combine climatic and wind wave models [1] and to use assimilated wind velocity field data to simulate wind waves and swell which occur in a particular region of ocean and also to simulate evolution of wave climate between normal and storm weather. Another option is to simulate water streams, ice cover, wave deflection and wave diffraction. However, none of these options were implemented in software to a full extent and often used wind wave models are capable of generating only linear sea. So, virtual testbed approach takes marine object behaviour simulations one level higher than

level offered by towing tank, however, not all the potential of this approach is realised.

Not only different weather scenarios are not implemented in a virtual testbed but wind wave models such as Longuet—Higgins model are capable of generating only linear sea and more effective models can be developed. An alternative autoregressive model is a wind wave model proposed by Rozhkov, Gurgenidze and Trapeznikov [2] and it is advantageous in many ways over Longuet—Higgins model when conducting simulations in a virtual testbed. First, it allows generating realisations of arbitrary amplitude ocean waves whereas Longuet—Higgins model formulae are derived using assumptions of small-amplitude wave theory and are not suitable to generate surfaces of large-amplitude waves [3]. Second, it lacks disadvantages of Longuet—Higgins model: it has high convergence rate, its period is limited only by period of pseudo-random number generator and it can model certain nonlinearities of wave motion such as asymmetric distribution of wavy surface elevation [4]. Finally, autoregressive model has efficient and fast numerical algorithm compared to Longuet—Higgins model which reduces simulation time [5]. However, autoregressive model formulae are not derived from partial differential equations of wave motion but instead represent non-physical approach to wavy surface generation and to prove adequacy of such an approach series of experiments were conducted to show that wavy surface generated by this model possesses integral characteristics as well as dispersion relation of real ocean waves and an ability to reproduce storm weather [3].

Theory of small amplitude waves is also used to determine pressures under sea surface and methods for determining pressures should also be modified to match autoregressive model.

2. Determining pressures

2.1 Two-dimensional case

The problem of pressure determination under real sea surface in case of inviscid incompressible fluid is reduced to solving Laplace equation with dynamic and kinematic boundary conditions [6] and in two-dimensional case an analytical solution can be obtained. In two-dimensional case the corresponding system of equations

$$\begin{aligned} &\varphi_{xx} + \varphi_{zz} = 0, \\ &\varphi_t + \frac{1}{2}\left(\varphi_x^2 + \varphi_z^2\right) + g\zeta = \frac{p_0}{\rho} \qquad at\ z = \zeta(x,t), \\ &\zeta_t + \zeta_x \varphi_x = \varphi_z \qquad at\ z = \zeta(x,t). \end{aligned} \tag{1}$$

can be solved in three steps. The first step is to solve Laplace equation using Fourier method and obtain solution of the form of Fourier integral

$$\varphi(x,z,t) = \int_{-\infty}^{\infty} E(\lambda) e^{\lambda(z+ix)} d\lambda. \tag{2}$$

The second step is to determine coefficients $E(\lambda)$ by substituting this integral into the second (kinematic) boundary condition. The boundary condition is held on the free wavy surface $z=\varsigma(x, t)$ so that velocity potential derivative $\varphi_z(x, t)$ can be evaluated using the chain rule.

After performing these steps the equation

$$\frac{\zeta_t}{\zeta_x + \zeta_t - \zeta_x(\zeta_x + i)} = \int_{-\infty}^{\infty} \lambda E(\lambda) e^{\lambda(\zeta+ix)} d\lambda$$

which represents Laplace transform formula can be obtained and inverted to obtain formula for coefficients $E(\lambda)$:

$$E(\lambda) = \frac{1}{2\pi i}\frac{1}{\lambda}\int_{-\infty}^{\infty} \frac{\zeta_t}{\zeta_x + \zeta_t - \zeta_x(\zeta_x + i)} e^{-\lambda(\zeta+ix)} dx.$$

The final step is to substitute formula for coefficients into (2) which yields equation

$$\begin{aligned} \varphi(x,t) = &\frac{1}{2\pi i}\int_{-\infty}^{\infty} \frac{1}{\lambda} e^{\lambda(\zeta+ix)} d\lambda \\ &\times \int_{-\infty}^{\infty} \frac{\zeta_t}{\zeta_x + \zeta_t - \zeta_x(\zeta_x + i)} e^{-\lambda(\zeta+ix)} dx \end{aligned} \tag{3}$$

Using this equation an explicit formula for pressure determination can be obtained directly from the first boundary condition:

$$p(x_{0,}z_0) = -\rho\varphi_t - \frac{\rho}{2}\left(\varphi_x^2 + \varphi_z^2\right) - \rho g z_{0.}$$

Analytical solution was compared to the solution

$$\frac{\partial\varphi}{\partial x}\Big|_{x,t} = -\frac{1}{\sqrt{1+\alpha^2}} e^{-I(x)} \int_h^x \frac{\partial\dot{z}/\partial z + \alpha\dot{\alpha}}{\sqrt{1+\alpha^2}} e^{I(x)} dx,$$

$$I(x) = \int_h^x \frac{\partial\alpha/\partial z}{1+\alpha^2} dx$$

obtained for small-amplitude waves [7] and numerical experiments showed good correspondence rate between resulting velocity potential fields. In order to obtain velocity potential fields realisations of the wavy sea surface were generated by autoregressive model differing only in wave amplitude. In numerical implementation infinite outer and inner integral limits of (3) were replaced by the corresponding wavy surface size (x_0, x_1) and wave number interval (λ_0, λ_1) so that inner integral converges (this interval contained only those wave numbers which were present in wave energy spectrum of the realisation). Experiments were conducted for waves of both small and large amplitudes and in case of small-amplitude waves both solutions produced similar results, whereas in case of large-amplitude waves only general solution (3) produced stable velocity field (Figure 1–2). Therefore, general solution works for different wavy sea surfaces and does not impose restrictions on the wave amplitude.

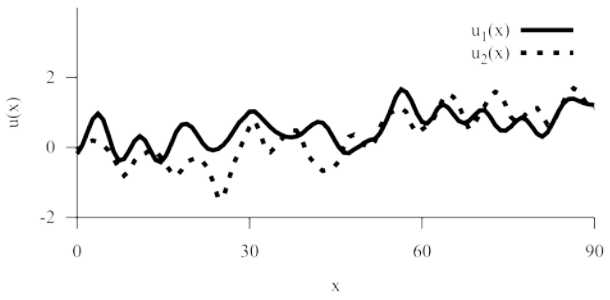

Fig. 1 – Velocity field for small-amplitude case, u_1 – general solution, u_2 – solution for small-amplitude waves.

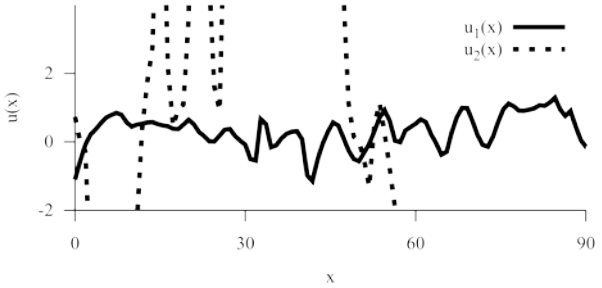

Fig. 2 – Velocity field for large-amplitude case, u_1 – general solution, u_2 – solution for small-amplitude waves.

Resulting solution (3) can be used to compute impact of hydrodynamic forces on a ship's hull and is advantageous in several ways. First, it can be used for wavy surfaces of arbitrary amplitudes to support simulations for small-sized ships or storm weather in a virtual testbed. Second, the formula is analytical and explicit so that no numerical scheme is needed to implement solution of initial system of partial differential equations (1) on a computer; hence, resulting algorithm is fast and easily scalable on a multiprocessor computer.

2.2 Three-dimensional case

The system of equations

$$\varphi_{xx} + \varphi_{yy} + \varphi_{zz} = 0$$

$$\varphi_t + \frac{1}{2}\left(\varphi_x^2 + \varphi_y^2 + \varphi_z^2\right) + g\zeta = \frac{p_0}{\rho} \qquad at\ z = \zeta,$$

$$\zeta_t + \zeta_x\varphi_x + \zeta_y\varphi_y = \varphi_z \qquad at\ z = \zeta$$

for three-dimensional case is solved in a way similar to the two-dimensional problem, however, it involves some additional steps. The first step is to obtain the solution of Laplace equation using Fourier method in a form of

$$\varphi(x,y,z,t) = \int_{-\infty}^{\infty}\int E(\lambda,\gamma) e^{i(\lambda x+\gamma y)+z\sqrt{\lambda^2+\gamma^2}} d\gamma d\lambda.$$

The second step is to substitute this integral into the kinematic boundary condition, however, here integral

transform can not be readily applied. In order to circumvent this wave numbers *(λ, γ)* can be written in polar coordinates *(r, θ)* and space coordinates *(x, y, ζ(x, y))* converted to cylindrical coordinates *(ρ, ψ, ζ(ρ, ψ))*:

$$\zeta_t = \int_0^{\infty} dr \int_0^{2\pi} d\theta \left[f_1 + f_2 \cos(\psi - \theta) + f_3 \sin(\psi - \theta) \right] \times E_1(r,\theta) \exp\left[ir\rho \cos(\psi - \theta) + r\zeta \right],$$

where $f_1 = \zeta_\rho (\cos\psi + \sin\psi) + \frac{1}{\rho}\zeta_\psi (\cos\psi - \sin\psi)\zeta_\rho^2 - \frac{1}{\rho}\zeta_\psi^2,$

$$f_2 = -i\zeta_\rho,\ f_3 = -i\frac{1}{\rho}\zeta_\psi,\ E_1 = r^2 E.$$

After performing these steps the integral on the right hand side can be written as two-dimensional convolution and then Fourier transform can be applied (see Appendix):

$$\frac{\mathsf{F}\zeta_t}{\mathsf{F}\left\{ f_1 g_1 + f_2 g_2 + f_3 g_3 \right\}} = \mathsf{F}E_2,$$

where $g_1 = \exp[ir\cos\theta],\ g_2 = g_1 \cos\theta,$

$g_3 = g_1 \sin\theta.$

The final expression is written as follows.

$$\varphi(x,y,t) = \int_0^{\infty} \int_0^{2\pi} \mathsf{F}^{-1} \left\{ \frac{\mathsf{F}\zeta_t}{\mathsf{F}\left\{ f_1 g_1 + f_2 g_2 + f_3 g_3 \right\}} \right\} \times \exp\left[ir\left(x\cos\theta + y\sin\theta \right) + r\zeta \right] dr d\theta.$$

The explicit formula for pressure determination

$$p(x_0, y_0, z_0) = -\rho\varphi_t - \frac{\rho}{2}\left(\varphi_x^2 + \varphi_y^2 + \varphi_z^2 \right) - \rho g z_0.$$

is obtained from the first boundary condition the same way it is done for two-dimensional case.

Compared to the solution for small-amplitude waves new solution not only works for arbitrary wave amplitudes but also has a number of computational advantages of corresponding numerical algorithm. The solution for small-amplitude case is written as an elliptic partial differential equation

$$\frac{\partial^2\varphi}{\partial x^2}\left(1 + \alpha_{x^2}\right) + \frac{\partial^2\varphi}{\partial y^2}\left(1 + \alpha_{y^2}\right) + 2\alpha_x\alpha_y \frac{\partial^2\varphi}{\partial x \partial y} + \left(\partial\alpha_x / \partial z + \alpha_x \partial\alpha_x / \partial x + \partial\alpha_x / \partial y\, \alpha_y \right)\frac{\partial\varphi}{\partial x} + \left(\partial\alpha_y / \partial z + \alpha_x \partial\alpha_y / \partial x + \partial\alpha_y / \partial y\, \alpha_y \right)\frac{\partial\varphi}{\partial y} + \partial\dot{z} / \partial z + \alpha_x\dot{\alpha}_x + \alpha_y\dot{\alpha}_y = 0$$

which can be solved using multi-grid method [7]. Compared to this formula the new solution requires only numerical integration and fast Fourier transform (FFT) implementations which are well-known, simple, and already available in scientific software libraries. The other advantage is that these algorithms have efficient GPU implementations which allow constructing very efficient computational CPU–GPU pipeline because autoregressive model shows high performance only on CPU [5].

3. Conclusions

Obtained solutions for two- and three-dimensional problems can be used to compute hydrodynamic pressures exerted on a marine object in a seaway, they do not pose restrictions on wave amplitude and are analytical thus having efficient implementations on hybrid CPU & GPU computer architectures.

The future work is to implement three-dimensional problem solution on GPU and measure performance of CPU–GPU computational pipeline.

References

[1] A. Degtyarev, A. Reed, Synoptic and Short-Term Modeling of Ocean Waves, Proceedings of 29th Symposium on Naval Hydrodynamics, 2012.

[2] V. Rozhkov, Yu. Trapeznikov, Stochastic models of oceanological processes, Gidrometeoizdat, 1990 (in Russian: В. Рожков, Ю. Трапезников, Стохастические модели океанологических процессов, Гидрометеоиздат, 1990).

[3] A.B. Degtyarev, A.M. Reed, Modelling of Incident Waves Near the Ship's Hull (Application of autoregressive approach in problems of simulation of rough seas), Proceedings of the 12th International Ship Stability Work-shop, 2011.

[4] A. Boukhanovsky, Stochastic wind wave modeling considering its heterogeneity and non-stationarity: PhD thesis, AANII, 1997.

[5] A. Degtyarev, I. Gankevich, Efficiency Comparison of Wave Surface Generation Using OpenCL, OpenMP and MPI, Proceedings of 8th International Conference "Computer Science & Information Technologies", 2011, p. 248-251.

[6] N. Kochin, I. Kibel, N. Roze, Theoretical hydromechanics, NY: Interscience Publishers, 1965.

[7] A. Degtyarev, I. Gankevich, Evaluation of hydrodynamic pressures for autoregression model of irregular waves, Proceedings of the 11th International Conference on the Stability of Ships and Ocean Vehicles, 2012, p. 842-852.

Appendix

Forming two-dimensional convolution

Two-dimensional convolution on the right hand side of equation

$$\zeta_t = \int_0^{\infty} dr \int_0^{2\pi} d\theta \left[f_1 + f_2 \cos(\psi - \theta) + f_3 \sin(\psi - \theta) \right] \times E_1(r, \theta) \exp\left[ir\rho \cos(\psi - \theta) + r\zeta \right]$$

can be made by applying the following transform.

$$r = \exp r', \ \rho = \exp[-\rho'], \ \zeta = \rho\zeta, \ E_2 = E_1 \exp r'.$$

Now equation can be written as

$$\zeta_t = \int_0^{\infty} dr' \int_0^{2\pi} d\theta \left[f_1 + f_2 \cos(\psi - \theta) + f_3 \sin(\psi - \theta) \right] \times E_1(r', \theta) \exp\left[\exp\left[r' - \rho' \right] \left(i \cos(\psi - \theta) + \zeta \right) \right]$$

and two-dimensional convolution can be applied:

$$\zeta_t = f_1 (E_2 * g_1)(\rho', \psi) + f_2 (E_2 * g_2)(\rho', \psi) + f_3 (E_2 * g_3)(\rho', \psi),$$

where $g_1 = \exp\left[\exp \rho' \left(i \cos\psi + \zeta \right) \right]$,

$g_2 = g_1 \cos\psi, g_3 = g_1 \sin\psi.$

Example of Validation of Statistical Extrapolation

Timothy Smith [1*]

1. David Taylor Model Basin (NSWCCD) USA

Abstract: Statistical extrapolation is a method to predict extreme, rare events from smaller, more common events using relatively short duration data sets. The validation of such methods requires a multi-tier validation approach consistent with the true value data structure. This paper provides a full demonstration of the multi-tier validation approach using roll ship motion with the Generalized Pareto Distribution.

Key words: statistical extrapolation, validation, ship motion

1. Introduction

The validation of numerical simulations is a large field of interest and spans many engineering disciplines. Various professional societies and governmental bodies have outlined verification and validation processes to assist their members [1,2,3]. These processes are often generalized with details left to the engineers actually performing the verification and validation. However, in all cases some comparison is made between the simulation and the "true value," and becomes the basis for a validation decision. The true value comes from scale model testing or higher fidelity simulations.

There are some phenomena, such as large rolling or capsizing, that are at once non-linear and rare. The simulation of these phenomena requires advance, hydrodynamic blended method prediction tools due to the non-linearity involved. The ITTC parametric roll study [4] showed the uncertainty can be quite large due to practical non-ergodicity.

This paper continues Smith and Campbell [5] by providing a worked example to demonstrate the multi-tiered validation approach.

2. Test Case

This test case considers ship roll motion for a range of relative wave heading in a high sea state. Extrapolations are made based on a sub-set of time history data and compared to a directly counted true value at a motion level not necessarily seen in the data set.

2.1 Extrapolation Method

The Generalized Pareto Distribution (GPD) can be used to approximate a tail of any distribution that makes use of a scale and shape parameter to fit the data. There are various implementation details in terms of selecting a threshold and determining the scale and shape parameter. This paper uses the GPD as implemented in [6] as the extrapolation method.

The confidence intervals for the extrapolated estimate were calculated using assumption of the normal distribution of the GPD parameters. This follows the confidence interval method from [6], except the logarithm of the scale parameter was used instead of the scale parameters itself. The use of the logarithm of the scale parameter ensures its positive value.

2.2 True Value

The true value was determined by calculating hundreds of thousands of hours of ship motion simulation using a fully coupled, 3 degree of freedom simulation tool based on volume calculation [7]. This model assumes constant radiation and diffraction

*** Corresponding author:** Timothy Smith, research field: dynamic stability and seakeeping, E-mail timothy.c.smith1@navy.mil

The work described in this paper has been funded by the Office of Naval Research (ONR) under Dr. Ki-Han Kim.

forces with non-linear hydrostatics on 2D strip hull representation. As such it captures essential hydrostatic non-linearity and maintains very fast computation time.

The peaks were extracted using envelope approach [8]. This method ensures independent data samples as required to apply GPD.

The true value of the exceedance rate is found using a direct counting procedure studied in detail in [8]. It compared favourably with theoretical results available from upcrossing theory [9].

3. Validation Approach

This example uses a multi-tier validation approach consisting of a parameter, condition and set criteria [5, 10]. This reflects typical scale model data structures of individual motion channels, a run condition of speed-heading-seaway, and a test consisting of many conditions. Criteria are set to determine an acceptable parameter comparison, and what constitutes an acceptable condition and set.

A parameter comparison is the elemental comparison between the simulation and true value. It refers to a single motion or response. Typically, a condition is the environmental parameters, speed and heading used to define the simulation and the motion response. So a set of environmental parameters, speed and heading and two motions would be two conditions due to the two motions. Thus, condition can be defined as a deterministic vector:

$$\vec{S} = \left(H_S, T_m, V_S, \beta, i_{dx}\right) \tag{1}$$

where H_S is a significant wave height, T_m modal frequency, V_S, forward speed, β- heading, i_{dx} –motion index (say, i_{dx}=4 corresponds to roll). Repeating multiple parameter comparisons for the same condition makes the second tier.

The third tier, the set comparison, defines how many conditions have to pass for the simulation to pass the validation criteria.

For this example, the parameter comparison is the comparison of a statistical extrapolation to the true value at a specified critical motion level. The parameter comparison passes the test if the extrapolation confidence interval captures the true value. Multiple extrapolations are made from different data sets all representing the same condition, that is speed-heading-seaway-motion combination. That condition passes if the true value is captured by the confidence interval at a percentage roughly equal to the confidence level. This is repeated for a number of different conditions. The extrapolation method is considered valid if a high percentage of conditions pass.

Other parameter comparisons besides confidence interval capture to the true value may be used depending on what is important to the application. For instance, the amount of conservatism or absolute distance may be used as a metric. A change of the parameter comparison could change the condition criteria. The multi-tier validation definition used in this study provides a check on both the extrapolation and the confidence interval formulation as both are included in the parameter comparison.

It is also possible to consider the response independently of the environmental conditions in Tier II, the condition level. Then the number of passing responses becomes a criterion to condition passing. This is essentially a bookkeeping issue, but may be conceptually more appealing to some in formulating acceptance criteria.

4. Results

One hundred extrapolations based on different 100 hours of simulation were made using GPD. They were compared to the true value at an evaluation level corresponding to a high motion level in the true data set. The comparison was based on overlap of the 95% confidence interval with the true value.

The evaluation level was selected as the highest level in the true data set that had more than 30 data samples. Thirty samples are enough to have meaningful uncertainty. With less than 30 samples,

the uncertainty becomes very large and the true value has not stabilized.

Fig. 1 shows an example of the parameter comparisons for near following seas, 15 deg heading. In this figure, the true value is represented by a solid line ($1.47x10^{-8}$). Each extrapolation confidence interval is represented by a vertical line. The extrapolation captures the true value if these lines cross. The mean crossing rate is denoted by a circle and the most probable crossing rate is denoted by a cross. The confidence intervals are asymmetric relative to the mean or most probable crossing rate. This is a property of GPD and different than the symmetric confidence intervals more commonly seen with the Normal distribution.

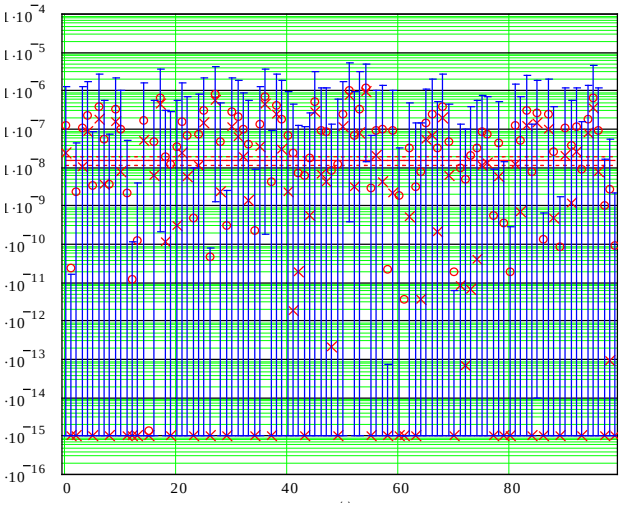

Fig. 1 – Extrapolation-true value comparison plot for roll, 15 deg heading using log normal confidence interval method.

The results for roll are presented in Table 1. The passing rate is the percentage of data sets that pass the parameter comparison, that is, capturing the true value. This table shows an average passing rate, 93.35, that is near the expected confidence level of 95%. Each condition, except for near following seas, 15 deg heading, was also acceptably close to the expected confidence interval. Given only 100 samples, it is unreasonable to expect exactly 95% due to the statistical uncertainty [5]. The 15 degree heading had the lowest roll angles, and the low passing rate could indicate a change in non-linearity at the evaluation level that is not represented at the GPD threshold level.

Most of conditions (6/7) have acceptable passing rates indicating a successful validation of both the mean value extrapolation and the confidence interval. The large confidence intervals certainly contributed to capturing the true value. The fact that the passing rate is not universally 100% indicates the confidence interval is not too large. A complete validation of the extrapolation method would consider many more conditions and motions representing the expected operational scenarios.

Table 1 – Extrapolation results for roll motion and range of headings.

Wave Heading (deg)	Simulation Time (hours)	GPD Threshold Level (deg)	Evaluation Level (deg)	Average Passing Rate
15	230,000	6.947	15	84
30	100,000	12.877	30	91
45	230,000	17.094	60	94
60	100,000	18.754	50	100
90	230,000	16.055	32.5	99
135	230,000	7.359	17.5	92

4.1 Other Considerations

As a point of further discussion, the evaluation level changed based on what was present in the true value data set. This is appropriate for validation. In practice, the true value is not known, and the evaluation level is set arbitrarily at some critical level.

In order to use a validated extrapolation, a further check is required based on the threshold selected for the GPD fit and the evaluation level or critical level. If this difference is too large, there is an indication that the extrapolation is meaningless and should be ignored.

The determination of "too large" requires some understanding of the physical properties involved. Fortunately, for these conditions the motion levels are low enough to be able to ignore them as "too small to care about." Alternatively, more data may be added to increase the GPD fit threshold in borderline cases. This will also reduce the uncertainty.

For the sake of argument, if the passing rates had not been near the desired 95%, the culprit could be the extrapolation method or the confidence interval formulation. A separate investigation would be required to confirm the confidence interval formulation as the comparison is based on confidence interval. For instance, the confidence interval can be evaluated using synthetic data with a known distribution.

6. Conclusions

This paper demonstrated the applicability of a multi-tier validation approach to a statistical extrapolation method based on the Generalized Pareto Distribution. The first tier, parameter comparison, was made by comparing the 95% confidence interval from a GPD extrapolation to the true value. This was done 100 times to determine a passing rate for the second tier, condition, comparison. Lastly, most of the conditions passed the second tier criterion, which passes the third tier, or set, comparison. The extrapolation method would be considered validated. A rigorous validation effort would specify passing percentages at Tiers I and II.

The use of confidence interval for the Tier I comparison implies a working confidence interval formulation. Other comparison metrics, e.g., mean to true value distance, can be used instead if confidence interval is not useful.

The ratio of the GPD threshold and the evaluation level provides a metric for practical use. The conditions with low motions can either have more data added, in the hope of increasing the GPD threshold level, or ignoring the condition as having negligible motions.

Acknowledgments

The author is grateful to Dr. V. Belenky for providing the data and analysis tools for the numerical example and thorough editing of the manuscript.

References

[1] AIAA, Guide for the Verification and Validation of Computational Fluid Dynamics Simulations. American Institute for Aeronautics and Astronautics, Reston, VA (1998).

[2] ASME, Standard for Verification and Validation in Computational Fluid Dynamics and Heat Transfer, American Society of Mechanical Engineers, New York (2009).

[3] ITTC Loads and Responses Seakeeping, Verification and Validation of Linear and Weakly Nonlinear Seakeeping Computer Code, Procedure 7.5-02-07-02.4 Rev 1 (2011).

[4] The Specialist Committee on Stability in Waves, Final Report and Recommendations to the 26th ITTC, Proc. 26th International Towing Tank Conference, Vol II, Rio de Janeiro, Brazil (2011).

[5] T. Smith and B. Campbell, On the Validation of Statistical Extrapolation for Stability Failure Rate, Proc. 13th Intl. Ship Stability Workshop, Brest, France (2013).

[6] B. Campbell, V. Belenky, and V. Pipiras, On the Application of the Generalized Pareto Distribution for Statistical Extrapolation in the Assessment of Dynamic Stability in Irregular Waves, Proc. 14th Intl. Ship Stability Workshop, Kuala Lumpur, Malaysia (2014).

[7] Weems, K. & D. Wundrow, "Hybrid Models for Fast Time-Domain Simulation of Stability Failures in Irregular Waves with Volume-Based Calculations for Froude-Krylov and Hydrostatic Force", Proc. 13th Intl. Ship Stability Workshop, Brest, France (2013).

[8] Belenky, V. & B. Campbell,. Evaluation of the Exceedance Rate of a Stationary Stochastic Process by Statistical Extrapolation Using the Envelope Peaks over Threshold (EPOT) Method. Naval Surface Warfare Center Carderock Division Report NSWCCD-50-TR-2011/032 (2011).

[9] Kramer, H., and Leadbetter, M.R., Stationary and Related Stochastic Processes, John Wiley, New York (1967).

[10] Smith, T. C., "Approaches to Ship Motion Simulation Acceptance Criteria" Proc. of 11th Intl Conference of the Stability of Ships and Ocean Vehicles, Athens, Greece pp 101-114 (2012).

Critical Distance on a Phase Plane as a Metric for the Likelihood of Surf-Riding in Irregular Waves

Vadim Belenky[1*], Kostas Spyrou[2] and Kenneth Weems[3]

1. *David Taylor Model Basin (NSWCCD), USA*
2. *School of Naval Architecture, National Technical University of Athens, Greece*
3. *Leidos, Inc., USA*

Abstract: The paper addresses the formulation of a metric for the likelihood of surf-riding in irregular waves. This likelihood is a critical element of the split-time method that allows the inclusion of physics in statistical extrapolation. The candidate metric is the distance on the phase plane between the current position and the instantaneous boundary of attraction to the stable surf-riding equilibrium. The distance is measured along the line connecting the position of the dynamical system and the stable surf-riding equilibrium at the initial moment.

Key words: Surf-riding, dynamical system, equilibrium, attraction.

1. Introduction

The split-time method [1] is a procedure for evaluating the probability of a rare stability failure in irregular waves from relatively short samples of time domain data. The application of the method requires the formulation of a metric for the likelihood of stability failure that can be computed at certain, non-rare instances in the time domain. For the case of capsizing due to pure loss of stability, the metric is the difference between the observed and critical roll rate at the instant of upcrossing of an intermediate threshold. The objective of the present study is to formulate such a metric for surf-riding in irregular waves.

The physical mechanism of surf-riding includes the appearance of dynamical equilibria and a ship's attraction to the stable equilibrium [2]. The equilibria appear when the wave surging force becomes large enough to offset the difference between the ship's thrust and its resistance at wave celerity. The equilibrium points are the positions of the ship on the waves where the forces balance exactly. The dynamics of surf-riding in regular waves is fairly well understood [3], but surf-riding in irregular waves is to large extent *terra incognita*. Some advances in the understanding of surf-riding in multi-frequency waves are described in [4]. One of the most significant issues in this area has been the development of an effective definition of wave celerity in irregular waves and practical procedures for calculating it. Unlike the regular wave case where wave celerity is constant, celerity in irregular waves will vary in both space and time and must be considered as a stochastic process of its own. In a similar fashion, the magnitude of the maximum wave surging forces in irregular waves will be varying in space and time.

With this time-dependence of both the wave celerity and the maximum surging forces in irregular waves, a balance of the wave surging, thrust and resistance forces may not always be possible, so the surf-riding equilibrium may exist for only a limited time. Because the time of the existence of equilibrium is not usually limited in mechanics, it would be more

[*] **Corresponding author:** Vadim Belenky, research field: dynamic stability, stochastic dynamics of ships.
E-mail: vadim.belenky@navy.mil

The work described in this paper has been funded by the Office of Naval Research (ONR) under Dr. Ki-Han Kim and ONR Global under Dr. Woei-Min Lin This support is gratefully acknowledged by the authors.

appropriate to use the term "quasi-equilibrium" in relation to surf-riding in irregular waves.

Indeed, the existence of the quasi-equilibrium is a necessary, but not sufficient, condition for surf-riding, as actual surf-riding includes ship's attraction. In the case of regular waves, the appearance of the system inside the area of attraction to the equilibrium is the sufficient condition of surf-riding. The formulation of the sufficient conditions for irregular waves is more difficult. Even while the quasi-equilibrium exists, there is no reason to believe that the area of attraction stays the same. It is quite possible also that the topology of phase plane may change back and forth between "coexistence of surging and surf-riding" and "surf-riding only." To accommodate this, the sufficient condition for surf-riding can be formulated in terms of the distance, in the phase plane, between the instantaneous positions of the quasi-equilibrium and the dynamical system. This formulation may be further extended with a requirement for the dynamical system to spend a certain amount of time in the vicinity of the quasi-equilibrium, thus allowing time for the ship to reach surf-riding condition. This condition is especially important when considering broaching-to following surf-riding, as it may take some time for the yaw instability (if it exists) to develop into broaching-to.

If the quasi-equilibrium does exist at an arbitrary instant of time, there is a neighborhood around the quasi-equilibrium that corresponds to surf-riding and that will exist while the quasi-equilibrium exists. Consider the position of the dynamical system on the phase plane at this instant. If this position is located within the neighborhood, then surf-riding occurs. The distance to the boundary of such a neighborhood can therefore be considered as a possible candidate for the metric of the likelihood of surf-riding. The distance can be measured by the line between the ship's position and the quasi-equilibrium, but must account for the time dependence of the equilibrium and the neighborhood.

2. Mathematical Model

Consider a simple model for one-degree-of-freedom nonlinear surging:

$$(M + A_{11})\ddot{\xi}_G + R(\dot{\xi}_G) - T(\dot{\xi}_G, n) + F_X(t, \xi_G) = 0 \qquad (1)$$

Here M is mass of the ship, A_{11} is longitudinal added mass, R is resistance in calm water, T is the thrust in calm water, n is the number of propeller revolutions, F_X is the Froude-Krylov wave surging force, and ξ_G is longitudinal position of the center of gravity in the Earth-fixed coordinate system; the dot above the symbol stands for temporal derivative. Polynomial presentations are used for the resistance and thrust:

$$\begin{aligned} R(U) &= r_1 U + r_2 U^2 + r_3 U^3 \\ T(U, n) &= \tau_1 n^2 + \tau_2 n U + \tau_3 U^2 \end{aligned} \qquad (2)$$

The coefficients r and τ are meant to be fit to the appropriate calm water curves [5].

As the model is meant at this stage to be qualitative, a linear wave-body formulation is appropriate. Therefore,

$$F_X(t, \xi_G) = \sum_{i=1}^{N} A_{Xi} \cos(k_i \xi - \omega_i t + \varphi_i + \gamma_i) \qquad (3)$$

Here A_{Xi} is the amplitude of the surging force for each component frequency of the incident wave, while γ_i is the phase shift between the wave elevation and the force components. Details of the surging force calculation can be found in [1].

3. Candidate Metric – Distance to the Manifold

First, consider the case of regular waves. The boundary for the domain of attraction to a stable equilibrium is the unstable invariant manifold. It can be computed by integration in inverse time from unstable equilibrium, as illustrated in Fig. 1.

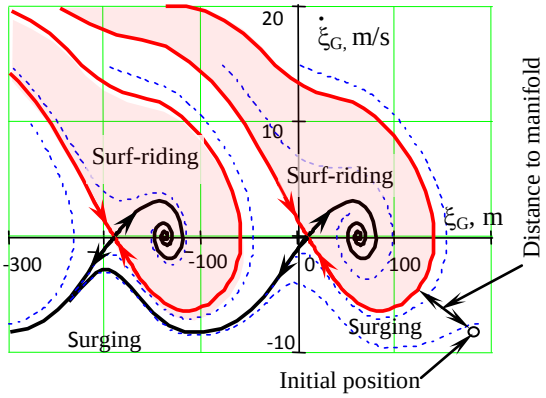

Fig. 1 – Phase plane for co-existence of surging and surf-riding in regular waves

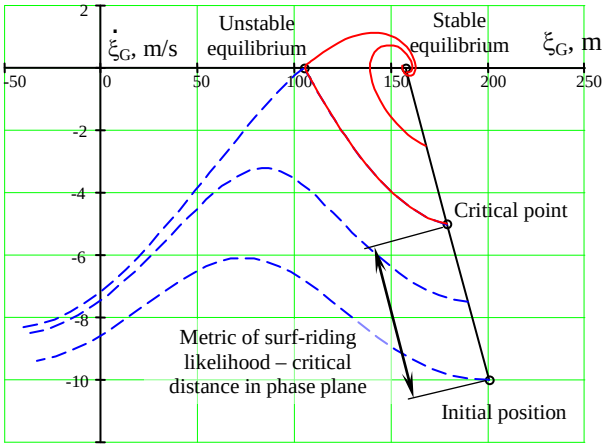

Fig. 2 – Perturbation algorithm to find a "distance to manifold"

However, the direct calculation of the invariant manifold may be not trivial in numerical sense. It requires careful management of the step of integration. In principle, such an approach can be extended to irregular waves [6], but the calculation cost renders such an approach impracticable.

However, it is not necessary to know the entire manifold in order to evaluate the distance. To find the single point on the manifold that characterizes the distance, one may consider a perturbation algorithm, similar to [1]. Fig. 2 illustrates such a calculation that consists of short simulations. Initial conditions for these simulations lie on the line connecting the dynamical system's position and the stable equilibrium at an arbitrary instant of time.

The initial position in Fig. 2 corresponds to surging. The variation of the initial conditions along the line (between the initial position and the stable equilibrium) defines an iterative process that converges to the critical point, at which the difference between initial conditions leading to surging and surf-riding falls below a pre-defined tolerance. These calculations converge after 9~12 iterations with the relative tolerance at 0.1%, and they take about a second on a single processor of a standard laptop computer.

5. Metric in the Time Dependent Dynamical System

The introduction of the irregular waves into the dynamical system defined by equation (1) essentially makes it time dependent [7]. Prior to the full implementation of irregular waves, the concept can be tested by considering an artificial time dependence consisting of simultaneous changes of wave frequency and amplitude, as illustrated in Fig.3. These changes alter the balance between thrust and resistance (see Fig.4). As a result, the surf-riding equilibria cease to exist around t=280 seconds, and surf-riding becomes impossible after that time. Fig.5 shows the evolution of the surf-riding equilibria caused by these changes to the waves.

The introduction of time dependence into the dynamical system changes the situation significantly. The surf-riding equilibria move, the domain of attraction changes, and the boundaries of the attraction move and are no longer invariant. However, the calculation result for the metric with perturbations looks very similar to the regular wave case, as shown in Fig. 6.

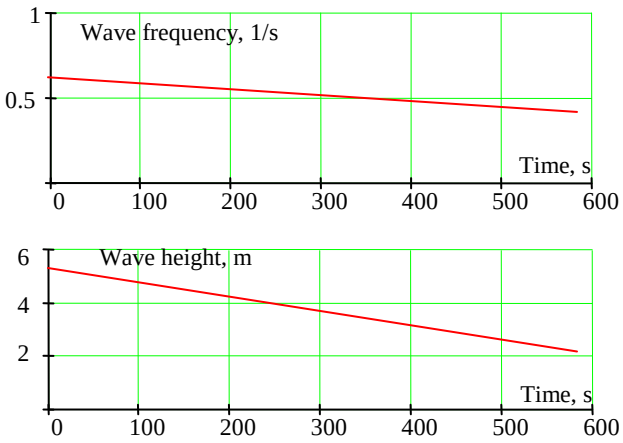

Fig. 3 – Wave parameters for artificial time-dependence

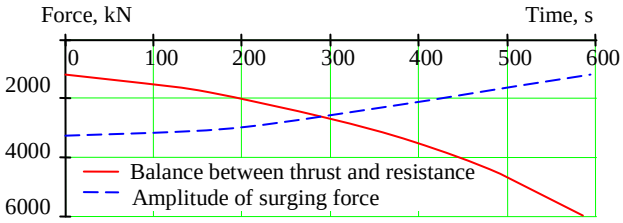

Fig. 4 – Changes in forces caused by time dependence

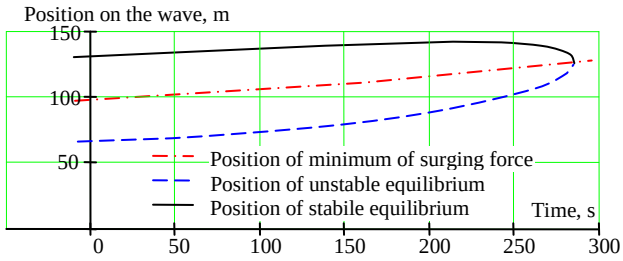

Fig. 5 – Evolution of surf-riding equilibria

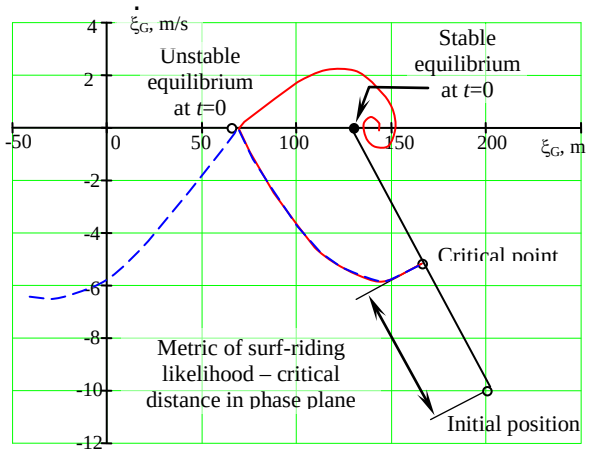

Fig. 6 – Perturbation algorithm to find a "distance to manifold"

However, some changes can be seen. The initial positions of the equilibria are no longer in the centers of the saddle and focus points. Indeed, the saddle point is located where the unstable equilibrium will be when the dynamical system will reach that position in phase plane. The same statement can be made with regard to the position of the stable equilibrium and the focus point.

6. Conclusions and Future Work

The present study addresses the formulation of a metric for the likelihood of surf-riding that could be applied to the case of irregular waves. Indeed this formulation implies existence of surf-riding equilibria at the time instance when the metric is evaluated.

The candidate metric is a distance between a given position of the dynamical system in the phase plane and the boundary of attraction to the stable surf-riding equilibrium. The metric is measured along the line between the position of the dynamical system and stable equilibrium at the same instant of time. It has been demonstrated that the candidate metric can be computed for a model of the dynamical system incorporating a time-dependence of the wave parameters.

The next step is to determine if the metric can be computed for the dynamical system under stochastic excitation and then whether the occurrence of surf-riding in a long series of simulations can be predicted by extrapolation of this metric from a short series of simulations.

Acknowledgements

The authors are grateful to Dr. Art Reed, Tim Smith, and Brad Campbell of David Taylor Model Basin and to Nikos Themelis and Ioannis Kontolefas of the National Technical University of Athens for fruitful discussion of this work.

References

[1] Belenky, V.L., Weems, K.M., Lin. W.M., & Spyrou, K.J. "Split Time Method for the Probabilistic Characterization of Stability Failures in Quartering Seas," *Intl. Shipbuilding* (2013), 60:579-612

[2] Makov, Yu. L. "Some results of theoretical analysis of surf-riding in following seas", *Transactions of Krylov Society*, "Manoeuvrability and Seakeeping of Ships" (1969) Vol. 126, Sudostroenie publishing, Leningrad, pp.124-128 (in Russian)

[3] Spyrou, K.J. "Dynamic instability in quartering seas: The Behavior of a Ship During Broaching," *J Ship Research* (1996), Vol. 40, No 1, 46-59

[4] Spyrou, K.J., Belenky, V., Themelis, N., & Weems, K.M., "Detection of Surf–Riding Behavior of Ships in Irregular Seas," *Nonlinear Dynamics* (2014)

[5] Spyrou, K.J., "Asymmetric Surging of Ships in Following Seas and its Repercussions for Safety," *Nonlinear Dynamics* (2006), 43: 149-172

[6] Vishnubholta, S., Falzarano, J., & Vakakis, A. "A New Method to Predict Vessel / Platform Critical Dynamics in a Realistic Seaway," *Phil. Trans. of the Royal Soc. Of London. Series A – Mathematical Physical and Engineering Sciences* (2000), 358:1967-1981

[7] Spyrou, K., Themelis, N., & Kontolefas, I. "What is surf-riding in an irregular sea?" *Proc. of 14th Intl. Ship Stability Workshop*, Kuala Lumpur (2014)

On the Application of the Generalized Pareto Distribution for Statistical Extrapolation in the Assessment of Dynamic Stability in Irregular Waves

Bradley Campbell[1], Vadim Belenky[1], Vladas Pipiras[2]

1. *David Taylor Model Basin (NSWCCD), USA*
2. *University of North Carolina at Chapel Hill, USA*

Abstract: Stability failures of intact ships can be characterized as the exceedance of some critical level of roll, pitch, and accelerations. The events that need to be characterized for a probabilistic assessment generally have a level of rarity so that they cannot be observed in a reasonable amount of model test runs or simulations. The Peaks Over Threshold (POT) method is a promising technique in the assessment of these rare stability failures. POT methods model the tail of the distribution of peaks as a Generalized Pareto Distribution, which is formally derived from the Generalized Extreme Value distribution. Using Generalized Pareto Distribution in a POT framework allows for the assessment of the probability (with confidence intervals) of these rare events through statistical extrapolation.

Key words: Dynamic Stability, Capsize, Extreme Event, Direct Assessment, Statistical Extrapolation, Probabilistic Assessment

1. Introduction

In the assessment of the dynamic stability of ships, probabilistic frameworks are generally employed to quantify, in some way, the risk of stability failure. For intact ships a stability failure can be characterized by the exceedance of some high level of the roll, pitch, or acceleration of the ship.

As the large amplitude motion of a ship can be a highly nonlinear process, the assumption of a Gaussian process does not hold. Since the rich set of tools accompanying a Gaussian process are not applicable, other approaches are needed in order to characterize the nature of the extreme events. In severe cases (i.e. very high sea states) descriptive statistics may suffice if enough failures can be observed in physical model tests or Monte Carlo simulations. For seaways where extreme events are sufficiently rare but the risk is still not negligible, the amount of model test runs or Monte Carlo simulations (given the requirements of a hydrodynamic code for this task [1]) becomes intractable. Inferential statistics provide ways of dealing with these types of cases through techniques of statistical extrapolation and extreme value theory.

2. Peaks Over Threshold Methods

The extreme value theorem (sometimes referred to as the Fisher-Tippet-Gnedenko theorem) states that the largest value of a set of independent and identically distributed data (IID) in a fixed time period, *T*, will (for "large" values of T) be distributed via the Generalized Extreme Value (GEV) distribution [2]. While this theorem is extremely valuable, its asymptotic nature (with respect to the size of the time window) means it makes poor use of available data.

The second extreme value theorem (the Pickands–Balkema–de Haan theorem) states that distribution of exceedances of a sufficiently high

* **Corresponding author:**, Bradley Campbell research field: dynamic stability, stochastic dynamics of ships. E-mail: bradley.campbell@navy.mil

The authors wish to thank Dr. Pat Purtell and Dr. Ki-Han Kim at the Office of Naval Research for their support of this work. Participation of Dr. Pipiras was facilitated by the summer faculty program supported by ONR and managed by Dr. Jack Price of David Taylor Model Basin..

threshold can be approximated using the Generalized Pareto distribution (GPD). Use of the GPD, which is derived from the GEV distribution [3] [2], also relies on the peaks also satisfying the IID condition.

3. Peaks Over Threshold For Dynamic Stability Assessment

The general framework for the use of POT methods for stability assessments is discussed in [4], [5], and [6]. In order to ensure the IID requirement is satisfied, the peaks of the piece-wise linear envelope, rather than the peaks of the signal, are used. The theoretical envelope (derived through a Hilbert transform) is not used as its peaks are not always a subset of the signal peaks. As the level is increased the exceedance rate computed using either envelope or signal peaks approach each other, but the IID condition will only be met using the envelope peaks for intermediate level thresholds. The envelope peak extraction process is illustrated in Figure 1.

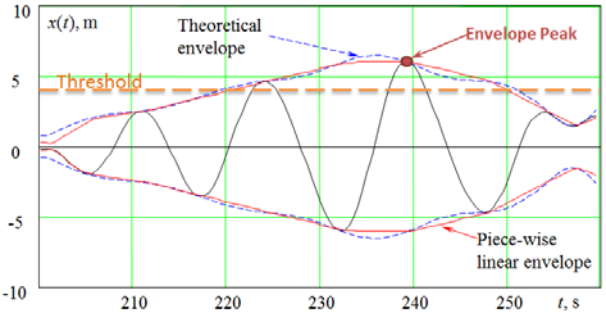

Figure 1. Envelope Peak Selection

The exceedance rate of level a is then given by:

$$\lambda_a = \lambda_\mu \cdot (1 - F(x > a | x > \mu)) \qquad (1)$$

Where a is the level of interest, μ is the threshold, λ_μ is the rate of exceedance of threshold μ, and $F(x>a|x>\mu)$ is the conditional probability that a will be exceeded given that μ has been exceeded. It is this conditional probability that needs to be computed accurately for this type of method to work, since the level of interest (defined as a stability failure) may be higher than the any peak observed during a model test or set of simulations, as shown by sample histogram and GPD fit in Figure 2.

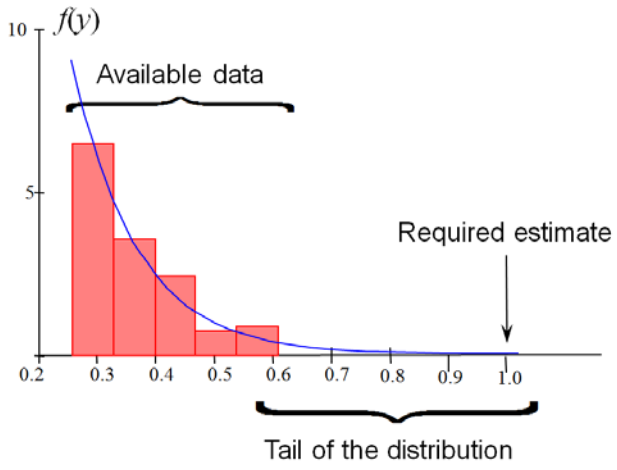

Figure 2. Histogram in GPD Fit of Ship Motions Data

4. Modeling the Distribution of Peaks Over Threshold

4.1 Definition of the Probability Density Function

As stated in section 2, the GPD is used to model the conditional distribution of peaks over the threshold. The probability density function of the GPD has three parameters, location (μ), shape (k) and scale (σ). The location parameter is generally taken as the assumed threshold. The probability density function is given by equation (2).

$$f(x) = \begin{cases} \frac{1}{\sigma} \cdot \left(1 + k \cdot \frac{x-\mu}{\sigma}\right)^{-\left(1+\frac{1}{k}\right)} & k \neq 0 \\ \sigma \cdot e^{-\sigma \cdot (x-\mu)} & k = 0 \end{cases} \qquad (2)$$

The associated cumulative density function is given by equation (3).

$$F(x) = \begin{cases} 1 - \left(1 + k \cdot \frac{x-\mu}{\sigma}\right)^{\frac{-1}{k}} & k \neq 0 \\ 1 - \exp\left(\frac{x-\mu}{\sigma}\right) & k = 0 \end{cases} \qquad (3)$$

When the shape parameter k is zero, the GPD reduces to the exponential distribution. The tail of a normal process will behave in this way. When k is positive the tail is said to be heavy and higher levels become more likely than as modeled with the exponential distribution. Conversely, when k is negative the tail is said to be light, and higher levels have a smaller probability of exceedance.

4.2 Light Tails

For cases where the tail is light ($k < 0$), the GPD has a right bound, x_B, which is given by:

$$x_B = \mu - \frac{\sigma}{k} \quad (4)$$

Above x_B the probability of exceedance is identically 0. It is important to note that the derivative of the cumulative density function (CDF) gets very steep in the vicinity of x_B. This means that small changes in x lead to large changes in the probability of exceedance. The practical implication is that the confidence interval on the predicted exceedance rate can be very large near x_B.

4.2 Parameter Estimation

The parameters of the GPD are estimated using the Maximum Likelihood Estimation (MLE) method. The MLE method is based on the assumption that the observed data is the most likely data. The Maximum Likelihood (ML) estimator for a probability density function, f, with parameter set $\bar{\theta}$, is given by:

$$L(\bar{\theta}) = \prod_{i=1}^{n} f(x_i|\bar{\theta}) \quad (5)$$

where the x_i values are the observed data. The value of the L is maximized with respect to the parameters $\bar{\theta}$. In practice the natural logarithm of the likelihood function is used as certain algebraic simplifications that ease the complexity of the calculations can be achieved and the product operator becomes a summation operator. The estimates the distribution parameters, k and σ, from the MLE method are approximately normally distributed.

4.3 Confidence Interval of the Distribution Parameters

The confidence interval on the distribution parameters, k and σ, may be calculated using the delta method. The delta method assumes the parameters are normally distributed and that the ML estimator is a deterministic function of random arguments. The ML estimator is linearized and the variances of the parameters are computed by, first, computing Fisher Information matrix, M_F, a 2x2 matrix of the 2nd partial derivatives of the likelihood function. The covariance matrix is the inverse of M_F and the variances of the parameters are the diagonal elements of covariance matrix. The off-diagonal terms give the covariance of the parameter estimates. The confidence interval on the parameters is obtained assuming the parameter estimates are the mean value of a normal distribution with variances from the covariance matrix.

The profile log-likelihood method is another method for determining the confidence intervals on the distribution parameters [7]. The profile log-likelihood method has the advantage that the resulting confidence intervals need not be symmetric, but the computational cost is much higher. For the calculation of the parameter confidence intervals, this computational burden likely does not yield much gain.

4.4 Threshold Selection

A critical part of using the GPD effectively is selecting an appropriate threshold. Tanaka et. al. provide an overview of several commonly used methods and compare their performance [8]. Typical methods of threshold selection are graphical in nature, as many applications only deal with one dataset.

These methods include:

- Shape parameter plot (see Figure 3 - Top)
- Modified scale parameter plot (see Figure 3 – Bottom)
- Mean excess plot

In order to be useful for the probabilistic assessment of ship stability failure, the threshold selection method must be automated. The shape and modified scale parameter plots can be easily automated, while the mean excess plot (sometimes call the mean residual life plot) is a little more difficult to automate in a sensible fashion. For the shape and modified scale

parameter plots, the main idea is that above the minimum threshold, these values should be (statistically) constant with respect to the threshold.

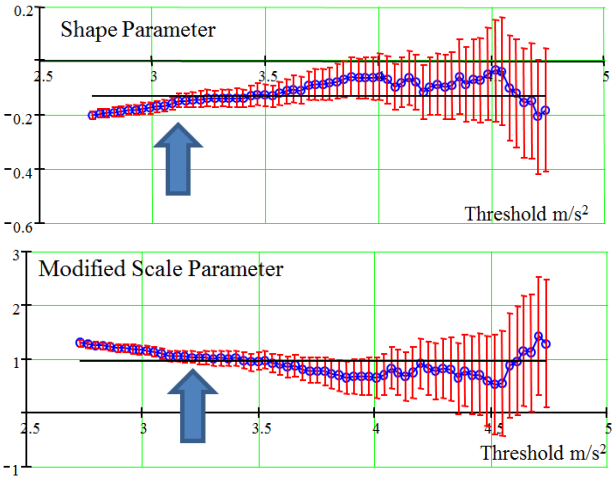

Figure 3. Sample Shape Parameter Plot (Top) and Modified Scale Parameter Plot (Bottom)

Additionally Reiss and Thomas [9] suggest two related alternative methods based on minimizing the difference between the shape parameter at a given threshold and the mean or median of the shape parameter for all of the thresholds above.

All of these methods give a lower bound on the threshold choice. The selected threshold must therefore be at least as high as the highest low bound from this set of methods. Additionally, given the sensitivity of the probability near the x_B when the tail is light, selection of the threshold with the highest shape parameter can help shrink the size of the confidence interval to some extent.

5. Extrapolation of the Conditional Probability of Exceedance

The conditional probability of exceedance is computed using equation (3). This value of the probability is based on the mean value of the parameter estimates. As the equation (3) is a non-linear function and can be treated as a deterministic function with random arguments, the mean probability will not be equal to the probability computed using the mean of the parameter estimates.

There are several techniques to compute the confidence interval on the probability estimate. The CDF of the extrapolated probability of exceedance, F_p, may be computed using equation (6). The confidence interval would then be assessed from the quantiles of the CDF.

$$F_P(z) = \begin{cases} \int_{-\infty}^{\infty} \left(\int_{-\infty}^{\sigma_{\lim}(k;z\geq 0)} f(k,\sigma) d\sigma \right) dk & z \geq 0 \\ 0 & z < 0 \end{cases}$$

Where:

$$\sigma \leq \sigma_{\lim}(k; z > 0) = \begin{cases} \frac{k}{z^{-k} - 1}(c - a) & ; \quad k \neq 0 \\ -\frac{(c-k)}{\ln(z)} & ; \quad k = 0 \end{cases} \tag{6}$$

The parameter space contained by the parameter confidence intervals may contain area where the computed probability is zero. If this is the case, then there is a discontinuity in the CDF of probability of exceedance. This is visible in Figure 4, where $F_P(0)$ is the amount of area where F_p is zero. In this case the lower bound of the confidence interval on the probability of exceedance will be zero.

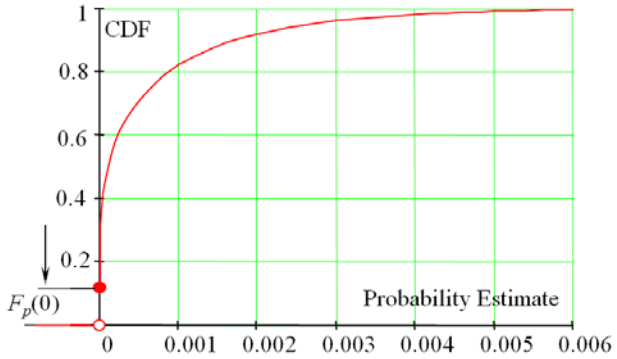

Figure 4. CDF of the Probability of Exceedance

Another method to be considered is an indirect method using the Profile Log-likelihood method mentioned earlier. The confidence intervals are developed for the return level and then mapped to the corresponding probability. This indirect use of the Profile Log-likelihood Method seems to be the more

accurate than the CDF based technique based on investigations using data sampled from a parent GPD. Issues still arise near the right bound in the case of a light tail.

6. Validation Considerations

Some work has been done on the validation of statistical extrapolation methods for use in ship dynamics. Smith discussed some initial validation results [10]. Generally these types of methods fair well, though more work needs to be done in this area.

7. Conclusions

Peaks Over Threshold methods can be very effective in the prediction of large ship motions or stability failures for intact ships. The Generalized Pareto distribution has some behaviors which need to be understood, particularly for light-tailed processes, in order to make proper use of it. The study of light-tailed processes and the behavior of the confidence interval for the probability of exceedance have been given some treatment in the present work, but have not been studied as deeply as heavy-tailed processes and return levels in available literature.

Acknowledgments

The authors also wish to thank Dr. A. Reed and T. Smith, (David Taylor Model Basin, NSWCCD), Prof. P. Spanos (Rice University) and Prof. M. R. Leadbetter (University of North Carolina) for many fruitful discussions.

References

[1] R. F. Beck and A. M. Reed, "Modern Computational Methods for Ships in a Seaway," *SNAME Transactions*, vol. 109, pp. 1-48.

[2] M. R. Leaderbetter, G. Lindgren and H. Rootzen, Extremes and Related Properties of Random Sequences and Processes, New York: Springer-Verlag, 1983.

[3] J. Pickands, "Statistical Inference Using Extreme Order Statistics," *The Annals of Statistics*, vol. 3, no. 1, pp. 119-131, 1975.

[4] B. Campbell and V. Belenky, "Assessment of Short-Term Risk with Monte-Carlo Method," in *Proceedings of the 11th International Ship Stability Workshop*, Wageningen, NL, 2010.

[5] B. Campbell and V. Belenky, "Statistical Extrapolation for Evaluation of Probability of Large Roll"," in *Proceedings of the 11th International Symposium on Practical Design of Ships and Other Floating Structures*, Rio de Janeiro, Brazil, 2010.

[6] V. Belenky, K. Weems, C. Bassler, M. Dipper, B. Campbell and K. Spyrou, "Approaches to Rare Events in Stochastic Dynamics of Ships," *Probabilistic Engineering Mechanics*, vol. 28, pp. 30-38, 2012.

[7] S. Coles, An Introduction to Statistical Modeling of Extreme Values, London: Springer-Verlag, 2001.

[8] S. Tanaka and K. Takara, "A Study on Threshold Selection in POT Analysis of Extreme Floods.," in *The Extremes of Extremes: Extraordinary Floods*, Reykjavik, 2002.

[9] R.-D. Reiss and M. Thomas, Statistical Analysis of Extreme Values, Boston: Birkhäuser, 1997, pp. 137-138.

[10] T. C. Smith, "Example of Validation of Statistical Extrapolation," in *Proceedings of the 14th International Ship Stability Workshop*, Kuala Lumpur, Malaysi, 2014.

- SESSION 5 -

STABILITY OF OFFSHORE FLOATING PLATFORMS

An Experimental Investigation on Reduction of List Angle of a Semi-submersible Platform in Head Sea

Nam Woo Kim[1], Bo Woo Nam[1], Young Myung Choi[1], Sa Young Hong[1,2,*]

1. *Offshore Plant Research Division, Korea Research Institute of Ships and Ocean Engineering, Daejeon, Korea*
2. *Dept. of Ship and Ocean Plant Engineering, University of Science and Technology, Daejeon, Korea*

Abstract: In this study, an experimental investigation has been made to investigate reduction of second-order roll motion of a semi-submersible platform in head sea condition by adding hull damping. The second-order heave drift force and roll drift moment are known as main triggers inducing the list angle (Hong et al., 2010). Hong et al. (2013) showed the possibility of reduction of list angle by changing pontoon shape and adding damping device on the hull by numerical calculations. One of their findings was that the reduction of the list angle due to increasing pontoon surface damping is significant. A series of model tests with a 1:50 scaled model of semi-submersible were carried out at the wave basin of KRISO. It was experimentally found that adding damping on hull surface is effective for suppression of list angle.

Key words: List angle, semi-submersible, model test, nonlinear roll, reduction of list angle

1. Introduction

As oil and gas exploration region has been moving to deeper and deeper water regions, the use of semi-submersible platforms is expected to increase both for drilling and production. Two new concepts of semi-submersibles can be found, the one with deeper draft and non-uniform pontoon for deep water production platform and the other one with shallow draft for deep water drilling rig.

The deep water semi-submersible with increased draft and large damping plate was devised to use dry tree. The shallow draft semi-submersible was designed for deep water drilling in relatively mild sea states. For shallow draft semi-submersible platforms, so called list angle has been reported by Voogt et al. (2002, 2007). The list angle is defined as the steady roll angle under head sea condition.

Their model experiments revealed that the list angle occurs only for specific wave periods and the existence of current magnifies the list angle.

Hong et al. (2010) showed that the second-order heave drift force and roll drift moment are main triggers inducing the list angle. Hong et al. (2013) showed that the reduction of the list angle can be possible by changing pontoon shape and adding damping device on the hull. But their conclusions were drawn from numerical results only. One of their findings was that the reduction of the list angle by increasing pontoon surface damping is significant. This is an important design point of view since adding hull damping is relatively an easy job compared with changing hull design.

In this study an experimental investigation has been made to investigate reduction of second-order roll motion of a semi-submersible platform in head sea condition. A series of model tests with a 1:50 scaled model of semi-submersible were carried out at the KRISO Ocean Engineering Basin. The effect of adding hull surface damping on the list angle was

*** Corresponding author:** Sa Young Hong, Principal Researcher, Professor, research fields: floating body dynamics, hydroelasticity, offshore plant and position keeping system. E-mail: sayhong@kriso.re.kr

investigated by changing hull surface roughness. The effect of plate barriers equipped to the pontoon top on the list angle was also discussed in view of suppression of trapped waves over the pontoons.

2. Model Tests

2.1 Test Set-up

The model test was carried out for a 1/50 scaled semi-submersible drilling rig with four columns and twin pontoons. Fig. 1 shows the semi-submersible model. The model test was conducted under the condition of the survival draft.

Fig. 1 Photo of Semi-submersible Model

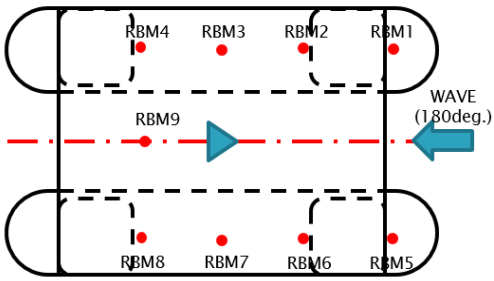

Fig. 2 Position of wave height meters (RBM)

6-DOF motions were measured with a non-contacting type motion sensor (RODYM), wave run-ups were measured for locations near front and back of columns. Fig. 2 shows the positions of wave probe (RBM). The test model was positioned with a 4-point soft spring mooring. The water depth was set to be 3.2m. Fig. 3 is a schematic view of the model setup and the model scene in the Ocean Engineering Basin is shown in Fig. 4.

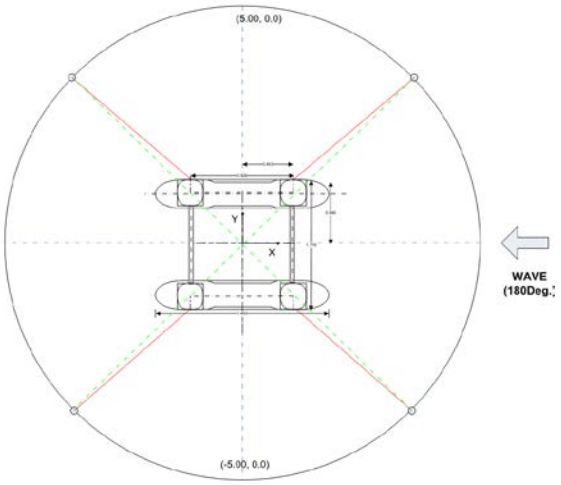

Fig. 3 Schematic View of the model setup

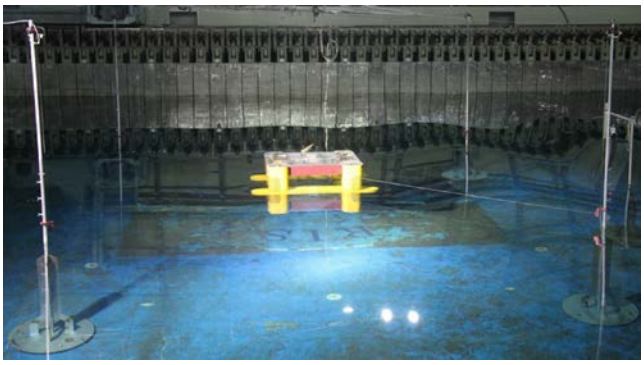

Fig. 4 Photo of Semi-submersible model setup

Table 1 Conditions of Experiment

Item	*Bare hull*	*w/* plates	*w/* damper
Wave height	2m, 4m, 6m	4m	4m
Wave period	6.5, 7.0, ~, 17.0, 19.0(s)	8.0, 8.5, ~, 11.0, 12.0(8)	8.0, 8.5, ~, 11.0, 12.0(8)
Draft	Survival (14.5m)	Survival (14.5m)	Survival (14.5m)

2.2 Test Conditions

The model test was conducted for three hull conditions, bare hull, pontoon with vertical barriers (plates) and pontoon with viscous damping device

(sponge layer). The details are summarized in Table 1. For bare hull condition wave period ranges from 6.5 seconds to 19 seconds with 1.0 second interval. Wave heights were 2m, 4m, and 6m for each wave condition. For the hull with appendages, wave period ranges from 8.0 seconds to 12 seconds with focus on the occurrence of list angle. Fig. 5 presents the models with appendage (vertical plate) and damping layer, respectively.

(a) Vertical plated hull model

(b) Sponge layered hull model

Fig. 5 The model hull with appendages and damping layer

3. Results and Discussions

3.1 Motion Response

Heave and pitch responses in regular waves are shown in Fig. 6 for three hull shapes; bare hull, pontoon with vertical plates and hull with sponge layer on the upper surface. No noticeable response change is observed for change of hull conditions. Numerical results by using HOBEM (Higher Order Boundary Element Method) show generally good agreement with experimental values. Slight discrepancy around wave frequency 0.4 ~ 0.6 rad/s, which can be explained by shallow draft effects where nonlinear effect is not negligible.

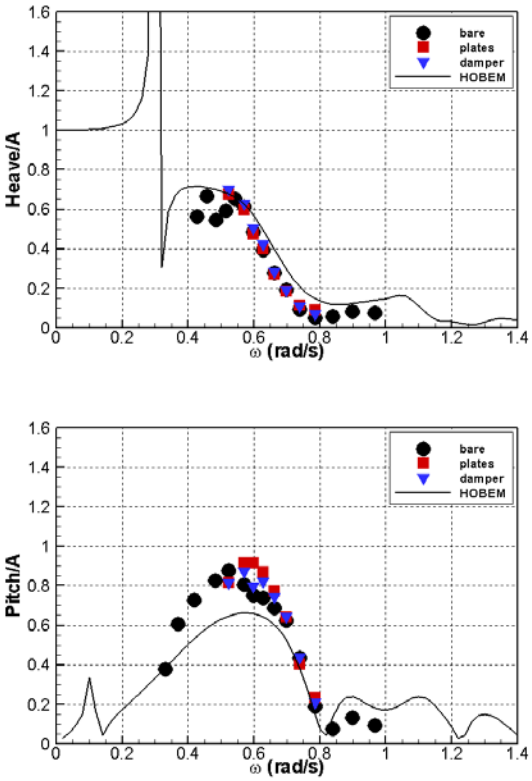

Fig. 6 Comparison of heave and pitch responses in regular waves for three hull shapes of semi-submersible

3.2 List Angle

The list angle of bare hull model was measured for wave heights of 2m, 4m and 6m, respectively. For the cases of hulls with vertical barriers and sponge layer on the pontoon top, wave height of 4m was applied. Two typical time histories of roll and heave motions are shown in Figs. 7 and 8. The case for wave height of 4m and period of 8.5s is shown in 7. It can be clearly seen that heave motion is small but mean

heave motion is significant, which implies that upward heave drift force is one of important parameters of list angle. The measured list angle is about 1.0°. The other case for wave height of 4m and period of 11s is shown in Fig. 8, in which large heave motion but smaller mean value is observed. The measured list angle is about 1.8°. The survival draft is 14.5m while pontoon height is 9.6m, so the effective draft from the top of pontoon is just 4.9m which is very shallow considering wave length and wave height. Two results show that the magnitude of mean heave and amplitude of heave motion are both important in occurrence of list angle.

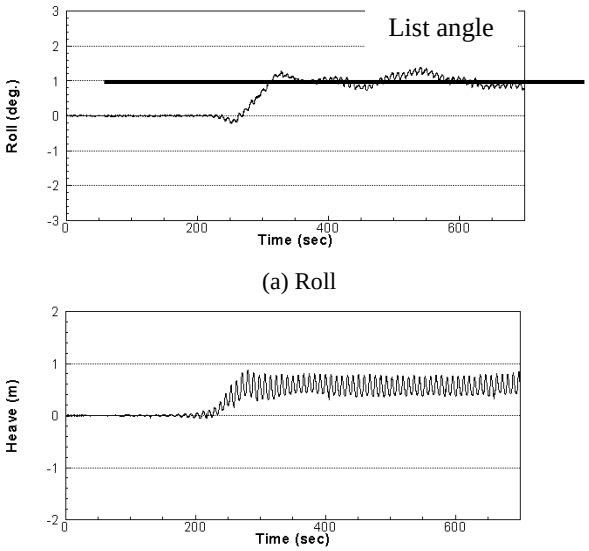

(a) Roll

(b) Heave

Fig. 8 Time histories of wave height 4m, wave period 8.5s

Fig. 10 summarizes the list angle of bare hull case for wave heights of 2, 4 and 6m. It can be seen that list angle occurrence is different for wave heights. For wave height of 2m, the list angle is noticeable for relatively high wave frequency, around 0.7~0.8 rad/s. For wave height of 4m, noticeable list angle occurs at wide wave frequency range 0.55 ~ 0.8 rad/s which corresponds to wave periods of 8.0 ~ 11seconds where upward heave drift force is dominant. It is interesting to observe list angle is not noticeable for wave height of 6m in which wave breaking was observed in the model test presumably due to shallow draft over the pontoon top.

Fig. 11 shows measured and predicted heave drift forces for the same condition as Fig. 10. The calculated value was obtained by using HOBEM, initial heeling angle 3 degrees was assumed (Hong et al., 2013). The measured value shows qualitatively and quantitatively similar trend with the calculations but the measured value shows a little bit broader distribution. This means that viscous effect should be considered in the calculation for more detailed analysis.

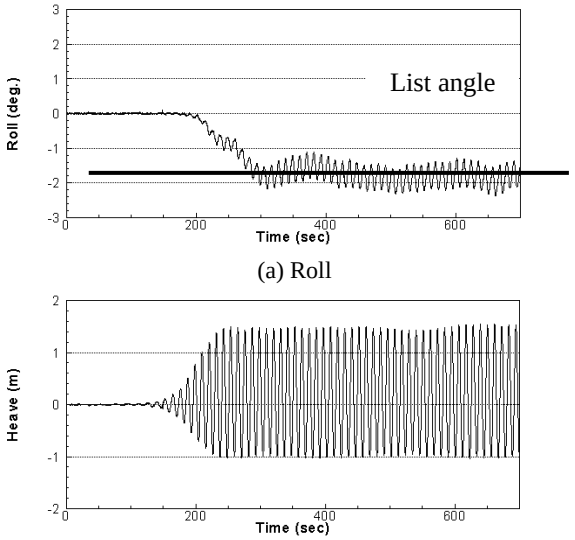

(a) Roll

(b) Heave

Fig. 9 Time histories of wave height 4m, wave period 11.0s

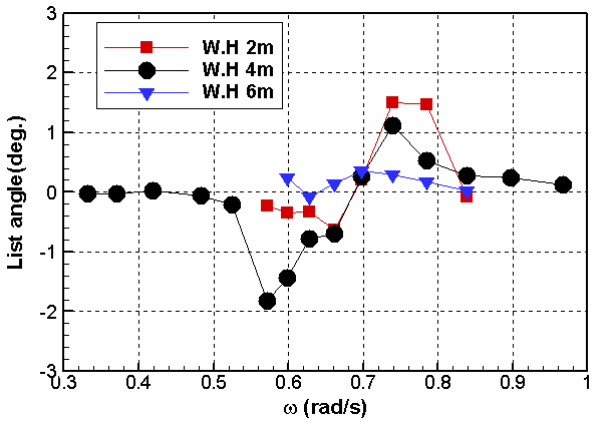

Fig. 10 List angle of bare hull, wave height 2, 4, 6m

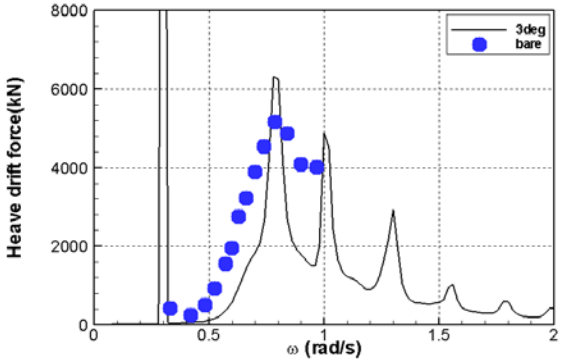

Fig. 11 Comparison of measured and calculated heave drift forces

3.3 Effect of Appendages

Two appendages were equipped as shown in Fig. 5, the vertical plate and sponge layer were devised to dissipate trapped wave energy between main columns. As shown in Fig. 12, two different types of appendages show noticeable effect on suppression of list angles. The sponge layer damping device show list angle suppression effect over wide range of wave frequencies while the vertical damping plate show the effect for specific wave frequency. This result implies that the surface damping device is more efficient for suppressing list angle in practice considering application of this kind of damping device.

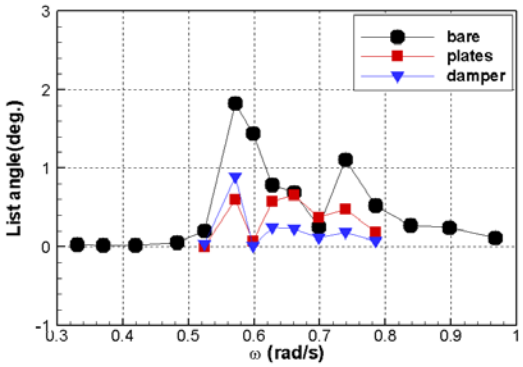

Fig. 12 Comparison of measured list angle for three different pontoon appendages

Fig. 13 shows comparison of time histories of roll and heave motions for two typical list angle occurrences. In the figure, reduction of list angle by adding damping such as vertical plates and sponge layer is significant. But it is interesting to observe that heave motion is not sensitive to adding appendages. This explains that adding damping is only effective to suppressing initial heel, not mean heave motion. This is quite reasonable because the damping does not contributes to mean value.

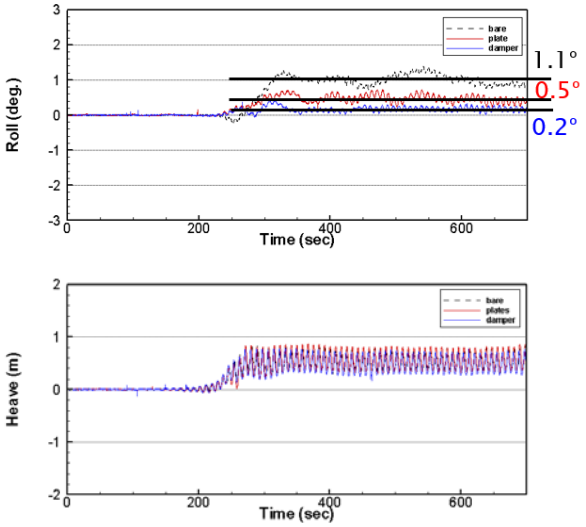

(a) Wave period =8.5s, H=4m

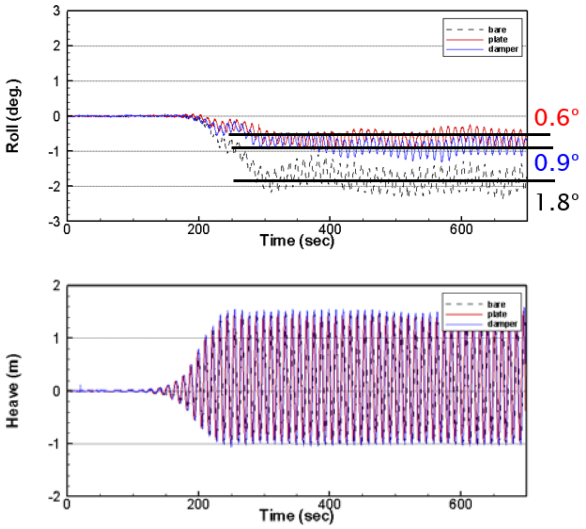

(b) Wave period =11s, H=4m

Fig. 13 Time history of roll in head sea for three different pontoon appendages

Figs. 14 and 15 compare waves measured at mid of pontoons, RBM 3 and 7 locations for wave periods of 8.5 and 11 seconds, respectively. Appendages change the patterns of trapped waves significantly. Uneven bare hull trapped waves become symmetric wave patterns to center plane by virtue of appendages. The vertical plates disturbed trapped waves more than sponge layer damper.

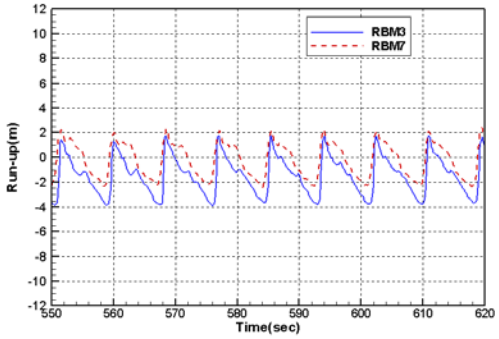

(a)Bare hull

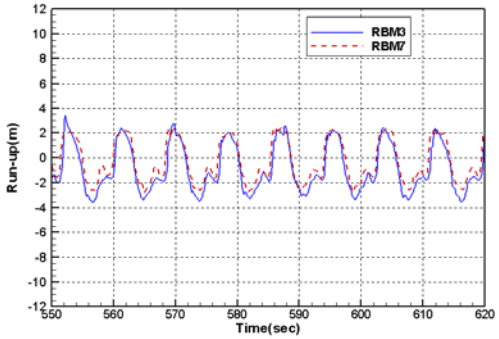

(b)Vertical plate

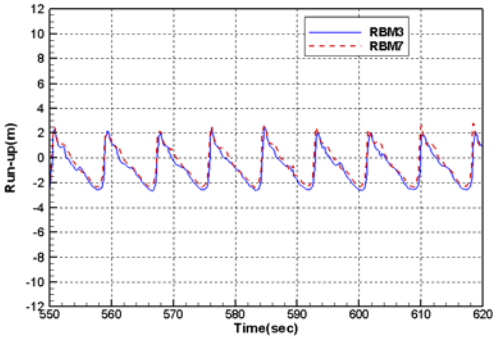

(c)Sponge damper

Fig. 14 Comparison of trapped wave at mid of pontoons for three different pontoon appendages (8.5 seconds)

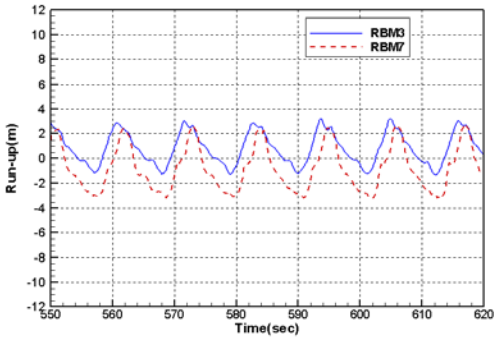

(a)Bare hull

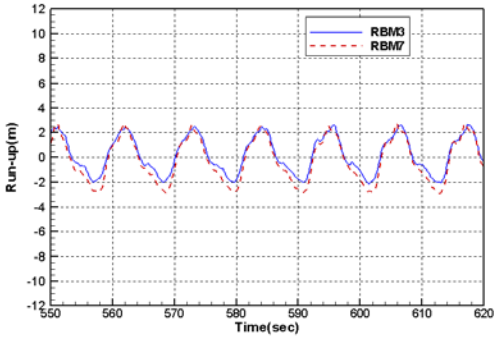

(b) Vertical plate

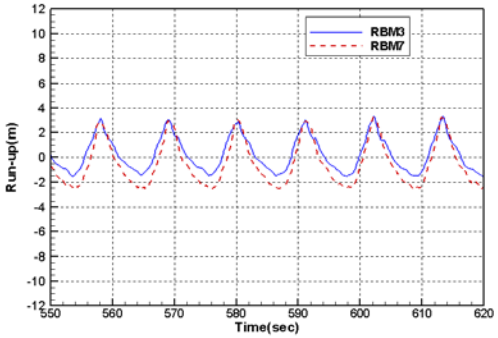

(c) Sponge damper

Fig. 15 Comparison of trapped wave at mid of pontoons for three different pontoon appendages (11 seconds)

In case of wave period of 11 seconds, similar behaviors can be observed. The area between starboard wave and portside wave can be interpreted as heeling moment. It can be seen that the area between both side waves is reduced by damping

devices. Fig. 15 shows trapped wave patterns for outside of list angle occurrence wave periods, both side wave are symmetric to each other.

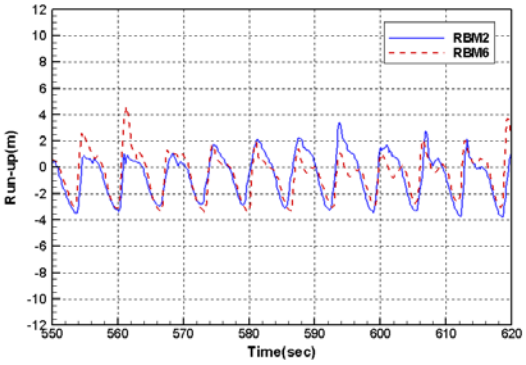

(a) Wave period = 6.5 seconds

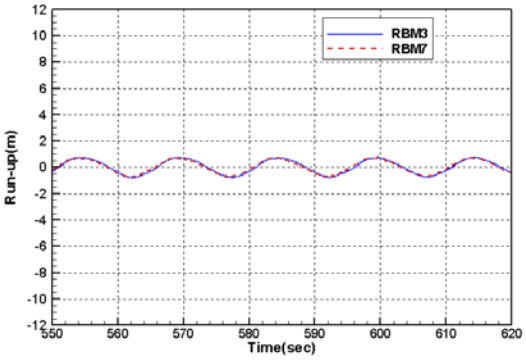

(b) Wave period = 15 seconds

Fig. 15 Comparison of trapped wave at mid of pontoons for bare hull

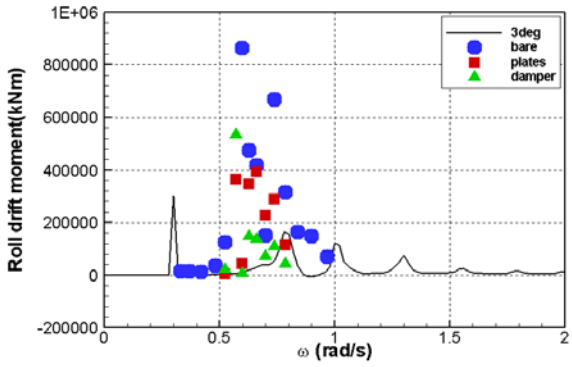

Fig. 16 Comparison of measured and calculated roll drift moments in head waves for different pontoon appendages

Fig. 16 compares roll drift moment for different hull appendages, solid line denotes calculated value by using HOBEM assuming 3 degrees initial heeling. Overall trends are similar between measured roll drift moments and calculated one but measured moment is much larger. Such discrepancy can be explained by the limited capability of potential flow model to this kind of problem.

6. Conclusions

The results of the model test for suppression of list angles of semi-submersible drilling rig were discussed. It was shown that the list angles noticeably reduced by adding appendages such as vertical barriers (plates) and viscous damping devices (sponge layer). The list angle suppressed significantly with sponge damper for wide range of wave periods, while vertical plates was only effective for specific waves, relatively longer waves. It was experimentally confirmed that adding damping on hull surface is effective for suppression of list angle, which was numerically predicted by Hong et al.(2013).

Adding damping contributes to make uneven trapped wave symmetric both side, which enhances stability to suppress initial heel due to heave motion. No noticeable changes wave observed for heave motion by adding damping to hull surface.

Acknowledgments

The present work was supported by a Grant-in-Aid for Strategy Technology Development Programs from the Korea Ministry of Trade, Industry and Energy (No.10038598, “Development of deep water installation design and analysis technology”). This work was supported by the principal R&D program of KIOST: “Performance Evaluation Technologies of Offshore Operability for Transport and Installation of Offshore Structures” granted by Korea Research Council of Public Science and Technology.

References

[1] Voogt, AJ, Soles, JJ and Dijk, RV (2002). "Mean and Low Frequency Roll for Semi-submersibles in Waves", Proc 12th Int. Offshore and Polar Eng Conference, ISOPE, Kita-Kyushu, pp 379-384

[2] Voogt, AJ and Soles, JJ (2007). "Stability of Deepwater Drilling Semi Submersibles," Proc 10th Int Symp on Practical Design of Ships and Other Floating Structures, Houston

[3] Hong, SY, Nam, BW, Kim, JH, Hong, SW, Kim, YS (2010a). "Secon-order motion characteristics of a semi-submersible platform in waves," Proc 11th PRADS, pp. 266–274

[4] Hong, SY, Nam, BW, Kim, NW and Cho, YS (2013). "Investigation of Nonlinear Roll Motion Characteristics of a Shallow Draft Semi-submersible" Proc 13th ISSW, pp28-35

- SESSION 6 -

MANEUVERABILITY AND STABILITY CONSIDERATIONS IN ADVERSE CONDITIONS

A Numerical Study on Maneuverability under Steady Equilibrium Condition in Waves for Free-running Model Ship

Ryosuke Suzuki [1, *], Michio Ueno [1] and Yoshiaki Tsukada [1]

1. *Dept. of Fluids Engineering and Ship Performance Evaluation, Marine Dynamics Research Group, National Maritime Research Institute, Japan.*

Abstract: Authors developed a method; rudder effectiveness and speed correction (RSC), which makes both speed response in waves and rudder response of free-running model ships similar to those of full scale ships by using an auxiliary thruster.

In this paper, the speed and the maneuvering responses of free-running model ships applied RSC in waves on steady straight-running equilibrium condition and those of full scale ships are compared by numerical simulations. As the result, authors revealed that the speed decrease in waves as well as the maneuvering response of free-running model ships applied RSC are able to be precisely similar to those of actual full scale ships. In addition, they also revealed the applicability of RSC in extreme severe seas and showed possibility to evaluate speed decrease and maneuverability for full scale ships in these seas experimentally.

Key words: Speed response and rudder effectiveness similarity, Scale effect, Speed decrease in waves, Maneuverability in adverse conditions, Maneuverability Auxiliary thruster.

1. Introduction

Because of the introduction of EEDI regulations for new built ships, it is said that ships which have a small engine compared with their size are built to pass regulations easily. Therefore, determining minimum propulsion power to maintain the maneuverability in severe seas is encouraged. In order to determine them, evaluation of speed decrease in severe heading waves for full scale ship is necessary as International Maritime Organization (IMO) proposes [1]. Those evaluation depends on only numerical calculations, since speed response in waves on free-running model experiments can't be similar to that of full scale ships because of the large difference of Reynolds number between model ships and full scale ships.

Although methods to estimate the speed decrease in waves for full scale ships near designated speed are in adequate level thanks to many successful researches regarding added resistance in waves, for example Tsujimoto et al. [2], it is required to estimate added resistance at not designated speed but low ship speed in order to evaluate speed decrease in severe heading waves by numerical calculations. In addition, wave drift sway forces and yaw moments are also needed to be formulated for the evaluation of maneuverability not only in heading seas but also in the other wave direction like oblique heading waves. However, methods to estimate them have not been developed enough yet because of the difficulty in model experiments to measure them [3]. Moreover, large different phenomena between in clam water and in severe seas, for example change of wake coefficient in waves, should be revealed enough for reliable sophisticated numerical tools. For these reasons, it is obvious that alternative more accurate methods to evaluate maneuverability in adverse conditions are necessary instead of numerical simulations.

Authors have proposed RSC [4][5] which is the method to make both speed response and rudder response of free-running model ships in clam seas and waves similar to those of full scale ships by using a

*** Corresponding author:** Ryosuke Suzuki, Researcher, research fields: marine engineering, marine dynamics. E-mail: suzuki-r@nmri.go.jp

duct fun type auxiliary thruster which can generate time varying longitudinal force for free-running model tests [6]. They have showed by numerical simulation that RSC can estimate maneuvering response of full scale ships by free-running maneuvering model tests.

In this report, the speed and the maneuvering responses of free-running model ships applied RSC in waves on steady straight-running equilibrium condition and those of full scale ships are estimated by numerical simulations for the aim of evaluating maneuverability in adverse conditions experimentally. As the results, authors disclosed that RSC can evaluate the speed decrease and the maneuvering responses in waves for full scale ships on straight-running conditions by free-running model tests and it can be applied in extreme rough seas in which ship speed decrease largely and drift angle and rudder angle become quite large. Since not only wave drift forces and moments but also all of actual phenomena in rough seas which are difficult to consider are reflected in the model experiment, these results imply they are not needed to be formulated thanks to RSC.

2. Methods of the Numerical Simulation

2.1 Algorithm and governing equations

Equations of surge and sway, yaw motions on steady straight-running equilibrium condition (1) according to the concept of MMG [7] are solved for ship speed V and drift angle β, rudder angle δ by Newton's method. Coordinate system in the simulation is body fixed axis system showed in Fig.1.

$$\begin{aligned} X &= X_0 + X_P + X_D + X_R + X_W + X_A + T_A = 0 \\ Y &= Y_D + Y_R + Y_W + Y_A = 0 \\ N &= N_D + N_R + N_W + N_A = 0 \end{aligned} \quad (1)$$

where, an item of subscript *0* means resistance in clam seas and an item of subscript *P* is thrust by propeller, items of subscript *D* and *R, W, A* are maneuvering forces and moment and those by rudder, and waves (wave drift forces and moments), wind respectively. T_A is longitudinal force by auxiliary thruster.

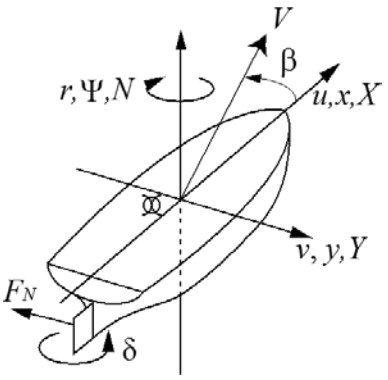

Fig. 1 – Coordinate system in the simulations

2.2 formulations of each items in governing equations

Resistance in clam water X_0 is calculated by (2).

$$X_0 = -\frac{\rho}{2} S_w u^2 \{C_W(Fn) + (1+k)C_{F0}(Rn) + \Delta C_F\} \quad (2)$$

where, ρ is density of fluid, S_W is wetted surface area, u is longitudinal ship speed, C_W is wave resistance coefficient, $1+k$ is form factor, C_{F0} is frictional resistance coefficient of a corresponding plate, ΔC_F is roughness allowance coefficient and zero in model scale. C_{F0} is calculated by ITTC procedures [8].

Thrust by propeller is calculated by (3).

$$X_P = (1-t)\rho K_T D_p^4 N_p^2 \quad (3)$$

where, t is thrust deduction fraction and constant value at self propulsion point, D_P is diameter of a propeller, N_P is propeller race of revolution, K_T is thrust coefficient and can be described by (4).

$$\begin{aligned} K_T &= a_0 + a_1 J + a_2 J^2 \\ J &= u(1-w)/nD_P \end{aligned} \quad (4)$$

where, 1-w is wake coefficient and this is a function of drift angle, J is propeller advance ratio.

Maneuvering forces and moments are calculated by Kang's method [9] which is applicable in large drift angle ($-90\text{deg} \leqq \beta \leqq 90\text{deg}$). Derivatives for Kang's Method are estimated by Kang's regression model for a blunt-body ship [9].

Forces and moments by rudder are described as (5).

$$\begin{aligned} X_R &= -(1-t_R)F_N \sin\delta \\ Y_R &= -(1+a_H)F_N \cos\delta \\ N_R &= -(x_R + a_H x_H)F_N \cos\delta \end{aligned} \quad (5)$$

where, x_R is the location of a rudder (=-L/2), a_H and x_H are interactive force coefficients among hull, propeller and rudder, t_R is coefficient of additional drag force. These coefficients were assumed constant. F_N is rudder normal force and can be described as the following (6).

$$F_N = \frac{\rho}{2} A_R f_\alpha U_R^{\ 2} \sin \alpha_R \qquad (6)$$

where, A_R is rudder area, f_α is the gradient of the lift coefficient of rudder, U_R and α_R represent rudder inflow velocity and angle respectively.

Longitudinal wave drift force X_W is estimated by Tsujimoto's proposal [2]. Y_W and N_W at any ship speed are estimated by interpolating the database whose wave drift forces and moments at zero ship speed are calculated by three-dimensional panel method [10], and they are interpolated by using ship type and principals. Y_W and N_W in all ship speed are assumed not to change from values at zero ship speed.

Wind forces and moments are calculated Fujiwara's method [11] and coefficients for the method are estimated by statistical equations (Ueno et al. [12]).

Auxiliary thruster force for models is described by (7) [13] and it is zero in case of full scale ships.

$$T_A = f_{TA} T_{SFC} = f_{TA}(X_{0m} - X_{0S}\big|_{us'=um'}) \qquad (7)$$

where, T_{SFC} is the force required for skin friction correction (SFC), f_{TA} is defined auxiliary thruster coefficient and it depends on the way to use the auxiliary thruster, for example f_{TA}=1 in SFC. f_{TA} in the simulations are showed in section 3.2.

3. A Ship and Conditions in the Simulation

3.1 A ship for simulations

Principal dimensions of tanker for simulations, KVLCC1 [14], whose model length and scale ratio are 2.909m and 1/110.0 respectively are listed in Table 1. *1+k* and C_W for models are from model tests by Kim et al. [15]. *1-w* and *1-t*, K_T of a model, coefficients for forces and moments by rudder are from Yoshimura et al. [16]. Scale effects for full scale ships are considered in *1-w* and K_T, ΔC_F and they are estimated in accordance with the ITTC procedures [8]. The other coefficients are assumed to have no scale effects.

A full scale ship condition and four model conditions of KVLCC1: model point and ship point applied SFC, rudder effectiveness correction (REC) [13], RSC, were simulated.

Table 1 Principal dimensions of tanker, KVLCC1

item	Full scale	Model
Scale ratio	1	1/110.0
Length b.p.s. L [m]	320.0	2.909
Breadth [m]	58.0	0.527
Draft, d [m]	20.8	0.189
Wetted surface area [m^2]	27320	2.258
Propeller diameter, D_P [m]	9.86	0.090
Propeller pitch ratio	0.721	0.721
The number of a propeller blade	4	4
Rudder type	Horn rudder	
Movable rudder area[m^2]	112.26	0.00928
Rudder height[m]	15.8	0.144

3.2 conditions of propellers and auxiliary thrusters

The full scale ship was considered maneuvering with constant propeller rate of revolution corresponding to the designated ship Froude number, 0.142. Therefore, those for models at model point and ship point, REC are also given as constant values corresponding to the designated ship Froude number and they are listed in Table2. That for RSC is given as a function of Froude number in waves by following RSC definitions [4][5] to make speed and maneuvering response of models similar to those of full scale ships and showed in Fig.2, though the revolution for full scale ships is considered to be constant.

Auxiliary thruster coefficient f_{TA} of RSC is also given as a function of Froude number in waves and showed in Fig.2. This value also determined by following the definitions of RSC [4][5]. On the other hands, f_{TA} in the other cases are constant value listed in Table2. Although *1-w* was assumed a function of drift angle in the numerical simulation, f_{TA} and propeller rate of revolution for RSC were calculated

by assuming that *1-w* was constant at self propulsion point for the simplification.

Table 2 Propeller rates of revolution and Auxiliary thruster coefficients f_{TA} in the simulation

	Scale	N_P[RPM]	f_{TA}
Full scale ship	Full	75.7	-
Model at model point	Model	1049.6	0.0
Model at ship point	Model	747.9	1.0
Model, REC [11]	Model	893.7	0.566
Model, RSC	Model	Function of Froude number (Fig. 2)	Function of Froude number (Fig. 2)

3.3 Wave and wind conditions

Waves in simulations were considered regular waves and short-crested irregular waves without swells. Ratio of wave height H_W to ship length L in regular waves is 1/72 and wave direction is 30 deg (oblique heading waves). Significant wave heights and mean wave periods in short-crested irregular waves correspond to the values of Beaufort scale of wind in state 8 ($H_{1/3}$=5.5m, T_W=9.1sec for full scale) and 11 ($H_{1/3}$=11.5m, T_W=13.1sec for full scale). Their frequency spectrums are ISSC spectrums and directional distributions are $\cos^2$.

Wind is not considered in regular waves and that in short-crested irregular waves is assumed uniform. The wind speed correspond with BF8 (U_A=19.0m/s) and BF11 (U_A=30.6m/s) respectively. Wind direction was assumed to correspond with principal wave direction.

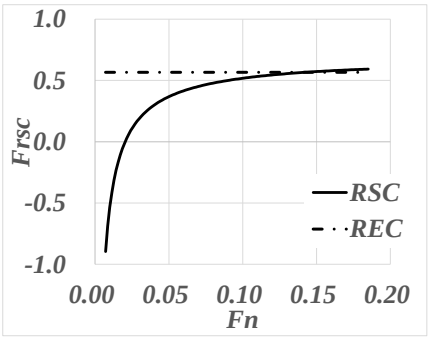

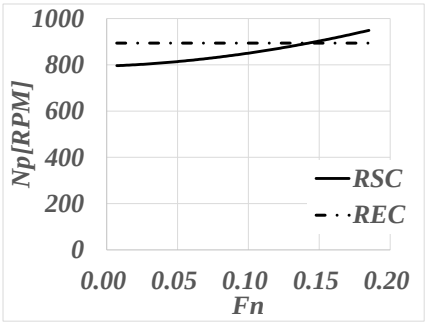

Fig. 2 – Propeller rate of revolution and Auxiliary thruster coefficient f_{TA} for RSC

4. Simulation Results

4.1 Results in regular waves

The simulation results; speed ratio V/V_0, drift angle β, rudder angle δ, on steady straight-running equilibrium condition in regular waves are showed in Fig.3-5. Simulation results at model point indicate that speed response in waves and maneuvering response of free-running models without corrections cannot be similar to those of full scale ships. It is caused that self propulsion points are different between models and full scale ships because of the large difference of Reynolds number between them.

According to the model, ship point (SFC) in Fig.4, although V/V_0 of SFC become closer to those of full scale ships than those of no correction, there is still difference. It is caused that propulsive thrust of model applied SFC cannot be similar to that of full scale ships when ship speed decrease in waves because of the difference of *1-w*. Rudder angle at ship point in Fig.5 indicates that it becomes larger than that of full scale ships.

Because forces of REC generated by auxiliary thruster are smaller than that of SFC, difference of speed response in waves between REC and full scale ships become larger than those between SFC and full scale ships as showed in Fig.4. Since rudder effectiveness by REC on straight-running condition in clam water is made similar to that of full scale ships, rudder response applied REC in waves is closer to that of full scale ships than that of model point and ship

point. However, difference is still exist since speed response in waves is different between REC and full scale ships.

On the other hand, results applied RSC in Fig.3-5 indicate that both speed and maneuvering response in waves become similar to those of a full scale ship precisely regardless λ/L.

4.2 Results in short-crested irregular waves and winds

The simulation results in short-crested irregular waves BF8 with wind are showed in Fig.6-8. According to these figures, tendencies same as the results in regular waves were also obtained in irregular waves and RSC can satisfy both speed and maneuvering response similarity to those of full scale ships. These results indicate that RSC is applicable not only regular waves but also irregular waves with wind regardless the wave and wind direction.

The simulation results in short-crested irregular waves with wind BF11 are showed in Fig.9-11. In these environmental conditions, ship speed decrease up to about 20% of designated ship speed and absolute values of drift angle and rudder angle increase to about 40deg and 30deg respectively. Fig.9-11 indicate that RSC is applicable even in these extreme adverse condition. It is implied that RSC has the possibility to be able to estimate maneuverability or required minimum propulsive power for full scale ships in adverse condition experimentally.

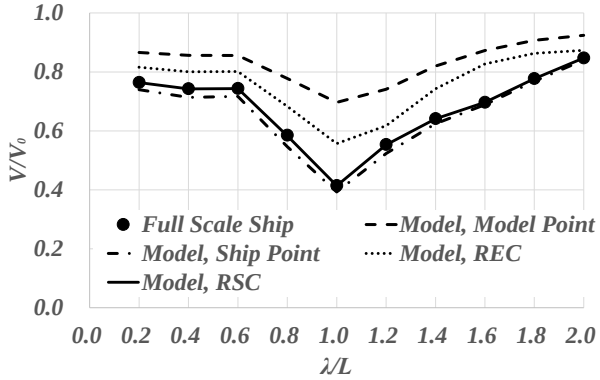

Fig. 3 – Speed ratio in regular waves (Oblique heading wave 30deg, H_W/L=1/72)

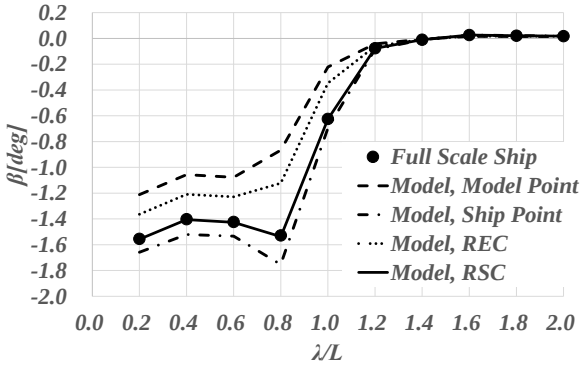

Fig. 4 – Drift angle in regular waves (Oblique heading wave 30deg, H_W/L=1/72)

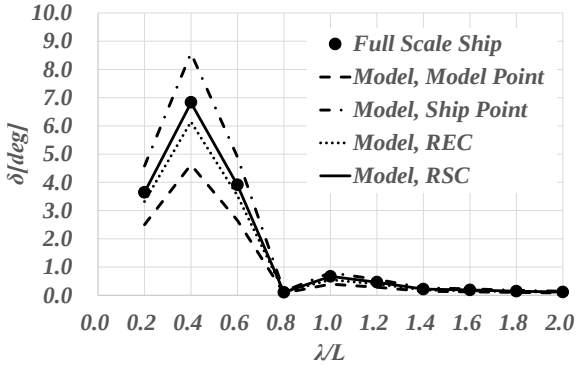

Fig. 5 – Rudder angle in regular waves (Oblique heading wave 30deg, H_W/L=1/72)

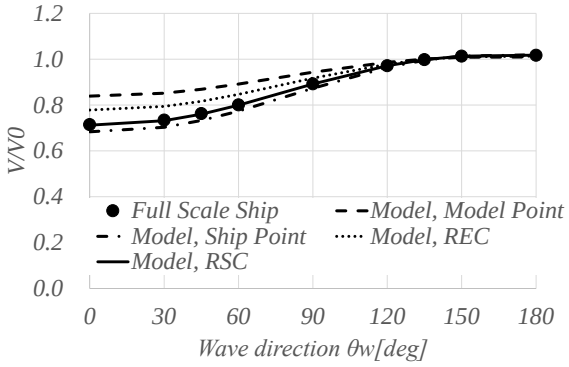

Fig. 6 – Speed ratio in irregular waves (BF8)

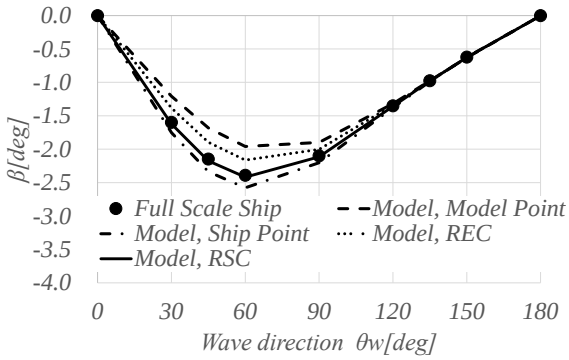

Fig. 7 – Drift angle in irregular waves (BF8)

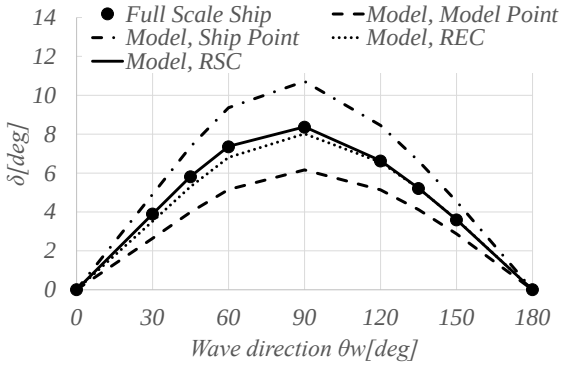

Fig. 8 – Rudder angle in irregular waves (BF8)

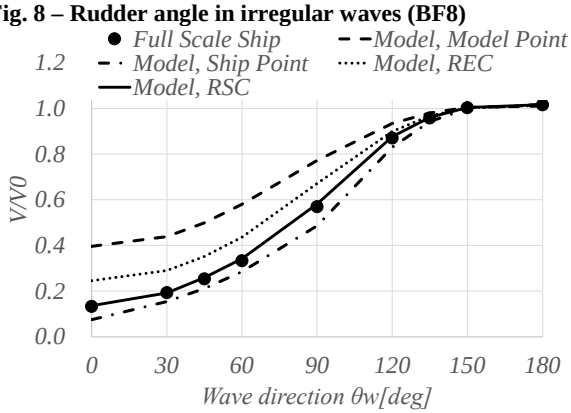

Fig. 9 – Speed ratio in irregular waves (BF11)

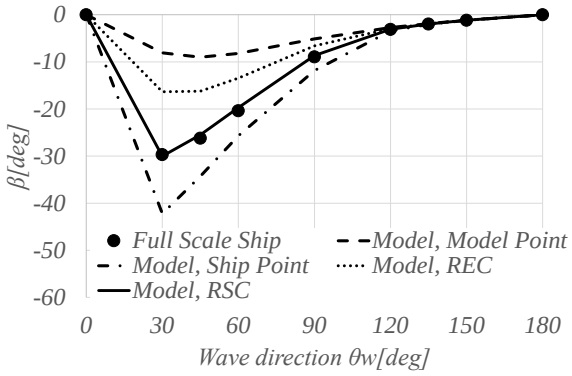

Fig. 10 – Drift angle in irregular waves (BF11)

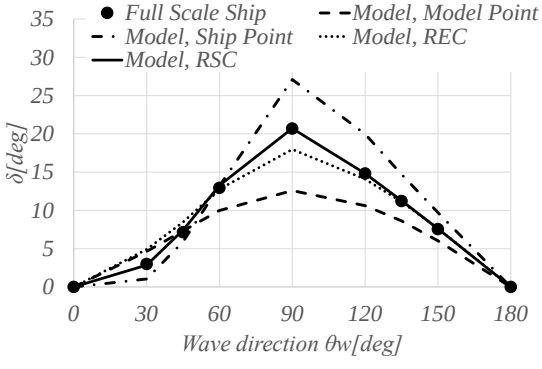

Fig. 11 – Rudder angle in irregular waves (BF11)

5. Conclusions

Authors have simulated speed and maneuvering response in waves for free-running model ships applied RSC and full scale ships on steady straight-running equilibrium condition. They have disclosed numerically that RSC is an experimental method which is able to make ship speed and drift angle, rudder angle on those condition similar to those of full scale ships regardless wave direction and whether regular or irregular waves, and the other kind of auxiliary thruster usage in free-running model test, for example SFC and REC, can't realize them.

In addition, Authors have conducted simulations in extreme adverse seas. As the result, they have also suggested that RSC is applicable in these conditions. Therefore, RSC may be able to estimate maneuverability for full scale ships in adverse conditions.

Important points of these conclusions are that speed decrease in waves or maneuverability and required minimum propulsive power in adverse conditions for full scale ships may be able to be measured directly by free-running model tests instead of estimation by numerical simulation. This implies that they can be evaluated without overcoming the difficulties in order to formulate wave drift forces and moments and all of difference between in clam water and in rough seas, changes of self propulsion factors etc., since all of those phenomena which are reflected in actual ships and seas are also included in free-running model tests.

Acknowledgments

This research was supported by the Grant-in-Aid for Scientific Research [KAKENHI (23246152)] of the Japan Society for the Promotion of Science (JSPS).

References

[1] 2013 interim guidelines for determing minimum propulsion power to maintain the maneuverability of ships in adverse condition, MEPC65/22 Annex16 p.p1-7, IMO,2013.

[2] M. Tsujimoto, M. Kuroda, N. Sogihara., Development of Calculation Method for Fuel Consumption of Ships in Actual Seas with Performance evaluation, Proc. of 32nd OMAE pp.1-10，2013.

[3] M. Ueno, T. Nimura, H.Miyazaki, K.Nonaka, On Steady Horizontal Forces and Moment Due to Short Waves Acting on Ships in Manoeuvring Motion, Proceedings of thePRADS2001, pp.671-677, 2001

[4] M. Ueno, Y. Tsukada, Similarity of rudder effectiveness and speed response of a free-running model ship, Proceedings of the 33rd OMAE2014, 2014.

[5] M. Ueno, Y. Tsukada, On Rudder Effectiveness and Speed Corection for Free-running Model Ship Tests, Proceedings of JASNAOE 2013 annual spring meeting, pp.-,2014

[6] Y. Tsukada M. Ueno, H. Miyazaki, T. Tatakimoto, An auxiliary thruster for free-running model ship test, Proceedings of the 32nd OMAE 2013, 2013.

[7] A. Ogawa, H. Kasai, On the Mathematical Model of Maneuvering Motion of Ship, ISP, 25, 292, pp.306-319,1978

[8] Report of performance committee, 1978, Proceedings of 15th International Towing Tank Conference, pp. 359-404.

[9] D. Kang, K. Hasegawa, Prediction method of hydro--dynamic forces acting on the hull of a blunt-body ship in the even keel condition, J Mar Sci Technol, Vol.12, 2007, pp.1-14.

[10] T. Haraguti, T. Nimura, Measurement of Wave Drift Forces Acting on Tugs and Barge at Zero Froude Number, Papers of national maritime research institute, Vol.31 No.3, 1994.

[11] T. Fujiwara, M.Ueno, Y. Ikeda, A New Estimation Method of Wind Forces and Moments acting in Ships on the basis of Physical Component Models, journal of the Japan Society of Naval Architects and Ocean Engineering, pp.243-255, 2005.

[12] M. Ueno, F. Kitamura, N. Sogihara, T. Fujiwara, A Simple Method to Estimate Wind Loads on Ships, the 2012 World Congress on Advances in Civil, Environmental, and Materials Research, pp.2314-2322, 2012.

[13] M. Ueno, Y. Tsukada, Numerical Study on Rudder Effectiveness Correction of a Free-running Model Ship, Proceedings of the PRADS 2013, pp.1120 – 1127, 2013.

[14] Stern F., and Agdrup K. (Eds.), KVLCC1, Proc. of Workshop on Verification and Validation of Ship Manoeuvring Simulation Methods, Part G: Comparison of Results for Free Manoeuvre Simulations - Systems and CFD Based Methods, 2008.

[15] Kim Wu-Joan, Kim Do-hyun, Van Suak-ho, Comparison of Turbulent Flows around Two KRISO 300K VLCCs with Stern Frameline Modification, Journal of Ships & Ocean Engineering, Vol. 28, pp. 1-14, 1999.

[16] Y. Yoshimura, M. Ueno, Y. Tsukada, Analysis of Steady Hydrodynamic Force Component and Prediction of Maneuvering Ship Motion with KVLCC1,KVKCC2 and KCS, Proceedings of SIMMAN 2008, Vol. 1, pp.E80-86, 2008.

Criteria for Minimum Powering and Maneuverability in Adverse Weather Conditions

V. Shigunov[1] and A. Papanikolaou[2]

1. *DNV GL Maritime, Hamburg, Germany*
2. *Ship Design Laboratory, National Technical University of Athens, Athens, Greece*

Abstract: The 2012 guidelines on the method of calculation of the attained Energy Efficiency Design Index (EEDI) for new ships, MEPC.212(63), represent a major step forward in implementing energy efficiency regulations for ships, MEPC.203(62), through the introduction of specifications for calculating the EEDI for various types of ships. There are, however, concerns regarding the sufficiency of propulsion power and steering devices to maintain manoeuvrability of ships in adverse conditions, hence safety of ships, if the EEDI requirements are achieved by simply reducing the installed engine power. In the frame of a review of current EEDI provisions, the paper discusses possible criteria required to ensure ship's manoeuvrability and safety under adverse conditions and proposes a way ahead regarding the implementation of these criteria by numerical methods and model tests.

Key words: Manoeuvrability; Minimum Power; Adverse Conditions; EEDI; Ship Safety

1. Introduction

The introduction of EEDI regulations in MARPOL facilitates drastic improvement of energy efficiency of ships and reduction of GHG impact of shipping operations. There are, however, concerns regarding the sufficiency of propulsion power and steering devices to maintain manoeuvrability of ships under adverse conditions, hence the safety of ships, if the EEDI requirements are achieved by simply reducing the installed engine power. Following a proposal from the International Association of Classification Societies (IACS), the following requirement was added to the Reg. 21, Ch. 4 of MARPOL Annex VI: *For each ship to which this regulation applies, the installed propulsion power shall not be less than the propulsion power needed to maintain the manoeuvrability of the ship under adverse conditions as defined in the guidelines to be developed by the Organization*. Work carried out by IACS to develop such guidelines [1-4] served as basis for the Interim Guidelines for Determining Minimum Propulsion Power to Maintain the Manoeuvrability of Ship in Adverse Weather Conditions, MSC-MEPC.2/Circ.1 (2012), updated in Res. MEPC.232 (65) [5].

In relation to this, a new European research project called SHOPERA [6], funded by the European Commission in the frame of FP7, was launched in October 2013, aiming at addressing the challenges of this issue by in-depth research studies and submission of main results for consideration to IMO-MEPC in 2016. A strong European RTD consortium was formed, representing the whole spectrum of the European maritime industry, including classification societies, universities, research organisations and model basins, ship designers, shipyards and ship operators. The project will

- develop and fine-tune hydrodynamic analysis methods for manoeuvring of ships in complex environmental conditions
- perform seakeeping and manoeuvring model tests in seaway to provide basis for the validation of numerical methods
- integrate hydrodynamic analysis tools into a ship design software platform and perform multi-objective holistic optimisation, balancing economy, efficiency and safety
- develop new guidelines for sufficient manoeuvrability in adverse weather conditions

- put together teams of designers, shipyards, owners, classification societies and national administrations to conduct investigations on the impact of the proposed guidelines on design and operation of various ship types

2. Definitions

The following terminology is used herein:

- *functional requirements* (avoiding collision, maintaining and changing speed or course, transit, stopping, rescue etc.) are used to set up the framework of new guidelines;
- *criteria* refer to ship characteristics which are defined in idealized situations (e.g. turning and course-keeping and -changing abilities);
- corresponding *measures* quantify ship's performance in idealized situations (turning diameter, stopping distance, maximum wave height for course-keeping etc.) and
- *standards* (or *norms*) set the limits on these measures for the ship to be considered fulfilling the defined requirements.

3. Existing Regulations

Manoeuvrability in waves is an issue of both ship's powering and manoeuvrability in waves, thus also of seakeeping. Ship's powering and efficiency are regulated by the EEDI provisions; manoeuvrability has been considered in the past more as an issue of operation rather than design; however, once it was realized that some uniform minimum requirements to manoeuvrability are necessary, IMO introduced the Interim Standards for Ship Manoeuvrability, A.751(18), which were revised and finally adopted in 2002 [7]. These standards address turning, initial turning, yaw-checking, course-keeping and emergence stopping abilities by geometrical measures of selected standard manoeuvres in calm water (advance and tactical diameter in turning circle, distance for heading change by 10° due to rudder angle change by 10°, first and second overshoot angles in 10°/10° and the first overshoot angle in the 20°/20° zig-zag manoeuvres and advance until full stop in emergency stopping).

IMO's Manoeuvrability Standards have been criticized by some authors, e.g. [8], for not addressing ship manoeuvrability at low speed, in restricted areas and in wind, waves and currents[8]. Because the task of steering is not only turning, course-keeping and stopping, but also withstanding environmental forces (e.g. to keep or change course and speed), and because different ships react in a different way to environmental forces, norming ship's steering ability in waves seems an *essential* part of *minimum manoeuvrability requirements.*

However, this issue has not been addressed by regulations so far. IACS gathered requirements of classification societies regarding redundancy of the propulsion system [9] as a preparation to the development of performance criteria for safe navigation in adverse conditions. In general, these requirements require the ability to change heading into position of less resistance to the waves and wind and maintain this heading, to keep a prescribed minimum advance speed, or a combination of these two requirements. IACS work towards 2013 Interim Guidelines [5] elaborated on functional requirements to manoeuvrability in adverse conditions [1,2], which led to the following two criteria in [3,4]: the ship must be able to keep a *prescribed course* at *advance speed of at least 4.0 knots* in waves and wind from any direction, which are elaborated in the following.

4. Manoeuvrability in Adverse Conditions

Ship's master knows the performance of his ship in adverse conditions; thus, at least in the open sea, he can decide how close the ship can come to a storm, depending on the ship size and type, freeboard, type of cargo, dynamic stability, engine power and steering devices. However, reliable weather forecast and routing are not always possible. In violent weather conditions, no engine power will help as the ship will be mainly driven by the weather; however, turning against the seaway will still be possible, for which a period of less severe seas is selected, and the heading is changed as fast as possible.

Manoeuvring in coastal waters is more demanding and important, than in the open sea. The usual practice in a growing storm in coastal waters is to look for a shelter or, if there is no safe escape, move away from the coast and take a position with enough room for drifting away; grounding, stranding and contact accidents in heavy weather suggest however that there are notable exceptions. The most frequent cause of grounding accidents in a growing storm is waiting at anchor until it starts dragging; after that, engine may be started too late or at too low power. However, in several occasions [10-13] vessels were not able to move away from the coast despite full engine power applied. Although in accident [10] full engine power was not available due to failure of one of the engines, in accident [11] forward speed was reduced in the approach channel to the port to wait for entrance clearance by an outward-bound vessel, and in accidents [12,13] full engine power was available and applied, such accidents suggest that there is a minimum limit for the installed power for a ship to be able to leave a coastal area in a growing storm.

Experience shows that a specific manoeuvring problem of ship types with large windage area is manoeuvring at low speed in restricted areas in strong wind (and usually current) without significant seaway.

An indicative sample of results of a comprehensive statistical analysis [14] of ship accidents[1] in adverse sea conditions is given in Figures 1 to 4.

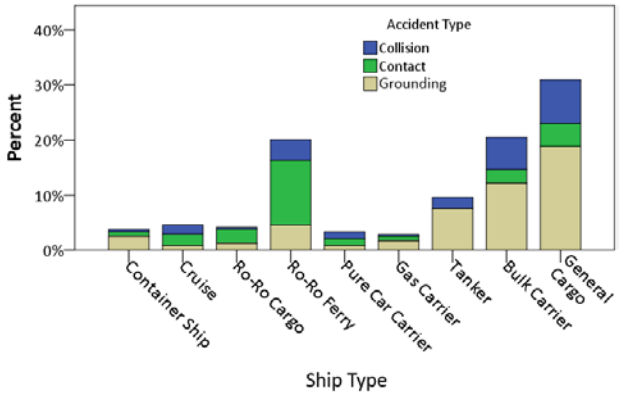

[1] Accident period 1980-2013; ships over 400GT built after 1980; accidents related to adverse/heavy weather conditions, excluding poor visibility (e.g. fog)

Figure 1. Percentage of ship types by accident types

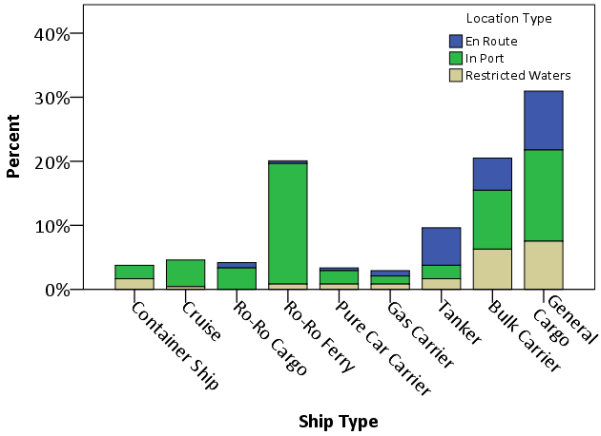

Figure 2. Percentage of ship types by accident location

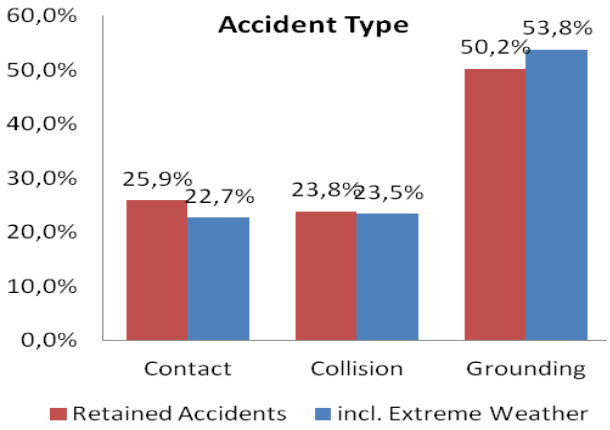

Figure 3. Comparison of distribution of accident types with included very extreme (abnormal) weather conditions

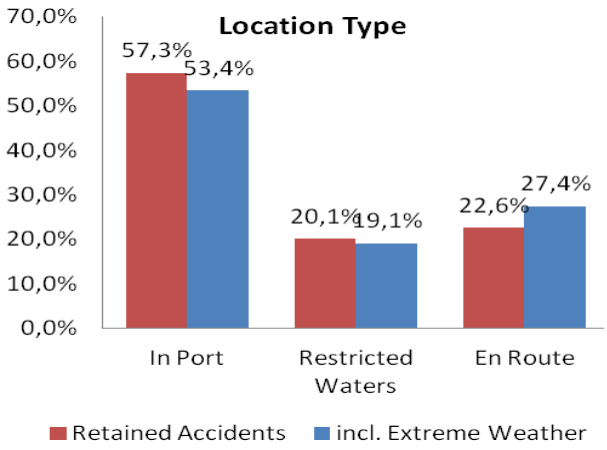

Figure 4. Comparison of accident location with included very extreme (abnormal) weather conditions

In view of the above findings, we consider three groups of criteria:

1. Manoeuvring in extreme conditions in open sea
2. Manoeuvring in coastal areas in a growing storm
3. Low-speed manoeuvring in wind and current in restricted waters

5. Manoeuvrability in Extreme Conditions in Open Sea

In the open sea, the ship must be able to turn into a favourable heading towards the seaway to limit excessive ship motions and to maintain this heading. Arguably, even uncontrolled drifting with waves and wind may be acceptable for some time. For container ships with low metacentric height, this practice is considered as one of the safest ways to weather-vane, if there is enough room available for drifting. Anyway, if the ship is forced to drift in beam waves and wind without being able to turn into seaway, her stability will be controlled by the Severe Wind and Rolling Criterion (Weather Criterion) [15].

However, is some situations it might be not acceptable for a ship to simply drift away without possibility of weather-vaning, for example, in loading conditions with deck cargo and large initial GM, because direct exposure to resonance roll excitation can lead to large lateral accelerations, loss or damage of cargo or even to injuries to the crew, or to water on deck for vessels with low freeboard. Another argument for the need to norm weather-vaning ability in extreme conditions is the preservation of the present safety level: the present rate of intact stability failures in dead ship condition is low because, first, combinations of extreme weather and engine failure are rare and, second, the Weather Criterion is sufficiently conservative. If, however, majority of ships would be uncontrollable in extreme weather due to reduced installed power (as a possible consequence of reducing EEDI), *the level of safety provided by the Weather Criterion alone might become insufficient.*

A counterargument to this reasoning, related to seakeeping and stability problems, can be in the way of adopting other design measures, not concerning manoeuvrability in extreme seaway; for example, adjusting the strictness level of the Weather Criterion, which will inherently lead to more severe seakeeping criteria, likely increase of required roll damping, stronger deck cargo securing etc.

If a criterion for manoeuvrability in extreme open sea weather conditions is required, the following is proposed: *the ship should be able to keep heading in head to bow-quartering extreme*[2] *waves and wind up to 60° off-bow to avoid synchronous rolling and water on deck.* Testing and adjustment of this criterion is required, as well as the definition of the "extreme weather" conditions. For the latter, benchmarking of existing ships against the proposed criterion, as well as accident investigations seem as possible way ahead and are planned within project SHOPERA.

6. Manoeuvrability in Escalating Storm in Coastal Areas

Operation in coastal areas places greater requirements on manoeuvrability than in the open sea: the ship must be able to change the course to the required one and maintain it; she should also maintain some minimum advance speed to leave the coastal area before the storm escalates. Because of possible navigational restrictions, all this must be possible in waves, wind and possible currents from any direction.

If a ship *can keep* any course with respect to the seaway, including seaway directions which are most unfavorable with respect to course-keeping, the ship will also be *able to perform any course change*. Thus, the requirement *to keep any course is more stringent than the requirement to change course*. However, course changing must happen in a short enough time, thus the requirement of some minimum advance speed in seaway from any direction is also necessary. The requirement of some minimum advance speed is also necessary to enable leaving coastal area before the storm escalates.

[2] The severity level of extreme weather conditions is arguable, considering that the ship may nowadays avoid crossing through violent weather conditions (hurricanes, typhoons etc.) and should by design and operation remain a cost effective transportation vehicle

These considerations led, during the work of IACS on minimum power requirements [3,4], to the following criteria:

- *ship must be able to keep any prescribed course in waves and wind from any direction*
- *ship must be able to keep advance speed of at least 4.0 knots in waves and wind from any direction*

Note that the use of port tugs in such situations is unlikely, because port tugs may not be available away from ports, and because port tugs cannot operate in heavy seaway; open sea tugs are used seldom in normal operations.

Whereas the compliance with the IMO Manoeuvrability Standards [7] is demonstrated in full-scale trials, evaluation of criteria concerning adverse weather conditions is impracticable in full-scale trials. Alternatives to full scale tests are model experiments and numerical computations. Because the assessment procedure will be routinely used by designers and verified by Administrations, it must be reasonably simple, inexpensive, transparent and verifiable. Ideally, the procedure should allow using both calculations and equivalent model tests interchangeably and complementarily, in such a way that any assessment can be verified, if necessary; this is only possible if experiments and computations are performed in simple and well-controlled conditions.

In principle, evaluation of the course-keeping and advance speed criteria requires transient model tests with self-propelled models in simulated irregular waves and wind, for all possible wave and wind directions with respect to the ship course. Such experimental techniques are however not mature enough; besides, few facilities exist worldwide able to carry out such tests, which makes them impracticable for routine ship design and approval. Further, reliable predictions in irregular seaways require repetition of tests in multiple realisations of the same seaway in a seakeeping basin, Fig. 5, which is expensive. Finally, the time history of the applied helm in each seaway realization is deciding for the results, and impact of its variability is difficult to quantify, especially for regulatory purposes. Despite some progress in the State of the Art, available numerical methods for the simulation of transient ship manoeuvres in waves are still not mature enough for routine use in ship design and approval.

Figure 5. MARINTEK's 80mx50m Ocean Basin facility (project SHOPERA)

Therefore, a practical assessment procedure should be based on *steady model tests or calculations, under well-controlled conditions*. A possible simplification is to neglect oscillatory wave forces and moments because their time scale is shorter than the time scale of manoeuvring motions, and thus to consider only average in time forces, moments and other variables, such as propeller thrust, torque and rotation rate, required and available power, drift angle and rudder angle. The second possible simplification is to use spectral methods to calculate wave drift forces and moments, which requires only measurements or calculations of drift forces in regular waves. Encounter-frequency wave-induced motions and forces can influence manoeuvring, especially in high waves, in several ways:

- At high speeds in stern waves, encounter frequency motions can induce broaching-to; however, broaching-to can be handled in operation (speed reduction) and is, moreover, not relevant to minimum power requirements.
- Neglecting oscillations of propeller thrust, of required and available power and jumps of the required power above the torque-speed limit

(engine overload) due to encounter-frequency motions and forces, we introduce a non-conservative error. This error is to some degree compensated by the conservativeness of the course-keeping requirement in any wave and wind direction; besides, short overload is possible without damage to the engine.

- Propeller pitching reduces available time-average thrust; besides, it leads to the drop of the mean available power due to dynamic response of a diesel engine after ventilation events and can even lead to engine shutdown. These effects are particularly relevant in ballast loading conditions and can be ignored if the assessment is done for full load condition, not extreme seaways and at low forward speeds.
- Rudder is used in seaway both to ensure course-keeping with respect to the steady effects and to compensate the dynamic yaw motions due to waves and wind gusts. To take these dynamic effects into account in the procedure, the maximum available average rudder angle should be slightly lower than the maximum possible rudder angle (by 3-5° to 10° according to different sources).

Any practical procedure inevitably involves simplifications, each of which leads to either conservative or non-conservative bias. The overall safety level as an outcome of the adopted assessment procedure can still be fine-tuned by the adjustment of the standards: in this case, the environmental conditions used in the assessment should lead to an appropriate classification of existing ships into safe and unsafe. The only trivial requirement to the procedure is that it should be sensitive to ship-specific factors, which are important for the manoeuvring in waves.

One of important ship-specific factors in this respect is the under way drift motion: in response to seaway-induced lateral forces and yaw moment, the ship will sail at a certain average drift angle and with average rudder angle; this increases the required propeller thrust and the required power. Thus, the assessment procedure should take into account at least three degrees of freedom (horizontal motions and yaw); the hydrodynamic problem may be then solved as a steady equilibrium problem in the horizontal plane for the ship advancing with constant forward speed and course under the action of average wave and wind forces, calm-water drift forces and rudder and propeller forces. The solution of the system of equations provides the required average propeller thrust, drift angle and rudder angle. From the propeller thrust, average advance ratio and rotation rate of the propeller are found using open-water propeller curves; then the average in time required power is calculated, as well as the average available power (which will be less than MCR due to reduced rotation rate in seaway). The procedure takes into account longitudinal and lateral forces and yaw moments due to

- *Wind*: can be defined from wind tunnel tests, RANSE simulations or empirical data
- *Waves*: seakeeping tests in regular waves, perhaps potential flow computations or empirical formulae
- *Calm-water*: steady model tests, RANSE simulations, empirical data or formulae
- *Rudder*: steady model tests, RANSE simulations, semi-empirical models
- *Propeller* (open-water propeller curves): steady model tests, propeller series, potential or RANSE computations

The procedure checks whether the required average rudder angle is less than the maximum allowed rudder angle (taking into account margin for steering in waves) and whether the average required power does not exceed the average available power. Example of assessment results in Fig. 6 shows in axes ship speed (radial coordinate) – wave and wind direction (circumferential coordinate) achievable operational conditions (grey area) in waves with significant wave height 6.0 m; in this example, the ship can fulfill the course-keeping criterion with the installed engine and rudder, but fails to keep advance speed of 4.0 knots in waves and wind from directions against the course to about 60 degree off the course.

The advantage of this procedure is that the time-average forces and moments due to different factors (wind, waves, calm water, rudder and propeller) can be computed or measured separately, in simple well-controlled steady tests, and combined in a simple steady mathematical model. If necessary, separate force components can be verified in additional model tests.

Several observations can be made regarding environmental conditions to be used with these course-keeping and advance speed criteria.

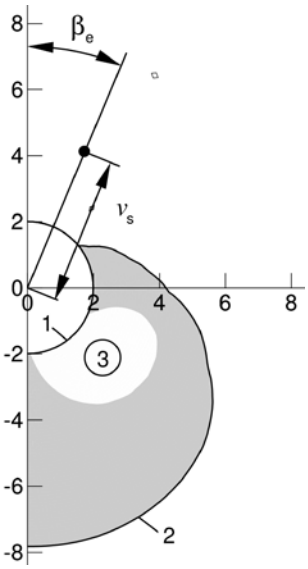

Figure 6. Example of assessment results for a handysize bulk carrier for significant wave height 6.0 m: line 1 – advance speed of 4.0 knots, line 2 – required power equal to available power, area 3 – rudder angle greater than 25°, v_s is ship speed, β_e is wave and wind direction (ship course is to the north)

First, these conditions cannot be too severe because ships usually leave to the open sea or search for a shelter before storm escalates. Second, although ship masters know the capabilities of their ships and, if weather forecast is available, they can decide when they have to search for shelter or leave to the open sea, practice shows that in the majority of accidents, ships wait at anchor in a growing storm and thus, anchor dragging defines very frequently the environmental conditions for leaving coastal areas in practice. Figure 7 shows the dependency of the number of ships remaining at anchor as percentage of the initial number of vessels at anchor vs. significant wave height during an increasing storm, based on data [13].

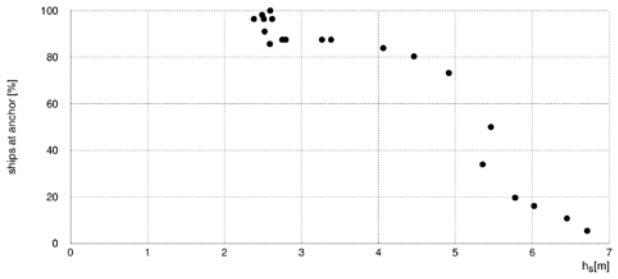

Figure 7. Number of vessels at anchor as percentage of the initial number of vessels vs. significant wave height during an increasing storm according to data in [13]

About 80% of vessels were still at anchor at the significant wave height of 4.5 m, whereas at 6.0 m, the majority of vessels have already left to the open sea only about 20% remained at the anchor. In this case, all vessels left anchorage only after they have dragged anchor in the increasing storm. An argument against using the anchor holding power to define the environmental conditions for leaving to the open sea is the fact that anchoring equipment is intended for temporary mooring of a vessel, and not designed to hold the vessels off exposed coast in rough weather, even though in practice this is frequently the case.

Another consideration is the idea to use statistics of *environmental conditions during groundings, contacts and collisions*; a similar approach was used to choose the wave height for the definition of survival probability in the SOLAS damage stability requirements. According to the results of HARDER project, concerning statistics of weather conditions at the time of *collision* for all ship types, Fig. 8, 80% of collisions happened at significant wave heights below 1 m, i.e. practically in calm water, and very few accidents happen at significant wave heights in excess of 4 m.

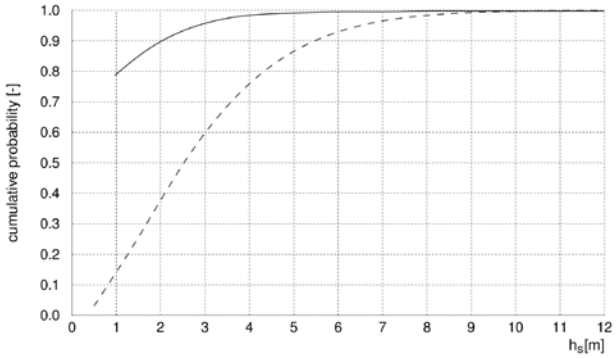

Figure 8. Cumulative probability of significant wave height during collisions according to HARDER database (—) in comparison with North Atlantics wave climate (- - -)

Note that Figures 1-4 from the SHOPERA project [14] show that adverse environmental conditions are more relevant for contact, grounding and stranding accidents than for collisions; the corresponding statistics of environmental conditions is to be evaluated yet.

As final consideration, a practical approach to the definition of environmental conditions to be used in the assessment is the benchmarking of existing ships against the new criteria; the advantage of this approach is the possibility to calibrate the assessment procedure and thus compensate for all biases due to inevitable simplifications. Such an approach, which relied on the assumption that only a small percentage of existing vessels in service might have insufficient manoeuvrability in adverse weather conditions, led to the following environmental conditions in [5]: significant wave height 4.0 to 5.5 m for ships with length between perpendiculars less than 200 and more than 250 m, respectively, and corresponding wind speeds of 15.7 to 19.0 m/s, respectively; modal wave periods vary from 7 to 15 s in all cases. The reduction of significant wave height to 4.0 m for small vessels followed from applying the course-keeping and advance speed criteria to small (about 20000 t dwt) bulk carriers and tankers.

7. Low-Speed Manoeuvrability in Wind

Manoeuvrability at low forward speed in strong wind is critical for ships with large windage area, such as container ships, cruise vessels, RoPax and car carriers, during approach to and entering ports (where also strong current is frequently relevant). There are several specific considerations in this respect. First, low-speed manoeuvrability does not seem to be an issue of safety for most ship types, but an operational issue: because these criteria concern port entrance, availability of port tugs can be assumed. Some vessels are towed during the complete port entry, so they might not need low-speed manoeuvrability[3]. Second, such criteria will lead to additional requirements on the steering performance, but not to restrictions on the minimum installed power, thus there is no potential conflict with EEDI. Still, these criteria are considered in the project SHOPERA for completeness. According to proposals in the literature, the following criteria seem to be suitable:

- *course-keeping in strong wind at specified reduced speed in loading condition maximizing lateral windage area*
- *course-keeping in shallow water near channel wall or bank at specified reduced speed in load case maximizing hydrodynamic forces*
- *course-keeping on shallow water at reduced forward speed during overtaking by a quicker ship in load case maximizing hydrodynamic forces*

In these criteria, no waves are considered but strong wind and, perhaps, strong current. In addition to steering devices dimensioning, these criteria provide important guidance to operators, e.g. up to what speed the ship can manoeuvre itself in a given wind and beyond what wind force tug assistance is required.

Low-speed manoeuvrability criteria require specification of the wind speed and, perhaps, current. Reference [8] recommends wind speed of 20 knots for general use and 30 knots for ferries and cruise ships, as the wind speed at which the ship should be able to leave the quay.

[3] Important exemption to this rule are RoPax and passenger ships in general, commonly not calling for tug assistance; the insufficiency of tugs in small ports should also be considered.

8. Way Ahead to Fill Gaps

Most of the *accident reports* studied so far [14] are from the IHS Sea-Web Marine Casualty Database and the public area of Marine Casualties and Incidents Database of the IMO Global Integrated Shipping Information System (GISIS). Information collected from these sources was cross-referenced, whenever possible, with accident reports acquired from the following sources:

- Marine Accident Investigation Branch (MAIB), United Kingdom
- Swedish Maritime Safety Inspectorate
- Federal Bureau of Maritime Casualty Investigation, Germany
- Panama Maritime Authority
- Marine Accident Inquiry Agency (MAIA), Japan
- Transportation Safety Board of Canada
- Accident Investigation Board Norway (AIBN)
- Maritime Safety Authority of New Zealand
- Maritime Safety Investigation Unit, Malta

We believe that the collected data are sufficient to evaluate the risk of the operating worldwide fleet with respect to the maneuverability in adverse conditions.

Another activity is to complete initiated interviews with ship masters: so far, masters of about 30 container ships and about 5 bulk carriers were consulted. Thus, interviewing masters of RoPax and passenger ships, bulk carriers, tankers and especially general cargo vessels is an important activity to verify criteria and environmental conditions.

Finally, available statistics and accident reports show that adverse weather conditions in coastal areas are especially relevant for grounding and stranding accidents and for contacts with fixed installations. However, the only available processed statistical data on wave heights during accidents (HARDER database) concerns collisions, for which poor visibility in calm-water conditions is most relevant. Thus, statistics of environmental conditions relevant to grounding, stranding, and contact accidents is required to define environmental conditions for all three groups of criteria.

Development of Criteria: One of the main strengths of the IACS proposal [3,4] is the three-tiered approach, allowing better flexibility to designers and evaluators in meeting the requirements. The considerations presented in this paper concern only Level 3 procedures (*Comprehensive Assessment*). Note that in the final version of Guidelines [5], comprehensive assessment was dropped because of the insufficient state-of-the-art of numerical methods for the assessment to be used for regulatory purposes. Implementation of Level 3 procedures in the new Guidelines requires the following: first, three groups of criteria (for growing storm in coastal areas, extreme waves in the open sea and low-speed manoeuvring in wind) should be tested and updated as necessary; this especially concerns criteria and corresponding environmental conditions for extreme waves in the open sea. Second, the proposed simplifications in the assessment procedure should be validated and, if necessary, revised; transient simulations of course change in waves, taking into account first-order forces and other dynamic effects can be used for validation. Third, further simplifications of the proposed Level 3 procedure should be considered. Environmental conditions should be defined and justified for all three groups of criteria.

To develop Level 2 procedure (*Simplified Assessment*), a possible approach is to use empirical formulae for all forces and moments, including the horizontal wave drift forces and yaw wave drift moment. Level 1 assessment procedure is supposed to be simple and based on some empirical formulae or graphs, which are to be developed after processing results of application of the Level 3 procedure to a sufficiently large number of ships; this procedure should take into account installed power as well as steering and propulsion efficiency.

Numerical Methods: For the horizontal forces and yaw moment due to wind and calm-water motions, the existing SoA of numerical methods seems adequate. For a practical procedure, empirical data can be used

for wind forces; for calm-water forces, such empirical recommendations exist for VLCCs but still have to be developed for other ship types. Also desirable is the development of validated semi-empirical models for rudder forces in propeller race; some existing models [16,17] can be used as a starting point and fine-tuned.

Problematic is the determination of the horizontal drift forces and drift yaw moment due to waves. For a practical procedure, their computation with potential theory panel methods is desired in the long-term, which requires development, fine-tuning and validation of such methods; in the short term, semi-empirical solutions can be an alternative.

Impact of New Manoeuvrability Standards: Because the proposed criteria address only the ability of ships to withstand environmental conditions, ships subject to the new criteria will also have to fulfill IMO Manoeuvrability Standards [7]. In this respect, it has to be checked how the reduction of installed power influences the fulfillment of the IMO Manoeuvrability Standards: it is well known that turning circle parameters (transfer and advance) are nearly identical for different engine sizes for the same rudder area (time scale of turning is of course different); however, zig-zag manoeuvres are affected by the reduction of the engine size, thus it is interesting to see to what degree reduced installed power will influence the ability of ships to fulfill the requirements of 10°/10° and, especially, 20°/20° zig-zag in calm water. Another important check is whether the existing fleet in service is evaluated in a feasible way by the new criteria; otherwise, criteria and environment will have to be adjusted.

Design and Optimisation: An important question for ship designers in the EEDI era will be to manage possible contradictions between EEDI requirements, especially in Phases 3 and 4 of EEDI implementation, and minimum power requirements (which will have to be based on the present navigational practice). An important task of SHOPERA is to elaborate on optimal design solutions, demonstrate their feasibility and assess them through case studies involving multiple criteria. There may be the possibility to employ emergency means of manoeuvring and propulsion, e.g. emergency rating of the engine, which should not be used for propulsion in normal operation and thus not included in the EEDI calculation, and should be only activated in adverse weather conditions.

Acknowledgements

The work presented in this paper was partly supported by the Collaborative Project SHOPERA (Energy Efficient Safe SHip OPERAtion), Grant Agreement number 605221, co-funded by the Research DG of the European Commission within the RTD activities of the FP7 Thematic Priority Transport, FP7-SST-2013-RTD-1, Activity 7.2.4 Improving Safety and Security, SST.2013.4-1: Ships in Operation. The European Community and the authors shall not in any way be liable or responsible for the use of any knowledge, information or data of the present paper, or of the consequences thereof. The views expressed in this paper are those of the authors and do not necessary reflect the views and policies of the European Community.

References

[1] MEPC 62/5/19 (2011) Reduction of GHG emissions from ships - Consideration of the Energy Efficiency Design Index for New Ships. Minimum propulsion power to ensure safe manoeuvring in adverse conditions, Submitted by IACS, BIMCO, CESA, INTERCARGO, INTERTANKO, WSC

[2] MEPC 62/INF.21 (2011) Reduction of GHG emissions from ships - Consideration of the Energy Efficiency Design Index for New Ships. Minimum propulsion power to ensure safe manoeuvring in adverse conditions, Submitted by IACS, BIMCO, CESA, INTERCARGO, INTERTANKO, WSC

[3] MEPC 64/4/13 (2012) Consideration of the Energy Efficiency Design Index for new ships – Minimum propulsion power to maintain the manoeuvrability in adverse conditions, Submitted by IACS, BIMCO, INTERCARGO, INTERTANKO and OCIMF

[4] MEPC 64/INF.7 (2012) Background information to document MEPC 64/4/13, Submitted by IACS

[5] IMO (2013) Interim guidelines for determining minimum propulsion power to maintain the manoeuvrability in adverse conditions, Res. MEPC.232(65), in MEPC 65/22, Annex 16

[6] SHOPERA (2013-2016) http://www.shopera.org
[7] IMO (2002) Standards for ship manoeuvrability, Res. MSC.137(76)
[8] F.H.H.A. Quadvlieg and P. van Coevorden (2008) Manoeuvring criteria: more than IMO A.751 requirements alone!
[9] EE-WG 1/4 (2010) Minimum required speed to ensure safe navigation in adverse conditions, submitted by IACS
[10] N. N. (2009) Report on the investigation into the grounding, and subsequent loss, of the roro cargo vessel Reverdance, Shell Flats – Cleveleys Beach, Lancashire, 31. January 2008, Marine Accidents Investigation Branch
[11] N. N. (1996) Report on the investigation into the grounding of the passenger roro ferry Stena Challenger on 19 September 1995, Blériot-Plage, Calais, Marine Accidents Investigation Branch
[12] N. N. (2012) Report on the investigation of the grounding of the cargo ship Carrier at Raynes Jetty in Llanddulas, North Wales on 3 April 2012, Marine Accidents Investigation Branch
[13] Australian Transport Safety Bureau (2008) Independent investigation into the grounding of the Panamian registered bulk carrier Pasha Bulker on Nobbys Beach, Newcastle, New South Wales, 8 June 2007, ATSB Rep. Marine Occurrence Investigation No. 243
[14] Ventikos et al. (2014) Database of ships and accidents, project SHOPERA, D1.3.
[15] International Code on Intact Stability, 2008 (2008 IS Code), IMO, MSC 85/26/Add.1, Annex 2
[16] Brix, J. E. (1993) Manoeuvring Technical Manual. – Seehafen Verlag, Hamburg
[17] H. Söding (1998) Limits of potential theory in rudder flow predictions, Proc. Symp. Naval Hydrodynamics, Washington

- SESSION 7 -

NUMERICAL APPROACHES TO SHIP STABILITY

Design and Construction of Computer Experiments in Fluid Mechanics and Ship Stability

Alexander Degtyarev*, Vasily Khramushin and Vladimir Mareev

Dept. of Computer Modelling and Multiprocessor Systems, Faculty of Applied Mathematics and Control Processes, St.Petersburg State University, Russia

Abstract: The paper considers a generalized functional and algorithmic construction of direct computational experiments in fluid dynamics. Tensor mathematics naturally embedded in the finite- operation in the construction of numerical schemes. As an elementary computing object large fluid particle which has a finite size, its own weight, internal displacement and deformation is considered. The proposed approach focuses on the use of explicit numerical schemes. The numerical solution of the problem is divided into several stages that are a combination of Lagrange and Euler methods.

Key words: Fluid mechanics, direct computational experiment, computational efficiency

1. Introduction

In the paper mathematical basis for direct computational hydroaeromechanic experiment formation is considered. In contrast to the traditional approach of finite difference numerical schemes construction that are output from analytical models in the form of partial differential equations [1], the proposed techniques are focused on the construction and use of direct computational experiments. For these purposes fundamental laws of motion [2] are applied to large fluid particles [3], which have a finite size, their own weight, internal displacement and deformation [4, 5]. Each particle is represented in world (global) and local coordinate systems [6, 7]. It gives opportunity to examine them as free particles with strictly defined laws of neighbor interaction and with alternation of modeling stages of independent internal transformation processes [8, 9]. Such modeling is carried out in accordance with the basic conservation laws of energy, mass and fluid continuity [10, 11]. With this approach mathematical description of physical processes in aerohydrodynamics is greatly enhanced. It is the better than the traditional mathematical models based on differential calculus of infinitesimal elements [12], which basically do not allow direct control of internal state of measurable fluid volumes. At the same time the proposed approach differs from the well known smooth particle hydrodynamics (SPH) simulation [13-16], which is a purely Lagrangian method. For better numerical realization we combine Lagrangian and Eulear approaches at different stages.

Strict and mutually reversible mathematical definition of properties and description of mechanics of finite fluid volumes transformations are possible using classical tools of tensor calculus. This instrument sufficiently specifies transformation of complex fluid flows through first-order spatial approximations.

It is shown in the paper that with the proposed approach hydromechanics problems can be reduced to the use of explicit numerical schemes. At the same time tensor form of state control of three-dimensional computational objects and processes allows to tailor the solution to the real laws of motion or to the empirical and the asymptotic dependences. Apparatus of three-dimensional tensor mathematics in a natural way is embedded in the finite-difference operations of

large particles (final volume) method. This is done in a strict and an unambiguous representation of the physical laws in the nearest vicinity of an elementary particle continuum. In the paper carrying out of numerical experiments in a natural way comes down to three conditionally independent physical processes. This fact, combined with predominant use of explicit numerical schemes, enables natural parallel computing with the ability to dynamically select appropriate hydrodynamics laws. This choice is carried out depending on the characteristics of transformation and interaction of considered computational objects (particles).

In practice, the constructions of direct computational experiments are usually obtained from close analogs of the numerical schemes from systems of partial differential equations. However, these analogs differ as short canonical result expressions in the final difference form [17]. For them, the results of the calculations are more appropriate for comparisons with physical or full scale experiments than for analytically accurate but simplistic solutions of classical mathematical physics.

It should be noted that the above considerations are not new or unexpected. This work is focused on overcoming of two "eternal" questions in computational fluid mechanics:

1. incomplete adequacy of the Navier-Stokes equations;
2. problems arising in discretization of the equation.

The essence of the first question is that the Navier-Stokes equation is not closed [19]. Therefore at the solution of these equations in different cases various closing ratios are put into practice [1, 22]. These ratios have character of conservation laws. Thus, the first problem of hydrodynamics is isolation of physical model of considered system from the actual situation.

The problems arising at discretization of the model equations of hydrodynamics, are also quite serious. Firstly, equation change-type at its finite-difference representation is possible [22, 23]. Secondly, the hydrodynamic nature of the studied phenomena is far from concept of infinitesimals with which we work at consideration of any differential equations [12, 17]. In contrast to the problems of strength and elasticity of solid body, where deflections, shifts, turns may be considered in the finite-difference representation as smalls, shift of particles in continuous medium hydrodynamic problems even with a small impact may be finite.

Thus, as a result we not only have fundamentally wrong equation as a model, but we often incorrectly numerically solve it. Therefore our task, in essence, consists in tearing off calculations from representation of model of physical system. For the solution of this problem methods of the direct computing experiment based on the modern computer architecture are developed in the paper.

2. Numerical construction of continuous medium objects

Direct numerical experiments in continuum mechanics using digital discrete computers are based on a limited set of numeric objects which interpolate parameters of the state of the physical fields in time. Computational processes with such numerical objects have to take place in accordance with physical laws in the mesh areas (including nonregularized ones). At the same time each mesh cell is represented as independent corpuscle actively interacting with the surrounding cell particles [12].

Let us call one mesh cell as elementary computational object (large particle of continuous medium of finite volume). All internal transformation of such particle within linear approximations is strictly and uniquely determined by the rules of tensor arithmetics. This is a convenient tool for geometric and kinematic description of a large particle. Apart from its position in space, classical tensor calculus

describes more complex transformation: rotation, compression, elastic deformation etc. Its functional apparatus is sufficient for development of strong forward and reverse mathematical description of physical processes of fluid mechanics in the finite mesh area.

For description of large mobile elementary particles in a three-dimensional space we introduce two coordinate systems: absolute and mobile local (associated with the particle) (Fig. 1).

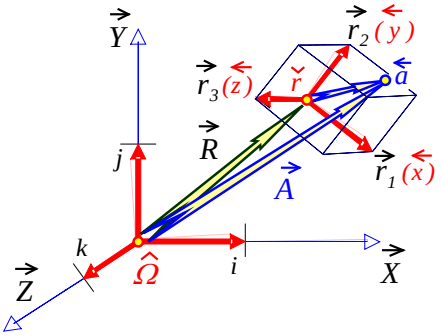

Fig. 1 – Local basis r_i is formed by triad of basis vectors, ijk – unit vectors of global coordinate system (XYZ); *R* – radius vector of the moving system; *A* - radius vector of the point in global coordinate system; $\breve{a}$ - the same point in local coordinate system

Let us initially restrict our consideration of distant mechanical interference. Then mechanical laws for local interaction set big external force interactions, intensive inertial reactions and sufficient internal deformations. All laws of fluid kinematics and mechanics of its transformation are represented as linear spatio-temporal dependencies in the simplest tensor-vector form.

Let us distinguish the following notations of vector and tensor quantities for the convenience of representation of analytic expressions in their direct relationship with finite-difference representations and earlier restrictions [12]:

A – value measured in a global coordinate system (may be scalar or vector only)

a – value measured in a local basis, it refers to small volume or contiguous particles only (differential differences, can be scalar, vector or tensor)

$\vec{R},\vec{r}$ – values projected on global basis

$\breve{R},\breve{r}$ – values projected on local basis

$\hat{r}$ – local tensor in projections of global system

$\breve{r}$ – local tensor in projections of local system

Detailed notation is in appendix 1.

With this alphabet, capital letters for values in global coordinate system are used. Lower letters are used for small quantities at local bases projections in spatial location and current time. Basic mathematical operations are tensors products and products of tensors and vectors. They define the ratio of local reactions of the fluid particles to external influences of the environment. Formally possibility of rank increasing of tensor-vector objects is excluded. They have not immediate physical interpretation.

Absolute or full velocity vector of a large particle is introduced as a shift of the center of mass in the global coordinate system:

$$\vec{V}\cdot t = {}^{\Delta}\vec{R} = {}^{t}\vec{R} - {}^{0}\vec{R} = {}^{T-t}\vec{R} - {}^{T}\vec{R} \qquad (1)$$

Tensor of instantaneous velocities relative to the conditional center of large particle in projections on absolute coordinate system is assembled by direct geometric constructions. Obviously, such tensor contains components of rotation and speed of mutual deformation of the basis vectors for the adjacent dots in the fluid flow:

$$\hat{\omega} = \vec{\omega}^{i} = {}_{\Delta}\vec{V}_i = {}_{+}\vec{V}_i - {}_{\Omega}\vec{V}_i \qquad (2)$$

At the initial moment tensor internal flow velocities equal to zero. This is acceptable on the Euler stages of computational experiment.

Kinematics of internal flows in elementary fluid particle is also algorithmically constructed as differential velocity tensor (Fig. 2).

This is tensor of basis vectors form of large fluid particle moveable in time:

$$\hat{v}\cdot t = \vec{v}_i \cdot t = {}^{\Delta}_{\Delta}\vec{r}_i = {}^{t}_{+}\vec{r}_i - {}^{o}_{\Omega}\vec{r}_i \quad [m^3] \qquad (3)$$

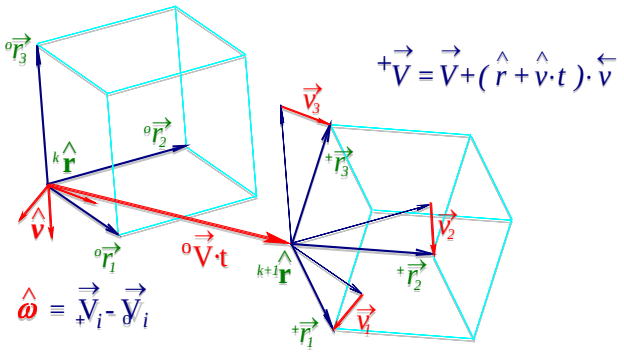

Fig. 2 – Tensor of local velocities is formed by deformation displacements of basis vectors of large fluid particle for rated time interval

Tensor $\hat{v}$ sets current speed of the unit vectors in the local basis (lower case) with respect to the global coordinate system (subscripts). For traditional analysis it can be transferred to the local reference system (normalization of geometric measurements):

$$\hat{v} = \hat{v} \cdot \hat{r} = \hat{v} / \hat{r} \quad [s^{-1}] \qquad (4)$$

Here the known tensor of convective velocities is automatically formed. Traditional definition of an affinor is applicable to it and the theorem of Helmholtz [4] for decomposition on small increments in time is fair: expansion (divergence); turn (rotor) and deformation (shift).

3. Definition of space operations over the elementary particles of fluid

Computing objects are created at a stage of initial formation of hydrodynamic fields in the form of mesh area. The mesh area is supposed dynamically changeable and the irregular depending on current regimes in local areas and features of the problem. These objects are under construction immediately during computing experiment. Their appearance is the result of special logical procedures that control specific regimes of fluid flow and control progress of computational experiment on a functional level. A striking example of such procedure is the change of mesh area in zones of cavitation and vortex breaks and also on the free surfaces. Computing objects cannot be generated or destroyed as a result of mathematical manipulations (generation of vector dyads or tensors of the third rank are excluded by logic of creation of computing objects) [17].

Control of physical state of considered objects (large particles) allows to choose type of computing operations dynamically. For correct carrying out direct computing experiment it is necessary to set the following requirements to mathematical models:

1. Elementary spatio-temporal objects and the basic physical phenomena must be described in the dimensional form;
2. Physical properties of the environment and mechanics laws for the modelled phenomena are formulated in canonical form. Transition to demanded reference systems is carried out automatically at algorithmic level.
3. Properties of arithmetic operations and elementary numerical objects are invariantly defined in global coordinate system and definitely correspond to calculated values in local bases. It is carried out by multiplication operations

Taking into account the history of the movement, "not free" fluid particle is governed by vector analog of the Newton law [5] (fig.3)

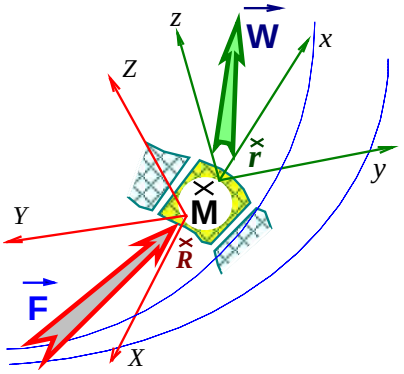

Fig. 1.

$$W_i = F_j \cdot M^{j}{}_{i} \quad \text{or} \quad \vec{W} = \vec{F} \cdot \overset{<}{M}, \qquad (5)$$

where external force $\vec{F}$ affects the large fluid particle allocated from stream $\overset{>}{M}$ and causes

reaction $\vec{W}$. $\times$ icon above the letters in fig.3 means that it can be both $\wedge$ and $\vee$. Value and direction of $\vec{W}$ depend both on internal state (inertia) of this particle, and on its ability to be deformed, to absorb or to strengthen external manifestations of motion energy. Linking mass tensor with the fluid particles $\overset{>}{M} = \hat{r} \cdot \check{\rho}$ we obtain the definition of density or internal energy, which imparts fluid environment anisotropic properties:

$$\vec{F} = r_{ik} \cdot \rho^{kj} \cdot \vec{W} = \hat{r} \cdot \check{\rho} \cdot \vec{W}, \qquad (6)$$

where $\hat{r}$ [m^3] is tensor of large fluid particle form; $\check{\rho}$ [kg/m^3] is density tensor characterizing the internal state of a fluid particle, taking into account the dynamic interaction with the continuous medium.

Small spatial movements historically are determined by the calculus of fluxions underlying Newtonian mechanics. In kinematic problem fluxions determine the speed forming difference differential (by Newton – the moment) in a product with calculated step in time.

Within such views large particle kinematics is given by differential (moment) of velocities in the absolute coordinate system subject to small displacements in the local basis:

$$^{+}\vec{A} = \vec{R} + \vec{V} \cdot t + \vec{Z}, \qquad (7)$$

where t is calculated time moment; $\overleftarrow{a}$ is coordinates of the control point (see fig.1) in local reference system; $\vec{R}$ is location of the local basis in the absolute coordinate system; $\vec{V}$ is speed of forward shift of local basis (of large fluid particle); $\vec{Z}$ may be in different form in dependence of mode of current. In simplest case $\vec{Z} = \overleftarrow{a} \cdot (\hat{r} + \hat{v} \cdot t)$. Then we represent (7) as $^{+}\vec{A} = {}^{0}\vec{A} + (\vec{V} + \overleftarrow{a} \cdot \hat{v}) \cdot t$ or in the form of system of scalar equations [6]:

$$^{+}A_x = {}^{o}A_x + \left(V_x + a^x v_{xx} + a^y v_{yx} + a^z v_{zx}\right);$$
$$^{+}A_y = {}^{o}A_y + \left(V_y + a^x v_{xy} + a^y v_{yy} + a^z v_{zy}\right);$$
$$^{+}A_z = {}^{o}A_z + \left(V_z + a^x v_{xz} + a^y v_{yz} + a^z v_{zz}\right).$$

In case of vortex flow in accordance with Cauchy-Helmholtz theorem [4] $^{+}\vec{A} = \vec{R} + \vec{V} \cdot t + \overleftarrow{a} \cdot (\hat{r} + \hat{v} \cdot t) + \overleftarrow{\omega} \cdot (\hat{r} + \hat{v} \cdot t) \cdot t$. Here $^{+}\vec{A}$ and $^{0}\vec{A}$ are new and initial location of control point in global system; $\hat{r}$ is tensor of large fluid particle form; $\hat{v}$ is tensor of speeds of local motions of basic axes of the tensor defining deformation of a large fluid particle; $\overleftarrow{\omega}$ is speed of internal shift.

Let us present equation for motion of arbitrary point (7) near large fluid particle in convenient dynamic form. Here we take into account deformation and energy of internal forces: $\overset{>}{m}$ [kg^{-1}]. We have to consider multiple nature of such forces: external distributed $\hat{f}$ [*N m^2, kg m^3/s^2*] and mass $\vec{F}$ [*N, kg m/s^2*]:

$$^{+}\vec{A} = \vec{R} + \vec{V} \cdot t + \overset{>}{m} \cdot \vec{F} \cdot t^2/2 + (\hat{r} + \hat{v} \cdot t + \overset{>}{m} \cdot \hat{f} \cdot t^2/2) \cdot \overleftarrow{a}, \qquad (8)$$

The resulting expression contains the traditional system of Euler differential equations and an additional term describing the deformation of a large fluid particle under the influence of stress on its borders.

4. Algorithmic realization of hydrodynamic laws

The Algorithmic implementation is based on computational schemes of mixed Lagrangian and Eulerian approaches [4,5]. This is expressed similar to the methods of "large particles" [3] and "final volume" [18] in the double integration of first order motion equations. Thus the time cycle of computing experiment is divided into three conditional stages:

1 stage – Kinematic parameters are calculated for the centers of large fluid particles. For this purpose, the current source data into fixed nodes of Eulerian coordinates are used;

2 stage – Lagrangian or large deformable fluid particles are involved in free motion. They redistribute the internal properties of the original Euler cells to adjacent space;

3 stage – Laws of conservation of mass and energy are consistent. This is achieved by deformation of

shifted fluid particles. The next step makes reinterpolation of characteristics of current in initial nodes of the fixed Euler computational mesh.

Computational experiment is generally presented as a process of integral transformation of the velocity field in absolute time:

$$^{+}\vec{V} = \vec{V} + \vec{W} \cdot t \,, \tag{9}$$

Thus the construction of computational experiment is reduced to difference derivation of the first order. This is the main feature of the Lagrangian-Eulerian approach for the numerical solution of problems in fluid mechanics. In other words, it is possible to call this approach a method of splitting of the decision on physical processes, which can be formed by three conditional stages of the numerical solution of applied problem:

1 stage. Basing on the current velocity field the condition of large fluid particles on the following instant is specified:

$$^{+}\overset{<}{M} = \overset{\vee}{\rho} \cdot (\hat{r} + \hat{v} \cdot t) \,, \tag{10}$$

where $\hat{v}$ is tensor of map of the current velocity field on local basis of a large particle; $\overset{\vee}{\rho}$ is tensor of internal state of a fluid particle at the current time moment.

2 stage. After specification of resultant vector of all external forces influencing a large fluid particle, calculation of new velocity field is carried out:

$$^{+}\vec{V} = \vec{V} + \overset{<}{M}^{-1} \cdot \vec{F} \cdot t \,, \tag{11}$$

3 stage. As a result of the first two phases spatial displacement of large fluid particles takes place. New hydrodynamic fields partly no longer satisfy the conditions of continuity and isotropic of source environment. Depending on task the type of problem, at the final stage it is necessary to make relaxational amendments to absolute properties and interaction conditions between fluid particles. It is necessary to carry out walkthrough control of quality of the solution. We must, if necessary, apply scheme of adaptation or empirical substitution of solution in areas where the computational model gives a clearly incorrect results.

It is known that traditional approach to numerical solution fluid dynamics problems is most often reduced to application of implicit schemes [1, 10]. The described algorithmic approach, first of all because of the proposed splitting of the solution on physical processes, gives the chance of application explicit numerical schemes at the first two stages. In this case it is possible to increase essentially effectiveness of computing procedures through:

1. Natural parallelization of the computation process;
2. Possibilities of adaptive correction of mesh area depending on features of the problem;
3. Dynamic reconstruction of solution in accordance with fluid currents transformations in time.

5. Construction of explicit numerical schemes and features of computational operations

Let us construct numerical procedure basing on the made assumptions. It is necessary to note that proposed approach (first of all endows the elementary deformable particle with internal energy) expands possibilities of mathematical representation of fundamental mechanics laws.

1. Vector analog of Newton law for deformable particle – equation (6).
2. Viscous stress tensor for Newtonian fluids:
$$\overset{>}{f}_{н} = \hat{v}_{н} \cdot \overset{\vee}{\eta} / \Lambda = \overset{>}{v}_{н} \cdot \eta / \Lambda \,, \quad [N/m] \tag{12}$$
3. Elastic stress tensor for a solid (Hooke law):
$$\overset{>}{f}_{\Gamma} = (\hat{r} + \hat{v}_{\Gamma} \cdot t) \cdot \overset{\vee}{c} / \Lambda \quad = (\overset{\times}{1} + \overset{>}{v}_{\Gamma} \cdot t) \cdot \overset{>}{c} / \Lambda \,, [N/m] \tag{13}$$

where tensor of local velocities is constructed as $\hat{v} = {}_{+}\vec{V}_i - {}_{o}\vec{V}_i$ (fig.2); general rheological constants are formally constructed in tensor form, they satisfy the expressions of the type $\overset{<}{M} = M^{i}_{k} = \overset{\vee}{\rho} \cdot \hat{r} = \rho^{ij} \cdot r_{jk}$ – tensor of inertia in projection on global reference system; $\hat{r}$, $\overset{\vee}{\rho}$ – geometric tensor of form [m^3] and fluid density [kg/m^3] and energy accumulation inside

the particle; $\overset{>}{\eta},\overset{>}{c}$ – tensors of dynamic viscosity [kg/s] and rigidity [kg] of real fluid; Λ – conditional distance that defines distance of upstream direction of adjacent particles.

5.1 Properties of computational operations

For correct construction of numerical schemes it is necessary to define properties of computational operation basing on proposed approach. All operations are carried out exclusively in the dimensional form. It is necessary to provide automatic control of the physical correctness of the simulated processes. If necessary hybrid schemes in subareas where there is a change of modes of the currents demanding well-timed substitution of used laws of mechanics and their mathematical models are applied. Three groups of operations contact computing objects:

1. Logical and empirical operations. There are physical laws like "if we have tensor of convective velocities $\overset{>}{v}$ then it generates tensor of stress $\overset{\vee}{f}$ in accordance with law (12)", etc. Such operations set a way of formation and methods of analysis of tensor objects, and also a decision making about change of mathematical models during calculations.
2. Addition operations are applied only to values with identical physical dimensions. Thus the condition of their definition and construction in the same basis has to be satisfied. Addition can be applied to the complex objects also in conditions when operations of automatic coordination of reference systems and physical dimensions are defined.
3. The operation "multiplication" is applicable only to objects whose connected components lie in dual systems of references. Increase of rank of tensor in multiplication operations is forbidden. For creation of vector or tensor objects special algorithms basing on a physical problem definition have to be defined.

Computational objects are given by the following characteristics:

1. Scalar and invariant values (time for example) take part just only in multiplication operations with any objects;
2. Vector values take part in addition operations with comparable vectors, they can take part in operations with tensors if it necessary for transition from one reference system to another. Application of multiplication of vectors for creation of dyads is inadmissible;
3. Tensor values define physical properties of elementary fluid particles, their geometrical deformations, kinematic properties and other dynamic processes in a continuous medium. Tensors take part both in addition operations with comparable tensors, and in multiplication operations with associated (dual) vector or scalar objects.

5.2 Construction of explicit numerical schemes

As input for construction of computer simulations in fluid mechanics the following dimensional fields in global reference system will be defined: $\{\vec{R}\}$ [m] – the field of mesh coordinates points; $\{\vec{V}\}$ [m/s] – the speed field; $\{\overset{<}{M}\}$ [kg] – the tensor field of internal properties for each of the fluid particles.

In thus defined mesh area local computing objects are introduced. Let us repeat physical parameters of fluid described elementary fluid particles: $\hat{r}$ [m^3] – tensor of large particle form; $\hat{v}$ [m^3/s] – tensor of local velocities of basis axes deformation of the particle; $\hat{f}$ [N m^2] – stress tensor at its boundaries.

In this case computer simulation could be divided into three stages (in language of tensor mathematics [12]):

Stage 1. KINEMATICS.

New field of nodal points:

$$\left\{ {}^{+}\vec{R} = \vec{R} + \vec{V} \cdot t + \vec{F} \cdot \overset{<}{M} \cdot t^2 / 2 \right\} \qquad (14)$$

The field of convective speeds is formed by algorithmic creation of the tensor:

$$\left\{ \hat{v} \right\} = \left\{ +\vec{V}\,i - o\vec{V}\,i \right\} \qquad (15)$$

Estimated status of the new field of internal properties:

$$\left\{ +\overset{>}{M} \right\} = \left\{ \hat{r} + \overset{\vee}{\rho} \right\} = \left\{ (\hat{r} + \hat{v}\cdot t)\cdot\overset{\vee}{\rho} \right\}$$

$$\left\{ +\overset{\vee}{\rho} \right\} = \left\{ \overset{\vee}{\rho}\cdot(\overset{\times}{1} + \overset{>}{v}\cdot t) \right\} \qquad (16)$$

Thus calculations of the distributed current characteristics are carried out on the fixed Euler mesh.

Stage 2. DYNAMICS.

The basis of this stage is satisfaction of physical conservation laws. Here comparison of fluid rheology with current state of computing model is carried out. E.g. let the momentum conservation law is defined $^{+}\overset{>}{M}\cdot\vec{V} = \overset{>}{M}\cdot(\vec{V} + {}^{\Delta}\vec{V})$. In this case basing (16) we have

$$^{\Delta}\vec{V} = (^{+}\overset{>}{M} - \overset{>}{M})\cdot\overset{<}{M}\cdot\vec{V} = \overset{>}{v}\cdot\vec{V}\cdot t \qquad (17)$$

and vector Newton equation (6) in Euler form that true for large fluid particle on fixed nodes of calculated area:

$$\vec{F} = \overset{>}{M}\cdot\overset{>}{v}\cdot\vec{V} = \hat{r}\cdot\overset{\vee}{\rho}\cdot\overset{>}{v}\cdot\vec{V}$$

The resulting expression contains fluid stressed state, which can be explained by the rheological properties of a computational model of the flow:

$$\left\{ \hat{f} \right\} = \left\{ +\vec{F}\,i - o\vec{F}\,i \right\} \quad \text{or} \quad \hat{f} = \hat{r}\cdot\overset{\vee}{\rho}\cdot\overset{>}{v}\cdot\hat{v} = \overset{>}{M}\cdot\overset{>}{v}\cdot\hat{v}$$

In a form of the new equation corresponds to record of stresses in the Navier-Stokes equations. Rheology of a real fluid is made in the form of laws (12), (13) associated with the tensor of convective velocities $\overset{>}{v}$.

Accounting of other conservation law restores loss of volume component of acceleration in the expression (17). It leads us to consideration of particle motion with variable mass without deformation.

$$\mathrm{M} = \det(\overset{>}{M}), \quad \rho = \det(\overset{\vee}{\rho}),$$

$$^{\Delta}\vec{V} = \vec{V}\cdot(\frac{M}{^{+}M} - 1) = \vec{V}\cdot(\frac{\rho}{^{+}\rho} - 1)\ . \qquad (18)$$

This model takes possibility to consider different stress modes. If we extract diagonal tensor $\overset{>}{v}_0$ in such a way that trace of residue $\overset{>}{v}^{*}$ is equal to zero:

$$\overset{>}{v} = \overset{>}{v}_0 + \overset{>}{v}^{*} \quad (tr\ \overset{>}{v}^{*} = 0)$$

than we obtain tensor of spherical compression:

$$\overset{\vee}{f}_0 = \overset{\vee}{\varepsilon}\cdot\overset{>}{v}_0\cdot t \qquad (19)$$

Selection of skew-symmetric part of a tensor gives viscous stress tensor:

$$\overset{\vee}{f}_H = \overset{\vee}{\mu}\cdot\overset{>}{v}_H = \overset{\vee}{\mu}\cdot(\overset{>}{v}^{*} - \overset{>}{v}^{*T})/2 \qquad (20)$$

The remaining symmetric tensor is associated with elastic deformation:

$$\overset{\vee}{f}_\Gamma = \overset{\vee}{c}\cdot\overset{>}{v}_\Gamma\cdot t = \overset{\vee}{c}\cdot(\overset{>}{v}^{*} + \overset{>}{v}^{*T})\cdot t/2 \qquad (21)$$

Full tensor of internal stress:

$$\overset{\vee}{f} = (\overset{\vee}{\varepsilon}\cdot\overset{>}{v}_0 + \overset{\vee}{c}\cdot\overset{>}{v}_\Gamma)\cdot t/2 + \overset{\vee}{\mu}\cdot\overset{>}{v}_H \qquad (22)$$

Dynamic coefficients $\overset{\vee}{\mu}, \overset{\vee}{c}, \overset{\vee}{\varepsilon}$ differ from kinematic coefficient by scalar density ρ., Particle has increment of internal movement velocity under the influence of the stress tensor:

$$^{\Delta}\overset{\vee}{v} = \overset{\vee}{f}\frac{t}{\rho} \qquad (23)$$

If flow is stable then tensor of speeds increment $^{\Delta}\overset{\vee}{v}$ has to compensate tensor of convective speeds for a calculated time interval:

$$\hat{v}\cdot\overset{\vee}{r} + \overset{\vee}{r}\cdot{}^{\Delta}\overset{\vee}{v} = 0$$

At this stage of the calculations, this expression is accurate, because it does not take into account the displacement of large particles in a time t.

Stage 3. STATIC.

At the final stage it is necessary to recover velocity field in accordance with increments calculated at the second stage. Here deformation movements around static centers of particles are considered. So during Lagrangian steps centers of gravity of large particles are shifted. We have to carry out interpolation of flow characteristics from these centers to initial nodes of computational area (Euler approach). At this stage it is possible to consider conditions on free boundaries. Here we use extrapolation with the help of centers of transborder fluid particles instead of interpolation in breaking nodes of nonregularized mesh.

For these purposes it is necessary to turn to mixed tensor from tensor $\overset{\vee}{v}$ defined in local basis. Mixed tensor is based on global reference system:

$$\overset{<}{v}=\overset{\vee}{v}\cdot\hat{r} \tag{24}$$

For transition to initial mesh the new local basis on the fixed knot is constructed. Spatial points shifted in time are used as adjacent nodes:

$$\hat{r}=\vec{R}_i-\vec{R}_i \tag{25}$$

Expanding expression (15) used in the construction of the tensor of local speeds on new basis vectors, we obtain algorithm for new velocity field calculation:

$$\vec{V}=\vec{V}+\sum_i \hat{r}\cdot\overset{\leftarrow}{v}_i \tag{26}$$

Expressions (23) - (26) reveal the basic algorithmic constructions allowing to apply inverse Newton's laws $\vec{W}=\vec{F}\cdot\overset{<}{M}$.

6. Conclusions

In the paper approach for constructing procedures for direct numerical experiment in problems of hydrodynamics is described. Distinctive feature of the proposed approach is a successful combination of well-known computing technologies (such as the "method of large particles" [3, 11]) and algorithms of tensor mathematics [8, 12]. We use dualism of corpuscular and continual representation of continuous medium (approaches of Euler and Lagrange). Introduction of a large particle with many degrees of freedom (movements, rotations, compression, stretching, etc.) makes it possible to consider the final transformation of computing object. This is very important, especially in problems of hydrodynamics, where even small effects can lead to significant displacement. The proposed approach makes it possible to exclude from consideration the mathematical models of fluid mechanics in the form of differential equations in partial derivatives. Construction on their basis of finite-difference computational schemes makes proceed from the consideration of infinitely small quantities (when considering the approximation of derivatives in the equations). In the proposed approach, computational experiment is carried out on the basis of fundamental conservation laws.

The dualism of corpuscular and continual models of continuous medium allowed to present computing procedure in the form of three serial stages combining approaches of Euler and Lagrange. Such division is aimed at providing efficient computing procedure especially in the conditions of the multiprocessor computer environment. As the basis of computational efficiency the use of explicit numerical schemes can be considered. This makes the internal state through control of the corpuscular-continuous computing environment possible. In this case application of hybrid or empirical solutions in subareas, where there is a violation of conditions of smoothness or stability of numerical schemes, is possible.

The apparatus of tensor mathematics is developed for construction of direct computing experiments on the basis of explicit numerical schemes. It fully describes physical processes in the continuous environment by means of the linear interpolation relations.

Experience in the application of this approach allows to judge the viability of historical ideas of Isaac Newton about corpuscular and continual construction

of laws of a mechanics of continua by means of finite differences – calculations of fluxions in three-dimensional space.

Acknowledgments

The research was carried out using computational resources of Resource Center Computer Center of Saint-Petersburg State University and supported by Russian Foundation for Basic Research (project N 13-07-00747) and St. Petersburg State University (projects N 9.38.674.2013, 0.37.155.2014). The authors thank Prof. Bogdanov for discussion of the problem and good ideas.

References

[1] Pletcher R.H., Tannehill J.C., Anderson D.A. Computational fluid mechanics and heat transfer. 3rd ed. CRC Press, Taylor&Francis Group, 2013

[2] Astarita G., Marrucci G. Principles of Non-Newtonian Fluid Mechanics. McGRAW-HILL, 1974

[3] Belocerkovski O.M., Davidov Yu.M. Method of large particles in gas dynamics. M.: Nauka, 1982 (in Russian)

[4] Lamb H. Hydrodynamics. 6th ed. Cambridge Univ.Pres., 1975

[5] Zommerfel'd A. Mechanics of deformable media. M.: Foreign Literature Publishing House, 1954 (in Russian)

[6] Kochin N.E. Vector calculus and beginnings of tensor calculus. 9th ed. M.: Nauka, 1965 (in Russian)

[7] Kilchevski N.A. Elements of tensor calculus and its application to mechanics. M.: Gostechizdat, 1954 (in Russian)

[8] McConnell A.J. Applications of Tensor Analysis. Dover Publications, 2011

[9] Faux I.D., Pratt M.J. Computational Geometry for Design and Manufacture (Mathematics and Its Applications). Ellis Horwood, 1981

[10] Methods in Computational Physics: Advances in Research and Applications, ed. by B.Alder, S.Fernbach, M.Rotenberg. Vol. 3: Fundamental Methods in Hydrodynamics. Academic Press, 1964.

[11] Hockney R.W., Eastwood J.W. Computer Simulation Using Particles. Taylor & Francis, 1989.

[12] Khramushin V.N. 3D Tensor Mathematics for the Computational Fluid Mechanics Experience. Vladivostok: FEB RAS, 2005 (in Russian)

[13] Monaghan J.J. Smoothed particle hydrodynamics. *Rep. Prog. Phys.* **68** (2005) 1703-1759

[14] Kitsionas S., Whitworth A.P. Smoothed particle hydrodynamics with particle splitting applied to self-gravitating flows *Mon. Not. R. Astron. Soc.* **330** (2002) 129–36

[15] Violeau D. Fluid Mechanics and the SPH Method: Theory and Applications. Oxford University Press, 2012

[16] Liu M.B. Smoothed Particle Hydrodynamics: A Meshfree Particle Method. World Scientific Pub Co Inc, 2003

[17] Degtyarev A.B., Khramushin V.N. Design and construction of computer experiment in hydrodynamics using explicit numerical schemes and tensor mathematics algorithms. *Mathematical Modelling* **26**, №11 (2014) (to be printed)

[18] Patankar S.V. Computation of conduction and Duct Flow Heat Transfer. Innovative Research Inc., 1991

[19] Ladyzhenskaya O.A. Mathematical Theory of Viscous Incompressible Flow. Mathematics and Its Applications Vol. 2. Gordon & Breach Science Publishers Ltd, 1969

[20] Ortega J.M. Introduction to Parallel & Vector Solution of Linear Systems. Plenum Press New York, NY, 1988

[21] The Fourth Paradigm. Data-Intensive Scientific Discovery. /ed. by T.Hey, S.Tansley, K.Tolle, Microsoft Research, Redmond, Washington, 2009

[22] Dubrovskii V.G., Bauman D.A., Kozachek V.V., Mareev V.V., Cirlin G.E. Kinetic models of self-organization effects in lattice systems. *Physica A*, **260** (1998), №3-4, p.349.

[23] Porubov A.V.; Maugin G.A., Mareev V.V. Localization of two-dimensional non-linear strain waves in a plate. *International Journal of Non-Linear Mechanics*, **39** (2004), i.8, 1359-1370

[24] Gankevich I., Gaiduchok V., Gushchanskiy D., Tipikin Yu., Korkhov V., Degtyarev A., Bogdanov A., Zolotarev V. Virtual private supercomputer: Design and evaluation. *Ninth International Conference on Computer Science and Information Technologies (CSIT). Revised Selected Papers, 2013*. IEEE Conference Publication, DOI: 10.1109/CSITechnol.2013.6710358

[25] Bogdanov A., Degtyarev A., Nechaev Yu. Parallel Algorithms for Virtual Testbed. *Proceedings of 5th International Conference «Computer Science & Information Technologies»*, Yerevan, Armenia, 2005, pp.393-398

Appendix

Let us introduce geometrical notations adopted in this work [12].

Local tensor in the absolute frame of reference is written as a string of three basis vectors or three-column coordinate matrix:

$$\hat{r} = \overset{\rightarrow}{r_i} = \begin{Bmatrix} \overset{\rightarrow}{r_1} & \overset{\rightarrow}{r_2} & \overset{\rightarrow}{r_3} \end{Bmatrix} = \begin{Bmatrix} r_{1,1} & r_{1,2} & r_{1,3} \\ r_{2,1} & r_{2,2} & r_{2,3} \\ r_{3,1} & r_{3,2} & r_{3,3} \end{Bmatrix}$$ (index at a vector on the right)

Projections of simple basis vectors of global coordinate system in local basis are represented uniquely in the form of dual basis $\overset{\vee}{r} = \overset{\leftarrow}{r^j} = \overset{\wedge}{r^{-1}}$ (or inverse matrix)

$$\overset{\vee}{r} = \overset{\leftarrow}{r^j} = \begin{Bmatrix} \overset{\leftarrow}{r^1} \\ \overset{\leftarrow}{r^2} \\ \overset{\leftarrow}{r^3} \end{Bmatrix} = \begin{Bmatrix} r^{1,1} & r^{2,1} & r^{3,1} \\ r^{1,2} & r^{2,2} & r^{3,2} \\ r^{1,3} & r^{2,3} & r^{3,3} \end{Bmatrix} = \overset{\wedge}{r^{-1}}$$ (index at a vector on the right)

$\vec{\boldsymbol{A}} = \vec{\boldsymbol{R}} + \vec{\boldsymbol{a}} = \boldsymbol{A}_i$ - the big vector with covariant components where the capital letter *A* means that a vector is constructed, measured relatively common center Ω and scaled in a uniform global coordinate system. If arrow is to the right → or subscript designate than vector components are projected on coordinate axes of global reference system. If arrow is to the left or vector index is at the top (superscript) $_{\Omega}\overset{\leftarrow}{\boldsymbol{A}} = {}_{\Omega}\boldsymbol{A}^{\boldsymbol{j}}$ then vector components are contravariant. They are projected in the dual system of local coordinates $\overset{\vee}{\boldsymbol{r}}$ inside large fluid particle. The one-to-one association between dual bases is defined by multiplication operation with tensor of form of concrete $\overset{\wedge}{\boldsymbol{r}}$ fundamental particle: $\vec{\boldsymbol{R}} = \overset{\wedge}{\boldsymbol{r}} \cdot {}_{\Omega}\overset{\leftarrow}{\boldsymbol{R}}$ or ${}_{\Omega}\overset{\leftarrow}{\boldsymbol{R}} = \vec{\boldsymbol{R}} / \overset{\wedge}{\boldsymbol{r}} = \vec{\boldsymbol{R}} \cdot \overset{\vee}{\boldsymbol{r}}$.

The left-hand indexes unless otherwise stated can be used for a space binding of computing object and for its mark in current time:

${}^{T}_{\Omega}\vec{\boldsymbol{R}}$ are *coordinates of knot point*. Ω defines location of node in mesh of computational domain; *T* is time from the beginning of the computational experiment.

${}^{t}_{+}\vec{\boldsymbol{R}}$ is *reference to adjacent point* (relative to the direction '+' starting from the center of mass of the large fluid particle Ω offset in time by an amount *t*).

$\vec{A} = A_i$ – space point (vector) marked in global coordinate system [m];

$\overset{\leftarrow}{a} = a^k$ – vector counting in the local basis of an elementary fluid particle [m-2];

$\hat{r} = \overset{\rightarrow}{r_k} = r_{ik}$ – tensor of form of large fluid particle [m3];

$\overset{\vee}{\rho} = \overset{\leftarrow}{\rho^j} = \rho^{kj}$ – tensor of density [kg·m-3];

$\overset{<}{M} = M^i{}_j = \overset{\vee}{\rho} \cdot \hat{r}$ – mixed tensor which relates the internal state of the particle at global reference system [kg];

In this case it is possible to present brief table of general notations

T – absolute time counting; $t = \Delta T$ – calculated time interval	c
p – pointwise (scalar) pressure	N/m^2
${}_{\Omega}^{T}\vec{R}$ – coordinates of knot of mesh area Ω at time moment T	m
${}_{+}^{+}\vec{R}$ – coordinates of adjacent point at the next time moment	m
$\vec{V}$ – full speed of fluid particle in global reference system	m/s
v – velocity vector relatively moving center of fluid particle	m/s
w – vector of velocity increment (*acceleration*) for fluid particles	m/s^2
$\hat{r} = \vec{r_k} = r_{ik}$ – geometric tensor of form large fluid particle	m^3
$v = {}_{\Delta}^{\Delta}r_i$ – tensor of local velocities (*velocities increment*)	m^3/s
$\overset{>}{v} = \hat{v}\,\overset{\vee}{r} = \hat{v}/\hat{r}$ – tensor of convective velocities	1/s
$\overset{\wedge}{\omega} = {}_{\Delta}\vec{V}_i$ – tensor of flows inside large fluid particle	m^3/s
$\overset{\vee}{\rho} = \overset{\leftarrow}{\rho^j} = \rho^{kj}$ – tensor of density or internal state of fluid particle	kg/m^3

$\overset{<}{\ }\ \overset{\vee}{\ }\ \overset{\wedge}{\ }$

$M = \rho \cdot r = M^i_j$ – tensor mass of fluid particle (mixed tensor resulting internal state of fluid to global frame of reference) kg

$\vec{F}$ – resultant vector of mass (volume) forces N

$\hat{f}$ – tensor of stresses at the boundaries of fluid particle N m^2

$\overset{>}{f} = \hat{f} \cdot r$ – stress inside and in a vicinity of fluid particle N/m

$\overset{>}{f}_H = \eta \cdot \nu_H / \Lambda$ – conditional tensor of viscous stresses

$\overset{>}{f}_\Gamma = c \cdot \nu_\Gamma \cdot t / \Lambda$ – conditional tensor of elastic stresses

The Inertia Contributions due to Floodwater Mass

*Gyeong Joong Lee[1], Arthur M. Reed[2], Frans van Walree[3], Andrew Peters[4], Paola Gualeni[5], Toru Katayama[6] and WenYang Duan[7]

1. *KRISO, Korea*
2. *NSWC, USA*
3. *MARIN, Netherlands*
4. *QinetiQ, UK*
5. *University of Genoa, Italy*
6. *Osaka Prefecture University, Japan*
7. *Harbin Engineering University, China*

Abstract: The Stability in Waves committee of the 27th ITTC investigated how to deal with the ship inertia contributions due to floodwater mass from three points of view: (1) floodwater domain, (2) floodwater inertia itself, (3) floodwater entering the ship. The committee suggested three criteria indicating the concept of how to deal with floodwater and providing clues on what to consider as floodwater when examining damaged ships: (1) whether the water is moving with the ship and the mass of that volume of water, (2) whether there is a significant pressure jump across the compartment boundary, and (3) whether the dynamics of water can be solved separately. For floodwater inertia, the committee divided this into the partially flooded case and fully flooded case, and investigated the properties and showed how to deal with floodwater inertia for each case. For the case of the floodwater entering the ship, the treatment of the inertia change due to floodwater was derived using the momentum change principle. The related ITTC procedure was updated reflecting this work.

Key words: Floodwater, inertia of floodwater, domain of floodwater

1. Introduction

One of the tasks of the committee on Stability in Waves of the 27th ITTC is to investigate how to deal with the inertia due to the floodwater mass, and to update the relevant ITTC procedure for damage stability simulations. The committee investigated this task from three points of view: (1) floodwater domain, (2) floodwater inertia itself and (3) floodwater entering the ship.

The boundary of the floodwater domain is hard to determine for a large damage opening. The committee suggested three criteria indicating the concept of how to deal with floodwater and providing clues on what to consider as floodwater when examining damaged ships: (1) whether the water is moving with the ship and the mass of that volume of water, (2) whether there is a significant pressure jump across the compartment boundary and (3) whether the dynamics of water can be solved separately.

For the partially flooded compartment, the motion of floodwater is usually analysed by three techniques, namely quasi-static, quasi-dynamic and full dynamic analysis. Quasi-static and quasi-dynamic analyses consider only the centre of gravity of the floodwater, and the mass of floodwater should be included in the ship's mass. However, in full dynamic analysis, the pressure includes all static and dynamic pressure components, therefore the force derived from the pressure integration on the surface of the compartment includes all the effects of floodwater inertia and flow properties. This is subject to the condition that the body force includes the actual acceleration, that is, the gravitational acceleration and the acceleration of the

*** Corresponding author:** Gyeong Joong Lee, Principal Researcher, research fields: ship dynamics. E-mail: gjlee@kriso.re.kr

flood water. In this case, the mass of flood water should not be included in the ship's mass.

In the case of a fully flooded compartment, the floodwater is often treated as a solid and is included in the ship's mass in many studies for the motion dynamics of ships. In order to clarify this problem, the committee reviewed the work of Lee (2014). In his study, the inertial properties of a compartment fully filled with liquid were studied based on potential flow theory. An analytic solution was obtained for the rectangular tank, and the numerical solutions using Green's 2nd identity were obtained for other shapes. The inertia of liquid behaves like a solid in rectilinear acceleration. But under rotational acceleration, the moment of inertia of liquid becomes small compared to that of a solid. The shapes of the compartments investigated in his study were ellipsoid, rectangular, hexagonal and octagonal with various aspect ratios. The numerical solutions were compared with analytic solutions, and an ad hoc semi-analytical approximate formula is proposed which gives a very good prediction for the moment of inertia of the liquid in a tank of several different geometrical shapes. The results of his study will be useful in analysing of the motion of LNG/LPG tankers, liquid cargo ships and damaged ships.

For the case of the floodwater entering ship, the treatment of inertia change due to floodwater was made clear using the momentum change principle. The related ITTC procedure was updated reflecting this work.

2. Floodwater Domain

There is the problem of which region should be treated as floodwater if the damage opening is large enough. So we first need a more reasonable and clear definition of floodwater in the analysis of a damaged ship. If we focus on the inertia properties, the floodwater can be determined by looking at whether the water is moving with the ship or not. If we focus on the hydrodynamics, floodwater may be determined by investigating whether the pressure of it is strongly related with outside water level, and whether the hydrodynamic problem of floodwater can be analysed separately, provided that the boundary condition is given for the matching of the inner and outer flow domains.

Therefore the following may be criteria that will be used to determine the floodwater.

- Whether the water is moving with the ship and the mass of that water volume.
- Whether there is a significant pressure jump across the compartment boundary.
- Whether the dynamics of water can be solved separately.

The above three criteria indicate the concept of how to deal with floodwater and provide clues on what to consider as floodwater when examining damage ships.

3. Inertia of Floodwater

3.1 Partially Flooded Compartments

The hydrodynamics and the force on the compartment partially filled with flood water can be calculated by theory or numerical schemes, such as resonant mode analysis, potential theory, CFD with free surface, etc. In these methods, the force originated from floodwater is treated as an external force, and the motion of a ship is affected by it. However in this case, it is uncertain whether the mass of the floodwater should be included in the ship's mass or not.

The forces due to floodwater can be divided into three parts by considering their origins. The first is the one due to gravitational acceleration, the second one is due to the acceleration by the ship motion, and the third one is due to the dynamic pressure of the flow of floodwater. The interactions of floodwater and ship motion were summarised in the 26th ITTC report by the Stability in Waves committee. The interaction concept is given in Table 1, while the concepts of these three models are shown in Figure 1.

Table 1 Three models of interactions (from 26th ITTC report)

	Floodwater treatment	Interaction concept
Quasi-static	static	added weight
Quasi-dynamic	dynamic	added weight
Dynamic	dynamic	added force

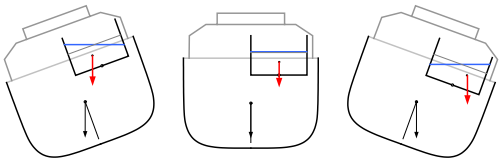

(a) quasi-static (free surface horizontal)

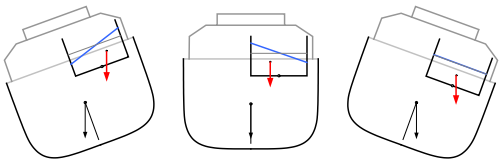

(b) quasi-dynamic (dynamic free surface)

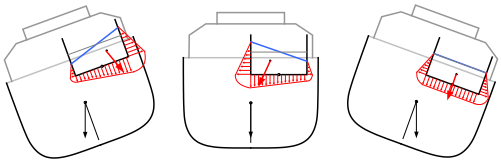

(c) dynamic (dynamic free surface, fluid pressure force)

Figure 1 Concept of floodwater and ship motion interaction (from 26th ITTC report)

In quasi-static or quasi-dynamic analysis, because it considers only the centre of gravity of the flood water and only the gravitational force, the mass of flood water should be included in the ship's mass in order to represent the inertia force, that is, the force due to the acceleration by the ships motion. However in fully dynamic analysis, the pressure includes all the static and dynamic pressure components, the force derived from the pressure integration on the surface of the compartment includes all the effects of floodwater inertia and flow properties. This is subject to the condition that the body force includes the actual acceleration, that is, the gravitational acceleration and the acceleration of the flood water due to the ship's motion. In this case, the mass of flood water should not be included in the ship's mass. The following conceptual equations of motion show how the floodwater inertia should be included.

Quasi-static, quasi-dynamic analysis,

$$(m + \boxed{m_F})\ddot{x} + b\dot{x} + cx = F_{ext} + F_G \quad (1)$$

Fully dynamic analysis,

$$m\ddot{x} + b\dot{x} + cx = F_{ext} + \boxed{F_{FL}} \quad (2)$$

As explained above, in quasi-static or quasi-dynamic analysis, the force due to the floodwater is a gravitational force, this is included in the right side as external force. In this case, the mass of floodwater, m_F should be included in the ship's mass, as in Eq. (1). And in fully dynamic analysis, if the floodwater force, F_{FL} includes all the forces due to gravitational acceleration, the acceleration due to the ship's motion, and dynamic pressure of the flow, the mass of floodwater should not be included into the ship's mass.

3.2 Fully Flooded Compartments

The flood water in a fully filled compartment is often treated as a part of the ship and treated as a solid. In rectilinear acceleration, the flood water acts like a solid. In rotational acceleration, the moment of inertia is smaller than that of a solid, because there is a part of water that does not rotate with the ship. Lee (2014) shows the ratio of the moment of inertia of flood water and that of solids for various shapes of compartments.

$$C_R = I_{Liquid} / I_{Solid} \quad (3)$$

where I_{Liquid} and I_{Solid} are the moment of inertias of the flood water when treated as liquid and solid respectively.

Figure 2 shows the shapes of compartments investigated in his study.

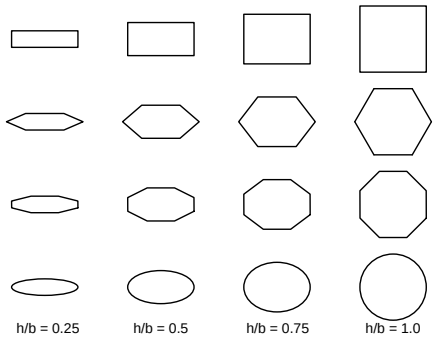

Figure 2 Various shapes of tanks useful for application from Lee (2014)

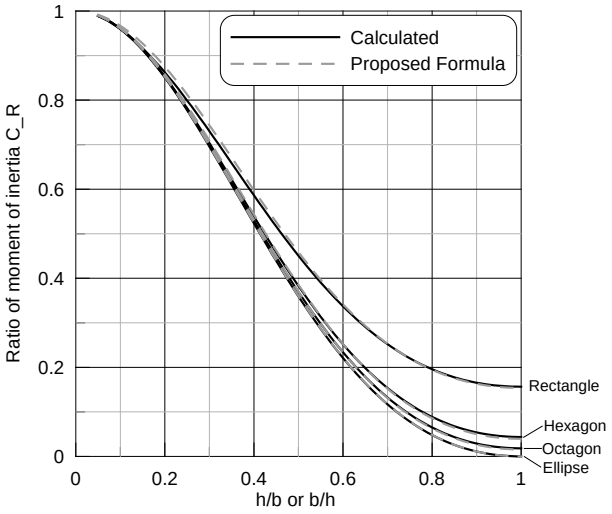

Figure 3 Moment of Inertia prediction of fully filled liquid for various shaped tanks; calculated and estimated from Lee (2014)

The inertias of the fluid in tanks of different aspect ratios and shapes become small as the aspect ratio goes to unity, see Figure 3. The solid lines in Figure 3 are analytical or numerical results while the dashed lines show an estimation formula that provides accurate results. The estimation formula is as follows:

$$I_{Liquid} = I_{Solid} - I_e = I_{Solid} - \rho k_e \frac{A^2}{\pi}\left(\frac{hb}{h^2+b^2}\right) \quad (4)$$

where the shape correlation factor k_e is

$$k_e = \left(\frac{A_{ellipse}}{A}\right)^{2/n} = \left(\frac{\pi hb}{4A}\right)^{2/n} \quad (5)$$

If we put the area A from Table 2, the factor k_e turns out as a coefficient dependent only on the type of the shape as follows,

$$k_e = \begin{cases} \left(\pi/4\right)^{1/2} & \text{for rectangle} \\ \left(\pi/2\sqrt{3}\right)^{1/3} & \text{for hexagon} \\ \left(\dfrac{\pi}{8(\sqrt{2}-1)}\right)^{1/4} & \text{for octagon} \\ 1 & \text{for ellipse} \end{cases} \quad (6)$$

Table 2 Area and moment of inertia of solid for various shapes from Lee (2014)

shape	Number of edges (n)	Area	Moment of inertia for roll
Rectangle	n=4	$A = hb$	$\frac{I_{Solid}}{\rho} = \frac{1}{12}A\left(h^2+b^2\right)$
Hexagon	n=6	$A = \frac{\sqrt{3}}{2}hb'$	$\frac{I_{Solid}}{\rho} = \frac{5}{72}A\left(h^2+b^2\right)$
Octagon	n=8	$A = 2\left(\sqrt{2}-1\right)hb$	$\frac{I_{Solid}}{\rho} = \frac{3-\sqrt{2}}{24}A\left(h^2+b^2\right)$
Ellipse	n=∞	$A = \frac{\pi}{4}hb$	$\frac{I_{Solid}}{\rho} = \frac{1}{16}A\left(h^2+b^2\right)$

4. Inertia of Floodwater Entering Ship

Newton's Second Law states that the force (moment) on a body is equal to its time rate-of-change of momentum (angular momentum). For a body of constant mass (moment of inertia) this translates to $\vec{F} = m\vec{a}$ ($\vec{M} = I\, d\vec{\omega}/dt$). However, for a body such as a rocket which is burning fuel and ejecting gas or a damaged ship in a seaway taking on and possibly discharging water, the $\vec{F} = m\vec{a}$ analogy is not correct, but in fact the time-rate-of-change of mass must be taken into account. As the force must remain independent of the coordinate system, a simple application of the rule for differentiation of the product of two functions is not correct. The contribution from the time-rate-of-change of mass term belongs on the left-hand side of the equation with

the force. In the context of rocket propulsion, the time-rate-of-change of mass contribution is the equivalent of the thrust of the rocket motor, and the entire system must be looked at as a constant mass system. Similar analogies apply to the time-rate-of-change of moment of inertia.

If we represent the momentum of the vessel as $\vec{p}$ and the angular momentum as $\vec{L}$, where $\vec{p}=m\vec{v}$ and $\vec{L} = I\vec{\omega}$, with m the mass of the ship, $\vec{v}$ the velocity, I the moment of inertial tensor and $\vec{\omega}$ the angular velocity, then Newton's second law can be written as:

$$\vec{F} = m\frac{d\vec{v}}{dt}, \qquad \vec{M} = I\frac{d\vec{\omega}}{dt}. \tag{7}$$

When the mass and hence the moment of inertia are constant, then these equations reduce to the traditional $\vec{F} = m\vec{a}$ form. However, in the damaged condition, the vessel's mass and moment of inertia vary with time and the equations of motion must be written in the above form. Rewriting equation (7) to account for the intake or discharge of floodwater as for a closed system yields:

$$F - \vec{v}'\frac{dm}{dt} = m\frac{d\vec{v}}{dt}, \qquad M - \vec{\omega}'\frac{dI}{dt} = I\frac{d\vec{\omega}}{dt}, \tag{8}$$

where $\vec{v}'$ and $\vec{\omega}'$ are the velocity and angular velocity of the flooding (discharging) water relative to the vessel, respectively. All of the quantities $\vec{v}'$, dm/dt, and $\vec{\omega}'$ can be determined from analysis of the flow at the damaged opening (if there is flow between flooded compartments, then the flow between the compartments must be incorporated in a similar manner.) The evaluation of dI/dt is somewhat more complex as it involves the actual shape of the compartment.

The above material dealing with the inertia change due to floodwater was included in the ITTC procedure 7.5-02-07-04.4.

5. Conclusions

The committee investigated how to deal with the inertia due to floodwater mass from three points of view: (1) floodwater domain, (2) floodwater inertia itself and (3) floodwater entering the ship.

For the floodwater domain, the committee proposed the criteria that will be used to determine the floodwater. For floodwater inertia, the committee divided this into the partially flooded case and fully flooded case, and investigated the properties and showed how to deal with floodwater inertia for each case. For the case of the floodwater entering the ship, the treatment of inertia change due to floodwater was made clear using the momentum change principle. The related ITTC procedure was updated reflecting this work.

Acknowledgments

The aim of this paper is to introduce the work of the ITTC Stability in Waves committee on the damage simulations. The present paper contains a chapter of the SiW report to the 27th ITTC in a rearranged format.

References

[1] Committee on Stability in Waves, 2014, Final Report and Recommendations to 27th ITTC, 27th ITTC.

[2] Committee on Stability in Waves, 2011, Final Report and Recommendations to 26th ITTC, 26th ITTC.

[3] Lee, G. J. (2014) Moment of Inertia of Liquid in a Tank. *Int. J. of Naval Architecture and Ocean Engineering*, Vol.6, No.1. pp.132-150.

Numerical Estimation and Validation of Shallow Draft Effect on Roll Damping

Toru Katayama[1], Burak Yildiz [2, *] and Jun Umeda [1]

1. *Dept. of Marine System Engineering, Graduate School of Engineering , Osaka Prefecture University, Japan*
2. *Dept. of Marine Engineering Operations, Faculty of Naval Architecture and maritime, Yildiz Technical University, Turkey*

Abstract: It is difficult to calculate roll damping of ships theoretically due to the effects of viscosity. Therefore, Computational Fluid Dynamics (CFD) has become a powerful tool for the prediction of roll damping recently. For ship roll damping, the bilge keel component accounts for the greatest part of the total roll damping. However, bilge keels are most effective when they are fully submerged and the contribution of bilge keel to the total roll damping decrease when the draft is shallow. In this paper, the flow around a forced rolling two dimensional body is analyzed to see the shallow draft effect on roll damping by using CFD code Fluent. In order to validate the CFD calculations, the results are compared with both the forced roll test results that were carried out by Katayama et al. (2010) [1] and Ikeda's estimation method. This study seeks to assess if the CFD code can correctly predict roll damping coefficients of a rolling vessel.

Key words: Roll damping, bilge keel, shallow draft, computational fluid dynamics

1. Introduction

The roll response of a ship is an important consideration in its design. Roll motion limits ship operability, affects crew performance and ship habitability and affects dynamic stability and it can lead to ship capsize. Roll motion is one of the most critical responses of a ship in waves. The roll motion of a ship can be determined by analyzing various kinds of moments acting on the ship, virtual and actual mass moments of inertia, roll damping moment, restoring moment, wave excitation and other moments caused by other modes of ship motion. Among them, the roll damping moment has been considered to be the most important term that should be correctly predicted.

Damping of roll motion strongly depends on viscous effects so that it is really significant to calculate damping forces correctly. Prediction of roll damping by using potential flow theories is hard due to viscous effects. Therefore, Computational fluid dynamics (CFD) have become an important tool for the estimation of roll damping. Many researchers have recently studied about prediction and validation of roll damping by using CFD. Jaouen et al. (2011) verified and validated MARIN's URANS code ReFRESCO for roll damping of 2D hull sections by comparing with the damping coefficients measured by Ikeda et al. (1978) [2]. Bonfiglio et al. (2011) by using the developed CFD code base on the open source libraries of OpenFOAM and Henning (2011) by using FLUENT evaluated the hydrodynamic damping and added mass coefficients of 2D ship-like hull sections in the case of forced oscillations [3][4]. Bangun et al. (2010) calculated the hydrodynamic damping and added mass coefficients of a 2-D rectangular sections with bilge keels and compared the predictions with measured results by Yago et al. (2008) [5]. Paap (2005) investigated verification of CFD calculations with forced roll test results for a circular cylinder with various types of bilge keels and a free surface [6]. Bassler (2013) analyses the hydrodynamics of large amplitude ship roll motion as components of the added inertia and damping based on the results of forced roll test and CFD. It is shown that the effects of the hull geometry, bilge keel geometry, deck edge and the free surface all affect the hydrodynamic components during large amplitude roll motions [7].

Large amplitude roll motions have the same effect on bilge keel with shallow draft. Bilge keel come closer to the free surface in both case.

Bilge keels have been used on ships to increase damping and reduce the roll motion. Bilge keel component is the biggest part of total roll damping so that it should be calculated accurately. There are some factors that affect the contribution of bilge keel to total roll damping. One of these factors is shallow draft effect. In the previous study by Tanaka et al. (1981), it is pointed out that bilge-keel component decreases when the draft is shallow [8].

In this study, the effect of shallow draft on roll damping is investigated by using a commercial CFD code and the CFD results validated with the experiment results of Katayama et al. (2010). The simulations are carried out for three different center of gravity (KG) and several draft values for each KG. Also the roll damping coefficients are calculated by using Ikeda's estimation method and it is observed that Ikeda's method does not consider shallow draft effect.

2. Theoretical Formulation

2.1 Definitions

The roll motion of the 2D hull section is forced around the z axis, perpendicular to the hull section. The description of the symbols used in this study is given in Table 1.

Table 1 Nomenclature

B	Breadth of the hull (m)
d	Draft of the hull (m)
g	Gravitational acceleration (m^2/s)
T	Roll period (s)
ρ	Density of water (kg/m^3)
ϕ_0	Roll Amplitude (rad)
ω	Roll angular frequency (rad/s)
$B_{\phi\phi}$	Damping coefficient (-)

2.2 Roll Damping Analysis

As many numerical simulations that indicate a body motion, a gradual start of the motion is needed in order to avoid strong transient flows at the earlier time-steps of the calculation. It can take considerable number iterations to get rid of those initial peaks. The final motion of the hull will be a pure sine:

$$\emptyset(t) = \emptyset_0 \sin \omega t \tag{2}$$

A start-up function is defined that slowly increases the amplitude from zero to the final value for the first 4 periods, the frequency will be constant during the whole computation. The start-up function f(t) is defined by

$$f(t) = \begin{cases} \frac{1}{2} sin\left(\frac{1}{4}.\frac{\pi}{T}.t - \frac{1}{2}\pi\right) + \frac{1}{2}, for\ t < 4T \\ 1 \qquad\qquad\qquad\quad , for\ t > 4T \end{cases} \tag{3}$$

The function that indicates the prescribed motion, f(t), is written with C^{++} programming language and fluent calls this function as an user defined function (UDF). UDF gives the rotational velocity as function of time and Fluent reads these values to force the body to harmonic oscillation, see in Fig.1.

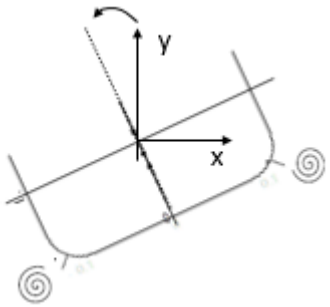

Fig. 1 – Description of the forced roll model

The roll angle $\emptyset(t)$ is now defined by

$$\emptyset(t) = f(t)\emptyset_0 \sin \omega t \tag{4}$$

The uncoupled equation of motion to describe the forced roll motion may be written as

$$a_{\emptyset\emptyset}\emptyset'' + B(\emptyset,\emptyset') + C(\emptyset) = M_E(t) \quad (5)$$

where $a_{\emptyset\emptyset}$ is the added mass for roll motion, $B(\emptyset,\emptyset')$ is the damping moment, $C(\emptyset)$ is the restoring moment and $M_E(t)$ is the time history of the computed moments and it is fitted with

$$M_E(t) = M_0 sin(\omega t + \varepsilon) \quad (6)$$

by applying the Fourier analysis, M_0 is the amplitude of the roll moment and ε indicates the phase angle between the prescribed roll angle and the roll moment. Time history of the computed moments are acquired via experiments and CFD simulations, then M_0 and ε can be calculated with Fourier transformation between time history of moments and roll angle. The final step is calculation of roll damping coefficient which can be expressed as follow:

$$B_{\emptyset\emptyset} = \frac{M_0 sin(\varepsilon)}{\emptyset_0 \omega} \quad (7)$$

To be able to compare these results with other research projects damping terms will be presented dimensionless. Dimension analyses give the following dimensionless representations of the damping coefficient.

$$\hat{B} = \frac{B}{\rho \nabla B_{WL}^2} \sqrt{\frac{B_{WL}}{2g}} \quad (1)$$

3. Forced Roll Experiments

In this study, the results of forced rolling test that is carried out by using two-dimensional model to observe the effects of shallow draft on roll damping is used to validate the CFD results.

Table 2 shows the principal particulars of the model with bilge keel. Fig. 2 shows some parameters for explaining experimental conditions. The measurements at systematically changed roll amplitudes, roll periods, drafts and height of roll axis (the center of rolling) are carried out. Bilge-keel component is obtained from subtraction measured data of hull without bilge keel from measured data of hull with bilge keel at the same condition.

Table 2 Principle particulars of two-dimensional model

length: L	0.80m
breadth: B	0.237m
depth: D	0.14465m
block coefficient: C_B	0.8
bilge radius	0.035m
length X breadth	0.01m x 0.80m

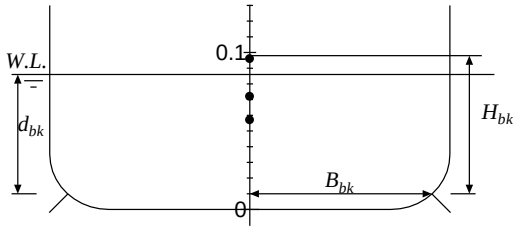

Fig. 2 – Cross section of two-dimensional model

4. Numerical Settings

CFD package Fluent is used for calculations, based on the specifications, should be able to perform 2D computations on a rolling midsection of a ship. It can include any kind of prescribed roll motion, radiation of waves, far field wave damping, grid refinement around the bilge keel, turbulence modeling and it can record the forces and moments on the body.

Fluent, viscous flow code, can be used for unsteady analyses. It is used to simulate incompressible flow around the rolling 2D section and it uses the finite-volume approach. This is based on control volume technique which all transport equations (mass and momentum equations) are solved numerically. The finite volume type solution method also calculates the equations for turbulence model and volume fraction of water-air. In this study, the segregated iterative solution method which is based on SIMPLE algorithm is preferred instead of coupled solution methods (Fluent Handbook). First order implicit scheme is used for time integration. To calculate the free surface effect a volume of fluid method (VOF) is applied. The k-ε-standard turbulence is used for all calculations.

The integral value of the energy dissipation during the forced roll motion can be calculated based on the flow simulation results. In the past, two groups of RANSE-simulation methods for estimating roll damping have been applied: one which uses a fixed roll axis as well as a sliding interface, and one which uses grid motion or deformation technique to simulate the free motion without an interface [9]. In this study 2D midsection is fixed to x axis and cylindrical mesh zone rotated around the roll axis. There is an interface between stationary zone and rigid moving zone which avoids cell-deforming issue, see Fig. 3.

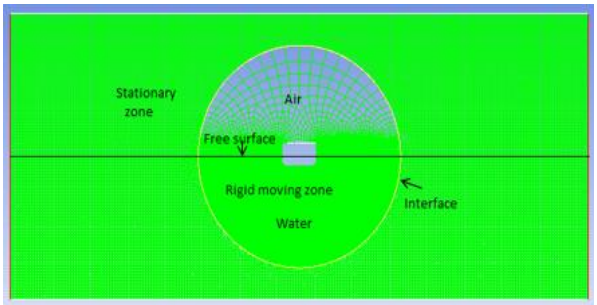

Fig. 3 – The geometry and computational mesh

Both experiment and CFD simulations are carried out for variable KG and draft values, also Ikeda's estimation method is used for calculations, see in Table 3.

Table 3 Principle particulars of experiments and simulations

KG	T	ϕ	d	CFD	Exp.	Ikeda
0.096	1.2	8.59	0.095	O	O	O
0.096	1.2	8.59	0.08	O	O	O
0.096	1.2	8.59	0.072	O	X	O
0.096	1.2	8.59	0.06	O	O	O
0.096	1.2	8.59	0.05	O	O	O
0.096	1.2	8.59	0.042	O	O	O
0.096	1.2	8.59	0.035	O	X	O
0.096	1.2	8.59	0.025	O	X	O
0.072	1.2	8.59	0.095	O	X	O
0.072	1.2	8.59	0.08	O	O	O
0.072	1.2	8.59	0.072	O	X	O
0.072	1.2	8.59	0.06	O	X	O
0.072	1.2	8.59	0.05	O	O	O
0.072	1.2	8.59	0.042	O	O	O
0.072	1.2	8.59	0.035	O	X	O
0.072	1.2	8.59	0.03	O	X	O
0.072	1.2	8.59	0.025	O	X	O
0.072	1.2	8.59	0.023	O	O	O
0.057	1.2	8.59	0.057	O	O	O
0.057	1.2	8.59	0.05	O	O	O
0.057	1.2	8.59	0.042	O	O	O
0.057	1.2	8.59	0.035	O	O	O
0.057	1.2	8.59	0.025	O	X	O
0.057	1.2	8.59	0.023	O	X	O

(O = Done, X = Not done)

5. Calculations and Validations

CFD computations have been carried out for 2D midsection for different draft values and results have been validated with both experiment results and Ikeda's estimation method.

Fig. 4 shows the harmonic oscillation of the body that slowly increases the amplitude from zero to the final value for the first 4 periods. Moments on hull

and bilge keels have been calculated by using CFD for this movement of body. It is observed that when the draft decreases, total roll damping decreases because free surface effect increases for shallow draft. Fig. 5 shows the time history of calculated moment on bilge keels. It is observed that when the draft becomes shallow. The moment on bilge keels decrease.

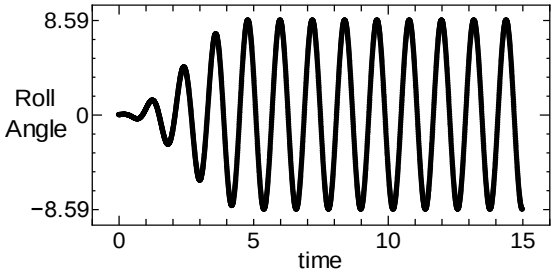

Fig. 4 – Time history of roll motion

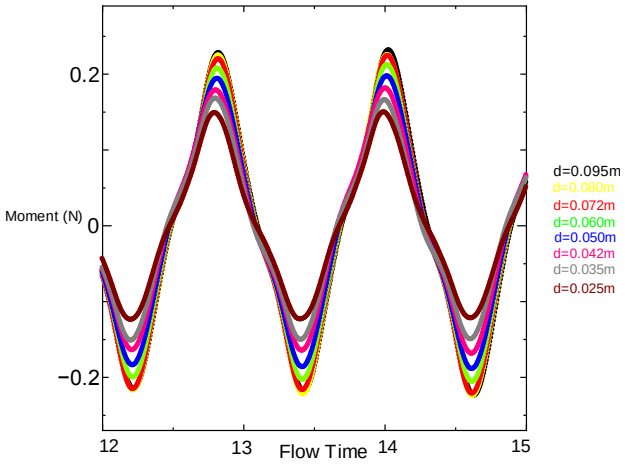

Fig. 5 – Time history of bilge-keel moment for different drafts

Comparison between CFD results and experiments and also Ikeda's method for different KG values are shown in Fig, 6-7 and 8. As it is shown in figures, CFD results show good agreement with experiment results. Non dimensional roll damping coefficients are shown for each draft values in figures. When the draft decreases, the difference between CFD results and Ikeda's estimation method increases, especially for Fig. 6 and 7. The reason of this difference is that Ikeda's method does not consider shallow draft effect.

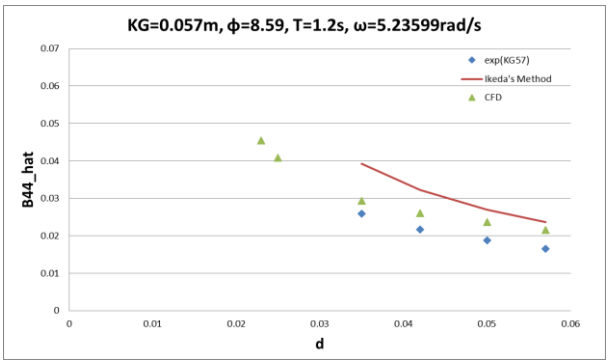

Fig.6 – Dimensionless roll damping coefficient (KG=0.057)

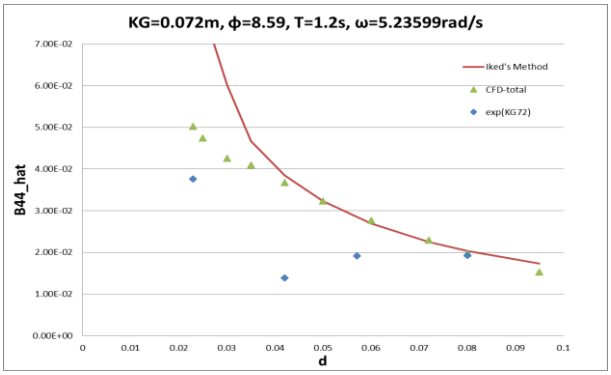

Fig. 7 – Dimensionless roll damping coefficient (KG=0.072)

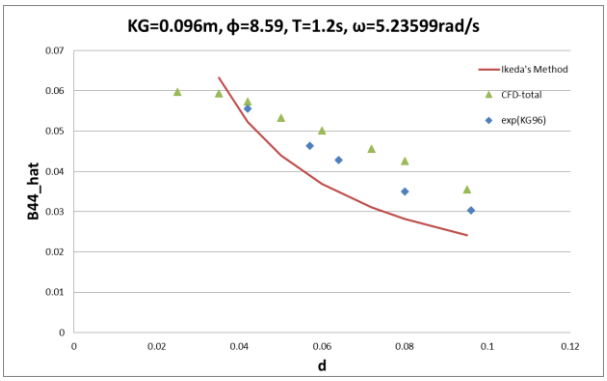

Fig. 8 – Dimensionless roll damping coefficient (KG=0.096)

6. Conclusions

In this paper CFD code Fluent has been used for the estimation of effect of shallow draft on roll-damping. The unsteady flow around a forced rolling 2D midsection with bilge keels is computed. Extensive numerical sensitivity studies are carried out and the viscous-damping coefficient is computed for various draft values. The numerical results of Fluent are compared to experimental values and Ikeda's

estimation method. It is found out that CFD can be used for accurate prediction of roll damping coefficient.

Calculations for shallow draft show that the roll damping moment decreases when the draft becomes shallow. It is because of that the bilge keel comes closer to the free surface when the ship rolled. This free surface effect decrease the total roll damping coefficient. Ikeda's estimation method does not consider this effect. However, CFD calculates this effect and results show good agreement with model tests.

There are a lot of options that directly affect the CFD results, especially mesh quality. In this study, medium mesh quality is used for calculations due to computational time. As a future work calculations will be carried out for a high quality mesh to have better results.

CFD is a practical and fast way to estimate ship roll damping but without validation CFD results are not essential. Therefore, as a first step of estimation of roll damping, experiment results needs to be provided to validate CFD results. After that we can develop a more accurate model to describe and predict roll motions in severe wave environments.

References

[1] T. Katayama, Y. Yoshioka, T. Kakinoki, Y. Ikeda, Some Topics for estimation of Bilge-Keel Component of Roll Damping, Proceedings of the 11th International Ship Stability Workshop, 2010, pp.225-230.

[2] F. Jaouen, A. Koop, G. Vaz, Predicting roll added mass and damping of a ship hull section using CFD, Proceedings of the 30th International Conference on Ocean, Offshore and Arctic Engineering (OMAE,), 20111, pp.1-11.

[3] L. Bonfiglo, S. Brizzolara, C. Chryssostomidis, Added mass and damping of oscillating bodies a fully viscous numerical approach, Recent Advances in fluid Mechanics, Heat & Mass Transfer and Biology, (2011), pp.210-215.

[4] H. L. Henning, Investigation of the Heave, Sway and Roll Motions of Typical Ship Like Hull Sections Using RANS Numerical Methods. Master Thesis, University of Stellenbosch.M, 2011.

[5] E. P. Bangun, C. M. Wang, T. Utsunomiya, Hydrodynamic forces on a rolling barge with bilge keels, Applied Ocean Research, 2010, (32):219-232

[6] M. Paap, Verification of CFD calculations with experiments on a rolling circular cylinder with bilge keels in a free surface. Master Thesis, Delft University of Technology & Bluewater Energy Services, 2005.

[7] C. C. Bassler, Analysis and Modeling of Hydrodynamic Components for Ship Roll Motion in Heavy Weather, Ph.D. Thesis, Virginia Polytechnic Institute and State University, 2013.

[8] N. Tanaka, Y. Himeno, Y. Ikeda and K. Isomura, Experimental study on Bilge-Keel Effect for Shallow-Draft Ship, Journal of the Kansai Society of Naval Architects, Japan, 1981, Vol. 180, pp. 69-75.

[9] S. Handschel, N. Kollisch, J. P. Soproni, M. Abdel-Maksoud, A numerical method for estimation of ship roll damping for large amplitudes, 29th Symposium on Naval Hydrodynamics, Sweeden, 2012.

Modelling of Extreme Waves Related to Stability Research

Janou Hennig[1] and Frans van Walree[1]

1. Maritime Research Institute Netherlands,(MARIN), Wageningen, the Netherlands

Abstract: The paper deals with several aspects of extreme wave modeling in model basins. The effects of directional spreading, steepness and distance from the wave maker on the probability of occurrence of extreme wave crest heights are shown and discussed. Next a method for calibration of directional waves is presented. Finally, the modeling of deterministic waves in a model basin is dealt with.

Key words: Extreme waves, wave crest distributions, wave generation

1. Introduction

When non-linear or extreme wave modeling is considered with respect to ship stability research, the following related questions can be raised:

1. How often do extreme waves occur and how relevant are they,
2. What are their typical shape and kinematics,
3. How can extreme waves be generated in wave basins.

These questions shall be treated in the following, looking both at state-of-the-art methods and at recent research.

2. Probability of Occurrence and Relevance of Extreme Waves

From the numerous data sets investigated during the CresT JIP, a Joint Industry Project on the effect of extreme wave impacts on offshore structures, it was concluded that a second order wave crest distribution function is a good basis for the estimation of a design wave crest, see Ref [1]. However, depending on parameters such as directional spreading, sea state steepness and propagation distance, crests may exceed the second order distribution in severe seas by some 10%. On the other hand, the very highest crests may be limited by breaking and even fall below a second order model.

2.1 Effect of directional spreading

For three different sea states at the same peak period, the effect of spreading is illustrated in Fig. 1. Three spreading increases from top to bottom. The sea states were measured in the MARIN Offshore Basin during the CresT project. The waves were steep, with a nominal significant wave height of 12 m and a peak period of 12 seconds. The model scale was 50. The measured crest height distribution lies above both the Rayleigh distribution and the standard second order distribution (Ref [2]) for the long-crested and the low spreading case. The measurements show that the deviation from second order theory is much less in short-crested waves. It should be noted that the figures correspond to one seed per sea state. In ongoing projects, corresponding investigations concern a large number of seeds.

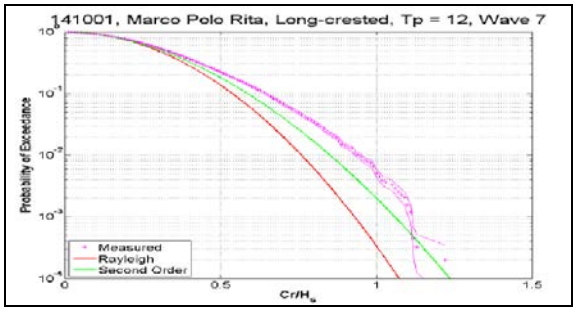

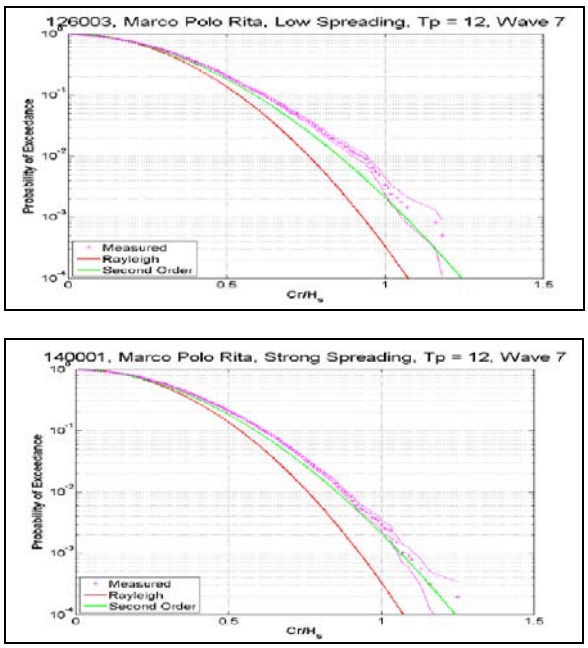

Figure 1 Wave crest distribution depending on spreading, from top to bottom: Long-crested, low spreading (s=15) and strong spreading (s=4).

2.2 Effect of sea state steepness

The effect of sea state steepness is illustrated in Fig. 2 (see also Ref [1]) showing the measured crest distributions for 4000 hours of field data. The steepness increases from top to bottom. The sea state steepness is defined on basis of the mean spectral period T_1:

$$S_1 = \frac{2\pi H_s}{g T_1^2} \qquad (1)$$

It can be seen that the wave crests become higher with increasing sea state steepness, starting from below the second order theory and increasing up to a significant deviation beyond second order. For the largest crests, wave breaking as counteracting effect limits a further increase. This effect of wave breaking as a limiting process is considered an important observation.

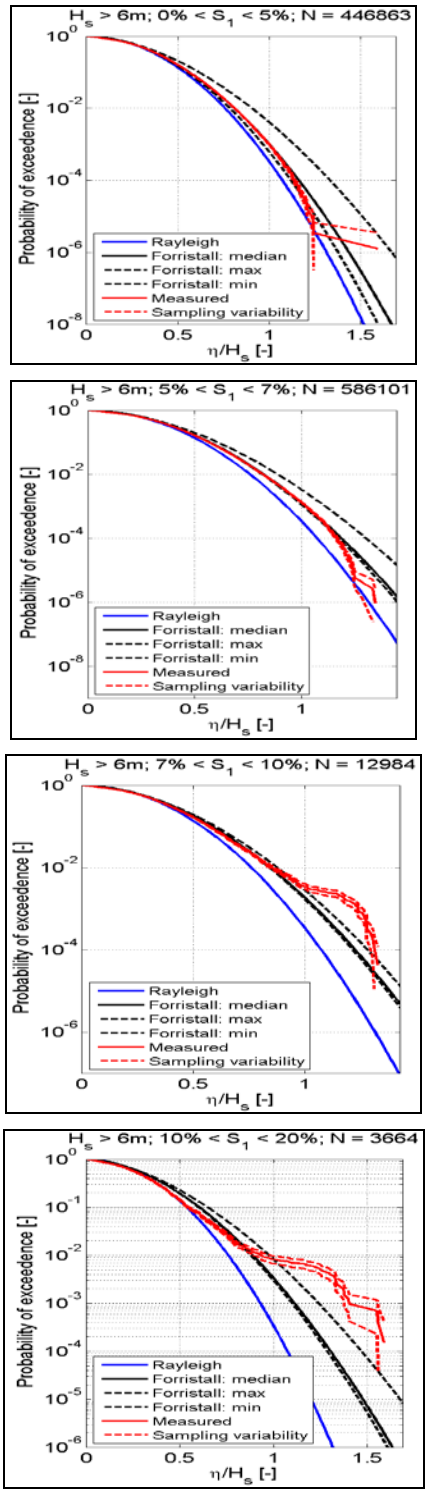

Figure 2 Wave crest distribution depending on sea state steepness, increasing from top to bottom.

2.3 Effect of distance (from the wave maker)

In order to investigate the effect of wave evolution with distance on the wave crest distributions, measurements at several locations along MARIN's Offshore Basin length were carried out. Fig. 3 shows the distribution of wave probes over the basin length.

Following the evolution of the wave with increasing distance from the wave generator, it can be observed that breaking does not stop the possible further development of extreme crests. Fig. 4 shows crest height distributions for the same test, but at greater distances from the wave generator. These measurements show that in long-crested waves it may take a few wave lengths to modify the crest height distribution. The observed growth may be due to third-order resonant interactions, or Benjamin-Feir instabilities, accompanied by a shift of spectral energy in frequency band and seems somewhat faster here than has been reported in some other studies – at scale 1:50, the MARIN Offshore Basin has a length of 5-10 wave lengths.

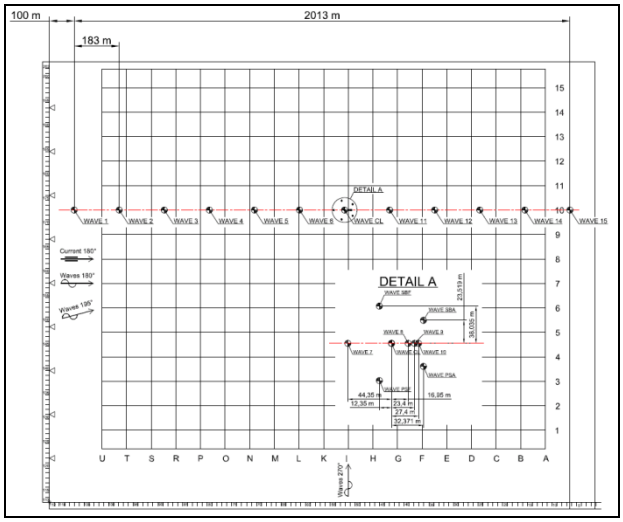

Figure 3 Distribution of wave probes along MARIN's Offshore Basin.

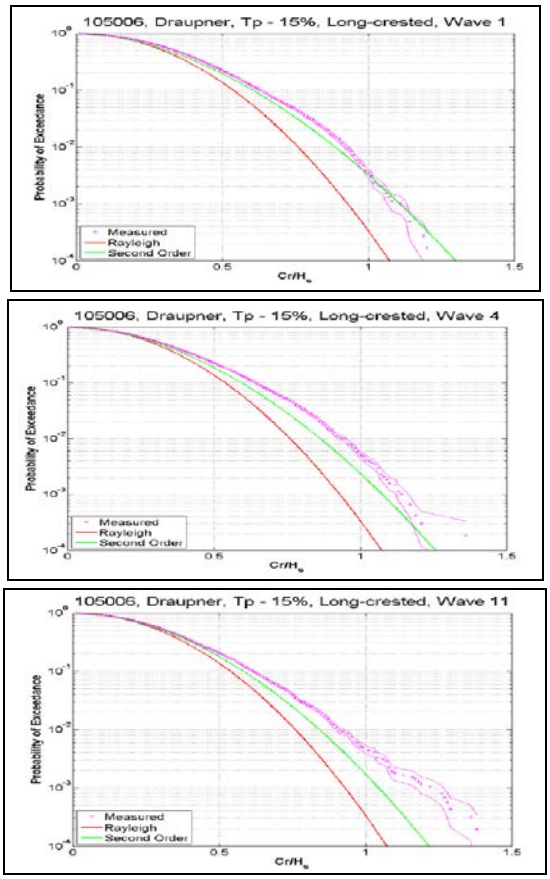

Figure 4 Crest height distribution observed for long-crested seas.

In summary, for the wave statistics, the following can be concluded from the research undertaken in CresT:

1. Use the Forristall distribution for the wave height.
2. Use the second order distribution as basis for the crest height.
3. Correct for observed deviations from second order. This is subject to ongoing research.

3. Calibration of Directional Waves

Understanding the processes described previously and giving useful recommendations demands an effort in defining the correct wave spectrum, understanding wave amplification and breaking, and generating fully non-linear crest statistics in a scheme useful for engineering application.

To improve the quality of the waves in a model basin a calibration loop can be used. For a target wave spectrum the wave maker control software determines the theoretical flap motions, leading to a wave realisation in the basin. Depending on the quality of the wave maker theory used, the resulting wave in the basin can differ from the target spectrum. In a typical calibration loop the generated wave is measured and analyzed. The resulting spectrum is compared against the target spectrum. Next the target spectrum sent to the wave maker can be adjusted in an attempt to obtain a better quality basin wave.

For long-crested waves the calibration procedure is well established and included in common wave generation software. For short-crested waves a similar approach was implemented and tested at MARIN. First the directional spectrum $S(\omega,\theta)$ is defined as a combination of a frequency dependent spectrum $S(\omega)$ and a frequency and direction dependent spreading function $D(\omega,\theta)$; in the correction procedure $S(\omega,\theta)$ and $D(\omega,\theta)$ are treated separately. In global overview the calibration works as follows:

1. Generate wave in the basin for the theoretical spectrum $St(\omega)$ and spreading function $Dt(\omega,\theta)$.
2. Measure and analyse the resulting realization to determine the measured spectrum $Sm(\omega)$ and measured spreading function $Dm(\omega,\theta)$.
3. Compute the corrections $CS(\omega)$ and $CD(\omega,\theta)$.
4. Generate a new wave attempt based on $CS(\omega).St(\omega)$ and $CD(\omega,\theta).Dt(\omega,\theta)$
5. Repeat from point 2 until satisfied.

To measure the waves, resistance type wave elevation probes are used. The probe layout consists of a number of small footprint arrays distributed over a larger area of the basin. To determine the wave spectral density, a mixture between two methods is used: EMLM (Extended Maximum Likelihood Method, see Ref [3] and MEM (Maximum Entropy Method, see Ref [4]) which are both implemented and tested for typical probe arrays. For the frequencies above 2.5 rad/s (18 s prototype) a slope based MEM method is used on each of the small footprint arrays to obtain local information on $Dm(\omega, \theta)$. At lower frequencies (longer waves) the slope falls within the resolution/measurement accuracy of the wave probes within a small footprint array. As an alternative a phase difference based EMLM method is used, based on single wave probes distributed over a larger area in the basin. Combining the two methods give a reliable analysis for a wide range of frequencies. The correction factor $CD(\omega,\theta)$ is computed using: $CD(\omega,\theta) = Dm(\omega,\theta)/Dt(\omega, \theta)$. The correction is only computed for the range of ω and θ values with sufficient spectral energy.

Fig. 5 shows the results of the directional wave calibration: Example for an Ewans' spread sea state calibrated in MARIN's Seakeeping and Manoeuvring Basin. Top left: Measured directional spectrum. Top right: Theoretical spectrum. Bottom figures: Directional distribution at a selection of frequencies

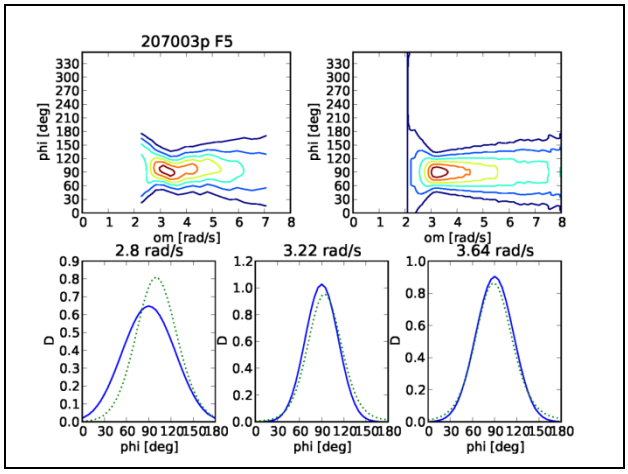

Figure 5 Example of directional wave calibration

4. Extreme wave modeling in model basins

To model extreme waves appropriately both in the basin and in numerical simulations, different approaches are required which are addressed briefly in the following sections.

4.1 Deterministic wave generation

Deterministic wave generation means to reproduce a predefined target wave train at a given position and time in a basin. For the generation of deterministic wave sequences in a model basin different types of wave makers are available. The wave generation process, as illustrated in Fig. 6 for the example of a double flap wave maker, can be divided into four steps:

1. Definition of the target wave train: the target position in time and space is selected – for example the position where a ship encounters the wave train at a given time. At this location, the target wave train is designed – based on defined parameters or a wave record.
2. Upstream transformation: the target wave train is transformed upstream to the position of the wave maker, e. g. by means of a non-linear wave propagation model.
3. Calculation of control signals: the corresponding control signals are calculated using adequate transfer functions of the wave generator.
4. Performing the model tests: the control signals are used to generate the specified wave train which is measured at selected positions in the tank.

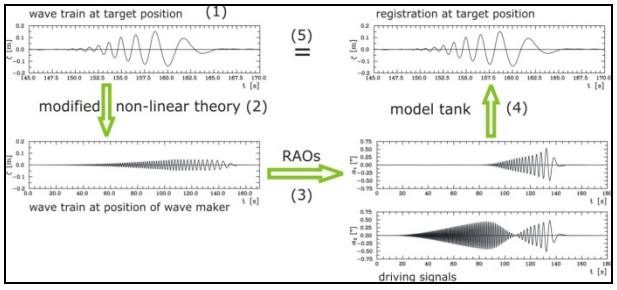

Figure 6 Process of deterministic wave generation

4.2 Optimization of wave realisations

Furthermore, the target wave can be achieved by optimization applied both to a numerical and a physical wave tank. In the figure below, for the example of the well-known "New Year Wave" as extreme directional wave, this optimization process is illustrated. The "New Year Wave" was measured on 01/01/95 in the Norwegian sector of the North Sea (Draupner) by a down-looking radar, see Ref [5]. It is a 20 min wave record, with T_P = 10.8 s, H_S = 11.92 m, H_{MAX} = 25.6 m ⇨ H_{MAX} / H_S = 2.15, Crest height 18.5 m, water depth = 70 m. The directional wave generation based on optimization works as follows:

1. Combining target wave train (time domain) and directional spectrum (frequency domain) to "fronts" as an unique parameter set of wave frequency, heading, amplitude and phase.
2. Upstream transformation of wave fronts using linear theory
3. Calculating motion of first wave board, then of neighboring boards
4. Generate, measure and analyse wave
5. Start optimization of wave board motions, based on comparison with target wave

Fig. 7 shows the result of the optimized basin realization of the short-crested New Year Wave.

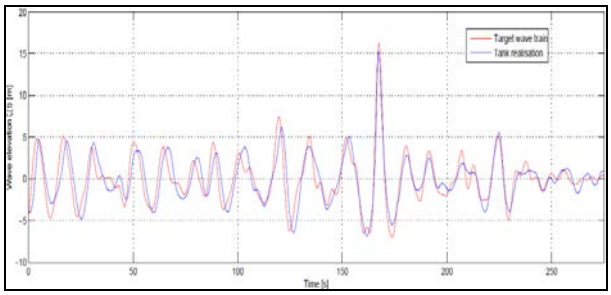

Figure 7 "New Year Wave".

5. Conclusions

The paper has shown that directional wave spreading reduces the probability of occurrence of extreme wave crest heights (for the same sea state steepness). Wave crests become higher with increasing sea state steepness, but wave breaking may reduce the crest height. However, wave breaking does not stop further development of extreme crests in downwind directions.

A calibration method for directional waves is discussed. Finally, the process used to generate deterministic waves in a model basin is discussed and an example is given.

Acknowledgments

The aim of this paper is to introduce the work of the ITTC Stability in Waves committee on the modelling of extreme waves. The present paper contains a chapter of the SiW report to the 27th ITTC in a rearranged format.

References

[1] B. Buchner, G. Forristall, K. Ewans, M. Christou and J. Hennig, "New Insights in Extreme Crest Height Distributions (A Summary of the Crest JIP)", Proceedings of OMAE 2011, Rotterdam, Netherlands.

[2] M. Provosto and G.Z. Forristall, "Statistics of Wave Crests from Models vs. Measurements", Proceedings of OMAE, Oslo Norway, 2002.

[3] O.J. Waals, A.B. Aalbers and J.A. Pinkster, " Maximum Likelihood Method as a Means to Estimate the Directional Wave Spectrum and the Mean Wave Drift Force on a Dynamically Positioned Vessel, 21st International Conference on Offshore Mechanics and Arctic Engineering, Oslo, Norway, 2002.

[4] M.J. Briggs, "Multichannel Maximum Entropy Method of Spectral Analysis Applied to Offshore Platforms", 14th Offshore Technology Conference OTC, Houston, TX, 1982.

[5] S. Haver, 'Evidences of Existence of Freak Waves', Rogue Waves Workshop, Vol. 1, 129-140, Brest, 2000

An Analysis of Bilge Keel Effects using RANS with Overset Grids Method

Motoki Araki[1], Kunihide Ohashi[1], Nobuyuki Hirata[1]

1. National Maritime Research Institute, Japan

Abstract: Roll damping effects due to bilge keels are one of the important topics for roll damping prediction. Since the mechanisms of the bilge keel effects are highly related to viscous phenomena, the roll decay with forward speed simulation of the US navy combatant DTMB5415 is conducted with URANS solver. Here the attached bilge keel is reproduced by using an overset grids method. The computed results show not quantitative but qualitative agreements with the experimental results. Moreover the CFD forced roll motion without bilge keels is simulated to analyze the bilge keel effects. From the comparison of the roll moment between these computed results, the model with bilge keels has larger roll rate component and smaller roll acceleration component than those of the model without bilge keel. The larger roll rate component could be caused by vortex shedding at the bilge keel tips and smaller roll acceleration component might be caused by interfering the accelerated flow around the body.

Key words: CFD, DTMB5415, roll decay,

1. Introduction

Bilge keel is one of the most basic and effective roll damping devices for ship stability. Since the roll damping is dominated by viscous effect and highly complex interactions with hull, bilge keels and free surface, potential flow simulations show some difficulties predicting roll damping on hull including bilge keels [1]. Therefore the semi-empirical roll damping prediction method is the most widely used for practical purpose e.g. Ikeda's method [2], which decomposes roll damping coefficients into various components. On the other hand, viscous computational fluid dynamics (CFD) has been developed and applied into dynamic ship motions such like Sakamoto et al. [3]. Moreover several URANS simulations have been done with overset girds method to reproduce the ship appendages including bilge keels e.g. Sadat-Hosseini et al. [4]. Therefore unsteady RANS (URANS) simulation could be one of the powerful tools to observe and predict the bilge keels effects on roll damping.

The first objective of this research is to validate the roll decay computed results using unstructured grid based URANS solver SURF [5] developed at NMRI with an overset grids method. The second objective is to analyze the bilge keel effects on roll damping by observing the flow fields and roll moments during CFD roll decay and forced roll motion simulations with/without bilge keels.

2. Subject Ship

The US Navy combatant DTMB5415 (Fig. 1) famous as benchmarking ship is selected in this research. The roll decay test with forward speed in calm water was conducted in Iowa Institute of Hydraulic Research (IIHR) for the Gothenburg 2010 CFD Workshop [6]. The ship conditions of the roll decay simulations are shown in Table 1 which is same as the experimental conditions [7]. The bilge keels are conventional type with tapered ends.

Fig. 1 The US navy combatant DTMB5415

Table 1 Principal particulars

	Model scale
Scale ratio	46.6
Length between perpendiculars: L_{PP} [m]	3.048
Breadth: B [m]	0.405
Draft: d [m]	0.132
Block coefficient: C_B	0.506
Metacentric height: GM [m]	0.043
Longitudinal position of center of gravity from F.P.: LCG [m]	1.536
Vertical position of center of gravity from waterline: VCG [m]	0.030
Roll radius of gyration: k_{44}=0.39B	0.158
Natural roll period: T_ϕ [s]	1.54
Bilge keel length: l_{BK}/L_{PP}	0.313
Bilge keel height at midship: b_{BK}/B	0.048

3. Computational Method

3.1 URANS Solver

The URANS solver SURF is applied in this research. The governing equations are continuity and incompressible URANS equations which are solved in the earth fixed coordinate system. A cell-centered finite volume method with unstructured grids is used for the spatial discritization. In this research all grids are constructed with hexahedral cells. The velocity-pressure coupling is accomplished with the artificial compressibility approach. The inviscid fluxes are evaluated by MUSCL typed 2nd-order upwinding scheme based on flux-difference-splitting of Roe [8], and the 2nd-order central differencing scheme is applied to the viscous fluxes. Following schemes are used for the time marching, the 2nd-order Euler backward differencing scheme for physical time step and 1st-order Euler backward differencing scheme for pseudo time step. More details on this solver can be found in the reference [5].

3.1 Overset Grids Method

An overset grid system UP_GRID [9] developed at NMRI is used as a pre-processor to generate overlapping assembly interconnecting each block. The basic algorithm of UP_GRID starts from searching in-wall cells located inside the solid surface of the other blocks by solving inverse problem in position space. Then the cells surrounding the in-wall cells are defined as receptor cells which receive flow information from the other cells. Moreover the outer boundaries of the each block are also set to be receptor cells to interconnect to the other blocks. After the receptor cells are settled, the non-in-wall and non-receptor cells vicinal to the other blocks' receptor cells are chosen to be donor cells which provide the flow information to the receptor cells. The cells of higher prioritized block are preferentially defined to be donor.

In this research 4 blocks in total (two bilge keel in starboard and port sides, bare hull, and background) are generated to express the model geometry. The highest priority is set to starboard sided bilge keel block, followed in order by port side bilge keel, bare hull, and background blocks. The details of the computational grids are given in Table 2 where 6.23M grid points are in total. The surface distributions and the slice of the midship section of the bilge keels, bare hull, and background blocks are shown in Fig. 2. Now the grid densities near the waterline are controlled to be higher than other parts for girth direction of the bare hull and the vertical direction of the background blocks are also controlled to resolve the wave elevation with single-phase level set method [10]. The minimum spacing of the solid walls are provided to be $y^+ < 1$ to resolve the boundary layer.

Figure 3 shows the grid assembly at the midship section. The upper figure shows the grid distribution before overset; the all blocks are overlapping together. The lower figure shows the non-in-wall and non-receptor cells after overset by UP_GRID. Comparing with the upper figure, the cells locating inside the solid surface and the outer boundary layers are removed while the outer boundary of the lowest

priority block, background block in this case, is maintained. Moreover the cells located in the region of the higher priority blocks are also removed.

Table 2 Grid sizes and decompositions

Block	i_m x j_m x k_m	Topology
Bilge keel Stb.	61x45x71 (0.19M)	H
Bilge keel Prt.	61x45x71 (0.19M)	H
Bare hull	141x157x81 (1.79M)	O-O
Background	249x161x101 (4.05M)	Cartesian

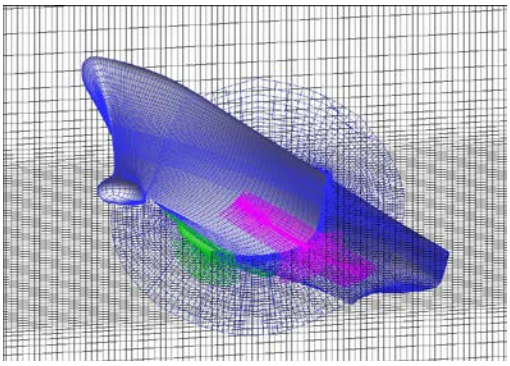

Fig. 2 Surface discretization and midship slice of the bilge keels, hull, and background blocks.

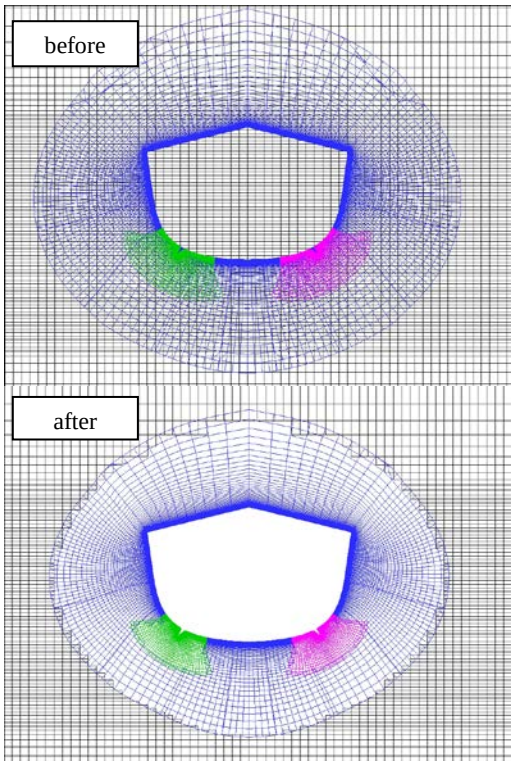

Fig. 3 UP_GRID overset grid assembly at midship section: before and after overset

4. Simulation Design

4.1 Test Case

The test conditions of the roll decay with forward speed simulations in calm water are shown in Table 3 same as the experimental condition [7] where U_c is constant towing speed and ϕ_0 is initial heel angle.

Table 3 Test condition

U_c [m/s]	Fr	Re [x10^6]	ϕ_0 [deg.]
0.754	0.138	2.56	-10.0

4.2 Grids and Simulation Design

The origin of the CFD coordinate system is at the intersection point of F.P., centerline, and undisturbed waterline. The x direction is from F.P. to A.P. and the y direction is the port to starboard, z direction is upward positive. Therefore it should be noted that the roll direction is reversed from the conventional ship stability coordinate.

The boundary conditions of the blocks are summarized in Fig. 4. The conditions of the solid walls are set to be no-slip conditions. In the background block, the upstream boundary is set to be inlet, the bottom, downstream, side boundaries are outlet and the top is far-field condition. Moreover wave damping zones are set at the outer boundaries of the background block to reduce the effects of the reflection wave. The distance from F.P. to upstream boundary of the background block is $1.5L_{PP}$, $2.5L_{PP}$ from A.P. to downstream boundary, $1.5L_{PP}$ from centerline to side boundaries, and $1.5L_{PP}$ from waterline to bottom.

The simulation procedure is as follows: first the ship is towed with static heel angle (-10 degrees) for a while; and then the roll motion is released to start the roll decay simulation which is similar to the experimental procedure. Now 1 DOF roll motion is solved in this simulation; fixed trim and sinkage were given in the experiment. The dynamic roll motion is computed with moving grid method [3] as shown in Fig. 5. During the grid morphing, the region around the connect boundary between bare hull and background blocks are kept to maintain the initial overset information provided by UP_GRID.

In this case, the size of the physical time step and the position of the morphing area are important factors for the roll decay simulation. The large time step and the far morphing area from the center of rotation cause the large mesh motion and that could affect the interpolation of the level set function which creates numerical waves disturbing the roll motion [11]. Therefore the small time step and close morphing area are selected. Now the computation is performed with almost 380 time steps per the natural roll period.

The k-ω form of two-equation nonlinear explicit algebraic stress model (EASM) [12] is used for the turbulence model.

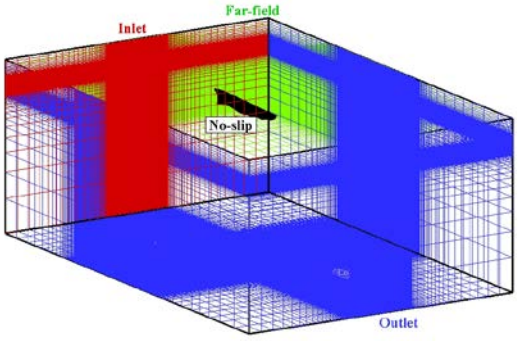

Fig. 4 Computational region and the boundary conditions

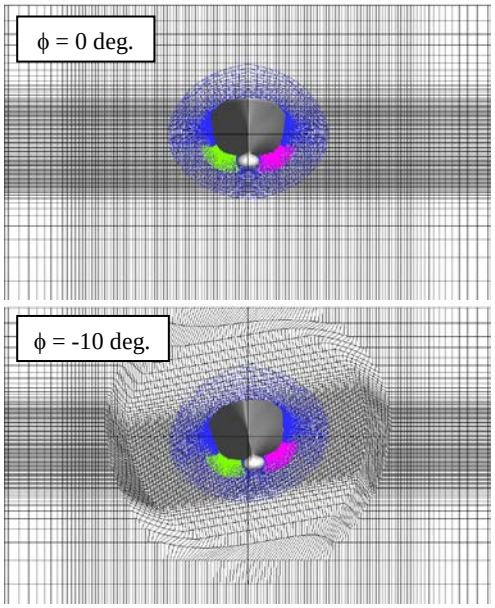

Fig. 5 Grid morphing by moving grid method at midship section (ϕ = 0 and -10 deg.).

5. Roll Decay Validation

5.1 Roll Motion and damping coefficients

The CFD roll decay simulation is executed according to the procedure of the previous section. Figure 6 shows the comparison of the EFD and CFD roll motion. The red circle symbol indicates the EFD result and the blue solid line shows the present CFD result. As shown in Fig. 6, the CFD result shows some agreements with the EFD. However the error of the roll amplitude and phase are increasing as time progress. Because the roll damping progress is one of the energy dissipation phenomena, the error is accumulating with the time progression. Therefore the small initial error could grow to the large error after a while.

The extinction coefficients *a, b, c* and equivalent linearlized roll damping coefficients α_e are estimated from the time history of the roll motion based on the Baker's expression (Eqs. 1-3) [2].

$$\Delta\phi = a\phi_n' + b\phi_n'^2 + c\phi_n'^3 \quad (1)$$

$$\alpha_e = \frac{\omega}{\pi}\left(a + b\phi_0 + c\phi_0^2\right) \quad (2)$$

$$where \begin{cases} \Delta\phi = \phi_n - \phi_{n+1} \\ \phi_n' = (\phi_n + \phi_{n+1})/2. \end{cases} \quad (3).$$

Here ϕ_n is the absolute values of the peak roll angles during the roll decay test and ω is the natural roll frequency. These coefficients are obtained with the first roll peak to the 11th peak (ϕ_1 to ϕ_{11}). The computed EFD and CFD extinction coefficients and the equivalent linearlized roll damping coefficient are shown in Table 4 and the extinction curves are shown in Fig. 7. As shown in Fig. 6 and the α_e values in Table 4, the CFD simulation overestimates the roll damping. Comparison of EFD and CFD flowfields could provide some guidelines for the better CFD results.

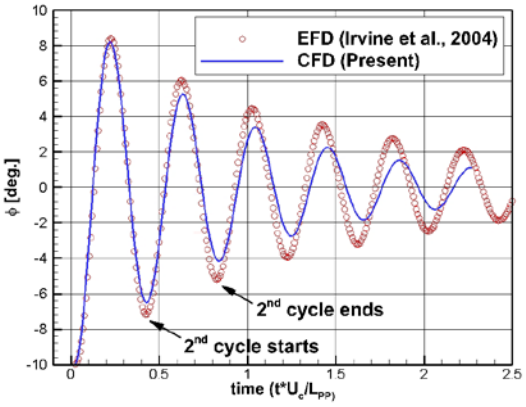

Fig. 6 Comparison of EFD and CFD roll motion during roll decay.

Table 4 EFD and CFD roll damping extinction coefficients and equivalent linearized coefficient

	EFD	CFD
a	0.06530	0.19413
b	0.02246	0.00296
c	-0.00128	0.00030
α_e	0.21026	0.32953

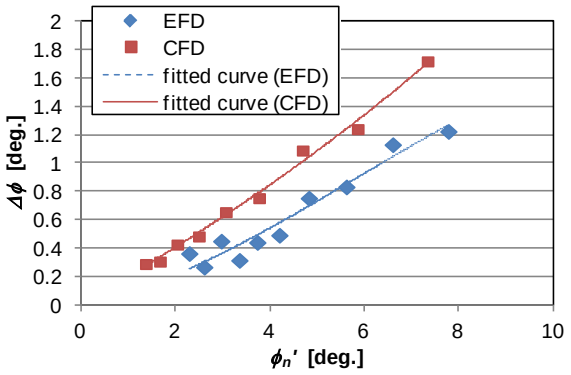

Fig. 7 Comparison of EFD and CFD extinction curves.

5.2 *Flowfield*

The EFD flowfield data during the roll decay was provided by Particle Image Velocimetry (PIV) measurements and servo wave probes (Irvine et al., 2004). Here Figs. 8-10 show the comparisons of EFD and CFD streamwise, horizontal, and vertical velocities (u, v, w) at x/L_{PP} = 0.675 section in vicinity of the port side bilge keel during the 2nd roll cycle. Now the 2nd roll cycle starts from the 2nd negative peak and ends at the 3rd negative peak as shown in Fig. 6. In Figs. 8-10, the velocity contours are shown when the roll angle reaches to the 1st negative peak (t/T_e=0/4), the 1st zerocross point (t/T_e=1/4), the positive peak (t/T_e=2/4), and the 2nd zerocross point (t/T_e=3/4) in the 2nd cycle.

Figure 8 shows distribution of the streamwise velocity at x/L_{PP} = 0.675. At the t/T_e=0/4, 1/4, 3/4, CFD results clearly show smaller low speed regions than the EFD which could indicate the strong numerical diffusion due to lack of the grid density near the bilge keels. On the other hand, the horizontal and vertical velocities in Figs. 9 and 10 show fairly good agreement with the EFD results similar to the other CFD results [6]. These results indicate the grid density in the streamwise direction could be not enough to resolve the vortex flow to the downstream. However, in total, CFD velocities seem to show qualitative agreements with the EFD results.

EFD and CFD wave elevations in the starboard side during the 2nd roll cycle are shown in Figs. 11 and 12. While the CFD results cannot simulate the wave propagation in far field, the trends of the variation of the wave elevation during the 2nd cycle in vicinity of the bow seem to be good agreement with the EFD results. Since the CFD fails to resolve the small waves in far field, the finer grid density might be required for all directions near the free surface. Moreover, since single O-O topology gird has difficulty clustering around the sonar dome, finer overset grid around the sonar dome might help simulating the vortex from the sonar dome.

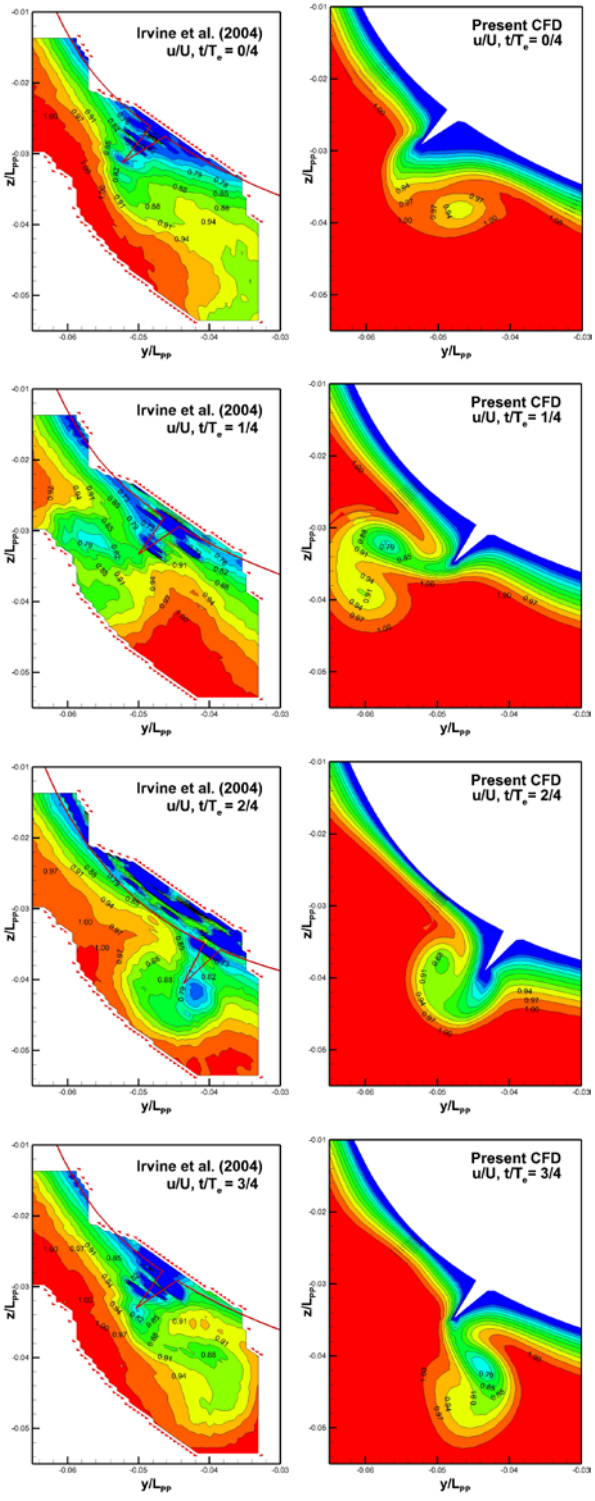

Fig. 8 Comparison of EFD and CFD streamwise velocity at $x/L_{pp}=0.675$ during the 2nd cycle of roll decay.

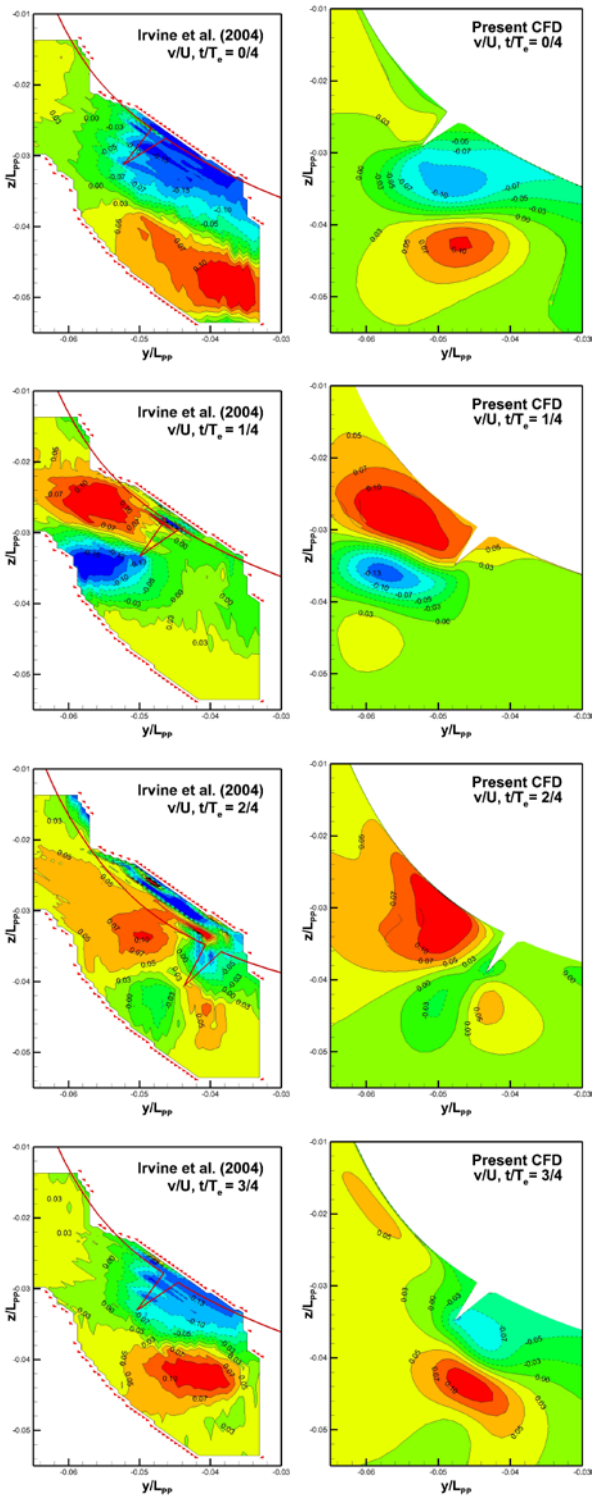

Fig. 9 Comparison of EFD and CFD horizontal velocity at x/L_{pp}=0.675 during the 2nd cycle of roll decay.

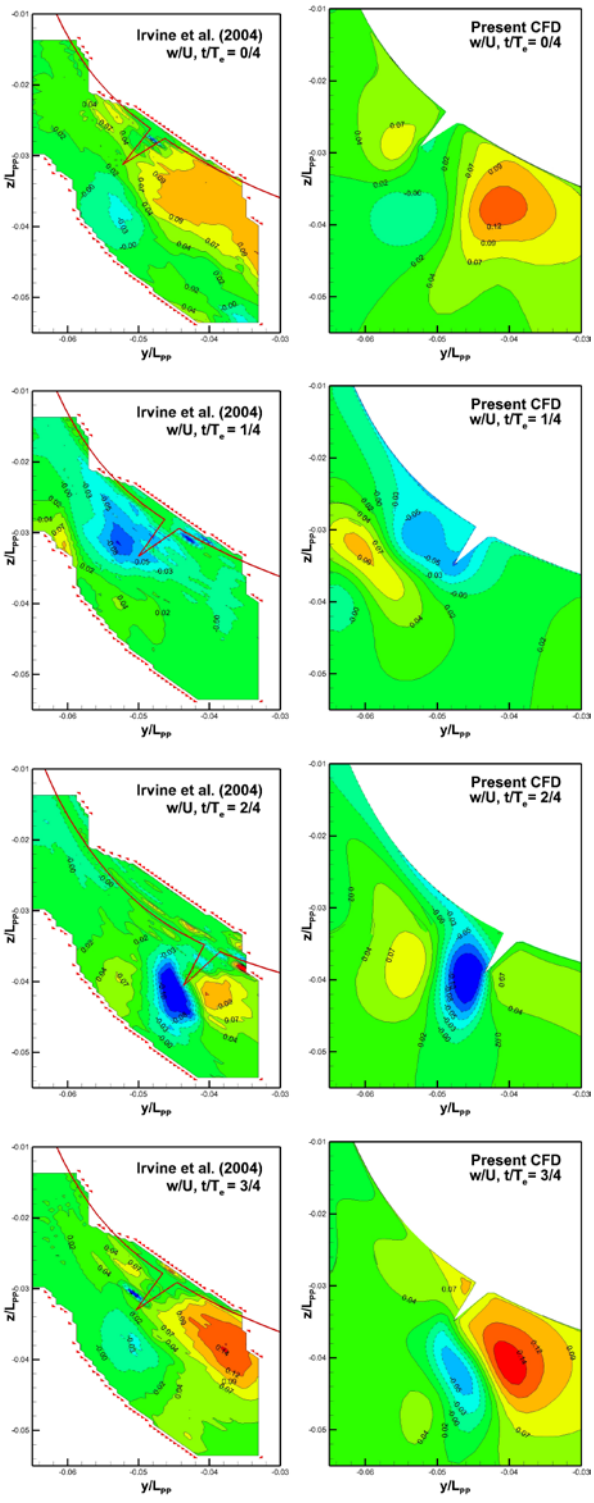

Fig. 10 Comparison of EFD and CFD vertical velocity at x/L_{pp}=0.675 during the 2nd cycle of roll decay.

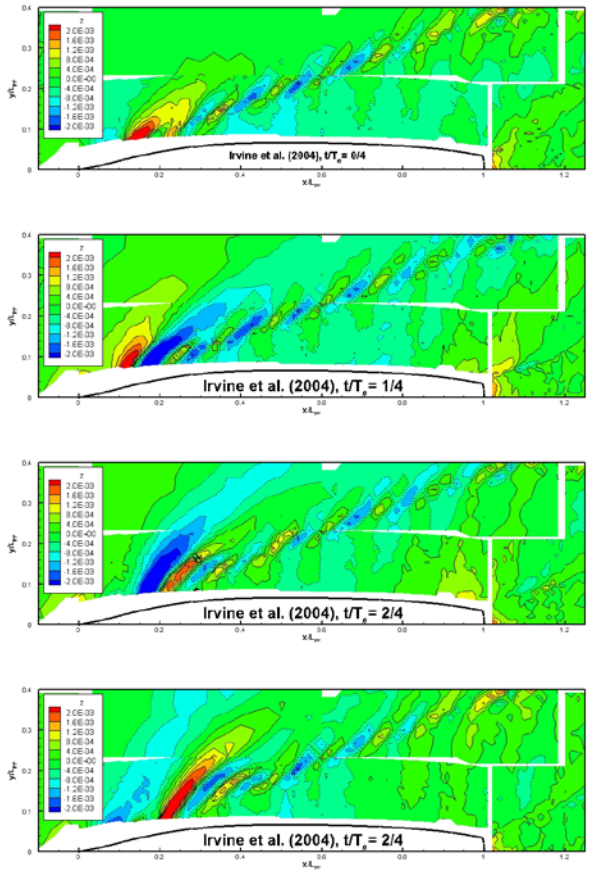

Fig. 11 Contours of the EFD wave elevation during the 2nd cycle of roll decay.

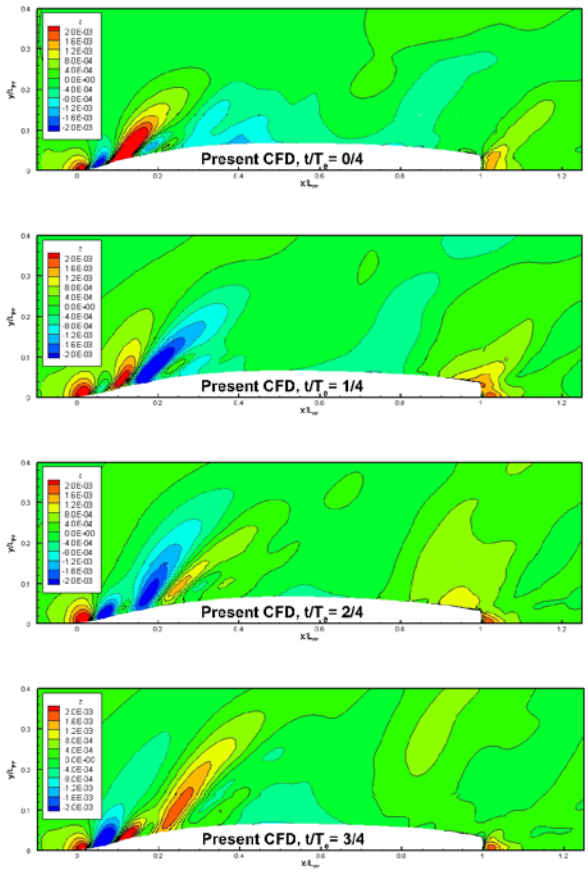

Fig. 12 Contours of the CFD wave elevation during the 2nd cycle of roll decay.

6. Bilge Keel Effects

6.1 Roll Decay and Forced Roll Motion without Bilge Keel

In this section, the bilge keel effects are evaluated by comparing the CFD roll decay and forced roll motion simulations with/without bilge keels. The previous CFD roll decay results are reused for the forced roll motion. Now the roll motion is forced to trace the CFD roll decay motion as shown in Fig. 6. Therefore the exactly same roll motion can be achieved in both cases with/without bilge keels.

The characteristics of the bilge keels could be demonstrated by comparing the roll moments, flowfield, and the pressure distribution on the hull surface with the same roll motion. Hereafter the roll decay simulations with/without bilge keels are termed RDwBK and RDwoBK, and the force roll motion without bilge keel is FRwoBK.

6.2 Comparison between RDw/woBK, and FRwoBK

Figure 13 shows the comparison of the roll moments at the CoG and roll angles between the RDw/woBK and FRwoBK. Now the roll moments are nondimensionalized with $0.5\rho U_c^2 L_{PP}^3$ and the hydrostatic restoring moments are extracted from the total roll moments and it is also assumed that the hydrostatic restoring moments of the RDw/woBK and FRwoBK are same. The RDwBK shows smaller roll angle than the RDwoBK due to the bilge keel effects. The roll moment of RDwBK has largest amplitude and the phase lag from the roll motion is very close to the 90 degrees which is identical for the roll damping. On the other hand, the moments of the RDwoBK and FRwoBK have smaller amplitude and the phase lag is larger than 90 degrees. The difference of the roll moment amplitudes between the RDwoBK and FRwoBK is caused by the slightly different roll rate between the two cases. Hereafter the comparison between RDwBK and FRwoBK is focused since the difference between the RDwoBK and FRwoBK is small. In Fig. 14, the roll moments of RDwBK and FRwoBK are plotted with the roll rate and roll acceleration in the horizontal axis. Note that the initial transition parts are extracted in Fig. 14. In Fig. 14a, RDwBK shows larger negative incline than the FRwoBK which indicates the RDwBK has larger roll rate component. In Fig.14b, The FRwoBK spiral shows the larger positive incline than the RDwBK spiral which indicates the FRwoBK has larger roll acceleration component. Moreover the roll moments are separated to the roll rate and roll acceleration components as Eq. (4) using the least square method.

$$K' = \alpha\dot{\phi} + \beta\ddot{\phi} \qquad (4).$$

Here the α is roll rate component and the β is roll acceleration component. The separated results are shown in Table 5. As mentioned in Fig. 14, the RDwBK shows larger roll rate component and smaller acceleration component than those of FRwoBK.

The x axial vorticity (ω_x) at x/L_{PP} = 0.675 section during the 2nd roll cycle is shown in Figs. 15 and 16. Figure 16 shows the large vortices generated from the bilge keel tips while Fig. 15 merely shows very thin vortex layer on the body surface. In Fig. 16, large and strong vortices are generated at t/T_e=1/4 and 3/4 which is the zero crossing points of the roll angle synonymous with the peaks of the roll rate. Meanwhile relatively small vortices are generated at t/T_e=0/4 and 2/4 almost zero roll rate. From these results, the main component of the bilge keel roll damping related to the roll rate could be the eddy-making component as mentioned by Ikeda et al. [13].

The comparison of the RDwBK and FRwoBK pressure distribution at x/L_{PP} = 0.675 section during the 2nd roll cycle is shown in Fig. 17. The red solid line shows the pressure distribution of the RDwBK and the green line indicates that of the FDwoBK. The sharp pressure peaks can be found at the RDwBK's bilge keels positions in Fig.17. Even in far from the bilge keels, some discrepancies are shown between the RDwBK and FRwoBK pressure distribution which

could be the interaction effects between bilge keels and hull. Unexpectedly the larger pressure peak can be found at the zero roll rate points (t/Te = 0/4 and 2/4) than those of the points at the peaks of roll rate (t/Te = 1/4 and 3/4). Moreover the discrepancies between the RDwBK and FRwoBK are increasing along with increase of the roll acceleration which could cause the difference of the added moment of inertia. Going back to Fig. 13, the roll moment of the RDwBK is almost zero at roll angle peaks while the moments of FRwoBK and RDwoBK remains in restoring direction. These remaining moments could be one factor for the delay of the roll damping in the RDwoBK. At the roll peaks (t/T_e=0/4 and 2/4) in Fig. 17, the pressure at the bilge keels is acting to the direction cancelling the remaining moment. For example, focusing into the port side bilge keel at t/T_e=0/4 in Fig. 17, the pressure distribution of the RDwBK shows larger negative pressure than FRwoBK in the inner surface of the bilge keel and smaller negative pressure in the outer surface which generate the roll moment in opposite to the restoring direction. The bilge keel in starboard also shows similar pressure distribution with smaller magnitude. From these results, it could be presumed that the bilge keel might interfere the flow accelerated by the hull movement and that could make the roll acceleration component smaller than that of the no bilge keel case in stationary points.

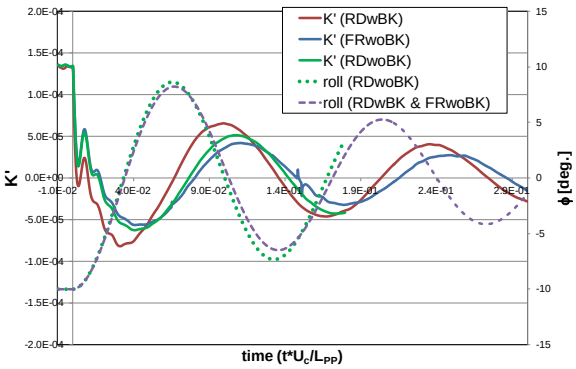

Fig. 13 Comparison of the RDwBK and FRwoBK roll moments.

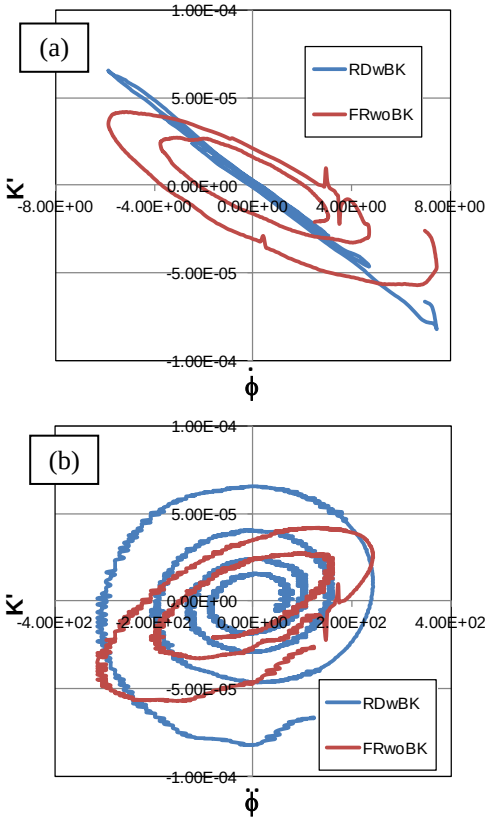

Fig. 14 Comparison of the RDwBK and FRwoBK roll moments with (a) roll rate, and (b) roll acceleration.

Table 5 The comparison of the roll rate and roll acceleration components between RDwBK and FRwoBK

	RDwBK	FRwoBK
α [x 10^{-5}]	-1.05	-0.59
β [x 10^{-7}]	0.04	0.96

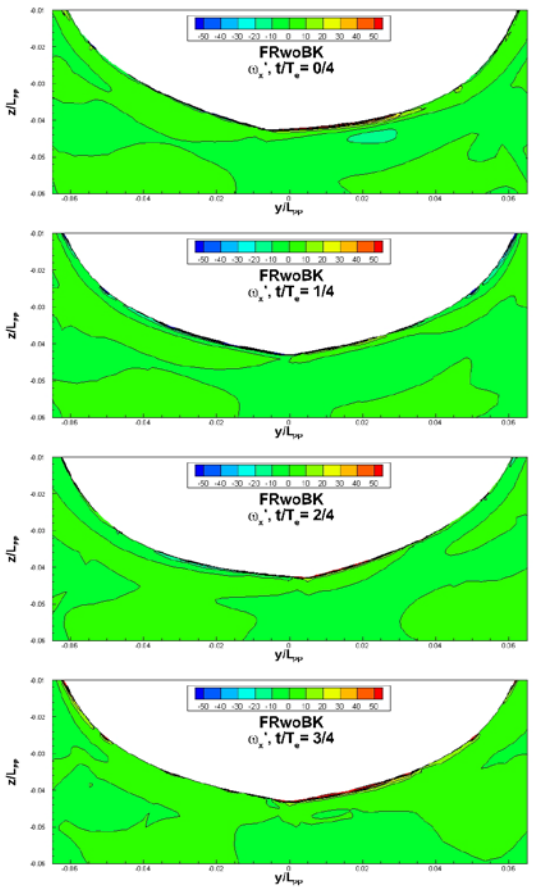

Fig. 15 Contours of the x axial vorticity (ω_x) at x/LPP = 0.675 section during the 2nd roll cycle in FRwoBK.

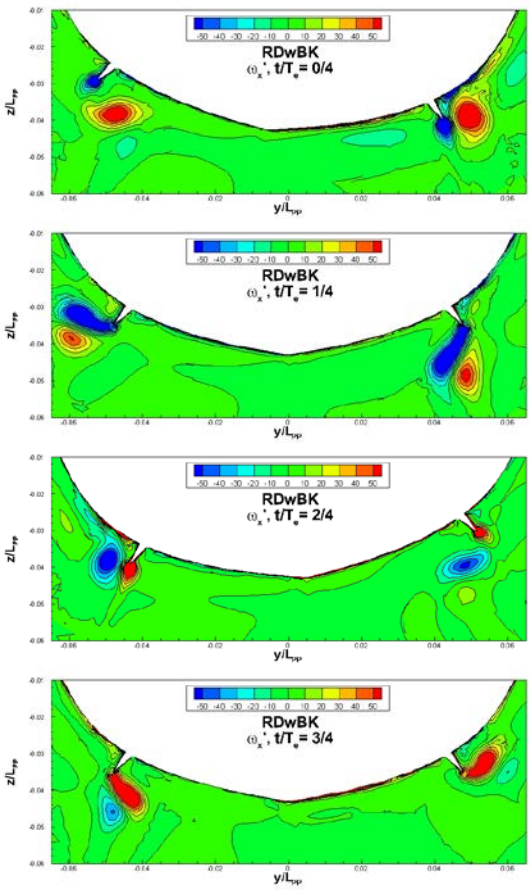

Fig. 16 Contours of the x axial vorticity (ω_x) at x/LPP = 0.675 section during the 2nd roll cycle in RDwBK.

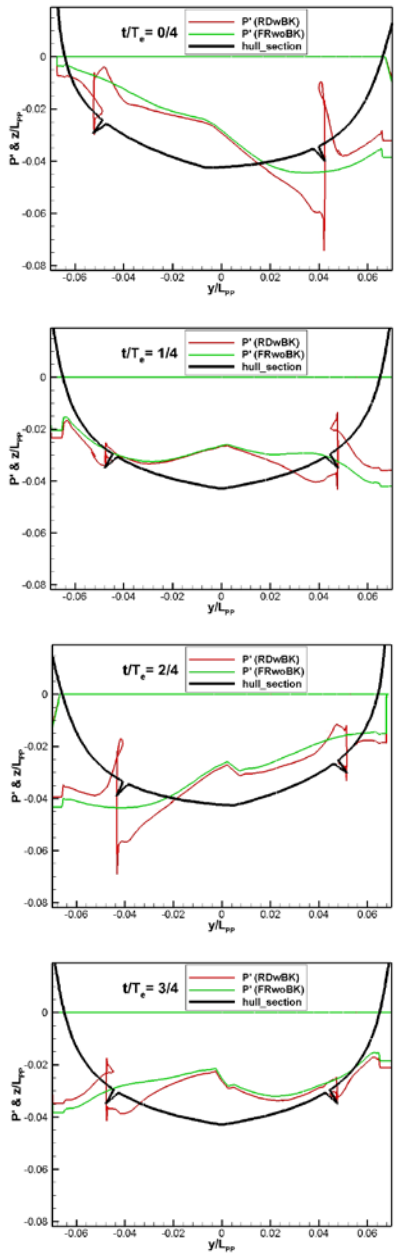

Fig. 17 Comparison of the RDwBK and FRwoBK pressure distribution at x/L_{PP}=0.675 during second cycle.

7. Conclusions

The CFD roll decay simulation using overset grids method is conducted with the US Navy combatant DTMB5415 installing bilge keels. The roll decay with forward speed simulation is validated with the experimental results. Moreover the CFD roll decay and forced roll motion simulation without bilge keels are conducted to evaluate the bilge keel effects. By comparing these simulation results, the model with bilge keel shows larger roll rate component and smaller roll acceleration component than those of no bilge keel cases. The large vortex shedding from the bilge keel tips can be found at the roll rate peaks and the large difference of the pressure distribution at the bilge keel are shown in the roll acceleration peaks.

Acknowledgments

The authors gratefully acknowledge to the members of CFD group, and Dr. Nobuaki Sakamoto at NMRI for suggestions and advices.

References

[1] Bassler, C., 2008, Roll Damping Mechanisms for a Wave-Piercing Tumblehome Hull Form, Proceeding of 6th Osaka Colloquium on Seakeeping and Stability of Ships.

[2] Himeno, Y., 1981, Prediction of Ship Roll Damping –State of the Art, Dept. of Naval Architecture and Marine Engineering, Univ. of Michigan, Report 239.

[3] Sakamoto, N., Ohashi, K., Kobayashi, H., Hirata, N., 2011, Analysis of non-linear/large-amplitude motions of submerged and floating bodies by URANS simulation with moving grid technique, Proceedings of 25th CFD Symposium, Osaka, Japan.

[4] Sadat-Hosseini, H., Carrica, P., Stern, F., Umeda, N., Hashimoto, H., Yamamura, S., Mastuda, A., 2011, CFD, system-based and EFD study of ship dynamic instability events: Surf-riding, periodic motion, and broaching, Ocean Engineering, Vol. 38, pp.88-110.

[5] Hino, T., 1997, A 3D unstructured grid method for incompressible viscous flows, Journal of the Society of Naval Architects of Japan, Vol. 183, pp. 9-15.

[6] Larsson, L., Stern, F., Visonneau, M., 2011, Numerical Ship Hydrodynamics, Proceedings of Gothenburg 2010 Workshop, December 8-10, Gothenburg, Sweden.

[7] Irvine, M., Longo, J., Sten, F., 2004, Towing-Tank Tests for Surface Combatant for Free Roll Decay and Coupled Pitch and Heave Motions, Proceedings of the 25th Symposium on Naval Hydrodynamics.

[8] Roe P.L., 1986, Characteristic-based scheme for the Euler equations, Annual Review of Fluid Mechanics, Vol. 18, pp. 337-365

[9] Kodama, Y., Ohashi, K., Umezaki, Y., Hirata, N., 2012, Development of UP_GRID, and Overset Grid System for Computing Flows past Ship Hulls with Appendages, Proceedings of the 26th Computational Fluid Dynamics Symposium , Tokyo, Japan, D08-1.

[10] Hino, T., 1999, An interface capturing method for free surface flow computations of unstructured grids, Journal of the Society of Naval Architects of Japan, Vol. 186, pp. 177-183.

[11] Deng, G. B., Leroyer, A., Guilmineau, E., Queutey, P., Visonneau, M., Wackers, J., 2010, Verification and Validation for Unsteady Computation, Proceedings of Gothenburg 2010 Workshop on Numerical Ship Hydrodynamics, Vol. 2, pp. 447-452.

[12] Rumsey, L.C., Gatski, B.T., 2001, Recent Turbulence Model Advances Applied to Multielemet Airfoil Computations, Journal of Aircraft, Vol. 38, No. 5, pp. 904-910.

[13] Ikeda, Y., Himeno, Y., Tanaka, N., 1978, Components of Roll Damping of Ship at Forward Speed, Journal of Kansai Society of Naval Architects, No. 176, pp. 33-45.

Numerical Investigation into Ship Stability Failure Events in Quartering Seas Based on Time Domain Weakly Nonlinear Unified Model

Liwei Yu, Ning Ma* and Xiechong Gu
State Key Laboratory of Ocean Engineering, Shanghai Jiao Tong University, China

Abstract: A 6-DOF weakly nonlinear unified model considering sea-keeping motion at low frequency, maneuvering motion and rudder propeller hydrodynamics is developed for the numerical analysis of ship stability failure events in quartering seas. In the model, the maneuvering and seakeeping models are solved in different time scale and combined together based on the Unified theory. The model is applied to the ITTC ship A2 fishing vessel. Motions in regular astern waves with possible stability failure are simulated and compared with experiment results obtained from the literature. Results show that the weakly nonlinear model is capable of reproducing stability failure events like steady surf-riding, capsizing due to broaching and capsizing without broaching. However the quantitative agreement between simulation and experiment results of the ITTC ship A2 are not good enough at the moment. The present model seems to overestimate the possibility of stability failure somewhat and the reasons are discussed consequently

Key words: Weakly nonlinearity, unified theory, stability failure mode, surf-riding, broaching

1. Introduction

Ship sailing in severe following/quartering seas may suffer from loss of control and stability. Such phenomena like surf-riding and broaching have been recognized as the causes of ship capsizing in high astern seas. Unlike normal periodic ship motion, surf-riding is non-periodic and occurs when ship is overtaken by wave astern and forced to sail with wave celerity. Broaching happens when ship heading changes suddenly and lose its course-keeping ability. Both phenomena are strongly nonlinear which often happens on small fishing vessels and can cause ship dynamic stability problems, even capsizing [1].

Theoretical study on surf-riding and broaching dates back to 1950s. Pioneering researches on surf-riding and broaching in following seas are done based on uncoupled surge equation with nonlinear wave induced surging force[2],[3]. Theoretical solutions in regular and irregular waves show the occurrence of surf-riding in a certain range of propeller thrust. Due to difficulties in getting an analytical solution for the nonlinear problem, steady state and bifurcation analysis in nonlinear dynamics are applied. Umeda and Kohyama [4], Umeda [5] conducted phase plane analysis on the nonlinear surge equation with different initial conditions on basis of the works done by a Russian researcher [6]. Lately, an analytical formula for prediction of surf-riding threshold is proposed based on the Melnikov's method [7].Furthermore, the nonlinear steady state analysis are applied on a surge-sway-yaw-roll model, recently a 6-DOF model [8-11]. Boundaries between periodic motion, surf-riding, broaching and capsizing are discussed. These analytic and nonlinear dynamic approaches show advantages in analyzing the dependence on initial conditions and determining the critical conditions for surf-riding and broaching.

Model experiments is useful for understanding the physical mechanism of ship surf-riding and broaching

in following/quartering seas. Moreover the experiment results can be used for the validation of numerical models. Umeda et al. [12] conduct model experiment to assess the stability of two fishing vessels in quartering sea. Broaching, broaching without capsizing, nearly broaching and capsizing due to bow diving were identified for ships satisfying IMO intact stability criteria. Min et al. [13] also conduct free running model test for broaching. Wave excited yaw moment in following sea is measured using captive model experiments.

With the development of computational capabilities, time domain numerical simulation of surf-riding and broaching based on 4-DOF [14] and 6-DOF [15] models are conducted, and results are compared with experiments. A qualitative analysis is done by repeating numerical runs with many combinations of initial and control values to clarify critical conditions of motion [16]. However the numerical models used in the previous studies calculate the wave excitation force using the simplified Froude-Kriloff hypothesis on the mean water surface. Given that Froude-Kriloff force is critical for the occurrence of surf-riding at low frequency, it is of crucial importance to calculate Froude-Kriloff and restoring forces over the instantaneous ship wetted surface.

In this work, a 6-DOF weakly nonlinear model proposed by Yu, Ma and Gu [17] in which Froude-Kriloff and restoring forces are calculated nonlinearly are developed for the simulation of ship motions in following and quartering seas. The model couples the maneuvering and seakeeping motion based on the unified theory and incorporates rudder and propeller modeling. Each component of the model is verified based on the experiment data of the ITTC ship A2 provided in ref. [18]. Finally, results of numerical simulation are compared with the results of model experiments qualitatively.

2. Mathematical Model

2.1 Coordinate System

Three coordinate systems are used for describing ship motion, namely the earth fixed coordinate O_e-$x_e y_e z_e$, the body fixed coordinate O-xyz and the horizontal body axes coordinate O-$x_h y_h z_h$. The coordinate O-$x_h y_h z_h$ moves along with ship while its axes parallel to the axes of the Earth-fixed co-ordinate, as shown in Fig.1. The origin O is chosen at the ship center of gravity.

Ship forward speed is $\tilde{U}$. The position, velocity and force vectors are defined as:

$$\begin{aligned}\boldsymbol{\eta} &= \left[x, y, z, \phi, \theta, \psi\right]^T \\ \mathbf{v} &= \left[u, v, w, p, q, r\right]^T \\ \mathbf{f} &= \left[X, Y, Z, K, M, N\right]^T\end{aligned} \tag{1}$$

The velocity vector $\mathbf{v}$ which is defined in body-fixed coordinate will be transferred to earth-fixed coordinate:

$$\dot{\boldsymbol{\eta}} = \left[\dot{x}, \dot{y}, \dot{z}, \dot{\phi}, \dot{\theta}, \dot{\psi}\right]^T = \left[U, V, W, P, Q, R\right]^T = \begin{bmatrix} \mathbf{R}_{3\times3} & \mathbf{0}_{3\times3} \\ \mathbf{0}_{3\times3} & \mathbf{Q}_{3\times3} \end{bmatrix} \mathbf{v} \tag{2}$$

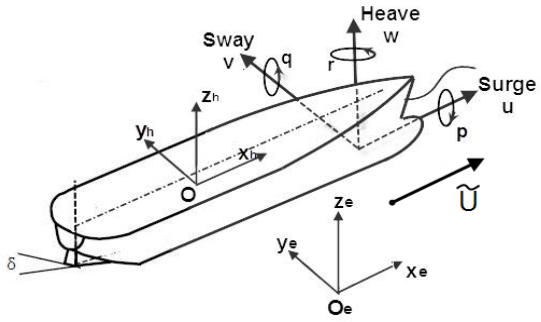

Fig. 1 Definition of coordinate system and ship motions

2.2 Maneuvering and Seakeeping Model

The maneuvering motion is simulated by a 3-DOF surge-sway-yaw MMG model, proposed by Japanese research group: Maneuvering Mathematical Modelling Group.

$$\begin{bmatrix} m-\bar{X}_{\dot{U}} & 0 & 0 \\ 0 & -m+\bar{Y}_{\dot{V}} & -mx_G+\bar{Y}_{\dot{R}} \\ 0 & -mx_G+\bar{N}_{\dot{V}} & -I_z+\bar{N}_{\dot{R}} \end{bmatrix} \begin{bmatrix} \dot{u} \\ \dot{v} \\ \dot{R} \end{bmatrix} + \begin{bmatrix} 0 & -mR & 0 \\ 0 & \bar{Y}_V & -mU+\bar{Y}_R \\ 0 & \bar{N}_V & -mx_G U+\bar{N}_R \end{bmatrix} \begin{bmatrix} u \\ v \\ R \end{bmatrix} = \begin{bmatrix} \bar{X}_{HO} \\ \bar{Y}_{HO} \\ \bar{N}_{HO} \end{bmatrix} + \begin{bmatrix} \bar{X}_\delta \\ \bar{Y}_\delta \\ \bar{N}_\delta \end{bmatrix} + \begin{bmatrix} -R(\tilde{U}) \\ +(1-t)T(\tilde{U}) \\ 0 \\ \\ 0 \end{bmatrix} \tag{3}$$

where *m* and *I* represent the ship mass and moment of

inertia, and(X_δ, Y_δ, N_δ), $R(\tilde{U})$ and $T(\tilde{U})$ are defined as rudder force, resistance and propeller thrust respectively. t is the propeller thrust deduction factor. (X_{HO}, Y_{HO}, N_{HO}) is higher order hull hydrodynamic force:

$$\begin{aligned}\bar{X}_{HO} &= X_{vv}v^2 + X_{vr}vr + X_{rr}r^2 \\ \bar{Y}_{HO} &= Y_{vvr}v^2r + Y_{vrr}vr^2 + Y_{vvv}v^3 + Y_{rrr}r^3 \\ \bar{N}_{HO} &= N_{vvr}v^2r + N_{vrr}vr^2 + N_{vvv}v^3 + N_{rrr}r^3\end{aligned} \tag{4}$$

The rudder forces are calculated:

$$\begin{aligned}\bar{X}_\delta &= -0.5(1-t_R)\rho A_R {U_R}^2 C_N \sin\alpha_R \sin\delta \\ \bar{Y}_\delta &= -0.5(1+a_H)\rho A_R {U_R}^2 C_N \sin\alpha_R \cos\delta \\ \bar{N}_\delta &= -0.5(GR_L + a_H x_H)\rho A_R {U_R}^2 C_N \sin\alpha_R \cos\delta \\ \bar{K}_\delta &= -GR\bar{Y}_\delta\end{aligned} \tag{5}$$

where K_δ is rudder moment on roll. A_R, U_R, GR, GR_L are the rudder area, the advance speed of rudder, the vertical and longitudinal distance between center of gravity and point of rudder force. And the rudder force coefficient C_N is determined empirically.

The sea-keeping motion is simulated by a 6-DOF model based on the IRF approach [19]. And the equation of motion can be written as:

$$\begin{aligned}&\sum_{j=1}^{6}\left[\left(m_{ij} + a_{ij}(\infty)\right)\dot{v}_j(t) + \int_0^t R_{ij}(t-\tau)v_j(\tau)d\tau + F_i^{res}(t)\right] \\ &= F_i^{FK}(t) + F_i^{dif}(t) + (\bar{K}_\delta, i=4)\end{aligned} \tag{6}$$

where m_{ij} and $a_{ij}(\infty)$ stand for the ship mass and the infinite-frequency added mass. And the nonlinear restoring forces, F-K forces and diffraction forces are denoted as $F_i^{res}(t), F_i^{FK}(t), F_i^{dif}(t)$. According to the IRF approach, the radiation and diffraction forces are calculated in frequency domain by the 2-D strip theory and transferred into time domain.

The restoring and Froude-Kriloff forces are calculated nonlinearly through pressure integration on instantaneous wetted surfaces. The hull and upper deck consist of several NURBS surfaces. Each surface has an area of A_i, a central point r_i=(x_i,y_i,z_i) with a normal vector n_i=(n_{xi},n_{yi},n_{zi}) in body-fixed axis. And the restoring forces and F-K forces are given as:

$$F_1^{FK\&res} = \sum_{i=1}^{N^*} A_i P(r_i^*, t) n_{xi}^* \tag{7}$$

$$P(r_i^*, t) = \rho g(d(x_i^*) - z_i^*) + A\rho g e^{k(z_i^* - d(x_i^*))}\cos(kx_i^* - \omega_e t)$$

$P(r_i,t)$ is the hydrodynamic pressure due to undisturbed waves. The superscript (*) indicates vectors in earth fixed coordinate system.

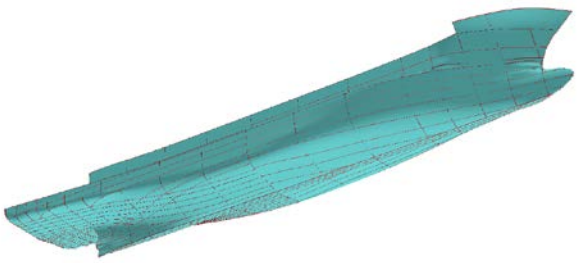

Fig.2 Hull NURBS sufaces of the ITTC ship A2

2.3 The Unified Model

In the unified model, the manoeuvring and seakeeping models described above are solved in different time scale. As a slowly varying motion, the manoeuvring motion is simulated using larger time step than the seakeeping motion. The seakeeping motion is simulated within each time step of the manoeuvring simulation assuming that the manoeuvring motion is constant. Then the total motion of the ship is calculated by combining the two motions referring to different coordinate system together:

$$\begin{aligned}&\left[X_T, Y_T, Z_T, \Phi_T, \Theta_T, \Psi_T\right] = \left[x^0, y^0, z^0, \phi^0, \theta^0, \psi^0\right] \\ &+\left[\int_0^t U_T dt, \int_0^t V_T dt, \int_0^t W_T dt, \int_0^t P_T dt, \int_0^t Q_T dt, \int_0^t R_T dt\right]\end{aligned} \tag{8}$$

where the subscript T indicates the total motion, and superscript 0 means the initial value for time t=0, and the seakeeping motion velocity in earth-fixed coordinate is given by:

$$[U_T, V_T, W_T, P_T, Q_T, R_T]^T = \begin{bmatrix}\mathbf{R}_{3\times3} & \mathbf{0}_{3\times3} \\ \mathbf{0}_{3\times3} & \mathbf{Q}_{3\times3}\end{bmatrix}[u_T, v_T, w_T, p_T, q_T, r_T]^T \tag{9}$$

Thus the sea-keeping and manoeuvring computations are coupled each other.

3. Model Verification

The model experiment data of the ITTC ship A2 provided in Ref. [18] are used for the verification of

the weakly nonlinear numerical model. Main particulars of the ship are shown in Tab. 1

Table 1 Main particulars of ITTC ship A2

	Ship	1/15 model
Length between per-pendiculars, Lpp(m)	34.5	2.3
Breadth, B(m)	7.60	0.507
Depth, D(m)	3.07	0.205
Fore draught, df(m)	2.5	0.166
Aft draught, da(m)	2.8	0.176
Mean draught, d(m)	2.65	0.186
Block coefficient, CB	0.597	0.597
Radius of gyration, roll, kxx/Lpp	0.108	0.108
Radius of gyration, pitch yaw, kyy/Lpp, kzz/Lpp	0.302	0.302
Longitudinal position of Buoyancy, LCB(m)	1.31m aft	0.087m aft
Longitudinal position of Floatation, LCF(m)	3.94m aft	0.263m aft
Metacentric height, GM(m)	1.00	0.0667
Natural roll period, TR (s)	7.4	1.9
	Bilge keel	model
Area, (m^2)	5.10 X2	0.023 X2
Position of fore end	6.22m fore	0.415m fore
Position of aft end	8.60m aft	0.573m aft
Breadth, (m)	0.35	0.023

All other data needed for the numerical simulation including hull geometry, hydrodynamic derivatives, rudder and propeller characteristics, roll viscous damping can be found in Ref. [18].

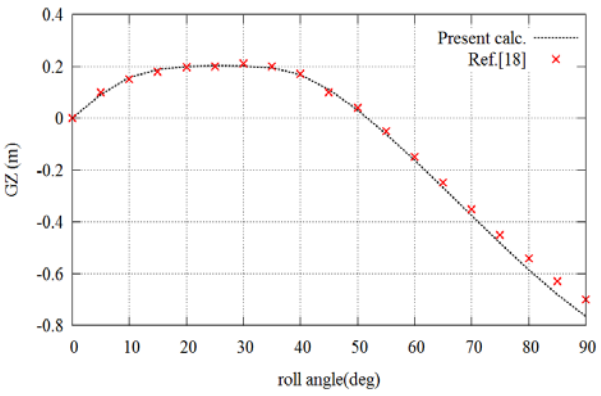

Fig.3 Comparison of GZ curve of Ship A2 in still water between present calculation and Ref.[18]

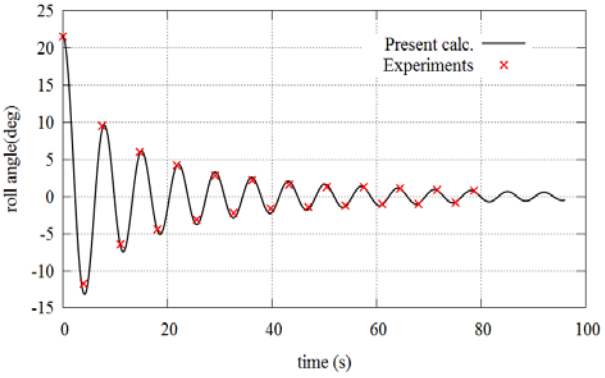

Fig.4 Comparison of roll decay test results between present calculation and experiments (Ref.[18])

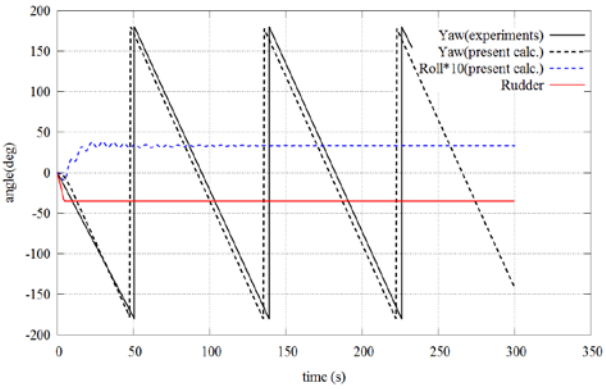

Fig.5 Comparison of -35 degree turning circle test results at Fn=0.30 between present calculation and experiments (Ref.[18])

GZ curve in still water is calculated using the code in which the pressure is integrated on instantaneous wetted surfaces and compared with the data provided in Ref. [18], and is shown in Fig.2. Roll decay test is also simulated to verify the seakeeping model. Results are compared with the roll decay experiment data and are shown in Fig.3. Moreover, the maneuvering model is verified by comparing with experiment results of the -35 degree turning circle test. However due to the lack of experiment data, only yaw angle in turning circle test is compared as shown in Fig.5. All the data is shown in full scale.

4. Numerical Simulation

According to Ref. [18], model experiments of ITTC ship A2 in quartering seas are conducted in various initial conditions with different ship speeds, wave lengths and autopilot courses. Periodic motion,

broaching, broaching without capsizing, nearly broaching and capsizing on a wave crest were identified from the experiment results. Four cases with full time series data are chosen for numerical simulation and they are shown in Tab.2.

Table 2 Cases for numerical simulation

No.	*Fn*	H/λ	λ/L_{pp}	χ	ω_e	Experiment results
1	0.3	1/8.7	1.127	-30	0.566	Periodic motion
2	0.3	1/10.0	1.637	-30	0.563	Periodic motion
3	0.43	1/8.7	1.127	-30	0.232	Capsize on a wave crest
4	0.431	0/10.0	1.637	-10	0.228	Capsize due to broaching

Where Fn is Froude number, H, λ, χ are wave height, length and heading angle, ω_e is encounter frequency. They satisfy the followings:

$$\omega^2 = gk(1+k^2H^2/4)$$
$$\lambda = 2\pi/k, \omega_e = \omega - kU\cos(\chi), U = \mathrm{Fn}\sqrt{gL_{pp}} \quad (9)$$

(1) Fn=0.3

For case No.1 and 2 with Froude number 0.3, numerical simulations are conducted with the same conditions as experiment. Results in full scale are demonstrated in Fig.6 and Fig.7.

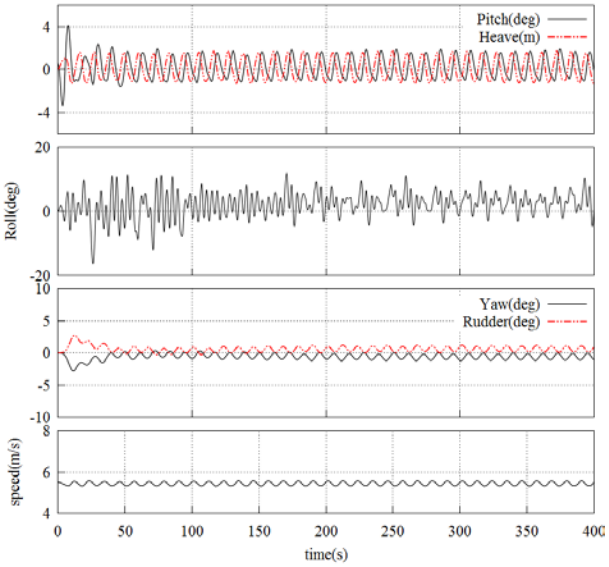

Fig.6 Result of case No. 1 in full scale with H/λ=1/8.7, λ/L_{pp}=1.127, *Fn*=0.3 and χ=-30 deg

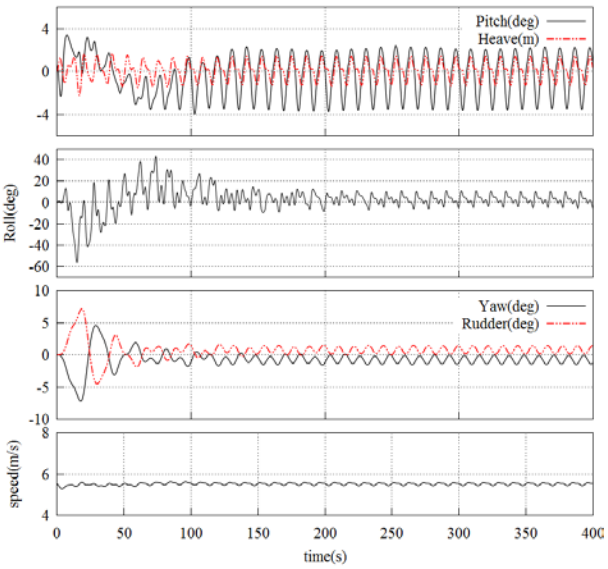

Fig.7 Result of case No. 2 in full scale with H/λ=1/10.0, λ/L_{pp}=1.637, *Fn*=0.3 and χ=-30 deg

As shown in Fig.6 and Fig.7, only periodic motion is observed for both cases with Froude number 0.3 and wave angle -30 degree, which is the same as experiment results.

(2) Fn=0.43

For case No.3 and 4 with Froude number 0.43, numerical simulations are conducted with the same conditions as experiment. Results in full scale are demonstrated in Fig.8 and Fig.9.

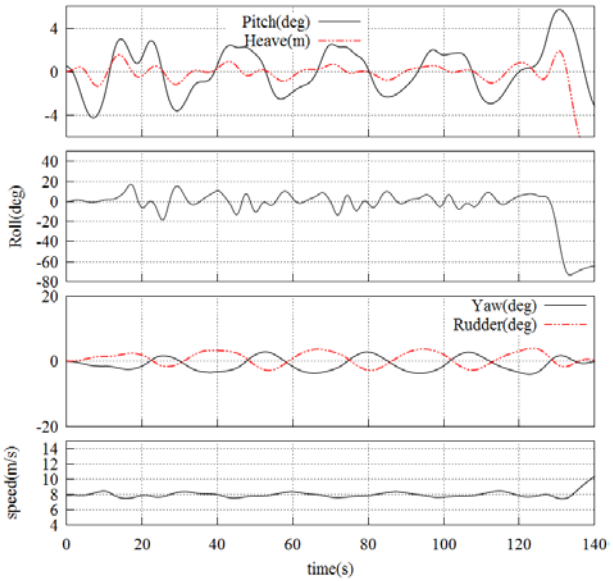

Fig.8 Result of case No. 3 in full scale with **H/λ=1/8.7**, λ/L_{pp}=1.127, *Fn*=0.43 and χ=-30 deg

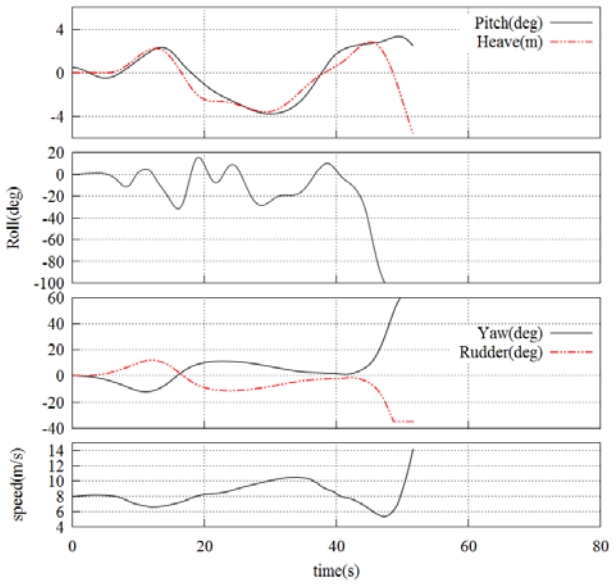

Fig.9 Result of case No. 4 in full scale with **H/λ=1/10.0**, λ/L_{pp}=1.637, *Fn*=0.43 and χ=-10 deg

From Fig.8, it is found that ship experiences very large heave and pitch motion after about 130s. This causes the reduction of restoring moment, and roll angle grows large consequently. Eventually ship capsizes due to loss of stability.

In Fig.9, the pitch angle keeps almost unchanged after 45s, and ship is sitting on the downslope of the wave. Meanwhile ship speed is accelerated to reach to wave celerity. This indicates that the ship is suffering surf-riding. At the same time, yaw angle increases suddenly and ship turns to port side, despite max rudder control is taken. Roll angle also starts to raise and eventually causes ship to capsize. Therefore, this implies that the phenomenon of capsizing due to broaching occurs, and broaching happens right after surf-riding.

Therefore, it has been shown that the weakly nonlinear model is capable of simulating ship stability failure events in quartering seas. However it should be noted that the actual wave heights used for numerical simulation in case No. 3 and 4 are H/λ=1/13.0 and 1/14.1, which is smaller than experiment. Because wave height higher than the value above will cause ship to capsize immediately. Thus the weakly nonlinear model tends to overestimate the possible stability failure events in following and quartering seas.

From results with different Froude number, it is found that ship tends to capsize at high Froude number in following and quartering seas. This is probably because that for high Froude number like Fn=0.43, the ship speed is close to wave celerity and ship may have encounter frequency close to zero. Hereby restoring and F-K forces are dominant; ship may be overtaken by wave from astern and experience stability loss. However for low Froude number like Fn=0.3, ship speed is much lower than wave celerity and it tends to do periodic motion. Therefore IMO Sub-Committee on Ship Design and Construction (SDC) suggests that a ship is considered not to be vulnerable to the broaching stability failure mode if Fn<0.3 [20].

5. Conclusions

In this work, a 6-DOF weakly nonlinear unified model considering nonlinear restoring and F-K forces over instantaneous wetted surfaces is applied for the numerical simulation of ship stability failure events in quartering seas. Due to the strong nonlinearity of broaching and surf-riding and lack of experimental data, the results are only compared with experiment results of the ITTC ship A2 qualitatively, but not quantitatively.

The weakly nonlinear model is proved to be capable of simulating ship stability failure events including broaching after surf-riding and capsizing due to loss of stability in quartering seas. However the weakly nonlinear model tends to overestimate the possibility of stability failure events in following and quartering seas.

It is also found that ship tends to capsize at high Froude number in following and quartering seas, due to the fact that ship may be overtaken by wave from astern with high speed close to wave celerity.

The weakly nonlinear model still needs to be improved and factors such as the reduction of rudder force, as well as the change of hydrodynamic derivatives and propeller characteristics in waves when surf-riding occurs should be investigated in

detail in the future.

References

[1] Mata-Álvarez-Santullano, F., Souto-Iglesias, A. (2014). Stability, safety and operability of small fishing vessels. Ocean Engineering, 79(0), 81–91.

[2] Grim, O. (1951). *Das Schiff in von achtern auflaufender See*. Schiffbau-Versuchsanstalt.

[3] Grim, O. (1963). Surging motion and broaching tendencies in a severe irregular sea. Deutsche Hydrografische Zeitschrift, 16(5), 201–231.

[4] Umeda, N., Kohyama, T. (1990). Surf-riding of a ship in regular seas. Journal of Kansai Society of Naval Architects.

[5] Umeda, N. (1999). Nonlinear dynamics of ship capsizing due to broaching in following and quartering seas. Journal of Marine Science and Technology, 4(1), 16–26.

[6] Makov, Y. (1969). Some results of theoretical analysis of surf-riding in following seas. T Krylov Soc, (126), 4.

[7] Maki, A., Umeda, N., Renilson, M., Ueta, T. (2014). Analytical methods to predict the surf-riding threshold and the wave-blocking threshold in astern seas. Journal of Marine Science and Technology, 1–10.

[8] Spyrou, K. J. (1995). Surf-riding and oscillations of a ship in quartering waves. Journal of Marine Science and Technology, 1(1), 24–36.

[9] Spyrou, K. J. (1996). Dynamic instability in quartering seas: The behavior of a ship during broaching. Journal of Ship Research, 40(1).

[10] Umeda, N., Hori, M., Hashimoto, H. (2007). Theoretical prediction of broaching in the light of local and global bifurcation analyses. International Shipbuilding Progress, 54(4), 269–281.

[11] Tigkas, I., Spyrou, K. J. (2012). Continuation Analysis of Surf-riding and Periodic Responses of a Ship in Steep Quartering Seas. In Proceedings of the 11th International Conference on the Stability of Ships and Ocean Vehicles (pp. 337–349).

[12] Umeda, N., Matsuda, A., Hamamoto, M., Suzuki, S. (1999). Stability assessment for intact ships in the light of model experiments. Journal of Marine Science and Technology, 4(2), 45–57.

[13] Min S. L., Ding Y., Zhao X. D. (1993). The tests on Broaching-to of a ship in following seas. Journal of Harbin Shipbuilding Engineering Institute, 14(3), 12–18.

[14] Umeda, N., Hamamoto, M. (2000). Capsize of ship models in following/quartering waves: physical experiments and nonlinear dynamics. Philosophical Transactions of the Royal Society of London. Series A: Mathematical, Physical and Engineering Sciences, 358(1771), 1883–1904.

[15] de Kat, J. O.,Pinkster, D.-J.,McTaggart, K. A. Random Waves and Capsize Probability Based on Large Amplitude Motion Analysis[J]. ASME Conference Proceedings, 2002, 2002 (36142): 685-694.

[16] Umeda, N., Hashimoto, H. (2002). Qualitative aspects of nonlinear ship motions in following and quartering seas with high forward velocity. Journal of Marine Science and Technology, 6(3), 111–121.

[17] Yu, L., Ma, N., Gu, X. (2012), “Study on Parametric Roll and Its Rudder Stabilization Based on Unified Seakeeping and Maneuvering Model”. 11th International conference on the Stability of Ships and Ocean Vehicles, Greece, 2012.

[18] Sample ship data sheet: ITTC A2 fishing vessel. Available online at http://www.naoe.eng.osaka-u.ac.jp/imo/a2

[19] Cummins, W.E., 1962. “The impulse response function and ship motions”, Schiffstechnik, 47(9), pp. 101-109.

[20] IMO SDC1/INF.8 ANNEX 15 (2014). Proposed Amendments to Part B of the 2008 IS CODE to Assess the Vulnerability of Ships to the Broaching Stability Failure Mode. London, UK: IMO SDC.

Deriving the Linear-Wave Spectrum from a Nonlinear Spectrum

Arthur M. Reed and John G. Telste
David Taylor Model Basin, Carderock Division, Naval Surface Warfare Center

Abstract: In extreme nonlinear seas, one cannot directly use the measured spectra, $S_T(\omega)$, from these seas in an analysis, or to derive a seakeeping prediction, but rather one must derive the underlying linear spectrum to describe the waves that should be simulated. At extreme wave heights theoretical spectra have nonlinear tails that are unrealizable in an experimental facility due to the breaking of high frequency waves. A technique for deriving the underlying realizable spectrum is described.

Keywords: Nonlinear spectrum, second-order spectrum, linear spectrum, linear spectrum from nonlinear spectrum

1 Introduction

In extreme nonlinear seas, one cannot directly use the measured spectra, $S_T(\omega)$, from these seas in an analysis, or to derive a seakeeping prediction, but rather one must derive the underlying linear spectrum to describe the waves that should be simulated. This is because nonlinear interactions between the linear waves will provide second-order, nonlinear contributions through the physics capturing wave-wave interactions.

At extreme wave heights theoretical spectra such as the Joint North Sea Wave Observation Project (JONSWAP) spectrum have nonlinear tails that are unrealizable in an experimental facility due to the breaking of high frequency waves. The underlying realizable spectrum may be derived as the corresponding linear spectrum by the tech- niques to be described.

The derivation of the linear spectrum underlying the nonlinear spectrum requires the solution of an integral equation describing the measured spectrum by either direct or indirect methods. This section will introduce two possible methods of solving this problem, with the assumption that the process involves only first- and second-order processes, a reasonable assumption in most circumstances.

2 Determining the Linear Spectrum

Wave processes are assumed to be homogeneous, stationary, and ergodic. This allows us to derive all statistical properties of the wave height and the power spectrum by examining wave records at just one position, which is taken as x = 0.

Only the case of unidirectional waves is considered here since an integral equation similar to the one that exists for unidirectional waves is not known for the case of multidirectional waves. A two-sided target spectrum $S_Q(\omega)$ is assumed to have been provided by the user. A two-sided linear spectrum $S_L(\omega)$ is sought which approximately satisfies the equation

$$S_Q(\omega) = S_L(\omega) + 2\int_{-\infty}^{\infty} d\sigma\, S_L(\sigma)\, S_L(\omega-\sigma) Z^2(\sigma,\omega-\sigma) \tag{1}$$

for real ω where

$$Z(\sigma,\omega) = \begin{cases} (\sigma^2+\omega^2)/(2g) & \text{if } \omega\sigma > 0 \\ -|\sigma^2-\omega^2|/(2g) & \text{if } \omega\sigma < 0 \end{cases}.$$

The details of the derivation are presented in Sclavounos (1992). The spectral density $S_L(\omega)$ is that of the linear model and is defined as follows:

$$\frac{1}{8}a_j^2 = S_L(\omega_j)\Delta\omega\,. \tag{2}$$

Therefore, the statistical inference of the second-order model reduces to the determination of the wave amplitudes a_j so that the second-order spectral density best matches the measured spectrum $S_Q(\omega)$. The linear spectral density $S_L(\omega)$ may be selected from any of the standard families with parameters such that the equality (1) is satisfied in a least squares sense.

For example, the ITTC spectrum may be used for the representation[1] of $S_L(\omega)$:

$$S_L(\omega) = \frac{0.110}{4\pi} H_{1/3}^2 T_1 \lambda^{-5} e^{-0.440\lambda^{-4}}, \qquad \lambda = \frac{\omega T_1}{2\pi}. \tag{3}$$

In (3) an accurate estimate of the modal period T_1 may be available from full-scale measurements. The significant wave height on the other hand must be selected so that (1) is satisfied as accurately as possible, given $S_Q(\omega)$. The amplitudes of the regular wave components then follow from (2).

A numerical approach such as the following might be considered. Using this definition of Z and assuming that the spectra $S_L(\omega)$ and $S_Q(\omega)$ are even functions of ω, the integral equation can be rewritten as

$$S_Q(\omega) = S_L(\omega) + 2\int_0^\infty d\sigma\, S_L(\sigma) \times \left[S_L(\omega+\sigma)Z^2(-\sigma,\omega+\sigma) + S_L(\omega-\sigma)Z^2(\sigma,\omega-\sigma)\right].$$

The integral equation has no solution if the target spectrum has content of higher than second order in the wave amplitude. This section describes how a least-squares approximation to the desired linear spectrum $S_L(\omega)$ may be obtained and thus avoids the issue of whether a solution exists or not.

The numerical scheme that follows requires that discrete frequencies be equally spaced. If this is not the case, then $\omega - \sigma$ in the discretized integral equation will not be one of the discrete frequencies ω_j and any numerical scheme becomes complicated. The discrete frequencies in this section are therefore not necessarily those for which linear wave amplitudes a_j are chosen in the next section, and the N used in the description of the numerical scheme is not necessarily the number of positive wave frequencies used in the next section.

To discretize this equation, it is assumed that $S(\omega)$ can be ignored for $|\omega| > \Omega$. Then N and $\Delta\omega$ are chosen so that $N\Delta\omega = \Omega$. Define the following quantities for $j = -N, -N+1, \ldots, N$:

$$\omega_j = j\Delta\omega$$
$$\sigma_j = j\Delta\omega$$
$$S_j = S(j\Delta\omega)$$

We need to define $S_{L,j}$ over the wider range of j values between $-2N$ and $2N$:

$$S_{L,j} = S_L(j\Delta\omega)$$

although it has been assumed that the target spectrum $S_T(\omega)$ is negligible for values of j greater than N in absolute value. (The linear part of it in $S_L(\omega)$ should be even more negligible.) The range of integration is truncated and trapezoidal quadrature is used to approximate the integral equation as follows:

$$\begin{aligned} S_Q(\omega) &\approx S_L(\omega) \\ &\quad + 2\int_{-\Omega}^{\Omega} d\sigma\, S_L(\sigma)S_L(\omega-\sigma)|Z(\sigma,\omega-\sigma)|^2 \\ &\approx S_L(\omega) + 2\Delta\sigma\left\{\frac{1}{2}S_L(\sigma_{-N})S_L(\omega-\sigma_{-N}) \times |Z(\sigma_{-N},\omega-\sigma_{-N})|^2 \right. \\ &\quad + \sum_{n=-N+1}^{N-1} S_L(\sigma_n)S_L(\omega-\sigma_n) \times |Z(\sigma_n,\omega-\sigma_n)|^2 \\ &\quad \left. + \frac{1}{2}S_L(\sigma_N)S_L(\omega-\sigma_N) \times |Z(\sigma_N,\omega-\sigma_N)|^2 \right\} \end{aligned}$$

$$\begin{aligned} S_{Q,\ell} &= S_{L,\ell} + 2\Delta\sigma\left\{\frac{1}{2}S_{L,-N}S_{L,\ell+N} \times |Z(-N\Delta\omega,(\ell+N)\Delta\omega)|^2 \right. \\ &\quad + \sum_{n=-N+1}^{N-1} S_{L,n}S_{L,\ell-n}|Z(n\Delta\omega,(\ell-n)\Delta\omega)|^2 \\ &\quad \left. + \frac{1}{2}S_{L,N}S_{L,\ell-N}|Z(N\Delta\omega,(\ell-N)\Delta\omega)|^2 \right\} \end{aligned}$$

Here $\Delta\sigma = \Delta\omega$. Taking account of where the target spectrum and its linear part are neglibigle, we have the following approximation of the integral equation:

$$S_{Q,\ell} \approx S_{L,\ell} + 2\Delta\omega \sum_{n=-N}^{N} S_{L,n}S_{L,\ell-n}Z_{n,\ell-n}^2 \tag{4}$$

[1] This representation can be obtained from equations on page 38 of Beck et al. (1989) if three significant digits are retained.

where $Z_{n,\ell-n} = Z(n\Delta\omega, (\ell-n)\Delta\omega)$.

A small error has been introduced at the two end points. When $|\ell-n| > N$, we can either ignore $S_{n-\ell}$ or set it equal to S_ℓ. The latter alternative is preferable. In view of the definition of the function Z and the evenness of S_L, (4) can be written as

$$S_{Q,\ell} \approx \begin{cases} S_{L,\ell} + 2\Delta\omega \sum_{n=1}^{N} S_{L,n} S_{L,|\ell-n|} Z^2_{n,\ell-n} & \text{if } \ell > 0 \\ S_{L,\ell} + 2\Delta\omega \sum_{n=-N}^{-1} S_{L,n} S_{L,-|\ell-n|} \times Z^2_{n,-\ell-n} & \text{if } \ell < 0 \end{cases} \tag{4'}$$

where the case $\ell = 0$ has been ignored since spectra are assumed to vanish as the frequency approaches zero.

Here $S_{L,p} = S_L(p\Delta\omega)$ and $S_{Q,p} = S_Q(p\Delta\omega)$. The series is truncated and the equations are written as

$$\begin{aligned} f_\ell \equiv\ & S_{L,\ell} - S_{Q,\ell} \\ & + 2\Delta\omega \left[\sum_{n=1}^{\ell-1} S_{L,n} S_{L,\ell-n} Z^2_{n,\ell-n} \right. \\ & + \sum_{n=\ell+1}^{N} S_{L,n} S_{L,n-\ell} Z^2_{n,\ell-n} \\ & \left. + \sum_{n=1}^{N-\ell} S_{L,n} S_{L,n+\ell} Z^2_{-n,\ell+n} \right] = 0 \end{aligned}$$

for $\ell = 1, 2, \ldots, N$. The frequency $\Delta\omega$ and the number N are provided by the user. The objective is to minimize the sum

$$\chi^2 = \sum_{\ell=1}^{N} f_\ell^2 .$$

An initial guess $S^{(0)}_{L,\ell}$ for the discrete linear spectrum is provided by the equation

$$S^{(0)}_{L,\ell} = S_{T,\ell} \quad \text{for } \ell = 0, 1, \ldots, N .$$

All iterates for the linear spectrum are assumed to vanish at $\omega = 0$ rad/sec:

$$S^{(p)}_{L,0} = 0 \quad \text{for } p = 0, 1, \ldots$$

It is now assumed that the p-th iterate, say $S^{(p)}_{L,m}$, is known. For $m = 1, 2, \ldots, N$, $S^{(p+1)}_{L,m}$ is chosen between $(1-\alpha)\, S^{(p)}_{L,m}$ and $(1+\alpha)\, S^{(p)}_{L,m}$ such that

$$\sum_{\ell=0}^{N} f_\ell^2 \left(S^{(p+1)}_{L,1}, \ldots, S^{(p+1)}_{L,m-1}, S^{(p+1)}_{L,m}, S^{(p)}_{L,m+1}, \ldots, S^{(p)}_{L,N} \right) .$$

is approximately minimized. The number α is somewhat arbitrary and can be provided by the user; it only serves to bound the interval in which a minimum of χ^2 is sought. Numerical tests for some spectra indicate that $\alpha = 0.1$ is acceptable for those spectra. To minimize χ^2, we can check the sum at several, say 10, evenly spaced points $S^{(p+1)}_{L,m}$ in the interval $[(1-\alpha)\, S^{(p)}_{L,m}, (1+\alpha)\, S^{(p)}_{L,m}]$ and make the change based on the 10 evaluations of χ^2. The number 10 is arbitrary and can be replaced by another value supplied by the user. Furthermore, the points do not have to be evenly spaced. The whole process is repeated for a specified number of iterations. The sum χ^2 can be monitored and the iterative process can be truncated when the fractional change in the sum is less than a user-specified tolerance or no longer decreases.

The desired values $S_{L,\ell}$ for the discrete linear spectrum are given by $S^{(p)}_{L,m}$ where p is the number of the most recent iterate. Interpolation is required if the spectral density function is desired at frequencies other than $\omega_m = m\Delta\omega$.

3 The Algorithm

The scheme proceeds as follows:

1. Choose the highest frequency Ω to be used in the discretization and a sufficiently large value of N. This defines $\Delta\omega = \Omega/N$.
2. Define the initial guess $S^{(0)}_{L,\ell}$ as the target spectrum: $S^{(0)}_{L,\ell} = S_{T,\ell}$. Also define $S^{(0)}_{Q,\ell}$ so that $S^{(0)}_{Q,\ell} = S^{(0)}_{L,\ell}$. Except for the zeroth iterate, the discrete function $S^{(m)}_{Q,\ell}$ is the right side of eq. (4) when $S_{L,\ell}$ is replaced by the m-th iterate $S^{(m)}_{L,\ell}$ for linear part of the target spectrum.
3. This is the start of a loop. Calculate a new guess $S^{(m)}_{L,\ell}$ for the linear part of the target spectrum from the equation

$$S^{(m)}_{L,\ell} = S_{T,\ell} \frac{S^{(m-1)}_{L,\ell}}{10^{-20} + S^{(m-1)}_{Q,\ell}} \tag{5}$$

4. Calculate the RMS difference between $S_{L,\ell}^{(m)}$ and $S_{L,\ell}^{(m-1)}$. If it is sufficiently small or there have been too many iterations, exit the loop.
5. Calculate the right side $S_{Q,\ell}^{(m)}$ of eq. (4) corresponding to $S_{L,\ell}^{(m)}$.
6. Go back to the beginning of the loop.

4 Numerical Test

The scheme was tested on the Bretschneider spectrum. Two tests were conducted, in the first, a quadratic target spectrum was constructed from the Bretschneider spectrum and the Bretschneider spectrum was extracted from this target spectrum. In the second test, the Bretschneider spectrum was treated and the target quadratic spectrum and the linear part of the Bretschneider was determined. In both cases, the Bretschneider spectrum was given by:

$$S(\omega) = A/\omega^5 e^{-B/\omega^4},$$

where $A = 173\,H_{1/3}^2/T_1^4$, $B = 691/T_1^4$, $T_1 = 0.773\,T_m$, $T_m = 2\pi/0.45$ sec and $H_{1/3} = 14.7$ m.

In these computations, the loop was not terminated for any value of the RMS difference between iterates. Instead, the loop was allowed to execute 30 times. The parameter Ω was set to 10 rad/sec and the number of subintervals into which the interval $[0,\Omega]$ was subdivided was set to 1023 so that $N = 1024$.

For the first test case, where a target quadratic spectrum was constructed from a Bretschneider spectrum, Fig. 1 compares the initial iterate (the target spectrum $S_T = S_L^{(0)}$) with the 10th, 20th, and 30th iterates for $S_L^{(m)}$. Figure 2 depicts the nonlinear part $S_T - S_L^{(m)}$ of the computed total spectrum at the mth iterate for for $m = 10, 20, 30$ and the target Bretschneider spectrum.

For the second test case, where the Bretschneider spectrum is considered to be the target spectrum, Fig. 3 compares the initial iterate (the target spectrum $S_T = S_L^{(0)}$) with the 10th, 20th, and 30th iterates for $S_L^{(m)}$. Figure 4 plots the computed linear spectrum $S_L^{(m)}$ and the computed total spectrum $S_Q^{(m)}$ at iteration $m = 30$. Figure 5 is a log plot of the RMS difference between successive iterates $S_L^{(m)}$ for the linear part of the target spectrum. Even though successive approximations $S_L^{(m)}$ appear to converge, Figs. 3 and 4 show

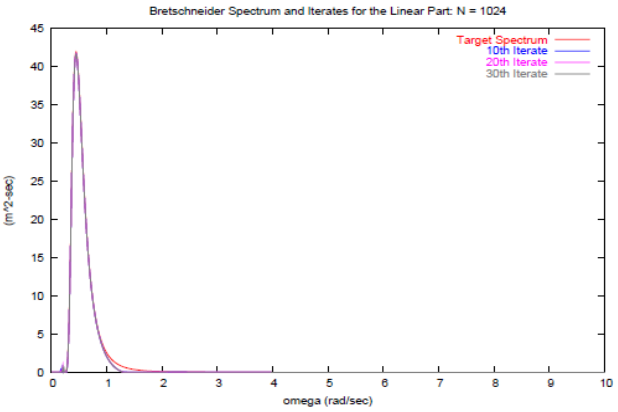

Fig. 1 The target spectrum and iterates for the linear part of the target spectrum. Spectral definition: $S(\omega) = A/\omega^5 e^{-B/\omega^4}$, $A = 173\,H_{1/3}^2/T_1^4$, $B = 691/T_1^4$, $T_1 = 0.773\,T_m$, $T_m = 2\pi/0.45$ sec and $H_{1/3} = 14.7$ m.

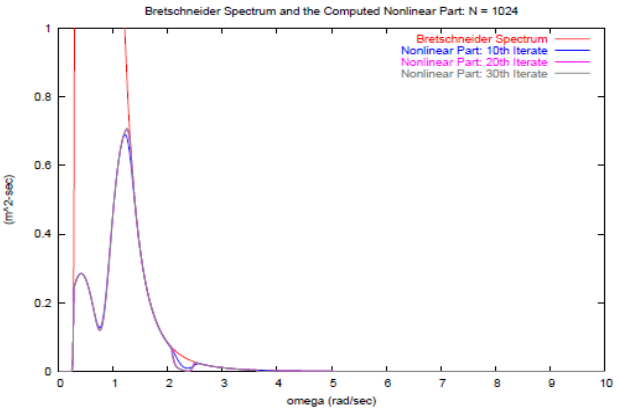

Fig. 2 The nonlinear part of the target spectrum calculated as the difference between the target Bretschneider spectrum and iterates for the linear part of the target spectrum. Spectral definition: $S(\omega) = A/\omega^5 e^{-B/\omega^4}$, $A = 173\,H_{1/3}^2/T_1^4$, $B = 691/T_1^4$, $T_1 = 0.773\,T_m$, $T_m = 2\pi/0.45$ sec and $H_{1/3} = 14.7$ m.

that the result for the linear part of the Bretschneider spectrum is not the limit of the successive approximations $S_{L\ell}^{(m)}$:

$$\lim_{m\to\infty} S_{L\ell}^{(m)} \neq S_{L\ell}\,.$$

The computed nonlinear spectrum is larger than the target Bretschneider spectrum in finite intervals, a phenomena which probably also occurs at higher frequencies. As an example, near the frequency $\omega \approx 7.5$ rad/sec in Figs. 3 and 4, it is clear that the computed nonlinear spectrum is larger than the target spectrum and that the linear part of it is identically zero (within a small tolerance). In this method a local change in the linear spectrum does not affect the computed nonlinear spectrum in the neighborhood of the change as much as at other frequencies due to the nonlinear nature of the integrand in the integral equation. In any case, the linear spectrum cannot be reduced below its current value near $\omega = 7.5$ rad/sec so that a beneficial local change in the linear spectrum is precluded. Thus, it is impossible to improve the solution when the next iterate is computed from (5).

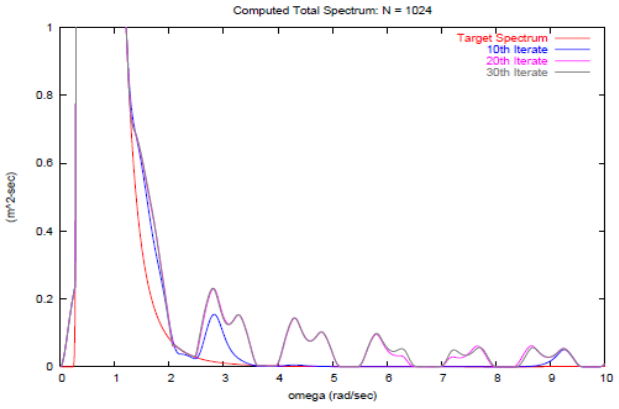

Fig. 3 The total computed nonlinear spectrum obtained while iterating for for the linear part of the Bretschneider spectrum. Spectral definition: $S(\omega) = A/\omega^5 e^{-B/\omega^4}$, $A = 173\,H_{1/3}^2/T_1^4$, $B = 691/T_1^4$, $T_1 = 0.773\,T_m$, $T_m = 2\pi/0.45$ sec and $H_{1/3} = 14.7$ m.

5 Conclusions

In extreme nonlinear seas, one cannot directly use the measured spectra, $S_T(\omega)$, from these seas in an anal-

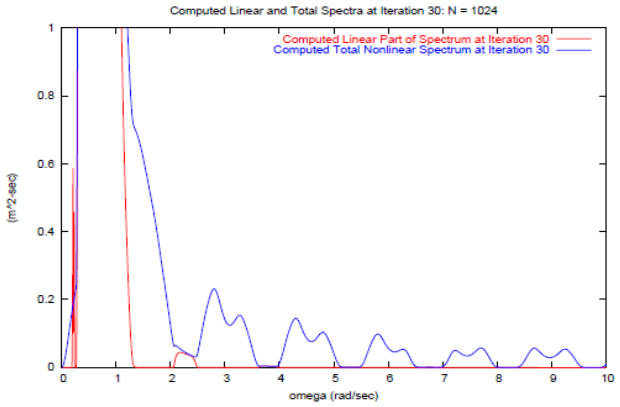

Fig. 4 Comparison of the total computed nonlinear spectrum with the linear part of the total computed nonlinear spectrum. Spectral definition: $S(\omega) = A/\omega^5 e^{-B/\omega^4}$, $A = 173\,H_{1/3}^2/T_1^4$, $B = 691/T_1^4$, $T_1 = 0.773\,T_m$, $T_m = 2\pi/0.45$ sec and $H_{1/3} = 14.7$ m.

Fig. 5 Log_{10} plot of the RMS difference between successive iterates for the linear part of the target Bretschneider spectrum. Spectral definition: $S(\omega) = A/\omega^5 e^{-B/\omega^4}$, $A = 173\,H_{1/3}^2/T_1^4$, $B = 691/T_1^4$, $T_1 = 0.773\,T_m$, $T_m = 2\pi/0.45$ sec and $H_{1/3} = 14.7$ m.

ysis, or to derive a seakeeping prediction, but rather one must derive the underlying linear spectrum to describe the waves that should be simulated. A technique for deriving the underlying realizable spectrum has been described.

Using the technique presented for deriving the linear spectrum from the quadratic spectrum via the solution of an integral equation, even though successive approximations $S_L^{(m)}$ appear to converge, the result for the linear part of the spectrum is not the limit of the successive approximations. It is clear that in some intervals, the computed nonlinear spectrum is larger than the target spectrum and that the linear part of it is identically zero (within a small tolerance). In this method a local change in the linear spectrum does not affect the computed nonlinear spectrum in the neighborhood of the change as much as at several other frequencies due to the nonlinear nature of the integrand in the integral equation.

References

Beck, R. F., W. E. Cummins, J. F. Dalzell, P. Mandel, and W. C. Webster (1989). "Principles of Naval Architecture Second Revision. Motions in Waves and Controllability". In: ed. by E. V. Lewis. Vol. III. 3 vols. Jersey City, NJ: Society of Naval Architects and Marine Engineers. Chap. Motions in Waves, pp. 1–190. ISBN: 0-939773-02-3.

Sclavounos, P. D. (1992). "On the Quadratic Effect of Random Gravity Waves on Floating Bodies". In: *Journal of Fluid Mechanics* 242, pp. 475–489.

High Performance Algorithms for Multiphase and Multicomponent Media

Bogdanov A., Stankova E., Mareev V.

Introduction. Although the main problem of multicomponent media dynamics still remains large difference of characteristic values of the processes, there are some indications, that it can very effectively be solved by the change of dynamic parameters, thus quasi-diagonalzing the rates of processes matrix. To overcome the difficulty of representing flow parameters in new variables one can use such procedure to all dynamic variables, not only with large difference of characteristic time. With the populations such approach is straightforward and intuitively clear, and it has support with a lot of effective examples in quantum mechanics. It is more interesting to do the same with flow variables. It is difficult to do this with standard representation of transport equations, but one can more effectively use the conservation laws in moving coordinates frame. In such a case one has simpler representation for derivatives in discreditized representation and thus a lot of possibilities for speed-up of computations. For efficient numerical implementation tensor representation in two coordinate systems (global and moving) is used. Proposed approach takes possibility to use explicit numerical schemes that result in natural parallelism of numerical procedure.

Mathematical Foundation. It is easy to understand bases of the proposed algorithm on the example of the evolution equation of the type

$$idu/dt = Pu, \tag{1}$$

with $\boldsymbol{P}$ being some operator, which we will suppose to be Hermitian. Any standard approach normally will transform it to the linear system of ordinary differential equations of the type

$$id\vec{v}/dt = \boldsymbol{P}\vec{v}, \tag{2}$$

with $\vec{v}$ being the large vector and $\boldsymbol{P}$ being symmetric matrix. The problem is not difficult for any size of $\vec{v}$, if $\boldsymbol{P}$ is almost diagonal, but for many important situations it is not the case. From the point of view of the theory of dynamic systems large nondiagonal members in $\boldsymbol{P}$ means bad choice of representation for Eq.(1), although often such representation is forced by physical considerations.

Usually it is not difficult to find the transformation, which will make $\boldsymbol{P}$ quasidiagonal, some of the beautiful approaches in the theory of nonlinear equations can have even natural physical background. At the same time some problems may cause the reverse transformation to original variables.

To find out what should be a correct dynamical approach let us look at one dimensional model that can be represented in simple form

$$u_t + uu_x - \mu u_{xx} = H(u,x),$$

with H being functional of flow parameters. Brilliant analyses of Prof. Ladyzhenskaya (1972) [1] on solution and uniqueness of this equation shows, that main problems can come from second term of lhs. If H can be represented as gradient of some functional, the problem can be solved by representing u as gradient of some v and integrating this equation one time. Actually exactly in such a way we can introduce famous Coul-Hopf transformation

$$u = -2\mu \frac{1}{v}\frac{dv}{dx}$$

that can linearize our equation in u in case of H being gradient of some functional. In general case it is not the case and we face all the problems of Navier-Stockes approach. One can imagine representation

$$K \equiv \frac{d}{dx}\left(\frac{d}{dx}\right)^{-1} K$$

and try to extract some sense from inverse operator of d/dx. It is very often done in quantum field theory, sometimes successfully, sometimes not [2]. The reason is non uniqueness of such operator. To give to it some foundation it is possible to return to foundation of hydrodynamic equations from kinetic ones and to obtain the way of regularization of such procedure [3]. In such a way one can come to new dynamical picture that we can illustrate on simple model.

Proposed approach. Here we shall study the problem on the base of one dimensional model, for which it is easy to make reverse transformation.

Let us assume, that *c* is any dynamical parameter and we shall discreditize it changing space coordinate x to index j. The system of transport equations, describing the flow in this one dimensional systems, consists in realistic cases of thousands of equations of the type

$$dc(j,t)/dt = I(j-1,t)I(j,t), \qquad (3)$$

with I being the current of this dynamic parameter in index space in and out of discreditization cell. It is always possible to present I as linear form of c, thus representing r.h.s of (3) in a way $I(j,t) = K(j,j+1)c(j,t) - K(j+1,j)c(j+1,t)$, where K may be a complex functional of all dynamical parameters.

The problems with Eq.(3) actually come from two factors — there are large nondiagonal members, corresponding to important physical transitions, and values of $I(j,t)$ are very large with difference between them in r.h.s. of Eq. (3) is relatively small. The situation becomes dramatic if you start integration with thermal equilibrium, when all *I*'s are equal.

To overcome those difficulties it is useful to introduce new variables $f(j,t) = c(j+1,t)/c(j,t)a(j,t)$ with $a(j,t)$ being the ratio of functionals $K(j,j+1)$ and

$K(j+1,j)$. f's are so called slow variables, which become constants at equilibrium conditions. The equations for f's are

$$df(j,t)/dt = \tilde{R}[f(j,t)] + H(j,t)f(j,t) + S(j)f(j,t), \quad (4)$$

with $\tilde{R}$ being the quadric term, that is diagonal in j, H is the source term, proportional to external fields, and S is the source of dynamical parameter change, the only term, that is nondiagonal in $f(j,t)$. The main advantage of Eq.(4) is, that not only the sum of three terms in r.h.s. (4) is small, but they are small separately and it is easy to determine their relative values beforehand. Moreover, it is important, that the major contribution in r.h.s. of (4) is diagonal that opens interesting opportunities for parallel algorithm.

Such notation makes it possible to rewrite numerical schemes in tensor form. Tensor mathematics naturally embedded in the finite- operation in the construction of numerical schemes.

Stages of the computation. The traditional computational scheme for the above described approach is already realized as a computer code for Power clusters and includes following phases:

1. Functional constants *K* computation,
2. Functional constants *K* parametrization,
3. Approximate system evolution,
4. Corrections for exact system evolution,
5. Populations and averages computations.

Since even in this new approach, the whole computational problem is prohibitively time consuming, in practice it is separated into three stages:

I. Stages 1 and 2,
II. Stages 3 and 4,
III. Stage 5

And usually it is realized on different systems. The stages I and II are the most difficult ones. We are not discussing here the realization of stage I, which is more or less standard.

It is enough to note, that the results of stage I are the input for stage II, and thus should be realized as Data Base, or Knowledge Base with pertinent gate to the system, realizing stage II. What we are proposing here is to use absolutely parallel nature of the algorithm, discussed above to realize substantial part of the computations in Items 3 and 4, which are actually reduced to the solution of huge amount of Ordinary Differential Equations, connected only by initial data. For that purpose we split this algorithm in separate blocks and realize it on different systems.

Important Example

For illustration of proposed approach we have taken thermal wave in mixture He-HF in one dimensional flow with initial temperature difference between plates of 1300K. The reason of this is obvious. There are not so large gradients involved and we can prepare and keep all necessary data for functional constants *K* on the same system. So we can skip the large part of Grid infrastructure

and concentrate only on peculiarities of computational algorithm. To check the real advantages of our approach and see possibilities for its migrating to Grid infrastructure we test it on a cluster with slow links.

To simulate this flow we must solve standard equations (3). It is very effective demonstration, since number of discretization boxes, which should be taken into account, is of the order of 80 with such temperature spread, so one needs not much time for convergence of flow solution. Computation was done on 8-processor linux cluster with slow 2Gb links to simulate importance of communications between computational processes.

The complete simulation of initial problem took about 20 min. The use of relaxational system (4) instead of (3) reduces that time to 2.4 min.

In this case it is possible to increase essentially effectiveness of computing procedures through:

1. Natural parallelization of the computation process;
2. Possibilities of adaptive correction of mesh area depending on features of the problem;
3. Dynamic reconstruction of solution in accordance with fluid currents transformations in time.

Conclusion. It is known that traditional approach to numerical solution fluid dynamics problems is most often reduced to application of implicit schemes. The described algorithmic approach, first of all because of the proposed splitting of the solution on physical processes, gives the chance of application explicit numerical schemes. It is even more interesting to see how all this arrangement works for more complex hydrodynamic flows, but that we will show in our next paper.

Acknowledgment. The research was carried out using computational resources of Resource Center Computer Center of Saint-Petersburg State University and supported by Russian Foundation for Basic Research (project N 13-07-00747) and St. Petersburg State University (projects N 9.38.674.2013, 0.37.155.2014).

References

[1]. G.B. Whitham. Linear and nonlinear waves. JOHN WILEY and SONS, 1974.
[2]. P. Ramond. Field theory. A modern primer. The Benjamin Cummings publishing, 1981.
[3]. V.Ya. Rudyak. Statistical theory of dissipative processes in gases and liquids (in Russian). Nauka, 1984.

- SESSION 8 -

HIGH SPEED AND SPECIALIZED CRAFT STABILITY AND SAFETY

A Study on Spinout Phenomena of Planing Craft in High Speed Turning with Radio Control Small Model

Toru Katayama [1 *] and Shun Ohashi [1]

1. *Dept. of Marine System Engineering, Graduate School of Engineering, Osaka Prefecture University, Japan*

Abstract: In this study, a free running model test system for measuring unstable phenomena of planing craft, which is an 1m radio controlled planing hull model including measurement devices and whose max speed is 12m/sec, is developed to inspect safely and easily the occurrence of instabilities instead of a real-craft test. And, by using the system, the occurrence running condition, the characteristics of motion and the mechanism of occurrence of Spinout phenomenon is investigated.

Key words: Planing craft, spinout, radio control model.

1. Introduction

Recently, high-speed planing craft, which can run at more than 100km/h, are developed owing to engine improvement and its hull weight reduction. At the high-speed running which most of a hull is exposed above the water surface, even if it runs in calm water, some peculiar unstable phenomena[1)2)] for planing craft occur. For example, Porpoising, Corkscrew, Transverse pure stability loss, Directional instability, Dutch-roll, Spinout and etc. The causes and mechanisms of some of these phenomena are not clear yet, so there are demands for development of estimation methods of their occurrence in design stage and suggestions on how to avoid their occurrence. It is important to understand the conditions of occurrence of an unstable phenomenon and the detail of motion of the phenomenon, as a first step of developing its performance estimation method. However, it is difficult to measure them by a real-craft, because it may cause capsizing, hull damage and/or crew's injury in the serious cases.

Spinout is one of the more serious consequences of high speed maneuvering, in its moderate form, Spinout is the maneuvering motion that a hull suddenly begins spinning by small disturbance in high speed turning or straight running and rapidly stops without capsizing. In the serious cases, it may cause capsizing, hull damage and/or crew's injury[3)]. In this study, in order to simulate Spinout occurring, the free running scaled model, which is a radio control planing hull 1.0m model and its maximum forward speed is 12m/sec and it includes several measurement devices, is developed. And, by using the system, the occurrence running condition, the characteristics of its motion and the scenario of occurrence of Spinout is investigated.

2. Free Running Model

2.1 Model

Fig.1 and Table 1 show the bodyplan and the principle particulars of the model. This is for an outboard engine. This type of craft is usually used in a lake or an enclosed bay, therefore its dead rise angle is small to take large vertical lift and to rise hull.

Fig.2 shows the radio control model, which is developed in this study. Its motion, track, ship speed are measured by AHRS (Attitude and Heading Reference System: Xsens MTi-G). Its Gyroscope and GPS antenna on s.s.7.43 and s.s.10 of hull. Number of motor's rotation is measured with Hyperion Emeter II, and rudder angle is measured with a potentiometer.

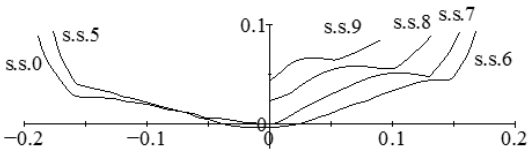

Fig. 1 – Bodyplan of the model

Table 1 Principal particulars of the model

overall length : L_{OA}[m]	1.03
breadth : B[m]	0.40
depth : D[m]	0.085
length to breadth ratio : L_{OA}/B	2.575
deadrise angle at ss5 : β_m [deg]	15
height of center of gravity : KG [m]	0.047
metacentric height : GM [m]	0.28
roll natural period : T_ϕ [sec]	0.56
pitch natural period : T_τ [sec]	0.63

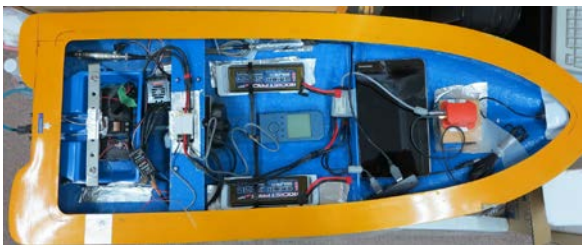

Fig. 2 – Picture of radio control model

2.2 Coordinate System

Fig.3 shows coordinate systems. They are an earth and a body fixed coordinate system. Before the model starting to run, the origins of them are the same, which is the center of gravity of the model, and the directions of x_0, y_0 and x, y axes are North and West, and direction of rotation around each axis is a right-handed screw.

3. Measurement of Spinout

3.1 Measurement Method

A free running model test with the radio control model is carried out in the pond of Osaka Prefecture University.

At first, the model is accelerated straight to reach a target speed. And rudder angle is changed to a target rudder angle with constant rudder speed. The time to reach a target rudder angle is one second for any target rudder angle. After the model starts turning motion, the control signals of forward speed and rudder angle are fixed. The measurement is continued from before starting running to after occurrence of Spinout. Table 2 shows the condition of experiment.

x_0y_0-O: earth fixed coordinate system
xy-O: body fixed coordinate system
X, Y, N: force or moment acting on craft
G: center of gravity ψ: heading angle
U, u, v: velocity r: yaw angular velocity
β: drift angle δ: rudder angle

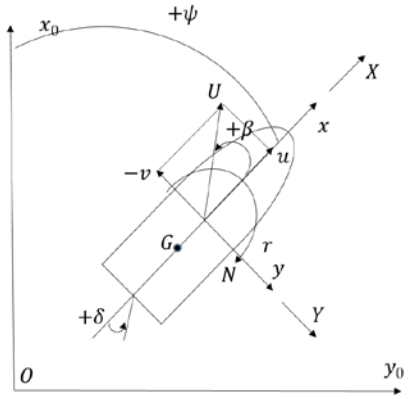

Fig. 3 – Coordinate system

Table 2 Experimental condition

displacement of the model [kgf]	6.08
initial trim angle [deg]	0
target forward speed [m/s]	7.0 ~ 11.0
maximum rudder angle δ_{max}[deg]	10.0 ~ 20.0
time for rudder turning to δ_{max} [sec]	1.0

3.2 Occurrence of Spinout

Fig.4 and 5 show typical time histories of number of propeller revolutions, rudder angles, yaw angular velocity and drift angle when Spinout occurs or does not. These data are measured for clockwise turning. When Spinout does not occur, yaw angular velocity increases just after starting steering, and it becomes a constant value after having a small peak. When Spinout occurs, yaw angular velocity rapidly increases just after starting steering, and it is continuously increase to a large peak value, and drift angle also increases and it reaches over 90 degrees.

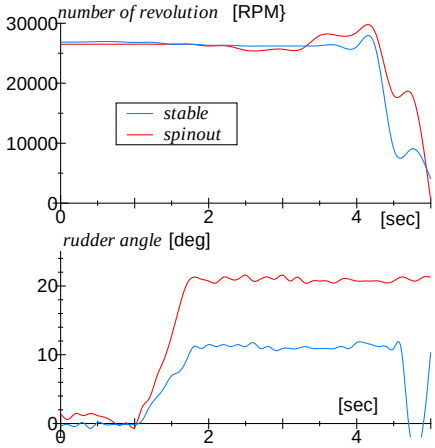

Fig. 4 – Time history of measured number of revolutions and rudder angle in the turning trial

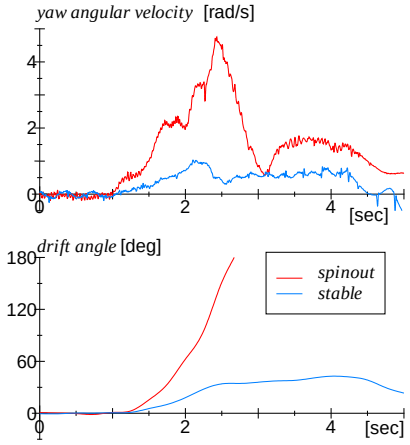

Fig. 5 – Time history of measured yaw angular velocity and drift angle in the turning trial

Fig.6 shows time histories of pitch angle, roll angle and velocity *U* in the same measurements shown in Fig.4 & 5. When Spinout occurs, after starting steering, velocity *U* decreases larger than one without occurrence of Spinout, and pitch angle rapidly decrease. The reason of this bow-down is supposed that a bow-down moment is caused by inertia force due to sudden deceleration by the change of thrust direction.

Fig.7 and 8 show a time histories of pitch angle roll angle, velocity *U*, number of propeller revolution and rudder angle when Spinout occurs without sudden deceleration. These data are measured for anti-clockwise turning. In this case, heel angle increases at first, and pitch angle rapidly decreases without sudden decrease of velocity *U*.

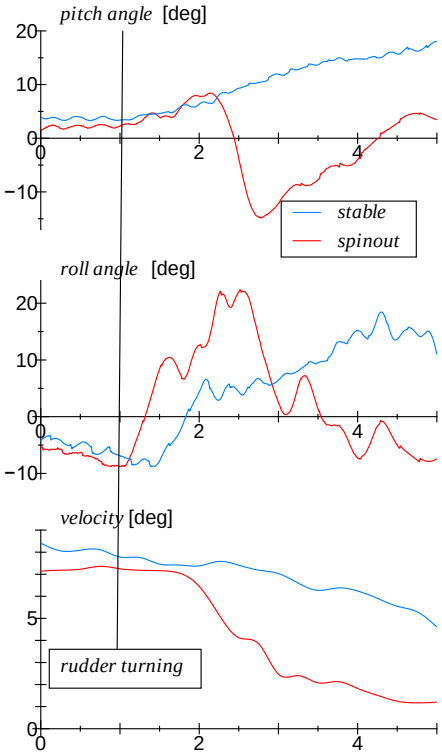

Fig.6 – Time history of measured pitch angle, roll angle, and velocity in the turning trial

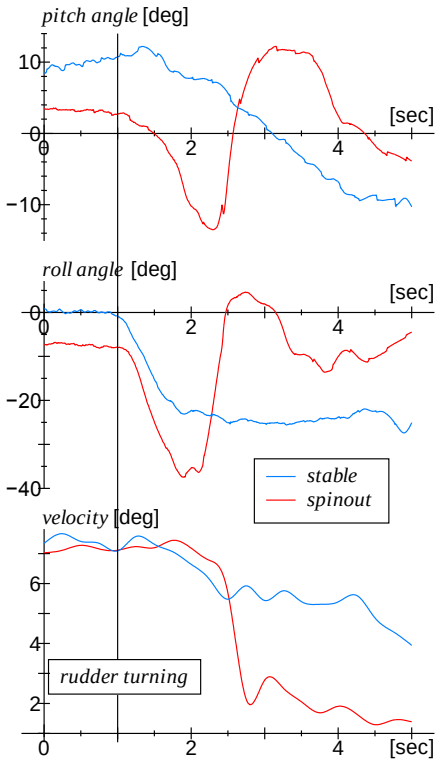

Fig.7 – Time history of measured pitch angle, roll angle and velocity at turning trial

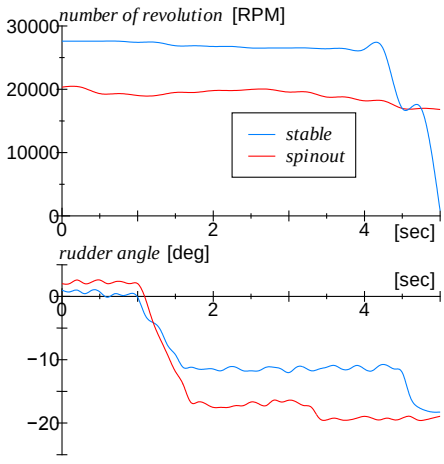

Fig.8 – Time history of measured number of revolution and rudder angle at turning trial

Fig.9 and 10 show occurrence of Spinout for all cases of measurements. From the figures, it is noted that Spinout occurs according to increase of a target rudder angle for the same forward speed. On the other hand, the occurrence speed of Spinout is different with turning direction for the same target rudder angle. The reasons of the differences is supposed that the hull is not necessarily symmetric, a moment is caused by propeller rotation of single screw etc.

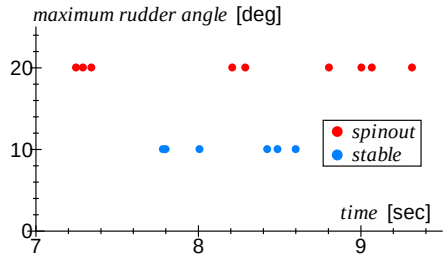

Fig.9 – Occurrence of Spinout in the right turning trial

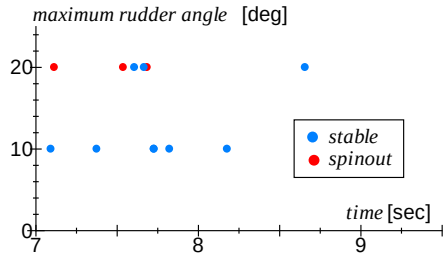

Fig.10 – Occurrence of Spinout in the left turning trial

3.3 Scenario of Spinout Occurring

From the measured data, a scenario of Spinout is discussed.

In the stable turning, the thrust cause the yaw moment which increases drift angle, and hydrodynamic forces acting on hull cause the yaw moment which decreases drift angle, usually, and these moments are balance.

When Spinout occurs, the bow-down caused by sudden deceleration or large heel angle just after starting steering moves forward the point of action of hydrodynamic forces passing the center of gravity as

shown in Fig.11. Therefore, the moment caused by hydrodynamic forces acting on hull becomes the moment which increases drift angle, and it causes a rapid spin.

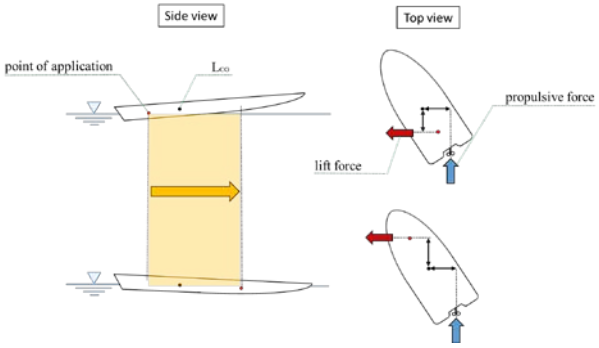

Fig.11 – Mechanism of occurrence of Spinout phenomena

4. Conclusions

In this study, a radio control free running model is developed and Spinout is measured by model test with the radio control model. Form the results, the following conclusions are obtained.

1. When Spinout occurs, the rapid deceleration or the large heel angle, which is caused by steering, cause a bow-down.
2. The rapid deceleration just after starting steering is caused by the change of thrust direction at high speed and large target rudder angle. And inertia force due to the deceleration causes bow-down.
3. For the same forward speed, larger rudder angle makes turning diameter smaller, and inside heel angle becomes larger and it is causes a bow-down.
4. The bow-down makes a wetted length longer, it moves the point of action of hydrodynamic force forward and the yaw moment, which causes drift angle, acts on a hull and Spinout occurs.

Acknowledgments

This work was supported by JSPS Grant-in-Aid for Scientific Research (C) 24560989. We are grateful for the support.

References

[1] Toru Katayama, Tomoki Taniguchi and Kazuya Habara: Tank Tests to estimate onset of Dynamic Instabilities of High-Speed Planing Craft, Transactions 2010, THE SOCIETY OF NAVAL ARCHITECTS AND MARINE ENGINEERS (2011) 106-121.

[2] Toru Katayama and Kazuya Habara: An Experimental Study on Instability of a Super High-speed Planing Craft with Outboard Engine at Straight Running, Proceedings of 11th International Conference on Fast Sea Transportation, FAST 2011 (2011) pp.850-856.

[3] Dag Pike: Fast Powerboat Seamanship, The McGraw-Hill Companies (2004) 180-183.

Stability Analysis of Hybrid Catamaran Fishing Vessel

P I Santosa [(1)], I K A P Utama [(2)] and T W Wuruk Pribadi[(2)]

[(1)] PhD Student, [(2)] Professor, and [(3)] Lecturer, Department of Naval Architecture and Shipbuilding Engineering,Institut Tenologi Sepuluh Nopember (ITS), Surabaya 6011, Indonesia

Abstract: The successful development of catamaran mode as passenger vessels has been extended to the development of catamaran fihing vessel. The study is combined with the development of hybrid power of the catamaran fihing vessel in order to minimize the use of fossil fuel and hence reduce greenhouse ga (GHG) effect. A combination power by using diesel engine, solar panels and sail is investigated. The study is focused on stability analysis with restriction to maintain its function as a fishing vessel.

Keywords : fishing vessel, hybrid power, stability, diesel engine, solar panel, sail.

1. Introduction

Development of environmentally friendly vessels has become very popular since the last 20 years. The reasons for this are attributed to the lack and high cost of oil. In the case of Indonesia, the situation has causal the fishermen into troubles with tendencies that they become bankrupt. There was a study reported that the growth of the construction of new fishing vessels in Indonesia reached about 6 % between 2001 and 2005 [1]. However, about half of those vessels have not been operated again recently the high cost of fuel oil.

Due to, there many efforts conducted by scientists, governments and IMO in order to reduce the spread of toxic gases to the atmosphere such as CO, CO_2, SO_2 and NO_2 which is caused by the use of fossil fuels by ships [2]. A new term called EEDI (energy efficiency design index) has been introducced by the IMO

(international maritime organization) in 2009 in order to measure the level of efficiency of the power (SEEMP) and its effect to the green house gases (GHG) impact [3]. These findings indicate that the use of fossil fuels should be reduced into a certain level in order to maintain the environment clear and healthy.

Many efforts have been made in order to reduce the use of fuel oil. A number of power systems have been developed such the reuse of sails in combination with the use of marine diesel engine; this is later known as sail assisted engine [4]. The powering vessel without using engine and fuel oil has become more popular in connection with environmental issues, later known as green economy concept. They are: (1) the use of sail, solar powered boat and wave power mechanism individually and (2) the combination of two or three of them [30]. Although the results of those developments are still far from economic benefits, research and development of those power systems has been carried out very intensive around the world such as reported in [5, 6].

In term of the vessel itself, the use of catamaran type of vessel as medium- and high-speed passenger carriers has been popularly known and reported in many papers [7, 8 and 9]. Those successes are being considered with the possibility to apply it into the development of fishing vessels, some work on itreported in [37]. If it is successful, it can help thousands of Indonesian fishermen to survive as well

*** Corresponding author:** Pramudya I Santosa, PhD student, research fields: naval architect and shipbuilding engineering and renewable energy. E-mail: mpic_pramudya@yahoo.com

.

as to reduce the effect of GHG hence cleaner and fresher.

2. LITERATURE REVIEW

2.1 The Catamaran Vessel

It has been reported in many papers that there is an increase growth on safer and more efficient ships and in particular as passenger carriers. Various types of vessel are further developed in order to satisfy those criteria. Among others, the concept of catamaran is preferred and becoming more popular [8][9][13][36]. In more details, the catamaran has unique characteristics in terms of stability, resistance, and seakeeping. Because the total width of catamaran is larger than that of equal monohull, this ship has better transverse stability [8].

2.2. Stability

Transverse Stability of vessel depends on KB, BM, KG and GM. Since Metacentre (M) is at the intersection of vertical lines through the centres of buoyancy in the initial and slightly inclined positions. GM is the most important.

As shown in Figure (A) and (B), a righting couple being formed when the vessel is heeled by the external force. The lever of the couple is known as the GZ or Righting lever. Stability or statical stability is the ability of a vessel to return to her initial position after being forcibly inclined. Moment of statical stability or righting moment is a measure of the vessel's ability to return to her initial position. It is always W*GZ tonnes-metres.

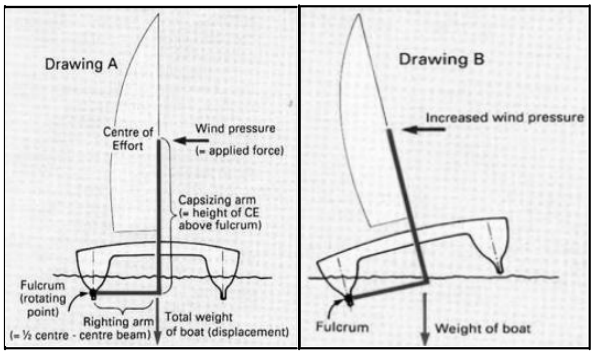

Fig.3 (A,) (B) - shows in a simple lever diagram the forces that act on a catamaran when sailing. (Source : Catamaran Stability, By James Wharram and Hanneke Boon,1991)

To balance :

W Boat x Right arm = Wind press x Capsize arm	(5)
(Righting moment) (Capsizing moment)	

3. METHODE

Stability analysis use Froude-Krylov Method.

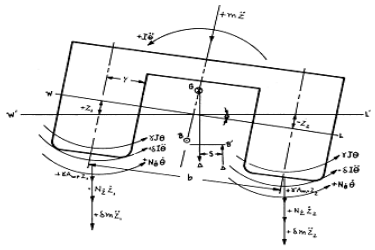

Fig.4 – Catamaran Moments and Forces

Useful formulae [34] :

$KM = KB + BM$ (6), $KM = KG + GM$ (7)

Substitute (6) to (7) : $GM = KB + BM - KG$ (8)

For a ship-shaped vessel : $KB \sim 0.535 \times d$ at each WL (9)

For a ship-shaped vessel : $BM_T = C_W^2 \times B^2/12 \times d \times C_B$ (10)

For a ship-shaped vessel : $BM_L = 3 \times C_W^2 \times L^2/40 \times d \times C_B$ (11)

$GZ = GM \times \sin\theta$ (12)

Righting moment = W x GZ (13)

$GZ = \sin\theta(GM + (BM \times \tan^2\theta)/2$ (14)

Useful formulae [35]:

Displ (mLDC) = 2 × BWL x LWL× T c × C p × Cm × 1025 (15)

Lwt (mLCC)= 0.7 × mLDC, after Construction (16)

Lwt (mmoc) = 0.8 × m LDC, for stability (17)

BMT = 2[(BWL3 × LWL xCw2 / 12) +(LWL × BWL× Cw x (0.5BCB)2)] ×(1025 / mLDC) (18)

BML = (2×0.92xLWL3×BWL x Cw2)/12 x(1025/mLDC) (19)

4. Result and Discussion

4.1 Set up Technical Data

Particulars of Boat :

Monohull : Lwl : 13.8 m, B : 2.88 m, H : 1.3 m, T : 0.65 m, Disp.: 11.80 ton, Cb : 0.498, Cp : 0,69, Cm : 0,69, Cwp : 0,72.

Catamaran : Lwl : 13.8 m, Bdemihull : 1.318 m, Btotal : 7.118 m, H : 1.44 m, T : 0.694 m, S/L : 0.4, Disp,demihull : 5.9 ton, Disp.total : 11.80 ton, Cb : 0.432, Cp : 0,550, Cm : 0,785, Cwp : 0,72.

4.2 Result

a. S/L = 0.2

Tabel 1 Result stability calc. of Hibrid CFV S/L = 0.2

ϕ'	GM	Stab. Statis	Stab. Dinamis
		GZ	INT
0	2.030	0	0
15	1.840	0.477	0.477
30	0.776	0.388	0.865
45	-0.285	-0.201	0.663
60	-0.898	-0.777	-0.114
75	-1.347	-1.301	-1.415
90	-1.735	-1.735	-3.150

Tabel 1 shown Result stability calcculate of Hibrid CFV S/L = 0.2 use Froude-Krylov Method, and than that result convert to become Stability Curve as shown in fig. 5.

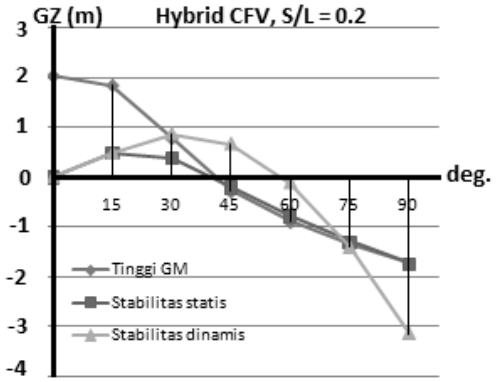

Figure.5 – Stability curve of Hybrid CFV, S/L = 0.2

Analysis :

The value of Initial Stabilty is positif, at Heel angel 0' GM value is 2.030. Pada harga roll angle of 15 'the value of GM fell to 1,840 and the return arm (GZ) has a value of 0.477 as well as the value of the dynamic stability = 0.477. On the roll angle 15 'static stability arm value equal to the value of dynamic stabiltas arms ship. GZ value = 0 at an angle of 46.12 shaky ', the value of GM = 0 at an angle of 38.70 shaky', dynamic stability Sleeve value = 0 at an angle of 48.11 shaky '. This means that the ship is really sinking in value roll angle of 48.11 'because it is intrinsically dynamic stabiltas an energy reserve that is used to return the ship to heel original position. Value of the dynamic stability of the arm is an integral of the value of static stability. According to CB Barras, the measurement arm roll static stability at small angles ($<15^0$) measured at Keel boats, while for large roll angles ($>15^0$) measured at the center of gravity (KG) ship.

b. S/L = 0.3

Tabel 2 Result of stability calc. of Hibrid CFV S/L = 0.3

ϕ'	GM	Stab. Statis	Stab. Dinamis
		GZ	INT
0	7.861	0	0
15	3.747	0.970	0.970
30	2.032	1.016	1.986
45	0.440	0.311	2.298
60	-0.479	-0.415	1.883
75	-1.153	-1.114	0.769
90	-1.735	-1.735	-0.966

Table 2 shows the results of stability calculations were computed using a hybrid CFV Froude-Krylov method, then from these results to curves stability as described in Figure 6.

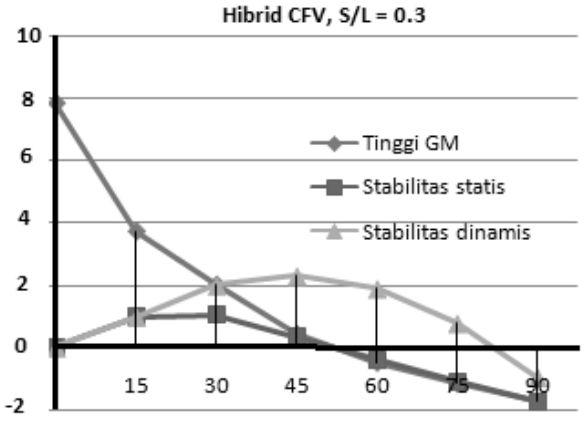

Figure 6. stability curve of Hibrid CFV SL = 0.3

analysis:
initial Stabilty of ship is positive, because the value of the angle 0^0 value of GM = 7,861. At the value of roll angle 15^0 value of GM fell to 3,747 and the return arm (GZ) has a value of 0.970 as well as the value of the dynamic stability = 0.970. On the roll angle 15 'static stability arm value equal to the value of dynamic stabiltas arms ship. GZ value = 0 at an angle of 53.57 shaky ', the value of GM = 0 at an angle of 52.28 shaky', dynamic stability Sleeve value = 0 at an angle of 83.35 shaky '. This means that the ship is really sinking in value roll angle of 83.35 'because in essence it is a dynamic stabiltas energy reserves used to back mengolengkan ship in its original position. Value of the dynamic stability of the arm is an integral of the value of static stability. According to CB Barras, the measurement arm roll static stability at small angles ($<15^0$) measured at Keel boats, while for large roll angles ($>15^0$) measured at the center of gravity (KG) ship.

c. S/L = 0.4

Tabel 3 Result of stability calc. of Hibrid CFV S/L = 0.4

ϕ'	GM	Stab. Statis	Stab. Dinamis
		GZ	INT
0	17.586	0	0
15	5.848	1.515	1.515
30	3.288	1.644	3.158
45	1.165	0.824	3.982
60	-0.061	-0.052	3.930
75	-0.959	-0.926	3.004
90	-1.735	-1.735	1.269

Table 3 shows the results of stability calculations CFV Hybrid S / L= 0.4, calculated using the Froude-Krylov method, then from these results to curves stability as described in Figure 7

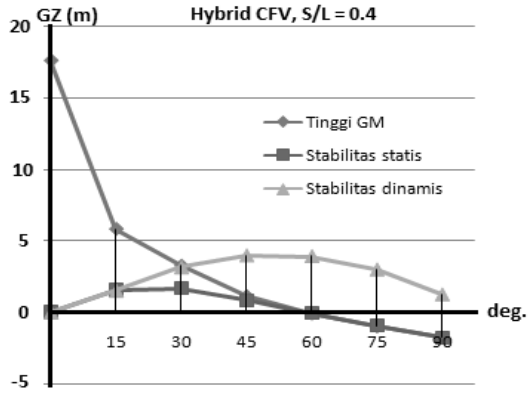

Figure 7. Stability Curve

analysis:

initial Stabilty of ship is positive, because the value of the angle 0 'value of GM = 17 586. At the value of roll angle 15 'value of GM fell to 5,848 and the return arm (GZ) has a value of 1,515 as well as the value of the dynamic stability = 1.515. On the roll angle 15 'static stability arm value equal to the value of dynamic stabiltas arms ship. GZ value = 0 at an angle of 45.89 shaky ', the value of GM = 0 at an angle of 45.74 shaky', dynamic stability Sleeve value = 1,269 m at an angle of roll 90 '. This means that the ship is really sinking in value roll angle> 90 'because it's intrinsically dynamic stabiltas an energy reserve that is used to return the ship to heel its original position. Value of the dynamic stability of the arm is an integral of the value of static stability. According to CB Barras, the measurement arm roll static stability at small angles (<15 ') measured at Keel boats, whereas for large roll angles (> 15 ') measured at the center of gravity (KG) ship.

d. Monohull – hybrid

Tabel 3 Result of stability calc. of Monohull-Hybrid

ϕ'	GM	Stab. Statis	Stab. Dinamis
		GZ	INT
0	-0.974	0.000	0.000
15	0.584	0.151	0.151
30	-0.116	-0.058	0.093
45	-0.819	-0.579	-0.486
60	-1.225	-1.061	-1.546
75	-1.522	-1.470	-3.017
90	-1.779	-1.779	-4.796

Table 4 shows the results of stability calculations Monohull-hybrid was calculated using the Froude-Krylov methods, the results described later became its stability curve as shown in figure 8.

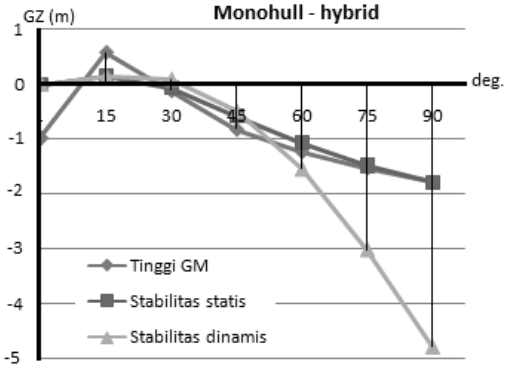

Figure 8. Stability Curve

Analisis :

initial Stabiltas of ship is negative, because the value of the angle 0 'value of GM = -0974. At the value of roll angle 15 'GM value increased to 0.584 and the return arm (GZ) has a value of 0.151 as well as the value of the dynamic stability = 0.151. On the roll angle 15 'static stability arm value equal to the value of dynamic

stabiltas arms ship. GZ value = 0 at 19:16 wobble angle ', the value of GM = 0 at 16:35 wobble angle', the dynamic stability Sleeve value = 0 at an angle of 42.59 shaky '. Since the beginning of the ship had experienced unstable equilibrium, so the stability condition of the vessel from the beginning was not bad need of further analysis.

4.3 Discussion

Resume

Descript	Initial Stab	Capsize degree			Remark
		GM	S-S	S-D	
S/L=0.2	Positif	46,12’	38.70’	48,11’	Capsize degree 48,11’
S/L=0.3	Positif	52.28’	53,57’	83.35’	Capsize degree 83,35’
S/L=0.4	Positif	45.74’	45.89’	> 90’	Capsize degree >90’
Monohl	Negatif	16.35’	19.16’	42.59’	Capsize degree 0’

Note : GM=Distance of Gravity Metacentre, S-S=Static Stability, S-D=Dynamic Stability

5. Conclusions

The development of hybrid vessel gave a promising hope. Application of hybrid technology is very useful when applied to catamaran fishing vessels The Hybrid CFV S/L= 0.4 have capsizing degree more than 90’ with initial stability is positive. KMt value is 17.586 m. . In more details, the catamaran has unique characteristics in terms of stability because the total width of catamaran is larger than that of equal monohull, this ship has better transverse stability.

Acknowledgments

The Authors would like to thank DP2M-Dikti of the Minister of Education and Culture of the Republic of Indonesia for funding the research under a research scheme called International Research Collaboration 2013-2014.

References

[1] Daniel, D and Chandra, H, *An Investigation into the Application of Solar Cell as Energy Resource to Power Vesses without Fuel*, Final Report of the PKPP Incentive Program (in Indonesian), 2010.

[2] Al-Harahsheh, A and Shawabkah, R, *SO2 Removal by Using Jordanian Oil Shale Ash*, 27th Oil Shale Symposium, Colorado School of Mines, 15-17 October 2007.

[3] Utama, IKAP and Molland, A F, *The Powering of Future Ships Taking Into Consideration Economic Viability and Environmental Issues*, ICSOT, Ambon, 7-8 November, 2012.

[4] Daniel, D and Chandra, H, *The Evaluation of Solar Power on Sea Trial Results of Catamaran Boat*, Jurnal Kelautan Nasional (in Indonesian), 2011.

[5] Satchwell, C J, *Windship Technology and Its Application to Motor Ships*, Transactions RINA, Vol. 131, 1989.

[6] Molland, A F, Turnock, S R and Hudson, D A, *Design Metrics for Evaluating the Propulsive Efficiency of Future Ships*, IMDC, Trondheim, Norway, 2009.

[7] Fry, E D and Graul, T (1972), *Design and Application of Modern High-Speed Catamarans*, Marine Technology, Vol.9, No.3, pp 345-357

[8] Utama, I K A P, *An Investigation into the Viscous Resistance Components of Catamarans*, PhD Thesis, University of Southampton, UK, 1999.

[9] Murdijanto, Utama, I K A P and Jamaluddin, A, *An Investigation into the Resistance/Powering and Seakeeping Characteristics of River Catamaran and Trimaran*, Makara Seri Teknologi, Vol 15, No. 1, April 2011

[10] IMO (2000). Marine Environmental Protection Committee. 44th session available at: http: www.imo.org/meeting/44.html.

[11] IMO. Guidelines on the method of calculation of the Attained Energy Efficiency Design Index (EEDI) for new ship. Resolution of the Marine Protection Environment Committee, MPEC212(63), 2012.

[12] IMO. Guidelines on Survey and Certification of the Energy Efficiency Design Index (EEDI). Resolution of the Marine Protection Environment Committee, MPEC214(63), 2012.

[13] Insel, M dan Molland, A F (1991), *An Investigation into the Resistance Components of High Speed Displacement Catamarans*, Meeting of the Royal Institution of Naval Architects.

[14] Marchaj, C A, *Sailing theory and practice*, Adlard Coles ltd, 1977.

[15] Claughton, A, Wellicome, J and Shenoi, R A (editors), *Sailing yacht design: theory*, Addison Wesley Longman Ltd, 1998.

[16] Claughton, A, Wellicome, J and Shenoi, R A (editors), Sailing *yacht design: practice*, Addison Wesley Longman Ltd, 1998.

[17] Nasirudin et al, Analysis of Size and Shape sail Type of Purse Seine Fishing Vessel; KM Maju Case Study. ITS,Surabaya, Indonesia, anasirudin@na.its.ac.id (in indonesia), 2009

[18] en.wikipedia.org/wiki/*Electric_boat*, retrieved 1 August 2012.

[19] Electrical Review Vol. 201 No. 7, 12 August 1977.

[20] Ru-Min Chao, Shih_Hung Ko, Photovoltaic dynamic MPPT on a moving vehicle, SciVerse Science Direc Solar Energy 86, 2013

[21] http://www.dasolar.com/solar-energy/solar-powered-boats

[22]http://www.nauticexpo.com/prod/aussiecat/power-catamarans-out-board-center-console-boats-twin- engine – 20734 - 47262.html

[23] Burnett, R F, *Wave energy for propelling craft – nothing new*, the Naval Architect, November 1979.

[24] Bose, N and Lien, J, *Energy absorption from ocean waves: a free ride for cetaceans*, Proceedings of the Royal Society of London, Volume B 240, pages 591-605, 1990.

[25] Vrooman, D, *Vibrating propeller*, US Patent 22, 097.Patented November 15, 1858.

[26] Schulze, O, *Wave motor*, US Patent, 1,033,476, Filed January 5, 1911, Patented July 23, 1912.

[27] Geoghegan, J J, *Boat, moved only by waves, sails to a seafaring first*, the New York Times, July 8, 2008.

[28] Jakobsen, E, *The foil propeller, wave power for propulsion*, Second international symposium on wave and tidal energy, 1981.

[29] Popular Science, *Wave runner*, March 2008, retrieved December 3, 2011.

[30] Utama, IKAP, Murdijanto and Yoghi, A, *Wave power mechanism to power catamaran*, 1st APTECS, Surabaya, December 2009.

[31] Geoghegan, J J, *Boat, moved only by waves, sails to a seafaring first*, the New York Times, July 8, 2008.

[32] Setyawan, D, Utama, I K A P, Murdijanto, Sugiarso, A and Jamaluddin, A, *Development of catamaran fishing vessel*, IPTEK – the journal for technology and science, Vol. 21, No. 4, November 2010.

[33] WINDTECH'85, International symposium on windship technology, University of Southampton UK, 1985.

[34]. Barrass C. B., Ship Stability for Masters and Mates, Sixth edition – Consolidated 2006

[35] Helmes T., Catamaran design, 2012]

[36] Dynamics G., Vol. II Catamaran study, 1969

[37] P I Santosa, I K A P Utama, W D Aryawan, D B Purwanto, R-M Chao, A Nasirudin, An Investigation into Hybrid Catamaran Fishing Vessel: Combination of Diesel Engine, Sails and Solar Panels, International Seminar on Applied Technology, Science, and Art (4th APTECS 2013).

[38] IKAP Utama, PI Santosa, RM Chao, A Nasirudin, New Concept of sola-powered Catamaran Fishing Vessel,

2013

[39] Pramudya Imawan Santosa and I Ketut Aria Pria Utama, Further study into the development of hybrid catamaran fishing vessel, Oceanic International Seminar- Situbondo, 2013.

Selecting Monohull, Catamaran and Trimaran as Suitable Passenger Vessels Based on Stability and Seakeeping Criteria

Richard B Luhulima [1], D Setyawan [2], and I K A P Utama [3]

1. *PhD Student Dept. of Naval Architecture and Shipbuilding Engineerin, Institut Teknologi Sepuluh Nopember (ITS), Indonesia*
2. *Senior Lecturer Dept. of Naval Architecture and Shipbuilding Engineering, Institut Teknologi Sepuluh Nopember (ITS), Indonesia*
3. *Professor Dept. of Naval Architecture and Shipbuilding Engineering, Institut Teknologi Sepuluh Nopember (ITS), Indonesia*

Abstract: The current paper describes the selection of monohull, catamaran and trimaran in order to operate as passenger vessel for calm water and oblique wave conditions. The three modes were built and modified based on the previous models developed at ITS which was applied for river and coastal areas. The analysis is focused on the evaluation of stability and seakeeping criteria. The stability criterion is based on IMO regulation and the seakeeping criterion is solved using Maxsurf and CFD analysis. The whole results are compared each other together with comparative analysis with published data in order to find out the most suitable vessel mode for the indicative seawaters.

Key words: monohull, catamaran, trimaran, stability, seakeeping, CFD

1. Introduction

Multihull vessels have been centre of attention in the last thirty years for their applications as passenger vessels, sporting craft, and oceanographic research vessels [1] and [2]. Reference [3] later developed catamaran form for the application of fishing vessels. The reasons behind the progressive development are due to the advantages of multihulls (catamaran and trimaran) such as their ability to provide lower drag and hence the size of main engine compared to monohull of similar displacement, having wider deck area and better transverse stability [2].

Multihull vessels also show good seakeeping characteristics compared to monohull type of vessel. Reference [4] conducted research on the seakeeping characteristics of catamarans in deep water, whilst Reference [2] investigated the seakeeping characteristics of catamaran and trimaran for river and coastal operation at Indonesian waters. However, both of them discovered that the seakeeping characteristics of catamaran, in particular, are rather poor in oblique waves. This is attributed to the configuration of catamaran when heeling aside due to rolling motion, the stability of catamaran relies only on the demihull, which is still underwater.

There are several tools that can be used to investigate the seakeeping characteristics of ships, including catamaran and trimaran, namely: (1) theoretical investigation, (2) the use of experimental model test, (3) the use of commercial software – Seakeepers from Maxsurf, and (4) the use of CFD package – ANSYS AQWA. The current paper is focused on the stability evaluation and seakeeping analysis of monohull and multihulls.

2. Ship Hull Form

The current work used a modified model which is developed by [2]. The previous models were designed for calm water condition such as river and coastal waters. In fact, slight modification was made to make it fit with oblique wave condition. Complete investigation was also included with the seakeeping characteristics of monohull for comparison purposes with the multihulls.

Body plan of the monoull is shown in Figure 1 together with its principal particular in Table 1.

*** Corresponding author:** Richard B Luhulima, PhD student, research fields: naval architect and shipbuilding engineering and renewable energy. E-mail: richard_luhulima@yahoo.com

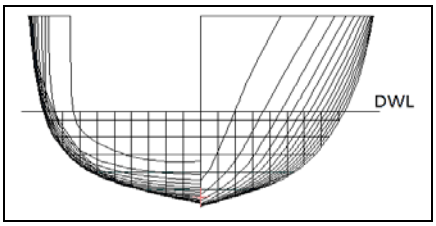

Figure 1 - Body plan of monohull

Table 1 Data particular of monohull

L (m)	B (m)	T (m)	V (knots)	C_P	L/B	B/T
68.55	11.93	3.24	20	0.79	5.75	4.10

Body plan of catamaran and trimaran were shown in Figures 2 and 3 and their particulars were given in Tables 2 and 3.

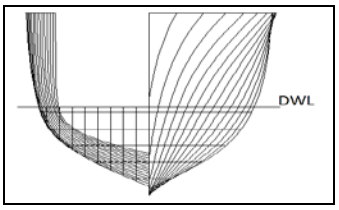

Figure 2 - Body plan of demihull catamaran

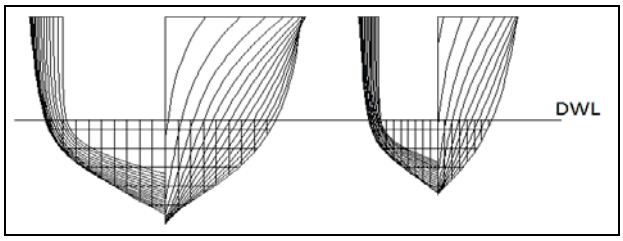

Figure 3 - Body plan of main-hull and side-hull of trimaran

Table 2: Data particular of demihull catamaran

L (m)	B (m)	T (m)	V (knots)	C_P	L/B	B/T
72.12	36.80	3.24	20	0.66	1.96	11.35

Table 3: Data particular of trimaran

L (m)	B (m)	T (m)	V (knots)	C_P	L/B	B/T
72.12	48.14	3.59	20	0.63	1.98	13.40

3. Stability Analysis

The term stability refers to the tendency of a body or system to return to its original state after it has suffered a small disturbance [5]. If a floating body is very stable it will return quickly to the upright and may produce motion sickness; if it is just stable a disturbance which is not small may cause it to capsize. The stability therefore must be just right in the range of conditions in which a vessel may find itself during its operation and life, even damaged or mishandled.

Transverse stability of a vessel depends on KB, BM. KG and GM. Since Metacentre (M) is at the intersection of vertical lines through the centres of buoyancy in the initial and slightly inclined positions, GM is the most important component.

The value of metacentre can be calculated as [5]:

$$KM = KB + BM \quad (1)$$

Where:

$$KB = 0.535T$$

$$BM_T = \frac{C_{WP}^2 B^2}{12TC_B} \quad (2)$$

The empirical value of KB was given by [6]. The values of BM for monohull, catamaran and trimaran can be obtained from the data given in Tables 1 to 3.

For monohull:

$$BM_T = \frac{0.79^2 x\, 11.93^2}{12 x\, 3.24 x\, 0.79 x\, 0.785} = 3.68 \text{ m}$$

For catamaran:

$$BM_T = \frac{0.79^2 x\, 36.8^2}{12 x\, 3.24 x\, 0.79 x\, 0.785} = 35.05 \text{ m}$$

For trimaran:

$$BM_T = \frac{0.79^2 x\, 48.14^2}{12 x\, 3.59 x\, 0.79 x\, 0.785} = 54.14 \text{ m}$$

Furthermore, the value of GZ at small angle (less than 15^0) and the righting moment are respectively:

$$GZ = GM\, x\, \sin\theta \quad (3)$$

$$Righting\ Moment = W\, x\, GZ\, x\, \sin\theta \quad (4)$$

The height of the initial metacentre above the keel (KM) depends upon a ship's underwater form. The vertical distance between G and M is referred to as the metacentric height. If G is below M, the ship is said to have positive metacentric height, and if G is above M the metacentric height is said to be negative.

Furthermore, during its voyage a ship can experience heeling and listing conditions [5]. A ship is said to be heeled when the ship is inclined by an external force, for example, when the ship is inclined by the action of the waves or wind. A ship is said to be listed when the ship is inclined within the ship, for example, when the ships is inclined by shifting a weight transversely within the ship. Catamaran and trimaran, which has higher BM, GM and GZ values, will have better characteristics on heeling and listing conditions.

4. Seakeeping Evaluation

Performance of ship at sea is popularly called seakeeping. This is among the most important factors when comparing competing vessels or types of vessel. This is due to the seakeeping criteria, which can influence important aspects such as passenger comfort, operational limits, speed loss and structural integrity [5].

Motion transfer functions for each vessel and wave energy spectra for the relevant sea area are necessary to perform spectral calculations. Reference [7] provides good information about wave spectrum of Indonesian water. This allows the calculation of statistical quantities such as the RMS values of the various motions and accelerations and the probabilities of an individual motion or acceleration exceeding a given value. This also assists ship designers to estimate vessel's seakeeping characteristics more realistic.

Seakeeping is simply known as the motions of ship at sea which is affected by external wave forces. Seakeeping is expressed as Figure 4 and consist of 3 sets of translational motions and 3 sets of rotational motions. The translational motions include heave, sway and surge, whereas rotational motions contain pitch, roll and yaw. Table 3 further describes the calculation of response of amplitude operator (RAO).

Examples of seakeeping estimation by using commercial software and CFD code were described. Three types of vessels were investigated: monohull, catamaran and trimaran. The tests were conducted at sea state 3 and 5 and represented calm water and oblique wave conditions.

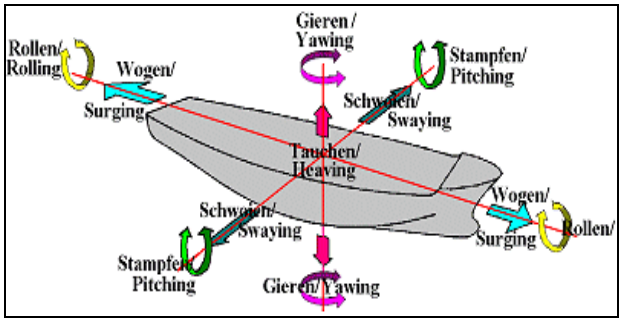

Figure 4 - 6 degrees of freedom of ship motions

Table 4 RAO equations of ship motion

No	Translational motion	RAO	No	Rotasional Motion	RAO
1	Surge	$(x_a/\delta_a)^2$	4	Roll	$(\emptyset_a/\delta_a)^2$
2	Sway	$(y_a/\delta_a)^2$	5	Pitch	$(\Theta_a/\delta_a)^2$
3	Heave	$(z_a/\delta_a)^2$	6	Yaw	$(\Phi_a/\delta_a)^2$

Surge and sway motions are motion of ship which accelerates and decelerates the motion of ship to move forward and backward from a certain position. Heave motion involves linear and vertical motion of going up and down. Similarly, pitch motion is also a motion which goes up and down but making a curve direction or a rotational motion. Roll motion involves motion from side to side of ship, whilst yaw motion involves rotational movement in vertical axis.

Based on the Second Law of Newton, the equation of motion of floating structure in 6 degrees of freedom can be expressed as follows:

$$F = Ma \tag{5}$$

Where:

F : resultant force on the structure

M : mass of structure

a : acceleration

Equation (1) can be written in other form, where the body acceleration (a) is the second differential of the body or structure position.

$$F = M\ddot{x} \tag{6}$$

Resultant of forces work on the structure consists of buoyancy and external forces. External forces comprise excitation and radiation forces. The mathematical equation can be written as follows:

$$FWJ + FRJ + FHSJ = M\ddot{x} \tag{7}$$

In order to estimate the seakeeping qualities of a vessel, the hydrodynamics responses of the vessel to hydrodynamics loading, must be known. At least two information, namely speed of vessel and wave angle of entrance, must be available [8]. Thus, the wave frequency within the operational area of the vessels can be found and this lead to the calculation of wave's magnitude. The behaviour of vessel is found based on the probability movement of the ship at the certain agreed level. The seawater condition is described using statistical model hence the wave height and wave energy will be known in relation with frequency and angle of entrance of the wave.

Furthermore, in order to estimate ship motion, the following items must be known: excitation force, added mass and damping radiation as functions of frequency and heading angle. Thus, the response amplitude operator (RAO), which is also known as transfer function, is obtained.

4.1 Heave Motion

Results from the calculation using ANSYS AQWA for each type of vessels at Froude Number (Fr) of 0.3 show that the trimaran at zero incidence has the most excessive heaving motion of about 0.43m. Similarly,

the calculation using Maxsurf code also provided the same condition, in which the displacement is about 0.58m. Other type of hull forms (monohull and catamaran) produce less heaving motions at the values of 0.47m and 0.14m (using Maxsurf) and 0.12m and 0.21m (using AQWA), respectively.

Table 5 Heave motion at sea state 5and Fr 0.3

Tool	Vessel type	Heave at various wave angle (m) 0	45	90	135	180
Maxsurf	Monohull	0.47	0.55	0.72	0.63	0.57
	Catamaran	0.14	0.12	0.18	0.19	0.19
	Trimaran	0.58	0.28	0.25	0.23	0.24
AQWA	Monohull	0.12	0.43	0.56	0.16	0.44
	Catamaran	0.21	0.03	0.26	0.06	0.11
	Trimaran	0.43	0.17	0.36	0.15	0.13

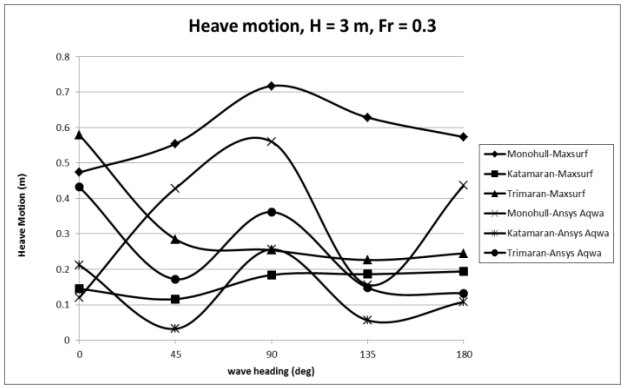

Figure 5 - Heave motion at sea state 5 and Fr 0.3

4.2 Pitch Motion

Results from the calculation using ANSYS AQWA for each type of vessels at Froude Number (Fr) of 0.3 demonstrate that the trimaran at zero incidence has the most excessive pitching motion of about 11.08 degrees at wave height about 5m (Figure 6).

Similarly, the calculation using Maxsurf code also provided the same condition, in which the displacement is about 11.77 degrees. Other type of hull forms (monohull and catamaran) produces less significant pitching motions.

Figures 5 and 6 demonstrated that the catamaran form has lower heave and pitch motions and this is attributed the effect of its width. The smaller the distance between hulls, the lower the response of heave and pitch. Monohull type of vessel, in general, has lower response at low frequency such as reported in [4].

Table 6 Pitch motion at sea state 5 and Fr 0.3

Tool	Vessel type	Pitch at various wave angle (degrees) 0	45	90	135	180
Maxsurf	Monohull	1.25	1.19	0.57	1.39	1.58
	Catamaran	1.78	0.86	0.55	0.75	0.86
	Trimaran	11.77	1.66	0.67	0.82	0.95
AQWA	Monohull	1.36	0.99	0.08	0.49	1.41
	Catamaran	0.94	0.56	0	0.63	0.49
	Trimaran	11.08	1.63	0.28	0.5	0.5

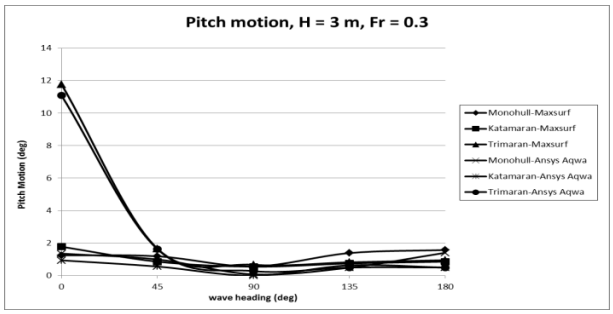

Figure 6 - Pitch motion at sea state 5 and Fr 0.3

The ship motion both for monohull and catamaran is significant when the direction of wave is from leeside (between 0 and 90 degrees) against the movement of ship. In details, Reference [9] stated that the motion of catamaran at S/L=0.2 was 18% lower than the motion of catamaran at S/L=0.4 at heading angle of 120 degrees. Fast catamaran has good characteristics at oblique wave condition and including at pitching motion condition. However, when wave comes from the side of vessel, the motion of catamaran is lower compared to the motion of monohull. This is believed to be due to the catamaran has relatively low rolling period [10].

4.3 Roll Motion

Results from the calculation using ANSYS AQWA for each type of vessels at Froude Number (Fr) of 0.3 demonstrate that the monohull at 90 degrees (beam sea condition) has the most excessive rolling motion of about 8.51 degrees at wave height about 5m (Figure 7).

Similarly, the calculation using Maxsurf code also provided the same condition, in which the displacement is about 8.61 degrees. Other type of hull forms (trimaran and catamaran) produces less significant pitching motion those are 1.14 and 4.07 degrees, respectively.

Table 7 Roll motion at sea state 5 and Fr 0.3

Tool	Vessel type	Roll at various wave angle (degrees) 0	45	90	135	180
Maxsurf	Monohull	0	4.16	8.61	5.13	0
	Catamaran	0	2.06	4.07	3.33	0

	Trimaran	0	1.97	4.41	3.11	0
Aqwa	Monohull	0	3.84	8.51	4.32	0
	Catamaran	0	0.8	1.14	0.8	0
	Trimaran	0	0.39	0.64	0.21	0

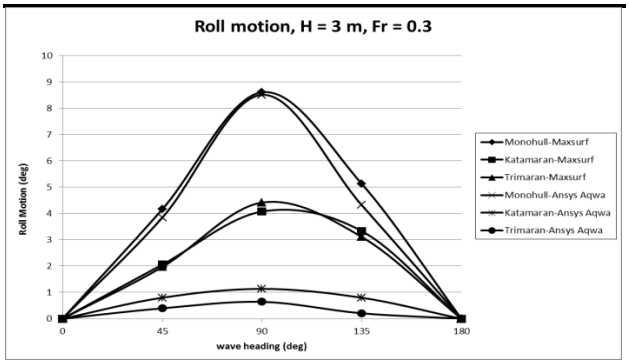

Figure 7 - Roll motion at sea state 5 and Fr 0.3

5. Conclusions

The current research has investigated the stability and seakeeping characteristics of monohull, catamaran, and trimaran. The stability analysis based on static stability was calculated using standard naval architecture criteria, whilst the seakeeping analysis was estimated using Maxsurf and ANSYS AQWA.

It is shown, from stability evaluation that both multihulls (catamaran and trimaran) has higher values of BM, GM and hence GZ thus causes the multihulls to be more stable than the monohull as well as providing better heeling and listing characteristics for the multihulls.

In terms of seakeeping, multihull vessels also demonstrate better characteristics on heave, pitch and roll motions. Both commercial softwares (Maxsurf and ANSYS AQWA) show similar results on the estimation of ship's seakeeping.

Acknowledgement

The authors wish to thank the Institute Technology of Sepuluh Nopember (ITS) for granted the current research under a scheme known as Laboratory Research Grant of the fiscal year 2013-2014.

References

[1] Molland, A.F. (2008), *A Guide to Ship Design, Construction and Operation*, The Maritime Engineering Reference Book, Butterworth- Heinemann, Elsevier.

[2] Murdijanto, Utama, IKAP and Jamaludin, A (2011), An Investigation into the Resistance/Powering and Seakeeping Characteristics of River Catamaran and Trimaran, *Makara Seri Teknologi*, Vol. 15, No. 1.

[3] Setyawan D., Utama I K. A. P., Murdijanto, Sugiarso A., Jamaluddin A. (2010), Development of Catamaran Fishing Vessel, IPTEK The Journal for Technology and Science, Surabaya, Indonesia

[4] Molland, A.F., Couser, P. R., and Wellicome, J. F.. (1995), *Experimental Measurement of the Seakeeping Characteristics of the Fast Displacement Catamaran in Long- Crested Head-Seas*, Ship Science Report, University of Southampton, UK.

[5] Rawson, K. J. And Tupper, E. C. (2001), Basic Ship Theory, Vol. 1, Longman Scientific and Technical, London, UK.

[6] Barrass, C. B. (2001), Ship Stability; notes & examples. ISBN; 0750648503. Plantatree. British

[7] Kurniawan, A. (2012), Long Term Wave Analysis Of Irreguler Wave For Long Term Sea State And Short Term Wave Analysis Using Fourier Transform for Spectrum Parametric Modification of Indonesian Waterways, M.Sc Thesis, Faculty of Marine Technology, ITS Surabaya, Indonesia

[8] Bhattacaryya, R. (1978), Dynamics of Marine Vehicles, John Wiley and soon, Toronto, Canada

[9] Wellicome P., Temarel P., Molland A.F., Cic J. and Taunton D.J. (1999), *Experimental Measurement of the Seakeeping Characteristics of the Fast Displacement Catamaran in Oblique Waves*, Ship Science Report, University of Southampton, UK.

[10] NATO Naval Group 6 (2009), Specialist Team on Small Ship Design, NATO Working Paper.

[11]

- SESSION 9 -

DAMAGE STABILITY STANDARD OF OLD SHIPS

Application of Second Generation IMO Intact Stability Criteria to Medium – Sized Fishing Vessels

Marcos Míguez González [1*], Vicente Díaz Casás [1], Luis Pérez Rojas [2], Fernando Junco Ocampo [1] and Daniel Pena Agras [1]

1. *Integrated Group for Engineering Research, University of A Coruña, Spain*
2. *Model Basin, ETSIN, Madrid Polytechnic University, Spain*

Abstract: In this work, a sample application of the draft criteria proposed in SLF 55/WP.3 for assessing pure loss of stability, parametric roll and broaching failure modes to medium sized fishing vessels, is presented. The sampled vessels consist of seven ships, including trawlers, longliners and purse – seiners, with lengths between 20 and 70 meters. This sample can be representative of the mid – sized Spanish current fishing fleet, including ships with quite different operative profiles and which are supposed to be safe from the static stability point of view (as they all comply with Torremolinos Protocol Requirements). On them, both loss of stability and parametric roll level 1 and 2 checks and broaching level 1 check have been carried out, analyzing the vulnerability of the different typologies to the three failure modes. Moreover, some comments regarding the applicability of these criteria to these types of ships and their use as a design tool to improve fishing vessels safety are included.

Key words: Second generation intact stability criteria, parametric roll, pure loss of stability, fishing vessels stability.

1. Introduction

Fishing is one of the industrial sectors with a higher number of fatalities, ranking between the most dangerous activities in many countries, such as the U.S., the U.K. or Spain [1]. Most of the accidents affecting the Spanish fleet of medium – sized vessels are due to stability issues (large heel and capsizing), usually due to reduced initial stability levels and crew lack of training in these matters. However, it is also well known that dynamic stability issues which affect this type of ships, such as parametric roll, broaching or loss of stability in stern seas, are not covered by any mandatory criteria. In addition, the ship tendency to being affected by one of these phenomena is not usually analyzed at any stage of its design.

The objective of the second generation intact stability criteria, is to set up methods which are aimed at evaluating the vulnerability of ships to some failure modes, mainly related to the aforementioned dynamic stability, which are not covered by existing criteria. Five are the failure modes under consideration, including loss of stability in stern seas, parametric resonance, broaching, dead ship condition and excessive accelerations.

These criteria, for each of the failure modes, follow a three-layer structure; the first one includes simple and easy to calculate criteria. If the ship fails to pass this first layer, a second one has to be evaluated, where a more accurate evaluation is proposed. Finally, if the vessel is considered as vulnerable under these two levels, a direct stability assessment is proposed, consisting on carrying out a detailed analysis of the ship behavior in the different sailing conditions and developing operational guidelines.

Work underdone in the last years in the SLF Sub - Committee of the IMO, which mainly began in 2005 during the 48th session of the SLF, involved the study and development of the requirements for each of the failure modes. An overview of the process could be found in [2]. In the SLF 55th session in 2013, agreement on pure loss of stability, parametric roll, broaching and dead ship stability modes was obtained

*** Corresponding author:** Marcos Miguez Gonzalez, Assistant Professor, research fields: parametric roll, ship stability. E-mail: mmiguez@udc.es

[3], although some points remained undecided. Excessive accelerations criteria were still not defined.

Although considered within then, second generation criteria are mainly focused on cargo and passenger vessels and not on fishing vessels. In fact, most of the applicability studies include only a few vessels of this type (three vessels in [4] and [5], two in [6]). One characteristic of the fishing fleet is its vast heterogeneity, as their typology largely changes depending on the fishing equipment and also depending on the geographical location under analysis (due to the existent regulatory framework and design tradition in that area). This fact makes it very difficult to generalize the obtained results for a small sample to the different typologies and locations.

The main objective of this work is to carry out a sample application of the current draft of the second generation stability criteria (contained on SLF 55/WP.3 [7]) to Spanish medium/large sized fishing vessels, in order to analyze its applicability and its possible use as a design tool to improve the fleet safety. The failure modes under consideration are pure loss of stability, parametric roll and broaching.

The sampled vessels are representative of the medium/large sized Spanish current fishing fleet. It includes ships with quite different operative profiles, and which are supposed to be safe from the static stability point of view (they all comply with Torremolinos Protocol requirements, in force in Spain for all fishing vessel of more than 12 meters). Moreover, some additional information regarding the dynamic behavior in waves of some of the vessels is also available, which can contribute to the analysis of the applicability of the criteria.

On all of them, both loss of stability and parametric roll Level 1 and 2 checks and broaching Level 1 check have been carried out, analyzing the vulnerability of the different typologies to the three failure modes.

2. Sample Vessels

The Spanish fishing fleet ranks first in terms of tonnage among all the UE countries, and it is composed by nearly 10.000 vessels [8]. From these, more than 540 vessels have lengths of more than 24 meters, and more than 900 have lengths of between 20 and 24 meters [9]. The fleet is divided mainly in seven vessel types: medium sized fresh trawlers, large freezer trawlers, medium sized coastal purse seiners, large tuna purse seiners, medium sized long liners and large freezer longliners and finally medium sized fixed fishing gear vessels.

This study has been performed on a series of fishing vessels representative of the aforementioned fleet, including two medium-sized trawlers, one large freezer trawler, one longliner, one medium sized purse seiner and one large tuna purse seiner. In addition, and for the sake of comparison, the well known TS trawler has been also included in the sample, although its arrangement doesn´t follow the Spanish standards.

From the above described vessels, towing tank tests in different conditions are available for a medium sized trawler [10,11] (named Trawler 2 in this work) and for the TS vessel [12].

Moreover, as fixed fishing gear vessels usually operate in coastal and protected waters, and its number is not very large, they have been excluded from this analysis.

The main characteristics of the analyzed vessels are included in Tables 1 and 2.

2.1 Tested conditions

In all cases, and in order to obtain a more conservative result, ships have been considered not to be equipped with bilge keels. Moreover, design speed has been the one considered in all cases to compute the reference ship speed (V_{PR}).

Table 1 Vessel characteristics (1)

Vessel	L_{Pp} (m)	B (m)	d (m)	C_b
Trawler 1	25,70	8,50	3,25	0,56
Trawler 2	29,00	8,00	3,30	0,57
Large Trawler	60,60	12,50	4,60	0,54
Longliner	24,00	8,20	3,20	0,68
Purse Seiner	21,00	7,00	2,70	0,67
Tuna Purse Seiner	67,60	14,00	4,80	0,53

TS Trawler (d_1)	22,00	6,90	2,30	0,47
TS Trawler (d_2)	22,00	6,90	2,46	0,48

Table 2 Vessel characteristics (2)

Vessel	L/B	B/D	D/d
Trawler 1	3,02	1,51	1,73
Trawler 2	3,63	1,38	1,76
Large Trawler	4,85	1,63	1,66
Longliner	2,93	1,41	1,81
Purse Seiner	3,00	2,19	1,19
Tuna Purse Seiner	4,83	1,54	1,90
TS Trawler (d_1)	3,19	2,06	1,46
TS Trawler (d_2)	3,19	2,06	1,36

Finally, regarding the loading conditions under analysis, the design draft has been the one considered. In the cases in which the real sailing conditions of the ship were available, the minimum GM of the different conditions has been selected for testing. Moreover, an additional IMO minimum required GM value of 350 mm has been also tested in these cases. For those ships with unknown sailing situations, the minimum required GM value for complying with the IMO Torremolinos Protocol (350 mm), has been considered.

3. 2nd Generation Intact Stability Criteria

As it has been already mentioned, 2nd generation intact stability criteria present a three tier structure for all of the five failure modes.

Table 3 Tested Conditions

Vessel	Fn	d (m)	GM_T (m)
Trawler 1 LC1	0,32	3,25	0,653
Trawler 1 LC2	0,32	3,25	0.350
Trawler 2	0,31	3,30	0,350
Large Trawler	0,31	4,60	0.350
Longliner LC1	0,34	3,20	0,495
Longliner LC2	0,34	3,20	0,350
Purse Seiner	0,36	2,70	0,350
Tuna Purse Seiner LC1	0,34	4,80	0,916
Tuna Purse Seiner LC2	0,34	4,80	0,350
TS Trawler LC1	0,32	2,30	0,730
TS Trawler LC2	0,32	2,46	0,436

In this work, the Levels 1 and 2 of the draft proposal contained in [7] for parametric roll resonance and pure loss of stability failure modes, and Level 1 for broaching, has been applied. The obtained results are shown in the following sections.

3.1 Parametric Roll

Autoparametric roll resonance, parametric roll resonance or simplifying, parametric roll, could be defined as a ship dynamic instability. It is caused by the variation of ship transversal restoring capabilities when waves pass along the hull, together with the effects of the coupling between roll, heave and pitch motion. It reaches its largest intensity in head or stern seas, when wave height exceeds a given threshold and when ship-wave encounter frequency approximately doubles the ship roll natural frequency.

In these conditions, roll motions could increase rapidly up to very large amplitudes, leading, in the worst cases, to the capsizing of the vessel. The intensity of this phenomenon depends also on many other factors, such as ship hull forms, wave amplitude and frequency, roll damping, etc. Of course, the possible consequences that derive from one of these episodes depend on that intensity, but well known incidents have shown that these can be devastating.

Second generation criteria regarding parametric roll resonance are based on the analysis of *GM* variation in longitudinal waves of given values of wavelength and height.

The first level criterion is based on the comparison of the amplitude of the variation of metacentric height as a longitudinal wave of wavelength $\lambda = L$ and wave height $h = L \cdot S_W$ passes the ship (ΔGM), where S_W is a constant wave steepness of 0.0167, with the metacentric height in calm water (GM). Under this condition, the ship is considered vulnerable if:

$$\frac{\Delta GM}{GM} > R_{PR} \tag{1}$$

Where R_{PR} represents roll linear damping, that may be taken as 0.5 or a value dependant on bilge keel area.

The second level is a two tier criterion. Regarding the first check, it is similar to that of the first level criterion; however, in this case *GM* variation is computed for a series of 16 different waves, and compared to the average *GM* on each of the wave cases, weighing the results according to a wave scatter database. Moreover, an additional requirement taking into account the effect of forward speed in the appearance of parametric roll is also considered. According to this first check, the ship will be considered vulnerable if:

$$C1 = \sum_{i=1}^{N} W_i C_i > R_{PR0} \tag{2}$$

Where *Wi* is the wave case weight and *Ci* is a coefficient equal to 1 if the ship is vulnerable under *GM* and speed checks, and 0 if not. *GM* vulnerability checks are the same as those of the first level criterion, but computed for each of the wave parameters. The ship is considered as vulnerable if:

$$GM(H_i, \lambda_i) < 0 \tag{3}$$

$$\frac{\Delta GM(H_i, \lambda_i)}{GM(H_i, \lambda_i)} > R_{PR} \tag{4}$$

The speed requirement consists on comparing the design speed of the ship (V_D) and a reference speed for parametric roll appearance (V_{PRi}), which depends on the metacentric height on waves and calm water, wave conditions and natural roll period. The ship is considered as vulnerable if:

$$V_{PRi} < V_D \tag{6}$$

Finally, the second check has a similar structure to the first check, and the vulnerability of the ship is evaluated obtaining the maximum roll motion of the ship in different head and stern longitudinal waves (306 cases), at different speeds, and by using an uncoupled equation of roll motion.

The ship, according to this two tier method, is considered not to be vulnerable if it complies with the first check or if it complies with the second check after failing the first one.

3.2 Pure Loss of Stability

Pure loss of stability failure mode is, as it happens with parametric roll resonance, caused by the effect of longitudinal waves passing along the hull, subsequently modifying waterplane area. This modification periodically alternates between wider and slender waterplanes (when a wave crest is situated in the ship bow and stern and amidships respectively), and is especially critical when wavelength is similar to ship length. The modification in flotation area implies a variation in transverse stability, which changes as wave passes along the hull.

Under these circumstances, when a ship sails in stern seas and spends time on the minimum stability condition (wave crest amidships), it may experience large roll angles and even capsizing if stability levels have been largely reduced due to the wave effect.

The pure loss of stability criteria are also divided into two levels. The first level criterion is based on the evaluation of the minimum value of the metacentric height as a longitudinal wave of wavelength $\lambda = L$ and wave height $h = L \cdot S_W$ passes the ship (GM_{min}), where S_W is the constant wave steepness, that in this case is 0.0334. Under this condition, the ship is considered vulnerable if:

$$GM_{\min} < R_{PLA} \tag{7}$$

where R_{PLA} is the minimum value between 0.05 m and a speed and draft dependant factor.

The second level check consists of three criteria (CR_j), computed for two possible set of waves (16 or 306 cases). Each CR_j is obtained by weighting the coefficients Cj_i, which are evaluated for each wave condition and that are equal to 1 if the angle of vanishing stability (φ_v) is over 30 degrees, the maximum loll angle (ϕ_{loll}) is over 25 degrees and if the maximum GZ value is under $8 \cdot (H/\lambda) \cdot d \cdot Fn^2$, respectively.

$$CR_{j=1:3} = \sum_{i=1}^{N} W_i Cj_i \quad (8)$$

So, the ship is considered to be vulnerable if:

$$\max(CR_1, CR_2, CR_3) > R_{PL0} \quad (9)$$

Where R_{PL0} is 0.06 for the first set of waves and 0.15 if the second option is adopted.

Pure loss of stability criteria are only applied to vessels with a Froude number exceeding a threshold value, still under consideration; the minimum of the different possibilities is 0.2.

3.3 Broaching

The phenomenon of broaching is caused by the effect of large stern waves acting on the ship, forcing it to travel at their own speed and generating a directional instability, which may lead to a large yaw motion and subsequent roll, while the ship deviates from its original course.

Broaching criteria is also divided in Level 1 and Level 2 tests. Level 1 is the same as that included in the IMO guidelines for avoiding dangerous situations in adverse weather (MSC.1 Circ. 1228), and stablishes a Froude number limit of 0.3. All ships sailing at speeds over this limit, are considered vulnerable to the broaching failure. Regarding level 2, a direct evaluation of the surf-riding sensibility of the ship is needed [3].

4. Application and Results

4.1 Parametric Roll

Regarding the evaluation of parametric roll vulnerability, both Level 1 criteria and Level 2 first check have been analyzed for all vessels. In all cases, no bilge keels have been considered; so, the Level 1 limiting factor R_{PR} has been taken as 0.5.

In Table 4, the results for Level 1 criterion are shown. On it, ΔGM represents the GM variation on the specified waves and ΔGM_{alt} represents the alternative GM variation in waves computed considering the waterplane inertias at drafts d_h and d_l [7].

In Table 5, the results for the first check of the Level 2 criterion are presented. On it, ΔGM_{max} represents the maximum GM variation for all the 16 wave cases, GM_{avg} is the corresponding average GM for that wave case and V_{PR} is the reference ship speed for resonance in that conditions.

As can be seen in Table 4, all ships pass the Level 1 criterion except the largest ones, and in the case of the Tuna Purse Seiner, the criterion is not fulfilled only in the minimum GM condition.

Regarding the Level 2 test, all vessels pass the criteria for all wave cases and positions along the hull, obtaining a $C1$ value of 0.

The criteria, for the sampled ships, are consistent, and none of the vessels found vulnerable under Level 1 requirements, was classified as vulnerable under Level 2.

Table 4 Parametric roll. Level 1 results

Vessel	ΔGM (m)	ΔGM_{alt} (m)	$\Delta GM/GM$	Level 1
Trawler 1 LC1	0,090	0,164	0,251	Pass
Trawler 1 LC2	0,090	0,164	0,468	Pass
Trawler 2	0,102	0,133	0,379	Pass
Large Trawler	0,109	0,251	0,718	Fail
Longliner LC1	0.051	0.062	0.126	Pass
Longliner LC2	0,051	0,062	0,178	Pass
Purse Seiner	0,035	0,046	0,130	Pass
Tuna Purse Seiner LC1	0,154	0,295	0,322	Pass
Tuna Purse Seiner LC2	0,153	0,295	0,843	Fail
TS Trawler LC1	0,095	0,205	0,281	Pass
TS Trawler LC2	0,107	0,181	0,414	Pass

Table 5 Parametric roll. Level 2 results. 1st check

Vessel	ΔGM_{max} (m)	GM_{avg} (m)	$\Delta GM_{max}/GM_{avg}$	V_{PR} (m/s)	Level 2
Trawler 1 LC1	0,075	0,650	0,115	1,186	Pass
Trawler 1 LC2	0,073	0,347	0,211	2,040	Pass
Trawler 2	0,085	0,353	0,241	0,728	Pass
Large Trawler	0,104	0,360	0,287	1,707	Pass
Longliner LC1	0.044	0.495	0.089	1.110	Pass
Longliner LC2	0,045	0,349	0,128	0,935	Pass
Purse Seiner	0,034	0,352	0,097	1,171	Pass
Tuna Purse Seiner LC1	0,152	0,895	0,169	2,090	Pass
Tuna Purse Seiner LC2	0,152	0,330	0,460	3,069	Pass
TS Trawler LC1	0,090	0,719	0,125	1,019	Pass
TS Trawler LC2	0,100	0,444	0,225	0,473	Pass

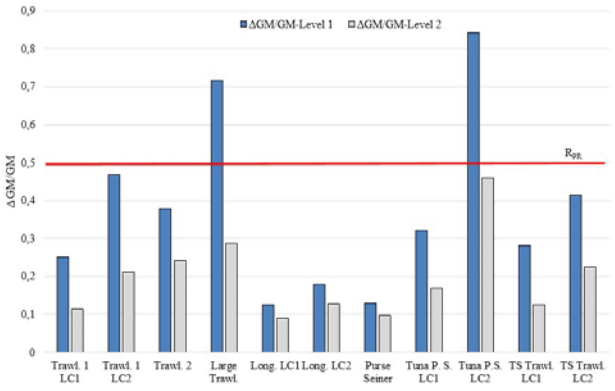

Fig. 1 – Parametric Roll Level 1 $\Delta GM/GM$ and Level 2 $\Delta GM_{max}/GM_{avg}$

One remark has to be made regarding the cases of Trawler 2 and the well known TS Trawler. Both vessels have a very large tendency to developing parametric roll resonance, even in wave the conditions evaluated in Level 1 and 2 tests, as can be observed in [11] and [12] and the two vessels have been judged as non-vulnerable under Level 1 and 2 tests.

Related to this, one main common characteristic of fishing vessels may be highlighted. Their hull forms don´t usually present very pronounced bow flares, as could be the case, for example, of containerships or Ro Pax vessels, although in many occasions transom and overhanging sterns are present.

In addition, in some occasions, as shown in [13], the changes in *GM* with wave passing are very small by themselves, and heave and pitch motions have more influence for triggering roll resonance than *GM* variation. This can be appreciated in the results presented in the aforementioned tables, where the values of the ΔGM seem to be quite small in comparison, for example, to the results shown in [14] for other types of ships.

The fact that both criteria are based on the analysis of *GM* variation in waves under the balance of trim and heave on waves approach, where dynamic pitch and heave effects are not included, may be the cause of this results.

Regarding the tuna purse seiner, a comparison with one of the ships tested in [15] can be made. Both ships have similar dimensional relationships, coefficients

and hull shape, and tests have shown that it is prone to capsizing in head waves of wavelength to ship ratio in the order of 1. Level 1 criterion seems to provide good agreement in this case.

If the different types of ships are compared, it can be concluded that trawlers and the large tuna purse seiner, are the ones more vulnerable to this failure mode. Two of them failed the stablished requirements, and the rest present the largest values of GM variation in waves among the ones fulfilling the criteria. The longliner and the purse seiner, with hull forms where little flare is present, are considered as non-vulnerable.

4.2 Pure Loss of Stability

In the case of pure loss of stability evaluation, the design speed have been chosen for all ships; in all vessels, Froude number is over 0.2, and so these set of criteria are of application. Level 1 and Level 2 tests have been carried out. Regarding Level 2 analysis, the option of 16 reference wave cases (Option A, [7]), instead of the 306 cases option, has been chosen.

In Table 6, the results for Level 1 criterion are shown. On it, GM_{min} represents the minimum *GM* as the specified wave passes the ship and GM_{min_alt} represents the alternative minimum *GM* computed considering the waterplane inertia at draft d_L [7].

In Table 7, the results for the Option A of the Level 2 criterion are presented. On it, GZ_{max} represents the minimum smallest *GZ* curve maximum for all the 16 wave cases, φ_v and ϕ_{loll} are respectively the vanishing stability and loll angles for that condition and R_{PL3} is the vulnerability limit for the presented GZ_{max}.

Table 6 Pure loss of stability. Level 1 results

Vessel	GM_{min}	GM_{min_alt}	Level 1
Trawler 1 LC1	0,452	0,488	Pass
Trawler 1 LC2	0,148	0,184	Pass
Trawler 2	0,172	0,075	Pass
Large Trawler	0,193	-0,147	Fail
Longliner LC1	0.391	0.342	Pass
Longliner LC2	0,246	0,197	Pass
Purse Seiner	0,276	0,231	Pass
Tuna Purse Seiner LC1	0,626	0,028	Fail
Tuna Purse Seiner LC2	0,060	-0,540	Fail
TS Trawler LC1	0,520	0,105	Pass
TS Trawler LC2	0,271	-0,113	Fail

Table 7 Pure loss of stability. Level 2 results. Option A

Vessel	GZ_{max}	φ_v	ϕ_{loll}	R_{PL3}	Level 2
Trawler 1 LC1	0,422	90	0	0,084	Pass
Trawler 1 LC2	0,199	70	0	0,085	Pass
Trawler 2	0,746	125	0	0,075	Pass
Large Trawler	0,187	51	0	0,115	Pass
Longliner LC1	0.392	82	0	0.088	Pass
Longliner LC2	0,293	73	0	0,089	Pass
Purse Seiner	0,269	78	0	0,086	Pass
Tuna Purse Seiner LC1	0,995	111	0	0,148	Pass
Tuna Purse Seiner LC2	0,451	95	0	0,136	Pass
TS Trawler LC1	0,254	70	0	0,056	Pass
TS Trawler LC2	0,144	58	0	0,060	Pass

In the case of pure loss of stability, the two vulnerable ships to parametric roll Level 1 are again vulnerable to pure loss of stability Level 1, although in this last case, the large tuna purse seiner is shown to be vulnerable in the two loading conditions under consideration. In addition, the TS Trawler, in one of its loading conditions, is also vulnerable according to the Level 1 test of this failure mode.

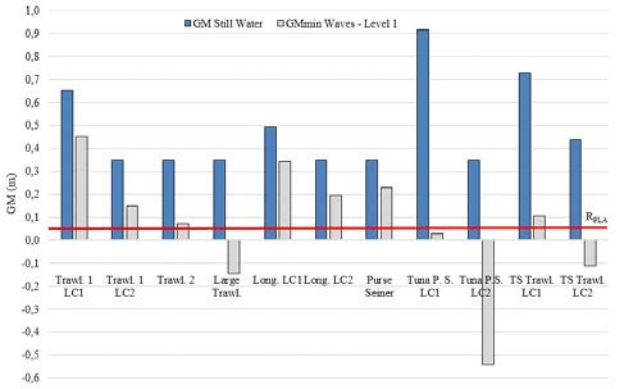

Fig. 2 – Pure loss of stability Level 1 minimum *GM* in waves and *GM* in still water

Again, as in the parametric rolling case, all vessels have been judged as non vulnerable under the Level 2 test, showing the consistency of the criteria.

In all wave cases and positions, all criteria have been fulfilled, and *C1*, *C2* and *C3* values are equal to 0.

Regarding the comparison of the obtained results with known data of the behavior of the tested ships, in [16] the tendency of the TS Trawler to capsizing in stern seas due to loss of stability is shown. In [15], it is shown that the purse seiner described in the previous chapter, is also vulnerable to this phenomenon.

Regarding the Trawler 2, it has been judged as non-vulnerable under both levels; in [17], the stability reduction in stern waves of this ship is demonstrated, although no capsizing is mentioned, as there is still a margin of positive stability.

According to this, it seems that pure loss of stability criteria could address the vulnerability of the type of vessels under analysis in a more accurate way than in the previous case, where pitch and heave have a larger influence on the behavior of the vessels.

Comparing the different typologies, again the trawlers and the tuna purse seiner are the most vulnerable ships, while both the longliner and the small purse seiner seem to be safe from the pure loss of stability failure point of view.

4.3 Broaching

Taking into account that all ships present a Froude number larger than 0.3, they are all classified as vulnerable according to Level 1 broaching criterion. In [18], it is shown that similar ships to those tested in this work have a large tendency to broaching. However, the analysis of Level 2 is needed to make any conclusions on this matter.

5. Conclusions

This work presented a sample application of the draft second generation intact stability criteria contained in the SLF55/WP.3 report, to a set of seven fishing vessels, which are representative of most of the typologies within the large Spanish fishing fleet.

The main objective of this work was to analyze the applicability of these criteria as a design tool that could improve the safety of the aforementioned vessels.

In order to do this, parametric roll resonance and pure loss of stability level 1 and Level 2 criteria, and broaching level 1 criterion, were applied to the 7 sample ships, considering a total number of 11 loading conditions.

As a first step, the consistency of the criteria was verified by checking that no discrepancy between Level 1 and Level 2 vulnerability results was found.

In a second step, the obtained results were analyzed, in order to determine the suitability of the criteria for evaluating the probability of the different types of ships of suffering the three phenomena, by comparing the obtained results with the known behavior of the different vessels.

Regarding parametric roll, only two vessels were vulnerable according to Level 1, and none according to Level 2. These two vessels were the largest of the sample. Some of the smaller ships, which are known for being prone to resonance, were qualified as safe under these criteria. Ships with small GM variation in waves, but with large amplitude pitch and heave motions, may have its vulnerability levels underestimated by these criteria.

Regarding pure loss of stability, three ships were found vulnerable under Level 1 test, and none according to Level 2. In this case, results show more consistency with the experimental data available for the different ships of the data base, and criteria seem to be applicable for all the different ship typologies.

With respect to broaching, all ships were judged as vulnerable according to Level 1 check.

From the results above, it can be concluded that the current draft version of the second generation intact stability criteria represents an easy to use tool for evaluating the possible vulnerability of medium sized fishing vessels. Its results show good agreement with

realistic data of the analyzed vessels for the case of pure roll of stability. For the case of parametric roll, a more detailed analysis is needed for the case of small trawlers, where some discrepancies have been shown.

Acknowledgments

The present work was supported by the Spanish Ministry of Economy and Competitiveness A-TEMPO contract with EDF funding.

References

[1] M. Míguez González, V. Díaz Casás, F. López Peña, L. Pérez Rojas, Experimental analysis of roll damping in small fishing vessels for large amplitude roll forecasting, Proceedings of the 13th Int. Ship Stability Workshop Brest (2013).

[2] W. Peters, V. Belenky, C. Bassler, K. Spyrou, N. Umeda, G. Bulian, B. Altmayer, The second generation intact stability criteria: an overview of development, SNAME Transactions (2011).

[3] N. Umeda, Current status of second generation intact stability criteria. Development and some recent efforts, Proceedings of the 13th Int. Ship Stability Workshop Brest (2013).

[4] SLF55/INF.15, Information Collected by the Correspondence Group on Intact Stability, submitted by Japan. Annex 6, Application and comments of vulnerability criteria on a large ship sample, IMO London (2012).

[5] P. Corrignan, C. Wandji, Sample application of second generation IMO intact stability vulnerability criteria as updated during SLF55, Proc.s of the 13th Int. Ship Stability Workshop Brest (2013).

[6] SLF55/INF.15, Information Collected by the Correspondence Group on Intact Stability, submitted by Japan. Annex 22, Sample calculations for vulnerability criteria on pure loss of stability, Level 2, IMO London (2012).

[7] SLF 55/WP.3, Report of the Working Group (Part 1), IMO London (2013).

[8] EU Maritime Policy: facts and figures. Spain, EU Commission, DG Fisheries and Maritime Affairs (2013).

[9] Estadísticas pesqueras. La flota pesquera. Número de buques pesqueros y eslora media, por tipo de pesca y caladero, Ministerio de Agricultura, Alimentación y Medio Ambiente Madrid (2013).

[10] J. De Juana Gamo, C. Arias Rodrigo, L. Pérez Rojas, On the parametric rolling of fishing vessels, 1st Int. Conf. on Marine Research and Transportation (2005).

[11] M. Míguez González, V. Díaz Casás, F. López Peña, L. Pérez Rojas, Experimental parametric roll resonance characterization of a stern trawler in head seas, Proceedings of the 11th Int. Conf. on the Stability of Ships and Ocean Vehicles Athens (2012).

[12] M. A. S. Neves, N. Pérez, O. Lorca, Experimental analysis on parametric resonance for two fishing vessels in head seas, 6th Int. Ship Stability Workshop New York (2006).

[13] A. Munif, N. Umeda, Numerical prediction on parametric roll resonance for a ship having no significant wave-induced change in hydrostatically-obtained metacentric height, Int. Shipbuilding Progress, 53(3) (2006) 183-203.

[14] C. Wandji, P. Corrignan, Test application of second generation IMO intact stability criteria on a large sample of ships, Proc. of the 11th Int. Conf. on the Stability of Ships and Ocean Vehicles Athens (2012).

[15] N. Umeda, A. Matsuda, M. Hamamoto, S. Suzuki, Stability assessment for intact ships in the light of model expermients. J. of Maritime Science and Technology, 4 (1999) 45-57.

[16] J. A. H. Paffett, Experiments with a model of MFV Trident and an alternative round-stern design, National Maritime Institute (NMI) UK (1976).

[17] L. Pérez Rojas, R. Abad, F. Pérez Arribas, C. Arias, Some experimental results on the stability of fishing vessels, Proc. of the 8th Int. Conf. on the Stability of Ships and Ocean Vehicles Madrid (2003).

[18] F. Mata-Álvarez-Santullano, A. Souto-Iglesias, Stability, safety and operability of small fishing vessels, Ocean Engineering, 79 (2014) 81–91.

Consideration of Risk Level in Terms of Damage Stability of Old Ship

Tomohiro Yuzui [1], and Yoshitaka Ogawa [1]

1. National Maritime Research Institute,Japan

Abstract: The risk analysis of passenger ships in terms of damage stability was conducted. Through this analysis, the relation between risk level and applied regulation was examined to clarify the effect of regulation for ensuring the safety. Consequently, it is clarified that risk level of SOLAS90 is generally low. It is also clarified that amendments of regulation improve the safety.

Key words: Damage stability, passenger ship, risk analysis, SOLAS90 and SOLAS2009, casualty database.

1. Introduction

The International Maritime Organization (IMO) is examining passenger ship safety. In this task, it is considered that safety level of passenger ships should be assessed for the further consideration.

Based on this background, the risk analysis of passenger ships, these are Cruise ships and RoPax vessels, in terms of damage stability was conducted utilizing IHS Fairplay Casualty and Ship databases (IHSF database) to contribute the technical background for the assessment.

Casualty data of collision, contact, wrecked, stranded and foundered accidents were focused in this analysis because these casualties have strong relation with the damage stability.

Through this analysis, the relation between risk level and applied regulation was examined to clarify the effect of regulation for ensuring the safety. In this study, data was separated into two kinds of ships. One is the ships built before application of SOLAS90. Another is the ships built in or after application of SOLAS90. The safety level of old ships, which was defined as the ships built before application of SOLAS90, was clarified based on this risk analysis. Currently, SOLAS2009 has been developed in the IMO. However, there are few casualty data, which makes it difficult to conduct a meaningful risk analysis. Furthermore, it is considered that safety level ensured by the SOLAS2009 is the same as that ensured by the SOLAS90.

Therefore, in this study, SOLAS90 was treated as an index for the examination of the effect of regulation on the safety revel in terms of damage stability.

Consequently, it is clarified that F-N curves for cruise ship of SOLAS 90 and pre-SOLAS 90 locate within ALARP (As Low As Reasonably Practicable) region. However, in the case of SOLAS90, it is found that only one serious accident raised the risk level and the risk level except this accident is quite low. It is also clarified that F-N curves for RoPax vessel of SOLAS 90 locates within NEGLIGIBLE region.

Based on the comparison of risk level, it is concluded that safety was relatively enhanced due to the revision of regulation. It is clarified that risk level of ships before implementation of SOLAS90 was not necessarily low.

*** Corresponding author:** Yoshitaka Ogawa, Head of Ship Structural Standards Group, Structural Strength Evaluation Department, National Maritime Research Institute, Japan. E-mail: ogawa@nmri.go.jp

2. Risk Analysis in terms of damage stability

2.1 Scope of this study

In this study, Risk analysis (step 2 of FSA[1]) was carried out based on IHSF database in order to consider the risk level in terms of damage stability of old ships. The subject ships of this risk analysis were following two types of passenger ships. One was the type which complied with SOLAS 90, and the other was the type which did not.

2.2 Used data

Based on the casualty and ship databases of IHSF, the risk analysis of Cruise ships and RoPax vessels 1,000GT or above was conducted.

2.3 Ships

This study focused on Cruise ships and RoPax vessels so that the following codes were collected in "STATCODE" of IHSF, for example A36 (RoPax) and A37 (Cruise/Passenger).

A36A2PR: Passenger/Ro-Ro Ship (Vehicles)
A36A2PT: Passenger/Ro-Ro Ship (Vehicles/Rail)
A36B2PL: Passenger/Landing Craft
A37A2PC: Passenger/Cruise
A37B2PS: Passenger Ship

2.4 SOLAS 90 ships

In this study, to clarify the relation between compliance of regulation and safety level, ships are categorized in accordance with following definition;

- ✓ Pre-SOLAS 90 ships: the ships built in or before 1989,
- ✓ SOLAS 90 ships: the ships built in or after 1990.

2.5 Casualties

The data of some categories of collision, contact, grounding and foundered were extracted for analysis in this study because they have strong relation with stability issue.

In the IHSF, they are categorized as the codes of CN (collision), CT (contact), WS (grounding), and FD (foundered). Table 1 shows the definitions of these 4 categorized casualties. In addition to those casualties, for the comparison, other 5 major casualties are shown in table 1.

Data from 1978 to 2012 are extracted as pre-SOLAS 90 ships. Data from 1990 to 2012 are extracted as SOLAS 90 ships.

Table 1 Casualty codes and their definitions (in IHSF)

Casualty (Category)	Casualty Code	Definition
Foundered(1)	FD	Includes ships which sank as a result of heavy weather, springing of leaks, breaking it two etc., and not as a consequence of categories 2-7 or 9.
Wrecked /Stranded (2)	WS	Includes ships reported hard and fast for an appreciable period of time and cases reported touching sea bottom. This category includes entanglement on under water wrecks.
Contact (3)	CT	Striking or being struck by an external substance but not another ship or the sea bottom (see categories 2/4). This category includes striking drilling rigs/platforms, regardless of whether in fixed position or in tow.
Collision (4)	CN	Striking or being struck by another ship, regardless of whether under way, anchored or moored. This category does not include striking under water wrecks.
Fire & Explosion (5)	FX	Where the fire and/or explosion is the first event reported (except where first event is a hull/machinery failure

		leading to fire/explosion). Note: It therefore follows that casualties involving fires and/or explosions after collisions, stranding etc., are categorized under 'Collision', 'Stranding'. Scavenge fires and crankcase explosions are included in this category.
Missing Vessel (6)	MG	After a reasonable period of time, no news having been received of a ship and its fate being therefore undetermined, the ship is posted as "Missing" at the Corporation of Lloyd's and is included in the Missing category on the data base together with similar cases reported by other reliable sources. Note: In peacetime, missing ships are considered as losses by marine perils.
War Loss /Damage During Hostilities (7)	LT	This category is intended to encompass damage or other incidents occasioned to ships by hostile acts.
Hull/ Machinery Damage (8)	HM	Includes ships lost or damaged as a result of hull/machinery damage or failure which is not attributable to categories 1-7 or category 9.
Miscellaneous (9)	XX	Includes ships which have been lost or damaged which, for want of sufficient information, or for other reasons, cannot be classified.

2.6 Review of the casualty data

The fatal accident data for foundered after damage and flooded is available for analysis in consideration of stability issue. However, the data for the accident of fire on the deck after damage is not available for the analysis of stability issue. Therefore, all fatal accident data one by one in the categories of CN (collision), CT (contact), WS (Wrecked/Stranded) and FD (foundered) were intensively checked. As a result, insufficient or inadequate data were removed. The detail of information of the removed data is shown in Table 2 and Table 3.

(1) Cruise ships

A casualty data shown in Table 2 was removed from 10 fatal accidents data of Cruise ships 1,000 GT or above both pre-SOLAS 90 and SOLAS 90 ships, which were categorized as CN, CT, WS and FD in IHSF data (1978-2012). This ship is among SOLAS 90 ship.

(2) RoPax

4 casualties (CN: 3 and FD: 1) shown in Table 3 were removed from the 33 fatal accidents data of RoPax vessels 1,000 GT or above. The accident in the first row of Table 3 was that of pre-SOLAS 90 ships. Other 3 accidents were those of SOLAS 90 ships.

Table 2 Detail of removed data from IHSF Casualty Database (1978-2012) (Cruise 1,000GT or above)

Casualty Code	No. of fatalities	Reason for removal
CN	4	This casualty is not related to the stability issue, because the crews on the deck were dead by the impact of collision [2].

Table 3 Detail of removed data from IHSF Casualty Database (1978-2012) (RoPax 1,000GT or above)

Casualty Code	No. of fatalities	Reason for removal
CN	18	This casualty is not related to the stability issue because of fire after collision [3].
FD	970	This ship was a government-owned and domestic vessel.
CN	1	This casualty is not the RoPax ships but the fishing vessel [4].
CN	1	This accident is excluded because of

duplication [5].

3. Methods of Calculating Risk

In this study, PLL (Potential Loss of Life) and F-N diagram were considered as risk. Calculating methods for them are shown in below.

3.1 PLL (Potential Loss of Life)

PLL [fatalities/(ship*year)] is given by eq.(1) where N is the total number of annual fleet of the subject ship in considered period, k is the total number of fatalities in considered period.

$$PLL = \frac{k}{N} \tag{1}$$

3.2 F-N diagram

F-N diagram is a continuous graph with the ordinate representing the cumulative frequency distribution of j or more fatalities and the abscissa representing the consequence (j fatalities)[1]. A value of a vertical axis in F-N diagram is obtained by eq. (2) where n_k is the number of casualties with exactly k fatalities, k_{max} is the maximum number of fatalities. F (j) shows frequency of accidents in which persons of j and above are killed.

$$F(j) = \sum_{k=j}^{k_{max}} \frac{n_k}{N} \tag{2}$$

4. Results of Calculating Risk of Cruise ships

4.1 Fleet

Fig.1 shows the results of calculation of fleet of Cruise ships and Table 4 provides the total number of annual fleet. It is found that the fleet of pre-SOLAS 90 ships decreases gradually from 1990, on the other hand, that of SOLAS 90 ships is increasing every year. The fleet of SOLAS 90 ships is larger than that of pre-SOLAS 90 ships from 2007.

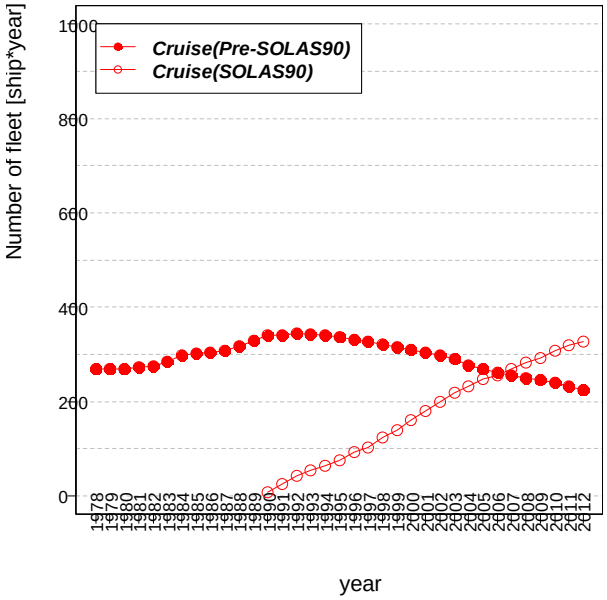

Fig.1 Chronological changes of fleet of Cruise ships (1,000GT or above)

Table 4 Total number of annual fleet of Cruise ships (1,000GT or above)

	Total number of fleet [ship*year]
Pre-SOLAS 90	10,291
SOLAS 90	4,019

4.2 PLL (Potential Loss of Life)

PLL of cruise ships of the above-mentioned 4 types of casualties are shown in Table 5 and Fig.2.

The following findings are derived:

- PLL of SOLAS 90 ships are lower than that of pre-SOLAS 90 ships except in the case of WS (Wrecked/Stranded).
- PLL of SOLAS 90 ships indicates zero except WS. The reason is that no accident with loss of life has happened except WS. On the other hand,

only the accident of Costa Concordia in January 2012 affects the PLL of WS.

- PLL of WS is the highest and that of CT (Contact) is the lowest in pre-SOLAS 90 ships.

Table 5 Number of fatalities and PLL of Cruise ships (1,000GT or above)

	Pre-SOLAS 90		SOLAS 90	
	No. of fatalities	PLL	No. of fatalities	PLL
CN	13	1.26×10^{-3}	0	0.00
CT	3	2.92×10^{-4}	0	0.00
WS	61	5.93×10^{-3}	32	7.96×10^{-3}
FD	15	1.46×10^{-3}	0	0.00

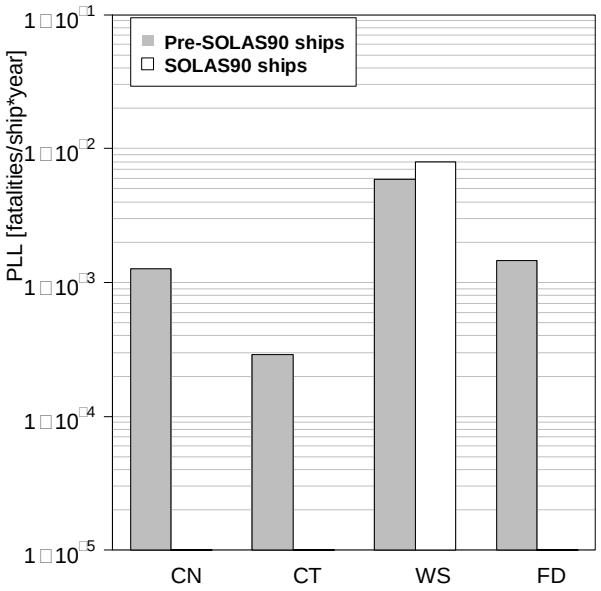

Fig.2 PLL of Cruise ships (>=1,000GT)

4.3 F-N diagram

F-N diagrams of cruise ships of the above-mentioned 4 types of casualties are shown in Fig.3. The ALARP limits[6] are also shown in Fig.3.

Following findings are clarified:

- Both F-N curves of SOLAS 90 and pre-SOLAS 90 locate within ALARP region.
- Maximum number of 58 fatalities of pre-SOLAS 90 ships is larger than that of SOLAS 90 ships.

  This accident of pre-SOLAS 90 ships is a grounding casualty.

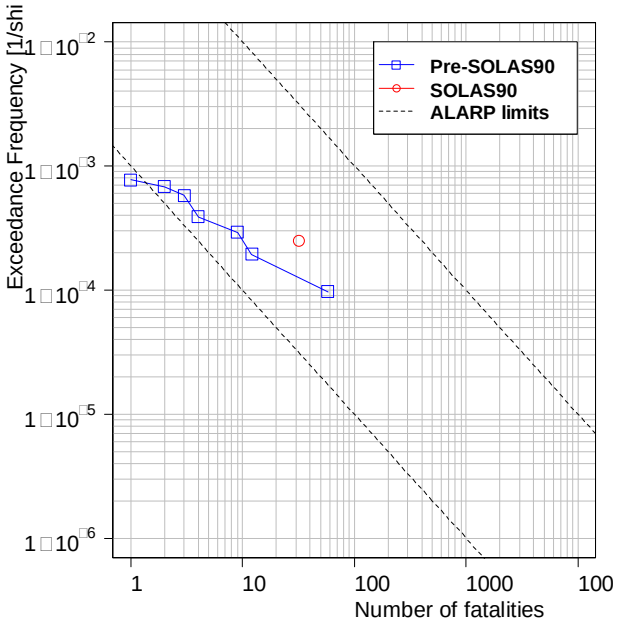

Fig.3 F-N curves of Cruise ships (1,000GT or above)

5. Results of Calculating Risk of RoPax vessels

5.1 Fleet

Fig. 4 shows the results of calculation of fleet of RoPax vessels under the above data and Table 6 provides the total number of annual fleet. It is found that the fleet of pre-SOLAS 90 ships decreases gradually from 1990. It is also found that the fleet of SOLAS 90 ships is increasing every year. The fleet of SOLAS 90 ships is larger than that of pre-SOLAS 90 ships from 2011.

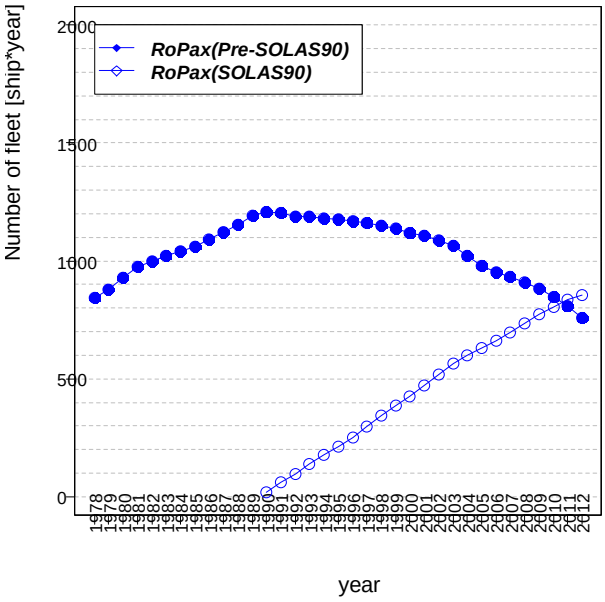

Fig.4 Chronological changes of fleet of RoPax vessels (1,000GT or above)

Table 6 Total number of annual fleet of RoPax vessels (1,000GT or above)

	Total number of fleet [ship*year]
Pre-SOLAS 90	36,543
SOLAS 90	10,554

5.2 PLL (Potential Loss of Life)

PLL of RoPax vessels of the above-mentioned 4 types of casualties are shown in Table 7 and Fig.5.

We can get a sense of the following from Table 7 and Fig.5:

- PLL of SOLAS 90 ships indicates zero except CT (Contact) because no accident with loss of life has happened except CT.
- PLL of FD (Foundered) is the highest and that of CT is the lowest in pre-SOLAS 90 ships.
- PLL of CT of SOLAS 90 ships is higher than that of pre-SOLAS 90 ships due to the difference of number of fleet. It is clarified that there is one fatality in each ship. Therefore, the difference of number of fleet induces the difference of PLL.

Table 7 Number of fatalities and PLL of RoPax vessels (1,000GT or above)

	Pre-SOLAS 90		SOLAS 90	
	No. of fatalities	PLL	No. of fatalities	PLL
CN	175	4.79×10^{-3}	0	0.00
CT	1	2.74×10^{-5}	1	9.48×10^{-5}
WS	1,381	3.78×10^{-2}	0	0.00
FD	1,692	4.63×10^{-2}	0	0.00

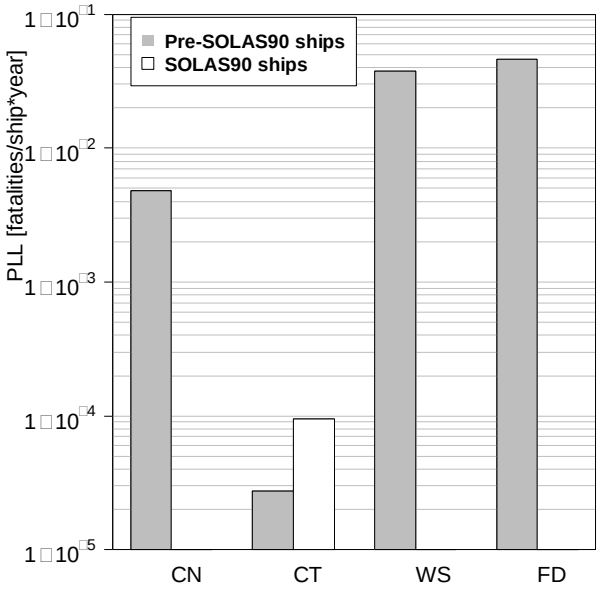

Fig.5 PLL of RoPax vessels (1,000GT or above)

5.3 F-N diagram

F-N diagrams of RoPax vessels of the above-mentioned 4 types of casualties are shown in Fig.6. The ALARP limits[6] are also shown in Fig.6.

Following findings are clarified:

- F-N curve of pre-SOLAS 90 ships locates within ALARP region.
- F-N curve of SOLAS 90 ships locates within NEGLIGIBLE region.
- Maximum number of fatalities of pre-SOLAS 90 ships is quite larger than that of SOLAS 90 ships.

This accident with maximum fatalities of pre-SOLAS 90 ships is a foundered casualty. This casualty is the accident of ESTONIA in September 1994. It is recorded that the total number of fatalities and missing is reported as 852 in IHSF.

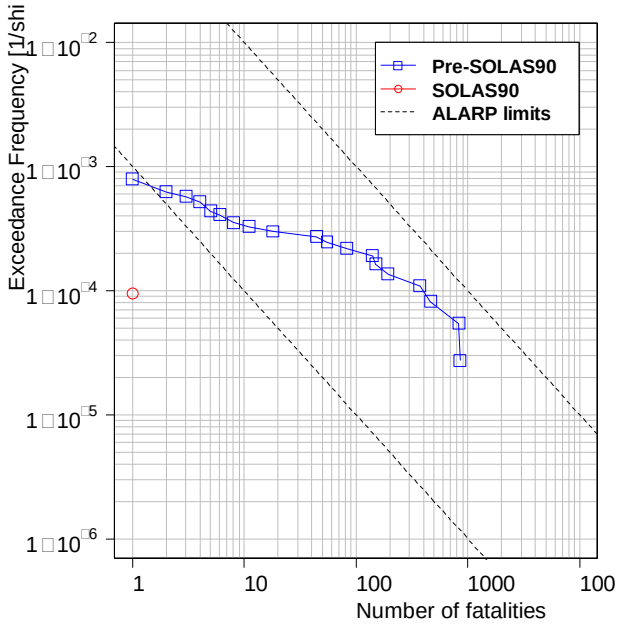

Fig.6 F-N curves of RoPax vessels (1,000GT or above)

6. Conclusions

Based on IHS Fairplay World Casualty Statistics database (hereinafter "IHSF"), risk level in terms of damage stability is investigated. Consequently, the following findings are clarified:

1) Regarding the accidents of collision, contact, grounding and foundered of Cruise ships, PLL of SOLAS 90 ships is lower than that of pre-SOLAS 90 ships except in the case of WS (Wrecked/Stranded). The reason is that no accident with loss of life has happened except WS. On the other hand, only the accident of Costa Concordia affects the PLL of WS.

2) In terms of the Cruise ships, both F-N curves of SOLAS 90 and pre-SOLAS 90 locate within ALARP region.

3) Regarding the accidents of collision, contact, grounding and foundered of RoPax vessels, PLL of CT of SOLAS 90 ships is higher than that of pre-SOLAS 90 ships due to the difference of number of fleet. It is clarified that there is one fatality in each ship. Therefore, the difference of number of fleet induces the difference of PLL.

4) In terms of the RoPAX vessel, F-N curve of pre-SOLAS 90 ships locates within ALARP region. On the other hand, F-N curve of SOLAS 90 ships locates within NEGLIGIBLE region. Particularly, Maximum number of fatalities of pre-SOLAS 90 ships is quite larger than that of SOLAS 90 ships due to the accident of ESTONIA, which is a pre-SOLAS 90 ship.

5) Consequently, it is concluded that safety is relatively enhanced due to the revision of regulation. It is clarified that risk level of ships before implementation of SOLAS90 is not necessarily low.

On the other hand, it is considered that not only damage stability aspects but also operational aspects should be considered for comprehensive measure of safety because serious accident, which raise the risk level, occurs due to the some kinds of accidental causes.

Acknowledgments

The present study was carried out in cooperation with the Japan Ship Technology Research Association through the Japanese project for the stability safety that was supported by the Nippon Foundation.

References

[1] IMO, REVISED GUDELINES FOR FORMAL SAFETY ASSESSMENT (FSA) FOR USE IN THE IMO RULE-MAKING PROCESS, MSC-MEPC.2/Circ.12, p. 43, 8 July 2013.

[2] http://www.tribuneindia.com/1998/98aug19/spotlite.htm.

[3] Aleik Nurwahyudy, “OVERVIEW TO THE HUMAN FACTOR CONTRIBUTION TO THE COLLISION ACCIDENT IN INDONESIA WATER. AN NTSC INVESTIGATION PERSPECTIVE”, 1st International

Conference on the Safety Investigation of Marine Casualty, pp.32-35.

[4] MARINE ACCIDNT INVESTICATION BRANCH, "FLYER TO THE FISHING INDUSTRY".

[5] Number 088 ****DAILY SHIPPING NEWSLETTER**** Thursday 03-07-2003, p.6.

[6] Norway, FORMAL SAFETY ASSESSMENT Decision parameters including risk acceptance criteria, MSC 72/16 ANNEX 1, p.10, 14 February 2000.

Stability of Grounded Ship

Apurba Ranjan Kar [1]

1. *Dept. of Hydrodynamics and Risk Analysis, Indian Register of Shipping, Mumbai*

Abstract: The objective of this paper is to present an algorithm for computerized calculation of hydrostatic stability of a vessel in grounded/stranded condition. This is based on the physics of floating bodies and follows the quasi-static approach of usual conventional Naval Architectural calculations.

Key words: Buoyoancy , Statical Stability , Dynamical Stability, Pinnacle, Equilibrium, Heel, Trim ,Capsizing, Stranding

1. Introduction

Grounding is defined as the ship being aground or hitting/touching shore or sea bottom or underwater objects (wrecks etc.). Ship stability in grounded condition is no less important than the same in free-floating condition. Grounding/Stranding of ships is not exception; in fact numerous cases of ships' grounding have indeed been reported in the past and contributed to the significant number of marine accidents so it deserves greater attention in maritime safety. The grounding of tanker Braer (1994) is worth mentioning in this context.

As far as the knowledge of the author goes, there exists no international rules/regulations as of today which explicitly addresses the issue of stability of ship in grounded condition.

The author feels this aspect warrants investigation in course of design of the ship. Further, this is of prime necessity during salvage operation in case of real accidents involving grounding/stranding of the ship and also during dry docking of ship. Calculations are to be made to establish intact and damaged statical and dynamical stability for the vessel in grounded condition.

If a ship runs aground in such a manner that the bottom offers little restraint to heeling and/or trimming, as illustrated in fig-1, the reactions of the bottom may produce a heeling and/or trimming moment. As the ship grounds, part of the energy due to its forward motion may be absorbed in lifting the ship, in which case a reaction, R, between the bottom and the ship would develop. This reaction may be increased later as the tide ebbs. Under these conditions, the force of buoyancy would be supported by the combination of buoyancy and the reaction of the bottom. The ship would heel and/or trim until the moment of buoyancy about the point of contact with the bottom became equal to the moment of the ship's weight about the same point.

In case a ship stranded/settles on a fairly flat bottom, the transverse stability is of no relevance.

There is less possibility of a stranded ship capsizing as the result of ebbing tide. For this to occur it would be necessary for the ship to be grounded on a bottom such that there is no restraint to heeling in one or both directions until a very large angle is reached, as, for example, on a peak which was considerably higher than the surrounding bottom. When a ship is aground in the manner, as illustrated in Fig - 1, the heel would increase as the tide ebbs.

An algorithm for developing suitable software in order to accomplish such calculations for the investigation of vessel's stability in grounded condition have been illustrated in this paper. The algorithm is based on the principles of rudimentary physics and conventional procedure of Naval Architectural calculations.

It is assumed that the reader of this paper is generally conversant with the aspect of ships' stability and related Naval Architectural calculation.

Two types of grounding have been considered in this paper – Grounding on 'One Pinnacle' and on 'Two Pinnacles' as illustrated in Fig-2 & Fig-3 , the latter (i.e. the two pinnacle case) can be extended to the case of shelf stranding.

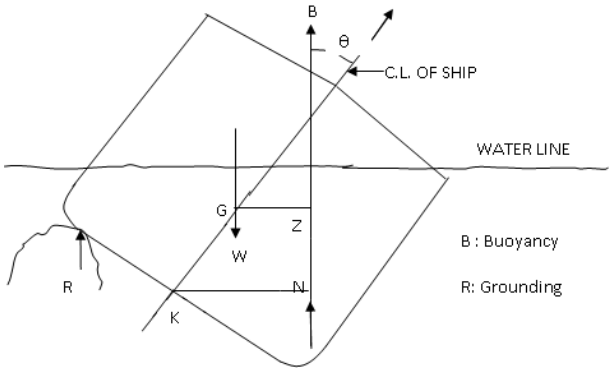

Fig: 1

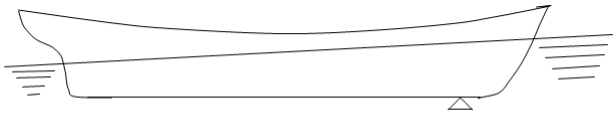

Fig – 2 : Grounded on Single Pinnacle

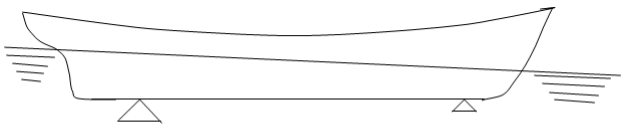

Fig – 3 : Grounded on Two Pinnacles

2. Method:

A step by step description of the algorithm has been presented here as follows. The description features some computer commands for explanatory purpose only, hence not to be looked for the syntactic correctness of the same. The illustration of the nomenclatures used in this paper has been given in Appendix - 3.

The flowchart as given in Appendix – 2 may also be referred for the logical sequence of the method.

Step 1:

A set of predefined values of the drafts (Tk=1,nd), angle of heels (θi=1,nh) and angle of trims (ϕj=1,nt) where nd = No. of drafts; nh = No. of heels; nt = No. of trims have been selected.

Step 2:

The array of hydrostatic parameters i.e. { WPA, LCF, TCF, IT, IL, VOL, LCB, VCB, TCB, KN } are determined for the vessel in the orientation at each of the combinations of predefined drafts, heel and trim conditions.

As it can be observed that a large amount of computation is involved in this step.

No. of calculation sets = No. of Drafts X No. of Heels X No. of Trims).

It is, therefore, obvious that manual calculation will be extremely tedious to accomplish, hence an appropriate computer routine is essentially needed for the task. The formulation for calculation is given in Appendix –1.

Step 3:

A data file is created compiling the values of the array of the hydrostatic parameters {WPA, LCF, TCF, IT, IL, VOL, LCB, VCB, TCB, KN} as obtained from Step-2.

This data file essentially contains ship-specific data as mentioned here below and is named in this paper as 'Vessel.inf'.

[Vessel.inf] ⟨ { θ(i) , ϕ(j) , T(k), WPA(i, j, k); LCF(i, j, k); TCF(i, j, k); IT(i, j, k); IL(i, j, k); VOL(i, j, k); LCB(i, j, k); VCB(i, j, k); TCB(i, j, k) ;KN(i, j, k) } i=1, nh; j=1, nt; k=1, nd

Another data file is created to store information with regards to the situation when the vessel is grounded. This data file is named in this paper as 'Situation.inf' and contains the variables as shown below -

[Situation.inf] ⟨ { ng; xg(i); yg(i); dg(i) } i=1, ng

Step 4:

In this step the mean draft at midship 'dref' for the vessel is determined.

Case-A: No. of Grounding Pinnacle = 1

```
        DO 10     j = 1, nt
        trim (j) = tan(ϕj)
10      dref (j) = dg (1)-xg(1) * trim(j)/LBP
```

Case-B: No. of Grounding Pinnacles = 2

```
        DO 11     j = 1, nt
        trim (j)=tan(ϕj)
11      dref (j)=dg(2)-xg(2)*
                (dg (2)-dg(1))/(xg(2)-xg(1))
```

Step 5:

Determine the hydrostatic parameters of the vessel for each of the combinations of, Heel and Trim conditions, and at the draft of 'dref (j)'.

```
        DO 20     i = 1, nh
        DO 20     j = 1, nt
        DO 30 k = 1, nd
        wpa1 (k) = WPA (i,j,k)
        lcf1 (k) = LCF (i, j,k)
        tcf1 (k) = TCF (i, j, k)
        it1 (k) = IT (i, j, k)
        il1 (k) =IL (i, j, k)
        vol1 (k) =VOL (i, j, k)
        lcb1 (k) =LCB (i, j, k)
        vcb1 (k) =VCB (i, j, k)
        tcb1 (k) = TCB (i, j, k)
30      kn1 (k) = KN (i, j, k)

        D = dref (j)
        wpad(i, j) = Intp { nd,T(k),
                    WPA1(k), D }
        lcfd(i, j) = Intp { nd,T(k),
                    LCF1 (k), D}
        tcfd(i, j) = Intp { nd,T(k),
                    TCF1 (k), D}
        itd(i, j) = Intp { nd,T(k),
                    IT1(k), D}
        ild(i, j) =  Intp { nd,T(k),
                    IL1(k),D}
        vold (i, j) = Intp { nd, T(k),
                    VOL1(k), D }
        lcbd(i, j) = Intp { nd,T(k),
                    LCB1(k), D}
        vcbd(i, j) = Intp { nd,T(k),
                    VCB1(k), D    }
        tcbd(i, j) = Intp{ nd,T(k), TCB1(k),D    }
20      knd(i, j) = Intp { nd,T(k), KN1(k), D    }
```

Step 6:

In case of grounding at one location (i.e. one pinnacle case) the lever ordinates to match the longitudinal moment about the grounding location for equilibrium trim at the defined angles of heel and at drafts = 'dref(j)' can be determined as follows.

```
        DO 40     i = 1, nh
        DO 40     j = 1, nt
40      TRMLEV(i, j, D) = vold(i, j) *ρ * (xg(1)
        –  lcbd(i, j)) - W*(xg(1)-LCG)
```

Step 7:

Now, the equilibrium trim and mean draft at midship corresponding to each of the predefined heel angle is determined

Case-A: No. of Pinnacles = 1

```
        DO 50     i = 1, nh
        DO 60     j = 1, nt
60      trmlev1 (j) = trmlev(i, j, D)
        etrm(i) = Intp { nt, trmlev1(j), trim(j),
        0.0 }
50      dref (i) = dg (1)-xg(1) * etrm(i)/LBP
```

Case-B: No. of Pinnacles = 2

```
        DO 70 i = 1 , nh
```

```
        etrm(i) = (dg(2)-dg(1))/(xg(2)-xg(1)) *
                  LBP
70      dref(i)=dg(2)-xg(2)*
        (dg(2)-dg(1))/(xg(2)-xg(1))
```

Step 8:

Determine hydrostatic parameters for each of the pre-defined heel angle at their corresponding equilibrium trim angle.

```
        DO 80    i = 1, nh
        DO 100   j = 1, nt
        vol2 (j) = vold (i, j)
        lcb2 (j) = lcbd(i, j)
        vcb2 (j) =vcbd(i, j)
        tcb2 (j) =tcbd(i, j)
100     kn2(j) = knd(i, j)
        etvol (i) = Intp { nj, trim(j), vol2(j),
        etrm(i) }
        etlcb (i) = Intp { nj, trim(j), lcb2(j),
        etrm(i) }
        etvcb(i) = Intp { nj, trim(j), vcb2(j),
        etrm(i) }
        ettcb(i) = Intp { nj, trim(j), tcb2(j),
        etrm(i) }
80      etkn(i) = Intp{nj,trim(j),kn2(j),etrm(i) }
```

Step 9:

Determine grounding reactions (R1 & R2) and the values of Vertical Centre of Gravity and Transverse Centre of Gravity (VCGG & TCGG) for the vessel in the grounded condition in the orientation of equilibrium trim and at each of the predefined heel angle.

```
        DO 150 i = 1, nh
        IF No. of Pinnacle = 1
        R1 = W – etvol(i) * ρ
       ettcg(i) = (W*TCG-R1 * yg(1))/(etvol(i) * ρ)
        etvcg(i) = (W*VCG)/(etvol(i) * ρ )
        ELSEIF No. of Pinnacles = 2
        R1 = { etvol(i) * ρ *(xg(2) – etlcb(i)) – W *
        (xg(2) – LCG) } ÷ { xg(1) – xg(2) }
          R2 = { (W – (etvol(i)) * ρ } – R1
        ettcg(i) = (W * TCG – R1 * yg(1) – R2 *
        yg(2))/(etvol(i) * ρ)
150     etvcg(i) = (VCG*W)/(etvol(i)* ρ)
```

Step 10:

Determine transverse moment lever and also the statical stability levers at each of the pre-defined angle of heel (θ).

```
        DO 170    i = 1, nh
        LEVHEEL (i) = (etvol(i) * ρ *ettcb(i) -
        etvol(i) * ρ * ettcg(i))
170     GZGR(i) = etkn(i) – ettcg(i) * Sin(θi) -
        ettcg(i) * cos(θi)
```

Step 11:

Now, the final condition of equilibrium is determined as follows.

θeq = Intp { nh, LEVHEEL(i), θ(i), 0.0 }
AND the equilibrium trim

ϕeq = Intp { nh, θ(i), etrm(i), θeq }
And the equilibrium draft

Teq = Intp { nh, etrm(i), dref(i), ϕeq }

The etrm(i) and dref(i) are obtained from Step - 7
Hence, the final equilibrium condition of the vessel is now established.

Step 12:

The hydrostatic parameters of the vessel at the final equilibrium condition are determined in this step

EQVOL = Intp { nh, θ(i), ETVOL(i), θeq }
EQLCB = Intp { nh, Q(i), ETLCB(i), θeq }
EQVCB = Intp { nh, Q(i), ETVCB(i), θeq }

Step 13:

R1, R2, EQTCG, EQVCG, EQGM and EQDraft are determined as follows.

If
No. of Pinnacle = 1
R1 = W – EQVOL * ρ
EQTCG = (W * TCG – R1 * yg(1))/ EQVOL * ρ
Else

No. of Pinnacles = 2

R1 = {EQVOL (i) * ρ *(xg(2) – EQLCB(i)) – W * (xg(2) – LCG) } ÷ { xg(1) – xg(2) }

R2 = W – (EQVOL (i) * ρ) – R1

EQTCG = {EQVOL * ρ * TCG – R1 * yg (1) – R2 * yg(2)} ÷(EQVOL * ρ)

End if

EQVCG = (VCG * W)/(EQVOL * ρ)

EQGM=(EQIT/EQVOL–(EQVCG–QVCB)/Cos(θeq)

Step 14:

Check for occurrence of grounding.

Occurrence of grounding can be verified from the simple principle of balance of forces.

We can simply say if the ground reactions are less than 0.0 then it is a free floating case.

Case-A:

No. of Pinnacles = 2

If (R1.LE.0). AND. (R2.LE.0) THEN NO GROUNDING

ELSE

GROUNDING HAS OCCURRED

ENDIF

Case-B:

No. of Pinnacle = 1

If (R1.LE.0.0) THEN NO GROUNDING

ELSE

GROUNDING HAS OCCURRED

ENDIF

Step 15:

The likelihood of capsizing with the expected variation in tide can also be evaluated.

Owing to the tidal variation, the values of one or more variable(s) in the data file {Situation.inf} may get modified, hence steps-4 through step-14 need to be repeated considering the changed situation.

3. Conclusions

The algorithm described above has dealt with all the essential aspects of statical stability of a vessel in the grounded condition.

The algorithm mainly involves very common interpolation and integration operations, as such can easily be programmed using any standard computer language for execution on an widely available personal computer.

The author hopes the readers will find the algorithm informative and complete for the purpose of writing an appropriate program.

Of course, adequate care needs to be taken in developing the codes with due regard to providing guidance to the user enabling him to select appropriate values of the predefined input parameters as stated in Step-1 for dependable and reliable result. The time requirement for execution of program on a personal computer will be negligible, matter of few seconds only.

The results which can be obtained from the software may be summarized as follows –

1) Ground reactions
2) Draft, Trim, Heel and the Metacentric height at the equilibrium state in the grounded condition.
3) Statical stability levers (GZ) in the grounded condition.
4) Consequence to tidal variation.

The author is unaware if there exists presently any standard criteria for the stability of the vessel in grounded condition. It is viewed by the author that the floating ship stability criteria cannot be applied to the grounded ship, hence the maritime regulatory bodies may look in to the matter of establishing criteria for stability in grounded condition to enable the comparison of ships as regards to their soundness against vulnerability towards capsizing/sinking in aground condition.

Acknowledgments:

Author of this paper is indebted to the authors of the references as listed above and to the Management of IRS for allowing me to present the paper at ISSW-14. Also the author expresses appreciation to Mr.Somesh Gupta of "Indian Register of Shipping" for providing support service to prepare this paper.

References

[1] Watson, D. G. M., Practical Ship Design, Elsevier Science Ltd., Oxford, UK, 1998.

[2] Rawson, K. J., and Tupper, E. C., Basic Ship Theory, Vol. 1 and Vol. 2, Longman, London, UK, 1983.

[3] E. V. Lewis (ed.), Principles of Naval Architecture, Vol. 1, 2, & 3, SNAME, 1988 and 1989.

[4] Semyonov – Tyan – Shansky V., "Statics and dynamics of the Ship"

Regulatory, Design, Operational and Emergency Response Measures for Improving the Damage Survivability of Existing RoPax

Dracos Vassalos, Evangelos Boulougouris[1]

Luis, Guarin, Andrzej Jasionowski[2]

John Garner[3]

[1]The Ship Stability Research Centre (SSRC), University of Strathclyde, Glasgow, UK

[2]Safety at Sea Brookes Bell

[3]P&O Ferries (INTERFERRY Board)

ABSTRACT

This paper describes the background and provides the rationale and the framework to embrace the whole spectrum of measures (regulatory, design, operational and emergency response) for improving the damage survivability of existing RoRo Passenger vessels. The damage stability workshop elaborated here is the first step of a process initiated by INTERFERRY Europe to assess impact on/options for existing ships of increasing the required subdivision index R should IMO decide to apply new damage stability requirements retrospectively. This, in turn, would provide the motivation for instigating and establishing a framework and propose an approach for alternative compliance to account for the contribution made to damage survivability by operational and active damage control measures that could be undertaken in case of a flooding accident. This represents a step change both in the mind-set of naval architects and in safety legislation but the impact will be immense and mostly positive.

KEYWORDS

RoPax damage stability workshop, alternative means of compliance, vulnerability management

INTRODUCTION

Recent discussions at IMO on the safety of passenger ships include a potential increase in the required subdivision index for all passenger ships. An initiative, started by INTERFERRY Europe, seeks to assess the impact of the above on existing vessels (if such changes were applied retrospectively) and propose an approach for alternative compliance based on a fair recognition and credit of the contribution to risk reduction afforded by operational and active damage control measures that would be undertaken in case of a flooding accident. This should be accounted for, in addition to the contribution made by traditional design measures. This approach was first presented in the 13th ISSW in BREST 2013, [1]. To this end, a tentative plan of action was prepared to carry out a study aimed at quantifying and validating the risk-reduction effectiveness potential of such measures. The proposal included a one-day workshop to discuss the context and the relevant issues on the subject as a first step in the process. This took place in London on 22 January 2014 with a participation of 19 persons representing 5 ferry operators, 1 class society, 1 yard, 2 Flag Administrations and a number of damage stability experts.

Following a brief description of the rationale in support of adopting an alternative compliance

approach that accounts for all meritorious contribution to enhancing damage survivability, the paper focuses on the objectives of and the key outcomes from the damage stability workshop.

BACKGROUND

Every time there is an accident with passenger ships, exposing their vulnerability to flooding as a result of collision/grounding accidents, societal outcry follows and industry and academia "buckle up", delving for design improvements to address the Achilles heel of this ship type, namely inadequate damage stability. However, any such improvements are targeting mainly newbuildings, which comprise a small minority of the existing fleet. Therefore, state-of-the-art knowledge on damage stability is all but wasted, scratching only the surface of the problem and leaving thousands of ships with severe vulnerability, that is likely to lead to further (unacceptably high) loss of life. This problem is exacerbated still further, today more rapidly, as the pace of scientific and technological developments is unrelenting, raising understanding and capability to address damage stability improvements of newbuildings cost-effectively, in ways not previously considered. As a result, SOLAS is becoming progressively less relevant and unable to keep up with this pace of development. This has led to gaps and pitfalls, which not only undermine safety but inhibit progress.

However, lack of retrospectively applied legislation (supported by what is commonly known as the Grandfather Clause) is not the only reason for damage stability problems with passenger ships. Tradition should share the blame here. In the quest for damage stability improvement, design (passive) measures have traditionally been the only means to achieve it in a measurable/auditable way (SOLAS 2009, Ch. II-1). However, in principle, the consequences from inadequate damage stability can also be reduced by operational (active) measures, which may be very effective in reducing loss of life (the residual risk). There are two reasons for this. The first relates to the traditional understanding that operational measures safeguard against erosion of the design safety envelop (possible increase of residual risk over time). The second derives from lack of measurement and verification of the risk reduction potential of any active measures. In simple terms, what is needed is the means to account for risk reduction by operational measures as well as measures that may be taken during emergencies. Such risk reduction may then be considered alongside risk reduction deriving from design measures.

Therefore, new measures for risk reduction (operational and in emergencies) should be considered in addition to design measures. What needs to be demonstrated and justified is the level of risk reduction and a way to account for it, the latter by adopting a formal process and taking requisite steps to institutionalise it.

LIFE-CYCLE RISK MANAGEMENT

Traditionally rules, as a risk control measure for damage stability improvement, always focus on design solutions, normally referred to as passive measures (**category 1 measures**), Figure 1, [1]. Operational/active measures (**category 2 measures**) whilst abundant in SOLAS Ch. II-2 (e.g. damage control), have not been validated to the same level of rigour as category 1 measures. Finally, measures/systems focusing on emergency response (**category 3 measures**), such as Decision Support Systems for Crisis Management, Evacuation, LSA, Escape and Rescue, whilst fuelling debates on being effective risk control measures or not, the cost-effectiveness of their risk reduction potential has never been measured nor verified. One of the reasons for this, arguably, derives from the fact that because these measures are there to address 'residual' risk and residual risk is by definition small, therefore risk reduction is also perceived to be small. However, this could not be further from the truth. The second is again lack of measurement and verification of such risk reduction.

Considering the above, a life-cycle perspective offers a framework for a holistic approach to damage stability, focusing on life cycle and encompassing all 3 categories of risk control options, accounting for these based on IMO cost-effectiveness criteria. This assumes that the risk reduction potential of all measures in the three categories is known and this is where there is a big gap in this approach that needs to be overcome before such a process can be formalised and adopted. This constitutes the kernel of the work to

be undertaken, with the workshop described in the following constituting and facilitating the first step.

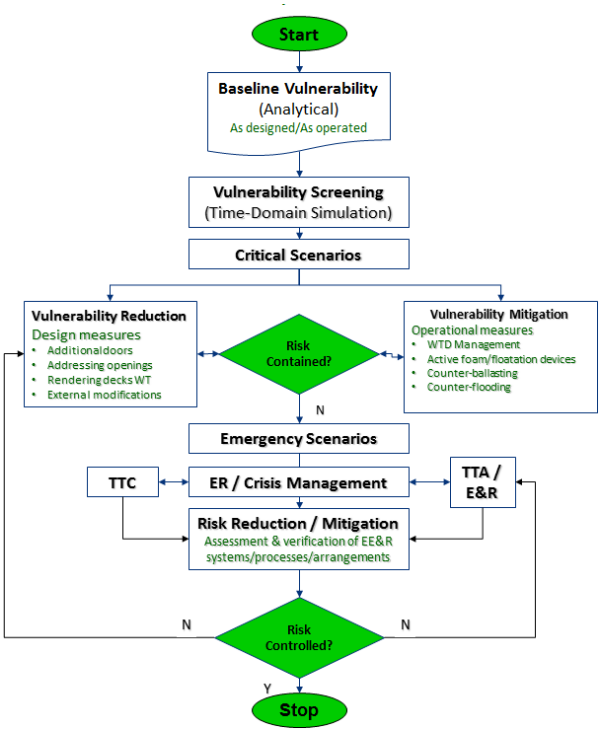

Fig. 1: Vulnerability Management, [1]

WORKSHOP – BRAINSTORMING SESSION

The brainstorming session was conducted on the basis of a number of basic premises related to risk as defined below. Mind maps were used to record the views of the participants. Whilst this method is relatively unstructured, it allows recording of high-level discussions of hazards, influencing factors and risk control measures.

Risk

- Risk can be quantified by the likelihood of undesirable consequences (e.g. fatalities per ship year, total losses per year, etc.)
- The range of undesirable consequences includes: impact on human life (fatalities and injuries) and impact on property (loss of and/or damage to the ship).
- For the purposes of this workshop, the accidental event that may lead to undesirable consequences is "flooding".

Accidental flooding events

- Water ingress and flooding may be the result of casualty incidents or systems failure including – but not limited to the following:
  1. Collision
  2. Contact (e.g. with quay)
  3. Bottom/side raking damage
  4. Failure (e.g. crack) of hull envelope
  5. Failure of overboard valve
- Incidents resulting in internal flooding (ballast water, fuel oils, etc.) may be the result of the following types of systems failures
  6. Internal structural failure (e.g. ballast tank, manhole, structural degradation, etc.);
  7. Failure of fire mains valve.

Risk Reduction

In order to reduce the risk associated with flooding, the likelihood of occurrence and/or the severity of the consequences need to be reduced.

<u>Reducing the likelihood of a flooding event</u>

- Although, it was agreed that this is an important element of the risk associated with flooding, this is out with the scope of the workshop. However, some of the factors affect both likelihood and consequences (e.g. crew competence).

<u>Reducing the severity of the consequences of a flooding event</u>

- The internal watertight subdivision is a passive barrier or risk control measure, the objective of which is to reduce the severity of the consequences should a flooding event occurs;
- However, as indicated in the foregoing, there are other measures that may reduce the severity of the consequences (mitigation) of a flooding event. Those measures are of operational and/or active nature and as such less amenable to statutory verification unless an alternative method is applied.

Risk Contributing Factors

- There are also other factors that can influence the severity of the consequence of flooding. These factors influence the sequence of events that occur after the accidental event. The

sequence of events can be generalised in terms of the following activities, see Table 1:

1. Flooding detection and alarm
2. Damage control
3. Muster of pax
4. Preparation of LSA
5. Abandon ship
6. Rescue to a place of safety

- Identification of the factors that influence the outcome of each of the above stages, is one of the key objectives of the brainstorming session. These factors can be of the following types:
  1. Human (crew, passengers)
  2. Hardware (e.g. ship, systems, equipment)
  3. Organisational (e.g. procedures)
  4. External (e.g. weather-related, SAR assets)
- In addition, human and organisational factors are significant in terms of Damage Control and Emergency Response performance.

Table 1
Generic sequence of events that may occur after a flooding event (typical muster list)

STAGE 1	STAGE 2	STAGE 3
INCIDENT (1) Detection & Alarm	(2) Damage control (3) Muster of Pax (4) Preparation of LSA	(5) Abandon Ship (6) Rescue

IDENTIFICATION OF HAZARDS

Risk contributing factors and potential hazards were identified as listed below. These lists only reflect the scope of the discussions and therefore are not exhaustive; they can however be regarded to be representative.

Stage 1: Detection and Alarm

Relevant hazards identified during the brainstorming session include:

1. Flooding in space not fitted with water alarms
2. No/difficult access for validation of alarm
3. Failure or impairment of automatic means of detection
4. Not effective (slow) means of detection
5. Trips, falls, exposure to flood water when trying to validate an alarm
6. Crew not familiar with layout of the ship
7. No information or uncertainty about the location and the extent of the damage
8. Unclear, ineffective procedures (reference to muster list)
9. Poor competence of crew – lack of training in flooding detection
10. Lack of crew preparedness in searching for water
11. Poor/ineffective internal and/or external communications
12. Initiation of mustering (general alarm) too soon – this will create MUSTERING hazards unnecessarily

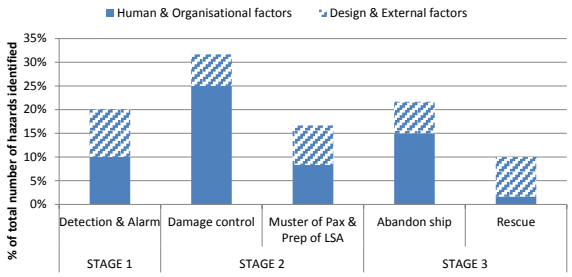

Fig. 2: Breakdown of identified hazards (60 hazards in total)

Stage 2: Damage Control

Relevant hazards identified during the brainstorming session include:

1. High vulnerability of watertight subdivision & arrangements to flooding
2. Impairment of watertight subdivision & arrangements (due to accidental event)
3. Ineffective/blocked scuppers in car deck
4. No/difficult access for effective damage control (e.g. vehicles on car deck, voids)
5. No/difficult access to damage control equipment.
6. Additional hydrostatic pressure on internal structures, doors and bulkhead penetrations
7. No redundancy of essential ship systems after flooding
8. Crew not prepared/not able to reconfigure systems for damage control
9. Trips, falls, exposure to flood water when trying to deploy damage control measures
10. Ship systems not dimensioned for dealing with damage control (e.g. pumps)

11. No information or uncertainty about the location and the extent of the damage, especially if flooding is escalating
12. Crew not able to effectively assess the criticality of the damage
13. Poor competence of crew – not trained in damage control
14. Lack of crew preparedness in damage control
15. Crew not familiar with layout of the ship
16. Crew not available for damage control (low crew redundancy)
17. Lack of effective leadership in an emergency situation
18. Breakdown of internal communication (due to language barriers, inappropriate use or failure of communications equipment)
19. Ineffective/unhelpful external support
20. Rough weather, cold climates.

Stage 2: Muster of Pax & Preparation of LSA

Relevant hazards identified during the brainstorming session include:

1. False alarm – muster initiation too soon, would create unnecessary hazards for pax
2. Impairment of escape routes, muster areas and/or LSA systems (due to accidental event)
3. Impairment or failure of lighting along escape routes and/or muster areas (e.g. due to blackout as a result of the flooding)
4. Impairment or failure of internal communication systems (e.g. due to blackout as a result of flooding)
5. Ship motions, heel, trim – making moving to muster areas difficult and hazardous
6. Trips and falls when moving to muster area
7. Exposure to weather (to pax if mustering externally; to crew when preparing LSA)
8. Inefficient internal communication (with pax)
9. Difficult pax behaviour – crew not prepared in crowd control
10. Not sufficient crew numbers available to assist pax (e.g. due to damage control efforts) and control of mustering.

Stage 3: Abandon Ship

Relevant hazards identified during the brainstorming session include:

1. Fast ship capsize
2. Poor/delayed decision by the Master
3. Impairment of embarkation areas and/or LSA (due to accidental event)
4. Failure of deployment of LSA systems
5. Impairment or failure of emergency abandonment systems (e.g. due to blackout as a result of flooding)
6. MOB situation
7. Lack of key crew redundancy
8. Rough weather
9. Large heel and trim angles (in excess of LSA design criteria)
10. Poor competence of crew – not trained in deployment and use of all LSA on-board
11. Lack of crew preparedness in LSA deployment and embarkation
12. Not sufficient competent crew numbers available to deploy and control LSA units
13. Poor/ineffective passage planning (with SAR in mind).

Stage 4: Rescue to Place of Safety

Relevant hazards identified during the brainstorming session include:

1. Ineffective/no SAR planning
2. Safe place (to transfer people) not available
3. Unavailability of adequate SAR assets (for the number of persons)
4. Lack of crew preparedness
5. Poor/ineffective communication with external stakeholders (safe port, class, Coastal and Flag State)
6. Rough weather

FLOODING RISK MITIGATION OPTIONS

Although it was acknowledged that it is always preferable to have passive or semi-automatic measures in place, the discussion was focused on active and operational damage mitigation options including the following (see Figure 1):

Design Modifications (Category 1)

The following observations can be made:

- Passive measures providing additional buoyancy (sponsons, ducktails, buoyancy tanks, etc.);
- The performance of design modifications is related to the effectiveness of flooding mitigation;

- The effectiveness of design modifications does not depend explicitly on crew performance;
- Design modifications reducing the inherent vulnerability to flooding; from all mitigation measures, they may have the highest potential for improving the value of the A-index (Figure 3)

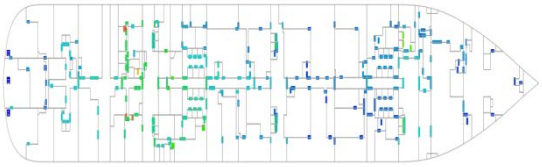

Fig. 3: Vulnerability Screening (identification of focal areas for improved survivability)

- Well known solutions and their implications – relating to the following
  - ✓ Double hull machinery room
  - ✓ Rendering decks watertight
  - ✓ Relocation of openings
  - ✓ SWT / Splash-tight doors (Fire doors)
  - ✓ Buoyancy tanks

Operational Measures (Category 2)

In relation to containment actions, the following observations were made:

- Containment actions limit the severity of the consequences of a flooding accident by preventing progressive flooding
- Limited experience on merchant ships –better experience on naval vessels
- Simple tools and equipment available on-board
- Crew competence and preparedness is a significant influencing factor in ensuring that containment actions are effective
- However, in terms of statutory A index calculations or flooding simulations, it is assumed that the existing watertight integrity performs as expected, e.g. watertight doors do not leak, penetrations in watertight bulkheads do not leak, etc.

In relation to active damage control, the following observations can be made:

- Counter ballasting and/or counter flooding measures limit the severity of the consequences of a flooding accident by preventing excessive heel/trim of the ship (Figure 4)

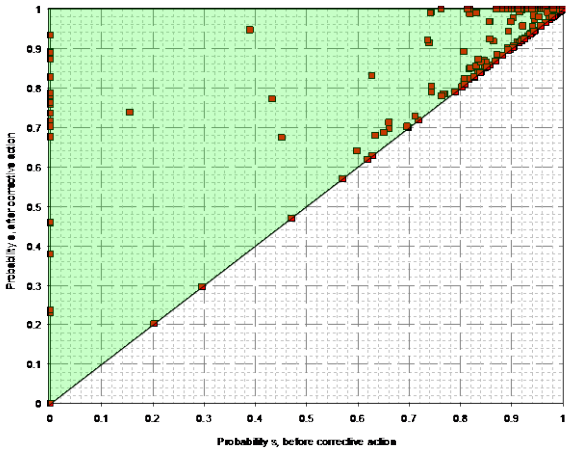

Fig. 4: Counter-ballasting capacity post-casualty (typical example)

- Damage-specific measures not possible in all cases
- Depends on tank and internal arrangements
- Relies on the availability of relevant ship systems (bilge, ballast, power, among others)
- Large number of possibilities – difficult to assess and do by the crew without support
- Hazard of significant hydrostatic loads on internal structures
- Potential for using new materials/technologies (e.g. foams, inflatable devices):
  - o Fast semi-automatic deployment, essential
  - o To be effective in critical damages where time to capsize less than say 20 minutes
  - o Requires type approval and additional maintenance and training
- Crew competence and preparedness as well as availability of relevant ship systems are significant influencing factors for ensuring that active damage control actions are effective
- The contribution to A-index can be assessed by means of flooding simulations (not by statutory calculations). However, in order to ensure that the actions can be accomplished effectively, crew performance and availability of relevant ship systems needs to be demonstrated.

Some radical actions were identified, for which the following observations can be made:

- Running the ship aground when/if possible
- Unloading cargo overboard when/if necessary
- Such actions will require additional planning and crew preparedness.

Emergency Response Measures (Category 3)

These relate mainly to escape, evacuation and rescue arrangements; for which the following comments were made:

- Measures reducing the severity of the consequences of a flooding accident by allowing the persons on-board to abandon the vessel.
- Effective evacuation requires the vessel to remain afloat and upright – to the limits of LSA systems
- Crew competence and preparedness as well as availability of relevant ship systems are significant influencing factors for ensuring that people on-board can be evacuated effectively

WORKSHOP OUTCOME

The outcome of the workshop discussions and subsequent analysis is presented under the following headings:

- Long-terms goals
- Ship vulnerability to flooding
- Active flooding mitigation
- Risk reduction

Long-terms goals

Although in the short to medium term, the goal of the initiative started by INTERFERRY EUROPE is related to the potential retrospective application of increased R-index requirements, the participants of the workshop agreed that the long-term goals and implications of the issues addressed in the workshop need to be established.

Key items that will be affected include:

1. Alternative arrangements and credit for operations/emergency response measures
2. Definition and interpretation of required subdivision index R, SOLAS Ch.II-1 Regulation 6.
3. Alternative methodology for the calculation of the A index value – in accordance with SOLAS Ch.II-1 Regulation 4.
4. Verification of essential ship systems redundancy for existing ships. This is in line with SOLAS Ch.II-2 Safe return to Port requirements for ship systems
5. Evacuation and LSA arrangements – considering that SOLAS Ch.III is under revision.
6. Verification and validation of crew preparedness and performance. ISM Code implementation is the minimum level or performance expected;
7. Contribution from INTERFERRY on potential changes to SOLAS and the ISM Code.

Ship vulnerability to flooding

In terms of the subdivision index, used for design verification of ship damage stability, the following observations can be made:

1. The required index of subdivision R expressed the accepted probability of a ship surviving a collision incident for 30 minutes or more. Consequently, the attained index A reflects the average probability of a ship surviving 30 minutes or more, such average deriving from consideration of damage statistics as described in SOLAS 2009.
2. On this basis, a ship attaining a value of A=0.8, implies that the ship has a 20% average probability of capsize within 30 minutes, following flooding of ship spaces as a result of collision damage.
3. The statutory calculation [1] of A-index encompasses many empirical approximations (e.g. s-factor) and conservative assumptions, some of which are not justified in practice (e.g. loading conditions).

Moreover, there is extensive knowledge and evidence to make the following assertions:

4. A method based on numerical (flooding) simulations and Monte-Carlo sampling techniques can be used reliably as an alternative approach to the statutory calculation of the A-index, in accordance with SOLAS Ch.II-1 Regulation 4.2.
5. Previous studies have shown that by using this alternative method, the simplicity and conservatism implicit in the statutory calculations may, in some cases lead to underestimation, while in other cases lead to overestimation of the attained index A. (Figures 5 and 6)

[1] Referred to as 'SOLAS2009' calculation

6. Furthermore, regarding these flooding cases in which a ship is likely to capsize within 30 minutes, it has been shown that in some cases, (i) the ship will have no damage stability at all: i.e. the ship will capsize fast, whilst in other cases (ii) the ship may be recovered with effective active damage control: i.e. the ship can be saved or the time to capsize can be extended to allow for evacuation (Figure 4)
7. The alternative approach is a better method for assessing the vulnerability of a ship to flooding, regardless of the type of accident (collision, grounding, raking damage, etc.).
8. The use of the alternative approach to assess ship vulnerability has many benefits; it allows the incorporation of realistic operating conditions and it allows the verification of active damage control actions such as counter-ballast and counter-flooding, and by providing information on time line of events, it allows assessing the effectiveness of the evacuation arrangements

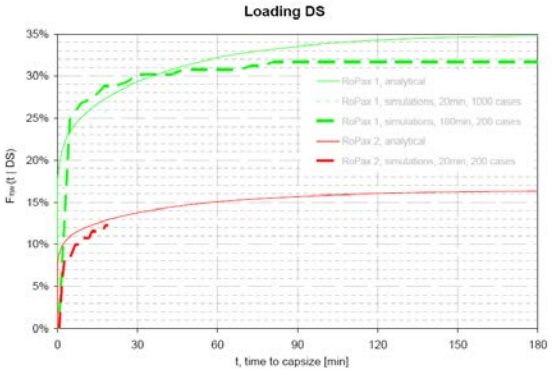

Fig. 5: SOLAS Vs Numerical Simulations (Reg. 4, Part B) – Simple Internal Architecture

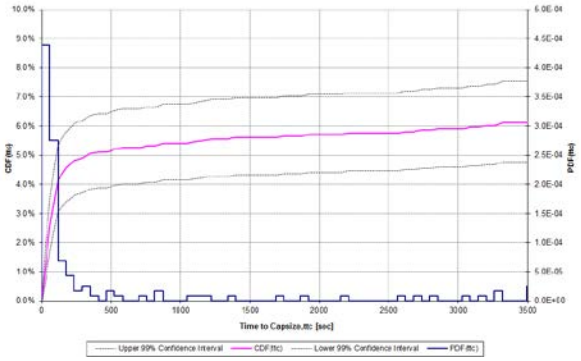

Fig. 6: SOLAS Vs Numerical Simulations (Reg. 4, Part B) – Medium Complexity Internal Architecture

Active Flooding Mitigation

Assuming that an alternative method for assessing ship vulnerability to flooding is adopted, active flooding mitigation options for which credit can be obtained in terms of the attained A-index (by simulation), include the following:

1. Design modifications – although not the preferred option for existing ships unless they are easy to implement and are cost-effective
2. Active, counter-ballasting, counter-flooding measures – these are damage-specific therefore, verification may be extensive. In order to realise the potential gains, additional verification is required:
   a. Relevant ship systems must be demonstrated to be available (Safe Return to Port concept of SOLAS Ch.II-2) – note that 16% of the hazards related to damage control relate to ship systems redundancy in case of flooding
   b. Crew competence and preparedness must be demonstrated (objective evidence as per or beyond SOLAS and ISM Code requirements). Note that 32% of the hazards identified relate to damage control. Of those, the majority (78%) can be controlled by effective crew performance and/or effective operating procedures.

Risk reduction

Effective evacuation and rescue (EER) arrangements also reduce the risk to people. These measures can be successful only if the ship remains afloat and upright for as long as necessary to complete the ship abandonment process. Therefore the following is required to demonstrate risk reduction:

1. Time line of key events in the flooding process – e.g. time to reach a heel angle of, say 20 degrees. This can be provided by the numerical flooding simulations (alternative approach)
2. A verification of the time required to carry out ship abandonment as per the ship's muster list. This includes quantification of the time for general alarm, response and mustering, embarkation of LSA, deployment of LSA and sail away from vessel.
3. Crew competence and preparedness must be demonstrated (objective evidence as per or beyond SOLAS and ISM Code requirements) – Note that 32% of the hazards identified relate to

ship abandon and rescue. Of those, the large majority (86%) can be controlled by effective crew performance and/or effective operating procedures.

CONLCUDING REMARKS

1. Building on the knowledge and understanding of damage stability fundamentals, a process has been elucidated to address the vulnerability to flooding of passenger ships from a life-cycle perspective and with focus on operational and emergency response measures alongside the more traditional design measures, with emphasis of application on existing ships.
2. An initiative undertaken by INTERFERRY Europe is putting this concept to test, starting with workshop to assess the impact of possible changes in the required subdivision index R and the potential implications for existing vessels should IMO decided to apply the new requirements retrospectively.

ACKNOWLEDGMENTS

The authors would like to express their gratitude to INTERFERRY for sponsoring this work and for their invaluable contribution to identifying and targeting cost-effective solutions to improving the damage survivability of RoRo passenger ships.

REFERENCES

Vassalos, D: "Emergency Response in Flooding Casualties", 13th Int. Ship Stability Workshoip, Brest, France, 21-26 September 2013.